Synthesis and Study of the Cyclic Lipopeptide Antibiotics Paenibacterin and Daptomycin

by

Michael Noden

A thesis
presented to the University of Waterloo
in fulfillment of the
thesis requirement for the degree of
Doctor of Philosophy
in
Chemistry

Waterloo, Ontario, Canada, 2021

Examining Committee Membership

The following served on the Examining Committee for this thesis. The decision of the Examining Committee is by majority vote.

External Examiner	Dr. Karine Auclair, PhD Professor, McGill University Chemistry
Supervisor	Dr. Scott Taylor, PhD Professor, University of Waterloo Chemistry
Internal-External Member	Dr. Zoya Leonenko, PhD Professor, University of Waterloo Biology, Physics and Astronomy
Other Members	Dr. Michael Palmer, MD, Dr. habil Associate Professor, University of Waterloo Biochemistry, Chemistry
	Dr. Adrian Schwan, PhD Professor, University of Guelph Chemistry

Author's Declaration

This thesis consists of material all of which I authored or co-authored: see Statement of Contributions included in the thesis. This is a true copy of the thesis, including any required final revisions, as accepted by my examiners.

I understand that my thesis may be made electronically available to the public.

Statement of Contributions

Michael Noden is the sole author for chapters 1, 3, and 6 which were written under the supervision of Dr. Scott Taylor. Chapters 1 and 6 were not written for publication. Chapter 3 has not yet been adapted for publication at the time of writing. At the time of writing Chapter 5 is being adapted for publication by Michael Noden and Dr. Scott Taylor. Additional details regarding specific contributions are included throughout this thesis.

Research presented in Chapter 2:

This work was carried out by Michael Noden under the supervision of Dr. Scott Taylor at the University of Waterloo. Dr. Michael Palmer provided additional supervision and materials for biological studies. Ryan Moreira provided a key reagent, the synthesis and characterization of which is published elsewhere. Dr. En Huang provided a sample of authentic paenibacterin isolated from OSY-SE, which he prepared under the supervision of Dr. Ahmed Yousef. Chapter 2 is an adapted pre-publication version of the paper.[1] The manuscript was written by Michael Noden with input and revisions primarily from Dr. Scott Taylor. Other listed authors approved the manuscript before submission.

Research presented in Chapter 4:

This work was carried out by Michael Noden under the supervision of Dr. Scott Taylor at the University of Waterloo. Chapter 4 is an adapted version of the paper that was submitted for review to the *Journal of Organic Chemistry*. The manuscript was written by Michael Noden with input and revisions primarily from Dr. Scott Taylor. Four fluorescent peptides were prepared by Carlee Montgomery and are mentioned in brief within this chapter.

Research presented in Chapter 5:

This work was carried out by several graduate students. Approximately half of the peptides within this section were prepared by Ghufran Barnawi under the supervision of Dr. Scott Taylor. These peptides were analyzed by Sara Schulz and David Beriashvili under the supervision of Dr. Michael Palmer. The remaining peptides were prepared either by Michael Noden, or by Olivia Schneider and Julian Marlyn—overseen by Michael Noden and under the supervision of Dr. Scott Taylor. Characterization of these compounds was carried out in-part or wholly by Michael Noden. The specific contributions of each individual are outlined throughout this chapter. Five peptides were prepared by Jeremy Goodyear, overseen by Ryan Moreira; these are mentioned in brief at the end of this chapter. The collected data was amalgamated by Michael Noden, who is also wrote chapter 5 in full with input and revisions by Dr. Scott Taylor. At the time of writing this chapter is being adapted for publication.

Abstract

Cyclic lipopeptides present a rich source of antimicrobial compounds with diverse modes of action. Paenibacterin is a cyclic lipopeptide antibiotic produced by *Paenibacillus thaminolyticus* that exhibits activity against a broad spectrum of bacteria. Paenibacterin's mechanism of action (MOA) against Gram-negative bacteria is thought to be similar to the clinically useful polymyxins; however, certain aspects of its MOA are still not understood, particularly with respect to its activity against Gram-positive bacteria. To facilitate MOA studies a method for the synthesis of paenibacterin and analogs was developed using solid-phase peptide synthesis (SPPS). One analog was prepared where costly D-Orn residues were replaced with D-Lys residues. This analog exhibited activity similar to or better than native paenibacterin and so was used as a scaffold for further analogs.

To establish structure-activity relationships (SARs) of paenibacterin, a series of analogs were synthesized and their *in vitro* antibacterial activity was evaluated. Several analogs were prepared with acyl tails reduced from 15 carbon atoms to 2 carbon atoms in length. Pentanoyl or acetyl tails resulted in loss of activity. Activity against Gram-positive bacteria gradually decreased as the tail length was reduced from 15 to 10 carbon atoms. Activity against Gram-negative bacteria remained consistent with a decanoyl tail. To determine the importance of each cationic lysine residue, they were individually replaced with alanine. Replacing any single lysine residue resulted in at most a two-fold loss in activity. We then prepared analogs with double Lys→Ala substitutions. This resulted in only a two to four-fold loss in activity against Gram-positive bacteria, but activity against Gram-negative bacteria was highly dependent on which lysine residues were replaced. Two fluorescent analogs were prepared, with either a 1-pyrenbutyric acid tail, or a tryptophan residue at position 6. An analog of a paenibacterin B series peptide was also prepared.

To facilitate MOA studies of paenibacterin and other peptide antibiotics, two environmentally sensitive fluorescent amino acids were prepared bearing a 7-dialkylaminocoumarin fluorophore. These amino acids were compatible with Fmoc-SPPS and were incorporated into a paenibacterin analog. The interaction of this analog with model membranes, lipopolysaccharide, and bacterial cells was examined using fluorescence spectroscopy and confocal microscopy.

Lastly a SAR study was conducted on an analog of the lipopeptide antibiotic daptomycin, Dap-K6-E12-W13. A series of substitutions were made at positions 8 and 11, and their effect on *in vitro* antimicrobial activity and calcium-dependent membrane binding was determined. Cationic residues were well tolerated at these positions, and these analogs exhibited good activity and membrane

binding at low calcium concentrations. When the same substitutions were introduced into daptomycin, they increased antibacterial activity.

Acknowledgements

The completion of this thesis was made possible by the support of many. I would like to express my sincere thanks to Professor Scott Taylor for accepting me into his research group and providing support and guidance throughout the course of my undergraduate and graduate studies. His insightful advice and genuine enthusiasm were both helpful and inspiring. I would also like to thank the members of my advisory committee. Dr. Michael Palmer, who opened his lab to me and other Taylor group members, and who provided invaluable advice throughout the duration of this project. Dr. Gary Dmitrienko and Dr. Adrian Schwan, who provided informative discussion and recommendations during meetings over the past few years. I also thank Dr. Karine Auclair and Dr. Zoya Leonenko, for agreeing to join my examining committee.

I extend my gratitude to members of the Taylor group with whom I have had the pleasure of working over the years: Dr. Chuda Lohani, Dr. Robert Taylor, Dr. Bowei Zheng, Dr. Braden Kralt, Dr. Jacob Soley, Bradley Scott, Yuhan Huang, Ghufran Barnawi, Ryan Moreira, Matthew Diamandas, Jeremy Goodyear, and the many undergraduate students who joined the group during my time. I would also like to thank the administrative and research staff at the University of Waterloo for their help and support.

Thank you to my family and friends for their love and support. I am especially grateful for the never-ending support of my parents, Evan and Lori, and my wife Kaylin.

Dedication

To Kaylin…

Table of Contents

List of Figures

List of Schemes

List of Tables

List of Abbreviations

2-MP	2-methylpiperidine
4-MP	4-methylpiperidine
ABC	ATP-binding cassette
A-domain	adenylation domain
Alloc	allyloxycarbonyl
AMP	antimicrobial peptide
ATP	adenosine triphosphate
Boc	*tert*-butyloxycarbonyl
BODIPY	4,4-difluoro-4-bora-3a,4a-diaza-*s*-indacene
BOP	benzotriazol-1-yloxytris(dimethylamino)phosphonium hexafluorophosphate
C1	coumarin 1
C311	coumarin 311
CCCP	carbonyl cyanide *m*-chlorophenylhydrazone
C-domain	condensation domain
cLPA	cyclic lipopeptide antibiotic
CMC	critical micelle concentration
COMU	(1-cyano-2-ethoxy-2-oxoethylidenaminooxy)dimethylamino-morpholino-carbenium hexafluorophosphate
Dab	2,4-diaminobutyric acid
Daba	(2*S*,3*R*)-diaminobutyric acid
Dapa	2,3-diaminopropionic acid
DCM	dichloromethane
Dde	1-(4,4-dimethyl-2,6-dioxocyclohex-1-ylidene)ethyl
DEACA	7-diethylaminocoumarin-4-alanine
DIC	*N,N'*-diisopropylcarbodiimide
DIPEA	*N,N*-diisopropylethylamine
$diSC_3(5)$	3,3'-dipropylthiadicarbocyanine iodide
DKP	diketopiperazine
DMACA	7-dimethylaminocoumarin-4-alanine
DMAP	4-dimethylaminopyridine
Dmb	2,4-dimethoxybenzyl
DMBA	1,3-dimethylbarbituric acid
DMF	*N,N*-dimethylformamide
DMPC	1,2-dimyristoyl-*sn*-glycero-3-phosphocholine
DMPG	1,2-dimyristoyl-*sn*-glycero-3-phospho-(1'-*rac*-glycerol) sodium salt
DOPC	1,2-dioleoyl-*sn*-glycero-3-phosphocholine
DOPG	1,2-dioleoyl-*sn*-glycero-3-phospho-(1'-*rac*-glycerol) sodium salt
DPPA	diphenylphosphoryl azide

EDT	ethanedithiol
EDTA	ethylenediaminetetraacetic acid
EtOAc	ethyl acetate
FlAA	fluorescent amino acid
Fmoc	fluorenylmethyloxycarbonyl
FRET	Förster resonance energy transfer
GlcNAc	*N*-acetylglucosamine
Gram-(−)	Gram-negative
Gram-(+)	Gram-positive
HBTU	hexafluorophosphate benzotriazole tetramethyl uronium
HCTU	*O*-(1h-6-chlorobenzotriazole-1-yl)-1,1,3,3-tetramethyluronium hexafluorophosphate
HDP	host-defense peptide
Hmb	hydroxymethylbenzyl
HMPA	hexamethylphosphoramide
HOAt	1-hydroxy-7-azabenzotriazole
HRMS	high resolution mass spectrometry
IC_{50}	half maximal inhibitory concentration
ITC	isothermal calorimetry
KDO	ketodeoxyoctonate
Kyn	kynurenine
LPS	lipopolysaccharide
LUV	large unilamellar vesicle
MDR	multi-drug resistant
MeGlu	(2*S*,3*R*)-3-methylglutamate
MIC	minimum inhibitory concentration
MOA	mechanism of action
MRSA	methicillin-resistant *Staphylococcus aureus*
MurNAc	*N*-acetylmuramic acid
NBD	7-nitro-2,1,3-benzoxadiazol
NMM	*N*-methylmorpholine
NRPS	non-ribosomal peptide synthetase
Orn	ornithine
PA	paenibacterin A
PAK	paenibacterin A1-D-Lys1-D-Lys4
PB	paenibacterin B
PBFI	potassium-binding benzofuran isophthalate
PBK	paenibacterin B-D-Lys1-D-Lys4
PBP	penicillin binding protein
PCP	peptidyl carrier protein
PE	phosphatidylethanolamine
PEG	polyethylene glycol

PEZ	pfefferminz
PG	phosphatidylglycerol
PMBN	polymyxin B nonapeptide
PMB-R	polymyxin B resistant
Ppan	4'-phosphopantetheine
PyAOP	(7-azabenzotriazol-1-yloxy)tripyrrolidinophosphonium hexafluorophosphate
RP-HPLC	reversed phase high-performance liquid chromatography
SAR	structure-activity relationship
SPPS	solid-phase peptide synthesis
t-Bu	*tert*-butyl
TDR	totally drug resistant
TFA	trifluoroacetic acid
THF	tetrahydrofuran
TIPS	triisopropylsilane
TIRF	total internal reflection fluorescence
TLC	thin layer chromatography
Trt	trityl
UDP	uridine diphosphate
VRE	vancomycin-resistant enterococci
VRSA	vancomycin-resistant *Staphylococcus aureus*
WHO	World Health Organization
XDR	extremely drug resistant

Chapter 1
Introduction & Literature Review

1.1 Microbial resistance and the need for new antimicrobials

The prevalence of antibiotic-resistant bacteria is increasing, and bacterial infections are becoming more challenging to treat. Antibiotic resistance has significantly increased the risk associated with routine medical procedures including surgery and cancer treatment. In spite of this, the development of new antimicrobials has stagnated due to high development costs and relatively low profitability of antimicrobial drugs.[2] Consequently, the World Health Organization (WHO) considers microbial resistance to antibiotics and the lack of development of new antibiotics as one of the greatest potential threats to human health.[2]

The emergence of multi-drug resistance (MDR) is prevalent among both Gram-positive (Gram-(+)) and Gram-negative (Gram-(−)) bacteria. Many recent antibiotic development efforts have been directed at the ESKAPE pathogens, which consist of *Enterococcus faecium*, *Staphylococcus aureus*, *Klebsiella pneumoniae*, *Acinetobacter baumannii*, *Pseudomonas aeruginosa*, and *Enterobacter* spp., with the first two species being Gram-(+) bacteria and latter four species being Gram-(−) bacteria.[3] These bacteria are responsible for a large fraction of infections in hospital environments, and exhibit resistance to many common antibiotics.

Treatment of infections resistant to common antibiotics typically involves a small number of so-called *drugs of last resort* or *last defense*. For treating resistant infections caused by Gram-(+) organisms, such antibiotics include: linezolid, quinupristin-dalfopristin, and daptomycin, which are used for treating vancomycin-resistant *Enterococcus* spp. (VRE); and vancomycin, linezolid, tigecycline, and daptomycin, used for treating methicillin-resistant *S. aureus* (MRSA).[4] Daptomycin is

a cyclic lipopeptide antibiotic (cLPA) (Figure 1.1) and represents one of the few new classes of antibiotics to be approved for clinical use in the last two decades.

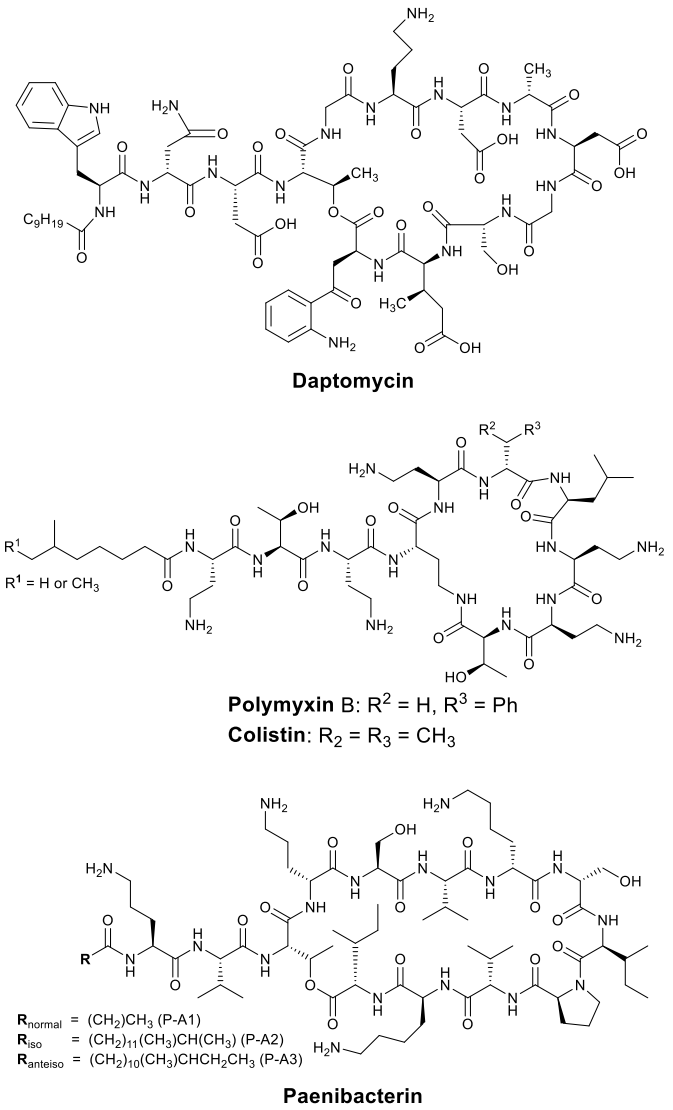

Figure 1.1 Structures of daptomycin, polymyxins B and E (colistin) and paenibacterin.

Resistance among Gram-(−) bacteria is arguably a more pressing issue, with extremely drug-resistant (XDR) and totally drug-resistant (TDR) strains emerging. Certain *P. aeruginosa* strains have developed resistance to all current antibiotics save the polymyxin class of antibiotics, such as colistin (polymyxin

E) and polymyxin B (Figure 1.1) which, like daptomycin, are also cLPAs.[4] The polymyxin-class of antibiotics still retain their activity against many MDR Gram-(−) strains; however, colistin-resistant *K. pneumoniae* strains have emerged.[4] The low degree of resistance to polymyxin antibiotics can in part be attributed to reduced use in the past due to nephrotoxic and neurotoxic effects upon intravenous injection. Even now, this relegates polymyxin B and colistin to use as a last resort treatment for internal infections, though toxicity is not observed in patients given the commonly recommended daily dosage.[5,6] This presents an obvious opportunity for the development of polymyxin-like cationic cLPAs with similar mechanisms of action (MOA), but more favourable pharmacokinetic properties.

Albeit rare, the number of clinical isolates exhibiting resistance to last resort antibiotics such as daptomycin and polymyxin is increasing steadily.[7,8] This is a cause for considerable concern as these antibiotics are among the last defense antibiotics against several very serious pathogens. It is crucial that new antibiotics be developed to address this problem. The overarching goal of this thesis is to develop new cLPA antibiotics that are active against the ESKAPE pathogens. These new antibiotics are derived daptomycin and a recently discovered cLPA called paenibacterin (Figure 1.1).

1.2 Bacterial Membranes

Daptomycin and paenibacterin are cLPAs that exert their antibacterial effects by acting upon bacterial membranes. A brief discussion of bacterial membranes is presented below.

Bacteria are divided into two categories based on the structure of their outer membranes: Gram-(+) and Gram-(−). Gram-(+) bacteria have only a single membrane surrounded by a thick cell wall, while Gram-(−) bacteria have both an outer and inner membrane (Figure 1.2), the latter of which closely resembles the Gram-(+) cytoplasmic membrane. The properties of bacterial cytoplasmic membranes are discussed below, followed by a discussion of Gram-(+) and Gram-(−) membranes in sections 1.2.1 and 1.2.2, respectively.

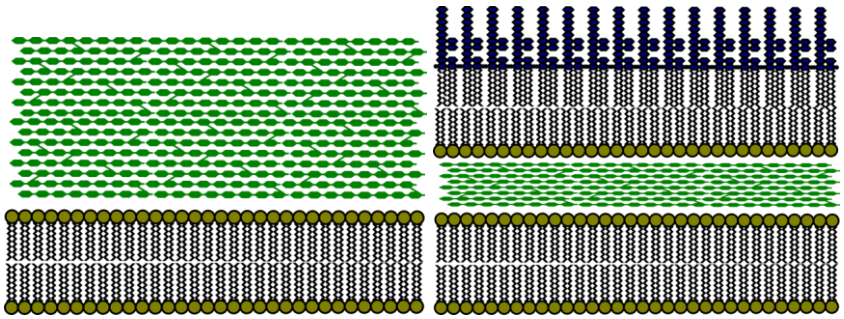

Figure 1.2 Bacterial membranes. Left: Phospholipid membrane (phospholipid headgroups shown in yellow) and peptidoglycan cell wall (green) of Gram-(+) bacteria. **Right:** Inner membrane (phospholipid bilayer) cell wall (green), and LPS (blue) containing outermembrane of Gram-(−) bacteria.

The bacterial cytoplasmic membrane consists of a phospholipid bilayer with embedded hydrophobic membrane proteins. The cytoplasmic membrane contains the cell's contents and separates them from the external environment. The membrane also serves as a permeability barrier, allowing the cell to control movement of nutrients, small ions, waste, and more through a variety of mechanisms.[9,10]

The fluid mosaic model of the cytoplasmic membrane was devised by Singer and Nicolson and published in 1972.[11] The membrane was described as a two-dimensional liquid containing embedded proteins, called *integral proteins*, which diffused freely throughout the membrane. Though lipids are capable of easy lateral diffusion, there is little movement of lipids from one face to the other i.e., lipid *flip-flop*. This results in an inner and outer leaflet with different lipid compositions. Lipid *flip-flop* is mediated by families of flippase enzymes.[12–15] The main components of bacterial cytoplasmic membranes are phosphatidylglycerol (PG), cardiolipin, and phosphatidyl ethanolamine (PE). Both PG and cardiolipin are anionic while PE is zwitterionic.[9] Since its inception, the fluid mosaic model has been refined considerably to incorporate organized membrane structures such as the lipid rafts found in eukaryotes. Lipid rafts are regions where cholesterol induces lipid segregation forming a sphingolipid rich domain of reduced fluidity in which specific proteins will accumulate. These domains play a role

in cell trafficking and signalling.[16] Analogous membrane domains have been identified in bacteria, and these domains accumulate proteins involved in signaling and transport.[17] Membranes also contain domains of increased fluidity. In bacteria the cell-wall synthesis machinery accumulates in such a region, and disruption of the fluidity of these domains is a mechanism by which cLPAs may exert their bactericidal activity.[18]

The cell membrane is also a source of energy, which is stored as a proton gradient.[10] Like in mitochondria, this so-called *proton motive force* can be harnessed for ATP synthesis, but it can also play a role in signaling.[19] The gradient is also important for certain modes of transport across the membrane. Some bacteria, particularly pathogenic species, make use of an analogous *sodium motive force* that can be used for energy production or transport across the membrane.[20] Some antibiotics function by disrupting these electrochemical gradients.

For the membrane to act as an effective permeability barrier, the import and export of nutrients, waste, etc. must be tightly controlled. There are three classes of transport systems for the movement of nutrients into the cell: simple transport, group translocation, and the ABC transporters.[10] The energy for simple transport comes from the proton motive force. A notable example of a simple transporter is *lac permease* in which internalizes lactose into *E. coli*. Group transport relies on chemical modification of the substrate. In the case of the phosphotransferase system sugars are phosphorylated upon reaching the cytoplasm. Finally, the ABC (ATP-binding cassette) system relies on a substrate-specific binding protein located between the peptidoglycan layer and the membrane which delivers the substrate to a transmembrane channel. The process is driven by ATP hydrolysis by associated proteins on the inner leaflet. Transport proteins can be further subdivided into uniporters (transport one molecule in one direction), symporters (couple the transported molecule with another, such as a proton), and antiporters (two molecules are transported in opposite directions). To reach an intracellular target, antibiotics must either be capable traversing cellular membranes by passive diffusion upon partitioning into the lipid

bilayer (e.g. tetracyclines or chloramphenicol), or be a compatible substrate for an active transport systems (e.g. aminoglycosides).[21] ABC transporters are used for excretion of peptide antibiotics, and this active efflux mechanism can provide self-immunity to antibiotic-producing bacteria.[22]

1.2.1 Gram-Positive Bacteria

Gram-(+) bacteria are characterized by their single membrane surrounded by a thick cell wall composed of peptidoglycan (also called murein). In addition to the common three phospholipids, modified PG can be found in the membrane of Gram-(+) bacteria, where it is acylated with lysine, alanine, or arginine.[23] These modifications alter the membranes properties and can play a role in resistance to antibiotics.

The cell wall of Gram-(+) bacteria is composed of a *N*-acetylglucosamine and *N*-muramic acid polysaccharides held together by short peptide linkages composed of D/L-Ala, D-Glu, and Lys or diaminopimelic acid. The cell wall provides structural integrity to the cell, counter-balancing the relatively intense osmotic pressure caused by high solute concentrations found in bacteria.[10]

Synthesis of peptidoglycan (Figure 1.3) begins in the cytoplasm with uridine diphosphate (UDP) linked *N*-acetylglucosamine (GlcNAc), which is converted to *N*-acetylmuramic acid (MurNAc), followed by the coupling of five amino acids—sequence: AE(K or diaminopimelic acid)AA. This is accomplished by a series of enzymes referred to as MurA-F.[24] The sugar-linked peptide is then transferred from UDP to a lipid carrier on the inner leaflet of the membrane by the integral membrane protein MraY giving Lipid I. MurG then transfers a GlcNAc subunit onto the MurNAc moiety giving Lipid II.[25] Lipid II is then transferred to the outer leaflet by a flippase. The identity of this flippase is a contentious issue, with three putative candidates: FtsW, MurJ (mentioned above), and AmJ. In a 2015 review Ruiz outlines the case for each of the candidates.[26] Briefly, FtsW has been shown to cause lipid II translocation *in vitro* but is not supported by *in vivo* evidence, and the opposite is true for MurJ and

AmJ. Following translocation, the glycosyltransferase enzymes incorporate the glycopeptide subunit into the peptidoglycan chains. Transpeptidases then catalyse cross-linking between strands through the peptide moieties. Interference with these later steps is a common and effective mechanism of action for antibiotics, highlighted by the naming of the *penicillin binding proteins* (PBPs) which catalyze this cross-linking step and are inhibited by the antibiotic penicillin.[27]

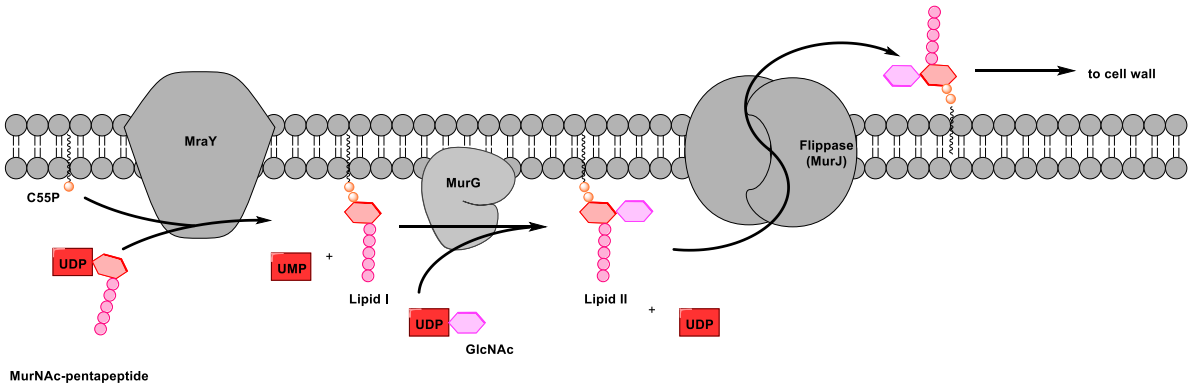

Figure 1.3 Biosynthesis of the cell wall precursor lipid II.

Another important component of Gram-(+) bacterial cell walls are teichoic acids. Teichoic acids are glycerol phosphate/ribitol phosphate-carbohydrate copolymers that may be incorporated into the cell-wall or anchored to bacterial membranes (lipoteichoic acids).[28,29] Wall teichoic acids serve many purposes including the regulation and localization of peptidoglycan biosynthesis proteins, metal ion binding, biofilm formation and cell adhesion, as well as simple modification of the cell wall's charge and hydrophobicity which plays a role in defence.[29] They also contribute to the overall negative charge of the cell surface.[10] Modifications to lipoteichoic acids can affect the properties of the cell membrane and is an important component of antibiotic resistance mechanisms.[28]

1.2.2 Gram-Negative Bacteria

Gram-(−) bacteria are characterized by a relatively thin peptidoglycan cell wall which is enclosed within an outer membrane. The outer membrane differs significantly from the inner membrane, mainly

due to the presence of lipopolysaccharide (LPS) on the outer leaflet.[10] In contrast to the cytoplasmic membrane, the outer membrane is permeable to small molecules thanks to transmembrane proteins called porins, which allow for passive diffusion in and out of the periplasm. The outer membrane is impermeable to larger molecules and proteins, which allows for the retention of periplasmic enzymes that can carry out their function outside of the cytoplasm.[10] This impermeability is in part responsible for the lack of susceptibility of Gram-(−) bacteria towards certain large antibiotics such as vancomycin, daptomycin, and rifampin. Another key component of the outer membrane are the lipoproteins found anchored into the inner leaflet, such as LpoB which participates in regulation of PBPs.[9,30]

The structure of LPS is divided into three components: furthest from the membrane is the O-specific polysaccharide (O-antigen), which is usually made up of galactose, glucose, mannose, rhamnose, and some dideoxyhexoses; next is the core polysaccharide composed of ketodeoxyoctonate (KDO), glucose, galactose, GlcNAc, and assorted heptoses; finally lipid A is composed of a diphosphorylated glucosamine disaccharide which is acylated with fatty acids typically 6–18 carbon atoms in length.[10] Peptide antibiotics that are active against Gram-(−) bacteria—several of which are mentioned in detail in this chapter—often rely upon interactions with this lipid A moiety. LPS is also referred to as endotoxin and plays a significant role in human illness. In particular, the lipid A component (see Figure 1.9 for more detail), is a powerful proinflammatory agent that can induce symptoms like fever, vomiting, diarrhea, and at high concentrations can induce potentially lethal septic shock.[31,32]

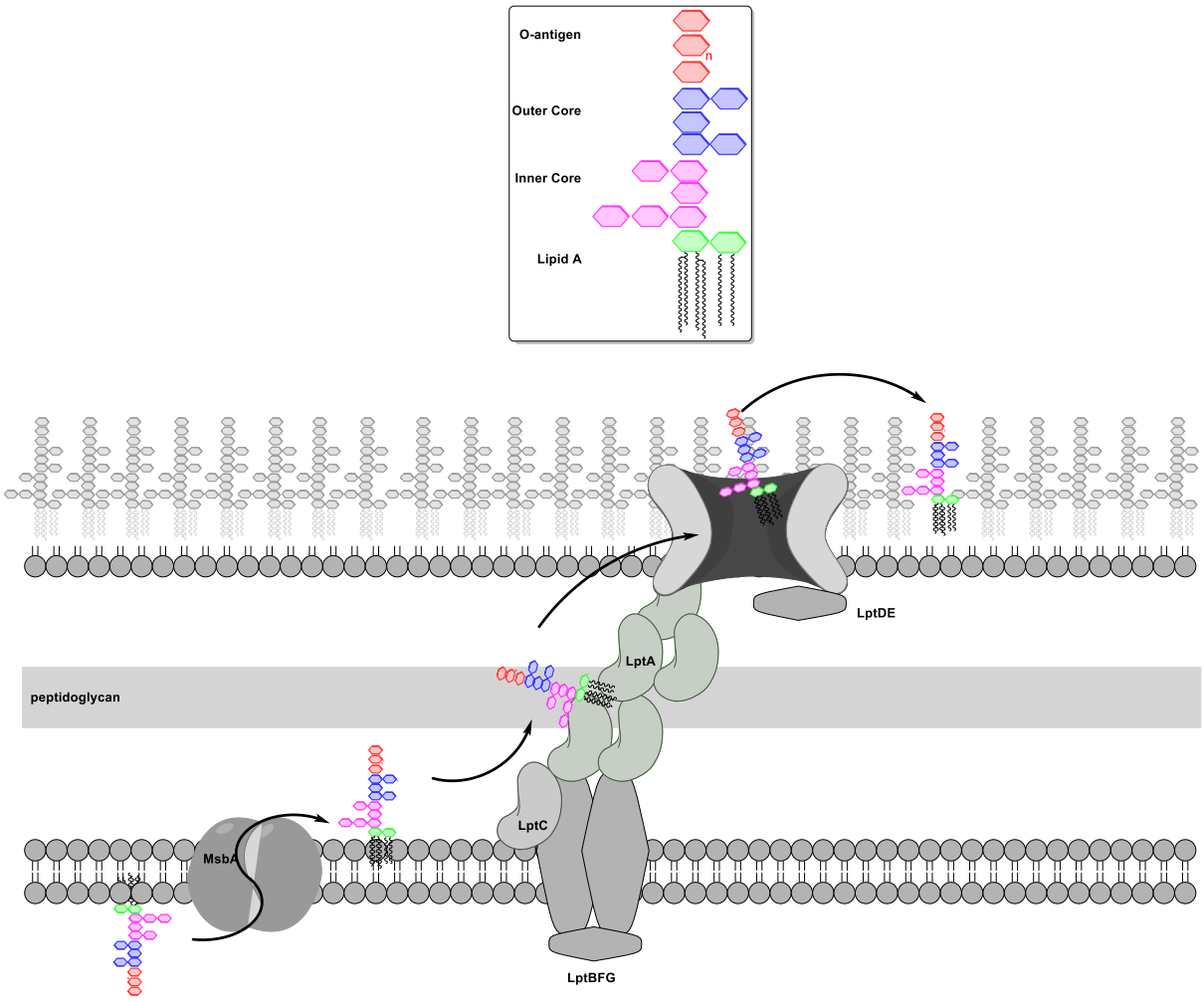

Figure 1.4 General structure of LPS and transport to the outer membrane.

LPS biosynthesis (Figure 1.4) starts at the inner leaflet of the cytoplasmic membrane, after which it is flipped to the outer leaflet by MsbA. This is followed by ATP-dependent extraction from the membrane by the LptBFG complex. Transport to the outer membrane is facilitated by a LptAC bridge that spans the periplasm and delivers LPS to the LpdDE complex. LptD has a β-jelly roll structure allowing it to orient LPS and deliver it through its lumen to the outer leaflet of the outer membrane.[33,34] Without an ion gradient across the outer membrane, or ATP in the periplasm, it is not obvious where the energy for this process comes from. It is thought that ATP hydrolysis in the cytoplasm by the

LptBFG complex drives the entire process, pushing successive LPS molecules all the way to the outer membrane. This model is likened to a PEZ® candy dispenser.[35] Outer membrane biogenesis is a promising target for antibiotic development, as seen with the novel antibiotic murepavadin which is in Phase III clinical trials.[36]

Bacteria of the genus *Mycoplasma* present an interesting case when it comes to classifying bacteria with the Gram stain. Though they lack an outer membrane, *Mycoplamsa* do not stain purple with crystal violet thanks to their complete lack of a cell wall and are thus technically Gram-(−). In general they either inhabit osmotically protected environments, such as inside animal hosts, or they have rigid sterol-containing membranes allow them to resist osmotic lysis.[10]

1.3 Cationic Antimicrobial Peptides (AMPs)

Daptomycin, paenibacterin and the polymyxins are examples of antimicrobial peptides (AMPs). AMPs are peptides produced by many different types of organisms and are found in all kingdoms of life. Many AMPs, such as paenibacterin and polymyxin, are cationic at physiological pH.[37,38] Bacteria are a rich source of these compounds, particularly members of the class *bacilli*.[39,40] These compounds are structurally diverse—ranging from non-lipidated linear peptides to lipidated cyclic peptides—but for the most part they kill bacteria in similar ways: by compromising the integrity of the cytoplasmic or outer membrane. With such a general MOA resistance can be slow to develop since it can require extensive modifications to the cellular membranes. This may appear to be a desirable trait for the development of broad-spectrum antibiotics; however, without a specific affinity for bacterial membranes, as opposed to human cell membranes, some cationic peptides can be quite toxic. Clinically useful cationic peptide antibiotics typically target specific membrane components that are more prevalent in bacteria.

This section contains a brief review of several types of cationic peptide antibiotics that differ significantly in their structure and/or mechanism of action. Special attention is given to paenibacterin as this cationic AMP is the focus of much of this thesis.

1.3.1 Paenibacterin

Paenibacterin is a recently discovered antimicrobial agent produced by the soil bacterium OSY-SE, a *Paenibacillus thiaminolyticus* strain. It was discovered through extensive screening for inhibition of *Listeria innocua* ATTC 33090 and *Escherichia coli* K-12 in Columbus, Ohio, USA.[41] Unlike most antibacterial peptides, which are usually active against just Gram-(+) or just Gram-(−) bacteria, paenibacterin exhibits activity against both Gram-(+) bacteria, including MRSA and VRE strains, and Gram-(−) bacteria.[41–43]

1.3.1.1 Paenibacterin Structure

Paenibacterin consists of an 11-residue macrocyclic ring containing an ester (*depsi*) bond between the side chain of the Thr3 residue and the α-carboxyl group of Ile13. There is an exocyclic dipeptide to which is attached a 15-carbon acyl tail. Paenibacterin sourced from *P. thiaminolyticus* (called the paenibacterin A-series) is a mixture of three homologous compounds with differing lipids.[41,42] Paenibacterin A1 (PA1, Figure 1.5) has a pentadecanoyl tail. Throughout this thesis, when we refer to paenibacterin, we are referring to the A-series mixture unless stated otherwise. Paenibacterin contains four non-proteogenic amino acid residues; D-Ser7, D-Lys6, D-Orn5, and D-Orn1. The configuration of each amino acid was inferred through sequencing of the corresponding non-ribosomal peptide synthetase domains (NRPS, see section 1.3.1.5) followed by bioinformatic analysis, comparing to NRPSs with known functions. This was followed by expression of select domains in *E. coli* to confirm function. The presence of an epimerization domain in an NRPS module (Figure 1.7) indicated the presence of a D-amino acid. Amino acid configuration was further confirmed by hydrolysis of

paenibacterin with aqueous HCl; the released amino acids were reacted with Marfey's reagent, followed by separation of the resulting modified amino acids using chiral HPLC.[42] Marfey analysis was unable to determine the position-specific configuration of each lysine and serine residue, so the stereochemistry at these positions was not confirmed.

The presence four basic residues (Orn, Lys) means that paenibacterin is cationic at physiological pH. It has been proposed that paenibacterin adopts a β-sheet structure with hydrophobic aliphatic side chains (Ile, Val) located on one side, giving rise to two separate faces, one hydrophobic, the other hydrophilic.[41] Contributing to its amphipathicity, the acyl tail of paenibacterin has been shown to be essential for activity.[41] These properties likely contribute to paenibacterin's mechanism of action, which is supported by many other examples of cationic, amphipathic peptides with antimicrobial activity.[44]

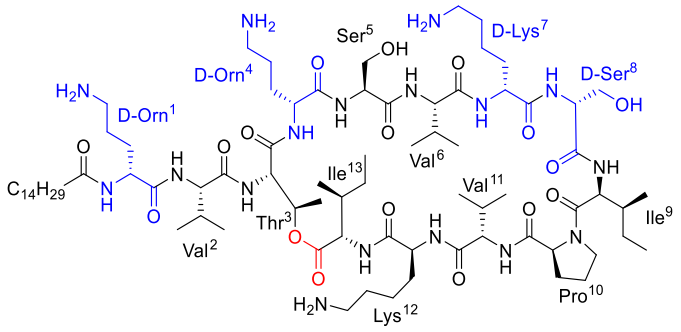

Figure 1.5 The structure of paenibacterin A1 (PA1). D-Amino acids are shown in blue. The ester/depsi bond is shown in red.

1.3.1.2 Antimicrobial Activity of Paenibacterin

Huang *et al.* examined the activity of paenibacterin against a series of Gram-(−) and Gram-(+) bacteria.[45] Their results (Table 1.1) compare paenibacterin activity with that of polymyxin B against Gram-(−) bacteria, and vancomycin against Gram-(+) bacteria. The wide range of strains susceptible to inhibition by paenibacterin is promising; however, the minimum inhibitory concentration (MIC) values are relatively high compared to those of clinically used antibiotics. Interestingly, paenibacterin

exhibited quite good activity against a polymyxin B resistant (PMB-R) strain of *A. baumannii* 2315. It also appears that in general, paenibacterin is more active against Gram-(−) than Gram-(+) bacteria, which is understandable given its proven affinity for bacterial LPS.

Table 1.1. Paenibacterin MICs from Huang *et al.* 2014[45]

Bacterial strain	MIC (µg/mL) Paenibacterin	Polymyxin B	Vancomycin
E. coli O157:H7 EDL933	8	0.25	
E. coli ATCC 25922	8	0.06	
E. coli 2276 (PMB-R, clinical isolate)	8	8	
Salmonella enterica serovar Typhimurium	8	1–2	
Pseudomonas aeruginosa ATCC 27853	8	0.125	
P. aeruginosa 999 (MDR, clinical isolate)	8	0.25	
P. aeruginosa 2325 (MDR, clinical isolate)	16	0.25	
A. baumannii ATCC BAA-747	2	0.06	
A. baumannii 1570 (MDR, clinical isolate)	2	0.06	
A. baumannii 2315 (MDR, PMB-R, clinical isolate)	2	8	
K pneumoniae ATCC 700603	8	0.125	
K. pneumoniae 2461 (MDR, PMB-S, clinical isolate)	4	2–8	
K. pneumoniae 2463 (MDR, PMB-R, clinical isolate)	8	0.06–0.13	
K. pneumoniae 2317 (PMB-R, clinical isolate)	64	>64	
S. aureus ATCC 29213	32		1
S. aureus ATCC 43300 (MRSA)	32		2
S. aureus 278 (DAP-R, MSSA)	32		2
S. aureus 1616 (DAP-R, MRSA)	32		0.2
S. aureus (MRSA, clinical isolate)	8		2
E. faecalis ATCC 29212	16		2–4
E. faecalis ATCC 700802 (DAP-S, VRE)	64		16–32
E. faecalis 2731 (DAP-R, VRE)	8		32
S. pneumoniae ATCC 49619	64		16
Bacillus cereus ATCC 14579	16		4
Listeria monocytogenes Scott A	2		2

1.3.1.3 The Mechanism of Action of Paenibacterin

Preliminary studies on the MOA of paenibacterin against Gram-(−) bacteria suggest that it is similar to that of polymyxins; i.e. binding LPS, displacing divalent cations, which facilitates further insertion of paenibacterin into the membrane of Gram-(−) bacteria (discussed in detail in section 1.3.3).[43] Like polymyxin, paenibacterin is both cationic and amphiphilic. It has been proposed that the charged amino acid side chains (Orn & Lys), and the hydrophobic aliphatic side chains orient themselves in a fashion that gives rise to both polar and hydrophobic faces, similar to polymyxin.[41]

It has been shown by Huang *et al.* that the presence of LPS in solution will reduce and even eliminate inhibition of *E. coli* growth by paenibacterin. This suggested that LPS might be capable of sequestering paenibacterin, an attribute shared with the polymyxins. The activity of ampicillin, a β-lactam antibiotic which functions through an unrelated mechanism, was unaffected.[43,46]

Huang *et al.* further confirmed the binding of paenibacterin to LPS using a fluorescence assay.[43] Polymyxin B fluorescently labelled with BODIPY-FL was combined with LPS purified from *E. coli*, which quenched fluorescence upon binding. They observed an increase in fluorescence upon addition of paenibacterin which suggested that it was displacing bound polymyxin. This effect was also observed when live *E. coli* cells were used.

Paenibacterin was also found to cause depolarization of both Gram-(+) *S. aureus* and Gram-(−) *E. coli* cell membranes, disrupting the electrical potential gradient required for ATP synthetase function.[10,43] Paenibacterin caused release of $diSC_3(5)$, a fluorescent dye which remains membrane-bound so long as hyperpolarization is present.[47]

Cell membrane permeabilization was further investigated using PBFI, a potassium-sensitive fluorescent probe.[43] Addition of paenibacterin to both *S. aureus* and *E. coli* resulted in an increase in fluorescence corresponding to intracellular potassium being released into the PBFI-containing

extracellular medium. Paenibacterin was also found to allow uptake of the nucleotide cell stain propidium iodide, which does not accumulate in live bacteria.[43] It was proposed that this was due to permeabilization of the membrane by paenibacterin, but since the dye is known to stain dead bacteria, this is likely an indicator that active extrusion (via ATP transporters) has halted following killing of the bacterium.

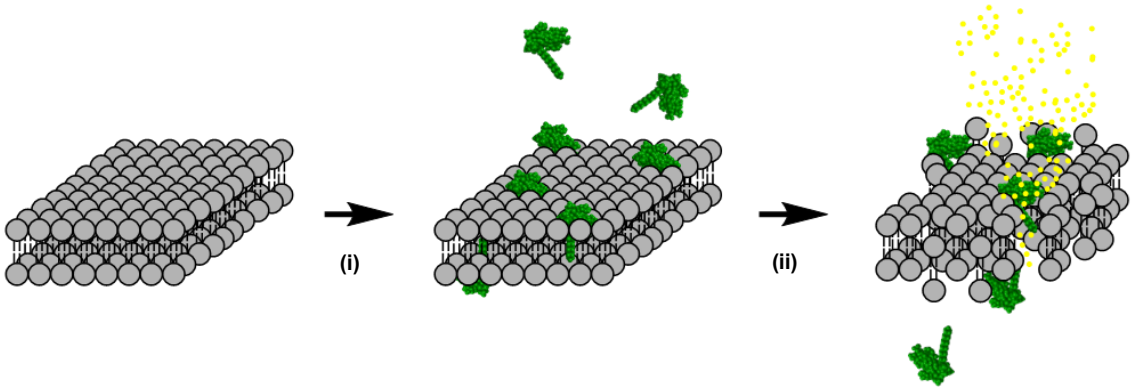

Figure 1.6 Proposed mechanism of cytoplasmic membrane disruption by paenibacterin
(i) Paenibacterin inserts into the bacterial membrane, mediated by insertion of the acyl tail. (ii) Insertion disrupts membrane integrity, promotes further uptake, and causes leakage of intracellular contents. The structure shown for paenibacterin (green) depicts an arbitrary conformation.

These observations are good evidence that paenibacterin disrupts cellular membrane integrity impeding normal cellular function in a similar fashion to polymyxin antibiotics (Figure 1.6). However, Huang *et al.* highlight the fact that no study to date has ruled out other potential MOAs.[43]

1.3.1.4 Paenibacterin: Toxicity, Animal Studies and Applications to Food Safety

The toxicity of paenibacterin against a human kidney cell line (ATCC CRL-2190) has been examined.[45] IC_{50} values fell into the 100–120 µg/mL range, significantly greater than most bacterial MICs indicating that paenibacterin may have a favourable, if modest, therapeutic index. Two 500 µg doses of paenibacterin increased the survival rate in mice inoculated with *P. aeruginosa* to 67.7% compared to

12.5% among mice who received no injections.[45] It was concluded that the mice were protected from septic shock by the ability of paenibacterin to sequester endotoxin.

Yousef and coworkers further investigated paenibacterin's potential for applications related to food-safety in 2018. *L. monocytogenes* is a particularly virulent food-borne pathogen that can form biofilms in food processing facilities. They found that relatively low concentrations of paenibacterin effectively suppressed *Listeria monocytogenes* within its biofilm matrix. They also demonstrated that treatment resulted in suppression of biofilm formation through the down-regulation of key genes as well as reduction of bacterial motility.[48]

Yousef and coworkers also investigated paenibacterin's potential as an agent for preventing *Salmonella enterica* contamination in low water-activity foods.[49] The *S. enterica* strains tested were capable of resisting dehydration. Treatment with paenibacterin, however, disrupted these desiccation resistance mechanisms. Pre-treatment at a concentration of 8 μg/ml was particularly effective. This effect was attributed to paenibacterin's ability to disrupt cell membrane integrity, and PBFI was again employed as an extracellular potassium probe to detect membrane leakage.

1.3.1.5 Biosynthesis of Paenibacterin

Paenibacterin is synthesized by non-ribosomal peptide synthetases (NRPS) in *P. thiaminolyticus* OSY-SE.[42] This is common among other cLPAs such as daptomycin, as well as other bacterial peptide derived antibiotics, such as β-lactam antibiotics and glycopeptides, such as vancomycin.[50–52] NRPSs are modular protein complexes, with one module for each amino acid residue of the peptide to be synthesized. Paenibacterin is synthesized by two 5-module NRPSs and a third 3-module NRPS, designated PbtA, PbtB, and PbtC, respectively.[42] PbtA is responsible for initial attachment of the acyl moiety to D-Orn1 and elongation to Ser5. PbtB then couples the Val6 residue through to Pro10; then the remaining residues, Val11, Lys12, and Ile13 are attached by PbtC as shown in Figure 1.7. The

composition of each module was elucidated through sequencing of the OSY-SE genome followed by analysis using bioinformatic methods to identify sequences similar to previously characterized NRPSs; the function of certain catalytic domains were further confirmed by transformation and expression in *E. coli*.[42]

Each module consists of a minimum of three individual catalytic domains. The adenylation domain (A-domain) is responsible for substrate selection, through ATP-dependent adenylation of the amino acid to be coupled. The activated amino acid is then transferred to a 4'-phosphopantetheine (PPan) cofactor bound in the peptidyl carrier protein (PCP) domain, which transports it to the condensation domain (C-domain). In the C-domain the activated amino acid is incorporated into the thioester bound peptide. Certain modules also contain an epimerization domain, which generate the D-amino acids from their corresponding L-isomers after incorporation. The terminal module also contains a thioesterase domain where the thioester linkage binding the peptide to the enzyme is cleaved. In the case of paenibacterin, this occurs with concomitant cyclization.

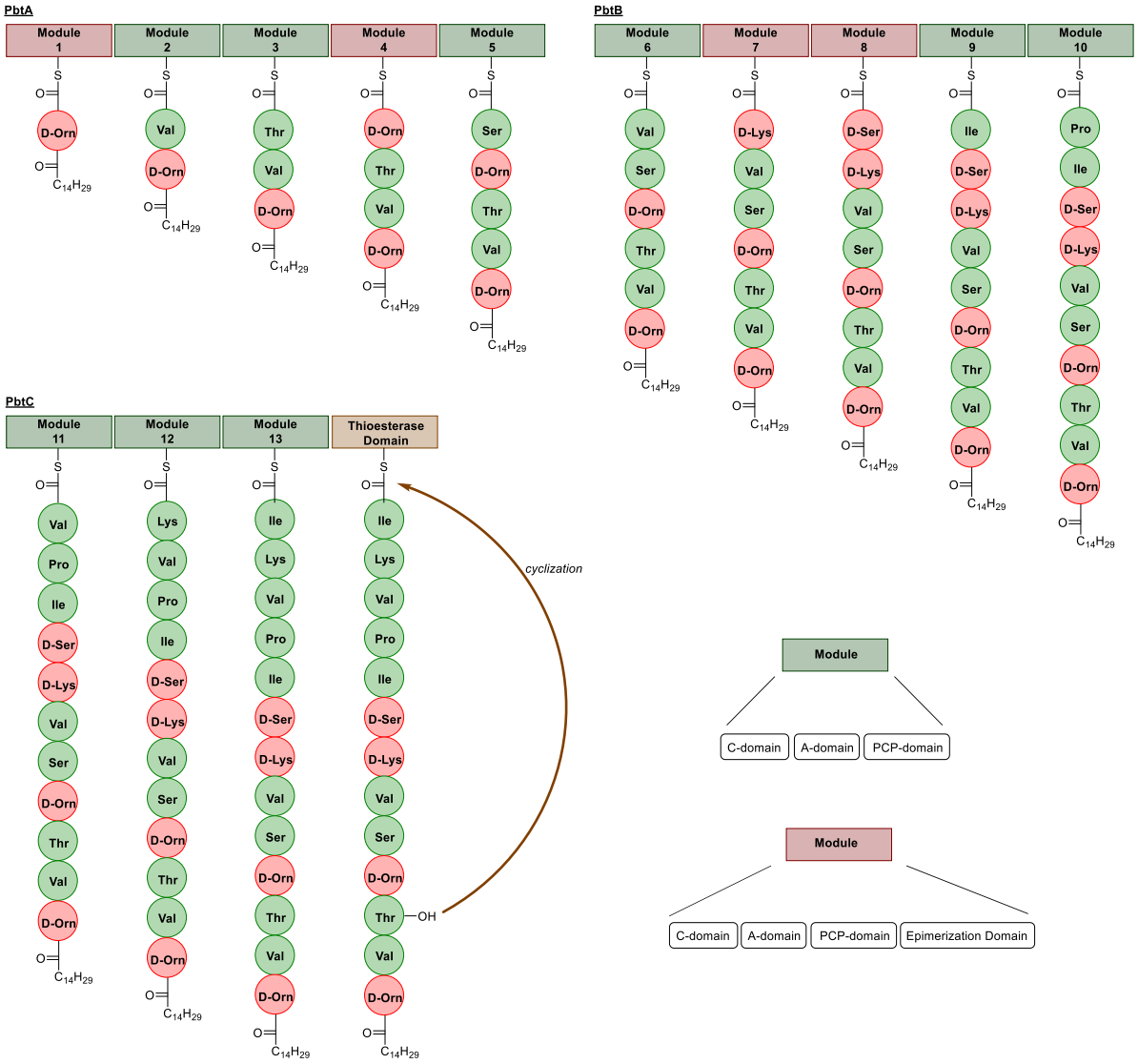

Figure 1.7 Biosynthesis of paenibacterin as described by Huang.[42]

Huang *et al.* have also identified two putative ABC transporters, PbtD and PbtE, with significant similarity to the known ABC transporters PmxC and PmxD, which are responsible for the secretion of polymyxins in *P. polymyxa*.[42,53,54] These proteins are suspected to be involved in the secretion of paenibacterin.

1.3.2 The Paenibacterin B-Series

A series of cLPAs have been recently discovered that closely resemble paenibacterin (called the paenibacterin B-series, Figure 1.8). These peptides were isolated from strains of *Paenibacillus alvei* and were characterized by tandem-mass spectrometry followed by genome mining.[55–57] Like paenibacterin, these peptides consist of an 11-amino acid macrocycle enclosed by an ester linkage between the side chain of threonine (position 3) and the *C*-terminal carboxyl group of isoleucine (position 13). The amino acid sequence of the B-series is similar to the A-series except D-lysine is replaced by D-Orn or vice versa, Val11 is substituted for Ile, and Val6 is substituted for either Phe or Tyr. One notable structural difference is the presence of a Pro residue at position 12, replacing Lys, and giving the peptide a reduced overall charge of 3+, and presumably affecting the peptides geometry in solution. There is also some variation in the size of the acyl tail, ranging from 10 to 15 carbons that may include a hydroxyl group. The exact structure of the lipid tails in the B-series have not been completely elucidated.

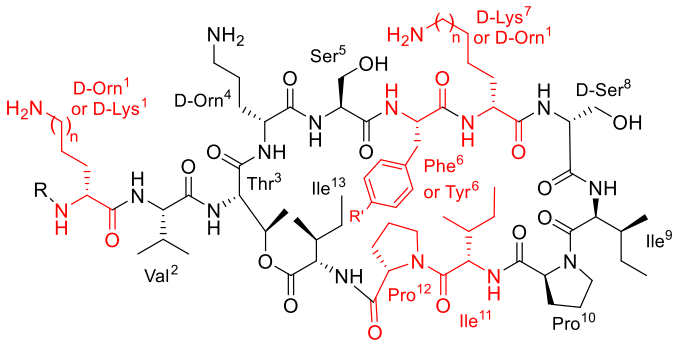

Figure 1.8 Structure of the paenibacterin B series. Residues that differ from the A-series are shown in red.

The evaluation of a few members of the B-series peptides against a very broad range of pathogens suggest that the B-series peptides may be more active than the A-series. For example, PB3-Y6 (PB3 with a Tyr residue at the 6-position) exhibited MICs ranging mainly from 4–8 mg/mL against a broad range of clinical isolates of MRSA and VRE and a very broad range of Gram-(−) bacteria.[55]

1.3.3 Polymyxin and Colistin

The polymyxins (A to E) are a group of five cLPAs isolated from *Paenibacillus polymyxa* in 1947. Two of them, polymyxin B and polymyxin E (colistin) (Figure 1.1) have been used in the clinic since the 1950's for treating serious infections caused by Gram-(−) bacteria. They are still in use today as last resort treatments for resistant Gram-(−) infections. Colistin use is more widespread.[5,58]

The fatty acid tail in polymyxin B and colistin is a mixture of (*S*)-6-methyl-octanoic acid (polymyxin B1 & colistin A1) and (*S*)-6-methyl-heptanoic acid (polymyxin B2 & colistin A2). Polymyxin B and colistin differ at the 6th position, with the former containing a D-Phe residue and the latter a D-Leu residue.[5,59]

One major drawback of the polymyxins is their toxicity. The polymyxins are actively taken up by renal cells leading to the formation of lesions and onset of nephrotoxicity. They are also somewhat neurotoxic. Consequently, the polymyxins fell almost completely out of favor in the 1970s when safer alternatives became available. However, due to widespread bacterial resistance to these safer alternatives in recent years, the polymyxins have made a dramatic comeback as last-defense antibiotics for treating severe infections caused by MDR Gram-(−) bacteria. Although the risk of kidney damage can be somewhat mitigated through a once a day dosing regimen, its toxicity still presents a significant downside to its use.[60] The MOA of polymyxins, while still somewhat speculative, has been studied extensively, and there are several reviews on the topic.[5,59]

Polymyxins are selective for Gram-(−) bacteria, interacting with lipopolysaccharides (LPS) in the outer membrane. The polymyxin B-LPS interaction has been investigated directly by isolating a stable complex of the two. The complexes could then be broken up with detergent or at low pH and the polymyxin quantified by dinitrophenylation of the amino groups and extraction into an organic solvent.[61]

The general structure of LPS is shown in Figure 1.4. The main components are a variable O-antigen polysaccharide domain, an inner core 2-keto-3-deoxycontonate (Kdo) domain, and lipid A (Figure 1.9) which is inserted into the outer membrane phospholipid bilayer. LPS in the outer leaflet of the bacterial outer membrane has a stabilizing effect on the membrane; with adjacent LPS molecules closely associating with one another, facilitated by divalent cations such as Ca^{2+} and Mg^{2+}.[62] The bacterial outer membrane acts as a permeability barrier, and the MOA of polymyxins is to disrupt this function through binding to lipid A. At physiological pH, polymyxin is cationic and interacts with the anionic LPS in the outer membrane. Divalent cations are displaced, resulting in destabilization of the LPS outer layer. The fatty acid tail and hydrophobic residues of polymyxin then insert into the membrane disrupting the uniformity of the lipid A acyl chain packing. Disruption of the outer membrane allows for further insertion of polymyxin into the membrane, where it translocates to the inner membrane. In the membrane polymyxin's amphiphilic character allows it to insert and displace phospholipids, causing membrane thinning.[5,59] It has also been proposed that polymyxin may cause the outer and inner membranes to come into contact, leading to phospholipid exchange. Altering the composition of each membrane and the inner/outer leaflets leads to cell death, possibly through lysis triggered by osmotic imbalance.[59]

The solution phase structures of polymyxin B and E when bound to LPS have been determined by NMR.[63] It was found that the 2,4-diaminobutyric acid (Dab) residues at positions 1, 5, 8 and 9 were involved in binding to the two phosphate groups in lipid A. The remaining Dab residue and two Thr

residues were positioned close to the polar Kdo-rich inner core. The hydrophobic moieties of polymyxin, namely the acyl tail and Phe/Leu residues were found to position themselves close to the acylated portion of lipid A. These hydrophobic sections are positioned on opposing sides of the molecule, and so requires polymyxin to adopt a folded conformation.

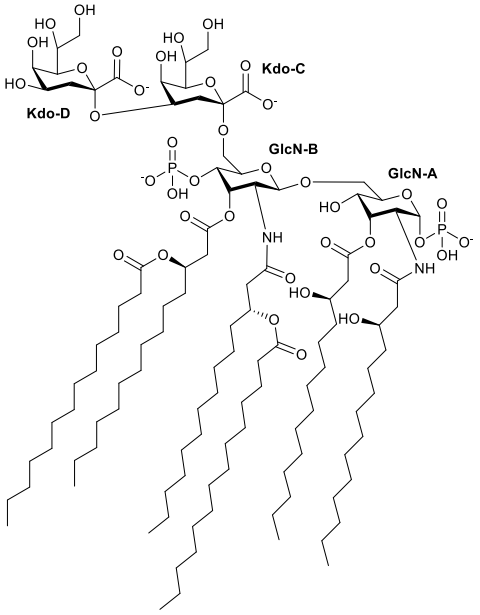

Figure 1.9 The structure of lipid A.

Van der Meijden and Robinson investigated polymyxin interactions with membrane proteins by incorporating into it the photoaffinity probe photoleucine.[64] Photoleucine is structurally similar enough to leucine that it can be incorporated by cell protein synthesis machinery, though in this case the amino acid was incorporated by SPPS. UV exposure triggers the formation of covalent linkages with nearby proteins.[65] The tail was also modified to include a terminal alkyne, which allowed for the attachment of a biotin tag by the CuAAC click-reaction. Photolabeling experiments with *Escherichia coli* ATCC25922 resulted in the photolabeling of several outer membrane proteins though it appears that these proteins have not yet been identified several years after publication of the initial findings.

A common method for studying the LPS binding affinity of polymyxin analogs is the displacement of a fluorescent probe.[59] This is commonly done with dansyl-polymyxin B which experiences increased fluorescence in a hydrophobic environment, and thus a decrease in fluorescence when being competitively displaced from LPS. Dansyl-polymyxin is typically prepared as a mixture of labelled compounds.[66]

Kanazawa et. al used an alanine scan to elucidate which amino acids in polymyxin were most important to its antibacterial activity.[67] This was done by preparing a series of analogs of polymyxin B3 in which each amino acid was, in-turn, replaced with alanine. For each analog, the MIC was determined as well as its LPS binding affinity—measured by observing the displacement of dansyl labelled polymyxin. They found that cationic residues within the cyclic portion of the molecule were more important to activity, with loss of the Dab residue at position 5 being the most important. The exocyclic Dab residues could be substituted without much of an impact on activity.[67] Previously, this same group had also investigated the effects of a variety of acyl tail modifications to polymyxin. Incorporating the fluorophore 1-pyrenebutyric acid at the *C*-terminal position (with both Dab1 and the acyl tail removed) only resulted in a 2-fold decrease in activity against *E. coli*.[68] This finding suggests that *N*-terminus acylation with pyrene butyric acid is likely a good way to incorporate a fluorophore into a lipopeptide without a large impact on activity. A similar pyrene-labelled analog of polymyxin has been used for studying interactions between polymyxin-like peptides within model membranes using FRET.[69]

Resistance to polymyxins typically arises through activation of a regulatory system like the PhoP-PhoQ pathway.[70,71] This system is activated under low Mg^{2+} conditions, modifying lipid A to compensate for the lack of divalent cations to bridge LPS molecules. When active, the phosphate groups on lipid A are modified with 4-amino-4-deoxy-L-arabinose, which bears a positive charge at physiological pH and allows for tighter LPS packing in the outer membrane, maintaining

impermeability in the absence of divalent cations.[5,59] Another mechanism of resistance involves phosphate group modification with phosphoethanolamine.[72] Cationic peptide antibiotics like polymyxin can trigger these lipid A modifications, which result in reduced affinities of the antibiotics for LPS, preventing membrane insertion.

It is known that activity of antimicrobial peptides against Gram-(−) bacteria typically depends on the peptide having a net positive charge. cLPAs such as daptomycin, which bear a net negative charge, are generally inactive against Gram-(−) bacteria since they cannot pass through the outer membrane.[52] Paenibacterin's positive charge suggests that, like polymyxin, it is able to traverse the outer membrane of Gram-(−) bacteria; however, paenibacterin's activity against Gram-(+) bacteria may suggest that it is not wholly dependent on specific LPS interactions, as is the case with polymyxin.

1.3.4 Polymyxin-B Nonapeptide

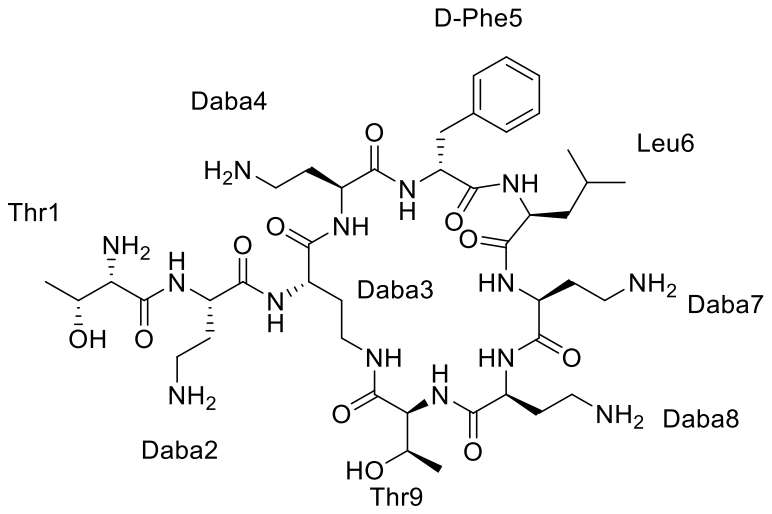

Figure 1.10 Structure of polymyxin B nonapeptide.

Polymyxin B nonapeptide (PMBN) and other polymyxin derivatives lacking the acyl tail serve as an interesting case-study for examining the different aspects of polymyxin's MOA. Developed by Vaara

and Vaara in 1983 using an enzymatic deacylation of polymyxin B, PMBN has no bactericidal activity.[73] Nevertheless, these authors found that it was still capable of compromising the integrity of the outer membrane of Gram-(−) bacteria. Co-treatment with large, membrane impermeable, antibiotics such as rifampin resulted in up to a hundred-fold decrease in MIC. PMBN also increased bacterial susceptibility to complement-cascade components (from guinea pig serum). The deacylated peptide was found to increase the susceptibility of a broad range of Gram-(−) bacteria to hydrophobic antibiotics, but was inactive against polymyxin resistant strains.[74] As one would expect, PMBN binds the outer membrane of Gram-(−) bacteria with a high affinity for LPS, although the binding affinity is less than that of polymyxin, which can have an inhibitory effect.[75,76] A later SAR study revealed that the peptide is highly specific for LPS binding, with any modifications resulting in decreased sensitization of Gram-(−) bacteria.[77] Vaara et al. later developed a PMBN derivative that was acetylated at the *N*-terminus, called NAB741, which exhibited similar ability to sensitize bacteria. With this truncated acyl tail, the peptide exhibited 400-fold higher renal clearance compared to colistin and 8-fold higher clearance than an octanoyl analog.[78] This poor retention likely limits the peptide's utility as a drug *in vivo*. In this peptide, the exocyclic Dab residue was replaced with D-Serine giving an overall charge of +3.

1.3.5 The Octapeptins

The octapeptins were initially isolated from *Bacillus circulans* and are grouped into four categories labelled A-D.[79,80] Currently, 19 octapeptins have been identified. As their name would suggest, the octapeptins are octapeptides. They consist of a 7-residue macrocycle enclosed by an amide linkage between the *C*-terminal carboxyl group of leucine and the side chain of a L-2,4-diaminobutyric acid residue (L-Dab). Categorization is based on variations at positions 1, 4, and 5. The exocyclic position 1 is populated with either D-Dab (A, B, C) or D-Ser (D) giving the peptides an overall charge of +4 or +3, respectively. Positions 4 and 5 are populated with hydrophobic amino acids D-leucine or

D-phenylalanine. Further variation within each category occurs with the 3-hydroxy acyl tail, which is typically 8–10 carbons in length and may be methylated.

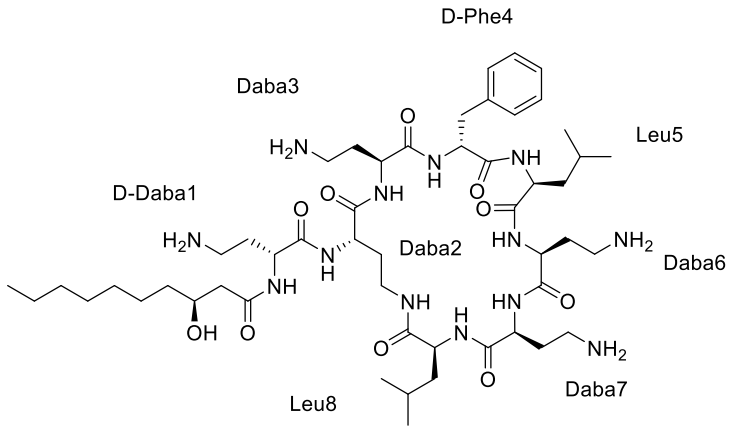

Figure 1.11 Structure of octapeptin C4.

Like paenibacterin, the octapeptins are active against both Gram-(−) and Gram-(+) bacteria, but they are also active against yeast, fungi, and protozoa. MICs against Gram-(−) bacteria are comparable to polymyxin B.[79] Octapeptins are presumed to exert their Gram-(−) bactericidal activity through interaction with lipid A, as is the case with polymyxin. Its activity against Gram-(+) bacteria suggests that it also binds and disrupts phospholipids (similar to polymyxin).[79] Studies by Velkov and coworkers confirmed this, demonstrating that octapeptin A3 interacts with lipid A and phospholipid headgroups through polar contacts followed by further insertion into the membrane.[81] Velkov, Gallardo-Godoy, et al. went on to identify the biosynthetic gene cluster for octapeptin then designed and studied a series of analogs of octapeptin C4 with linear, non-hydroxylated acyl tails sometimes truncated to 8-carbons in length using a newly developed SAR model based on the interaction of octapeptin C4 with modified lipid A. One resulting analog, FADDI-118 exhibited activity against polymyxin resistant strains of *P. aeruginosa* and reduced plasma protein binding.[82]

Supported membrane models have been used recently to investigate the MOA of octapeptin A3.[81] Neutron reflectrometry was used to observe a two stage process where octapeptin initially interacts with the headgroups of lipid A and phospholipids, then penetrates into the fatty acyl core. The membranes were constructed with a lower leaflet consisting of mostly DPPC and fixed to a solid-support, and an outer leaflet containing Lipid A.

1.3.6 Host-Defense Peptides

Bacteria are not the only source of AMPs. They are an important component of the innate-immune response of complex-organisms, including humans. These peptides are often cationic and amphipathic, and in addition to direct bactericidal activity, these peptides can play a role in modulation of the immune system.[83] This family of cationic amphipathic, ribosome-produced AMPs are briefly discussed in this section, and are referred to here as *host-defense peptides* (HDPs).

HDPs have been found with a variety of secondary structures, such as α-helical, β-sheet, hairpin, or extended secondary structure. In general HDPs range from small oligopeptides 5–10 residues up to 50 residues.[84–86] HDPs are ribosome synthesized and thus are typically constrained to common amino acids. They are important for early response to infection since they can be synthesized rapidly.[86] In addition to their direct bactericidal activity, human AMPs have been shown to modulate the immune response.[85]

Many HDPs exert their antibacterial effects via by forming pores in the bacterial membrane. This allows for the escape of intracellular cations, which leads to lethal cell depolarization and death. Three prevailing models exist for the formation of these pores: the barrel-stave pore, the toroidal pore, and the carpet model.[84,87] Regardless of the model, the first step is accumulation on the bacterial membrane. This can be mediated through specific interactions with negatively charged membrane components such as LPS or lipoteichoic acids.[85] To form a barrel-stave pore, peptides then insert vertically into the

membrane organizing into a cylindrical channel through which cellular contents can traverse the membrane.[88] To form a toroidal pore the peptide also inserts into the membrane but does not aggregate. Instead it induces local membrane curvature, forming a toroid the interior of which is lined with the peptide and the phospholipid head groups.[89] The carpet mechanism does not involve the formation of a defined pore, but instead upon the detergent effect of peptides at a certain concentration on the membrane's surface causing it to disintegrate.[90]

Several HDPs have been investigated in clinical trials; these include drugs derived from: human cathelicidin, magainin from the African clawed frog, and protegrin from porcine leukocytes.[85] The ability of certain HDPs to disrupt bacterial membranes has led to the investigation of possible synergistic effects with other antibiotics.[76,91] This is similar to the synergy studies performed with the polymyxin B nonapeptide discussed above.

To be clinically useful, drugs derived from HDPs must selectively disrupt bacterial membranes, and not those of mammalian cells—which leads to toxicity. This may be accomplished by developing AMPs that target specific bacterial membrane components. One example of such a drug is discussed below.

1.3.7 Murepavadin

Murepavadin is a cationic cyclic peptide antibiotic active against *Pseudomonas aeruginosa* currently undergoing clinical trials.[36] Though it is based on the β-sheet host defense peptide protegrin-I, which causes membrane lysis through pore formation, murepavadin has a non-lytic mechanism of action that targets the outer membrane protein LptD.[92]

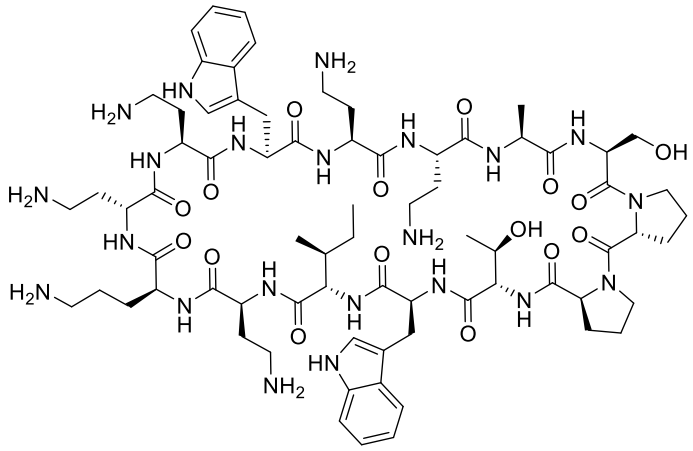

Figure 1.12 Structure of murepavadin.

A library of peptidomimetics based on a β-hairpin template were prepared and screened for increased antibacterial activity without toxicity for red blood cells. It was found that certain peptides adopted the key β-sheet structure only upon interactions with phospholipid membranes. The synthetic peptides were generally less potent than the natural protegrin-I or tachyplesin-I, but one mimetic (mimetic 4, cyclo-LRLKKRWKYRVPP) retained fairly good activity with dramatically reduced haemolysis.[93] This lead compound was extensively modified to determine the effect of amino acid substitutions on antibacterial activity and haemolysis establish a SAR. Antibacterial activity was generally retained or slightly improved, but some substitutions dramatically increased haemolysis.[94] The lead compound was then optimized for activity against P. aeruginosa using an iterative process where libraries of structural variants were tested for activity, the optimal hit was identified, and the process was repeated. The resulting compounds had MICs in the nanomolar range, but only against *P. aeruginosa*, pointing to a high affinity towards a specific target. The target was found to be LptD, a key outer membrane protein involved in LPS biogenesis.[92] Later structural studies and an alanine scan revealed that the β-hairpin structure and the two tryptophan residues are essential for activity.[95]

1.4 Membrane Modifications in Response to Cationic Peptides

Bacterial resistance to membrane-acting peptides and antibiotics typically arises from modifications to the membranes themselves. Resistance mechanisms have evolved to allow bacteria to handle exposure to a host of cationic AMPs. These mechanisms may be passive or inducible.[85] These resistance mechanisms have consequences relating to the effectiveness of clinical antibiotics as well, particularly large cationic peptides that have similar properties.

Gram-(+) bacteria can modify the charge of their cell surface to reduce the affinity of antibiotics that rely on electrostatic interactions with cell membrane or cell wall components.[85,96] These modifications are mediated by the *gra*RS (or *aps*) regulatory system, which can be induced by AMPs and regulates a series of genes involved in AMP resistance.[97] The *dlt* operon is responsible for appending D-alanine to hydroxyl groups of teichoic acids, giving an increased positive charge. This system is also inducible by low concentrations of the divalent cations that are typically bound within the peptidoglycan. Modifications to the lipid membrane are also induced through the activation of MprF which is responsible for incorporation of lysylphosphatidylglycerol (lysyl-PG) into the outer leaflet. Lysyl-PG bears a charge of +1 as opposed to the −1 charge of PG, which reduces the membrane's attraction towards cationic peptides.[98] The *aps* system also regulates the membrane transport proteins *vra*FG which expels AMPs from the cell.[97] A missense mutation in the *mprF* gene has been linked with increased expression of *vraSR*, a two-component regulatory system that regulates cell wall synthesis in response to damage. This resulted in increased resistance to even non-cationic peptides like daptomycin or vancomycin.[99]

AMP resistance in Gram-(−) bacteria is for the most part controlled by three regulatory systems, PhoPQ, PmrAB, and Rcs.[85,96] A common mode of resistance is modification of lipid A to give it a positive charge, similar to the cell wall modifications in Gram-(+) bacteria. PmrAB activation leads to 4-aminoarabinose being appended to lipid A by the action of the proteins encoded by the *pmr* operons,

as well as modification with phosphoethanolamine by PmrC. PhoPQ, in addition to regulating PmrAB, controls several other genes that encode proteins responsible for lipid A modifications like monophosphorylation or palmitoylation.[85] Finally the Rcs system regulates expression of a periplasmic protein YdeI that is important for AMP resistance but whose mode of action is unknown.[100] These mechanisms have implications for polymyxin resistance, since this antibiotic relies upon electrostatic interactions with lipid A. Gram-(−) bacteria carrying the gene *mcr*-1 and variants are of increasing concern as they confer polymyxin resistance. This gene is often plasmid-borne, and so has an increased likelihood of spreading between bacterial strains. It encodes a phosphoethanolamine transferase that modifies lipid A like PmrC.[72,101,102]

1.5 Daptomycin—An Anionic AMP

While the majority of the work presented in this thesis concerns the cationic AMP paenibacterin, in Chapter 5 we present a structure-activity relationship (SAR) study of a daptomycin analog. Daptomycin is an anionic AMP. A brief discussion of daptomycin is presented below.

Daptomycin, whose structure is shown again in Figure 1.13, is a calcium-dependent cLPA isolated from *Streptomyces roseosporus* in the early 1980s by researchers at Eli Lilly. The company initiated clinical trials, but discontinued them after discovering adverse effects. Cubist Pharmaceuticals later acquired the rights and resumed development. They found that adverse effects were mitigated by a modified dosing regimen and gained approval in 2003 for daptomycin's use for the treatment of serious Gram-(+) infections including methicillin-resistant *Staphylococcus aureus* (MRSA), vancomycin-resistant *Staphylococcus aureus* (VRSA) and vancomycin-resistant enterococci (VRE).

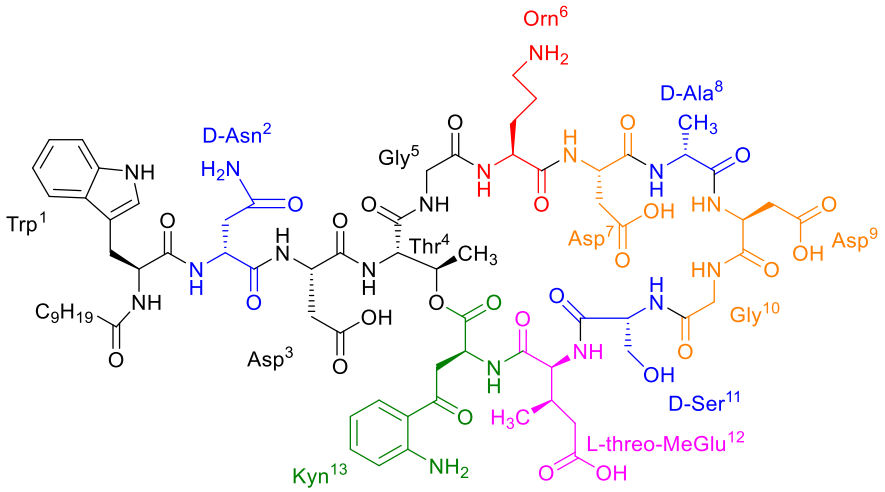

Figure 1.13 Structure of daptomycin. Uncommon amino acids: kynurenine (green), L-*threo*-MeGlu (magenta), ornithine (red). D-Amino acids are shown in blue. The DXDG binding motif consists of residues 7–10 (shown in orange with the exception of D-Ala8).

Daptomycin consists of a ten amino acid macrocycle to which is attached a lipidated linear tripeptide. It contains three unusual amino acids: kynurenine (Kyn), ornithine (Orn), and (2*S*,3*R*)-3-methylglutamate (MeGlu), in addition to three D-amino acids. The macrocycle is closed by an ester bond between the side chain of Thr4 and the α-COOH of Kyn13. Residues 7–10 make up the DXDG Ca^{2+}-binding motif which is found in most Ca^{2+}-dependent antibiotics.[103]

Although it is intrinsically anionic at physiological pH, daptomycin bears some similarities to the cationic peptides. Examination of calcium binding to daptomycin in the presence of large unilamellar vesicles (LUVs) using isothermal calorimetry (ITC) found that there were likely two calcium binding events.[104] A calcium-daptomycin stoichiometry of 2:1 gives daptomycin an overall positive charge at physiological pH. Straus and Hancock liken daptomycin to cationic AMPs in their 2006 review.[105]

1.5.1 The MOA of Daptomycin

Daptomycin acts upon the cytoplasmic membrane of Gram-(+) bacteria. The specific details of daptomycin's MOA are hotly debated. It is known that it binds calcium and inserts into the bacterial membranes where it interacts with PG and does not enter the cell. It is generally accepted that it changes the membrane's physicochemical properties, leading to cell death either through depolarization or interruption of the peptidoglycan biosynthesis machinery; however, key aspects of the MOA of daptomycin are still unknown, and what is known is not without controversy.

A major element of all proposed mechanisms of action for daptomycin is its ability to bind and disrupt bacterial membranes. This step has been extensively studied using a variety of techniques. Early studies on daptomycin demonstrated that its bactericidal effect correlated with dissipation of membrane potential, accompanied by potassium efflux from the cell.[106] This effect was also demonstrated to be calcium-dependent. It was later demonstrated that in the absence of liposomes, daptomycin binds calcium in a 1:1 molar ratio, forming a multimer or micelle.[107,108] This multimer then dissociates and daptomycin inserts into lipid membranes.[109] However, these studies used daptomycin concentrations in the millimolar range, many times what is required for antibacterial activity. So, the propensity of daptomycin to aggregate in solution may not relate to its mechanism of action under biologically relevant conditions.

Transcription profiling of *S. aureus* further supports the importance of membrane depolarization, with daptomycin inducing a response that was similar to responses induced by nisin and carbonyl cyanide *m*-chlorophenylhydrazone (CCCP)—which also cause depolarization. However, daptomycin was also found to induce a cell-wall stress response, also activated by vancomycin and oxacillin, which hinted towards a dual mode of action affecting both membrane polarization and cell wall synthesis.[110]

Considerable evidence has been amassed that indicates that daptomycin oligomerizes in membranes containing PG. Studies have shown that FRET occurs between the kynurenine residue of native

daptomycin and 7-nitro-2,1,3-benzoxadiazol (NBD)-labelled daptomycin (NBD label is attached to Orn7) in the presence of liposomes containing PG. This suggested that oligomerization was occurring upon insertion into bacterial membranes.[111] Kynurenine-NBD FRET was used to estimate the oligomer subunit stoichiometry, giving an initial value of 6–7 daptomycin subunits.[112] Muraih et al. made use of a perylene fluorophore incorporated into the acyl tail of daptomycin to study its oligomerization.[113] When perylene molecules are in close proximity, they can form an excited dimer (an excimer), resulting in red-shifted emission. Upon binding to liposomes, perylene excimer fluorescence was observed, which confirmed the presence of oligomers. This was also observed with live *B. subtilis* instead of liposomes. Excimer formation was also dependent on the presence of PG, further confirming that a daptomycin-PG interaction is key for its antibacterial activity.[104,114]

It has been proposed that the daptomycin oligomers form cation-selective pores, which in turn cause membrane depolarization.[115] It was later discovered that the presence of cardiolipin in LUVs prevented translocation of daptomycin to the inner leaflet.[116] Subsequent estimation of the subunit stoichiometry in these cardiolipin-containing LUVs found that they were likely tetramers. Additionally, cardiolipin was found to inhibit potassium influx into LUVs. This led to a proposed structure of a transmembrane pore formed by daptomycin, consisting of two tetramers on opposing leaflets, giving a subunit stoichiometry of 8.[116] It was proposed that the initial estimate of 6–7 subunits was the result of reduced FRET between fluorophores found in opposite leaflets. This pore-forming mechanism of action is illustrated in Figure 1.14 .

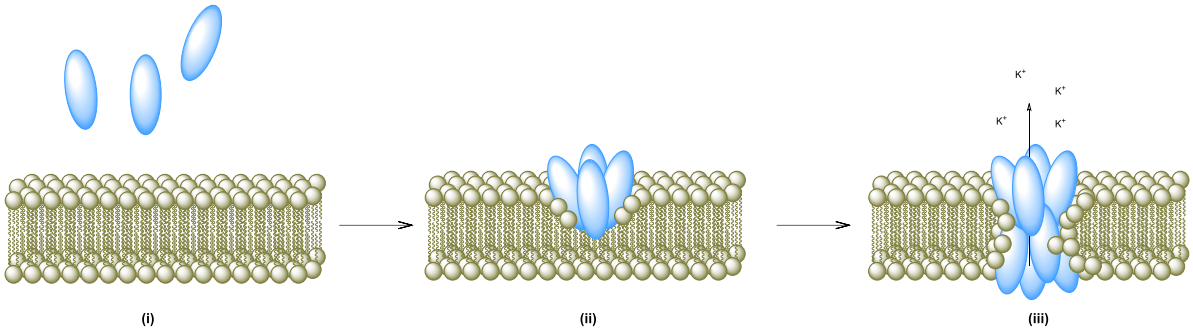

Figure 1.14 Proposed MOA of daptomycin via the formation of an octameric pore. (i) Calcium binding induces the formation of a multimer and association with the lipid bilayer. (ii) Binding of a second equivalent of calcium induces deeper insertion into the membrane and formation of a defined tetramer. (iii) Translocation to the inner leaflet and alignment with a second tetramer results in the formation of a cation channel.

Intrinsic fluorophores such as tryptophan or kynurenine are invaluable for studying the interactions of lipopeptides with bacterial membranes. It is relatively straightforward to monitor calcium-dependent binding of daptomycin and its analogs to liposomes by titrating in calcium and observing the resulting increase in fluorescence (Figure 1.15).[117] Tryptophan is a stronger fluorophore than kynurenine, but if both are present then Trp excitation results in FRET to the kynurenine residue. For this reason daptomycin binding is typically evaluated using kynurenine fluorescence while in analogs without kynurenine, tryptophan fluorescence is monitored.[117–119]

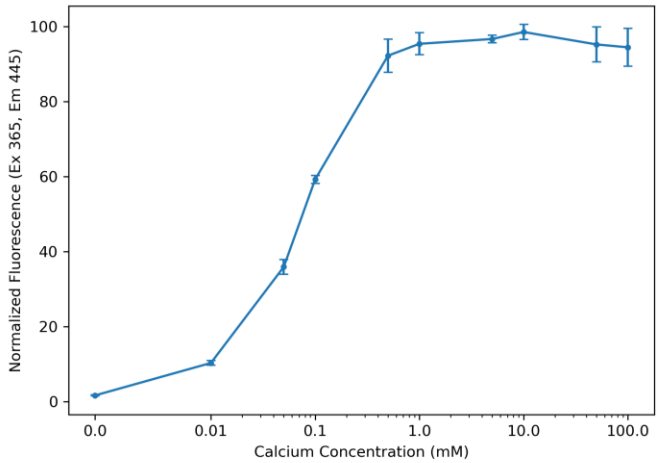

Figure 1.15 Calcium-dependent membrane binding of daptomycin. An increase in kynurenine fluorescence accompanies binding to 1:1 DMPC/DMPG LUVs (*Unpublished data*)

Intrinsic kynurenine fluorescence has also been used for direct imaging by fluorescent microscopy. Grein et. al recently used this method to discover an important new component to daptomycin's mechanism of action.[120] Daptomycin was directly observed accumulating at the division septum of *S. aureus* by fluorescence microscopy. The same effect was observed with BODIPY-labelled daptomycin. TIRF microscopy allowed the authors to directly observe labelled daptomycin binding to supported lipid bilayers, demonstrating that a combination of PG and undecaprenyl cell wall precursors dramatically increases the degree of binding.[120] They confirmed the formation of a tripartite complex using TLC analysis of lipid II, daptomycin and PG mixtures. They also observed reduced lipid II extraction into organic solvent as daptomycin concentration was increased, suggesting the formation of an extraction-stable complex. These results led to the proposal of an MOA that combines both interruption of cell wall biosynthesis and membrane disruption (Figure 1.16).

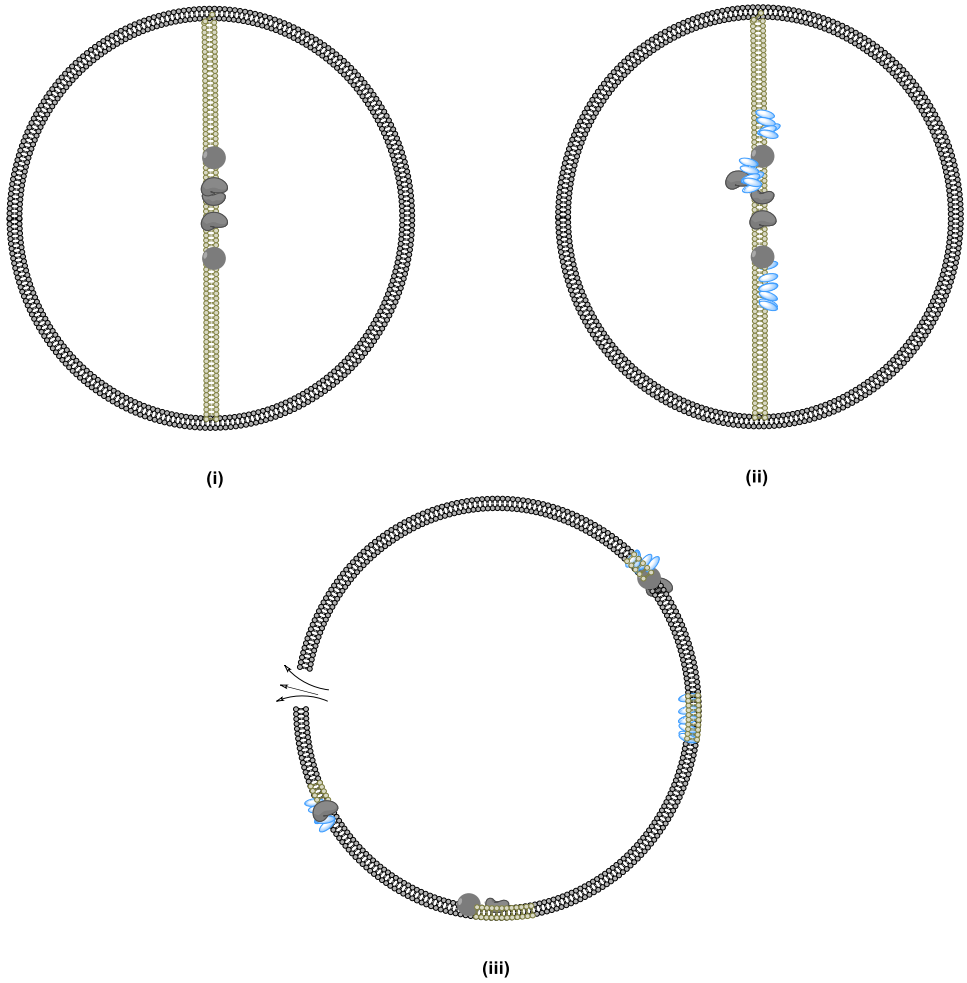

Figure 1.16 MOA of daptomycin proposed by Grein. (i) Cell wall biosynthesis machinery is located at the division septum, enriched in PG and undecaprenyl coupled cell wall precursors (yellow), e.g. lipid II. (ii) Ca^{2+} bound daptomycin oligomers bind PG and cell wall precursors, blocking cell wall synthesis. Accompanied by delocalization of the cell wall biosynthetic machinery. (iii) Daptomycin disperses throughout the membrane, causing its disintegration, leakage, and cell death.

Resistance to daptomycin is typically conferred by the modification of the bacterial membrane or the cell wall.[121,122] This is accomplished through incorporation of lysyl-PG, mediated by the *mprF* gene, or modification of lipotechoic acids with alanine, mediated by the *dlt* operon (see section 1.3.7).

1.6 Solid-Phase Peptide Synthesis

Central to this thesis is the synthesis of cLPAs using Fmoc solid-phase peptide synthesis (SPPS). A brief discussion of SPPS is provided below.

SPPS was initially developed by Bruce Merrifield who published his synthesis of a tetrapeptide using this approach in 1963.[123] Briefly, SPPS works by the iterative coupling of protected amino acids onto a peptide bound to a resin support. The amino acids are protected in a way that allows the α-amine to be unmasked without removing the protecting groups from any side chain functional groups. This way, following a coupling, the solid support is rinsed, filtered, and the *N*-terminus is easily deprotected for the next coupling (Scheme 1.1). There are two common protecting group schemes: the Boc/benzyl scheme and the Fmoc/*t*-Bu scheme. In the Boc/benzyl approach, the α-amino group is protected with an acid-labile Boc group and the side chains with groups (mainly benzyl derived) that can be removed with anhydrous hydrofluoric acid. In the Fmoc/*t*-Bu strategy, the base-labile Fmoc group is used to protect the α-amino group and the side chain functional groups are protected with acid-labile protecting groups—mainly derived from a *tert*-butyl group, but sometimes other types of acid labile groups are used—that can be removed with acid (usually TFA). The Fmoc/*t*-Bu approach is by far the most common approach used today, mainly because it provides peptides in higher yields and doesn't require the use of dangerous anhydrous HF. Resin linkers are typically chosen that allow the peptide to be cleaved from the resin under the same conditions used for side chain deprotection; however, it is sometimes desirable to effect cleavage without deprotection or vice versa. Protecting groups or linkers that can be removed independently of one another are commonly referred to as *orthogonal*. There are many review articles and books that cover the specific techniques and methods of SPPS.[124–127]

Scheme 1.1 Solid-phase peptide synthesis.

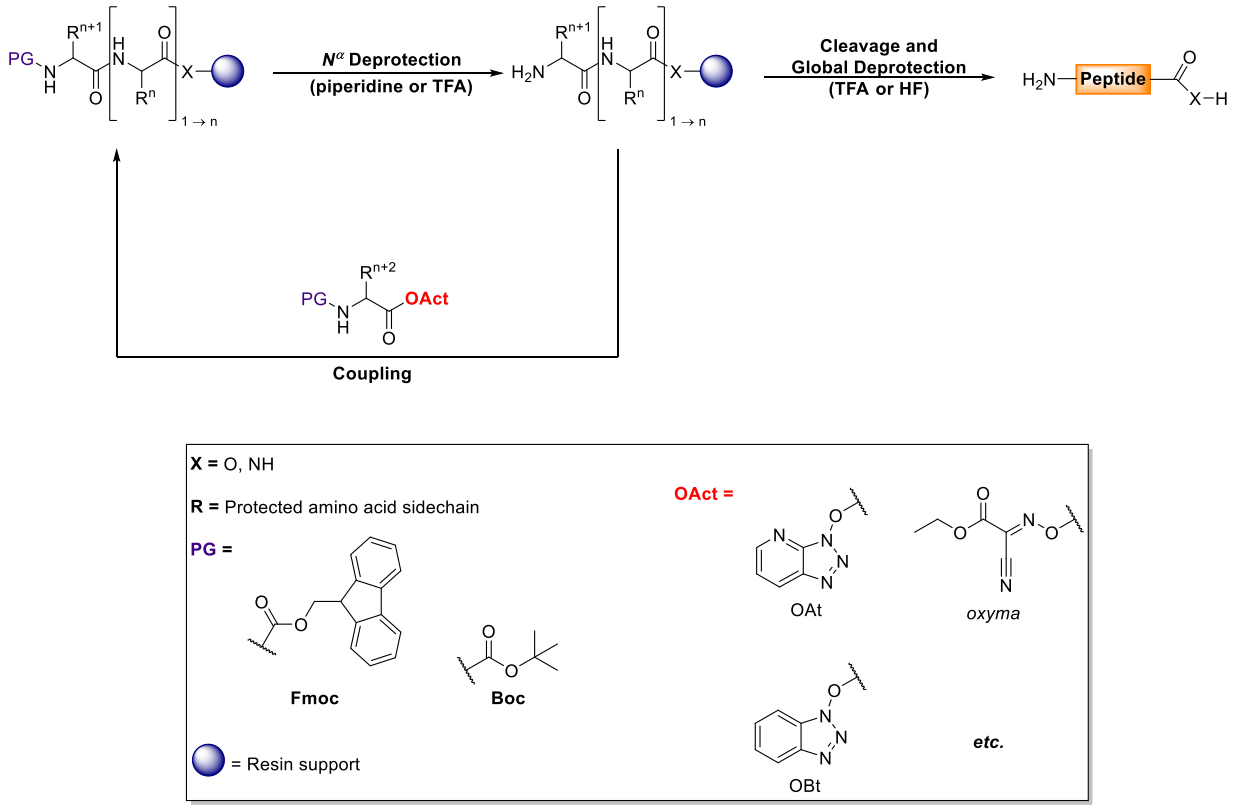

1.6.1 Synthesis of Difficult Peptide Sequences

When synthesizing peptides, there are many problems one may encounter. Many of these are sequence-dependent, only arising under certain conditions. While it is usually possible to predict certain problems by analyzing the sequence, there is always potential for a surprise. These problems can stem from side-reactions resulting in breakdown or premature termination of the peptide, or from the physical properties of the sequence itself. Two common side reactions encountered during routine peptide synthesis are aspartimide formation and diketopiperazine formation (Scheme 1.2). For the synthesis of sequences containing ester linkages, *N*→*O* acyl shifts must be taken into account. Epimerization during couplings, mainly via an oxazolone intermediate, can also occur (Scheme 1.2). Peptides containing many hydrophobic residues and peptides that are particularly lysine/arginine rich can be problematic

due to their low solubility or propensity to aggregate. Aggregation during SPPS can be a major problem. Many techniques have been developed to deal with these and other problems, some of which are discussed below.[128,129]

Scheme 1.2 Common side reactions encountered during SPPS.

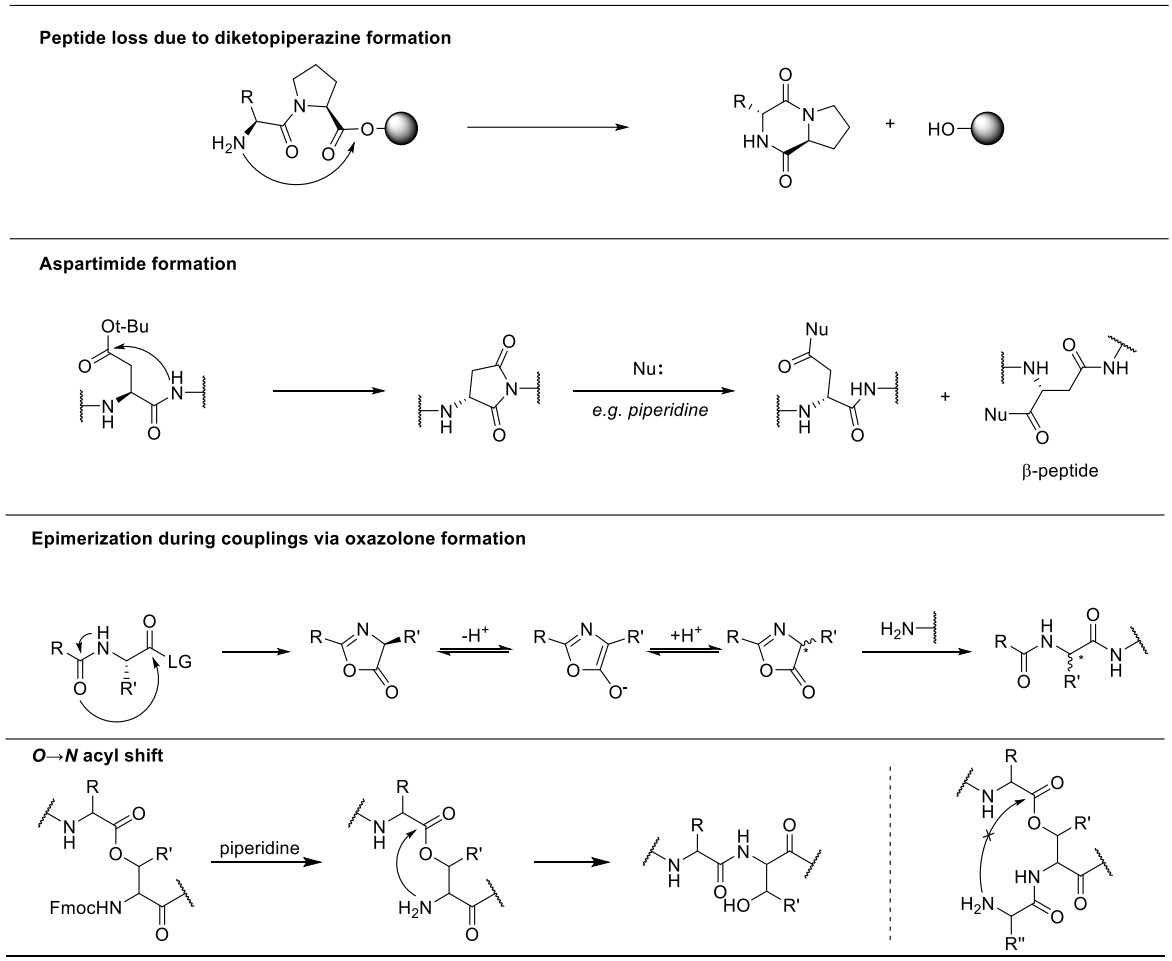

Peptide loss due to diketopiperazine (DKP) formation occurs following deprotection of the second residue when the peptide is linked through the resin via an ester bond (Scheme 1.2). Benzyl linkers are particularly prone to aminolysis by the newly deprotected *N*-terminus. DKP formation can be expected if a proline residue is located at the *C*-terminus. To minimize peptide loss, it is common to use a bulky trityl linker, and to use reduced deprotection times.[130]

The most straightforward approach to prevent aspartimide formation is the direct acylation of amide nitrogen atoms. Both hydroxymethylbenzyl (Hmb) and dimethoxybenzyl (Dmb) protecting groups are common, and glycine is most often the protected residue as aspartimide formation occurs most readily at Asp-Gly sequences. *N*-Acylated amino acids can be introduced to the sequence as a monomer but use of a dipeptide is preferable as the acylated amine is less nucleophilic and so couplings are slower. *N*-Acyl glycine is easily prepared by reductive amination. The backbone protecting groups are removed with TFA during global deprotection.

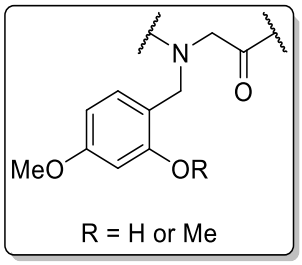

Figure 1.17 Hmb and Dmb backbone protecting groups.

For the synthesis of branched peptides containing ester linkages, deprotection of an amino group in close proximity to the ester bond may lead to an *O*→*N* acyl shift (Scheme 1.2). This is primarily a concern during Fmoc SPPS since the basic deprotection conditions favour the migration. Introduction of an ester linkage must be carefully planned to avoid the need to generate a nearby free amino group. This may be accomplished through the incorporation of an ester-containing oligopeptide building block, or simply by introduction of the ester linkage *after* elongation of the primary peptide sequence. Examples of these approaches are given in section 1.6.5.

Racemization of amino acid building blocks during couplings occurs primarily through the formation of an oxazolone intermediate (Scheme 1.2). Oxazolone formation is dependent on the electrophilicity of the activated ester, and so can be mitigated by the use of semi-stable esters derived from reagents such as 1-hydroxy-7-azabenzotriazole (HOAt, Scheme 1.1). Racemization is rare for urethane-

protected amino acid building blocks, but can be a major concern when coupling peptide fragments due to the presence of a relatively nucleophilic amide.[130]

Proline residues are known to disrupt aggregation by inducing conformational changes in the peptide backbone. A backbone modification strategy has been developed where serine, threonine, and cysteine residues are converted to *pseudoprolines* which have similar effects on peptide solubility. These oxazolidine or thiazolidines are most commonly derived from acetone, giving the corresponding dimethyl pseudoproline (denoted as $\Psi^{Me,Me}$Pro).[131–133] With the reduced nucleophilicity of the hemiaminal ether, it is most common for pseudoprolines to be introduced as a dipeptide, many of which are commercially available (Figure 1.18). The oxazolidines are cleaved during global deprotection with TFA. Thiazolidines, however, are typically more acid-stable though rapid deprotection has been observed.[134]

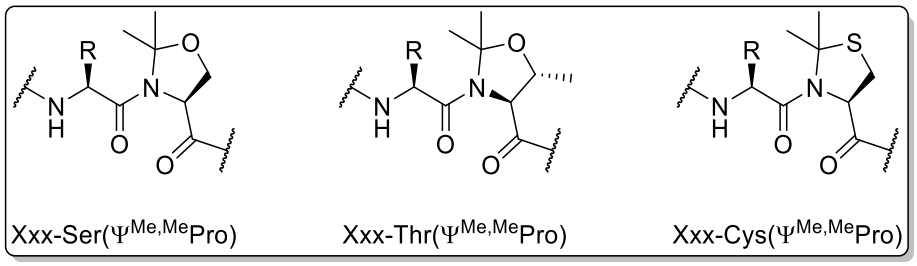

Figure 1.18 General structures of pseudoproline dipeptides.

A third common approach is the use of isopeptides, where the amide backbone is disrupted by incorporation of an ester linkage with the side chain of a serine or threonine residue. These depsipeptides are easily prepared by incorporating a pre-made isoacyl dipeptide, many of which are commercially available. The N^{α} of the serine or threonine residues are protected orthogonally to the Fmoc group typically used to protect the N^{α} of the *O*-acyl amino acid. A Boc protecting group is most common though azides have been used to mask the amine.[135] Like pseudoprolines, isopeptides disrupt aggregation by changing the peptide's secondary structure. Following deprotection and cleavage from

the resin and dissolution in an aqueous buffer solution, the peptide undergoes a pH dependent O→N acyl shift to give the desired native peptide (Scheme 1.3).

Scheme 1.3 Isopeptide rearrangement.

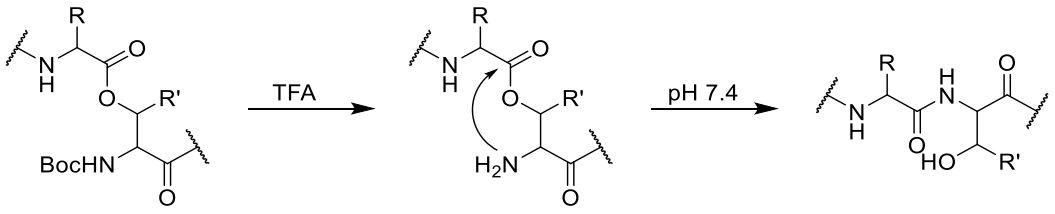

Often long reaction times can be avoided by heating the reaction mixture, typically using microwave irradiation. This improves peptide solubility and accelerates the rate of coupling reactions. Resin supports have been developed that contain a solubilizing polyethylene glycol (PEG) spacer between the linker and the core resin.[126,130]

1.6.2 Cyclic Peptides

The synthesis of cyclic peptides pushes the limits of classical solid-phase peptide synthesis, as they require more complicated protecting group schemes. Steps like branching, macrocyclization, and side chain functionalization often require the use of additional orthogonal protecting groups, often referred to as higher dimension orthogonal strategies.[136].

A key step in the synthesis of cyclic peptides is the macrocyclization. For this, there are two main strategies: the off-resin cyclization approach and the on-resin cyclization approach (Scheme 1.4). In both cases macrolactamization is preferable to macrolactonization since the formation of ester bonds is quite challenging as mentioned above. For on-resin cyclization, a carboxyl group and an amine/alcohol must be selectively deprotected. For cyclization onto the *C*-terminus, the peptide must be attached through the side chain a residue such as aspartate or glutamate. For off-resin cyclizations the peptide is

first cleaved from the resin, usually leaving the protecting groups intact. Off-resin cyclizations are typically conducted under dilute conditions to avoid oligomerization.

Scheme 1.4 Macrocyclization strategies.

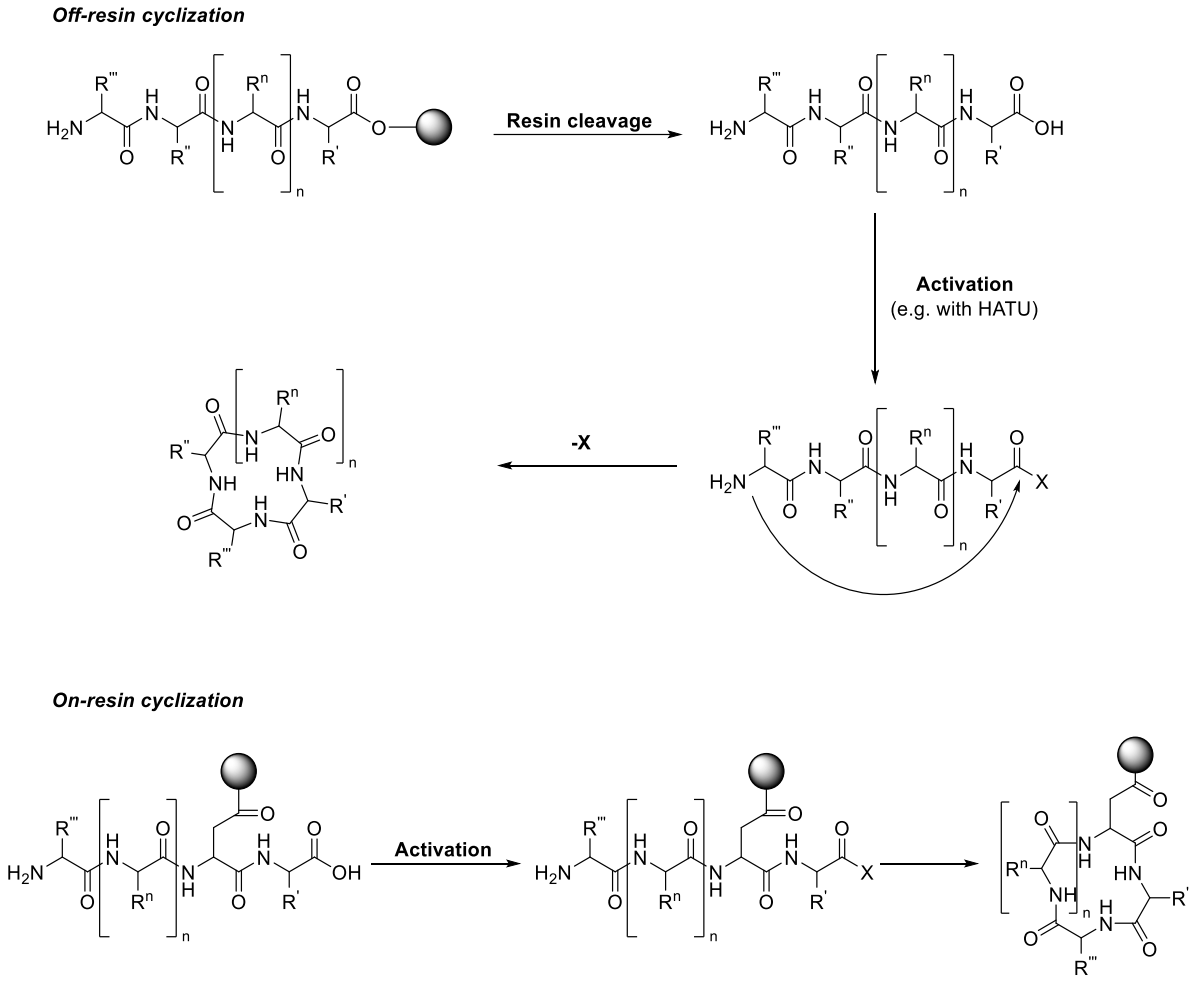

For the synthesis of a large number of analogs, it is often desirable to cyclize a peptide on-resin. Excessive dilution during the cyclization is not required due to the pseudo-dilution effect of the resin support, which favours intramolecular cyclization and reduces the waste and cost of each reaction.[130] On-resin cyclizations also open up the possibility for combinatorial approaches to the synthesis of cyclic peptide analogs. As seen in the syntheses of daptomycin described below (Scheme 1.12), on-resin cyclization requires that the *C*-terminus be orthogonally protected and so is unavailable for resin

attachment. Typically the peptide is attached to the resin by an appropriate side chain protecting group using a wide variety of strategies.[137]

Thakkar, Trinh, and Pei examined the effect of a peptide sequence on macrocyclization efficiency on-resin using a combinatorial approach.[138] They found that efficiency decreased dramatically if a large number of Boc-protected lysine residues or Pbf-protected arginine residues were present. This effect was attributed to aggregation promoted by the formation of bidentate hydrogen bonds between the side chains. Disruption of these hydrogen bonds with chaotropic salts, Triton X-100, or protic solvents improved cyclization efficiency.

The application of on-resin and off-resin cyclization strategies are nicely illustrated in the synthesis of the polymyxins, which is relevant to paenibacterin since they are structurally similar. These syntheses are discussed below.

1.6.3 Synthesis of Polymyxin

The first solid-phase total synthesis of polymyxin B1 was achieved in 1999 by Sharma et al (Scheme 1.5) using an off-resin cyclization strategy.[139] The peptide was attached to the highly acid-labile 2-methoxy-4-alkoxybenzyl alcohol resin (Sasrin™) via the α-carboxyl group of Thr1. The peptide (**1.1**) was elongated to the acyl tail using standard Fmoc SPPS, coupling protected amino acids with HBTU, DIPEA, and *N*-methylpyrrolidinone. The Dab4 residue was incorporated with the side chain amine protected with a Dde group, which was selectively removed from the complete linear peptide with dilute hydrazine in DMF. The protected peptide was then cleaved from the resin with dilute TFA, which leaves the side chain protecting groups intact. The peptide was cyclized with DPPA in a dilute acetonitrile solution to avoid polymerization. This is a common and reliable approach for the synthesis of macrolactam peptides, and the authors achieved a relatively high yield of 20%. Ramesh et al. used a

similar approach in their 2016 synthesis of a colistin-like peptide.[140] In this case an alloc group was used to protect the side chain of Dab4, and was selectively removed with a palladium catalyst.

Scheme 1.5 Total synthesis of Polymxyin B1 by Sharma using an off-resin cyclization strategy.

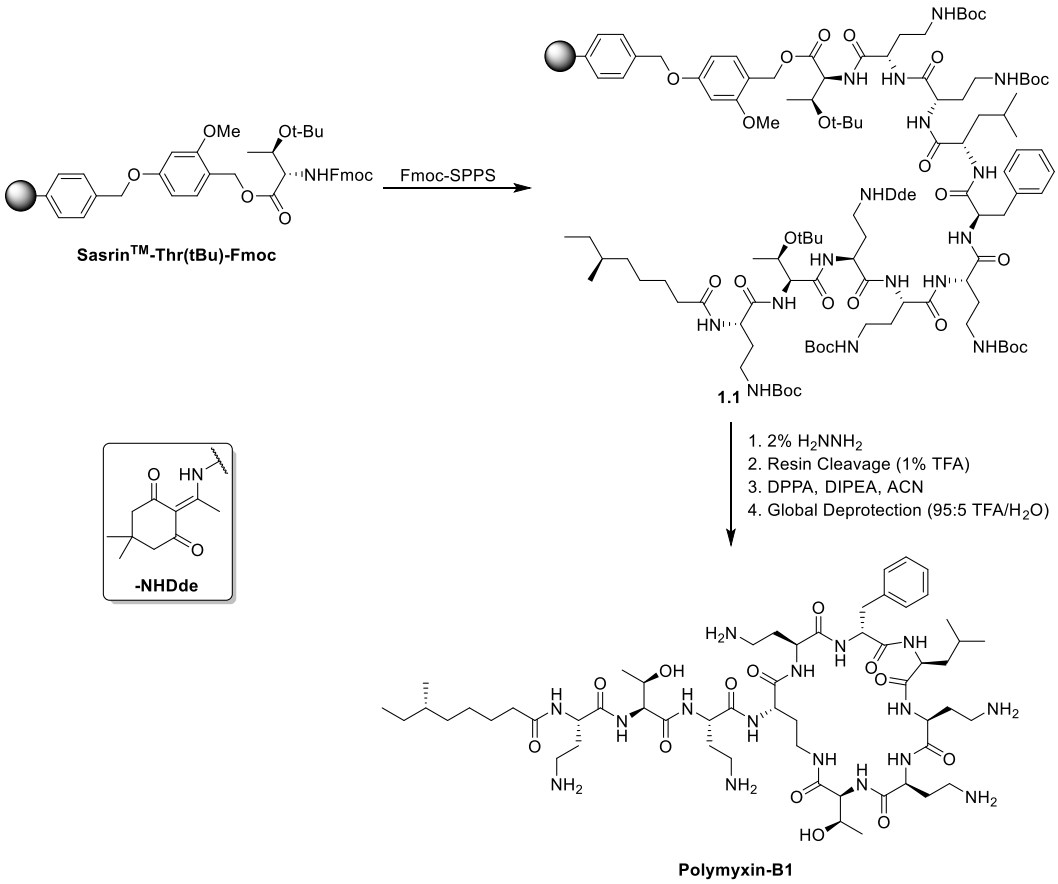

An on-resin cyclization strategy was later developed by Xu et al. that allowed the entire molecule to be synthesized on-resin (Scheme 1.6).[141] In this case the peptide was cyclized between Dab9 and Thr10. As with Sharma's approach, the side chain of Dab3 was protected with a Dde group (**1.2**) that could be selectively deprotected to allow the threonine residue to be coupled (**1.3**). To allow for on-resin cyclization (giving peptide **1.4)**, the *C*-terminus of the linear portion of the peptide was protected as an allyl ester, which could be selectively deprotected with a palladium catalyst. Since the peptide could not be attached to the resin through the *C*-terminus, it was loaded onto 2-chlorotrityl-resin through the side chain of a Dab residue. This is an example of a four-dimensional protecting group scheme.

Scheme 1.6 Synthesis of Polymyxin by Xu using an on-resin cyclization strategy.

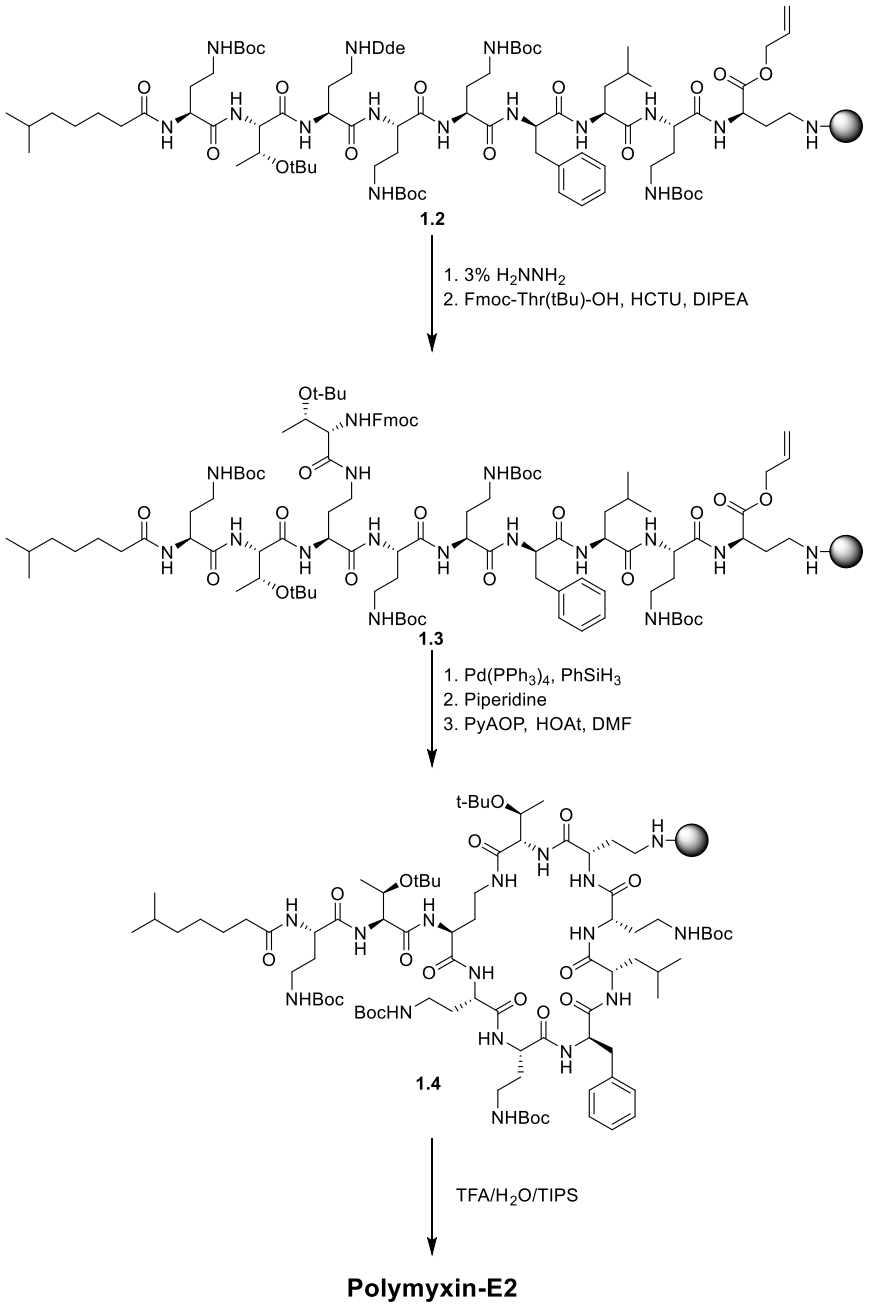

1.6.4 On-Resin Ester Coupling Reactions

A key structural difference between paenibacterin and polymyxin is the presence of an ester bond that gives rise to the macrocyclic portion of the peptide. Esterification steps are notoriously challenging in

the synthesis of natural products.[142] These couplings can be rendered even more challenging when done on resin-bound peptides where epimerization, slow couplings, and side reactions such as dehydration of unprotected asparagine residues are all of concern. The development of efficient esterification strategies has been a prominent area of research for the Taylor group in their pursuit of cyclic lipodepsipeptide target molecules. A good example of the difficulties that may be encountered when attempting to construct an ester bond on the solid phase is the synthesis of daptomycin, which is discussed below.

1.6.5 The Synthesis of Daptomycin

The first report describing a synthesis of daptomycin to appear in the primary scientific literature was by Lam et al.[143] Their initial attempt involved forming the ester bond between resin-bound linear peptide **1.5,** which was easily prepared using Fmoc SPPS, and a Kyn-containing building block **1.6** (Scheme 1.7). However, even though they tried a wide variety of coupling agents, they were unable to make the ester bond.

Scheme 1.7 Attempted synthesis of peptide 1.7 by Lam et al.

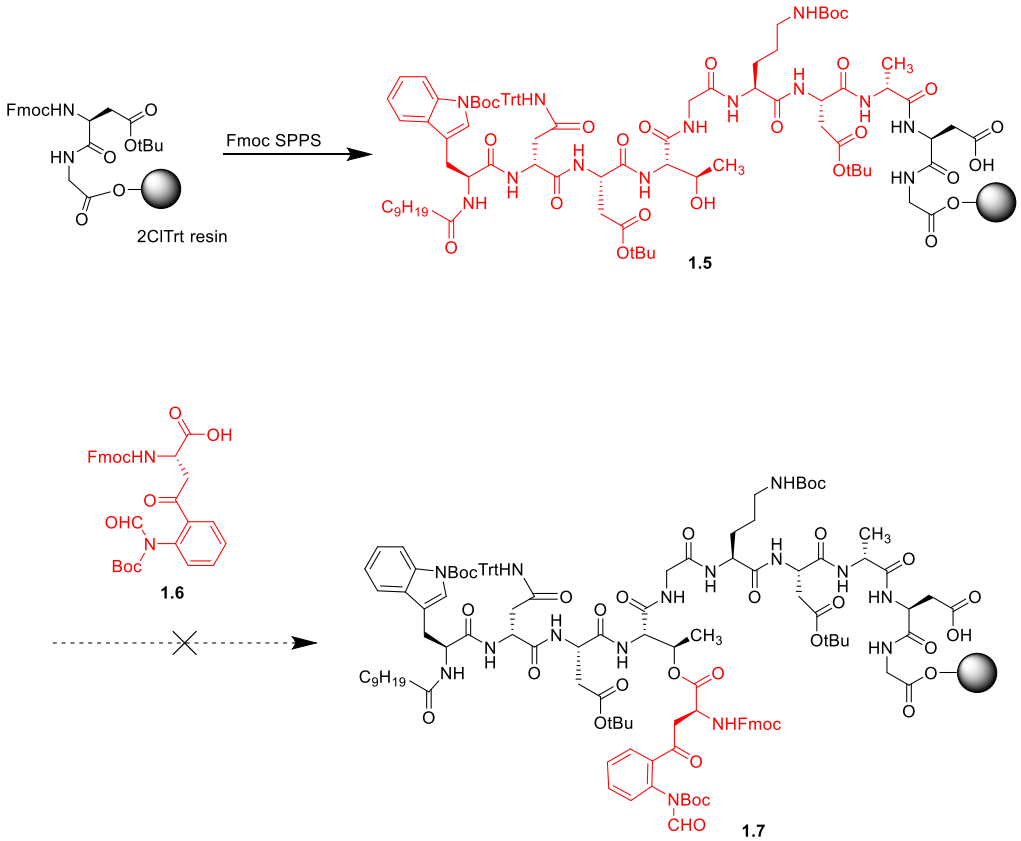

Next, they attempted a combined solution/solid phase approach in which ester bond formation would be achieved by coupling the Kyn residue to pentapeptide **1.8** in-solution (Scheme 1.8). The resulting branched hexapeptide (**1.9**) would be used as a building block for the solid phase synthesis of the rest

of the peptide. However, once again they were unable to make the ester bond. They attributed the failure of these attempts to the low reactivity of the Kyn building block.

Scheme 1.8 Attempted synthesis of peptide 1.9 by Lam et al.

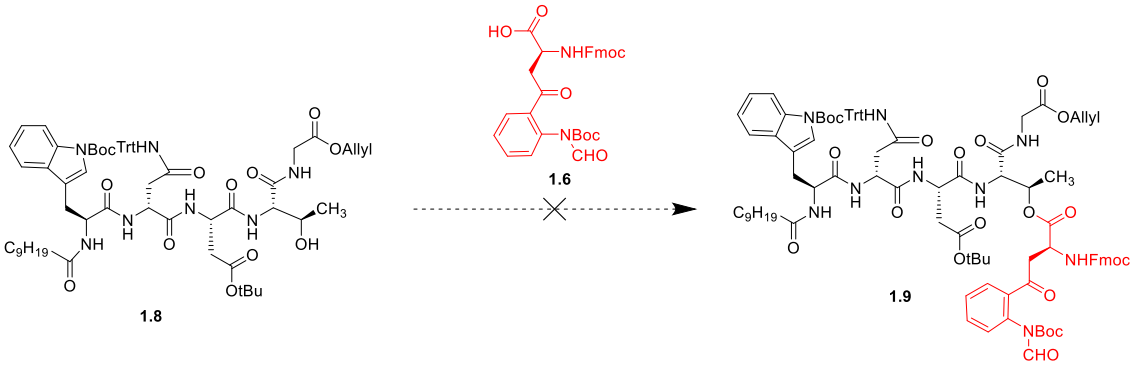

To get around the low reactivity of the Kyn building block towards ester bond formation, they decided to make the ester bond between Fmoc-Trp(Boc)-OH and tripeptide **1.10**, which contained residues 3 to 5 (Scheme 1.9). After allyl deprotection of the resulting peptide **1.11**, the Trp residue was successfully converted to a Kyn residue using ozonolysis to give tetrapeptide **1.12**.

Scheme 1.9. Synthesis of a kynurenine-containing tetrapeptide 1.12 by Lam et al.

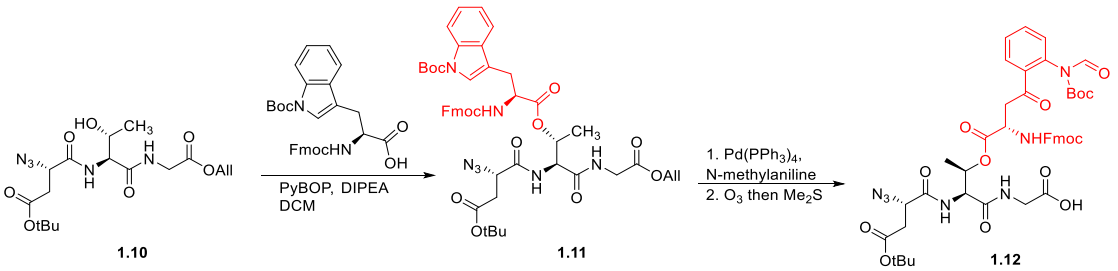

Peptide **1.13**, which contained residues 6 to 10, was attached to the resin via the α-COOH of Gly10, was prepared using standard Fmoc SPPS (Scheme 1.10). Tetrapeptide **1.12** was attached to peptide **1.13** to give peptide **1.14**. Coupling onto the α-COOH group of Gly5 residue of peptide **1.14** meant that epimerization upon formation of the active ester did not need to be considered. Residues 12 and 11 were installed into peptide **1.14** using Fmoc SPPS. The azido group in peptide **1.15** was then reduced and the peptide was elongated to the acyl tail to give peptide **1.16**. Peptide **1.16** was cleaved from the

resin using mild acid, the free *C*-terminus was functionalized with salicylaldehyde to give peptide **1.17**, and then all of the side chains protecting groups were removed. This allowed for solution phase macrocyclization via a serine-mediated ligation, giving daptomycin. Although this approach was successful it is somewhat labour intensive.

Scheme 1.10 Synthesis of daptomycin by Lam.

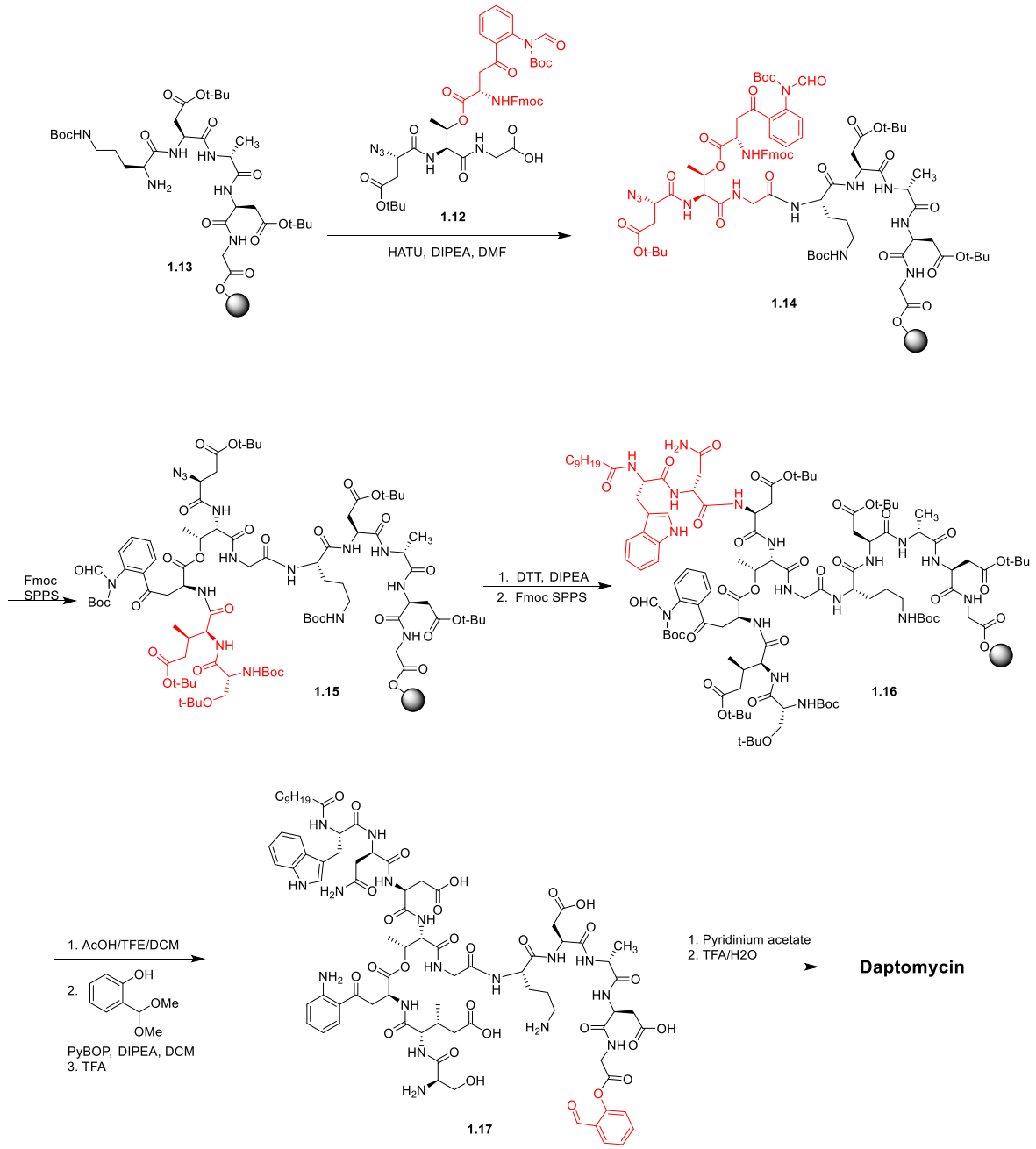

Shortly thereafter, the Taylor group reported an entirely solid phase total synthesis of daptomycin using an on-resin cyclization strategy. They began by attaching the peptide to the support via the side chain of Asp9 so that they could do an on-resin cyclization. The *C*-terminal Gly9 residue was protected with an allyl group. They found that the length of the resin-bound peptide dramatically affected the

efficiency of the coupling of the Kyn building block **1.6** onto the side chain of the Thr3 residue (Scheme 1.11).[144,145] Attempts to make the ester bond on a peptide containing residues 1–10 and the lipid tail (**1.18** and **1.19** in Scheme 1.11) were unsuccessful. However, they were able to obtain a 40% yield with peptide **1.20**, which did not contain the lipid, using DIC/DMAP to give peptide **1.21**. A quantitative yield was obtained using peptide **1.22**, which did not have the lipid tail or residues 1 and 2 (giving **1.23** in Scheme 1.11).

Scheme 1.11 Esterification conditions developed by Lohani et al.

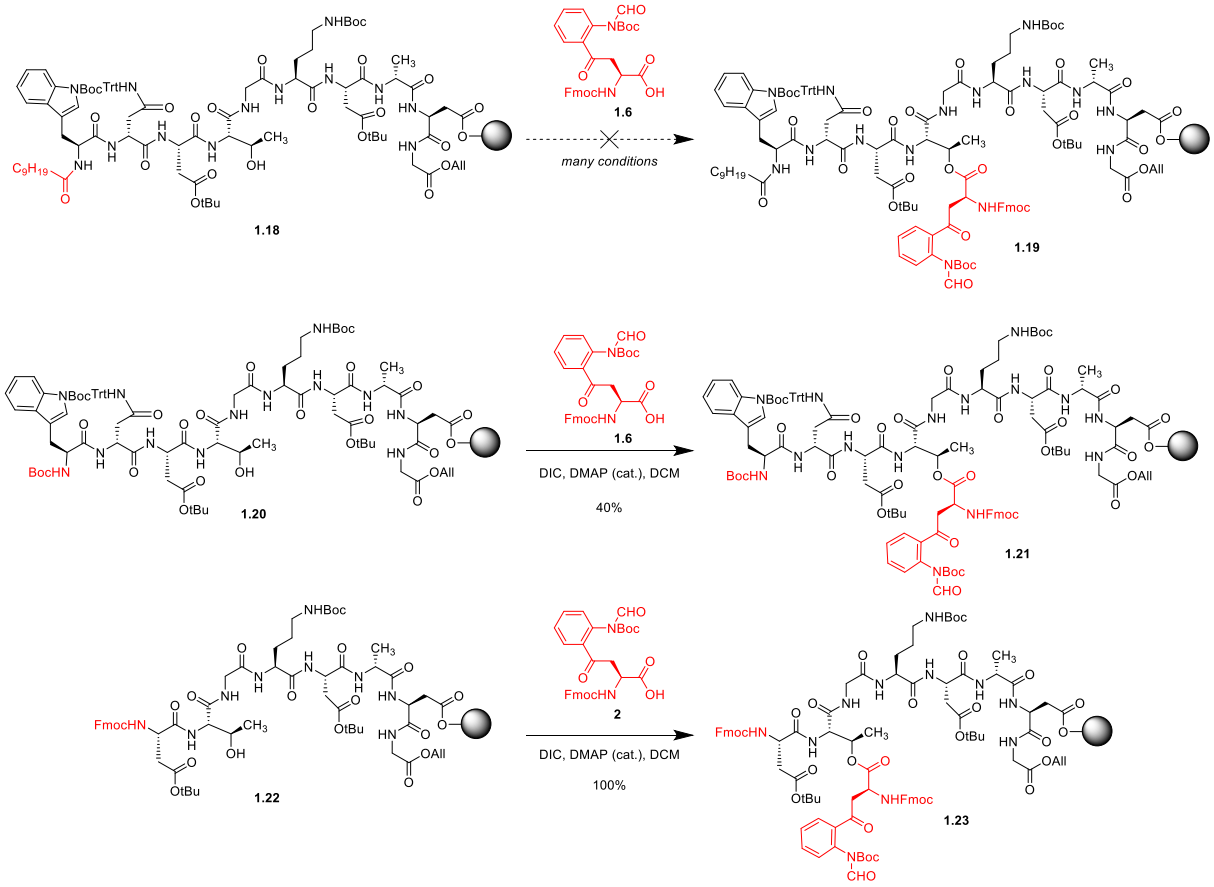

Armed with the knowledge that the ester bond could be formed on a 'short' (or *truncated*) peptide, they constructed peptide **1.24** (Scheme 1.12). This peptide contained residues 3 to 10 and an *N*-terminal azido group. This peptide had to be extended one residue beyond Thr4; otherwise, deprotection of the

N-terminus after ester bond formation would be followed by an unavoidable *O*→*N* acyl shift where the kynurenine would be transferred to the N^{α} of Thr4. Following esterification, the resulting peptide **1.25** was elongated to the acyl tail (peptide **1.26**) using an azide-SPPS approach which involved iteratively coupling of azido acids and deprotecting with aqueous trialkyl phosphine. Following acylation with decanoic acid the Fmoc group of kynurenine was deprotected and the remaining residues were installed using standard Fmoc-SPPS. The allyl group was removed with a palladium catalyst and a weak nucleophile prior to cyclization. Global deprotection gave daptomycin.

Scheme 1.12. Synthesis of daptomycin by Taylor and coworkers.

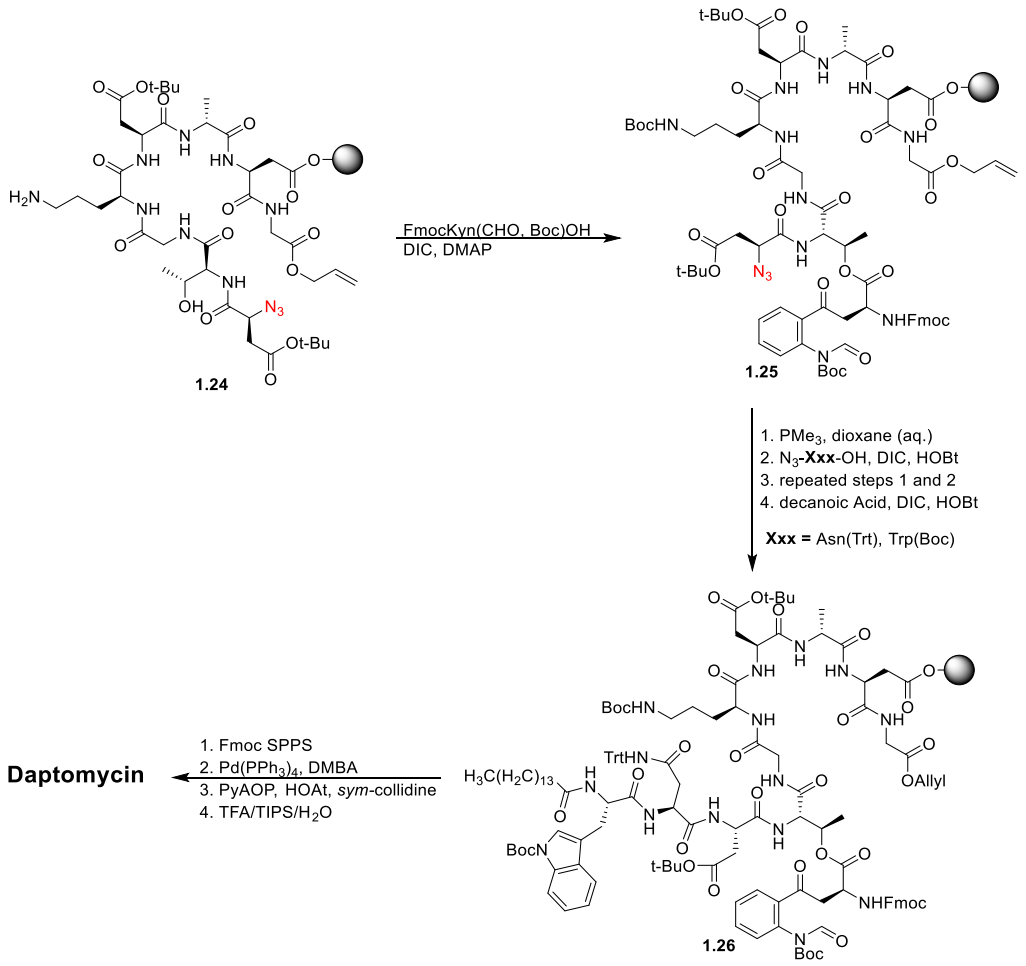

This approach was used by the Taylor group to prepare a number of daptomycin analogs, including one where the non-proteinogenic amino acids 3-MeGlu12 and Kyn13 were replaced with the readily

available and inexpensive Glu and Trp, respectively. This analog, Dap-E12-W13, was only 3 to 5-fold less active than daptomycin against the model bacterium, *B. subtilis* 1046.

A disadvantage of Taylor's initial approach was the use of several azido acids, which must be prepared individually. When synthesizing Dap-E12-W13 analogs the number of azido acids could be reduced by protecting Trp13 as an azide, allowing the peptide to be elongated to the *C*-terminus using standard Fmoc-SPPS. However, the reduction of an azido ester could be problematic and required special deprotection conditions to suppress cleavage of the ester bond.[146,147] A better approach for the synthesis of Dap-E12-W13 was later developed that did not require any azido acids (Scheme 1.13). It was found that Trp13 could be coupled onto the full-length linear portion of the peptide **1.27** to give peptide **1.28** if equimolar amounts of amino acid and DIC were used, and if chlorotrityl-Tentagel™ resin was used in place of a polystyrene solid-support. Tentagel is a copolymer, with a core of polystyrene attached to the linker with a PEG spacer. The PEG improves the solubility of the resin-bound peptide, and in general, improves reaction efficiency. This approach was used by Barnawi et al. to efficiently synthesize a large number of analogs and complete an alanine scan to identify key residues that are amenable to variation without loss of biological activity.[119] It was also found that the daptomycin analog, Dap-K6-E12-W13, in which all of the uncommon amino acids were replaced with their common counterparts, was only 1.5 to 3-fold less active than daptomycin against the model bacterium, *B. subtilis* 1046.

Scheme 1.13. Synthesis of a daptomycin analog by Taylor and coworkers.

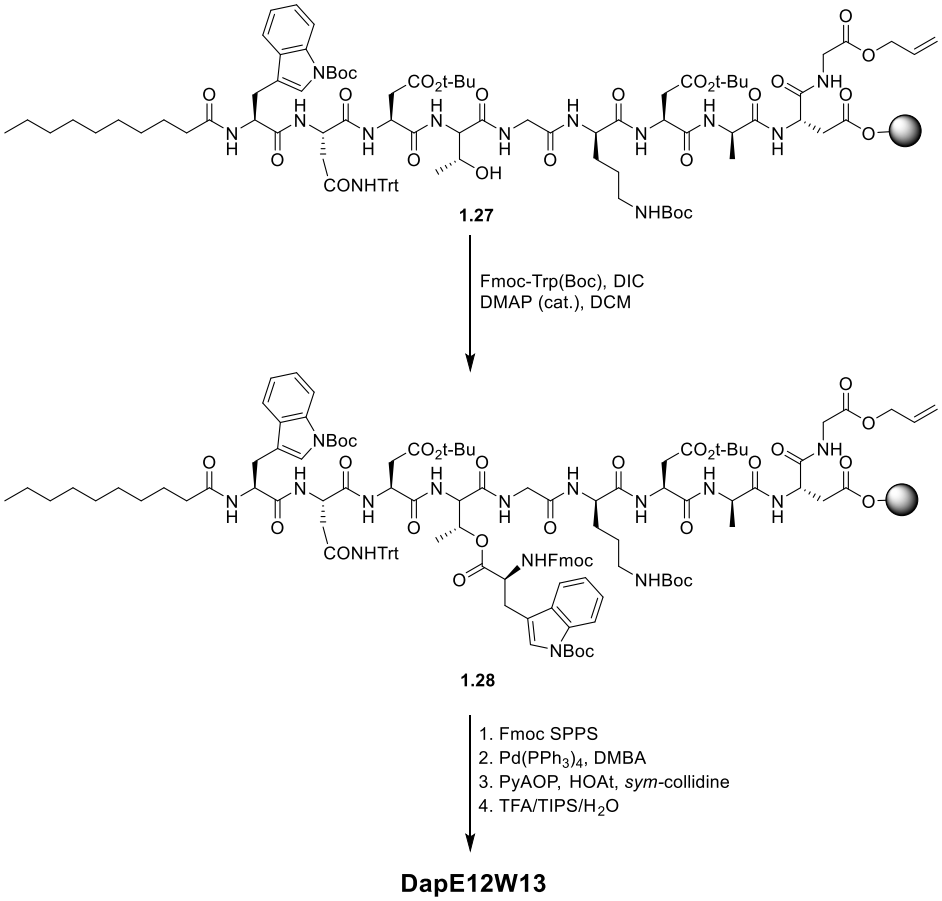

1.7 Research Goals and Thesis Outline

For clinical use, it is preferable that an antibiotic be highly active, having an MIC ≤ 1 μg/mL. Although the paenibacterins fall short in this regard, their above-mentioned characteristics (section 1.3.1) make them an attractive lead for the development of a clinically useful broad-spectrum antibiotic. However, until recently, the paenibacterins could only be obtained from bacterial cultures, an inefficient and time-consuming process. Furthermore, this did not allow for structural variation of the peptide. The goal of the work presented in Chapter 2 was to develop a robust and efficient method for the synthesis of paenibacterin A1 that could be applied to a wide variety of analogs. The development of this approach led us to solutions that overcame the difficult esterification and cyclization steps. In the process, we prepared analogs with minor structural variations such as an amide linkage in place of the ester bond.

The goal of the work presented in Chapter 3 was to use the synthetic methodology developed in Chapter 2 to prepare paenibacterin analogs that would enable us to probe the importance of hydrophobicity and overall charge to paenibacterin's antibacterial activity against both Gram-(+) and Gram-(−) bacteria. Remarkably, it was found that several cationic residues in paenibacterin could be substituted with L/D-Ala with little or no loss of activity when tested against two model bacteria, *B. subtilis* 1046 and *E. coli* K-12. Our synthetic method was also extended to synthesize an analog of paenibacterin B4.

In Chapter 4, we sought to develop a new solvatochromic fluorescent amino acid for studying the interactions of peptides, such as paenibacterin, with bacterial membranes and membrane components. Two 7-dialkylaminocoumarin-containing amino acids were designed, synthesized, and their photochemical properties were investigated. One of these fluorescent amino acids was incorporated into paenibacterin. The fluorescent paenibacterin analog had only slightly reduced biological activity and was found to be effective for investigating paenibacterin's interaction with model bacterial membranes, bacterial LPS, and intact bacterial cells.

In Chapter 5, a structure-activity relationship study on the daptomycin analog Dap-K6-E12-W13, mentioned in section 1.6.5, was conducted. This chapter builds on prior work that had identified two positions that were amenable to substitution. A series of analogs bearing a wide assortment of amino acids at these positions was prepared. The effect of these substitutions on antibacterial activity was determined. Cationic modifications were found to be particularly favoured at these two positions. This work also sought to probe the relationship between calcium-dependent binding to membranes and antibacterial activity. The results of this study enabled us to develop daptomycin analogs that were more active than daptomycin against *B. subtilis* 1046.

Chapter 2

Total Synthesis of Paenibacterin and Its Analogs[i]

2.1 Preface and Contributions

The work presented in this chapter was carried out primarily by myself under the supervision and guidance of Dr. Scott D. Taylor and Dr. Michael Palmer. Ryan Moreira, a graduate student in the Taylor group, prepared (2*S*,3*R*)-diaminobutyric acid (Daba), which was described in a prior publication. Dr. En Huang, under the supervision of Dr. Ahmed Yousef at Ohio State University, graciously prepared and provided a sample of authentic paenibacterin that was used in HPLC co-elution experiments.

The work described in this chapter was published in the *Journal of Organic Chemistry* (*J. Org. Chem.* **2019**, 84 (9), 5339–5347). I prepared initial drafts of the manuscript, which were then subjected to revisions primarily by Dr. Taylor. Much of this published manuscript has been reproduced below in accordance with the American Chemical Society's Policy on Theses and Dissertations. A letter of permission is included in the appropriate section. Select schemes have been rearranged for increased readability, and compounds have been re-numbered with a format consistent with the rest of the thesis.

---

[i] Reproduced (adapted) with permission from "Noden, M.; Moreira, R.; Huang, E.; Yousef, A.; Palmer, M.; Taylor, S. D. Total Synthesis of Paenibacterin and Its Analogues. *J. Org. Chem.* **2019**, *84* (9), 5339–5347. http://pubs.acs.org/articlesonrequest/AOR-9JJKmajHkFRVKFaYMZSr". Copyright © 2019 American Chemical Society.

2.2 Introduction

As stated in Chapter 1, one of the goals of this thesis was to develop a total synthesis of paenibacterin, as this antibiotic has properties that makes it a good lead structure for the development of new broad-spectrum antibiotics.

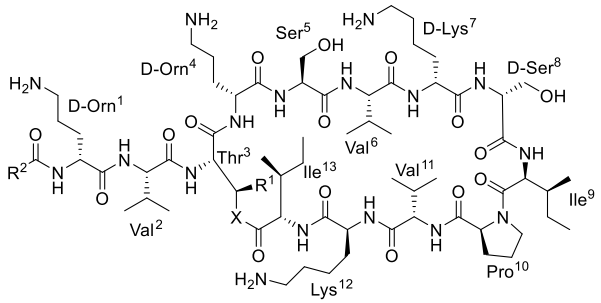

PA1, X = O, $R^1 = CH_3$, $R^2 = (CH_2)_{13}CH_3$
PA2, X = O, $R^1 = CH_3$, $R^2 = (CH_2)_{10}CH(CH_3)CH_2CH_3$ (anteiso)
PA3, X = O, $R^1 = CH_3$, $R^2 = (CH_2)_{11}CH(CH_3)CH_3$ (iso)
PA1-Dapa, X = NH, $R^1 = H$, $R^2 = (CH_2)_{13}CH_3$
PA1-Daba, X = NH, $R^1 = CH_3$, $R^2 = (CH_2)_{13}CH_3$

Figure 2.1 Structure of paenibacterin A1, A2 and A3, and Dapa and Daba analogs of PA1.

Paenibacterin sourced from *P. thiaminolyticus* is a mixture of three homologous compounds with isomeric 15-carbon acyl lipid tails designated PA1 (linear lipid), PA2 (anteiso lipid), and PA3 (iso lipid) (Figure 2.1).[41,42] PA2 and PA3 are the dominant isoforms produced by *P. thiaminolyticus*, with PA2 being produced in slight excess to PA3.

As mentioned in Chapter 1, paenibacterin is amphipathic, adopts a β-sheet conformation in solution, and requires its acyl tail for activity. Hydrolysis of paenibacterin with aq. HCl followed by reaction of the released amino acids with Marfey's reagent and HPLC analysis of the modified amino acids indicated that Val2, Thr3, Val6, Ile9, Pro10, Val11 and Ile13 are L-amino acids, while the two Orn residues and one of the Lys residues are of the D-configuration.[41] The peak of D-Ser in the HPLC profile overlapped with the Marfey's reagent; therefore, it was not possible to confirm the configuration of the

two serine residues using this approach. However, bioinformatic analysis suggests that Lys7 and Ser8 are of the D-configuration while Lys12 and Ser5 have the L-configuration.[42]

Herein we report the first total synthesis of PA1 and PA2, as well as the two analogs of PA1 in which the ring closing ester bond is replaced with an amide bond (PA1-Dapa and PA1-Daba, Figure 2.1). The antibacterial activity of these peptides against a Gram-(+) bacterium and a Gram-(−) bacterium is also reported.

2.3 Results and Discussion

Our initial approach to prepare PA1 and PA2 was via an on-resin cyclization strategy as illustrated for PA1 in Scheme 2.1. We envisioned attaching the peptides to a chlorotrityl (ClTrt) polystyrene resin via the side chain of Lys12 with the *C*-terminus protected as an allyl ester.[148] The linear peptide **1.6** would be assembled using Fmoc SPPS, incorporating Thr3 with an unprotected side chain, followed by formation of the ester bond between Thr3 and alloc-protected Ile13, to give peptide **2.2**. The alloc groups would be removed and the peptide cyclized. PA1 would be obtained by installation of D-Orn2 and the lipid tail followed by cleavage of the peptide from the resin and global deprotection.

Scheme 2.1 On-resin cyclization approach to PA1.

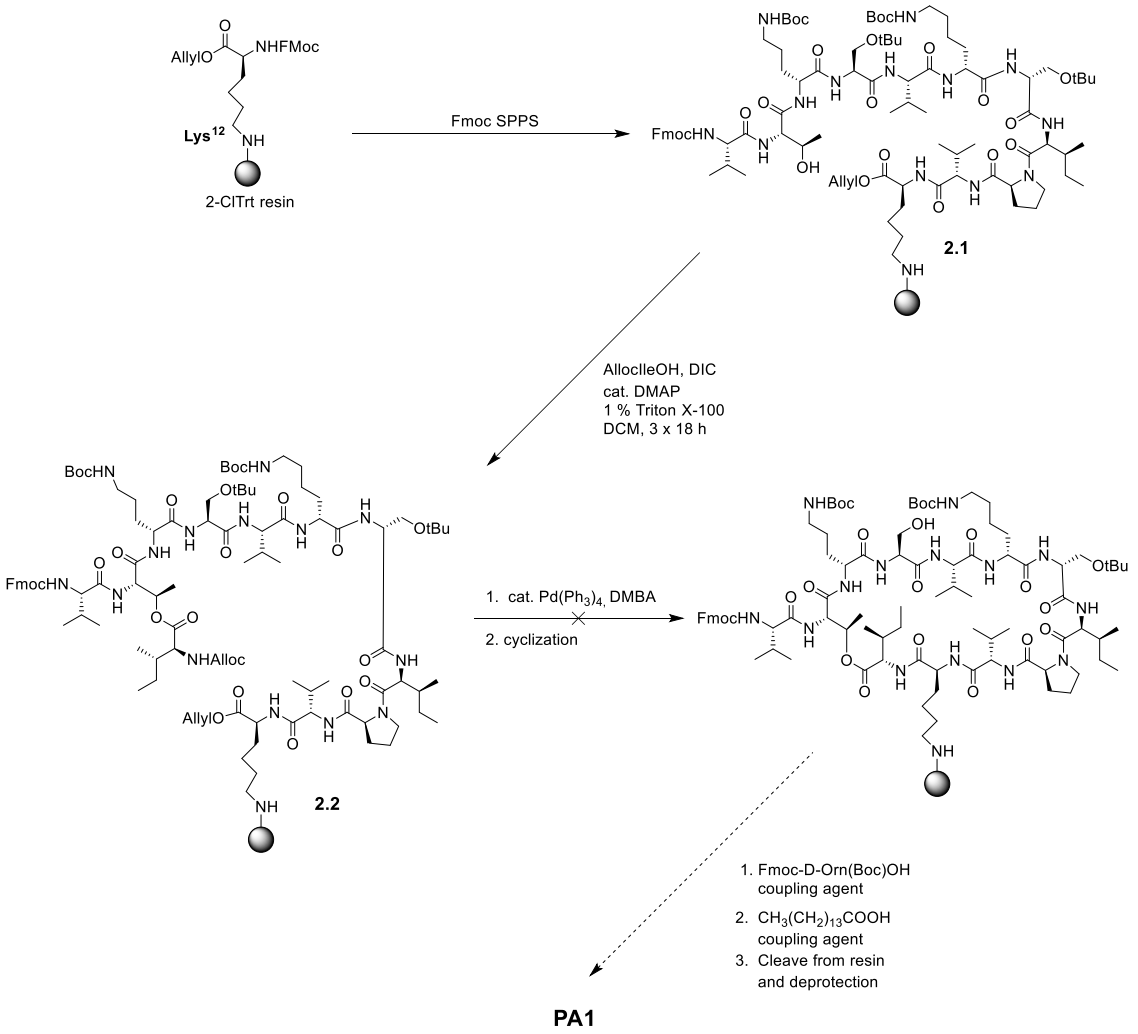

The synthesis of peptide **2.1** via standard Fmoc SPPS proceeded smoothly. On the other hand, formation of the ester bond to give peptide **2.2** proved to be challenging.[142] Nevertheless, after examining different coupling conditions, it was found that peptide **2.2** could be prepared in near quantitative yields after three 18 h couplings each using 10 equiv of allocIleOH and 10 equiv of DIC, 10 mol % DMAP, 1% Triton X-100 in DCM, which are conditions that we have found to be effective for forming depsi bonds during the synthesis of daptomycin (another cLPA) and its analogs.[119] We have recently shown that formation of the depsi bond during the synthesis of daptomycin analogs proceeded faster when using a Trt Tentagel® resin, which is a PEG-polystyrene copolymer, as opposed

to standard polystyrene resin.[119] This was not the case with peptide **2.2**: the esterification required three 18 h couplings regardless of the resin type.

The ester bond in peptide **2.2** was unusually susceptible to acid-catalyzed hydrolysis. Removing peptide **2.2** from the resin using TFA/TIPS/H_2O (1.5 h) resulted in complete hydrolysis of the ester bond, even when using shorter reaction times. Completely protected peptide **2.2** could be obtained by removing peptide **2.2** from the resin using AcOH/TFE/DCM (1:1:8).

The allyl groups in peptide **2.2** were removed using cat. $Pd(PPh_3)_4$ and excess *N,N*-dimethylbarbituric acid (DMBA). [119] However, we were unable to cyclize the resulting peptide in reasonable yield using a wide variety of different conditions including BOP/HOAt/DIPEA and PyAOP/HOAt/ DIPEA.[119,149,150] The cyclization was also proceeded poorly when using Trt Tentagel® resin.

Due to the difficulties encountered with the on-resin cyclization, we decided to prepare PA1 and PA2 using an off-resin cyclization strategy. Towards this end, and starting with Pro10 attached to 2-ClTrt polystyrene resin, peptide **2.3** was assembled by Fmoc SPPS (Scheme 2.2). The esterification conditions that were used to couple allocIleOH in Scheme 2.1 were used to couple FmocIleOH to peptide **2.3** (10 equiv of FmocIleOH, 10 equiv of DIC, 10 mol % DMAP, 3 × 18 h). Gauging the success of the esterification reaction proved to be difficult. The ester bond in peptide **2.4** was very susceptible to acid-catalyzed hydrolysis. Attempts to deprotect and remove peptide **2.4** from the resin using TFA/TIPS/H_2O resulted in complete hydrolysis of the ester bond. Although peptide **2.4** could be cleaved off the support with all of the protecting groups intact using AcOH/TFE/DCM, we found it difficult to obtain a good mass spectrum of the resulting hydrophobic peptide. However, it was found if residues 11 and 12 were installed, using 2-methylpiperidine (2-MP) in DMF for Fmoc removal to prevent ester bond aminolysis,[144,145] the ester bond in the resulting peptide **2.5** was stable enough such that it could be cleaved from the resin using TFA/TIPS/H_2O and its mass spectrum obtained.

Unfortunately, it was found that the esterification proceeded with only 60% efficiency and peptide **2.5** was produced as a 1:1 mixture of epimers. Similar results were obtained using a Trt Tentagel® resin. Racemization most likely occurred during installation of Ile13.

Scheme 2.2 Preparation of peptide 2.5.

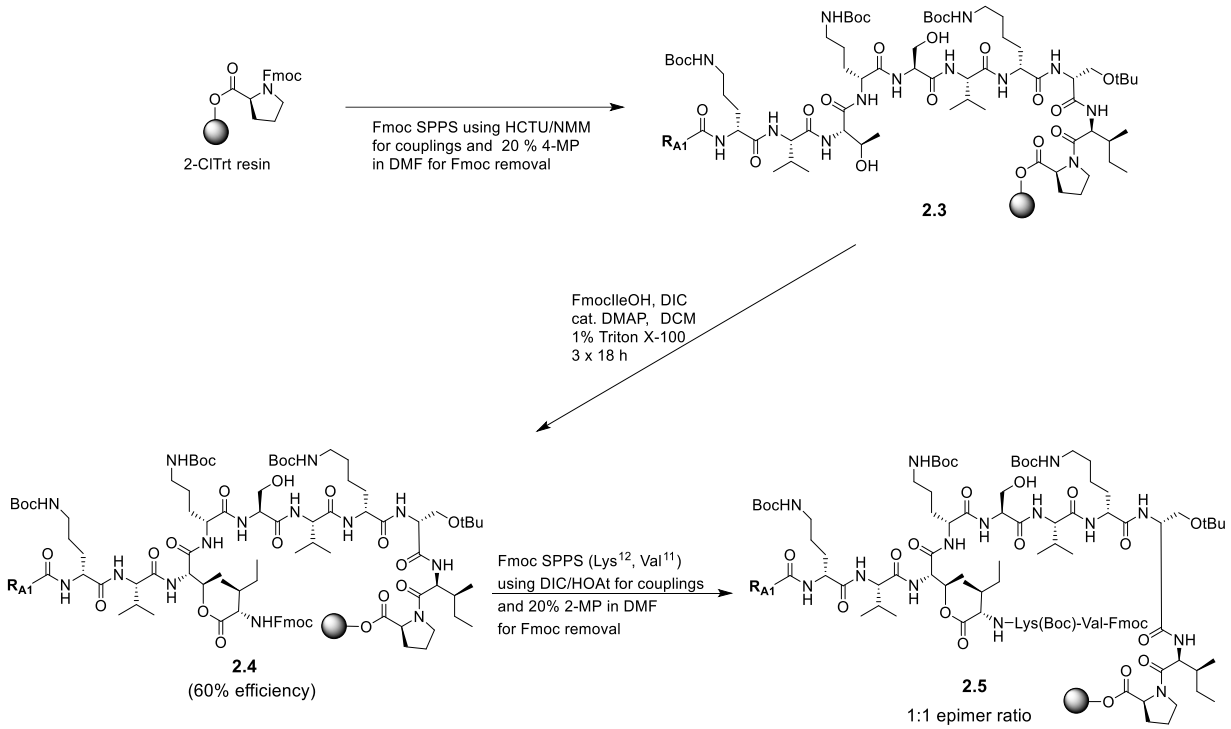

We attempted to improve the synthesis by performing the esterification reaction on a truncated peptide and using allocIleOH. Towards this end, peptide **2.6** was prepared using Fmoc SPPS.[151] To minimize epimerization, a single 18 h coupling, using the conditions outlined above for peptide **2.3**, was used to install allocIleOH into peptide **2.6** (Scheme 2.3). After elaboration to peptide **2.5**, it was found that the epimeric ratio of peptide **2.5** was improved to 4:1; however, the esterification reaction proceeded with an efficiency of only 50%. Similar results were obtained using a Trt Tentagel® resin. Nevertheless, we proceeded with the synthesis by removing the Fmoc group from **2.5** using 2-MP, cleaving the resulting peptide from the resin using HFIP (20% in DCM), followed by cyclization with BOP/HOAt/DIPEA to give peptide **2.7**. Peptide **2.7** proved to be stable to standard global deprotection

conditions (TFA/TIPS/H_2O), which enabled us to obtain PA1 from peptide **2.7** as a 4:1 mixture of epimers. The major epimer could be separated from the minor epimer and the linear peptide by RP-HPLC. The yield of the major epimer of PA1 was 5.6% based on resin loading.

Scheme 2.3 Synthesis of PA1 via an off-resin cyclization.

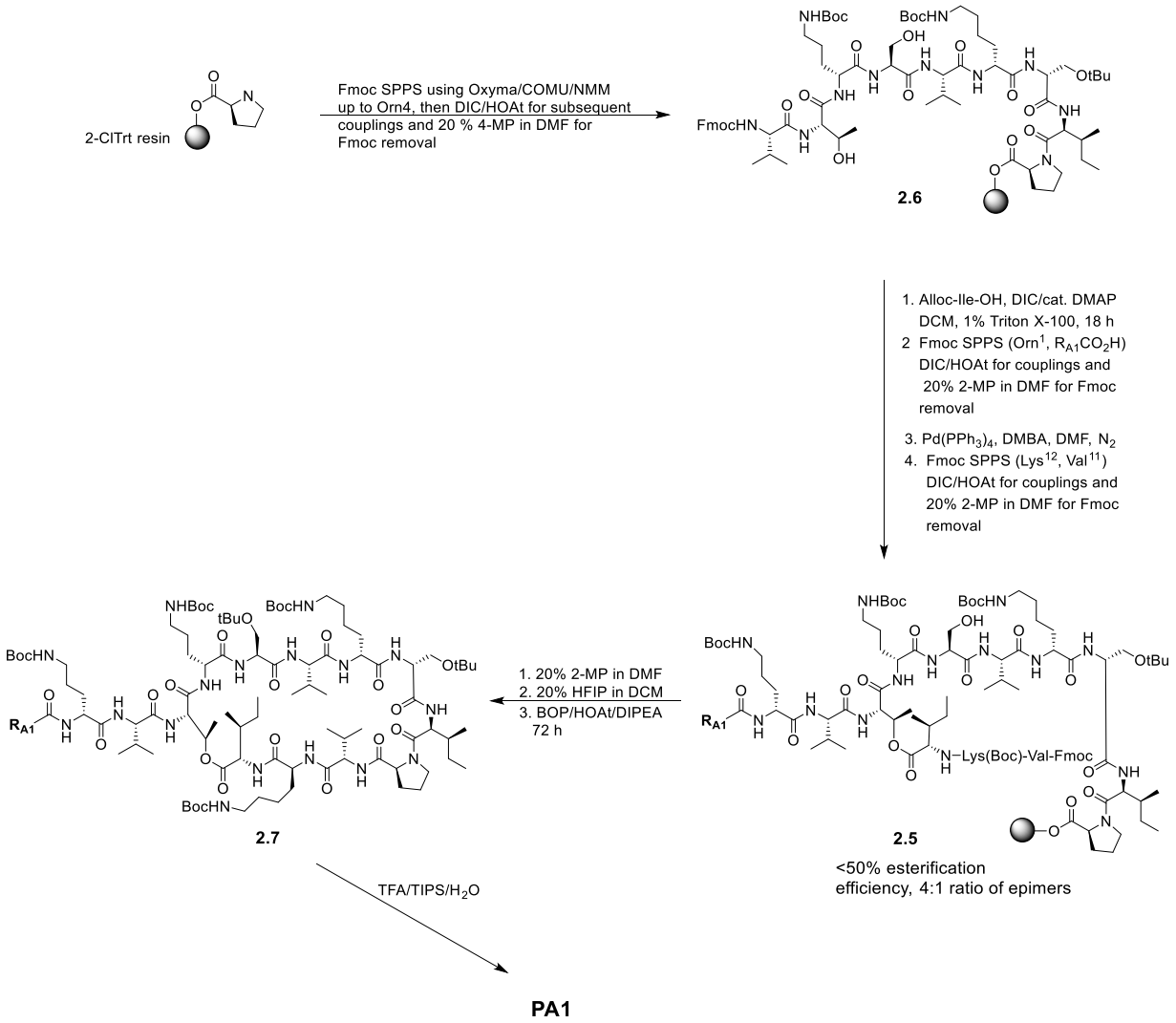

Although we could obtain PA1 using the approach outlined in Scheme 2.3, the overall yield was low. The low yield was mainly due to the poor efficiency of the esterification reaction and epimerization of Ile13 during the esterification reaction. We sought to circumvent the difficult esterification reaction by preparing analogs of PA1 in which Thr3 is replaced with L-2,3-diaminopropionic acid (PA1-Dapa) or

(2*S*, 3*R*)-2,3-diaminobutyric acid (PA1-Daba), converting the ring-closing ester bond to an amide bond. Similar analogs of daptomycin have been reported.[152,153] For the synthesis of PA1-Dapa, we prepared the linear peptide **2.8** using Fmoc-protected L-2-amino-3-azidopropionic acid (FmocDapa(N_3)OH) as a building block in place of FmocThr3 (Scheme 2.4). We elected to use the azido group as the protecting group for the 3-amino group of Dapa as we had found it to be an effective, atom-economic protecting group for the γ-amino group of Dapa when preparing amide analogs of daptomycin.[152] The azido group is reduced with DTT/DIPEA in DMF to the corresponding amino group usually within 4 h. [152] Unexpectedly, reduction of the azido group in peptide **2.8** to give peptide **2.9** required extended reaction times (2 × 20 h) which resulted in the formation of a considerable amount of byproducts.

Scheme 2.4 Reduction of the azido group in peptide 8 using DTT/DIPEA.

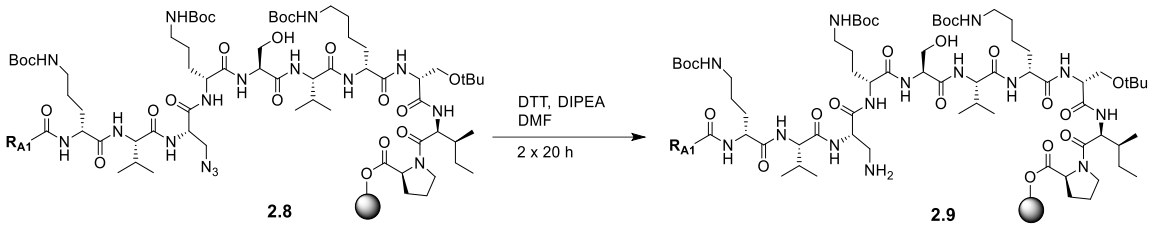

The slow rate of esterification of peptides **2.4** and **2.6,** and the sluggish rate of reduction of the azido group in peptide **2.8** suggested to us that these peptides were aggregating. We sought to address this issue by using a pseudoproline dipeptide as one of the building blocks. Pseudoprolines tend to favour a *cis*-amide, and the resulting peptide conformation is less prone to self-association.[131,132,150]

We modified our attempted synthesis of the PA1-Dapa by incorporating a D-Orn4-Ser5 pseudoproline dipeptide (Fmoc-D-Orn(Boc)-Ser($\Psi^{Me,Me}$Pro)OH) into the linear azido peptide **2.10** (Scheme 2.5). Subjecting peptide **2.10** to DTT, DIPEA in DMF resulted reduction of the azido group in **2.10** to the amine in just 4 h. It was also found that the reaction proceeded slightly faster and cleaner using a Trt Tentagel® resin as opposed to a standard polystyrene 2-ClTrt resin.

Scheme 2.5 Synthesis of PA1-Dapa.

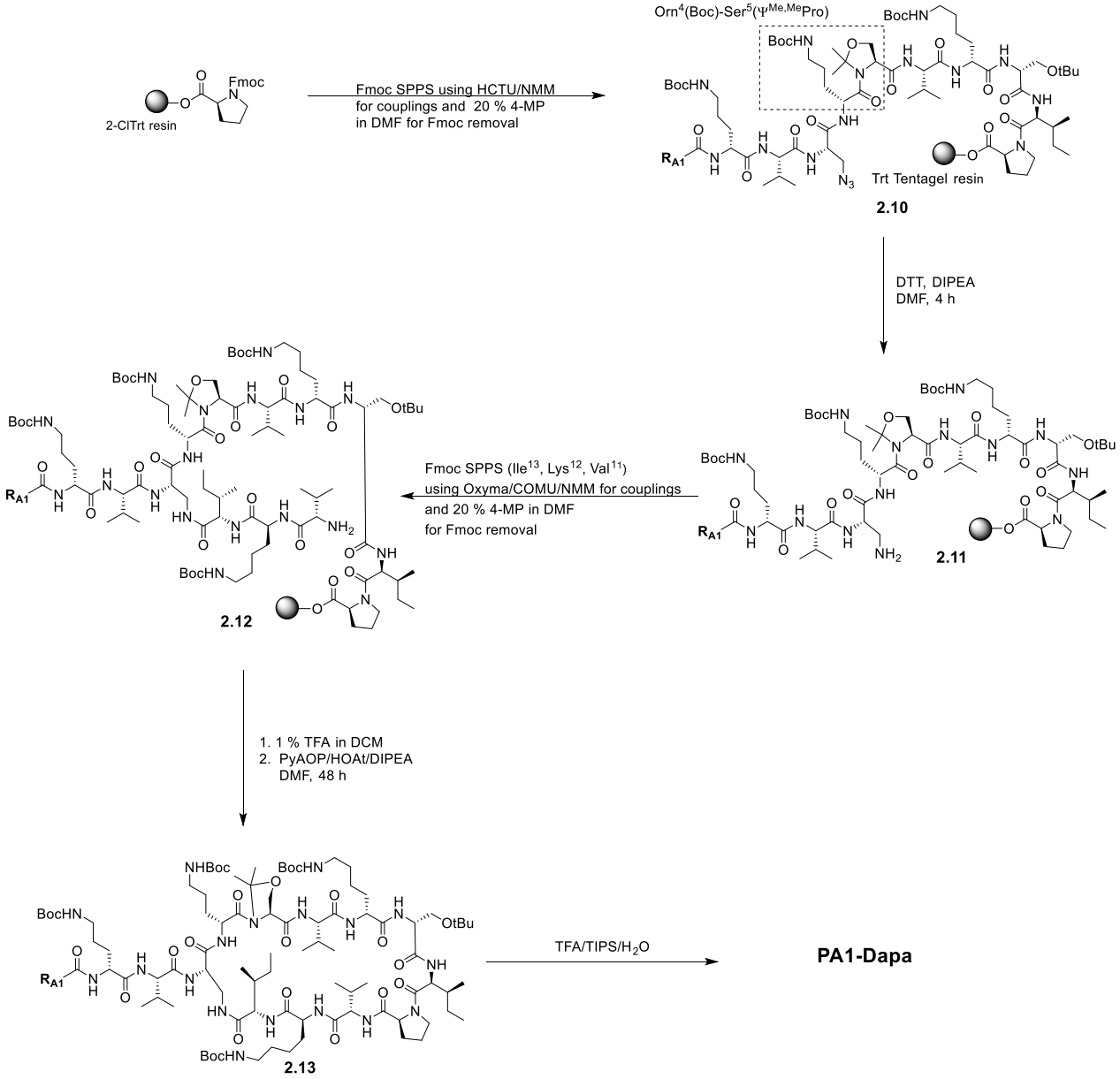

Ile13, Lys12 and Val11 were installed into peptide **2.11** to give peptide **2.12** using standard Fmoc SPPS. Couplings from the branch point were slightly sluggish using HCTU/NMM; however, by switching to the COMU/oxyma/NMM coupling system, these residues were readily introduced. Peptide **2.12** was cleaved for the support then cyclized to give peptide **2.13**. Cyclization with BOP/HOAt/DIPEA gave a complex mixture of products. However, cyclization with

PyAOP/HOAt/DIPEA proceeded cleanly. Global deprotection of **2.13** gave PA1-Dapa in an overall 31% yield based on resin loading. The same route, except Fmoc-protected (2*S*,3*R*)-2-amino-3-azidobutyric acid (FmocDaba(N_3)OH) was used in place of FmocDapa(N_3)OH and Trt Tentagel® resin was used instead of standard polystyrene resin, was employed to prepare PA1-Daba in an excellent 58% overall yield.[154]

Our success with using the pseudoproline dipeptide building block for the synthesis of PA1-Dapa and PA1-Daba prompted us to examine this approach for the synthesis of PA1 and PA2, as illustrated in Scheme 2.6 for the synthesis of PA1 in. Peptide **2.14** was prepared by Fmoc SPPS on Trt Tentagel® resin. FmocIleOH was quantitatively coupled onto peptide **2.14** to give peptide **2.15** after a single overnight coupling using our previously described conditions. Lys12 and Val11 were installed into peptide via Fmoc SPPS and using 2-MP for Fmoc removal, then the resulting peptide **2.16** was cleaved from the support with 1% TFA/DCM. Cyclization of **2.16** using PyAOP/HOAt/DIPEA proceeded cleanly to give cyclic peptide **2.17**. Global deprotection of cyclic peptide **2.17** gave PA1 as a 4:1 mixture of epimers that were separated by HPLC. The overall yield of the major epimer of PA1 was 15% based on resin loading. The same route, except anteisopentadecanoic acid was used in place of pentadecanoic acid, was employed to prepare PA2, with the major epimer being obtained in an overall 21% yield.

The NMR spectra of the synthesized PA1 and PA2 were essentially the same as that reported for an authentic PA1/PA2/P-A3 mixture by Guo et al (see **Figure A.15** to **Figure A.23**, **Table A.1** and **Table A.2)**.[41] This confirms that Lys7 and Ser8 are of the D-configuration while Lys12 and Ser5 are of the L-configuration.

Scheme 2.6 Synthesis of PA1 via an off-resin cyclization and using a D-Orn4-Ser5 pseudoproline dipeptide.

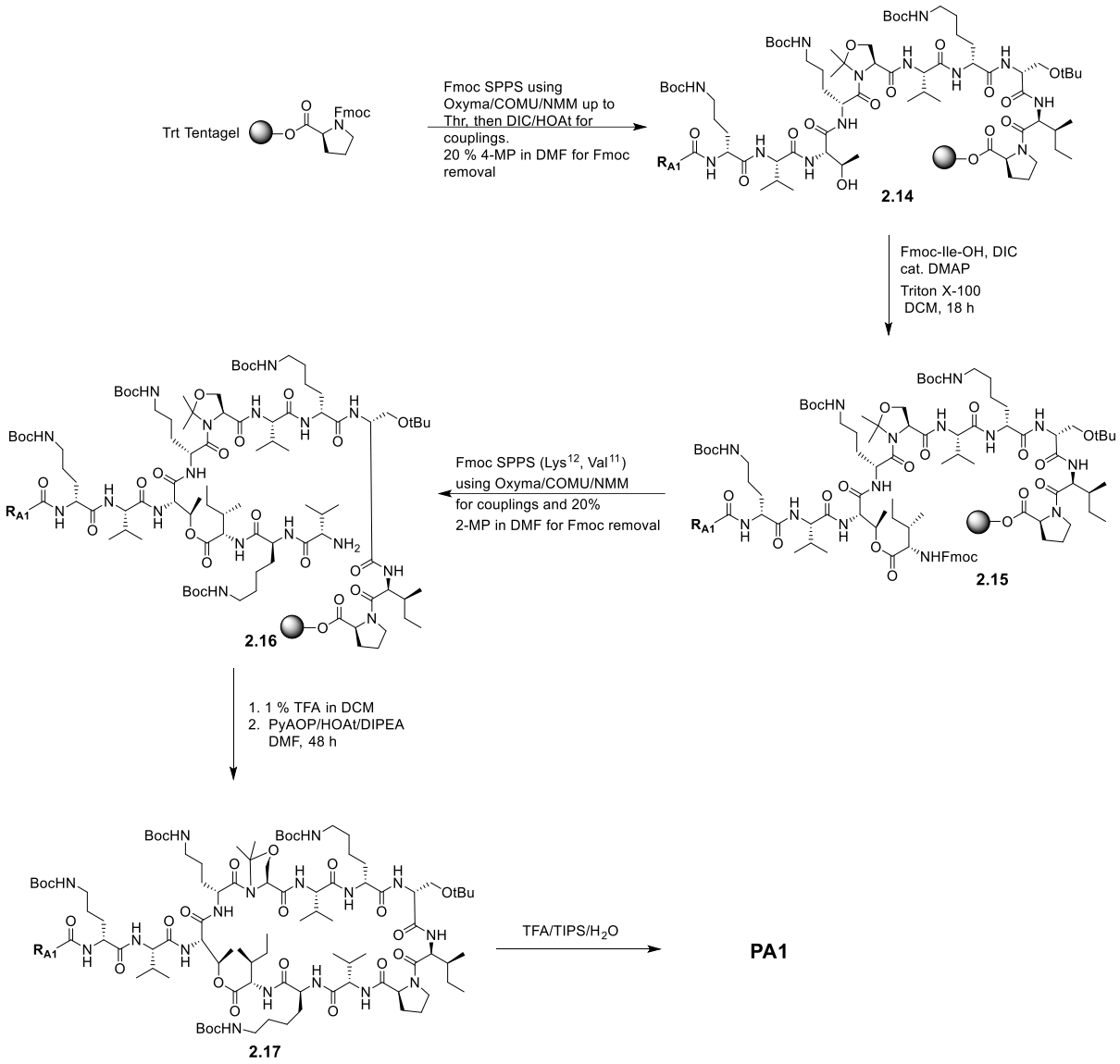

As stated in the introduction, paenibacterin is produced as a mixture of three isomers bearing either a 15-carbon linear (PA1, minor component), anteiso (PA2, major component), or iso (P-A3) lipid tail.[41] These three isomers can be partially resolved by HPLC, though baseline resolution is difficult to achieve (Figure 2.2). As expected, the retention time of synthesized PA2 matches that of the major component of authentic paenibacterin, and synthesized PA1, which elutes slightly later, has a retention

time matching that of the minor component of the authentic mixture (Figure 2.2). This is also clearly demonstrated by a coinjection of PA1, PA2 and authentic paenibacterin (Figure 2.2).

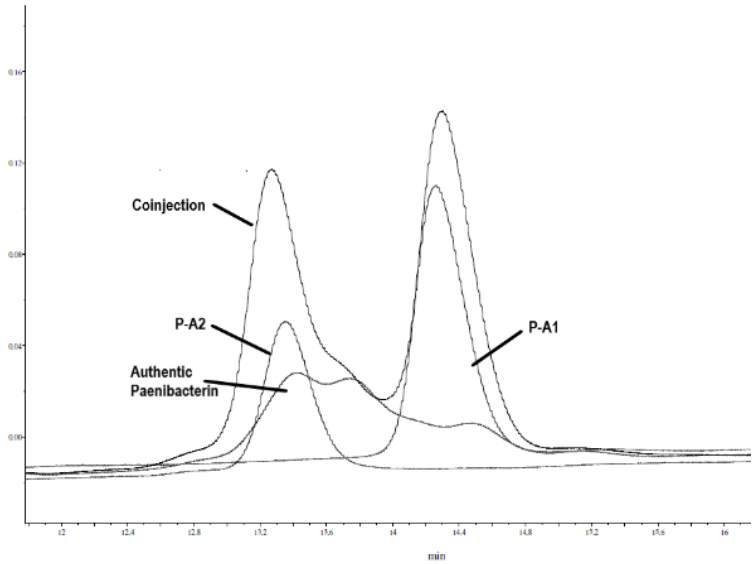

Figure 2.2 RP-HPLC chromatograms of synthetic PA1, PA2, and natural paenibacterin.

We determined the minimum inhibitory concentration (MIC) of each peptide against a strain of *Escherichia coli* (Gram-(−)) and of *Bacillus subtilis* (Gram-(+)) (Table 2.1). The MICs of the major epimers of PA1 and PA2 were the same despite the variation in the structure of the acyl tail, and were also identical to that of authentic paenibacterin. Moreover, the MIC of the minor epimer of PA1 was greater than that of the major epimer of PA1; therefore, it is reasonable to assume that the major epimers of PA1 and PA2 correspond to PA1 and PA2 in authentic paenibacterin, consistent with our NMR analyses. It is most likely that the minor epimers of PA1 and PA2 are a result of epimerization at Ile13, and so it appears that the stereochemistry at the α-carbon of Ile13 does not significantly impact activity. With *E. coli* K-12, the MICs of PA1 and PA2 fell well within the ranges reported by Huang *et al* with other Gram-(−) bacteria.[45] *B. subtilis* 1046 appears to be particularly susceptible to PA1 and PA2 when compared to the Gram-(+) bacteria previously investigated by Yousef and coworkers.[45] It is interesting

that replacing the ester bond with an amide bond had little or no effect on activity. While PA1-Dapa showed slightly reduced activity compared to PA1 and PA2, PA1-Daba matched that of PA1 and PA2. This is in contrast to daptomycin where it has been shown that replacing the ester bond with an amide bond severely impacts activity.[152]

Table 2.1 MICs[a] of PA1, PA2, PA1-Dapa and PA1-Daba and authentic paenibacterin.[b]

Antibiotic	*E. coli* K-12	*B. subtilis* 1046
Polymyxin-B	0.25	-
Daptomycin	-	0.75
Authentic paenibacterin	4	2
PA1 (major epimer)	4	2
PA1 (minor epimer)	8	4
PA2 (major epimer)	4	2
PA1-Dapa	8	8
PA1-Daba	4	2

[a]MICs are given in μg/mL. [b]Polymyxin-B and daptomycin are included for comparison.

2.4 Conclusions

In summary, we have developed the first total synthesis of paenibacterin A1 and A2, as well as the analogs, PA1-Dapa and PA1-Daba. The use of a pseudoproline dipeptide significantly improved the syntheses. We confirmed that the configurational assignments of residues 5, 7, 8 and 12, predicted by bioinformatics analysis, were correct. We demonstrated that paenibacterin retains its antibacterial activity when the ester bond is replaced with an amide (Thr3→Daba) although some activity is lost if the side chain methyl group is also removed (Thr3→Dapa). We also show that the activity of paenibacterin is the same whether the lipid tail is anteiso or linear. Overall, these studies suggest that paenibacterin may be amenable to further structural modification, with the aim of generating analogs with improved activity against either Gram-(+) or Gram-(−) bacteria, or both.

2.5 Further Studies

Following the successful synthesis of paenibacterin, we later modified our approach to minimize the epimerization during esterification. This was also accompanied by other minor improvements to our overall synthetic procedure. These improvements, and the rational behind them, are outlined in Chapter 3. This improved method was used to prepare a number of analogs of paenibacterin; described in Chapters 3 and 4.

2.6 Experimental

General. All reagents used for peptide synthesis were obtained from commercial sources including coupling reagents, resins, and the following amino acid building blocks: Fmoc-D-Orn(Boc)OH, Fmoc-Val-OH, Fmoc-Thr-OH, Fmoc-Lys(Boc)-OH, Fmoc-D-Lys(Boc)-OH, Fmoc-Ser(*t*-Bu)-OH, Fmoc-D-Ser(*t*-Bu)-OH, Fmoc-Ile-OH and Fmoc-Pro-OH. Fmoc-Dapa(N_3)-OH was prepared from Fmoc-Asn-OH following literature procedures.[155,156] Fmoc-Daba(N_3)-OH was prepared using the procedure of Moreira et al.[152] Alloc-Ile-OH was prepared according to a literature procedure.[157] Pentadecanoic acid was obtained for a commercial source. 12-Methyltetradecanoic acid was prepared from 10-undecenoic acid via a Friedel-Crafts alkylation as reported by Biermann and Metzger.[158] ACS grade, *N,N'*-dimethylformamide (DMF), 4-methylpiperidine (4-MP), 2-methylpiperidine (2-MP), TFA, triisopropylsilane (TIPS) were purchased from commercial suppliers and used without further purification. CH_2Cl_2 (DCM) was distilled from calcium hydride under nitrogen. THF was distilled from sodium metal and benzophenone under nitrogen. Peptide synthesis was performed manually using a rotary mixer for agitation.

Peptide syntheses were monitored by treating small aliquots of resin with 95:2.5:2.5 TFA/TIPS/H_2O for 1.5 h, concentrating under an N_2 stream, and precipitating the peptide with cold ether before re-dissolving in 1:1 CH_3CN/H_2O and analyzing by RP-HPLC and LRMS. To avoid loss of peptide to

adsorption onto glassware, polypropylene vessels were used for all steps following the deprotection of the crude peptide.

Analytical HPLC was accomplished with a reversed-phase C8 column (5µm, 250 mm × 4.6 mm, 1 ml/min flow rate). Peptides were purified by reversed phase semi-preparative HPLC using a C8 column (5µm, 150 mm × 20 mm, 8 mL/min flow rate). High resolution positive ion electrospray (ESI+) mass spectra were obtained using an orbitrap mass spectrometer, dissolving samples in 1:1 MeOH/H_2O + 0.1% formic acid. NMR spectra of purified peptides (~5 mg in 500µl CD_3OD) were obtained using a Bruker Avance 500 or 600 MHz NMR spectrometer in the case of PA1 and PA1-Dapa, and a 500 MHz NMR spectrometer for PA2 and PA1-Daba.

Resin loading was estimated using the procedure described by Gude et al.[159] After thoroughly drying, 10–20 mg of the loaded resin was treated with 2 mL of 2% DBU in DMF for 30 min, then diluted to 10 mL with CH_3CN. An aliquot of 1 mL was further diluted to 12.5 mL then absorbance was measured at 304nm. Approximate loading was then calculated using an extinction coefficient of 7624 $M^{-1}cm^{-1}$.

Fmoc-D-Orn(Boc)-Ser(Ψ^{Me,Me}Pro)OH. Synthesis of the pseudoproline dipeptide was adapted from literature procedures for the analogous FmocLys(Boc)-Ser(Ψ^{Me,Me}Pro)OH pseudoproline dipeptide.[131–133,160,161] Fmoc-D-Orn(Boc)OH (1.5 g, 3.3 mmol) was dissolved in dry THF (6.75 mL) and DMF (1.5 mL) then *N*-hydroxysuccinimide (760 mg, 6.6 mmol) was added, followed by EDC (1.27 g. 6.6 mmol) and stirred for 4 h at room temperature. The solution was then concentrated and re-dissolved in 1:1 ethyl acetate/hexanes (60 mL) and water (10 mL). Ethyl acetate was added until all solids dissolved, then the organic layer was washed with water (3 × 10 mL), dried over Na_2SO_4, and concentrated. The activated amino acid was dissolved in acetone (25 mL) to which L-serine, dissolved in 4.5 mL 10% Na_2CO_3(aq.), was added. The mixture was stirred for 18 h. The mixture was cooled to 0 °C and acidified to pH 3 with 5% HCl and concentrated to approximately half the volume. Ethyl acetate (50 mL) was

added then washed with water (3 × 25 mL) and brine, dried over Na_2SO_4, and concentrated. The crude dipeptide was dissolved in dry THF (50 mL) and 2,2-dimethoxypropane (2.03 mL, 16.5 mmol) and PPTS (166 mg, 0.66 mmol) were added. The solution was heated to reflux for 6 h, passing the condensate over 4Å molecular sieves. Upon cooling, triethylamine (100 µl) was added, then the solution was concentrated to a white foam. The crude product was purified by flash chromatography (R_f = 0.15 in 10% MeOH/90% DCM) using a gradient of 0–10% MeOH in DCM. The purified dipeptide was re-dissolved in a mixture of acetonitrile and water before lyophilizing to give a white powder (880 mg, 1.5 mmol, 46%) ^{1}H NMR (300 MHz, DMSO-*d₆*) δ 7.87 (d, *J* = 7.4 Hz, 2H), 7.70 (d, *J* = 6.8 Hz, 2H), 7.40 (t, *J* = 7.4 Hz, 2H), 7.30 (t, *J* = 7.4 Hz, 2H), 6.73 (t_{broad}, 1H), 4.91 (d, *J* = 5.6, 1H), 4.35–4.00 (m, 5H), 3.89 (q, *J* = 6.9 Hz, 1H), 2.85 (m, 1H), 1.65–1.17 (m, 20H); $^{13}C\{^1H\}$ NMR (75 MHz, DMSO-*d₆*) 172.9, 169.6, 156.8, 156.0, 144.3, 144.2, 141.2, 128.1, 127.5, 125.8, 120.6, 95.7, 77.9, 67.1, 66.2, 59.3, 53.8, 47.2, 40.3, 28.8, 26.6, 25.4, 23.5 HRMS-ESI-(+) calcd for $C_{31}H_{40}N_3O_8$ *m/z* = $[M+H]^+$, 582.2810; found,582.2824.

Synthesis of PA1-Dapa. 2'-Cl-TrtCl polystyrene resin (theoretical substitution = 1.5 mmol/g, 33.3 mg, 50 µmol, 1 equiv) was swollen in dry DCM then loaded with FmocProOH (4 equiv) and DIPEA (8 equiv) in 1 mL dry DCM for 5 h and capped with 17:2:1 DCM/DIPEA/MeOH (3 × 10 min). Loading efficiency was estimated to be 0.42 mmol/g. Fmoc protecting groups were removed with 4-MP (1.25 mL, 5 min, 20 min), and all Fmoc amino acids (5 equiv) were activated for one minute using HCTU (5 equiv) and NMM (5 equiv) in DMF (2.5 mL) then coupled for 1.5–2 h. After all couplings and deprotections, the resin was rinsed with DMF (6 × 1 min). Pentadecanoic acid was coupled using identical conditions and extending the coupling time to 10 h. The azido group was reduced using a solution of 2M DTT and 1M DIPEA in DMF (3 mL) under N_2 for 4 h or until complete reduction was confirmed by HPLC. The remaining amino acids were coupled using as described above, using COMU (5 equiv), oxyma (5 equiv), and NMM (10 equiv) in place of HCTU/NMM, and using an extended

coupling time of 16 h for Ile13. After the final Fmoc deprotection of Val11, the resin was rinsed (3 × 2 min) with MeOH, iPrOH, and DCM. The protected peptide was then cleaved from the resin with 1% TFA in DCM (2 mL, 3 × 2 min) draining into a flask containing 10% pyridine in MeOH (5 mL). The resin was rinsed (1–2 mL each, 2 × 2 min) with DCM, MeOH, iPrOH, then DCM again. The cleavage and rinsing process was repeated 3 times. The combined washings were concentrated by rotary evaporation, co-evaporating with toluene. The peptide was then re-dissolved in MeOH (1 mL) and precipitated with cold water (5 mL) and collected by centrifugation. Remaining water was removed azeotropically with toluene. To cyclize, the protected peptide was dissolved in DMF (50 mL, 0.1 M) that had been partially dried over 4Å MS. While stirring, DIPEA (8 equiv) was added followed by PyAOP (4 equiv) and HOAt (4 equiv) dissolved in DMF (3 mL). After stirring for 48 h, the DMF was removed by rotary evaporation, co-evaporating with heptane. The protected peptide was again precipitated from MeOH with water as described above. Protecting groups were removed by treating with 90:5:5 TFA/TIPS/H_2O (5 mL) for 2 h, then concentrating under N_2 stream and precipitating with cold MTBE. The crude peptide was re-dissolved in 4:1 H_2O/CH_3CN (5 mL) and purified by semi-preparative reversed phase HPLC (t_R = 42 min, linear gradient of 30:70 $CH_3CN:H_2O$ (0.2% TFA) to 50:50 $CH_3CN:H_2O$ (0.2% TFA) over 60 min). Fractions containing PA1-Dapa were pooled and lyophilized giving PA1-Dapa as a white powder (8.9 mg, 31% yield based on resin loading). PA1-Dapa was judged to be > 95% pure by analytical RP-HPLC (t_R = 28.8 min, linear gradient of 10:90 $CH_3CN:H_2O$ (0.2% TFA) to 90:10 $CH_3CN:H_2O$ (0.2% TFA) in 50 min. See Figure A.1 and Figure A.2). HRMS-ESI$^+$ (m/z) calcd for $C_{78}H_{146}N_{18}O_{16}$ $[M + H]^{2+}$, 795.5577; found, 795.5588. The peptide was also characterized by NMR (1D: ^{1}H and ^{13}C NMR, as well as 2D: ^{1}H-^{13}C HSQC, HMBC, COSY, TOCSY. See Figure A.24 to Figure A.28 and Table A.3).

PA1-Daba. PA1-Daba was prepared using a procedure identical to that used for PA1-Dapa except for the following. FmocDaba(N_3)OH was used in place of FmocDapa(N_3)OH. TrtCl Tentagel® (theoretical

substitution = 0.19 mmol/g, 263 mg, 50 μmol, 1 equiv) was used. Before use, this resin was activated with $SOCl_2$ (2.5 equiv) and pyridine (5 equiv) in dry DCM (2.5 mL) and heated to reflux for 2 h before rinsing with dry DCM (6 × 2 min) and drying under vacuum over 3Å MS for 14 h. The resin was then loaded with FmocProOH using the same procedure described for PA1-Dapa. Loading efficiency was estimated to be 58%. COMU (5 equiv), oxyma (5 equiv), and NMM (10 equiv) were used in place of the HCTU/NMM as coupling agents. Reduction of the azido group with DTT/DIPEA was extended to 16 h. Purification by reversed phase semi-preparative HPLC (t_R = 44 min, linear gradient of 30:70 CH_3CN:H_2O (0.2% TFA) to 50:50 CH_3CN:H_2O (0.2% TFA) in 60 min). Fractions containing PA1-Daba were pooled and lyophilized giving PA1-Daba as a white powder (27.0 mg, 58% yield based on resin loading). PA1-Daba was judged to be > 95% pure by analytical HPLC (t_R = 29.1 min, linear gradient of 10:90 CH_3CN:H_2O (0.2% TFA) to 90:10 CH_3CN:H_2O (0.2% TFA) in 50 min. See Figure A.9 and Figure A.10 in Appendix A. HRMS-ESI$^+$ (m/z) calcd for $C_{79}H_{148}N_{18}O_{16}$ $[M+H]^{2+}$, 802.5655; found, 802.5688. The peptide was also characterized by NMR (1D: ^{1}H and ^{13}C NMR, as well as 2D: ^{1}H-^{13}C HSQC, HMBC, COSY, TOCSY. See Figure A.29 to Figure A.34 and Table A.3).

Synthesis of PA1.

(a) Via the pseudoproline dipeptide approach (Scheme 2.6**).** TrtCl Tentagel® (theoretical substitution = 0.19 mmol/g, 526 mg, 100 μmol, 1 equiv) was activated with FmocProOH as described above for PA1-Daba. The resin was then loaded using the same procedure described above. Loading efficiency was estimated to be 84%. Amino acids up to and including the pseudoproline dipeptide were coupled using 5 equiv of the amino acid, COMU (5 equiv), oxyma (5 equiv), and NMM (10 equiv) in DMF (6 mL) for 1.5–2 h. Thr3, Val2, D-Orn1, and pentadecanoic acid residues were coupled using the 5 equiv of the free acid and DIC (5 equiv), HOAt (5 equiv) in DMF (3 mL) for 4 h. Up to this point, Fmoc deprotection were accomplished using 4-MP and rinsing steps were performed as described above for PA1-Dapa. To form the depsi bond, FmocIleOH (10 equiv) was dissolved in dry DCM (6

mL) then cooled to 0 °C before adding DIC (10 equiv) and stirring for 15 min. The mixture was warmed to rt then added to the resin along with DMAP (0.1 equiv) and Triton X-100 (60 µl) followed by agitating for 18 h. After installation of FmocIleOH, remaining couplings (FmocLys(Boc)OH and FmocValOH) were accomplished using the initial COMU/oxyma/NMM conditions. The Fmoc group was removed using 20% 2-MP in DMF + 1% formic acid (1 × 5 min, 1 × 7 min). After each coupling and Fmoc deprotection, the resin was rinsed as described above for PA1-Dapa. Following the coupling and Fmoc deprotection of Val11 the peptide was cleaved from the resin and cyclized as described above for PA1-Dapa. PA1 was purified by semi-preparative reversed phase HPLC (t_R = 39 min, linear gradient of 30:70 CH_3CN:H_2O (0.2% TFA) to 50:50 CH_3CN:H_2O (0.2% TFA) in 60 min). Fractions containing PA1 were pooled and lyophilized giving PA1 as a white powder (27.0 mg, 15% yield based on resin loading). PA1 was judged to be > 95% pure by analytical HPLC (t_R = 28.4 min, linear gradient of 10:90 CH_3CN:H_2O (0.2% TFA) to 90:10 CH_3CN:H_2O (0.2% TFA) in 50 min, see Figure A.3 and Figure A.4). HRMS-ESI$^+$ (m/z) calcd for $C_{79}H_{147}N_{17}O_{17}$ $[M+H]^{2+}$, 803.0575; found, 803.0587. The peptide was also characterized by NMR (1D: ^{1}H and ^{13}C NMR, as well as 2D: ^{1}H-^{13}C HSQC, COSY, TOCSY. See Figure A.15 to Figure A.19). NMR data was consistent to that reported by Guo et al for paenibacterin (a PA1/PA2/P-A3 mixture. See **Table A**.1, and Table A.2).[41]

(b) Via the route outlined in Scheme 2.3. 2-ClTrtCl resin (theoretical substitution = 1.5 mmol/g, 42 mg, 62.5 µmol, 1 equiv) was loaded with FmocProOH as described above for PA1-Daba. Loading efficiency was estimated to be 0.75 mmol/g. Amino acids up D-Orn4 were coupled using 5 equiv of the amino acid, HCTU (5 equiv), and NMM (5 equiv) in DMF (6 mL) for 1.5–2 h. Thr3 and Val2 residues were coupled using the 5 equiv of the free acid and DIC (5 equiv), HOAt (5 equiv) in DMF (3 mL) for 4 h. Up to this point, Fmoc deprotection were accomplished using 4-MP and rinsing steps were performed as described above for PA1-Dapa. To form the depsi bond, allocIleOH (10 equiv) was dissolved in dry DCM (6 mL) then cooled to 0 °C before adding DIC (10 equiv) and stirring for 15

min. The mixture was warmed to rt then added to the resin along with DMAP (0.1 equiv) and Triton X-100 (60 μL) followed by agitating this was repeated (3 × 16 h). After installation of allocIleOH, D-Orn1 and pentadecanoic acid were coupled with DIC/HOAt for 4 h and 16 h, respectively. The Fmoc group was removed using 20% 2-MP in DMF (3 × 10 min). After each coupling and Fmoc deprotection, the resin was rinsed as described above for PA1-Dapa. The resin was rinsed with DMF (3 × 2 min) and DCM (3 × 2 min), then the reaction vessel was flushed with dry Ar or N_2. To the vessel was added 1,3-dimethylbarbituric acid (DMBA, 10 equiv) and cat. $Pd(PPh_3)_4$ (0.2 equiv) as a solution in 1:3 DMF/DCM. The resin was agitated by bubbling inert gas for 1–2 h then the resin was filtered and rinsed with DCM (3 × 2 min) followed by a 1.0% solution of sodium diethyldithiocarbamate trihydrate in DMF (3 × 3 min), then DMF (3 × 2 min) and DCM (3 × 2 min). Lys12 and Val11 were then coupled, again using DIC/HOAt (4 h couplings). Val11 was deprotected then the peptide was cleaved from the resin with 20% HFIP in DCM. The peptide was concentrated then dissolved in DCM (125 mL), then BOP (4 equiv), HOAt (4 equiv), and DIPEA (4 equiv) were added before stirring for 3 days. After cyclization the solvent was removed by rotary evaporation and PA1 was purified by semi-preparative reversed phase HPLC as described above. Fractions containing PA1 were pooled and lyophilized giving PA1 as a white powder (2.8 mg, 5.6% yield based on resin loading). PA1 was judged to be > 95% pure by analytical HPLC (t_R = 30.5 min, linear gradient of 90:10 CH_3CN:H_2O + 0.1% TFA to 70:30 CH_3CN:H_2O + 0.1% TFA in 40 min. See Figure A.11 and Figure A.12. HRMS-ESI$^+$ (m/z) calcd for $C_{79}H_{146}N_{17}O_{17}$ $[M+H]^+$, 1605.1077; found, 1605.1080.

Paenibacterin A2. PA2 was prepared using a procedure identical to that used for PA1 (pseudoproline dipeptide approach) except 12-methyltetradecanoic acid was used instead of pentadecanoic acid. PA2 was purified by reversed phase semi-preparative HPLC (t_R = 38 min, linear gradient of 30:70 CH_3CN:H_2O (0.2% TFA) to 50:50 CH_3CN:H_2O (0.2% TFA) in 60 min). Fractions containing PA2 were pooled and lyophilized giving PA2 as a white powder (12.4 mg, 21% based on resin loading.)

PA2 was judged to be > 95% pure by analytical HPLC. HPLC (t_R = 28.1 min, linear gradient of 10:90 CH_3CN:H_2O (0.2% TFA) to 90:10 CH_3CN:H_2O (0.2% TFA) in 50 min, see Figure A.7 and Figure A.8). HRMS-ESI$^+$ (m/z) calcd for $C_{79}H_{147}N_{17}O_{17}$ $[M+H]^{2+}$, 803.0575; found, 803.0606. The peptide was also characterized by NMR (1D: ^{1}H and ^{13}C NMR, as well as 2D: ^{1}H-^{13}C HSQC, COSY, see Figure A.20 to Figure A.23). NMR data was consistent with that reported by Guo et al for paenibacterin (PA1/PA2/P-A3 mixture).[41]

Antibacterial assays. The antibacterial activity of the synthetic peptides and authentic paentibacterin was determined by a broth microdilution assay.[162] Overnight bacterial cultures were grown in LB broth then diluted to approximately 1×10^6 CFU/mL according to the measured optical density at 600 nm (OD_{600}). Two-fold serial dilutions were used to prepare a series of peptide solutions in LB broth which were then inoculated with an equal volume of diluted bacterial culture in 96-well microplates. Plates were incubated for 24 h at 37 °C then the MIC was determined by the lowest concentration at which there was no visible growth of bacteria.

Chapter 3

A Structure-Activity Relationship Study of Paenibacterin: Effect of Lipid Tail Length and Cationic Residues on Activity

3.1 Preface

The majority of the results presented in this chapter were acquired after or alongside the results presented in Chapter 4; however, this work most closely relates to the contents of Chapter 2, and so has been included out of chronological order. Also included early in this chapter are some findings that led to a series of improvements to our synthesis of paenibacterin described in Chapter 2. These improvements were employed in Chapter 4 as well.

3.2 Introduction

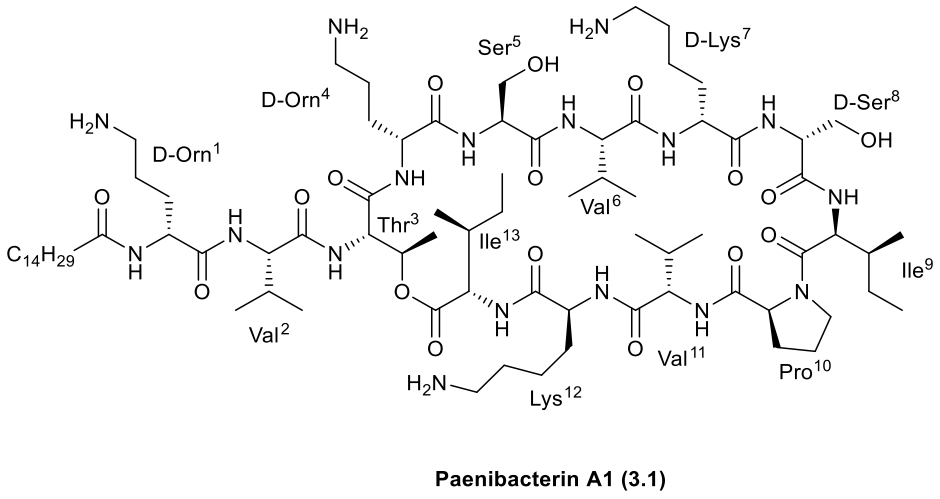

Figure 3.1 Structure of paenibacterin A1 (3.1).

Following our successful synthesis of paenibacterin A1 (PA1, **3.1**) we sought to further our understanding of its structure-activity relationships (SARs). Previous studies on small lipopeptides have identified hydrophobicity and net positive charge as key parameters affecting not only

antibacterial activity, but also potential toxicity, measured as hemolytic activity.[163,164] Highly hydrophobic and/or cationic peptides tend to be more toxic than their less hydrophobic or cationic counterparts. This tendency for toxicity is a well-known obstacle to the development of lipopeptide drugs.[39] To develop analogs of paenibacterin that are clinically useful antibiotics, it is crucial that we understand how to tune its activity to give the highest possible specificity for bacterial membranes over those of human cells.

The most straightforward approach to modifying the overall hydrophobicity of paenibacterin is to alter the length of the acyl tail. Many analogs of polymyxin with acyl tails of different length and structure have been prepared.[165] As mentioned in Chapter 1, polymyxin B loses all antibacterial activity if the acyl tail and an adjacent (2,4)-diaminobutyric acid (Dab) residue are removed. This analog (polymyxin B nonapeptide) does however retain the ability to permeabilize the membranes of Gram-(−) bacteria towards other antibiotics.[77] Incorporation of an acetyl group at the *C*-terminus also results in a considerable decrease in potency.[166] Polymyxin B analogs acylated with 2-chlorophenyl urea retain good activity but interestingly the same is not true for a similarly acylated nonapeptide analog.[167] For polymyxin, ideal activity is found with acyl tails ranging from 7–9 carbon atoms in length, which coincides with the variants found in nature.[5]

In order to obtain paenibacterin analogs with a reduced charge, it is necessary to first identify which cationic residues are required for activity. One way of doing this is via an alanine scan in which each cationic residue is replaced with Ala. This has previously been done with polymyxin, and this study identified the Dab residue at position 5 as the most important to antibacterial activity as well as LPS binding.[67] In general substitution of the exocyclic Dab residues had the least impact on activity compared to substitutions within the ring.

3.3 Objectives

The objectives of the work described in this chapter were: (1) to develop an improved approach to the synthesis of paenibacterin; (2) apply this improved approach to the synthesis of several paenibacterin analogs in which the length of the lipid tail is varied and the cationic residues are substituted with alanine; (3) to determine the effect of these modifications on activity, as tested against *B. subtilis* 1046 and *E.coli* K-12; and (4) synthesize an analog of one of the paenibacterin B-series and determine its activity against *B. subtilis* 1046 and *E.coli* K-12.

3.4 Results and Discussion

3.4.1 Esterification Onto a Truncated Linear Peptide

Prior to preparing a library of paenibacterin analogs, we first wished to improve our synthesis of PA1. As shown in Chapter 2, we demonstrated that we could successfully form the ester bond between Fmoc-Ile and Thr3 if a pseudoproline moiety was incorporated at residue 5 (see Scheme 2.6 in Chapter 2). In this case, Ile was coupled to decapeptide **2.14**, which included the pentadecanoyl tail. This resulted in partial epimerization, likely the result of the slow esterification reaction. We reasoned that the esterification would proceed more rapidly on the shorter, nonacylated nonapeptide **3.2** (Scheme 3.1), leaving the *N*-terminal amino group Fmoc protected. Without the acyl tail and penultimate lysine residue, this peptide should be less prone to aggregation. Indeed, we found that this allowed for complete esterification after one overnight coupling using DIC/DMAP, with little to no epimerization. To allow for selective removal of the Val2 Fmoc group, the α-amino group of Ile13 was orthogonally protected. We found that protection of N^{α}-Ile as an allyl carbamate (**3.3**) or as an azido acid (**3.4**) were both equally viable. The alloc group could be removed by a palladium-catalyzed Tsuji-Trost reaction, and reduction of the azide was accomplished by a Staudinger reduction using PBu_3 in THF/H_2O and in the presence of the symmetric anhydride of Fmoc-Lys(Boc)-OH.[147,168] This method for azide reduction was developed by the Taylor group, and inclusion of the anhydride prevents ester bond cleavage while

giving in partial acylation of the amino group. The requirement for 10 equivalents of the subsequent amino acid building block presents a significant disadvantage. Overall, allyl protection was deemed more efficient and convenient.

Scheme 3.1 Esterification on truncated peptide 2.

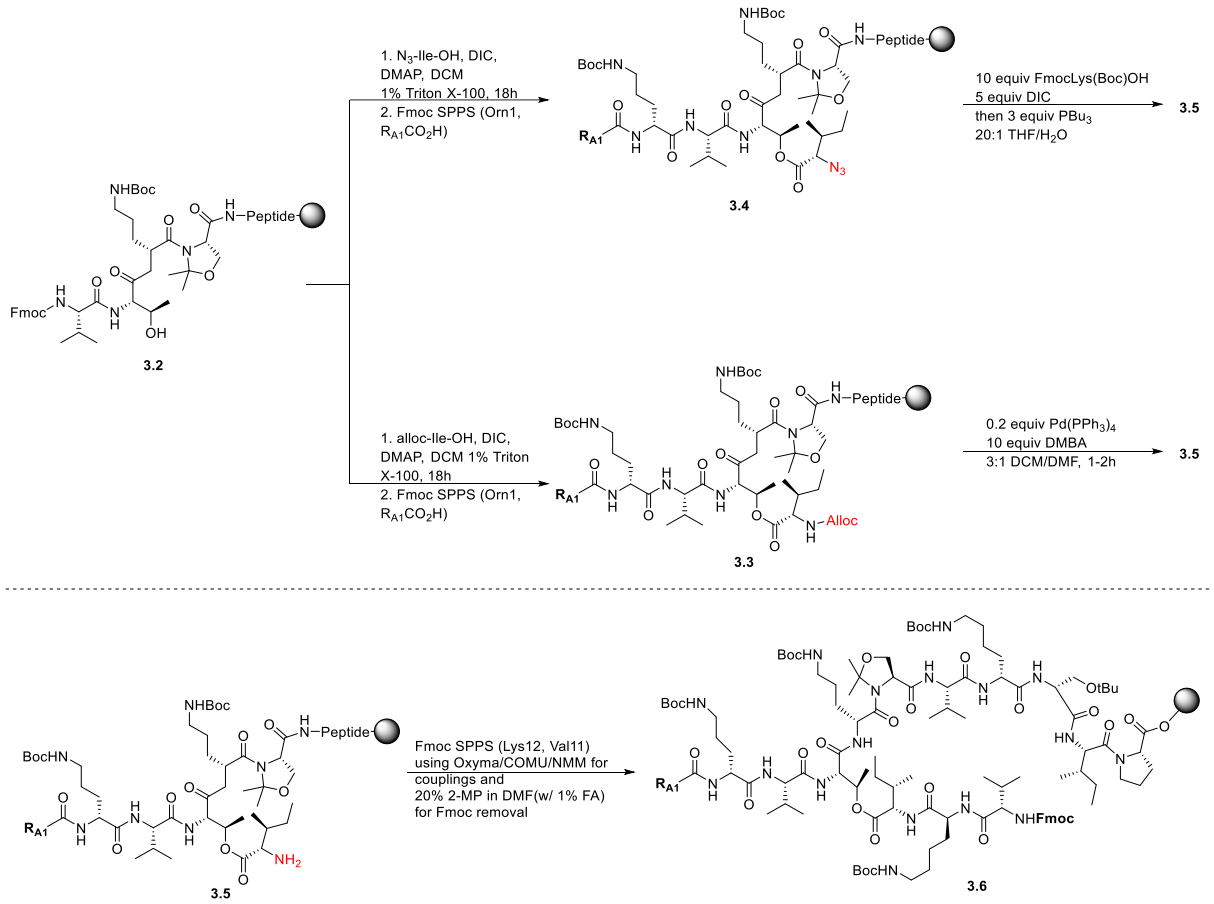

Following deprotection of the amino group, Lys12 and Val11 were coupled onto peptide **3.5** to give the intermediate peptide **3.6** in higher purity, i.e. with less epimerization, than if the same peptide was obtained using the route described in Scheme 2.6.

Furthermore, HPLC analysis of samples obtained after cleavage/deprotection with TFA/TIPS/H_2O showed that this intermediate was of very similar purity when obtained from the azido or the alloc protected peptide (Figure 3.2).

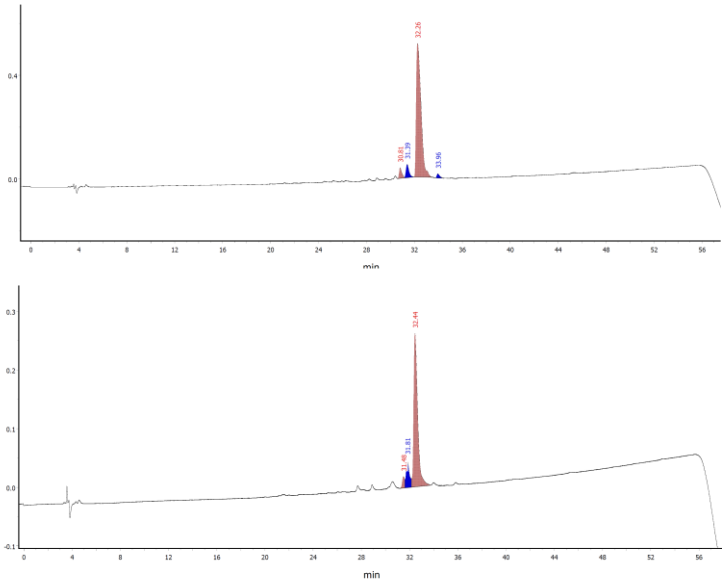

Figure 3.2 Analytical RP-HPLC of peptide 3.6, cleaved and deprotected. (top) *via* peptide **3.3**; (bottom) *via* peptide **3.4**.

This new and improved method for the synthesis of paenibacterin complements the method described in Chapter 2. The obvious advantage is that reduced epimerization both simplifies purification and improves yield. However, the requirement for non-Fmoc protected amino acids limits the possibility of adapting this method for use with an automated peptide synthesizer.

3.4.2 Attempted Development of an Fmoc-Ser($\Psi^{Me,Me}$Pro)-OH Building Block

The requirement for a D-Lys- or D-Orn-containing pseudoproline dipeptide (i.e. Fmoc-D-Orn(Boc)-Ser($\Psi^{Me,Me}$Pro)OH) presents a shortcoming of our synthesis as these building blocks are not commercially available, their synthesis is generally low yielding, and the Fmoc-D-Orn(Boc)/Fmoc-D-Lys(Boc) precursors are costly.

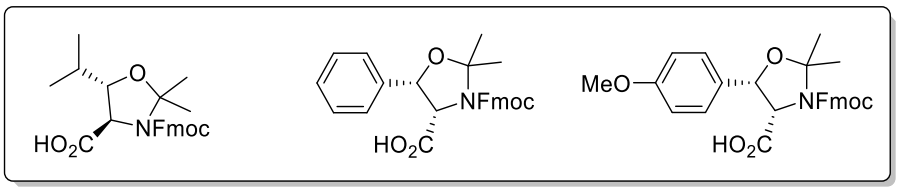

Figure 3.3 Pseudoproline building blocks used for the synthesis of skyllamycins A–C.[169]

Inspired by Giltrap et al.'s use of the pseudoproline building blocks shown in Figure 3.3 during their successful synthesis of the skyllamycins,[169,170] we hoped that we could use Fmoc-Ser($\Psi^{Me,Me}$Pro)-OH (**3.7**, Scheme 3.2) as a more accessible building block for the synthesis of paenibacterin. This building block was easily prepared from Fmoc-Ser-OH and 2,2-dimethoxypropane in a 71% yield (Scheme 3.2).

Scheme 3.2 Preparation of Fmoc-Ser($\Psi^{Me,Me}$Pro)-OH.

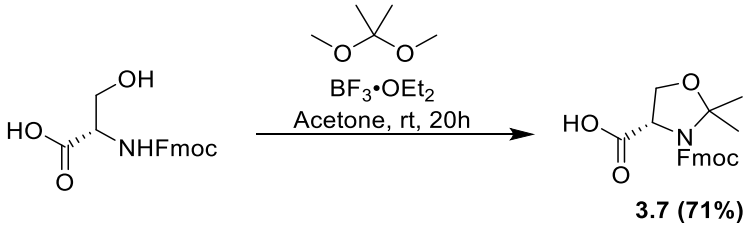

Initial results using **3.7** were promising, as we found that it could be incorporated into a linear precursor of paenibacterin by SPPS (**3.8** in Scheme 3.3). Following Fmoc deprotection of **3.8** and coupling of Fmoc-Lys(Boc) with HCTU/NMM, we cleaved/deprotected a portion of the resulting peptide, which was assumed to be intermediate **3.9**, with TFA/TIPS/H_2O. Analytical HPLC analysis of the cleaved material revealed a single peak which corresponded to peptide **3.10** as determined by MS (Scheme 3.3).

Scheme 3.3 Incorporation of 3.7 into a linear peptide.

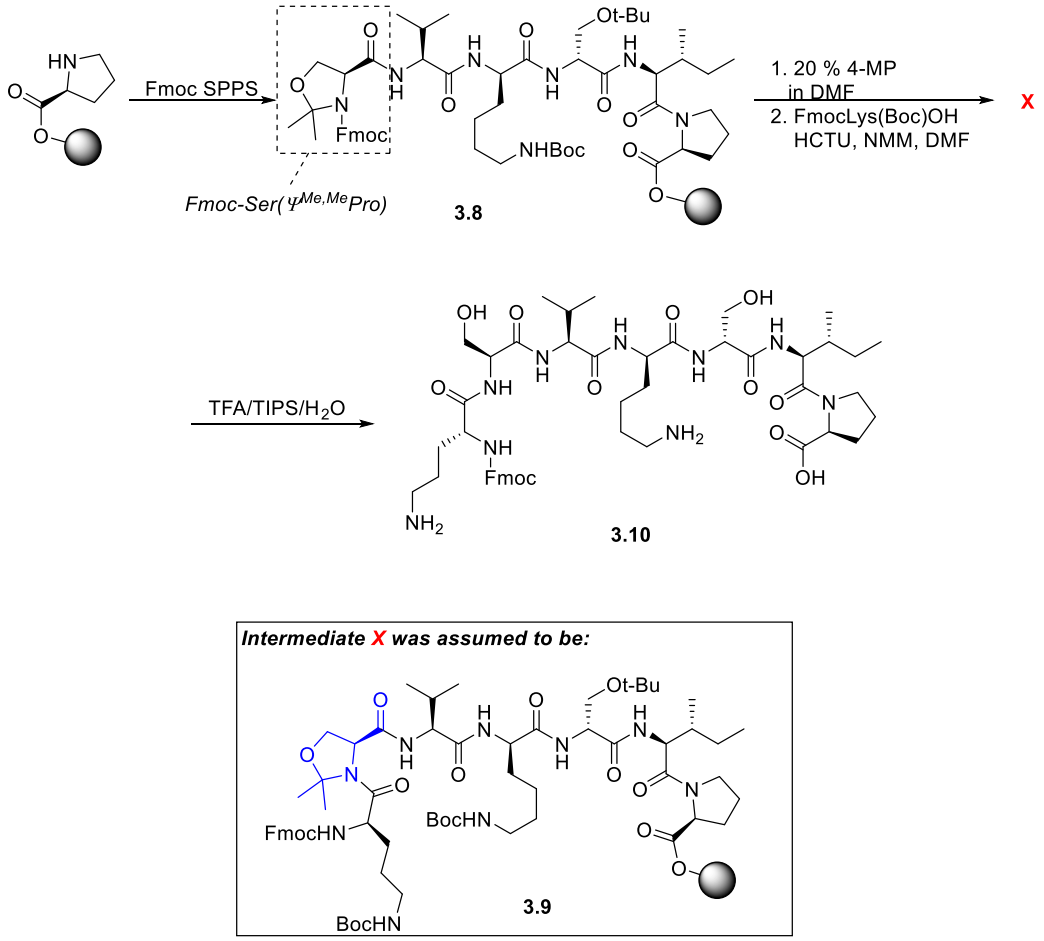

The synthesis was continued as described in Scheme 3.1, including coupling of Thr3 and Val2 to give **3.11**, followed by esterification with Alloc-Ile-OH (Scheme 3.4). After coupling of Val11, the quality of the peptide (**3.12**) was examined by HPLC and MS after cleavage/deprotection. Unfortunately, a complex mixture of products was observed. Some of these products had *m/z* values that indicated they were the result of undesired amino acid couplings onto the Ser6 side chain (for example peptide **3.13**.

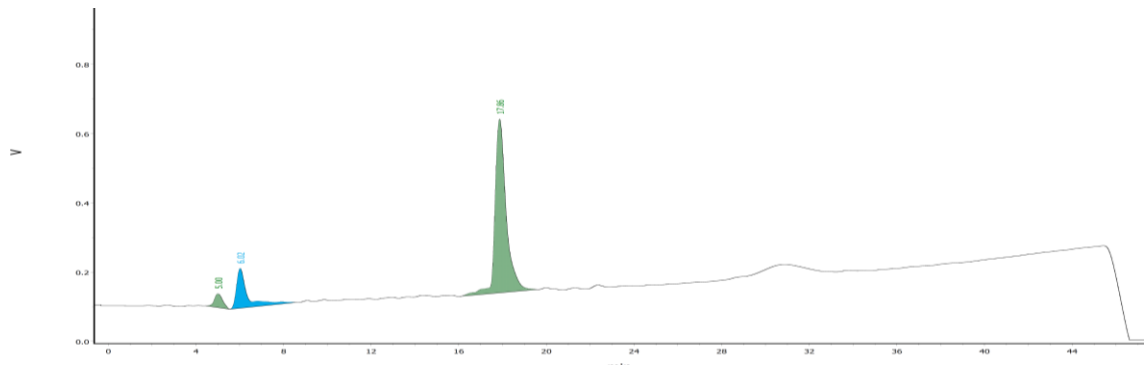

Figure 3.4 Analytical RP-HPLC of peptide 3.10. A mass of 966.58, corresponding to $[M + H]^+$ was detected by +ESI-MS.

This suggested that the pseudoproline was decomposing to the corresponding serine residue at some point following the Fmoc deprotection of **3.8** with 4-MP. It is likely that decomposition occurs during the following coupling, and so intermediate ***X*** in Scheme 3.3 must be peptide **3.14** (Scheme 3.4). The high purity of **3.10** can likely be attributed to the lower reactivity of the free serine alcohol compared to the terminal amino group. However, during esterification of the Thr residue, a competing esterification reaction with the unprotected Ser side chain took place. With the serine alcohol unprotected, selective esterification of the Thr3 side chain is impossible, and so the Fmoc-Ser($\Psi^{Me,Me}$Pro)-OH building block is unusable for the synthesis of paenibacterin analogs.

Scheme 3.4 Continued synthesis from peptide 3.9.

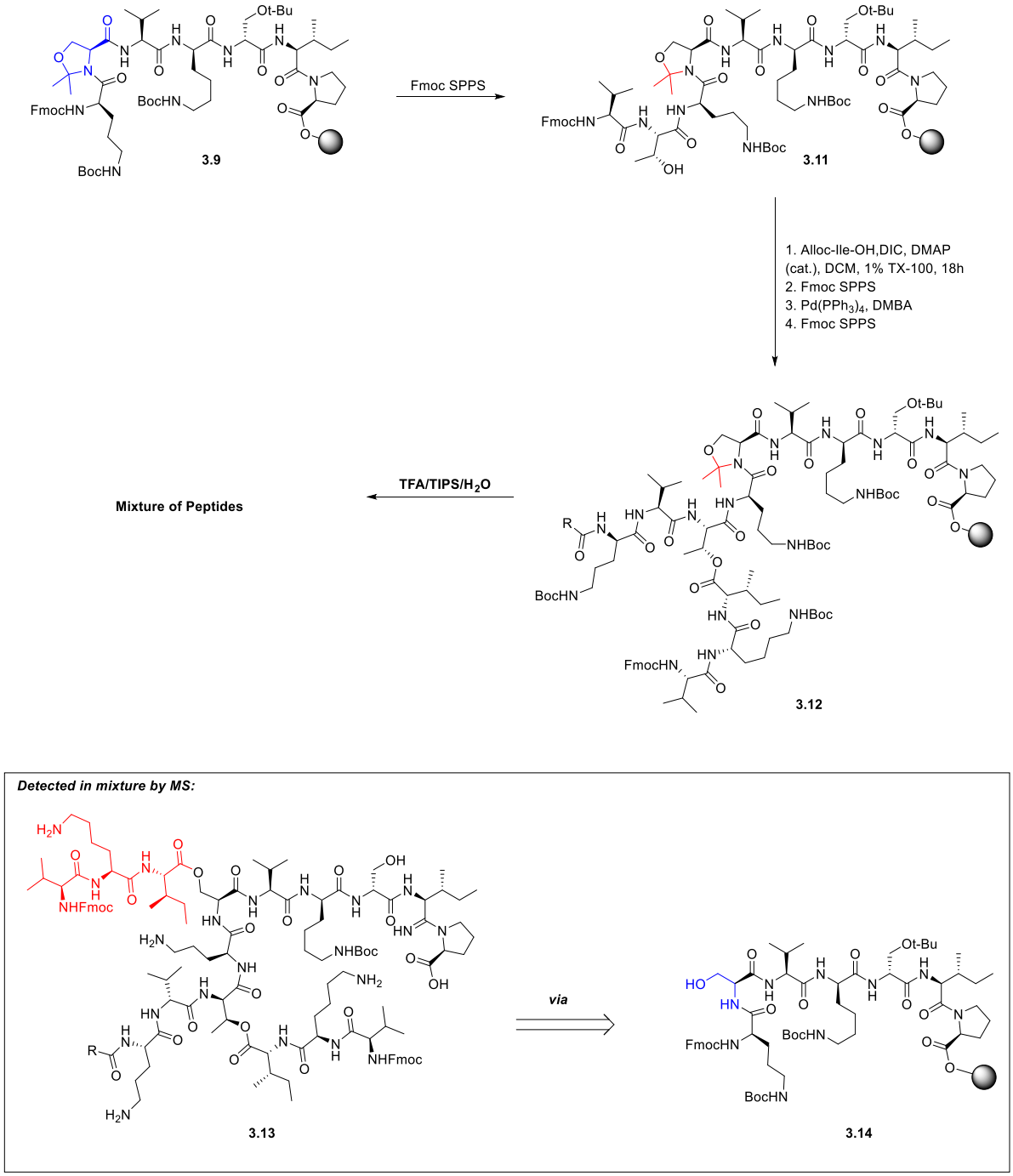

The method described in Chapter 2 allowed for the preparation of paenibacterin in relatively good yield. However, later attempts to prepare analogs of paenibacterin gave very low yields (<1%). The cause was later found to be long-term storage of Fmoc-Pro loaded Tentagel-Trt resin, but before this cause was identified, we closely examined many aspects of our synthesis, looking for ways to improve yields. One step that garnered attention was the palladium-catalyzed alloc deprotection using DMBA as a scavenger. DMBA (pK_a = 4.7) is similar in acidity to acetic acid (pK_a = 4.8), which is commonly used to cleave trityl ester linkers.[171] A more common scavenger for allyl deprotections on trityl resin is phenylsilane.[82,140,172] A third common scavenger for palladium-catalyzed allyl deprotections is dimedone (pK_a = 5.2), which is slightly less acidic than DMBA.[168]

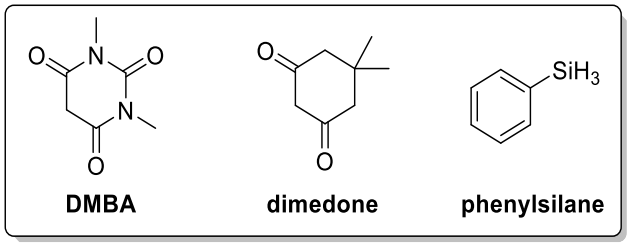

Figure 3.5 Common scavengers for allyl deprotections.

We compared two allyl deprotection methods, using either dimedone or phenylsilane as a scavenger. As a further precaution for the dimedone-method we also rinsed the resin with a dilute DIPEA solution in DCM immediately following filtration of the palladium/dimedone mixture. When approximately equal volumes of resin were cleaved for analysis, we observed no substantial difference in the amount of peptide observed by RP-HPLC. This suggests that either method is suitable. Dimedone was chosen as the preferred scavenger since it is an inert crystalline solid, so preparation of the deprotection solution is more convenient.

Another minor modification to our previously published method for the synthesis of paenibacterin was the use of hexafluoroisopropanol (HFIP) instead of dilute TFA in DCM for cleavage of the

protected peptide from the resin. If TFA is used, it must be neutralized with pyridine and a precipitation step is required to remove the resulting pyridinium trifluoroacetate salt. HFIP on the other hand can be directly removed *in vacuo*, and so is considerably more convenient.

3.4.3 An Analog of PA1 Containing Lysine in Place of Ornithine

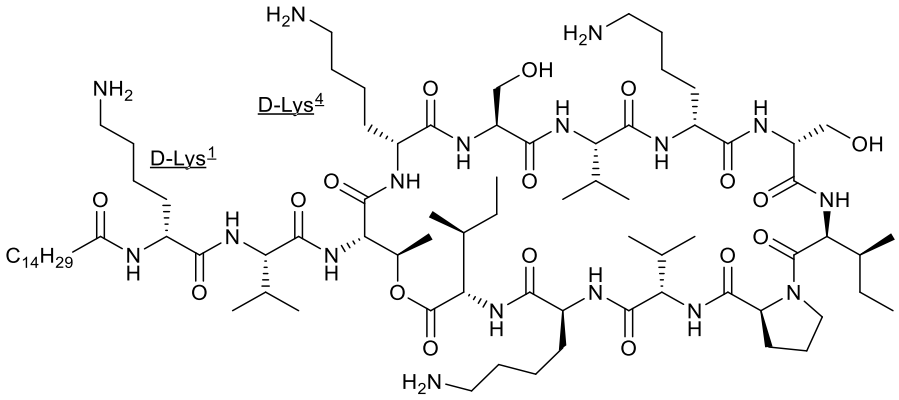

Figure 3.6 Structure of PA1-D-Lys1-D-Lys4 (PAK).

Since D-Lys costs less than D-Orn, we wished to determine if the D-Orn residues in paenibacterin could be replaced with D-Lys. We applied our improved method for the synthesis of PA1 to the synthesis of this analog, abbreviated **PAK** (**3.15**, Figure 3.6). This analog was obtained in a 40% yield, and details of its preparation are described in Chapter 4. The activity of PAK against both Gram-(−) and Gram-(+) bacteria was determined by measuring the minimum inhibitory concentrations (MICs) against *Escherichia coli* K-12 or *Bacillus subtilis* 1046, respectively. The MIC of both PA1 and polymyxin B sulfate (PmxB) against these strains were also determined. Table 3.1 contains the more recently determined MIC values for both PA1 and PAK, as well as PmxB and tetracycline. PAK and PA1 exhibited similar activity against Gram-(+) *B. subtilis* 1046 while PAK displayed improved activity against Gram-(−) *E. coli* K-12. The MICs of PA1 and PmxB had been previously determined in Chapter 2.[1] However, when the MICs of PA1 and PmxB were re-evaluated alongside PAK, we found that the

activity of both peptides was higher (i.e. the MIC was lower) than what had been previously observed. We are unsure of the cause of this discrepancy. A possibility is that the discrepancy arose from some change in the procedure or materials used. It is well known that the MIC of cationic peptides can be affected significantly by binding to plastic and glass.[173–175] Even if the material used is the same (e.g. polystyrene), microplates from different suppliers can result in drastically different MICs.[175] Regardless of the cause, the MIC values presented within this chapter, though lower than expected, were consistent between trials and using different frozen bacterial stocks.

Table 3.1 MICs of PA1, PAK, and controls.

Antibiotic	MIC (µg/ml)	
	***E. coli* K-12**	***B. subtilis* 1046**
Polymyxin B Sulfate[a]	0.03	—
Tetracycline HCl	—	4
PA1[a,b]	2	1
PAK[b] (**3.15**)	1	1

[a] MICs values are considerably lower than previously reported values. MICs are consistent even if different frozen bacterial stocks are used. [b] Stock peptide concentration has been corrected to account for 1 equivalent of TFA for each lysine residue.

Scheme 3.5 General synthesis of PAK analogs.

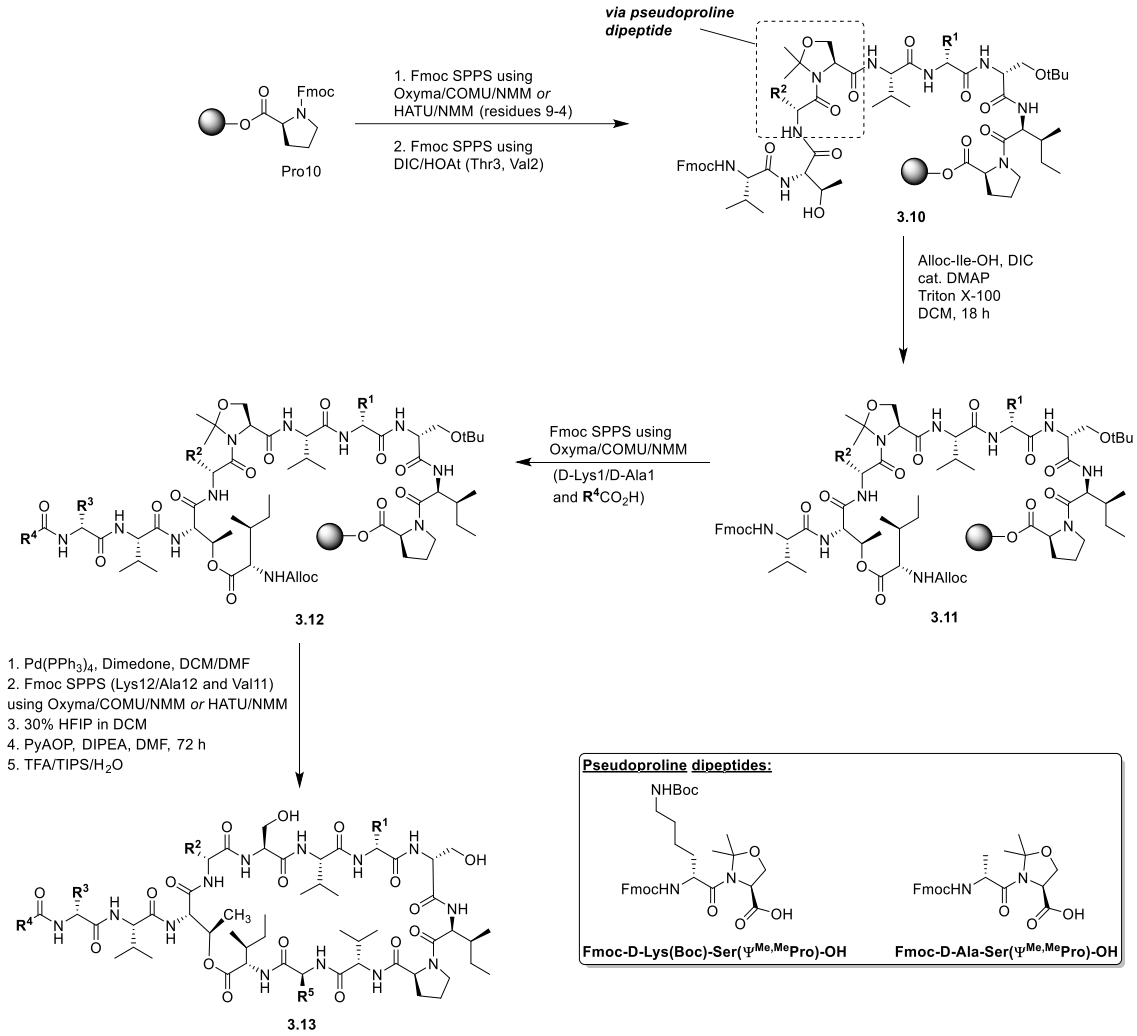

3.4.4 Synthesis of PAK Analogs

Because of the improved activity and lower cost, PAK was used as the scaffold for all further analogs of paenibacterin. Scheme 3.5 outlines the general approach for the synthesis of analogs of PAK and the positions of variation. In this approach, epimerization was minimized by forming the ester bond between the side chain of Thr3 in truncated peptide **3.16** and Alloc-Ile13. The resulting peptide **3.17** was then elongated to the acyl tail (**3.18**). Allyl deprotection then allows for the coupling of residues 12 and 13 before the peptide is cleaved from the resin and cyclized in solution. Global deprotection with concentrated TFA gives peptides **3.19**.

3.4.5 Modification of the Acyl Tail.

PAK analogs having lipid tails of varying lengths were prepared and their MIC values were determined against *B. subtilis* 1046 and *E. coli* K-12 (Table 3.1). The MIC values against *E.coli* K-12 did not change upon decreasing the length of the lipid from 15 to 10 carbons. The MIC values against *B. subtilis* 1046 increased 2-fold upon decreasing the length of the lipid from 15 to 13 or 12 carbons and increased 4 and 8-fold when the length was reduced to 11 to 10 carbons, respectively. Analogs containing a 5-carbon or 2-carbon tail were inactive against both *E. coli* K-12 and *B. subtilis* 1046 at 128 μg/mL. Surprisingly, we found that a 1-pyrenebutyric acid (Pba) tail could be accommodated with only a 2-fold loss of activity against *E. coli* K-12 and no loss of activity against *B. subtilis* 1046. Incorporation of the pyrene fluorophore is attractive because of its ability to form excimers when two molecules are in close proximity. Excimer fluorescence has been used to study the aggregation of the lipopeptide antibiotic daptomycin and we anticipate that **3.26** will prove useful in future studies on the aggregation of paenibacterin.[114] FRET studies on a similarly labelled polymyxin analog have provided evidence for self-association in model membranes.

Table 3.2 MIC of PAK with different acyl tails.

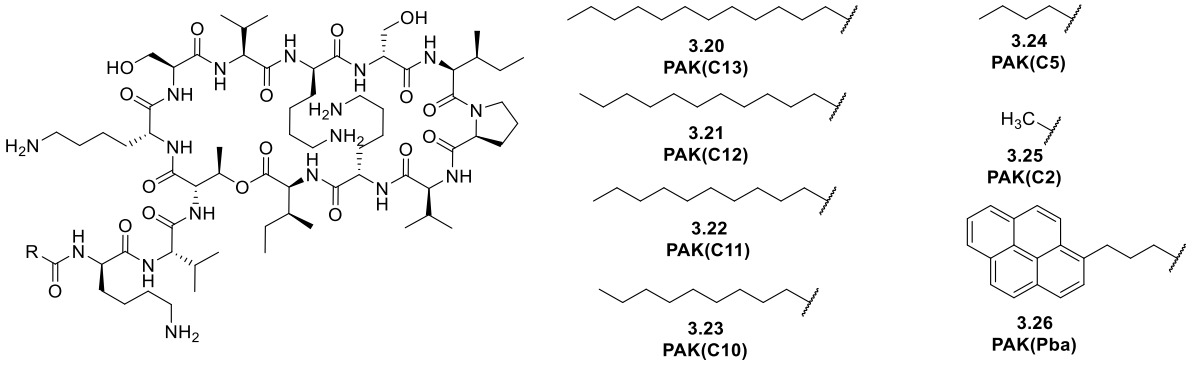

Peptide[a]	MIC (µg/ml)	
	E. coli K-12	*B. subtilis* 1046
PAK(C13) (**3.20**)	1	2
PAK(C12) (**3.21**)	1	2
PAK(C11) (**3.22**)	1	4
PAK(C10) (**3.23**)	1	8
PAK(C5) (**3.24**)	128	>128
PAK(C2) (**3.25**)	>128	>128
PAK(Pba) (**3.26**)	2	2

[a] Stock peptide concentration has been corrected to account for 1 equivalent of TFA for each lysine residue.

These results suggest decreasing the length of the acyl tail from 15 to 10 carbons correlates directly with the ability of paenibacterin to disrupt the cytoplasmic membrane of Gram-(+) bacteria, but does not have a noticeable impact on its mechanism of action against Gram-(−) *E. coli*. The lack of any observable effect on activity against Gram-(−) bacteria means that variation in the acyl tail length will allow us to tune the specificity of paenibacterin-analogs, narrowing their spectrum of activity. We

anticipate that reduced acyl tail length will also result in reduced haemolytic activity. If this proves to be true then **3.23** may provide the desired balance between potent activity against Gram-(−) bacteria and reduced toxicity at the expense of lower activity against Gram-(+) strains.

3.4.6 Alanine-Scan of All Cationic Residues

To examine the effect of reducing the cationic character of PAK on its activity, as well as the importance of each specific cationic residue, we conducted an alanine-scan where alanine was incorporated in place of each lysine residue in turn. The natural configuration was preserved at each position, meaning D-Ala was incorporated at position 7, position 4, and position 1; while L-Ala was incorporated at position 12. Substitution at position 4 necessitated the preparation of a D-Ala containing pseudoproline dipeptide (Fmoc-D-Ala-Ser($\Psi^{Me,Me}$Pro)-OH, Scheme 3.5).

Surprisingly, these analogs were all quite active against both Gram-(−) vs. Gram-(+) bacteria (Table 3.3). For *E. coli*, alanine substitution at position 7 (**3.27**) resulted in no loss of activity, while only a two-fold reduction was observed if alanine was substituted at position 4 (**3.28**), position 1 (**3.29**), or position 12 (**3.30**). As for *B. subtilis*, there was no lost activity when alanine was incorporated at position 7 (**3.27**) or position 4 (**3.28**); and a two-fold reduction at position 1 (**3.29**) or position 12 (**3.30**).

Considering the correlation between net charge and toxicity of cationic lipopeptides, it is promising that a reduction to an overall charge of +3 has little impact on activity. We can also tentatively conclude that the lysine residues at positions 4, 1, and 12 are more important for activity than the Lys at position 7 against Gram-(−) bacteria; while lysine at positions 1 and 12 are more important for activity than lysine at positions 4 and 7 against Gram-(+) bacteria.

Table 3.3 MIC of peptides bearing a single alanine substitution.

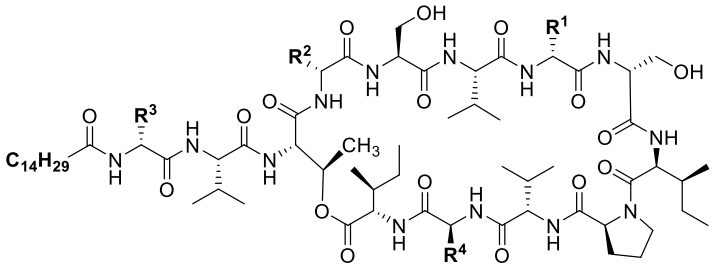

3.27: $R^1 = -CH_3$ $R^2, R^3, R^4 = -(CH_2)_4NH_2$

3.28: $R^2 = -CH_3$ $R^1, R^3, R^4 = -(CH_2)_4NH_2$

3.29: $R^3 = -CH_3$ $R^1, R^2, R^4 = -(CH_2)_4NH_2$

3.30: $R^4 = -CH_3$ $R^1, R^2, R^3 = -(CH_2)_4NH_2$

Peptide[a]	MIC (µg/ml)	
	***E. coli* K-12**	***B. subtilis* 1046**
PAK-D-Ala7 (**3.27**)	1	1
PAK-D-Ala4 (**3.28**)	2	1
PAK-D-Ala1 (**3.29**)	2	2
PAK-Ala12 (**3.30**)	2	2

[a] Stock peptide concentration has been corrected to account for 1 equivalent of TFA for each lysine residue.

3.4.7 Double-Substitution Alanine Scan of All Cationic Residues

To further establish which lysine residues were essential for activity, we then prepared a series of PAK analogs where two lysine residues were simultaneously substituted with alanine. Again, stereochemistry at each position was preserved. Six peptides were prepared, with every possible combination of substitutions at positions 7, 4, 1, and 12 (**3.31**-**3.36**). The antibacterial activity of these analogs is given in Table 3.4.

Table 3.4 MIC of peptides bearing a double alanine substitution.

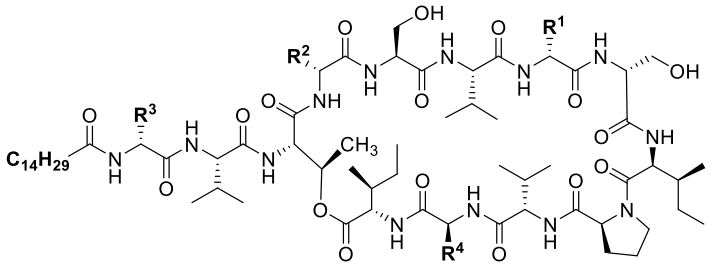

3.31: R^3, R^2 = $-CH_3$ R^1, R^4 = $-(CH_2)_4NH_2$

3.32: R^3, R^1 = $-CH_3$ R^2, R^4 = $-(CH_2)_4NH_2$

3.33: R^3, R^4 = $-CH_3$ R^1, R^2 = $-(CH_2)_4NH_2$

3.34: R^2, R^1 = $-CH_3$ R^3, R^4 = $-(CH_2)_4NH_2$

3.35: R^2, R^4 = $-CH_3$ R^1, R^3 = $-(CH_2)_4NH_2$

3.36: R^1, R^4 = $-CH_3$ R^2, R^3 = $-(CH_2)_4NH_2$

	MIC (µg/ml)	
Peptide[a]	***E. coli* K-12**	***B. subtilis* 1046**
PAK-D-Ala1-D-Ala4 (**3.31**)	32	2
PAK-D-Ala1-D-Ala7 (**3.32**)	4	2
PAK-D-Ala1-Ala12 (**3.33**)	>64	4
PAK-D-Ala4-D-Ala7 (**3.34**)	4	2
PAK-D-Ala4-Ala12 (**3.35**)	32	2
PAK-D-Ala7-Ala12 (**3.36**)	4	2

[a] Stock peptide concentration has been corrected to account for 1 equivalent of TFA for each lysine residue.

Unexpectedly, all analogs retained good activity against *B. subtilis*. The majority of the disubstituted peptides exhibited only a two-fold loss in activity, with the exception of **3.33** which was four-fold less active than PAK. This analog contained alanine residues at positions 1 and 12, which further confirms the finding that D-Lys1 and Lys12 are most important for activity against Gram-(+) bacteria.

Against *E. coli*, the effects of certain alanine substitutions were considerably more pronounced. If alanine was incorporated at positions 1 and 12 (**3.33**) then no antibacterial activity was observed up to 64 µg/ml. Similarly, the analogs with alanine at positions 1 and 4 (**3.31**) or positions 4 and 12 (**3.35**)

displayed poor activity (MIC = 32 μg/ml). These results also fit well with the observation that lysine residues at positions 4, 1, and 12 are important for activity against Gram-(−) bacteria. The other analogs exhibited only a four-fold reduction in activity. D-Lys7 appears to be the least important for activity, since all analogs containing alanine at position 7 remained quite active (**3.32**, **3.34**, **3.36**). This is somewhat unexpected since for polymyxin, cationic residues within the ring are known to be more important for activity.[67]

Another purpose of this alanine scan is the identification of which lysine residues could likely be labelled with some fluorophore without impacting activity significantly. Labelling at position 7 would likely impact activity the least, but the results of the single-alanine substitutions suggest that the impact of labelling at any position should have little effect.

These results show that it is possible to drastically reduce the net charge of paenibacterin to +2 while retaining good activity. In contrast to the effect of varying tail-length, eliminating select cationic side chains allows for the tuning of paenibacterin's selectivity towards Gram-(+) bacteria, though this property is likely not particularly useful. More important is the fact that the overall charge of paenibacterin can be significantly reduced with only a moderate reduction in activity, so long as certain residues are preserved. This may allow for the modulation of the potential toxicity of paenibacterin analogs since haemolytic activity often correlates with the cationic character of a peptide.

The fact that the specific location of each alanine substitution had little effect on the activity against *B. subtilis* suggests that paenibacterin's MOA against Gram-(+) bacteria may not depend on any specific intermolecular interaction, but instead depends on the overall amphipathic nature of the molecule. On the other hand, the fact that activity against *E. coli* was eliminated when alanine was incorporated at certain positions suggests that the MOA against Gram-(−) bacteria does involve some specific interaction, most likely with LPS.

3.4.8 Paenibacterin B Series Analog

The general approach for the synthesis of PAK analogs was applied to the synthesis of a D-Orn→D-Lys analog of a member of the paenibacterin B series with a tridecanoyl acyl tail, abbreviated **PBK(C13)**. The paenibacterin B family of peptides have acyl tails of varying lengths, from 10 to 15 carbons. The 13 carbon tail was chosen for no particular reason other than that it lies in the middle of this length distribution.[57] Some members of the paenibacterin B series have reportedly been chemically synthesized, though no experimental details were provided.[55]

Scheme 3.6 Synthesis of PBK(C13).

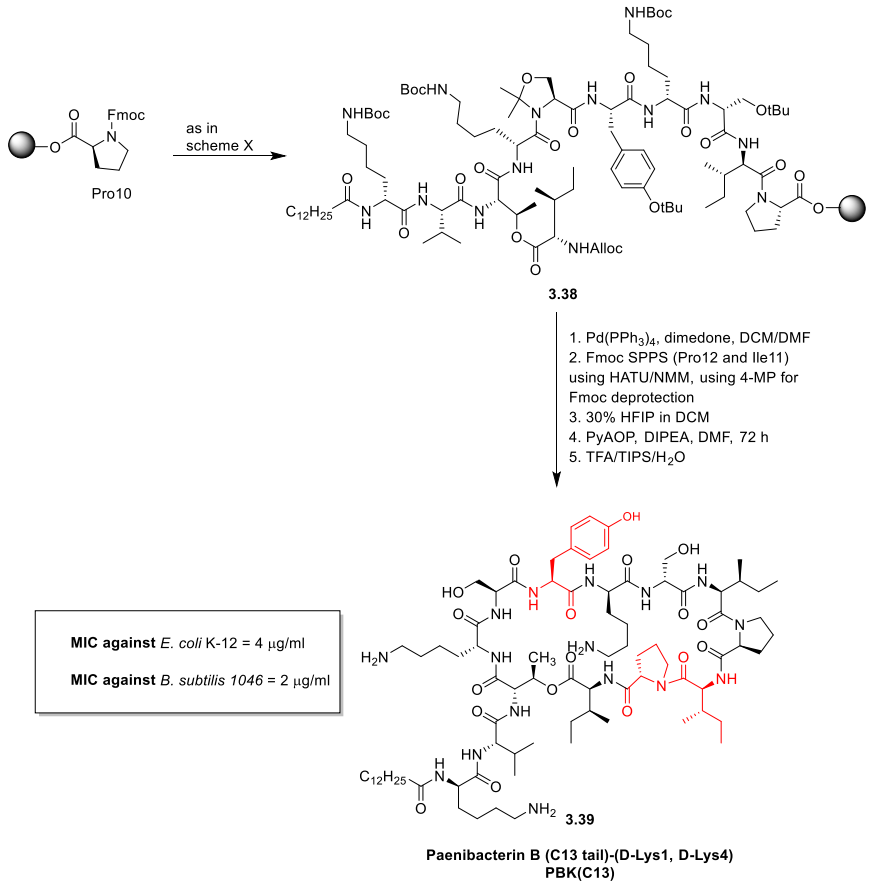

Peptide **3.37** was prepared using the same method for the preparation of peptide **3.16**, incorporating Fmoc-Tyr(*t*-Bu)-OH at position 6 (Scheme 3.6). The alloc protecting group on Ile13 was removed followed by coupling of Pro12 and Ile13. To remove the N^{α}-Fmoc protecting group of Pro12 we used

4-MP in DMF. Typically, at this point 2-MP is used as a precautionary measure to avoid any possible aminolysis of the ester bond; however, in our experience 2-MP can be slow to deprotect proline residues. We were pleased not to observe ester bond cleavage. Deprotection of Ile11 with 2-MP yielded a weakly positive ninhydrin test, used to detect the resulting free amine. This led us to 4-MP for the final Fmoc deprotection as well, though the ninhydrin test remained weakly positive. The weak ninhydrin test appears to be a misleading result, as PBK(C13) (**3.38**) was obtained in good purity and 26% yield[i]. We found that PBK(C13) was four-fold less active against *E. coli* K-12 than the analogous PAK(C13) (**3.20**) but was just as active against *B. subtilis* 1046 (Scheme 3.6).

3.4.9 PAK Analog with Tryptophan at Position 6

To facilitate the study of paenibacterin's mechanism of action, we wished to include a fluorescent amino acid into an analog of PAK. The existence of the paenibacterin B family of peptides, with aromatic residues at position 6, suggested to us that we could likely incorporate an aromatic amino acid at this position without a large loss of activity. Tryptophan was chosen, as it is aromatic, intrinsically fluorescent and readily available.

The precursor to this peptide, **3.39**, was prepared by esterification onto a truncated linear peptide using the general approach outlined in Scheme 3.5. Fmoc-Trp(Boc)-OH was incorporated at position 6. This peptide was prepared before some improvements had been made to the procedure, so allyl deprotection was performed using DMBA as a scavenger, while cleavage from the resin was accomplished with 1% TFA in DCM. The purity of PAK-Trp6 (**3.40**) was good, but it was isolated in poor yield (1%). As mentioned in section 3.4.2 this was attributed to the use of Trt-Tentagel resin that

---

[i] For this peptide—and all those prepared using Method B in the experimental section—faulty climate-control in the laboratory led to significant solvent evaporation during the esterification step. This caused some epimerization (detected in the crude peptide by RP-HPLC), likely caused by the increase in DMAP concentration. The major product was easily isolated during purification.

had been pre-loaded with Fmoc-Pro. Even though the resin was kept at −20 °C, it appears that long term storage resulted in decomposition, as all peptides prepared using this resin were obtained in very low yield. Looking closer at the literature, we found that it is recommended that, upon loading to trityl resins, Fmoc amino acids be immediately deprotected.[130] Reportedly with the Fmoc group in place, the trityl ester linkage is highly unstable. Confusing this matter is the fact that several pre-loaded trityl resins bearing Fmoc-amino acids are sold. Indeed, for the other analogs described in this chapter, we found that immediate deprotection resulted in dramatically improved yields.

Scheme 3.7 Synthesis of PAK-Trp6.

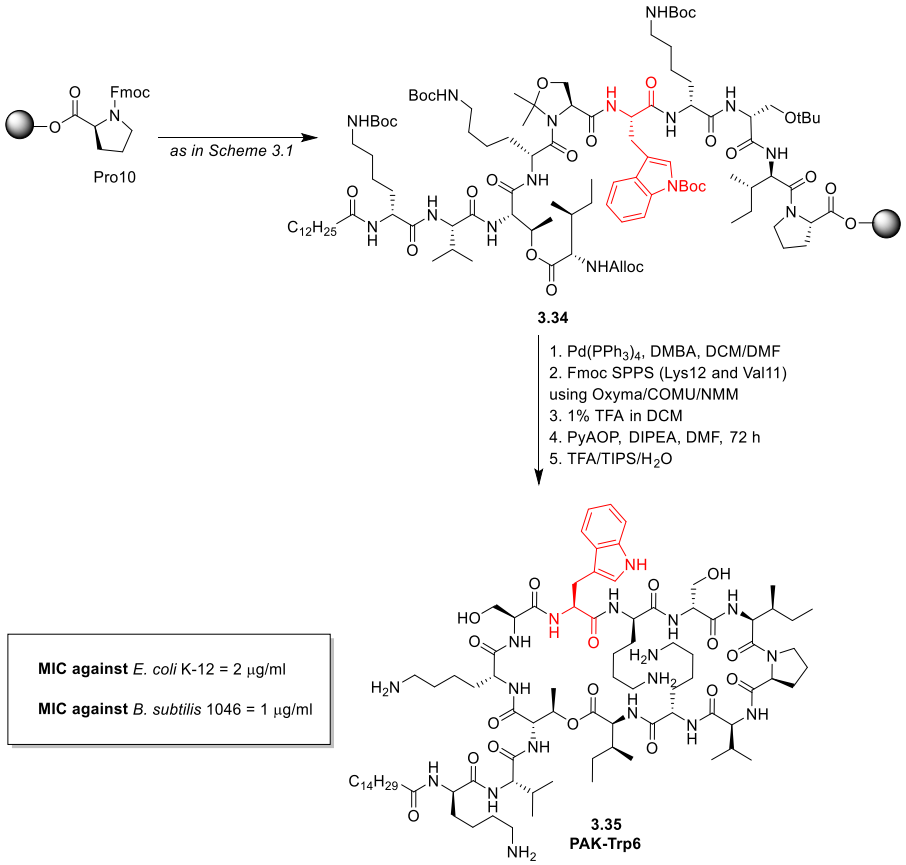

PAK-Trp6 was quite active against both *E. coli* K-12 (MIC = 2 μg/ml) and *B. subtilis* 1046 (MIC = 1 μg/ml). This confirmed to us that position 6 was amenable to substitution with aromatic amino acids.

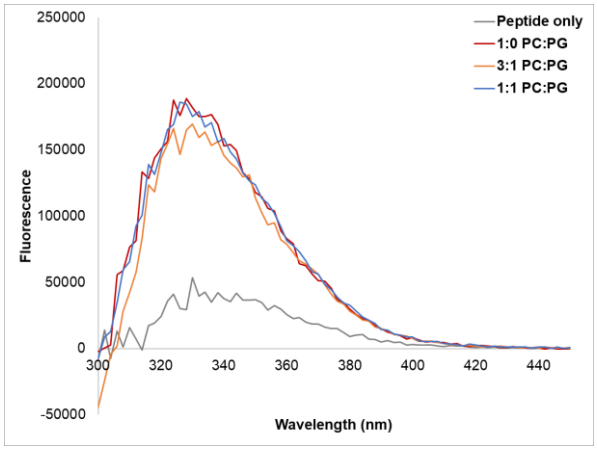

Figure 3.7 Interaction of 3.40 (3µM) with DMPC/DMPG liposomes (250 µM). Studies were conducted in 20 mM HEPES, 150 mM NaCl, pH 7.4 at 37 °C. λ_{ex} = 280 nm, λ_{em} = 300–450 nm.

We briefly examined the change in fluorescence of PAK-Trp6 in the presence of DMPC/DMPG liposomes. In the presence of liposomes, we saw a substantial increase in tryptophan fluorescence, corresponding to a decrease in environment polarity—likely caused by peptide insertion into the lipid bilayer. The sensitivity of this assay was quite low, which manifested in the noise seen in the emission spectra. Tryptophan fluorescence was equally affected for all the lipid compositions tested. Chapter 4 explores this concept further and discusses the incorporation of a highly fluorescent, environmentally sensitive amino acid into PAK.

3.5 Conclusions & Future Studies

In conclusion, an improved synthesis of PA1 was developed, which lends itself to the preparation of analogs with a range of substitutions. It was shown that replacing the two D-Orn residues in PA1 with D-Lys provides an analog with unchanged antibacterial activity. A gradual reduction in activity against *B. subtilis* occured as the tail length was reduced from 15 to 10 carbon atoms. Against *E. coli*, the activity was unaffected when reduced from 15 to 10 carbons in length. A pentanoyl or acetyl tail resulted in essentially complete loss of activity against both bacteria. It was found that any single lysine

side chain could be eliminated with only a minimal effect on antibacterial activity. Simultaneous elimination of two lysine side chains again had minimal effect on the activity against *B. subtilis*, but the activity against *E. coli* was strongly dependent on the location of each substitution. The lysine side chain at position 7 was identified as the least important for antibacterial activity, while positions 1 and 12 were found to be the most important.

Taken together, these results suggest that the mechanism of action of paenibacterin against Gram-(−) bacteria depends on fairly specific interactions between certain lysine side chains and some target, likely LPS. Against Gram-(+) bacteria, it appears that the mechanism of action depends on more general interactions of the peptide with the membrane, governed by the length of the acyl tail and the net cationic charge.

The ability to easily tune its physical properties should facilitate the creation of derivatives with high specificity for bacterial membranes and low toxicity. However, in this work the antibacterial activity was only measured against two bacterial species. While we believe that this gives a good indication of the relative activity of each analog against Gram-(±) bacteria, it will be important to screen new analogs against a wide variety of bacterial genera, species, and strains. To this end, many of the analogs described in this chapter have been submitted to the Community for Open Antimicrobial Drug Discovery for screening against the ESKAPE pathogens. In future work we also hope to determine the effects of these modifications to paenibacterin on haemolytic activity.

We anticipate that some of the analogs we have prepared will prove useful for studying certain aspects of paenibacterin's mechanism of action. We have prepared PAK(Pba) (**3.26**), a model compound that will be used for future studies on the aggregation of paenibacterin within membranes. We also plan to examine the ability of the inactive peptide PAK(C2) (**3.25**) to permeabilize the outer

membrane of Gram-(−) bacteria to other antibiotics, inspired by the work being done on polymyxin B nonapeptide.[74,75,77]

We have also demonstrated that our method for the synthesis of paenibacterin extends to a lysine-analog of paenibacterin B. Furthermore, we have confirmed that position 6 in PAK is amenable to substitution with aromatic amino acids. This finding ties directly into Chapter 4.

3.6 Experimental

General. Reagents available from commercial sources were used without further purification. Alloc-Ile-OH was prepared according to a literature procedure.[157] Fmoc-D-Lys(Boc)-Ser($\Psi^{Me,Me}$Pro)-OH was prepared as previously described.[1] Dry THF was obtained by distillation from sodium metal and benzophenone; DCM was distilled from calcium hydride. High resolution mass spectrometry was performed on an Orbitrap instrument in positive electrospray ionization mode (+ESI).

Determination of minimum inhibitory concentration. Peptide stock solutions were prepared by dissolving 1–3 mg of peptide TFA salts in water. The concentration of peptide in solution was corrected to account for one equivalent of TFA for each lysine residue. MICs were then determined by broth microdilution.[162] Overnight cultures of *B. subtilis* 1046 or *E. coli* K-12 were diluted to *ca.* 1×10^6 CFU/ml (determined by measuring OD_{600}). Peptide solutions were further diluted in LB broth, then two-fold serial dilutions were performed in a 96-well polystyrene plate. Finally an equal volume of diluted bacterial culture was added to each well. The plates were then incubated at 37 °C for 24h. The MIC was determined to be the lowest concentration with no detectable growth.

Interaction of PAK-Trp6 (3.40) with DMPC/DMPG liposomes. Small unilamellar vesicles were prepared exactly as described in the experimental section of Chapter 4 using 1,2-dimyristoyl-sn-glycero-3-phosphocholine (DMPC) and 1,2-dimyristoyl-sn-glycero-3-phospho-(1'-rac-glycerol) sodium salt (DMPG) in either 1:0, 3:1, or 1:1 ratios. Solutions of peptide **3.40** (3 μM final) and lipid solution (5 μM final) were mixed in a 96-well plate containing warm HEPES buffered saline (20 mM HEPES, 150 mM NaCl, pH 7.4). Emission spectra were collected using a Tecan M1000 plate reader at 37 °C, exciting at 280 nm.

Fmoc-Ser($\Psi^{Me,Me}$Pro)-OH (3.7). Fmoc-Ser-OH (3.93 g, 12 mmol, 1 equiv) was dissolved in acetone (100 ml). 2,2-dimethoxypropane (14.8 ml, 120 mmol, 10 equiv) was added followed by $BF_3 \cdot OEt_2$

(148 µl, 1.2 mmol, 0.1 equiv) and stirred for 20h before pouring into saturated NH_4Cl (300 ml). The solution was extracted with 6 × EtOAc (400 ml total) then concentrated to a red oil. The residue was taken up in 100 ml Et_2O then extracted with half-saturated $NaHCO_3$ (3 × 50 ml). The combined aqueous fractions were cooled to 0 °C then acidified with 6M HCl to pH 2–3. The solution was then extracted with Et_2O (3 × 50 ml) and the combined organic fractions were washed with brine, dried over Na_2SO_4, filtered and condensed. The product was purified by silica gel flash chromatography (80:20:5 heptane/EtOAc/AcOH) to give the product as a white solid (3.17 g, 71%). ^{1}H NMR ($(CD_3)_2SO$, 300 MHz): rotameric mixture δ 7.89 (d, 2H, J = 7.1), 7.75–7.59 (m, 2H), 7.49–7.26 (m, 4H), 4.80 - 3.75 (m, 6H), 1.7–0.5 (m, 6H); ^{13}C NMR ($(CD_3)_2SO$, 75 MHz): rotameric mixture δ 172.5, 172.0, 152.2, 151.8, 144.5, 144.5, 144.0, 144.0, 141.5, 141.4, 141.0, 141.0, 128.1, 127.8, 127.5, 127.5, 125.7, 125.5, 124.7, 124.7, 120.5, 120.4, 120.4, 94.7, 93.9, 67.0, 66.8, 66.3, 66.0, 59.1, 58.7, 47.1, 46.9, 31.6, 28.7, 25.3, 25.3, 23.9, 23.8, 22.4, 15.5, 14.3; MS (+ESI) m/z: $[M + Na]^+$ Calcd for $C_{21}H_{21}NO_5Na$ 390.13; Found 390.25.

Fmoc-D-Ala-Ser($\Psi^{Me,Me}$Pro)-OH. Fmoc-D-Ala pentafluorophenyl ester (769 mg, 1.6 mmol, 1 equiv) was dispersed in acetone (8 ml), then L-serine (504 mg, 4.8 mmol, 3 equiv) was added as a solution in 2.4 ml Na_2CO_3 (10% aq.) and the solution was stirred for 16h. The solution was then cooled to 0 °C then acidified to pH 1 with HCl (1N), partially concentrated, then extracted with EtOAc (2 × 20 ml), dried over Na_2SO_4, filtered, then concentrated.

The residue was then dissolved in dry THF (70 ml), then 2,2-dimethoxypropane (980 µl, 8 mmol, 5 equiv) and PPTS (80 mg, 0.32 mmol, 0.2 equiv) was added. The solution was refluxed for 12 h, passing the condensate through a Soxhlet extractor loaded with 4Å molecular sieves. The solution was then cooled to room temperature, and triethylamine (70 µl) was added before condensing. The residue taken up in EtOAc (50 ml), washed with H_2O (2 × 30 ml) and brine, dried over Mg_2SO_4, filtered and condensed. The product was isolated by silica gel flash chromatography (Gradient of 0 to 10% MeOH

in DCM) to give the pseudoproline dipeptide (634 mg, 91%). ^{1}H NMR ($CDCl_3$, 300 MHz): δ 7.73 (d, 2H, *J* = 7.7 Hz), 7.54 (d, 2H, *J* = 7.7 Hz), 7.37 (t, 2H, J = 7.5 Hz), 7.28 (t, 2H, J = 7.6 Hz), 5.72 (d, 1H, J = 8.6), 5.07 (d, 1H, J = 6.1 Hz), 4.44 - 4.10 (m, 6H), 1.66 (s, 3H), 1.56 (s, 3H), 1.33 (m, 3H); ^{13}C{^{1}H} NMR ($CDCl_3$, 75 MHz): δ 173.3, 170.7, 156.3, 143.6, 141.3, 127.8, 127.1, 125.1, 120.0, 96.9, 67.4, 67.0, 59.3, 49.5, 47.0, 24.9, 23.1, 18.0; HRMS (+ESI) m/z: $[M + H]^+$ Calcd for $C_{24}H_{27}N_2O_6$ 439.1864; Found 439.1891.

General method for esterification with Ile13. To form the ester bond, Alloc-Ile-OH or N_3-Ile-OH (10 equiv) was dissolved in dry DCM (1.5 ml) then cooled to 0 °C prior to the addition of DIC (10 equiv). The solution was warmed to RT over 30 min, then 1% Triton X-100 was added and the mixture was added to the dry resin followed by DMAP (0.1 equiv). The resin was mixed for 18 h before rinsing with DCM and DMF (3 × 1 ml each, 1–3 min).

General method for alloc deprotection with DMBA. Under N_2, $Pd(PPh_3)_4$ (0.2 equiv) and *N, N*-dimethylbarbituric acid (10 equiv) in 3:1 DMF/DCM (giving a concentration of 0.1 M DMBA) for 90 min, mixing by bubbling N_2 and adding dry DCM as needed to maintain a consistent volume. Following deprotection, the resin was rinsed with DCM, 1% sodium diethyldithiocarbamate in DMF, then DMF, then DCM (3 × 1 ml each, 1–3 min).

General method for alloc deprotection with dimedone. This method is essentially identical to that described above, with special consideration given to the acidity of the solution. Under N_2, $Pd(PPh_3)_4$ (0.2 equiv) and dimedone (10 equiv) in 3:1 DMF/DCM (to give a concentration of 0.1 M dimedone) for 90 min, mixing by bubbling N_2 and adding dry DCM as needed to maintain a consistent volume. Following deprotection, the resin was rinsed with 0.5% DIPEA in DMF, 0.5% sodium diethyldithiocarbamate in DMF, DMF, then DCM (3 × 1 ml each, 1–3 min).

General method for alloc deprotection with phenylsilane. Under N_2, $Pd(PPh_3)_4$ was dissolved in dry DCM (to give a concentration of 0.3 M phenylsilane) and $PhSiH_3$ (24 equiv) was added. This solution was transferred by cannula to the resin cartridge that had been flushed with N_2. The resin was then mixed by bubbling N_2 for 1h before rinsing with DCM, 0.5% sodium diethyldithiocarbamate in DMF, DMF, then DCM (3 × 1 ml each, 1–3 min).

Azide deprotection of N_3-Ile13. A similar method has been described by Lohani et al.[147] Fmoc-Lys(Boc)-OH (10 equiv) was dissolved in dry THF (0.125 M relative to lysine) then DIC (5 equiv) was added and the solution was mixed for 30 min to allow the symmetric anhydride to form. The solution was then added to the resin, followed by PBu_3. After 5 min H_2O was added (50 µl for 1 ml of THF) followed by mixing for 18h before rinsing with THF, DCM, and DMF.

General method A for synthesis of paenibacterin A analogs. Tentagel Trt-Cl resin (max loading 0.2 mmol/g, 25–50 µmol, 1 equiv) was loaded with Fmoc-Pro-OH (4 equiv) and DIPEA (8 equiv) in dry DCM (0.1 M of Pro), stirring for 18 h then rinsing with DCM/MeOH/DIPEA (17:2:1, 3 × 5 min). A small sample of resin was then set aside for estimation of the loading efficiency.[159] The loaded resin was then immediately treated with 2 × 4-MP (20% in DMF) for 5 min then 20 min, followed by rinsing with DMF (6 × 1 min). For all rinsing and deprotection steps, the volume of solution added was approximately 3 to 5 fold the volume of the swollen resin.

Fmoc-Ile-OH (residue 9), Fmoc-D-Ser(*t*-Bu)-OH (residue 8), Fmoc-D-Lys(Boc)-OH or Fmoc-D-Ala-OH (residue 7), and Fmoc-Val-OH (residue 6) were coupled by activating the amino acid (4 equiv) with COMU (3.9 equiv), oxyma (3.9 equiv), and NMM (8 equiv) in DMF (0.1 M relative to the amino acid) then mixing with the resin for 1–2 h or until complete as indicated by the ninhydrin test. For Fmoc removal the resin was treated with 2 × 4-MP (20% in DMF) for 5 min then 20 min. Between each coupling or deprotection step the resin was rinsed with DMF (6 × 1 min).

Fmoc-D-Lys(Boc)-Ser($\Psi^{Me,Me}$Pro)-OH or Fmoc-D-Ala(Boc)-Ser($\Psi^{Me,Me}$Pro)-OH (residues 4 & 5) were coupled using reduced equivalents, by activating the dipeptide (2.5 equiv) with COMU (2.4 equiv), oxyma (2.4 equiv), and NMM (5 equiv) using the same method.

Fmoc-Thr(OH)-OH (residue 3) and Fmoc-Val-OH (residue 2) were coupled by activating the amino acid (4 equiv) with DIC (4 equiv) and HOAt (4 equiv), mixing for 15–30 min prior to addition to the resin and further mixing for 3 h.

The ester bond was formed with Alloc-Ile-OH (residue 13) according to the general method outlined above. Fmoc-D-Lys(Boc)-OH or Fmoc-D-Ala-OH (residue 1) was coupled using the routine COMU/oxyma/NMM conditions. These conditions were also employed to couple the acyl tail, by activation of the appropriate carboxylic acid. For these couplings the Fmoc deprotection steps were accomplished with 2 × 2-MP (20% in DMF) for 5 min then 20 min.

Alloc deprotection was achieved using the general method for alloc deprotection with dimedone described above. Fmoc-Lys(Boc)-OH or Fmoc-Ala-OH (residue 12), and Fmoc-Val-OH (residue 11) were coupled with COMU/oxyma/NMM. The Fmoc groups of residues 12 and 13 were deprotected using freshly prepared 2-MP (20% in DMF + 1% formic acid) for 2 × 5 min.

Following removal of the final Fmoc protecting group, the resin was rinsed thoroughly with DMF, DCM, iPrOH, then DCM again before drying *in vacuo*. The peptide was then cleaved from the resin using 30% HFIP in dry DCM (3 × 30 min). DCM, iPrOH, and DCM again were used to rinse the cleaved peptide from the resin (3 × 1 min each) and the resin was again dried. The collected washings were concentrated by rotary evaporation to give the protected, uncyclized peptide which was then dissolved in dry DMF. Additional dry DMF was used to extract any remaining peptide from the dry resin. These were combined, and additional DMF was added to give a peptide concentration of 1 mM. DIPEA (8 equiv) was added followed by HOAt (4 equiv) and PyAOP (4 equiv) dissolved in 1–2 ml

DMF. The solution was then stirred for 72 h, before concentrating by rotary evaporation. The residue was then dispersed in minimal MeOH, precipitated with cold water (5 × the volume of MeOH), and collected by centrifugation. The peptide was then dried azeotropically with toluene, then transferred to a polypropylene vessel before deprotecting with TFA/TIPS/H_2O (90:5:5) for 90 min. The cleavage solution was then concentrated under an N_2 stream and the crude peptide was precipitated with cold MTBE and collected by centrifugation.

General method B for synthesis of paenibacterin A analogs. This method only differs from Method A in that HATU was used in place of oxyma/COMU. Routine amino acid couplings were accomplished by activating the N^{α}-Fmoc amino acids (4 equiv) with HATU (3.8 equiv) and NMM (8 equiv). To couple pseudoproline dipeptides, reduced equivalents of these reagents were used: dipeptide (2.5 equiv), HATU (2.4 equiv), NMM (5 equiv).

An HATU/NMM activator solution was prepared in DMF, then prior to each coupling the activator was added to a solution of the amino acid in DMF (giving a final amino acid concentration of 0.1 M).

PA1-D-Lys1-D-Lys4 Pba tail (3.26). Prepared according to Method A as described above from TrtCl-Tentagel resin (25 µmol, 1 equiv). Resin loading efficiency was estimated to be 42%.[159] 1-Pyrenebutyric acid was coupled onto residue 1. The crude peptide was purified by semi-preparative RP-HPLC (C8, linear gradient of 70:30 to 50:50 H_2O/MeCN + 0.1% TFA over 60 min). Collected fractions were pooled and lyophilized to give the TFA salt of peptide **3.26** as a white powder (6.5 mg, 29% based on estimated resin loading). Purity of the peptide was verified by analytical RP-HPLC (t_R = 18.9 min, linear gradient of 90:10 to 10:90 H_2O/MeCN + 0.1% TFA over 40 min (Figure B.1). HRMS (+ESI) *m/z*: $[M + H]^+$ calcd for $C_{86}H_{136}N_{17}O_{17}$ 1679.0295; found 1679.0256.

PA1-D-Lys1-D-Lys4 decanoyl tail (3.23). Prepared according to Method A as described above from TrtCl-Tentagel resin (25 µmol, 1 equiv). Resin loading efficiency was estimated to be 42%.[159] Decanoic

acid was coupled onto residue 1. The crude peptide was purified by semi-preparative RP-HPLC (C8, linear gradient of 70:30 to 50:50 H_2O/MeCN + 0.1% TFA over 60 min). Collected fractions were pooled and lyophilized to give the TFA salt of peptide **3.23** as a white powder (8.3 mg, 39% based on estimated resin loading). Purity of the peptide was verified by analytical RP-HPLC (t_R = 17.8 min, linear gradient of 90:10 to 10:90 H_2O/MeCN + 0.1% TFA over 40 min (Figure B.3). HRMS (+ESI) *m/z*: $[M + H]^+$ calcd for $C_{76}H_{140}N_{17}O_{17}$ 1563.0608; found 1563.0611.

PA1-D-Lys1-D-Lys4 pentanoyl tail (3.24). Prepared according to Method A as described above from TrtCl-Tentagel resin (25 µmol, 1 equiv). Resin loading efficiency was estimated to be 42%.[159] Valeric acid was coupled onto residue 1. The crude peptide was purified by semi-preparative RP-HPLC (C8, linear gradient of 80:20 to 60:40 H_2O/MeCN + 0.1% TFA over 60 min). Collected fractions were pooled and lyophilized to give the TFA salt of peptide **3.24** as a white powder (5.8 mg, 28% based on estimated resin loading). Purity of the peptide was verified by analytical RP-HPLC (t_R = 13.4 min, linear gradient of 90:10 to 10:90 H_2O/MeCN + 0.1% TFA over 40 min (Figure B.5). HRMS (+ESI) *m/z*: $[M + H]^+$ calcd for $C_{71}H_{130}N_{17}O_{17}$ 1492.9825; found 1492.9809.

PA1-D-Lys1-D-Lys4 acyl tail (3.25). Prepared according to Method A as described above from TrtCl-Tentagel resin (25 µmol, 1 equiv). Resin loading efficiency was estimated to be 42%.[159] Acetic acid was coupled onto residue 1. The crude peptide was purified by semi-preparative RP-HPLC (C8, linear gradient of 80:20 to 60:40 H_2O/MeCN + 0.1% TFA over 60 min). Collected fractions were pooled and lyophilized to give the TFA salt of peptide **3.25** as a white powder (8.9 mg, 44% based on estimated resin loading). Purity of the peptide was verified by analytical RP-HPLC (t_R = 12.5 min, linear gradient of 90:10 to 10:90 H_2O/MeCN + 0.1% TFA over 40 min (Figure B.7). HRMS (+ESI) *m/z*: $[M + H]^+$ calcd for $C_{68}H_{124}N_{17}O_{17}$ 1450.9356; found 1450.9351.

PA1-D-Lys1-D-Lys4 undecanoyl tail (3.22). Prepared according to Method B as described above from TrtCl-Tentagel resin (25 µmol, 1 equiv). Resin loading efficiency was estimated to be 85%.[159] Undecanoic acid was coupled onto residue 1. Epimerization was observed by HPLC analysis following esterification, likely caused by significant solvent evaporation during the esterification step. The major product was easily isolated by RP-HPLC. The crude peptide was purified by semi-preparative RP-HPLC (C8, linear gradient of 70:30 to 50:50 H_2O/MeCN + 0.1% TFA over 60 min). Collected fractions were pooled and lyophilized to give the TFA salt of peptide **3.22** as a white powder (14.0 mg, 32% based on estimated resin loading). Purity of the peptide was verified by analytical RP-HPLC (t_R = 18.9 min, linear gradient of 90:10 to 10:90 H_2O/MeCN + 0.1% TFA over 40 min (Figure B.9). HRMS (+ESI) *m/z*: $[M + 3H]^{+3}$ calcd for $C_{77}H_{144}N_{17}O_{17}$ 526.3637; found 526.3616.

PA1-D-Lys1-D-Lys4 dodecanoyl tail (3.21). Prepared according to Method B as described above from TrtCl-Tentagel resin (25 µmol, 1 equiv). Resin loading efficiency was estimated to be 85%.[159] Lauric acid was coupled onto residue 1. Epimerization was observed by HPLC analysis following esterification, likely caused by significant solvent evaporation during the esterification step. The major product was easily isolated by RP-HPLC. The crude peptide was purified by semi-preparative RP-HPLC (C8, linear gradient of 70:30 to 50:50 H_2O/MeCN + 0.1% TFA over 60 min). Collected fractions were pooled and lyophilized to give the TFA salt of peptide **3.21** as a white powder (11.9 mg, 27% based on estimated resin loading). Purity of the peptide was verified by analytical RP-HPLC (t_R = 20.0 min, linear gradient of 90:10 to 10:90 H_2O/MeCN + 0.1% TFA over 40 min (Figure B.11). HRMS (+ESI) *m/z*: $[M + 3H]^{+3}$ calcd for $C_{78}H_{146}N_{17}O_{17}$ 531.0355; found 526.0333.

PA1-D-Lys1-D-Lys4 tridecanoyl tail (3.20). Prepared according to Method B as described above from TrtCl-Tentagel resin (25 µmol, 1 equiv). Resin loading efficiency was estimated to be 85%.[159] Undecanoic acid was coupled onto residue 1. Epimerization was observed by HPLC analysis following esterification, likely caused by significant solvent evaporation during the esterification step. The major

product was easily isolated by RP-HPLC. The crude peptide was purified by semi-preparative RP-HPLC (C8, linear gradient of 70:30 to 50:50 H_2O/MeCN + 0.1% TFA over 60 min). Collected fractions were pooled and lyophilized to give the TFA salt of peptide **3.20** as a white powder (14.2 mg, 32% based on estimated resin loading). Purity of the peptide was verified by analytical RP-HPLC (t_R = 21.1 min, linear gradient of 90:10 to 10:90 H_2O/MeCN + 0.1% TFA over 40 min (Figure B.13). HRMS (+ESI) *m/z*: $[M + 3H]^{+3}$ calcd for $C_{79}H_{148}N_{17}O_{17}$ 535.7074; found 535.7048.

PA1-D-Lys1-D-Lys4-D-Ala7 (3.27). Prepared according to Method A as described above from newly purchased TrtCl-Tentagel resin (25 µmol, 1 equiv). Fmoc-D-Ala-OH was incorporated at position 7.

The crude peptide was purified by semi-preparative RP-HPLC (C8, linear gradient of 60:40 to 40:60 H_2O/MeCN + 0.1% TFA over 60 min). Collected fractions were pooled and lyophilized to give the TFA salt of peptide **3.27** as a white powder (15.5 mg, 32% based on resin loading). Purity of the peptide was verified by analytical RP-HPLC (t_R = 25.4 min, linear gradient of 90:10 to 10:90 H_2O/MeCN + 0.1% TFA over 40 min (Figure B.15). HRMS (+ESI) *m/z*: $[M + H]^+$ calcd for $C_{78}H_{143}N_{16}O_{17}$ 1576.0812; found 1576.0780.

PA1-D-Lys1-D-Ala4 (3.28). Prepared according to Method A as described above from newly purchased TrtCl-Tentagel resin (25 µmol, 1 equiv). Fmoc-D-Ala-OH was incorporated at position 4. The crude peptide was purified by semi-preparative RP-HPLC (C8, linear gradient of 60:40 to 40:60 H_2O/MeCN + 0.1% TFA over 60 min). Collected fractions were pooled and lyophilized to give the TFA salt of peptide **3.28** as a white powder (15.1 mg, 31% based on resin loading). Purity of the peptide was verified by analytical RP-HPLC (t_R = 25.2 min, linear gradient of 90:10 to 10:90 H_2O/MeCN + 0.1% TFA over 40 min (Figure B.17). HRMS (+ESI) *m/z*: $[M + H]^+$ calcd for $C_{78}H_{143}N_{16}O_{17}$ 1576.0812; found 1576.0773.

PA1-D-Lys4-D-Ala1 (3.29). Prepared according to Method A as described above from newly purchased TrtCl-Tentagel resin (25 μmol, 1 equiv). Fmoc-D-Ala-OH was incorporated at position 1. The crude peptide was purified by semi-preparative RP-HPLC (C8, linear gradient of 60:40 to 40:60 H_2O/MeCN + 0.1% TFA over 60 min). Collected fractions were pooled and lyophilized to give the TFA salt of peptide **3.29** as a white powder (24.3 mg, 51% based on resin loading). Purity of the peptide was verified by analytical RP-HPLC (t_R = 26.6 min, linear gradient of 90:10 to 10:90 H_2O/MeCN + 0.1% TFA over 40 min (Figure B.19). HRMS (+ESI) *m/z*: $[M + H]^+$ calcd for $C_{78}H_{143}N_{16}O_{17}$ 1576.0812; found 1576.0790.

PA1-D-Lys1-D-Lys4-Ala12 (3.30). Prepared according to Method A as described above from newly purchased TrtCl-Tentagel resin (25 μmol, 1 equiv). Fmoc-Ala-OH was incorporated at position 12. The crude peptide was purified by semi-preparative RP-HPLC (C8, linear gradient of 60:40 to 40:60 H_2O/MeCN + 0.1% TFA over 60 min). Collected fractions were pooled and lyophilized to give the TFA salt of peptide **3.30** as a white powder (23.5 mg, 49% based on resin loading). Purity of the peptide was verified by analytical RP-HPLC (t_R = 27.3 min, linear gradient of 90:10 to 10:90 H_2O/MeCN + 0.1% TFA over 40 min (Figure B.21). HRMS (+ESI) *m/z*: $[M + H]^+$ calcd for $C_{78}H_{143}N_{16}O_{17}$ 1576.0812; found 1576.0787.

PA1-D-Ala1-D-Ala4 (3.31). Prepared according to Method B as described above from TrtCl-Tentagel resin (25 μmol, 1 equiv). Resin loading efficiency was estimated to be 85%.[159] Fmoc-D-Ala-OH was incorporated at positions 1 and 4. Epimerization was observed by HPLC analysis following esterification, likely caused by significant solvent evaporation during the esterification step. The major product was easily isolated by RP-HPLC. The crude peptide was purified by semi-preparative RP-HPLC (C8, linear gradient of 60:40 to 40:60 H_2O/MeCN + 0.1% TFA over 60 min). Collected fractions were pooled and lyophilized to give the TFA salt of peptide **3.31** as a white powder (9.5 mg, 26% based on estimated resin loading). Purity of the peptide was verified by analytical RP-HPLC (t_R = 29.1 min,

linear gradient of 90:10 to 10:90 H_2O/MeCN + 0.1% TFA over 40 min (Figure B.23). HRMS (+ESI) *m/z*: $[M + 2H]^{+2}$ calcd for $C_{75}H_{137}N_{15}O_{17}$ 760.0153; found 760.0132.

PA1-D-Lys4-D-Ala1-D-Ala7 (3.32). Prepared according to Method B as described above from TrtCl-Tentagel resin (25 µmol, 1 equiv). Resin loading efficiency was estimated to be 85%.[159] Fmoc-D-Ala-OH was incorporated at positions 1 and 7. Epimerization was observed by HPLC analysis following esterification, likely caused by significant solvent evaporation during the esterification step. The major product was easily isolated by RP-HPLC. The crude peptide was purified by semi-preparative RP-HPLC (C8, linear gradient of 60:40 to 40:60 H_2O/MeCN + 0.1% TFA over 60 min). Collected fractions were pooled and lyophilized to give the TFA salt of peptide **3.32** as a white powder (8.2 mg, 22% based on estimated resin loading). Purity of the peptide was verified by analytical RP-HPLC (t_R = 28.5 min, linear gradient of 90:10 to 10:90 H_2O/MeCN + 0.1% TFA over 40 min (Figure B.25). HRMS (+ESI) *m/z*: $[M + 2H]^{+2}$ calcd for $C_{75}H_{137}N_{15}O_{17}$ 760.0153; found 760.0127.

PA1-D-Lys1-D-Lys4-D-Ala1-Ala12 (3.33). Prepared according to Method B as described above from TrtCl-Tentagel resin (25 µmol, 1 equiv). Resin loading efficiency was estimated to be 85%.[159] Fmoc-D-Ala-OH was incorporated at position 1 and Fmoc-Ala-OH was incorporated at position 12. Epimerization was observed by HPLC analysis following esterification, likely caused by significant solvent evaporation during the esterification step. The major product was easily isolated by RP-HPLC. The crude peptide was purified by semi-preparative RP-HPLC (C8, linear gradient of 55:45 to 35:65 H_2O/MeCN + 0.1% TFA over 60 min). Collected fractions were pooled and lyophilized to give the TFA salt of peptide **3.33** as a white powder (13 mg, 35% based on estimated resin loading). Purity of the peptide was verified by analytical RP-HPLC (t_R = 33.2 min, linear gradient of 90:10 to 10:90 H_2O/MeCN + 0.1% TFA over 40 min (Figure B.27). HRMS (+ESI) *m/z*: $[M + 2H]^{+2}$ calcd for $C_{75}H_{137}N_{15}O_{17}$ 760.0153; found 760.0126.

PA1-D-Lys1-D-Ala4-D-Ala7 (3.34). The crude peptide was purified by semi-preparative RP-HPLC (C8, linear gradient of 60:40 to 40:60 H_2O/MeCN + 0.1% TFA over 60 min). Collected fractions were pooled and lyophilized to give the TFA salt of peptide **3.34** as a white powder (8.1 mg, 22% based on estimated resin loading). Purity of the peptide was verified by analytical RP-HPLC (t_R = 27.5 min, linear gradient of 90:10 to 10:90 H_2O/MeCN + 0.1% TFA over 40 min (Figure B.29). HRMS (+ESI) *m/z*: $[M + 2H]^{+2}$ calcd for $C_{75}H_{137}N_{15}O_{17}$ 760.0153; found 760.0132.

PA1-D-Lys1-D-Ala4-Ala12 (3.35). Prepared according to Method B as described above from TrtCl-Tentagel resin (25 µmol, 1 equiv). Resin loading efficiency was estimated to be 85%.[159] Fmoc-D-Ala-OH was incorporated at position 4 and Fmoc-Ala-OH was incorporated at position 12. Epimerization was observed by HPLC analysis following esterification, likely caused by significant solvent evaporation during the esterification step. The major product was easily isolated by RP-HPLC. The crude peptide was purified by semi-preparative RP-HPLC (C8, linear gradient of 60:40 to 40:60 H_2O/MeCN + 0.1% TFA over 60 min). Collected fractions were pooled and lyophilized to give the TFA salt of peptide **3.35** as a white powder (8.5 mg, 23% based on estimated resin loading). Purity of the peptide was verified by analytical RP-HPLC (t_R = 29.3 min, linear gradient of 90:10 to 10:90 H_2O/MeCN + 0.1% TFA over 40 min (Figure B.31). HRMS (+ESI) *m/z*: $[M + 2H]^{+2}$ calcd for $C_{75}H_{137}N_{15}O_{17}$ 760.0153; found 760.0131.

PA1-D-Lys1-D-Lys4-D-Ala7-Ala12 (3.36). Prepared according to Method B as described above from TrtCl-Tentagel resin (25 µmol, 1 equiv). Resin loading efficiency was estimated to be 85%.[159] Fmoc-D-Ala-OH was incorporated at position 7 and Fmoc-Ala-OH was incorporated at position 12. Epimerization was observed by HPLC analysis following esterification, likely caused by significant solvent evaporation during the esterification step. The major product was easily isolated by RP-HPLC. The crude peptide was purified by semi-preparative RP-HPLC (C8, linear gradient of 60:40 to 40:60 H_2O/MeCN + 0.1% TFA over 60 min). Collected fractions were pooled and lyophilized to give the

TFA salt of peptide **3.36** as a white powder (8.7 mg, 23% based on estimated resin loading). Purity of the peptide was verified by analytical RP-HPLC (t_R = 30.0 min, linear gradient of 90:10 to 10:90 H_2O/MeCN + 0.1% TFA over 40 min (Figure B.33). HRMS (+ESI) *m/z*: $[M + 2H]^{+2}$ calcd for $C_{75}H_{137}N_{15}O_{17}$ 760.0153; found 760.0132.

Paenibacterin B-D-Lys1-D-Lys4 tridecanoyl tail (3.38). Beginning from TrtCl-Tentagel resin (25 µmol, 1 equiv), this peptide was prepared using a method very similar to Method B described above with some deviations. Fmoc-Tyr(*t*-Bu)-OH was incorporated at position 6, Fmoc-Pro-OH was incorporated at position 12, and Fmoc-Ile-OH was incorporated at position 11. N^{α} of D-Lys1 was acylated with tridecanoic acid. To remove the N^{α}-Fmoc group of Pro12 and Ile11 2 × 4-MP (20% in DMF) for 5 min and 10 min with 4-MP (20% in DMF + 1% formic acid). Resin loading efficiency was estimated to be 85%.[159] The crude peptide was purified by semi-preparative RP-HPLC (C8, linear gradient of 60:40 to 40:60 H_2O/MeCN + 0.1% TFA over 60 min). Collected fractions were pooled and lyophilized to give the TFA salt of peptide **3.38** as a white powder (11.5 mg, 26% based on estimated resin loading). Purity of the peptide was verified by analytical RP-HPLC (t_R = 25.4 min, linear gradient of 90:10 to 10:90 H_2O/MeCN + 0.1% TFA over 40 min (Figure B.35). HRMS (+ESI) *m/z*: $[M + 3H]^{+3}$ calcd for $C_{83}H_{142}N_{16}O_{18}$ 551.3635; found 551.3615.

PA1-D-Lys1-D-Lys4-Trp6 (3.40). For this peptide the cleavage and cyclization were accomplished as described previously for the synthesis of paenibacterin A1.[1] Pre-loaded Fmoc-Pro-Trt-Tentagel resin (33 µmol, 1 equiv) was swollen in DCM followed by rinsing with DMF and deprotection of the Fmoc group with 2 × 4-MP (20% in DMF) for 5, 20 min. Fmoc-Ile-OH (4 equiv) was then coupled with HOAT and DIC (4 equiv each) for 16h. The resin was then rinsed with DMF (6 × 1 ml, 1–3 min) and deprotected with 2 × 2-MP (20% in DMF) for 5 min, 7 min. Fmoc-D-Ser(*t*-Bu)-OH, Fmoc-D-Lys(Boc)-OH, and Fmoc-Trp(Boc)-OH were coupled by activating the amino acid (4 equiv) with COMU (4 equiv) and NMM (8 equiv) before adding to the resin and mixing for 1–2 h or complete by ninhydrin

test. Each coupling was preceded by deprotection with 4-MP (20% in DMF) for 5 then 20 min and between each coupling/deprotection the resin was rinsed with DMF (6 × 1 ml, 1–3 min). The pseudoproline dipeptide was coupled using the same method but reduced equivalents: Fmoc-D-Lys(Boc)-Ser($\Psi^{Me,\ Me}$Pro)-OH/COMU/NMM (2.5/2.5/5 equiv). Fmoc-Thr(OH)-OH and Fmoc-Val-OH (5 equiv) were each coupled for 3–4 h using HOAt (5 equiv) and DIC (5 equiv). Alloc-Ile-OH was coupled according to the general method for esterification described above.

Following the esterification step, Fmoc removal was effected with 2 × 2-MP (20% in DMF) for 5 then 20 min. Fmoc-Lys(Boc)-OH and pentadecanoic acid (5 equiv) were coupled with DIC (5 equiv) and HOAt (5 equiv) for 3.5 h or until complete by ninhydrin test. The allyl group was removed with $Pd(PPh_3)_4$ (0.2 equiv) and *N, N*-dimethylbarbituric acid (10 equiv) in 3:1 DMF/DCM (2 ml) for 90 min, mixing by bubbling N_2. Following allyl deprotection the resin was rinsed with DCM, 1% sodium diethyldithiocarbamate in DMF, then DMF (3 × 1 ml each). Fmoc-Lys(Boc)-OH and Fmoc-Val-OH were coupled with DIC/HOAt using the same method; for Fmoc deprotections the resin was treated with 2 × 2-MP (20% in DMF) for 5 then 7 min. Following removal of the final Fmoc protecting group the resin was thoroughly rinsed with MeOH, iPrOH, and DCM then dried. The peptide was cleaved from the resin with 1% TFA in DCM (1 ml, 3 × 2 min), draining into a solution of 10% pyridine in MeOH (5 ml). The resin was further rinsed with DCM, MeOH, iPrOH, then DCM (1 ml each, 2 × 2 min). Cleavage was repeated 3 times, then the solution was concentrated *in vacuo*. The crude peptide was precipitated from MeOH (0.5 ml) with ice cold water (2.5 ml), collected by centrifugation, and azeotropically dried with toluene. For cyclization, the peptide was dissolved in dry DMF (30 ml) and DIPEA (8 equiv) was added followed by a solution of HOAt (4 equiv) and PyAOP (4 equiv) in 3 ml DMF. The solution was stirred for 72 h before concentration by rotary evaporation. The peptide was again precipitated from MeOH with water, then the protecting groups were cleaved with 3 ml

TFA/TIPS/H_2O (90:5:5) for 90 min. The cleavage solution was concentrated under an N_2 stream then the peptide was precipitated with cold MTBE.

The crude peptide was purified by semi-preparative RP-HPLC (C8, linear gradient of 70:30 to 50:50 H_2O/MeCN + 0.1% TFA over 60 min). Collected fractions were pooled and lyophilized to give the TFA salt of peptide **3.40** as a white powder (0.8 mg, 1% based on estimated resin loading). Purity of the peptide was verified by analytical RP-HPLC (t_R = 24.1 min, linear gradient of 90:10 to 10:90 H_2O/MeCN + 0.1% TFA over 40 min (Figure B.37). HRMS (+ESI) *m/z*: $[M + H]^+$ calcd for $C_{87}H_{151}N_{18}O_{17}$ 1720.1499; found 1720.1468.

Chapter 4

Enantioselective Synthesis and Application of New Small and Environmentally Sensitive Fluorescent Amino Acids for Probing Biological Interactions[i]

4.1 Preface

The work presented in this section has been submitted for publication in the *Journal of Organic* chemistry at the time of this writing. Portions of the manuscript have been reproduced here in accordance with the American Chemical Society's Policy on Theses and Dissertation and the Prior Publication Policy of the *Journal of Organic Chemistry*. The work herein was carried out by myself under the guidance of Dr. Scott Taylor. The initial drafts of the manuscript was also prepared by me, with revisions provided by Dr. Taylor. The incorporation of the fluorescent amino acids into daptomycin analogs and the determination of their MICs and interactions with model membranes was accomplished by Carlee Montgomery, a former undergraduate student in the Taylor Group.

4.2 Introduction

Extrinsic fluorescent labels are often incorporated into peptides and proteins to probe their structure and function using fluorescence spectroscopy, and for visualizing molecular interactions and intracellular processes using fluorescence microscopy.[176] These labels are attached to reactive side chains or to the *N*- or *C*- terminus, which has the potential to significantly impact the characteristics of the peptide or protein.[177] Some peptides and proteins do not require labelling as they contain

---

[i]Reproduced (adapted) with permission from "Noden, M.; Taylor, S. D. Enantioselective Synthesis and Application of Small and Environmentally Sensitive Fluorescent Amino Acids for Probing Biological Interactions. *J. Org. Chem.* **2021**, *86* (17), 11407–11418.". Copyright © 2021 American Chemical Society.

intrinsically fluorescent amino acids, such as tryptophan[119,178,179] and kynurenine,[104,180] which can be used to study interactions with model biological systems and sometimes live cells. However, experiments with cells are complicated by the background fluorescence of cellular proteins that contain these amino acids. Furthermore, these naturally fluorescent amino acids often lack the sensitivity required for biological studies. As an alternative to extrinsic labelling, fluorescent amino acids (FlAAs) may be directly incorporated into peptides or proteins, minimizing added bulk and potentially reducing the impact of the structural change on the peptide's biological properties and function.[181–183] Solvatochromic FlAAs, which exhibit a change in fluorescence intensity and/or wavelength as the environment surrounding the amino acid changes from polar to apolar or vice versa, are particularly useful for probing interactions between biomolecules. A number of such amino acids have been developed and used to study peptide-protein interactions and peptide-membrane interactions.[184–189]

For our studies on cyclic lipopeptide antibiotics, we had need of a solvatochromic FlAA that had the following properties: (1) displays a large *increase* in fluorescence upon its transfer from a polar to an apolar environment; (2) is small and resembles a natural amino acid, such as tryptophan, as much as possible; and (3) can be readily incorporated into peptides using standard Fmoc SPPS. There are a number of FlAAs, such amino acids **4.1**-**4.5** in Figure 4.1, that meet the first and third criteria.[181,186–189] Some of them, such as 4-DAPA (**4.3**), exhibit very large increases in fluorescence upon transfer from polar to apolar media, and all are readily incorporated into peptides using standard SPPS. However, these FLAAs are either conjugates of diaminopropionic acid to various fluorophores (**4.1**-**4.4**) or, like DANA (**4.5**), have a ketone moiety in between the a-carbon and the aromatic group (DANA), or are very large (DMNA, **4.4**), and therefore, do not resemble a natural amino acid such as tryptoaphan. L-(7-Hydroxycoumarin-4-yl)ethylglycine (7-HC, **4.6**) is often the FlAA of choice for incorporation into peptides and proteins due to its small size and high fluorescence quantum yield. [185,190–192] However, the fluorescence intensity of this amino acid decreases as the polarity of the environment decreases.

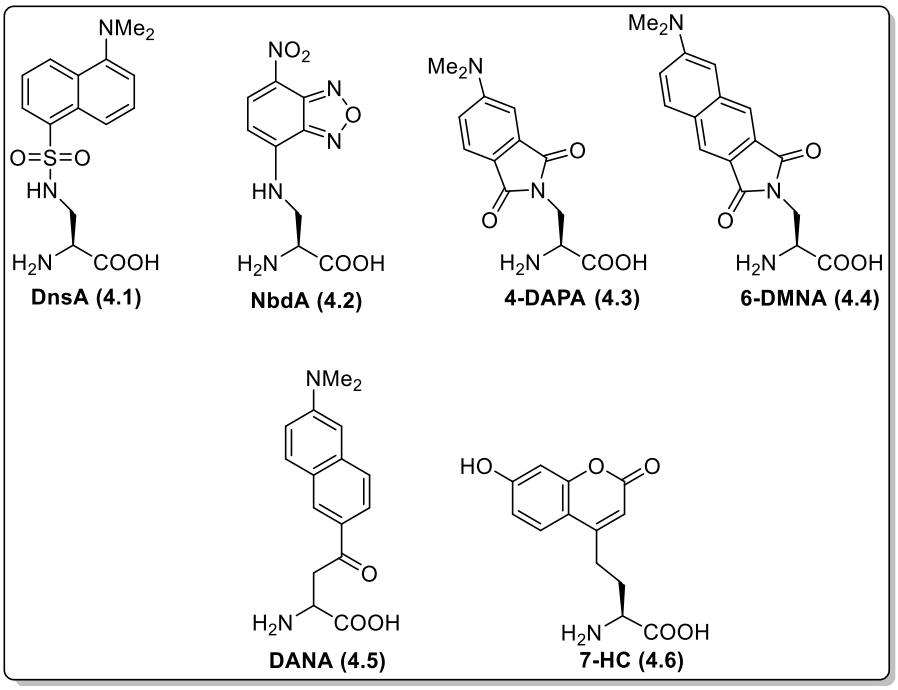

Figure 4.1 Literature examples of solvatochromic FlAAs (4.1-4.6).

4.2.1 7-Aminocoumarin Fluorescence

The 7-aminocoumarin family of fluorophores are extremely useful due to their strong solvatochromism, exhibiting increased and blue-shifted fluorescence as solvent polarity decreases.[193,194] Compared to hydroxycoumarins, 7-aminocoumarins are relatively unaffected by solvent acidity between pH 4–10.[195] 7-dialkylaminocoumarins are of particular interest for labeling experiments since the reactive aniline nitrogen is effectively protected. Many coumarins of this type have found use as laser dyes, and their photophysical properties have been studied extensively.[195–198] Some examples are shown in Figure 4.2.

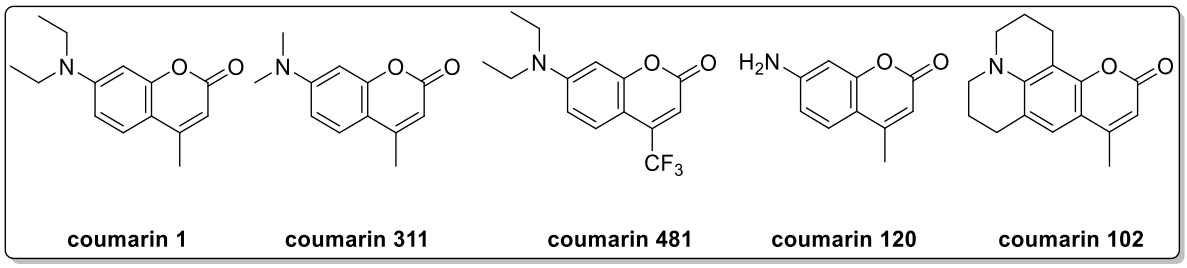

Figure 4.2 Select 7-aminocoumarin laser dyes and their respective common names.

Typically, increased solvent polarity results in lower quantum energy fluorescence emission. This effect can be attributed to the larger dipole moment of most excited states relative to the ground state. Reorientation and relaxation of the surrounding solvent dipoles lowers the excited state energy (Figure 4.3). The result is that the Stokes shift often dependent on solvent polarity, with increasing polarity accompanying red-shifted emission.[199] Additionally, specific solvent-fluorophore interactions can further stabilize the excited state, e.g. through hydrogen bonding or the stabilization of charge-transfer states, further affecting the emission spectrum.[199]

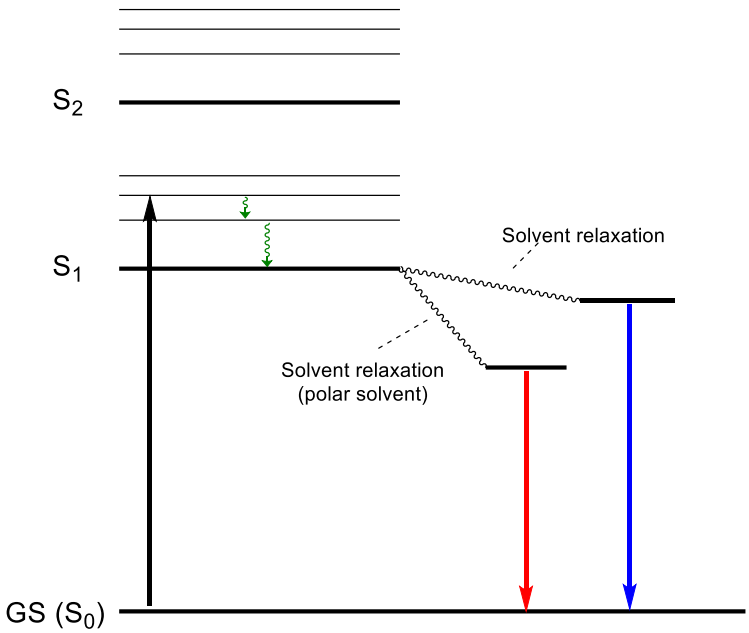

Figure 4.3 Jablonski diagram depicting polarity-dependent solvent relaxation. Excitation from the ground state (GS) to an excited vibrational state (black, 10^{-15} s) is followed by vibrational relaxation (green, 10^{-12} s), then solvent relaxation (10^{-10} s) and emission (blue/red, 10^{-9} s)[199]

The reduced fluorescence quantum yield of compounds like coumarin 1 (C1) or coumarin 311 (C311) in polar solvents has been attributed to relaxation of the excited state to a twisted intramolecular charge transfer (TICT) state.[196] In this TICT state the amino group acts as an electron donor, with the carbonyl-containing ring acting as an electron acceptor. Bond rotation results in increased charge separation, followed by rapid non-radiative decay to the ground state.[200] Polar solvents, and solvents capable of hydrogen bonding favour formation of the TICT state.[201,198] This effect of reduced quantum yield in polar solvents is enhanced if the electron withdrawing groups are added to the *acceptor* region of the fluorophore (as in coumarin 481). Conversely, restriction of rotation (as in coumarin 102) results in reduced fluorescence quenching in polar solvents.[196,201] Such rotation-restricted aminocoumarin fluorophores have been used for peptide labeling.[202,203] Representative resonance structures depicting

the locally excited (LE), intramolecular charge transfer (ICT), and TICT states of a C1 or C311-type coumarin are depicted in Figure 4.4.

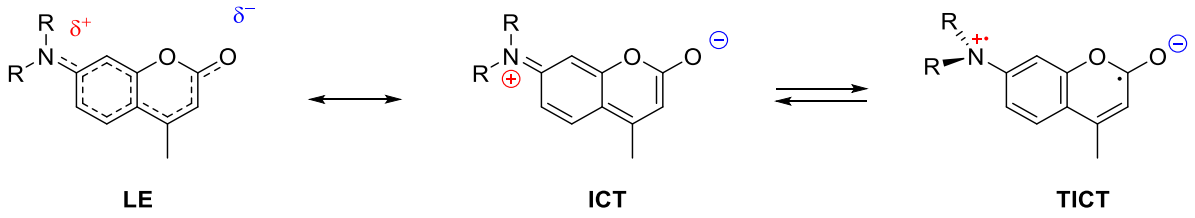

Figure 4.4 Representative resonance structures depicting the LE, ICT, and TICT states of a 7-aminocoumarin dye.

It has been demonstrated that coumarin 481 forms dimers and trimers in solution. Interestingly, in these aggregates the rotation of the amino group, and thus conversion to the TICT state, is hindered by steric interactions. This results in much longer fluorescence lifetimes for the dimer.[204] This effect is somewhat atypical, since often dimerization of fluorophores results in fluorescence quenching and shorter lifetimes.[205] Indeed the evidence was found for the formation of parallel H-type aggregates, accompanied by blue-shifted absorption and emission, and a shorter fluorescence lifetime for the trimer compared to the dimer—since quenching via exciton-exciton annihilation increases with aggregate size.[204] The formation of H-dimers is often also accompanied by self-quenching of fluorescence, and can be promoted by protic solvents or by the conformation of a protein bound to a fluorophore.[206,207]

4.2.2 Objectives

The favourable fluorescence properties of the 7-aminocoumarins and their small size led us to design *minimal* solvatochromic FlAAs 7-dimethylaminocoumarin-4-alanine (**4.7**, DMACA) and 7-diethylaminocoumarin-4-alanine (**4.8**, DEACA) (Figure 4.5). The objectives of the work presented in this chapter were multifold. The first was to develop enantioselective syntheses of these two amino acids suitably protected for Fmoc SPPS. The second was to characterize the photophysical properties

of simple peptides bearing these amino acids. The third was to demonstrate that these amino acids could be incorporated into complex peptides, such as paenibacterin and daptomycin. The fourth and final objective was to demonstrate the potential of these FlAAs for probing biological interactions by monitoring the insertion of paenibacterin containing DMACA into model liposomes, lipopolysaccharide and live bacteria using fluorescence spectroscopy/microscopy.

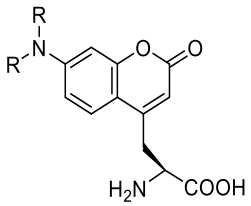

4.7, R = Me (DMACA)
4.8, R = Et (DEACA)

Figure 4.5 DMACA (4.7) and DEACA (4.8).

4.3 Results and Discussion

4.3.1 Synthesis of DMACA and DEACA.

Chiral coumarin amino acids can be accessed by acid-catalyzed von Pechmann condensation between substituted phenols and aspartate- or glutamate-derived β-ketoesters.[208] Although this is a fairly direct route to these types of compounds, the purification of the coumarin amino acid can be challenging, sometimes requiring preparative HPLC.[190] Therefore, we elected to examine a chiral auxiliary approach to the synthesis of **4.7** and **4.8**. Since Williams' auxiliary has been used for the enantioselective synthesis of coumarin amino acids, we anticipated that this approach could be used for the preparation of **4.7** and **4.8**.[209,210] Starting coumarin **4.10** is commercially available while coumarin **4.9**, which is not readily available, was prepared from 3-(dimethylamino)phenol and ethyl acetoacetate using a method initially reported by von Pechmann (Scheme 4.1).[211] Coumarins **4.9** and **4.10** were brominated on the methyl group using with LiHMDS and NBS to give bromomethyl coumarins **4.11** and **4.12**.[212]

Williams' auxiliary[213] was treated with NaHMDS and the resulting metalated auxiliary was reacted with **4.11** and **4.12** in THF or THF/HMPA which gave compound **4.13** in low yield (38%) and **4.14** in good yield (74%) which was probably due to the limited solubility of **4.11** in THF/HMPA. Unfortunately, compounds **4.13** and **4.14** exhibited very limited solubility in most organic solvents and we were unable to effect the removal of the auxiliary and isolate the free amino acids.

Scheme 4.1 Attempted synthesis of 4.7 and 4.8 using Williams' auxiliary.

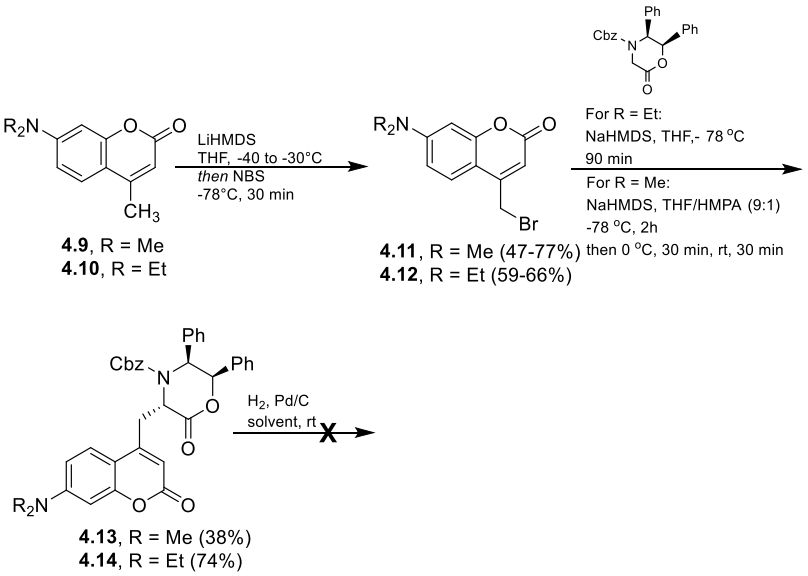

We then decided to prepare **4.7** and **4.8** via the alkylation of a chiral Ni(II) glycine Schiff base complex (**4.15** in Scheme 4.2). This auxiliary has been used extensively for the preparation of a wide variety of unnatural amino acids, and the absolute configuration can be inferred from extensive literature precedent.[214,215] Alkylation of the auxiliary with **4.11** and **4.12** proceeded smoothly in DMF with *dr* values of 86:14 and 84:16, respectively. Pleasingly, the major diastereomers, **4.16** and **4.17**, readily dissolved in organic solvents. They were isolated by column chromatography and then decomposed by acidic hydrolysis to give compounds **4.7** and **4.8**. The amino acids were insoluble in both organic solvents and in water, and so could be separated from both residual nickel salts and the (*S*)-2-[*N*-(*N'*-benzylprolyl)amino]benzophenone ligand without the use of ion exchange

chromatography. Protection of **4.16** and **4.17** with Fmoc-OSu gave **4.18** and **4.19**, suitable building blocks for solid phase peptide synthesis (SPPS).

Scheme 4.2 Synthesis of DMACA and DEACA using auxiliary 4.15.

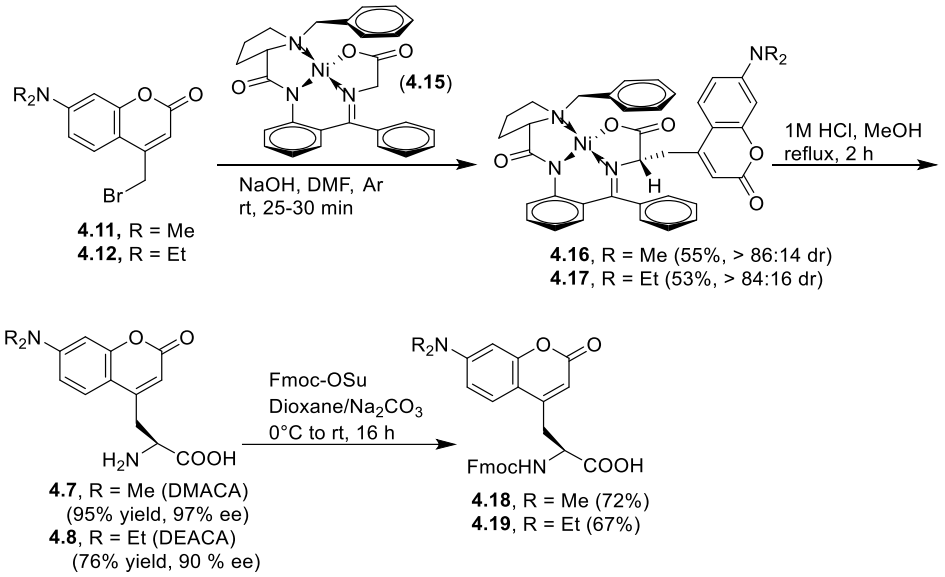

4.3.2 Determination of Enantiomeric Purity.

The enantiomeric purity of DMACA (**4.7**) and DEACA (**4.8**) was determined using the respective racemic amino acids for reference. These were prepared by alkylation of diethyl acetamidomalonate with bromocoumarins **4.11** or **4.12** in a refluxing sodium ethoxide-ethanol solution (Scheme 4.3).[209,210] This reaction was highly inefficient and resulted in a mixture of several compounds that were not easily separable by flash chromatography. Regardless, column fractions deemed to contain mostly the desired alkylation product were subjected to acidic hydrolysis and decarboxylation. Fortunately, due to the low solubility of the free amino acids we were able to separate them from the majority of contaminants simply by filtration. Racemic DMACA was isolated in low yield and high purity, while racemic DEACA was isolated as a mixture with a 7-(diethylamino)-4-hydroxymethylcoumarin impurity. This impurity does not contain a primary or secondary amine and so it was decided that it would not interfere

with Marfey analysis. Likewise, Marfey analysis requires only a small amount of each amino acid, and therefore the low yield was of little concern.

Scheme 4.3 Synthesis of Racemic DMACA/DEACA.

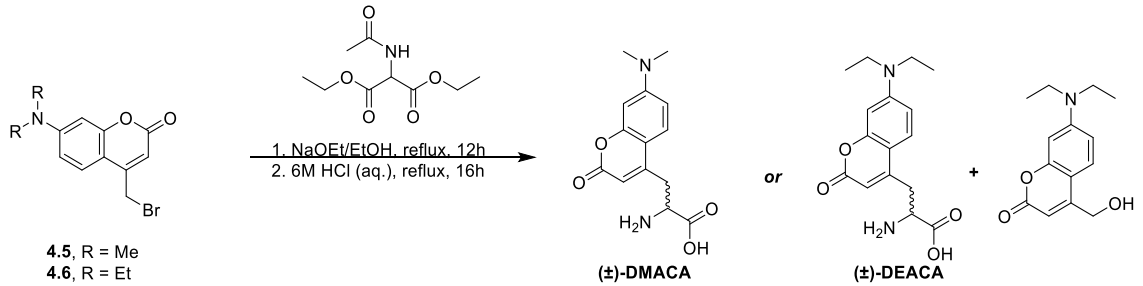

The racemic and L-enantiomers of each amino acid were derivatized with Marfey's reagent. Shown in Scheme 4.4, Marfey's reagent reacts with the α-amino group to give a pair of diastereomers that can be separated by HPLC.[215–218] Intramolecular hydrogen bonding exclusive to the (L, L)-diastereomer generally causes it to be eluted before the (D, L)-diastereomer when analyzed by RP-HPLC.[218]

Scheme 4.4 Derivatization of coumarin amino acids with Marfey's reagent.

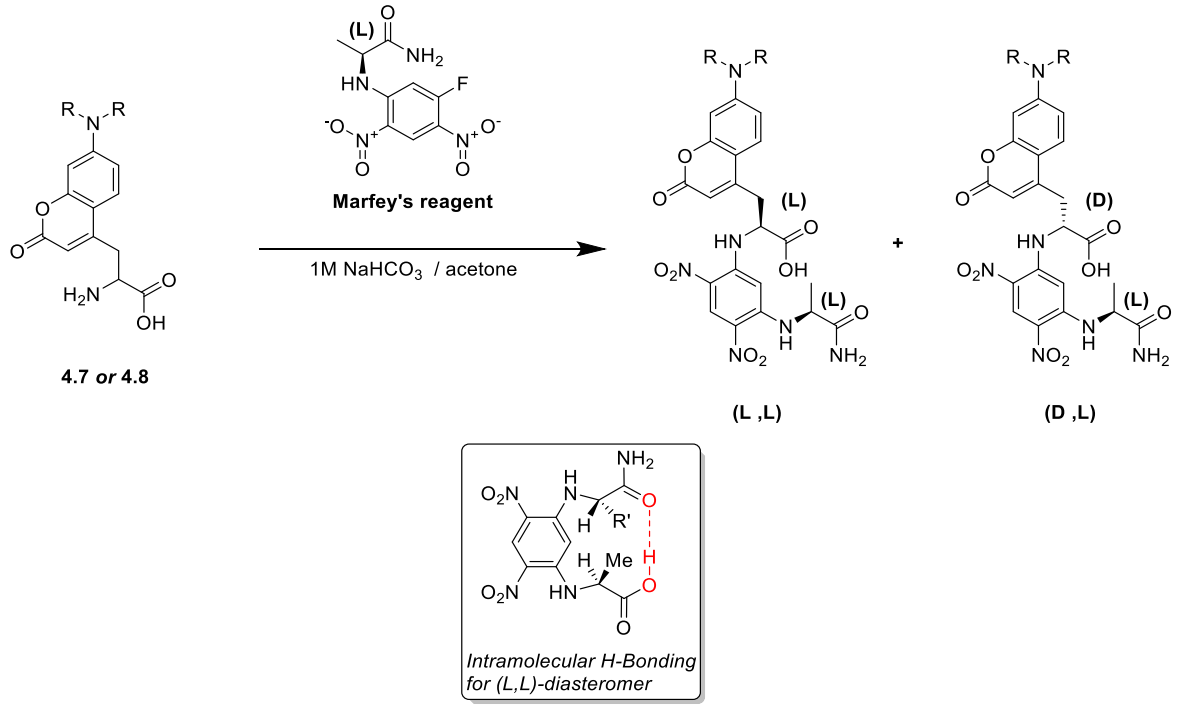

When DMACA was derivatized with Marfey's reagent and analyzed by RP-HPLC we indeed found that the major diastereomer eluted before the minor (Figure 4.6). This supports the stereochemistry assignment we inferred from literature precedent for the Ni-Schiff base auxiliary.[214,215] Pleasingly the enantiomeric purity of DMACA was 97%.

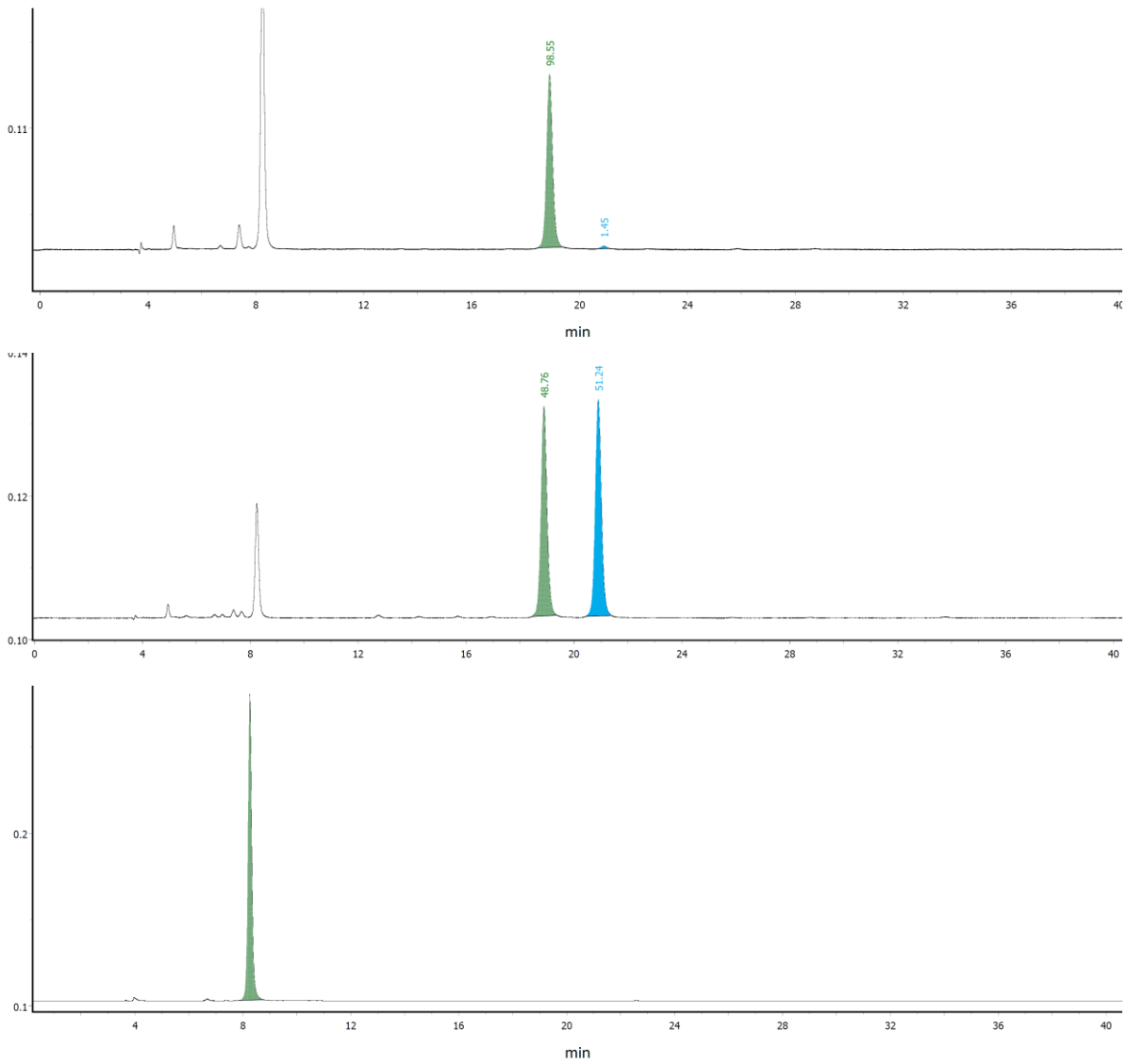

Figure 4.6 Marfey Analysis of DMACA (4.7). Analytical HPLC of L-DMACA (**4.7**) following derivatization with Marfey's reagent (top); racemic-DMACA following derivatization with Marfey's reagent (middle); Marfey's reagent (bottom)

The major enantiomer of DEACA was also found to elute before the minor enantiomer (Figure 4.7). In this case the enantiomeric purity was lower (90%) than for DMACA. The separation of diastereomers was perhaps less efficient following the alkylation of **4.15**. It is also possible that the difference is due to the use of recovered *N*-benzyl proline benzophenone ligand, which may have racemized to some extent, though the use of recovered ligand has been reported in the literature.[214,219]

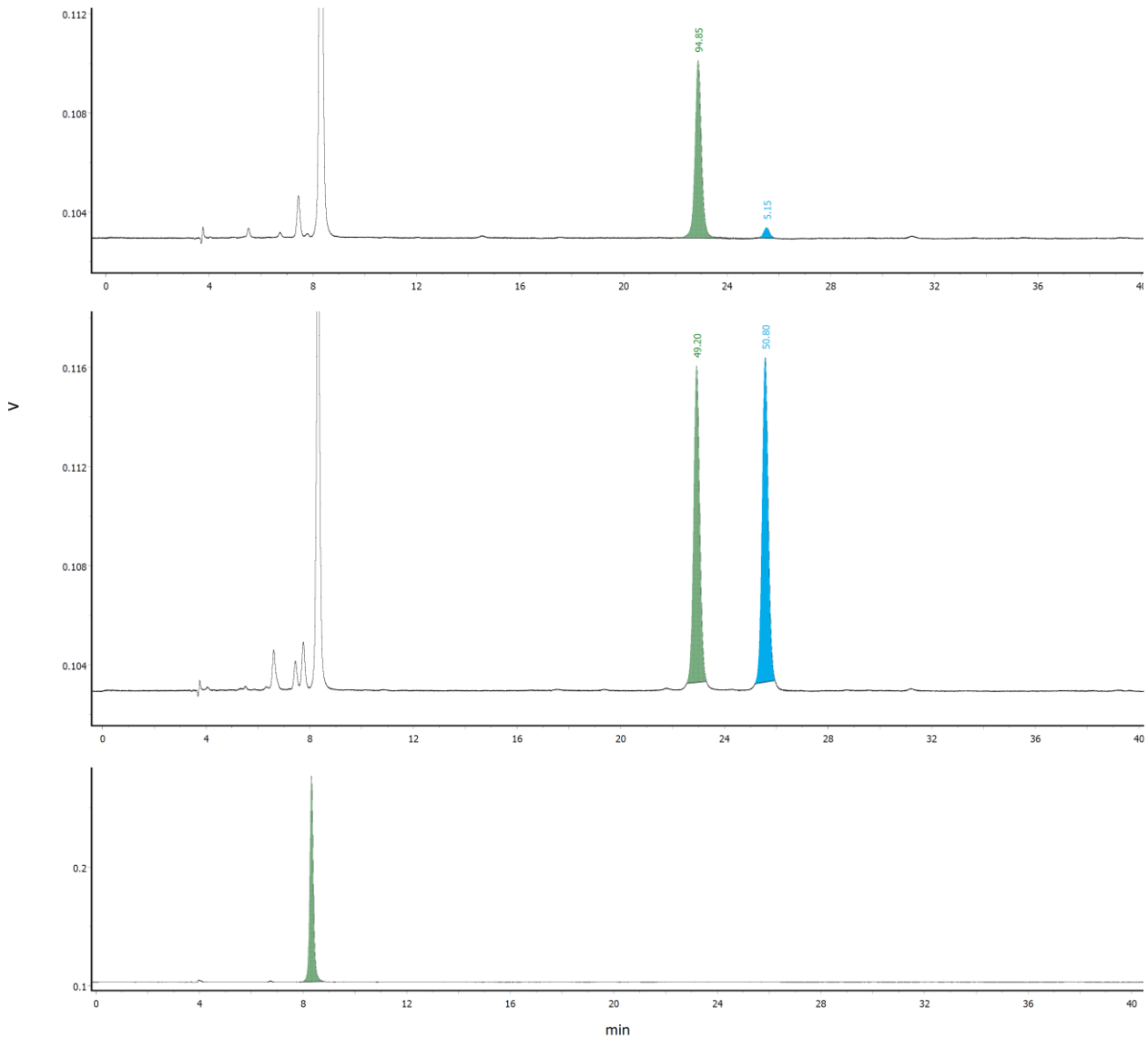

Figure 4.7 Marfey analysis of DEACA (4.8). Analytical HPLC of L-DEACA (**4.8**) following derivatization with Marfey's reagent (top); racemic-DEACA following derivatization with Marfey's reagent (middle); Marfey's reagent (bottom)

4.3.3 Incorporation of DEACA and DMACA into Peptides and their Photophysical Properties

To investigate their photophysical properties and suitability for Fmoc-SPPS, compounds **4.18** and **4.19** were incorporated into simple tripeptides bearing Ala at the *N* and *C*-terminal positions (H-Ala-DMACA-Ala-OH (**4.20**) and H-Ala-DEACA-Ala-OH (**4.21**)). The fluorescent residues proved to be stable to 20% piperidine in DMF, coupling reagents, and deprotection with concentrated TFA and typical scavengers. Interestingly, a sample of **4.20** exhibited a loss of 14 amu (likely loss of an *N*-methyl group) after several weeks in a MeCN/H_2O solution on the benchtop. Dealkylation of 7-dialkyl-4-methylaminocoumarin by singlet-oxygen has been reported by von Trebra and Koch.[197] However, no decomposition of **4.18-4.21** was observed so long as reasonable precautions were taken; namely minimizing prolonged exposure to light and storing long-term at low temperature, preferably as a dry solid.

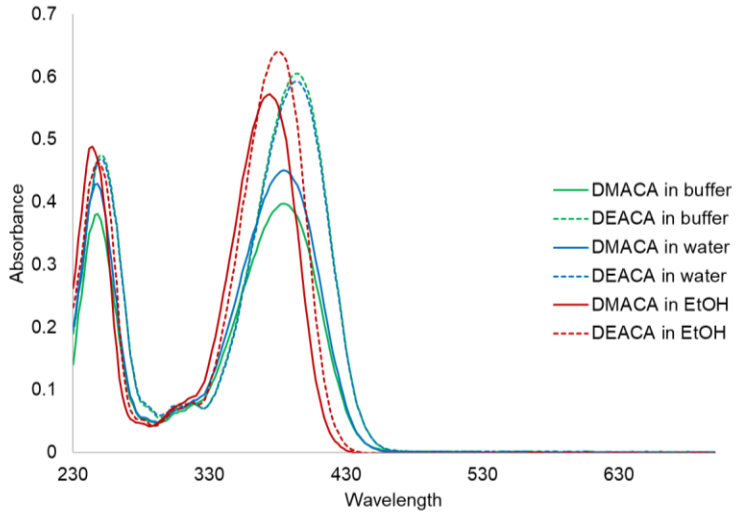

Figure 4.8 Absorbance spectra of tripeptides 4.20 & 4.21. Absorbance spectra (λ =230–700nm) were collected for tripeptides containing either DMACA (**4.20**) or DEACA (**4.21**) at position-2. A 4 mM peptide solution in ACN/H_2O (4:1) was diluted 100-fold in: 20 mM HEPES/150 mM NaCl pH 7.4 buffer (green), water (blue), or ethanol (red).

Both **4.20** and **4.21** exhibited absorption maxima near 380 nm in water or ethanol (Figure 4.8). Excitation at this wavelength resulted in fluorescence that was highly solvent-dependent. In aqueous solution both coumarins exhibited maximum fluorescence at approximately 480 nm. Decreasing solvent polarity resulted in a dramatic increase in fluorescence intensity, as well as a distinct blue-shift as shown in Figure 4.9. The spectroscopic properties of these coumarin-containing tripeptides in water and ethanol are given in Table 4.1. The quantum yields for **4.20** and **4.21** were 0.70 and 0.63, respectively in ethanol, and 0.21 and 0.12, respectively in water.

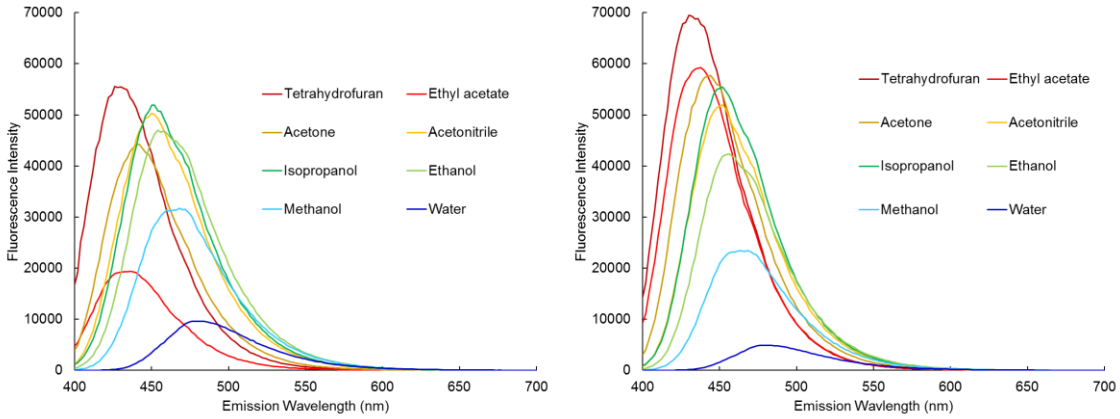

Figure 4.9 Emission spectra of tripeptides 4.20 (left) and 4.21 (right) in solvents of varying polarity. λ_{ex} = 380 nm.

Table 4.1 Spectroscopic properties of tripeptides 4.20 and 4.21.

Peptide	Solvent	$\lambda_{Abs.}$ max (nm)	$\lambda_{Em.}$ max (nm)	Stokes shift (cm^{-1})	ε ($cm^{-1}M^{-1}$)[a]	Φ_F [b]
4.20	H_2O	385	480	5140	1.5×10^4	0.21
	EtOH	373	457	4930	1.7×10^4	0.70
4.21	H_2O	393	483	4740	1.8×10^4	0.12
	EtOH	381	456	4320	2.0×10^4	0.63

[a] Extinction coefficient at $\lambda_{abs.}$ max. [b] Relative quantum yield using quinine sulfate in 0.5 M H_2SO_4 as a standard

4.3.4 Incorporation of DMACA and DEACA into Paenibacterin

To investigate the potential of these FLAAs for probing biological interactions, DMACA was incorporated into an analog of the broad-spectrum peptide antibiotic paenibacterin A1 (PA1, Figure 4.10).[41] PA1 is a one member of a family of recently discovered cyclic lipodepsipeptide antibiotics (cLPAs) produced by the soil bacterium *Paenibacillus thiaminolyticus.* It is active against both Gram-negative (Gram-(−)) and Gram positive (Gram-(+)) bacteria including methicillin-resistant *Staphylococcus aureus* and vancomycin-resistant enterococci.[45] The antibiotic activity of PA1 has been attributed to disruption of the outer membrane of Gram-(−) bacteria and damage of the cytoplasmic membrane of both Gram-(−) and Gram-(+) bacteria (see section 1.3.1.3).[43]

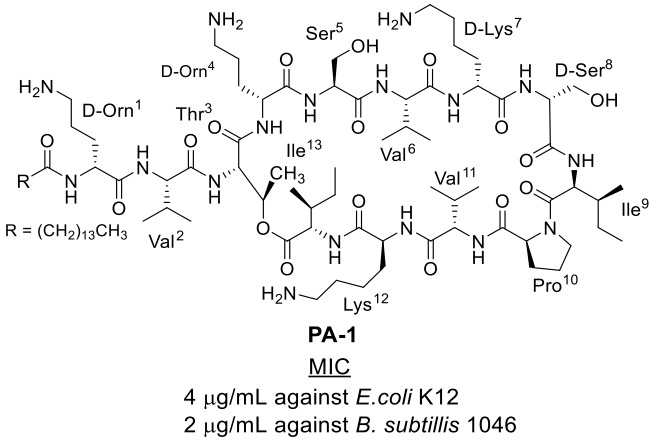

Figure 4.10 Structure of paenibacterin A1.

We have previously reported an Fmoc solid phase total synthesis of PA1 (see Chapter 2).[1] In this synthesis, a linear peptide was prepared that started with Pro10 attached to the resin and extended to lipidated D-Orn1. The ester bond was then formed between Thr3 and Ile13 and the resulting branched peptide extended to include Lys12 and Val11. The use of a pseudoproline dipeptide at residues 4 and 5 was found to significantly increase esterification yields. Cleavage of the protected peptide from the resin followed by cyclization and global deprotection gave PA1. However, partial epimerization of the

Ile13 residue occurred during the esterification reaction. Although the resulting epimers were separable by semi-preparative HPLC, we sought a method to further reduce epimerization. We also wished to determine if the D-Orn residues at positions 4 and 1 could be replaced with more economical D-Lys residues. We expected that shortening of the linear peptide onto which Ile13 is coupled would further suppress aggregation. This would accelerate the esterification and should then reduce epimerization.[144] As expected, we found that formation of the ester bond on peptide **4.22**, which does not contain an acylated residue at position 1, using DIC/DMAP (cat.) in the presence of Triton X-100,[144] resulted in no detectable epimerization (Scheme 4.5). This approach required the use of an alloc group for protection of the Ile13 residue since it is orthogonal to the Fmoc protecting group and allowed for elongation of the resulting peptide **4.23** to the acyl tail (peptide **4.24**) before deprotection of N^{α}-Ile and further couplings. The remaining amino acid couplings, resin-cleavage, cyclization, and deprotection are essentially identical to the originally reported procedure with only minor deviations. Using this method, an analog of paenibacterin A1 (PA1) was prepared containing D-Lys residues in place of D-Orn at positions 1 and 4 (peptide **4.25**), in a very good yield of 40%. Unexpectedly, this analog exhibited somewhat improved activity against both *Escherichia coli* K-12 and *Bacillus subtilis* 1046 compared to native PA1 (Scheme 4.5).[1]

We elected to incorporate DMACA and DEACA into peptide **4.25** at position 6. We anticipated that this position would tolerate substitution with aromatic residues without major loss in activity, since a recently isolated family of peptides from *Paenibacillus alvei* bears a similarity to paenibacterin and contains Tyr or Phe residues at that position (the paenibacterin B series, see section 1.3.2).[57] The target peptides **4.26** and **4.27** were prepared in a 41% yield and 49% yield, respectively (Scheme 4.5). Peptide **4.26** was two-fold less active than peptide **4.25** against *B. subtilis* and *E. coli* (Scheme 4.5). Peptide **4.27** was two-fold less active than peptide **4.25** against *B. subtilis* and 4-fold less active against *E. coli*

(Scheme 4.5). Because of its better activity, the DMACA-containing analog, **4.26**, was selected for further studies instead of peptide **4.27**.

Scheme 4.5 Synthesis of peptides 4.25-4.27.

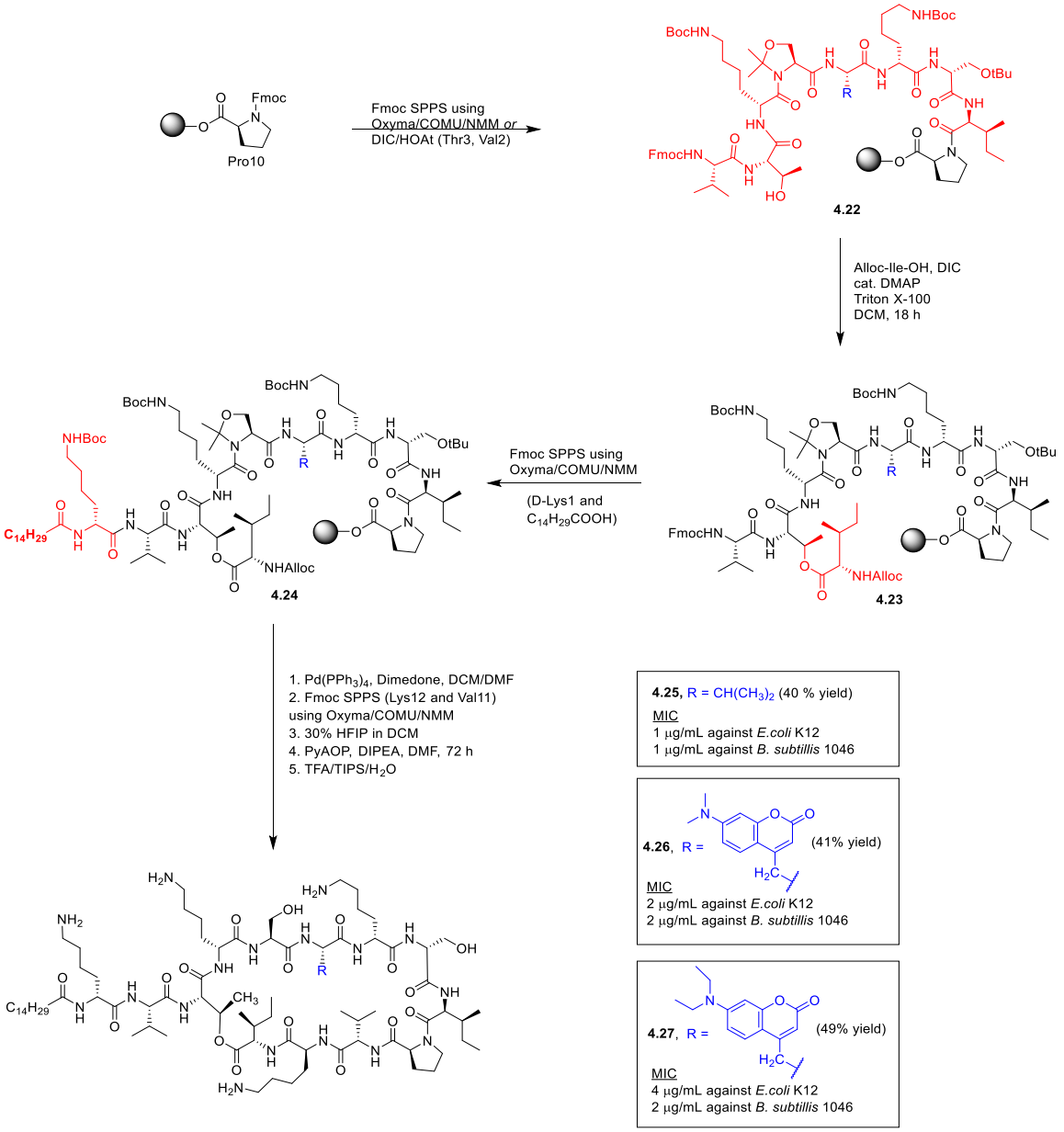

4.3.5 MOA Studies Using DMACA-Labeled Paenibacterin

Since it is known that paenibacterin disrupts the bacterial cytoplasmic membrane, we hypothesized that insertion of the peptide into the hydrophobic membrane interior would result in an observable increase in coumarin fluorescence intensity. As phosphatidylglycerol (PG) is a common component of Gram-(+) bacterial membranes, we prepared liposomes, consisting of either oleoyl or myristoyl lipids and varying amounts of PG or phosphatidyl choline (PC). An increase in fluorescence of peptide **4.26** was observed in the presence of these lipids as shown in Figure 4.11 A and B. We observed greater fluorescence intensity with liposomes containing 25% or 50% PG. This effect was more pronounced with the myristoyl lipids. It stands to reason that the presence of anionic PG would result in increased association of the cationic peptide, and this suggests that PG lipids may have a role in paenibacterin's mechanism of action against Gram-(+) bacteria as this lipid is present in the cell membranes of many Gram-(+) bacteria.

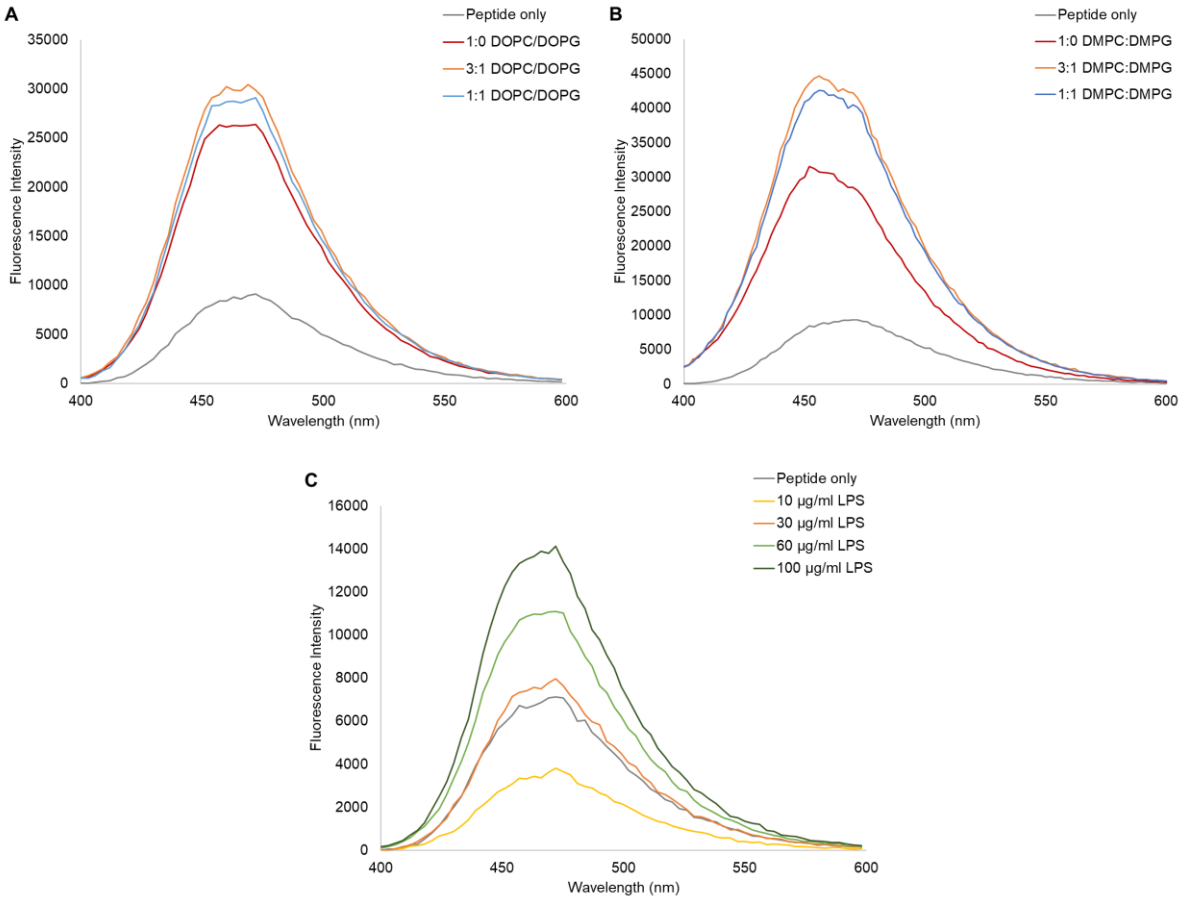

Figure 4.11 Interaction of peptide 4.26 (3 µM) with liposomes and LPS. A: DOPC/DOPG liposomes (250 µM). **B:** DMPC/DMPG liposomes (250 µM). **C:** *E. coli* LPS. Studies were conducted in 20 mM HEPES, 150 mM NaCl, pH 7.4 at 37 °C. λ_{ex} = 380 nm, λ_{em} = 400–600 nm.

Since studies suggest that paenibacterin interacts with lipopolysacharides (LPS, also known as endotoxins) in the outer membrane of Gram-(−) bacteria,[43,45] we also examined the interaction of peptide **4.26** with LPS. Based on prior studies of a similar nature conducted by others on the interaction between dansyl polymyxin and LPS, we expected to observe a large increase in fluorescence upon binding of **4.26** to LPS.[220,221] Instead, at 10 µg/ml of LPS, we observed quenching of fluorescence (Figure 4.11C). The expected increase in fluorescence was only observed at concentrations of LPS ≥

30 μg/ml (Figure 4.11C), which is above the range of typical critical micelle concentrations (CMC) reported for *E. coli* LPS (14–22 μg/mL).[222,223] The decrease in fluorescence at 10 μg/ml of LPS suggests that in the absence of LPS micelles or aggregates into which the peptide can insert, we instead see association with LPS that suppresses fluorescence emission. This can also be seen if LPS is titrated into a solution of peptide **4.26** (Figure 4.12). This results in a steady reduction in fluorescence until an LPS concentration of 12 μg/ml, at which point no further decrease occurs at 15 μg/ml LPS. The most probable explanation for this decrease in fluorescence is concentration-dependent self-quenching which is indicative of aggregation of the peptide-LPS complex. This explanation is supported by the finding that the extent of quenching is reduced when non-fluorescent peptide **4.25** is mixed with an excess of fluorescent peptide **4.26** before addition of LPS (Figure 4.13). Within the hybrid aggregates formed from these mixtures, the fluorescent peptides are separated from one another, and less quenching is observed (Figure 4.13 B & C). These results suggest that paenibacterin binds to free LPS, and the resulting paenibacterin-LPS complex readily aggregates.

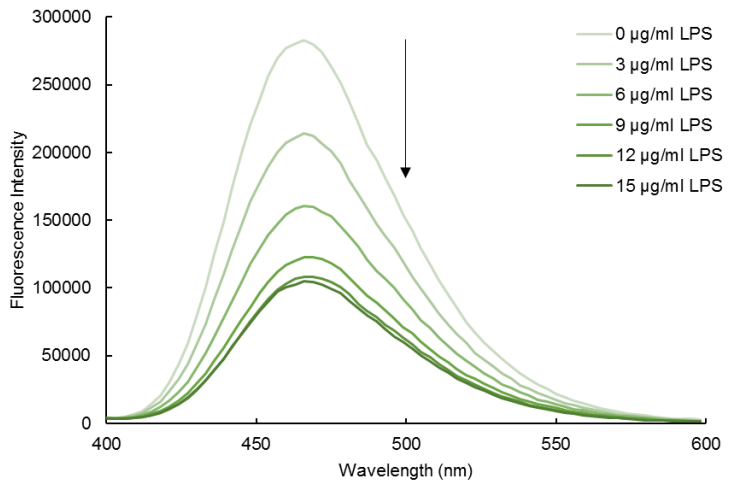

Figure 4.12 Titration of peptide 4.26 (3 µM) with LPS in buffer (pH 7.2, 5 mM HEPES). λ_{ex} = 380 nm, λ_{em} = 400–600 nm.

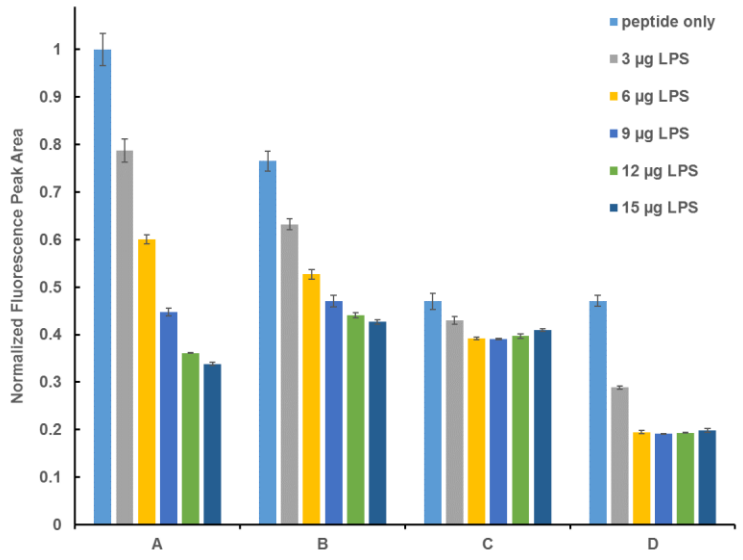

Figure 4.13 Effect of LPS on the fluorescence of peptide 4.26 in the presence and absence of peptide 4.25 in 5 mM HEPES. pH 7.2. λ_{ex} = 380 nm, λ_{em} = 400–600 nm. **A:** Peptide **4.26** (3 µM) alone. **B:** 3:1 mixture of peptide **4.26** and peptide **4.25** (3 µM total). **C:** 1:1 mixture of peptide **4.26** and peptide **4.25** (3 µM total). **D:** Peptide **4.26** (1.5 µM) alone.

To demonstrate that peptides containing these fluorescent amino acids can be used to image Gram-(+) and Gram-(−) bacteria by confocal microscopy, live *E. coli* or *B. subtilis* were suspended in a solution of **4.26**, then the suspension was added directly to an agarose pad. The staining procedure was very convenient, and no rinsing steps were necessary. As expected, DMACA appears to exhibit a large increase in brightness upon insertion into the cell. Because of this increase in brightness, the background fluorescence was negligible, and the stained bacteria were clearly visible. For *B. subtills*, the peptide appears to be capable of entering the cell. For *E. coli*, a modest increase in brightness was observed at the membrane, particularly at polar regions of the cell. The cause of this effect has not yet been determined but may indicate that paenibacterin accumulates at the cell poles. We anticipate that this fluorescent analog will facilitate the further study paenibacterin's mechanism of action, allowing us to observe its effects on bacterial cells over time. We also anticipate that DMACA or DEACA could be incorporated into other peptide antibiotics to give fluorescent analogs of sufficient brightness to be easily visualized by fluorescence microscopy.

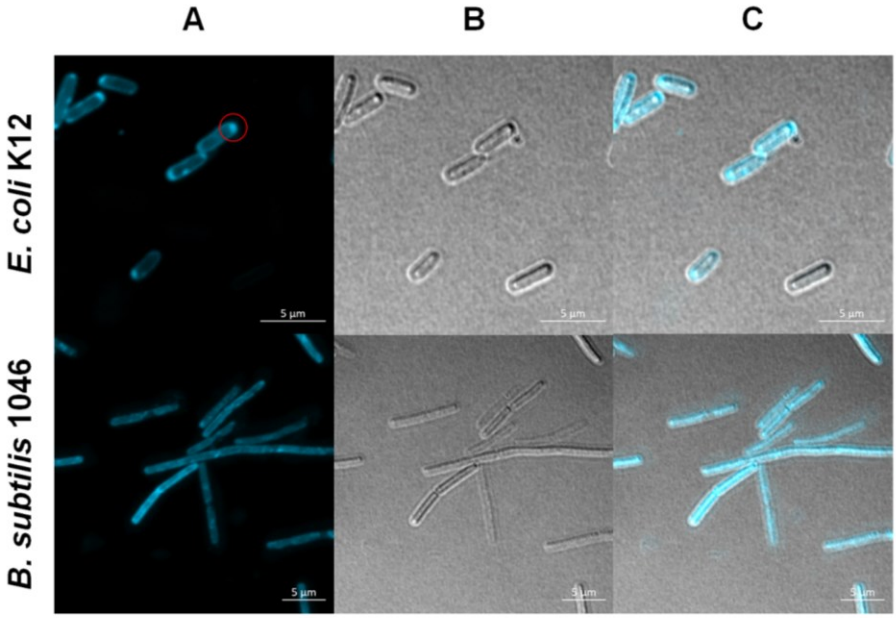

Figure 4.14 Micrographs of bacteria stained with 30 µg/ml peptide 4.26 in 1×PBS for 30 min. A: Confocal laser scanning micrograph (405 nm excitation). **B:** Differential interference contrast (DIC) micrograph. **C:** Merged image. Bacteria are immobilized on 1% agarose pads. The red circle highlights a bright spot found at the poles of *E. coli* cells.

Carlee Montgomery, an undergraduate in the Taylor group, incorporated DMACA and DEACA into a daptomycin analog at either position 1 or position 6. Unfortunately, the resulting peptides were inactive or poorly active against *B. subtilis* 1046 (MIC ≥ 32 µg/ml) at 1.25 mM Ca^{2+}. Of the analogs tested, only a Dap-DMACA6-E12-W13 analog was moderately active, with an MIC of 4 µg/ml; though this required elevated concentrations of calcium (5 mM). However, we were able to monitor calcium-dependent binding of these peptides to model membranes using DMACA fluorescence. Interestingly we observed the expected calcium-dependent increase in fluorescence or an unexpected calcium-dependent quenching effect depending on the position of the DMACA residue (position 1 or position 6, respectively). Clearly this quenching effect merits further study, since understanding of its root cause may provide some insight into the local environment of the fluorescent residues within a peptide.

4.3.6 Addition of Peptide 4.26 to Bacterial Cells

A modest fluorescence quenching effect is also observed if **4.26** is added to a suspension of bacterial cells. However, we observed an initial *increase* in fluorescence relative to a solution of buffer alone. In the presence of both Gram-(+) and Gram-(−) cells the magnitude of the increase in fluorescence decreases as the concentration of **4.26** approaches 3 µM (Figure 4.15).

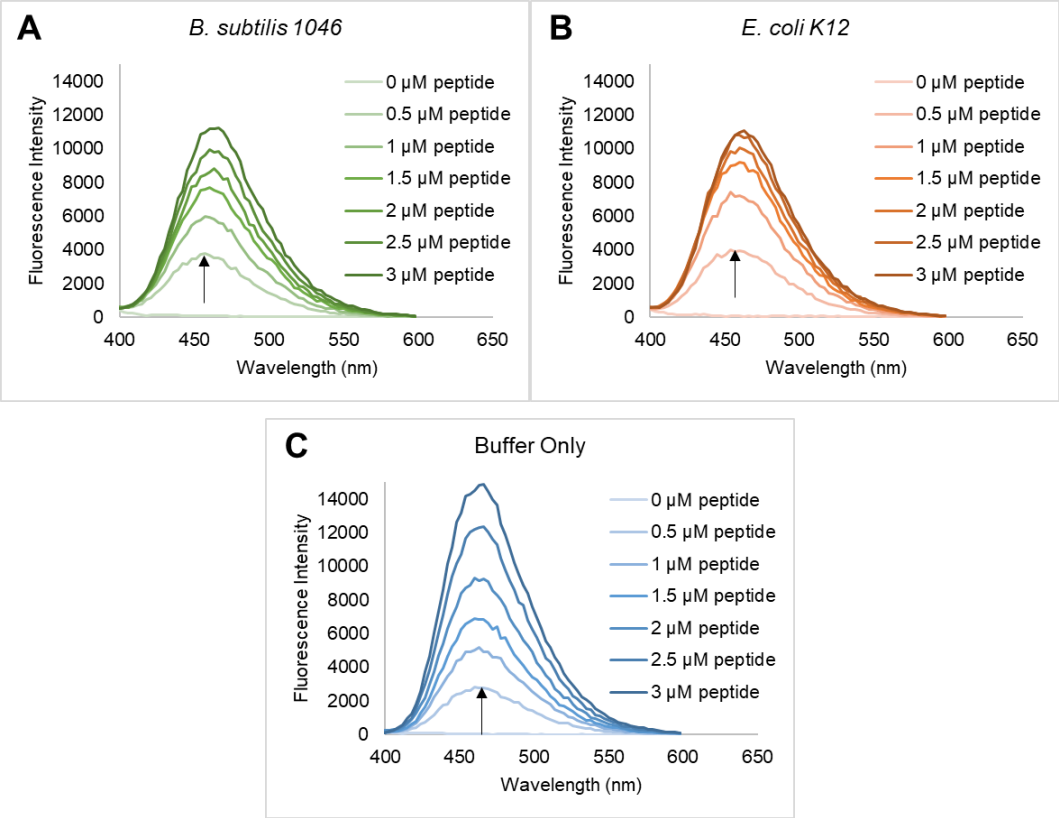

Figure 4.15 Interaction of peptide 4.26 with, (A) *B. subtilis* 1046; (B) *E. coli* K-12; and (C) buffer only. Studies were conducted in 20 mM HEPES, 150 mM NaCl, pH 7.4 at 25 °C. λ_{ex} = 380 nm, λ_{em} = 400–600 nm.

This effect is better visualized by plotting the peak area against the concentration of **4.26** (Figure 4.16). As expected, the increase in fluorescence upon addition to buffer appears linear, while in the

presence of bacteria there is an initial rapid increase in fluorescence, but at 2.5 µM of peptide the fluorescence intensity is less than that of the buffer control.

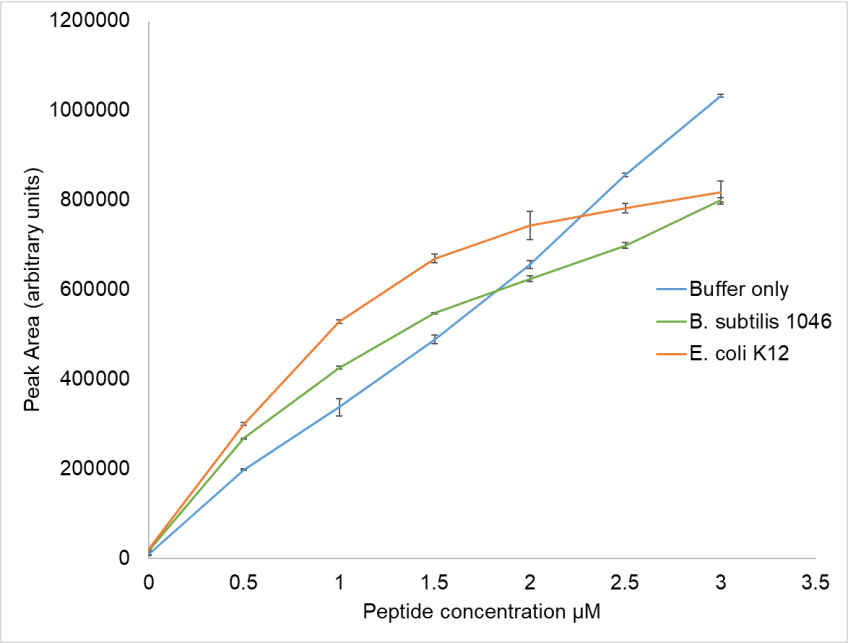

Figure 4.16 Fluorescence peak area when peptide 4.26 is added to a suspension of bacterial cells or buffer alone. Studies were conducted in 20 mM HEPES, 150 mM NaCl, pH 7.4 at 25 °C. λ_{ex} = 380 nm, λ_{em} = 400–600 nm.

The observed quenching effect may suggest that as the concentration of paenibacterin increases, it aggregates or self-associates in the bacterial membrane, resulting in fluorophore self-quenching. Whether paenibacterin oligomerizes in the membrane will be investigated in future studies.

4.4 Conclusions and future work

We have developed a facile method for the enantioselective synthesis of two 7-dialkylamino coumarin amino acids, DMACA and DEACA, suitable for use in Fmoc-SPPS. These amino acids function as environmental probes, exhibiting an increase in fluorescence as environment polarity decreases. We also report a synthesis of a highly active PA1 analog using an improved route employing mainly Fmoc chemistry. This route was used to prepare peptide **4.26**, a PA1 analog containing DMACA. Peptide **4.26** exhibited increased fluorescence in the presence of liposomes, and a greater increase if PG was present, suggesting that the presence of PG in bacterial membranes may promote membrane binding. Simple staining of bacterial cells with **4.26** allowed for direct visualization using fluorescence microscopy. Above the CMC of LPS, peptide **4.26** showed an increase in fluorescence consistent with the peptide inserting into a hydrophobic micelle or aggregate. In the presence of sub-CMCs of LPS, peptide **4.26** showed concentration-dependent self-quenching, which is indicative of binding to free LPS followed by aggregation of the peptide-LPS complex. LPS or endotoxins are powerful activators of septic shock. Inappropriate antibiotic treatment can induce the liberation of LPS into the circulation and cause septic shock.[224–226] Huang and Ahmed have suggested that paenibacterin may neutralise released LPS and thus may be capable of reducing sepsis during antibiotic treatment.[45] Our results lend support to this hypothesis as they indicate that paenibacterin is capable of binding to free LPS. Peptide **4.26** also allowed for direct visualization of the bacteria using fluorescence microscopy.

The results discussed in this chapter suggest that paenibacterin may aggregate when bound to LPS, resulting in fluorophore self-quenching. Future studies should probe this effect in more detail using the pyrene-labelled analog described earlier in chapter 3. Pyrene excimer formation between paenibacterin molecules would provide strong evidence for the formation of tight aggregates. These studies may also provide insight into why a large increase in fluorescence is observed in the presence of phospholipid vesicles, but not with Gram-(+) bacterial cells. Also, while peptide **4.26** is useful for immediate

visualization of the interaction of paenibacterin with bacterial cells, these imaging results should be supplemented with images of bacteria stained with a paenibacterin analog bearing a non-environmentally sensitive fluorophore (e.g., BODIPY). This would allow for more reliable localization of paenibacterin within the bacterium.

We anticipate that this fluorescent probe will facilitate further mechanism of action studies, allowing us to observe the effects of paenibacterin on bacterial cells over time. Immobilization on agarose gel allows for relatively simple imaging of live bacteria over prolonged periods of time.[227,228] This has been used to directly examine the insertion of antibacterial peptides into bacterial cells, providing timescales for penetration of bacterial membranes and accumulation within the cytoplasm.[229]

4.5 Experimental

General. Commercially available reagents were used without further purification. The Gly/Ni(II)/BPB auxiliary (**4.15**) was prepared as described in the literature.[230–232] Alloc-Ile was prepared following literature procedures.[157] DMF, 4-methylpiperidine (4-MP), 2-methylpiperidine (2-MP), TFA, were purchased from commercial suppliers and used without further purification. Tetrahydrofuran (THF) was dried over sodium metal and benzophenone. Dichloromethane (DCM) was dried over calcium hydride. High resolution mass spectra were acquired using an Orbitrap instrument in positive electrospray ionization mode (+ESI). Minimum inhibitory concentrations were determined by the broth dilution method as previously described.[1,162] For all reactions that required heating, the reaction flask was immersed in a hot oil bath.

7-(Dimethylamino)-4-methyl-2H-chromen-2-one (4.9). Compound **4.9** was prepared according to the procedure reported by von Pechmann.[211] To a solution of zinc chloride (2.50 g, 18.3 mmol, 0.5 equiv) in ethanol (10 ml) was added ethyl acetoacetate (5.35 ml, 42.3 mmol, 1.16 equiv) and 3-(dimethylamino)phenol (5.00 g, 36.4 mmol, 1.0 equiv). The solution was heated to reflux under nitrogen for 20 h. After cooling to room temperature, the mixture was poured into 75 ml of 0.5% HCl (aq.) and slowly stirred for 2 h. The resulting green solid was filtered and rinsed with water. The solid was dissolved in minimal concentrated HCl (aq.) then precipitated with 200 ml of water. The solid was collected by suction filtration then recrystallized from 90% EtOH to give compound **3** as purple-red crystals (4.52 g, 22.1 mmol, 61% yield). The NMR spectra of the product closely matched what had previously been reported.[233,234] ^{1}H NMR ($CDCl_3$, 300 MHz): δ 7.38 (d, 1H, J = 8.7 Hz), 6.60 (dd, 1H, J = 8.7 Hz, 2.1 Hz), 6.50 (s, 1H), 5.95 (s, 1H), 3.03 (s, 6H), 2.33 (s, 3H); HRMS (+ESI) m/z: $[M + H]^+$ calcd for $C_{12}H_{14}NO_2$ 204.1019; found 204.1037.

4-(Bromomethyl)-7-(dimethylamino)-2H-chromen-2-one (4.11). Compound **4.11** was prepared following a literature procedure for the bromination of coumarin **4.10**.[212] Compound **4.9** (1.4 g, 6.9

mmol, 1 equiv) was dispersed in dry THF (70 ml) then cooled to –41 °C in an acetonitrile-dry ice bath. LiHMDS was added as a 1M solution in THF (17.3 ml, 17.3 mmol, 2.5 equiv) then the bath was allowed to warm to –30 °C at which point the flask was transferred to an acetone-dry ice bath and cooled to –78 °C. *N*-bromosuccinimide (1.47 g, 8.28 mmol, 1.2 equiv) was added as a solution in dry THF (20 ml). After stirring for 30 min at –78 °C the reaction was quenched with 0.1 N HCl (100 ml). The mixture was extracted several times with DCM. The organic fractions contained an insoluble yellow solid. The combined organic extracts were concentrated by rotary evaporation then resuspended in EtOAc and concentrated again. The resulting orange-yellow solid was suspended in minimal EtOAc and filtered, rinsing with cold EtOAc which gave **4.11** as a yellow solid (1.50 g, 5.3 mmol, 77% yield). ^{1}H NMR (CD_2Cl_2, 300 MHz): δ 7.54 (d, 1H, *J* = 8.9 Hz), 6.72 (dd, 1H, *J* = 8.9, 2.5 Hz), 6.57 (d, 1H, *J* = 2.4 Hz), 6.14 (s, 1H), 4.44 (s, 2H), 3.06 (s, 6H); ^{13}C{^{1}H} NMR (CD_2Cl_2, 75 MHz): δ 161.1, 156.3, 152.9, 150.3, 125.2, 110.0, 109.1, 106.9, 98.5, 40.1, 27.3; HRMS (+ESI) *m/z*: $[M + H]^+$ calcd for $C_{12}H_{13}{}^{79}BrNO_2$ 282.0124; found 282.0149.

4-(Bromomethyl)-7-(diethylamino)-2H-chromen-2-one (4.12). Compound **4.12** was prepared in 59–66% yield from **4.10** according to the procedure reported by Li et al.[212] The NMR spectra of the product matched what was reported in literature. ^{1}H NMR ($CDCl_3$, 300 MHz): δ 7.47 (d, 1H, *J* = 8.9 Hz), 6.60 (dd, 1H, *J* = 8.9, 2.2 Hz), 6.49 (d, 1H, *J* = 2.2 Hz), 6.12 (s, 1H), 4.37 (s, 2H), 3.40 (q, 4H, *J* = 7.2 Hz), 1.20 (t, 6H, *J* = 7.0 Hz); ^{13}C{^{1}H} NMR ($CDCl_3$, 75 MHz): δ 161.7, 156.7, 150.9, 150.3, 125.3, 109.2, 108.6, 106.1, 97.8, 44.8, 27.1, 12.4; HRMS (+ESI) *m/z*: $[M + H]^+$ calcd for $C_{14}H_{17}{}^{79}BrNO_2$ 310.0437; found 310.0466.

Benzyl (3S,5S,6R)-3-((7-(dimethylamino)-2-oxo-2H-chromen-4-yl)methyl)-2-oxo-5,6-diphenylmorpholine-4-carboxylate (4.13). Bromocoumarin **4.11** (423 mg, 1.50 mmol, 1.06 equiv) and (5*S*,6*R*)-4-benzyloxycarbonyl-5,6-diphenylmorpholin-2-one (552 mg, 1.42 mmol, 1 equiv) were dispersed in dry THF (27 ml) and HMPA (3 ml) before cooling to –78 °C then 1M NaHMDS in THF

(1.5 ml, 1.5 mmol, 1.06 equiv) was added dropwise. After 2h the solution was warmed to 0 °C and stirred for a further 30 min before warming to room temperature. The reaction mixture was diluted in DCM (200 ml) and washed with water (3 × 50 ml) and brine before condensing. Dissolved the residue in a minimal volume of DCM by heating, then precipitated by the addition of heptane. The resulting suspension was decanted to separate the product from a red residue. The yellow solid was then collected by centrifugation, giving **4.13** (316 mg, 0.54 mmol, 38% yield). ^{1}H NMR ($(CD_3)_2SO$, 300 MHz): rotameric mixture δ 8.03 (d, 1H, *J* = 9.0 Hz), 7.50–6.98 (m, 12H), 6.84–6.44 (m, 6H), 6.18–6.05 (m, 1H), 5.42–5.31 (m, 1H), 5.21–4.86 (m, 3H), 3.65 (td_{app}, 1H, *J* = 11.7, 4.5 Hz), 3.42 (t, 1H, *J* = 11.7 Hz), 2.99 (m, 6H); $^{13}C\{^{1}H\}$ NMR ($(CD_3)_2SO$, 75 MHz): rotameric mixture δ 166.9, 161.1, 161.0, 156.0, 155.8, 154.4, 153.4, 153.1, 151.6, 151.4, 136.7, 136.4, 136.2, 136.0, 135.2, 135.1, 129.3, 129.1, 128.9, 128.7, 128.5, 128.4, 128.3, 128.0, 127.9, 127.7, 127.6, 126.9, 126.8, 126.0, 125.5, 110.6, 110.4, 109.9, 109.4, 108.3, 108.0, 98.2, 78.4, 68.2, 67.2, 60.5, 60.4, 57.0, 40.2, 35.3; ESI-MS *m/z*: $[M + H]^+$ calcd for $C_{36}H_{33}N_2O_6$ 589.2333; found 589. 2310.

Benzyl (3S,5S,6R)-3-((7-(diethylamino)-2-oxo-2H-chromen-4-yl)methyl)-2-oxo-5,6-diphenylmorpholine-4-carboxylate (4.14). Bromocoumarin **4.12** (310 mg, 1 mmol, 1 equiv) and (5*S*,6*R*)-4-benzyloxycarbonyl-5,6-diphenylmorpholin-2-one (387 mg, 1 mmol, 1 equiv) were dispersed in dry THF (20 ml) before cooling to –78 °C then 1M NaHMDS in THF (1.1 ml, 1.1 mmol, 1.1 equiv) was added dropwise. After 2h the solution was warmed to room temperature. The reaction mixture was diluted in DCM (100 ml), washed with water (3 × 20 ml) and brine, dried over Na_2SO_4 and condensed. The product (R_f = 0.26, 10:0.5:0.1 DCM/EtOAc/Triethylamine) was isolated by flash chromatography giving **4.14** (455 mg, 0.74 mmol, 74% yield). ^{1}H NMR ($CDCl_3$, 300 MHz): rotameric mixture δ 7.78 (d, 1H, *J* = 9.0 Hz), 7.46–6.39 (m, 17H), 6.00–5.62 (m, 2H), 5.50–4.90 (m, 5H), 3.78–3.48 (m, 6H), 1.19 (m, 6H); $^{13}C\{^{1}H\}$ NMR ($(CD_3)_2SO$, 75 MHz): rotameric mixture δ 161.1, 161.0, 156.5, 156.3, 154.4, 153.4, 151.5, 151.3, 150.9, 150.6, 136.7, 136.4, 136.2, 136.0, 135.2, 135.1, 129.5, 129.1, 128.9,

128.7, 128.5, 128.4, 128.0, 127.7, 127.6, 127.1, 126.9, 126.8, 126.6, 126.3, 125.8, 110.1, 109.9, 109.4, 108.8, 107.8, 107.4, 97.5, 79.3, 78.4, 68.3, 67.2, 66.9, 60.4, 57.1, 46.0, 44.5, 36.2, 35.4, 12.8; ESI-MS *m/z*: $[M + H]^+$ calcd for $C_{38}H_{37}N_2O_6$ 617.2646; found 617.2644.

(*S*)-BPB/Ni(II)/(*S*)-2-amino-3-(7-(dimethylamino)-2-oxo-2H-chromen-4-yl)propanoic acid complex (4.16). Bromocoumarin **4.11** (2.82 g, 10.0 mmol, 1 equiv) and Gly/Ni(II)/BPB auxiliary, **4.15**, (4.98 g, 10.0 mmol, 1 equiv) were dissolved in dry DMF (20 ml) and the solution was degassed by bubbling Ar through the solution. Ground NaOH (1 g, 25 mmol, 2.5 eq) was added and the solution was stirred at room temperature for 30 min. The solution was then poured into 0.5 M AcOH (aq., 100 ml) which was then extracted with DCM (3x). The organic extracts were concentrated by rotary evaporation then re-dissolved in EtOAc (200 ml) and washed with H_2O (6 × 70 mL) and once with brine. The major diastereomer (R_f = 0.27, 2:1 DCM/acetone) was isolated by flash chromatography (4:1 to 7:3 DCM/acetone) to give **4.16** as a red solid (3.84 g, 5.49 mmol, 55% yield). ^{1}H NMR ($CDCl_3$, 500 MHz): δ 8.22 (d, 1H, *J* = 8.7 Hz), 8.03 (d, 2H, *J* = 7.7 Hz), 7.53–7.43 (m, 2H), 7.40–7.27 (m, 4H), 7.19–7.12 (m, 2H), 6.90 (d, 1H, *J* = 8.7 Hz), 6.79 (d, 1H, *J* = 7.6 Hz), 6.68–6.59 (m, 2H), 6.46 (d, 1H, *J* = 2.3 Hz), 6.29 (dd, 1H, *J* = 8.8, 2.5 Hz), 5.87 (s, 1H), 4.40–4.31 (m, 2H), 3.52 (d, 1H, *J* = 12.8 Hz), 3.45–3.31 (m, 5H), 3.00 (s, 6H), 2.68–2.59 (m, 1H), 2.57–2.44 (m, 1H), 2.20–1.99 (m, 3H); ^{13}C{^{1}H} NMR ($CDCl_3$, 75 MHz): δ 180.2, 177.4, 171.3, 161.3, 156.0, 152.9, 150.3, 142.9, 133.6, 133.3, 133.2, 132.7, 131.5, 129.9, 129.0, 128.9, 128.2, 127.6, 125.9, 125.2, 123.6, 120.6, 111.0, 108.8, 108.7, 98.2, 70.4, 69.9, 63.2, 57.3, 40.1, 38.1, 30.8, 24.0; HRMS (+ESI) *m/z*: $[M + H]^+$ calcd for $C_{39}H_{37}N_4NiO_5$ 699.2112; found 699.2097. The minor diastereomer (R_f = 0.38, 2:1 DCM:acetone) was isolated as a mixture with an unidentified impurity and was not further purified.

(*S*)-BPB/Ni(II)/ (*S*)-2-amino-3-(7-(diethylamino)-2-oxo-2H-chromen-4-yl)propanoic acid (4.17). The Gly/Ni(II)/BPB auxiliary **4.15** (2.14 g, 5.00 mmol, 1 equiv) was alkylated with bromocoumarin 4.12 (1.55 g, 5.00 mmol) and NaOH (0.500 g, 12.5 mmol, 2.5 equiv) using the same procedure

described above for compound **4.16**. The major diastereomer (R_f = 0.39, 2:1 DCM/acetone) was isolated by flash chromatography (3:1 DCM/acetone) to give **4.17** as a red solid (1.94 g, 2.66 mmol, 53% yield). ^{1}H NMR ($CDCl_3$, 300 MHz): δ 8.22 (d, 1H, *J* = 8.8 Hz), 8.02 (d, 2H, *J* = 7.4 Hz), 7.52–7.28 (m, 6H), 7.19–7.09 (m, 2H), 6.89 (d, 1H, *J* = 9.1 Hz), 6.76 (d, 2H, J = 7.5 Hz), 6.69–6.57 (m, 2H), 6.43 (d, 1H, *J* = 2.5 Hz), 6.25 (dd, 1H, *J* = 9.2, 2.6 Hz), 5.84 (s, 1H), 4.42–4.31 (m, 2H), 3.52 (d, 1H, *J* = 12.8 Hz), 3.48–3.24 (m, 9H), 2.72–2.42 (m, 2H), 2.20–1.96 (m, 2H), 1.16 (t, 6H, J = 7.1); ^{13}C{^{1}H} NMR ($CDCl_3$, 75 MHz): δ 180.1, 177.5, 171.3, 161.4, 156.4, 150.6, 150.3, 142.9, 133.6, 133.3, 133.2, 132.7, 131.5, 129.8, 129.0, 128.9, 128.2, 127.6, 125.9, 125.5, 123.6, 120.6, 110.4, 108.5, 108.1, 97.6, 70.4, 69.9, 63.1, 57.2, 44.7, 38.2, 30.8, 23.9, 12.4; HRMS (+ESI) m/z: $[M + H]^+$ calcd for $C_{41}H_{41}N_4NiO_5$ 727.2425; found 727.2419. The minor diastereomer (R_f = 0.5, 2:1 DCM/acetone) was also isolated as a mixture with an unidentified impurity and was not further purified.

(*S*)-2-Amino-3-(7-(dimethylamino)-2-oxo-2H-chromen-4-yl)propanoic acid (DMACA, 4.7). A solution of compound **4.16** (3.74 g, 5.35 mmol) in MeOH (64 ml) and 1M HCl (aq., 32 ml) was heated to 55–60 °C for 2 h. The solution was allowed to cool to room temperature then neutralized with ammonium hydroxide. The solution was partially concentrated in vacuo, then the aqueous suspension was washed with 3 × 75 ml EtOAc to remove the BPB ligand. The aqueous fraction was lyophilized to give a green solid that was triturated with water several times, collecting by centrifugation, to give compound 1 as a yellow-green solid (1.41 g, 95% yield, 97% *ee*). ^{1}H NMR (D_2O with 5% DCl, 500 MHz): δ 7.59 (d, 1H, *J* = 8.8 Hz), 7.31 (s, 1H), 7.24 (d, 1H, *J* = 8.3 Hz), 6.21 (s, 1H), 4.05 (t, 1H, *J* = 6.7 Hz), 3.23 (dd, 1H, *J* = 15.2, 6.6 Hz), 3.00 (dd, 1H, *J* = 14.9, 8.2 Hz), 2.90 (s, 3H); ^{13}C{^{1}H} NMR (D_2O with 5% DCl, 75 MHz): δ 169.7, 161.7, 153.2, 149.5, 144.2, 126.9, 119.4, 117.8, 117.0, 110.1, 51.1, 46.2, 31.4; HRMS (+ESI) *m/z*: $[M + H]^+$ calcd for $C_{14}H_{17}N_2O_4$ 277.1183; found 277.1189. $[\alpha]_D^{20}$ = 10.3 (*c* 0.304, 1N HCl). Enantiomeric purity was determined by derivatization with Marfey's reagent.

(*S*)-2-amino-3-(7-(diethylamino)-2-oxo-2H-chromen-4-yl)propanoic acid (DEACA, 4.8). A solution of compound **4.17** (1.5 g, 2.06 mmol) in 2:1 MeOH/1M HCl (50 ml) was heated to 50–60 ºC for 2 h. After cooling to room temperature, the mixture was neutralized with ammonium hydroxide. The solution was partially concentrated *in vacuo*, filtered and the solid rinsed several times with water, dried, and then rinsed with EtOAc which gave compound **4.8** as a yellow solid (478 mg, 76% yield, 90% *ee*). ^{1}H NMR (D_2O with 5% DCl, 500 MHz): δ 7.44 (d, 1H, *J* = 8.2 Hz), 7.08 (s, 1H), 6.99 (d, 1H, *J* = 8.1 Hz), 6.04 (s, 1H), 3.88 (br t, 1H, *J* = 6.0 Hz), 3.18–2.99 (m, 5H), 2.81 (dd, 1H, *J* = 14.4 Hz, 7.7 Hz), 0.48 (s, 6H); ^{13}C{^{1}H} NMR (D_2O with 5% DCl, 75 MHz): δ 169.7, 161.6, 153.4, 149.5, 139.3, 126.9, 119.7, 118.7, 117.8, 111.8, 53.8, 51.1, 31.4, 9.5; HRMS (+ESI) *m/z*: $[M + H]^+$ calcd for $C_{16}H_{21}N_2O_4$ 305.1496; found 305.1508. $[\alpha]_D^{20}$ = 12.1 (*c* 0.105, 1N HCl). Enantiomeric purity was determined by derivatization with Marfey's reagent.

Fmoc-DMACA (4.18). Compound **4.7** (50 mg, 0.18 mmol, 1 equiv) was dispersed in 10% Na_2CO_3 (aq., 3 ml) and dioxane (2 ml) then cooled to 0 °C. Fmoc-OSu (73 mg, 0.22 mmol, 1.2 equiv) was added dropwise as a solution in dioxane (3 ml). The solution was allowed to warm to rt then stirred for 16 h then acidified with 1M HCl and extracted with EtOAc (3 × 10 mL). The combined organic extracts were washed with brine, dried over Na_2SO_4, filtered and concentrated in vacuo. Purification by flash chromatography (toluene/EtOAc/AcOH, 8:2:0.5,) gave **4.18** as a green solid (67 mg, 72% yield).^{1}H NMR ($(CD_3)_2SO$, 300 MHz): δ 7.88–7.77 (m, 3H), 7.70–7.52 (m, 3H), 7.41–7.20 (m, 4H), 6.71 (dd, 1H, *J* = 9.0, 2.0 Hz), 6.52 (d, 1H, *J* = 2.0 Hz), 5.99 (s, 1H), 4.33–4.04 (m, 4H), 3.30–3.10 (m, 2H), 2.96 (s, 6H); ^{13}C{^{1}H} NMR ($(CD_3)_2SO$, 75 MHz): δ 173.1, 161.0, 156.4, 156.0, 153.3, 153.2, 144.2, 144.1, 141.1, 128.1, 27.5, 125.7, 125.6, 120.5, 109.7, 109.3, 108.1, 98.2, 66.2, 53.5, 47.0, 40.1, 33.1; HRMS (+ESI) *m/z*: $[M + H]^+$ calcd for $C_{29}H_{27}N_2O_6$ 499.1863; found 499.1845. Alternatively, following acidification the precipitate could be filtered then rinsed with water and ether. The resulting product is sufficiently pure for use in Fmoc-SPPS.

Fmoc-DEACA (4.19). Compound **13** was prepared from **4.8** (20 mg, 0.066 mmol, 1 equiv) using the same procedure described above for the preparation of compound **4.18**. Purification by flash chromatography (toluene/EtOAc/AcOH, 8:2:0.5) gave **4.19** as a yellow solid (23 mg, 67% yield). ^{1}H NMR ($CDCl_3$, 300 MHz): δ 7.70 (d, 2H, *J* = 7.3 Hz), 7.59 (d, 1H, *J* = 8.5 Hz), 7.52 (d, 1H, *J* = 7.4 Hz), 7.46 (d, 1H, *J* = 7.3 Hz), 7.39–7.17 (m, 4H), 6.52 (d, 1H, *J* = 8.6), 6.45 (s, 1H), 6.07 (s, 1H), 5.86 (d, 1H, *J* = 6.9 Hz), 4.72 (m, 1H), 4.37 (t, 1H, *J* = 8.0 Hz), 4.27 (t, 1H, *J* = 7.8 Hz), 4.14 (t, 1H, *J* = 6.7 Hz), 3.40–3.12 (m, 6H), 1.10 (t, 6H, *J* = 6.3 Hz); ^{13}C{^{1}H} NMR ($CDCl_3$,75 MHz): δ 173.2, 163.5, 156.2, 156.1, 152.6, 150.9, 143.6, 141.2, 127.7, 127.1, 125.6, 125.2, 125.1, 119.9, 109.3, 108.7, 108.3, 97.7, 67.4, 53.6, 47.0, 44.7, 34.3, 12.4; HRMS (+ESI) *m/z*: $[M + H]^+$ calcd for $C_{31}H_{31}N_2O_6$ 527.2177; found 527.2170. As with compound **4.18**, following acidification the precipitate could be filtered then rinsed with water and ether giving a product sufficiently pure for use in Fmoc-SPPS.

Ala-DMACA-Ala (4.20) and Ala-DEACA-Ala (4.21). 2'-Cl-TrtCl resin (0.25 mmol, 1 equiv, 167 mg, 1.5 mmol/g) was swelled in dry DCM then filtered. Fmoc-Ala-OH (234 mg, 0.75 mmol, 3 equiv) and DIPEA (349 µl, 2 mmol, 8 equiv) in dry DCM (2 ml) was added to the resin and agitated for 16 h. After filtration, the resin was capped by rinsing three times with DCM/MeOH/DIPEA (17:2:1) followed by rinsing with DCM and DMF. The *N*-terminus was deprotected with 4-methylpiperidine (20% in DMF, 5 min then 20 min) followed by filtration and washing with DMF. **4.18** (187 mg, 0. 375 mmol, 1.5 equiv) or **4.19** (198 mg, 0.375 mmol, 1.5 equiv) was coupled using HOAt (51 mg, 0.375 mmol, 1.5 equiv) and DIC (59 µl, 0.375 mmol, 1.5 equiv) in 3 ml DMF for 16 h. The resin was filtered and washed with DMF the *N*-terminus was deprotected with 4-methylpiperidine then filtered and washed. Fmoc-Ala-OH (311 mg, 1 mmol, 4 equiv) was coupled using HOAt (136 mg, 1 mmol, 4 equiv) and DIC (155 µl, 1 mmol, 4 equiv) in 3 ml DMF for 3 h. The resin was rinsed with DMF and the *N*-terminus deprotected with 4-methylpiperidine. The tripeptides were cleaved from the resin with 4 ml TFA/TIPS/H_2O (95:2.5:2.5) for 90 min. The cleavage solution was filtered, and the filtrate was

concentrated under an N_2 stream then the peptide was precipitated with cold ether. The crude peptide was collected by centrifugation and purified by semi-preparative RP-HPLC (C18, 10 µm) using a linear gradient of 90:10 to 60:40 H_2O/MeCN + 0.1% TFA over 40 minutes.

Ala-DMACA-Ala (**4.20**) was obtained as a yellow powder (18.9 mg, 18% yield). The purity of the peptide was verified by analytical RP-HPLC (t_R = 11.1 min, linear gradient of 10:90 to 90:10 MeCN/H_2O + 0.1% TFA over 40 minutes (see Figure C.28 in the supporting information). HRMS (+ESI) *m/z*: $[M + H]^+$ calcd for $C_{20}H_{27}N_4O_6$ 419.1925; found 419.1929.

Ala-DEACA-Ala (**4.21**) was obtained as a yellow powder (35.5 mg, 32% yield). The purity of the peptide was verified by analytical RP-HPLC (t_R = 12.2 min, linear gradient of 10:90 to 90:10 MeCN/H_2O + 0.1% TFA over 40 minutes (see Figure C.30 in the supporting information); HRMS (+ESI) *m/z*: $[M + H]^+$ calcd for $C_{22}H_{31}N_4O_6$ 447.2238; found 447.2242.

Paenibacterin A1-D-Lys1-D-Lys4 (4.25). TrtCl TentaGel resin (theoretical substitution = 0.23 mmol/g, 217 mg, 50 µmol, 1 equiv) was loaded using Fmoc-Pro (4 equiv) and disopropylethylamine (DIPEA, 8 equiv) in dry DCM (2 ml) for 16 h followed by filtration/rinsing with DCM/MeOH/DIPEA (17:2:1, 3 × 3 min) followed by DCM, DMF, and DCM again (2 ml, 3 × 3 min each). The resin loading was estimated to be 42% using the method of Gude et al.[159] The Fmoc group was removed using 20% 4-methylpiperidine (4-MP) in DMF (2 × 2 ml, 5 min then 15 min). The resin was rinsed between each coupling/deprotection step with DMF (2 ml, 6 × 1 min). Fmoc-Ile-OH (4 equiv) was installed using 1-[(1-(cyano-2-ethoxy-2-oxoethylideneaminooxy)-dimethylamino-morpholinomethylene)]methanaminium hexafluorophosphate (COMU, 3.9 equiv), ethyl (hydroxyimino)cyanoacetate (oxyma, 3.9 equiv), and *N*-methylmorpholine (NMM, 8 equiv) in DMF (2 ml) for 4 h. The Fmoc group was removed with 20% 2-methylpiperidine (2-MP) in DMF containing 0.1% formic acid (2 × 2 ml, 5 min then 7 min) followed by rinsing and coupling of Fmoc-D-Ser(O*t*-Bu)-

OH and Fmoc-D-Lys(Boc)-OH with COMU/oxyma/NMM for 2 h until complete by ninhydrin test. Fmoc-D-Lys-Ser($\Psi^{Me,Me}$Pro)-OH (2.5 equiv) was coupled with COMU (2.4 equiv), oxyma (2.4 equiv), NMM (5 equiv) for 2h. Fmoc-Thr(OH) (4 equiv) then Fmoc-Val (4 equiv) were each coupled with DIC (4 equiv) and HOAt (4 equiv) for 3 h. The Fmoc group was removed after each coupling using 4-MP as described above Prior to esterification the resin was rinsed with DCM and dried *in vacuo* over KOH. Alloc-Ile (10 equiv) was activated with DIC (10 equiv) in dry DCM (2 ml) at 0 °C and allowed to warm to room temperature over 30 min. The solution was added to the dry resin, then 1% triton X-100 and DMAP (0.1 equiv) were added before mixing for 20 h. Fmoc-D-Lys(Boc)-OH and pentadecanoic acid were coupled with COMU/oxyma/NMM and the Fmoc group removed using 20% 2-MP in DMF (5 min then 20 min). The resin was treated with $Pd(PPh_3)_4$ (0.2 equiv) and dimedone (10 equiv), mixing for 90 min by bubbling N_2. The resin was then rinsed with 0.5% DIPEA in DMF (3 × 2 ml) followed by 0.5% sodium diethyldithiocarbamate trihydrate in DMF (3 × 2 ml). Fmoc-Lys and Fmoc-Val were coupled with COMU/oxyma/NMM and 20% 2-MP in DMF containing 0.1% formic Acid (2 × 2 ml, 5 min then 7 min) was used for Fmoc deprotection. After the final Fmoc deprotection, the resin was rinsed with DCM, iPrOH, and DCM again before drying *in vacuo* over KOH. The peptide was cleaved from the resin with 30% HFIP in DCM (2 ml, 3 × 30 min) and the resin rinsed with DCM, iPrOH, and DCM. Residual peptide was isolated from the resin by further rinsing with DMF. The cleavage solution was concentrated by rotary evaporation, then the peptide was dissolved in DMF (50 ml) and DIPEA (8 equiv), HOAt (4 equiv), and PyAOP (4 equiv) were added. After stirring for 72 h at room temperature the solution was concentrated by rotary evaporation and the protected peptide was suspended in MeOH then precipitated with cold H_2O and collected by centrifugation. The peptide was deprotected with TFA/TIPS/H_2O (90:5:5) for 90 minutes followed by concentration under an N_2 stream and precipitation with cold MTBE. The crude peptide was purified by semi-preparative RP-HPLC (C8, linear gradient of 70:30 to 50:50 H_2O/MeCN + 0.1% TFA over 60 min). Collected fractions were pooled and

lyophilized to give the TFA salt of peptide **4.25** as a white powder (17.8 mg, 40% based on estimated resin loading). Purity of the peptide was verified by analytical RP-HPLC (t_R = 23.6 min, linear gradient of 90:10 to 10:90 H_2O/MeCN + 0.1% TFA over 40 min (Figure C.32). HRMS (+ESI) *m/z*: $[M + 2H]^{+2}$ calcd for $C_{81}H_{151}N_{17}O_{17}$ 817.0731; found 817.0749.

Paenibacterin A1-D-Lys1-D-Lys4-DMACA6 (4.26). Peptide **4.26** was prepared using the same method described above for peptide 19. Fmoc-DMACA-OH (**4.18**) (2.5 equiv) was installed at position-6 using COMU (2.4 equiv), oxyma (2.4 equiv), and NMM (8 equiv) in DMF (2 ml), for 2h. Lyophilization of RP-HPLC fractions gave the TFA salt of peptide **4.26** as a yellow powder (19.5 mg, 41% based on estimated resin loading). Purity of the peptide was verified by analytical RP-HPLC (t_R = 24.2 min, linear gradient of 90:10 to 10:90 H_2O/MeCN + 0.1% TFA over 40 min, Figure C.34). HRMS (+ESI) *m/z*: $[M + 2H]^{+2}$ calcd for $C_{90}H_{156}N_{18}O_{19}$ 896.5892; found 896.5913.

Paenibacterin A1-D-Lys1-D-Lys4-DEACA6 (4.27). This peptide was prepared using the same method described above for peptide 19. Fmoc-DEACA-OH (**4.19**) (2.5 equiv) was installed at position-6 using COMU (2.4 equiv), oxyma (2.4 equiv), and NMM (8 equiv) in DMF (2 ml), for 2h. Lyophilization of RP-HPLC fractions gave the TFA salt of peptide **4.27** as a yellow powder (23.5 mg, 49% based on estimated resin loading). Purity of the peptide was verified by analytical RP-HPLC (t_R = 24.8 min, linear gradient of 90:10 to 10:90 H_2O/MeCN + 0.1% TFA over 40 min, Figure C.34). HRMS (+ESI) *m/z*: $[M + 2H]^{+2}$ calcd for $C_{92}H_{160}N_{18}O_{19}$ 910.6048; found 910.6074.

Fmoc-D-Lys(Boc)-Ser(Ψ^{Me,Me}Pro)-OH was prepared from Fmoc-D-Lys(Boc)-OH following a procedure previously reported for the synthesis of the analogous D-Orn-Ser dipeptide.[1] The (D, L)-dipeptide was obtained as a white solid (2.07 g, 54%). NMR spectra closely resemble that of the (D,D) or (L, L)-dipeptides reported in literature.[160,161] ^{1}H NMR ($(CD_3)_2SO$, 300 MHz): δ 7.90–7.75 (m, 3H), 7.67 (d, 2H, J = 7.3 Hz), 7.38 (t, 2H, J = 7.5 Hz), 7.28 (t, 2H, J = 7.5 Hz), 6.69 (t br, 1H, J = 5.1 Hz),

4.90 (d, 1H, J = 5.7 Hz), 4.36–3.98 (m, 5H), 3.86 (q, 1H, J = 6.9 Hz), 2.95–2.75 (m, 2H), 1.64–0.98 (m, 21H); $^{13}C\{^{1}H\}$ NMR ($(CD_3)_2SO$, 75 MHz): δ 172.8, 169.7, 156.8, 156.0, 144.2, 144.2, 141.2, 128.1, 127.5, 125.7, 120.5, 95.6, 77.8, 67.0, 66.1, 59.2, 53.8, 47.1, 30.8, 29.8, 28.7, 25.3, 23.5, 23.2; HRMS (+ESI) m/z: [M + H]+ Calcd for $C_{32}H_{42}N_3O_8$ 596.2966; Found 596.3013.

Synthesis of racemic DMACA and DEACA and derivatization with Marfey's reagent.[209,210]

To prepare (±)-DMACA, bromocoumarin **4.11** (500 mg, 1.77 mmol, 1.1 equiv), diethyl acetamidomalonate (349 mg, 1.61 mmol, 1 equiv), and sodium ethoxide (225 mg, 3.3 mmol, 2.05 equiv) were dissolved in EtOH (20 ml) and heated to reflux for 12 h. The solution was then cooled and concentrated. When attempting to isolate the desired product by flash chromatography (SiO_2, 1–3% DCM in MeOH) it was found to elute along with residual diethyl acetamidomalonate. Fractions containing mostly product were pooled and concentrated before dissolving in 6M HCl (aq.) and heating to reflux for 16h. After cooling, the solution was neutralized with ammonium hydroxide then lyophilized. The resulting solid was dispersed in water and filtered and rinsed with water and ether to give racemic DMACA (37 mg). The proton NMR spectra matched that of the pure enantiomer. ^{1}H NMR (D_2O with 5% DCl, 300 MHz): δ 7.57 (d, 1H, J = 8.7 Hz), 7.29 (d, 1H, J = 2.4 Hz), 7.21 (dd, 1H, J = 8.6, 2.3 Hz), 6.19 (s, 1H), 4.03 (t, 1H, J = 7.0 Hz), 3.20 (dd, 1H, J = 15.1, 6.6 Hz), 2.97 (dd, 1H, J = 15.1, 8.1 Hz), 2.88 (s, 6H) *;* HRMS (+ESI) m/z: [M + H]+ Calcd for $C_{14}H_{17}N_2O_4$ 277.1183; Found 277.1189.

(±)-DEACA was prepared from bromocoumarin **4.12** (200 mg, 0.64 mmol) in the manner described above. The product (Rf = 0.12, 1:1 EtOAc/Hexane) was isolated by flash chromatography (SiO_2, 3:7 then 1:1 EtOAc/Hexane) though apparent instability resulted in partial decomposition. It was then dissolved in 6M HCl and refluxed for 12h before cooling, neutralizing with ammonium hydroxide and lyophilizing. The resulting solid was dispersed in water and rinsed with both water and ether to give a

yellow powder (79 mg) consisting of racemic DEACA contaminated with 7-diethylamino-4-(hydroxymethyl)coumarin, confirmed by ^{1}H NMR and ESI-MS; HRMS (+ESI) m/z: [M + H]+ Calcd for $C_{16}H_{21}N_2O_4$ 305.1496; Found 305.1509.; HRMS (+ESI) m/z: [M + H]+ Calcd for $C_{16}H_{21}N_2O_4$ 305.1496; Found 248.1266.

For determination of enantiomeric excess. Coumarin amino acids (2.5 µmol) were treated with Marfey's reagent (3.5 µmol) in acetone (100µL) and 1M $NaHCO_3$ (aq. 200µL), stirring at 40 °C for 1h before centrifuging. Samples of the supernatant were analyzed by RP-HPLC (linear gradient of 80:20 to 60:40 Water/MeCN + 0.1% TFA over 40 minutes) monitoring absorbance at 340 nm. (Figure 4.6**,** Figure 4.7**)** Peak labels represent the normalized area. The major enantiomer elutes before the minor, as expected since most L-amino acids elute before their respective D-enantiomers when reacted with Marfey's reagent.[215]

Determination of quantum yields and extinction coefficients for peptides 4.20 and 4.21. Absorbance and fluorescence measurements were performed on a Tecan M1000 instrument, with bandwidths set to 5 nm for all measurements. Corrected fluorescence spectra were acquired using identical settings for all samples. The excitation wavelength was the wavelength of maximum absorption. The extinction coefficients in Table 4.1 were determined by measuring the absorbance of two independently prepared stock solutions of known concentration. Each solution was measured in duplicate for a total of four separate measurements (error is estimated to be ± 10%). The concentration of tripeptide stock solutions was determined by weight, accounting for 1 equivalent of residual TFA. Relative fluorescence quantum yields (Φ_F) were measured using quinine sulfate in 0.5 M H_2SO_4 (Φ_F = 0.546)[235] as a standard. Solutions of **4.20** or **4.21** were prepared in either ethanol or water and diluted so that the maximum absorbance was less than 0.10. For each peptide/solvent combination, four solutions were prepared with maximum absorbance values ranging from 0.02–0.08. The solutions were briefly sonicated following dilution. The absorbance of each sample was plotted against the

fluorescence peak area from 400–600 nm and the slope of this line ($R^2 > 0.99$) was used to calculate quantum yield with the following equation[236,237]: $\Phi_x = \Phi_{st} \times (m_x/m_{st}) \times (\eta_x/\eta_{st})^2$ where *x* refers to the sample and *st* refers to the standard, *m* is the slope, and η is the refractive index[238] of the solvent. As a control, the quantum yield of 7-diethylamino-4-methylcoumarin (coumarin 1) in ethanol was found to be 0.61, which falls well within the range reported in the literature (Φ_F = 0.5–0.7,[196,239] depending on extent of quenching by O_2).

Interaction of peptide 4.26 with liposomes. Stock solutions of 1,2-dimyristoyl-sn-glycero-3-phosphocholine (DMPC), 1,2-dimyristoyl-sn-glycero-3-phospho-(1'-rac-glycerol) sodium salt (DMPG), 1,2-dioleoyl-sn-glycero-3-phosphocholine (DOPC), and 1,2-dioleoyl-sn-glycero-3-phospho-(1'-rac-glycerol) sodium salt (DOPG) were prepared in chloroform then mixed in the following PC/PG molar ratios: 1:0, 3:1, 1:1. The chloroform was removed under an N_2 stream then high-vacuum, leaving a thin film of lipid which was re-suspended in buffer (20 mM HEPES, 150 mM NaCl, pH 7.4) to give a total lipid concentration of 5 mM. The solution was sonicated above 35 °C for 30 min (or until mostly transparent) to generate small unilamellar vesicles (SUVs). A 100 µM stock solution of peptide **4.20** was prepared in buffer. A corning black 96-well plate was pre-loaded with buffer and preheated to 37 °C before aliquots of the lipid and peptide solutions were added to give final concentrations of 250 µM lipid and 3 µM peptide, and a volume of 200 µL. Emission spectra (λ_{ex} = 380 nm, λ_{em} = 400–600 nm) were collected using a Tecan M1000 plate reader. This was performed in triplicate for each mixture with a single representative emission spectrum being depicted in Figure 4.11.

Interaction of peptide 4.26 with LPS. Stock solutions containing 300 µg/ml LPS from *Escherichia coli* O127:B8 (obtained from Millipore-Sigma) were prepared in buffer (20 mM HEPES, 150 mM NaCl, pH 7.4). Similar to the procedure described above, a corning black 96-well plate was pre-loaded with HEPES buffered saline and preheated to 37 °C before aliquots of the LPS and peptide solutions were added to give final concentrations of 10, 30, 60, or 100 µg/ml LPS, 3 µM peptide, and a volume

of 200 µL. Emission spectra (λ_{ex} = 380 nm, λ_{em} = 400–600 nm) were collected using a Tecan M1000 plate reader. This was performed in triplicate for each mixture with a single representative emission spectrum being depicted in Figure 4.11.

Titration of peptide 4.26 with LPS. Peptide **4.26** was diluted with buffer (5 mM HEPES, pH 7.2) to a concentration of 3 µM in a 1 ml cuvette. LPS (300 µg/ml in the same buffer) was added in 10 µl aliquots. Emission spectra were collected using a PTI Quantamaster fluorimeter, with excitation at 380 and emission from 400–600 nm and a step size of 3 nm. This was performed in duplicate, representative results from a single trial are shown in Figure 4.12. In Figure 4.13 the peak area is the average of two repeated measurements at each concentration, with error bars depicting the deviation.

Staining of Bacteria with Peptide 4.26. LB media was inoculated with either *B. subtilis* 1046 or *E. coli* K-12 from an overnight culture, then incubated at 37 °C. When the OD_{600} reached *ca.* 0.1, bacteria were collected by centrifugation then rinsed three times with phosphate buffered saline (1×PBS[240]). The pellet was then resuspended in a 30 µg/ml solution of peptide 20 in 1×PBS (50–100 µl) for 30 min at room temperature. Then, 2 µl of this suspension was added to a 1% agarose pad on a microscope slide. Once the droplet had been absorbed, a coverslip was added. The edges were sealed with beeswax before imaging on a Zeiss LSM 700 confocal microscope. Images were collected with a ×100 oil immersion objective with additional zoom as needed. Coumarin fluorescence was recorded by exciting at 405 nm with the pinhole size set to 1 AU.

Titration of bacteria with peptide 4.26. LB media was inoculated with from an overnight culture of *B. subtilis* 1046 or *E. coli* K-12, then incubated at 37 °C for 2–3 h or until an OD_{600} of *ca.* 0.5 was reached. Bacteria were collected by centrifugation and rinsed 3 × with HEPES buffered saline (20 mM HEPES, 150 mM NaCl, pH 7.4) then resuspended in buffer to give an OD_{600} of 0.5. A cuvette was filled with 1 ml of the bacterial suspension (or buffer alone) and 5 µl aliquots of a solution of peptide **4.26**

(100 μM) were added up to a peptide concentration of 3 μM. Emission spectra were collected using a PTI Quantamaster fluorimeter, with excitation at 380 and emission from 400–600 nm and a step size of 3 nm.

Chapter 5

Structure-Activity Relationship Study of a Daptomycin Analog: Antibacterial Activity and Calcium-Dependent Membrane Binding

5.1 Preface and Contributions

This work was done in collaboration with several members of the Taylor group and the Michael Palmer group at the University of Waterloo. The majority of peptides containing substitutions at position 11 were prepared and characterized by Ghufran Barnawi. Sara Schulz and David Beriashvili of the Palmer group collected the membrane binding data for these peptides. Jeremy Goodyear and Ryan Moreira prepared daptomycin analogs **5.45-5.49** and determined their MICs. My contribution was the synthesis and characterization of several position 8 analogs and the position 8/11 analogs of Dap-K6-E12-W13. I provided oversight and assistance to undergraduate students Julian Marlyn and Olivia Schneider who each prepared several position 8 analogs. I carried out some or all the characterization for these position 8 analogs. I also adapted the membrane binding assay to be compatible with a plate reader and collected binding data for all position 8 analogs. I collated the fluorescence data and generated plots for all of the analogs.

5.2 Introduction

In Chapter 1 (section 1.5) we briefly discussed daptomycin, a cyclic lipodepsipeptide antibiotic (cLPA) isolated from the fermentation broth of *Streptomyces roseosporus* (the structure of daptomycin, which was shown in Figure 1.13, is reproduced in Figure 5.1 for the reader's convenience).[241] Daptomycin has been used in the clinic since 2003 for treating serious infections caused by Gram-(+) bacteria including methicillin-resistant *Staphylococcus aureus* (MRSA), vancomycin-resistant *Staphylococcus aureus* (VRSA) and vancomycin-resistant enterococci (VRE).[242] Although widespread resistance to daptomycin has yet to materialize, the number of reports describing daptomycin-resistant Gram-(+)

pathogens has increased in recent years and is very likely to rise further in the future.[243–248] Hence, there will be a need for second generation of daptomycin-based antibiotics that are active against daptomycin-resistant strains.

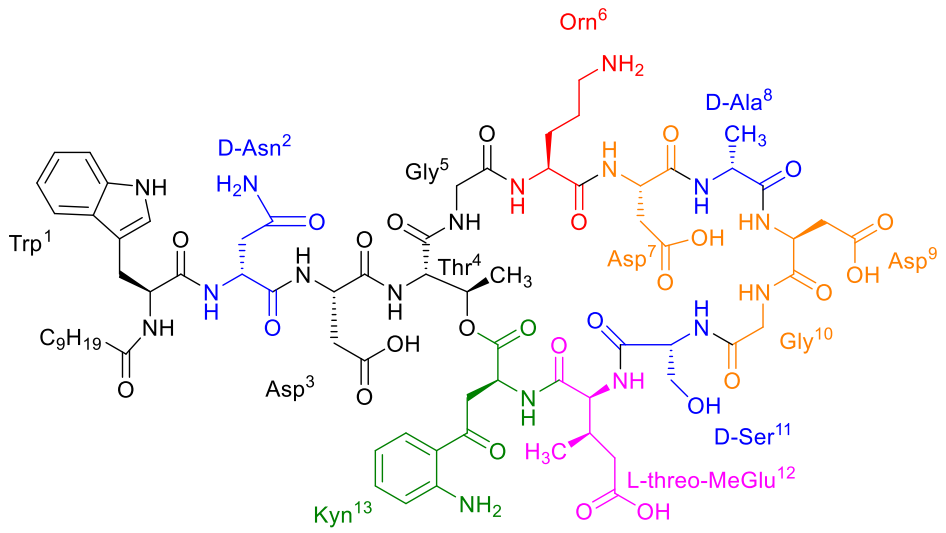

Figure 5.1 Structure of daptomycin. Uncommon amino acids: kynurenine (green), L-*threo*-MeGlu (magenta), ornithine (red). D-Amino acids are shown in blue. The DXDG binding motif consists of residues 7–10 (shown in orange with the exception of D-Ala8).

The development of a second generation daptomycin antibiotic requires a method for preparing daptomycin analogs. A large number of daptomycin analogs have been prepared using semisynthetic approaches in which the amino group of Orn6 has been functionalized, the lipid tail has been replaced with a wide variety of other hydrocarbons, and Trp1 has been replaced with unnatural aromatic amino acids.[249–253] However, none of these analogs were approved for clinical use.

Some of the earliest structure-activity relationship (SAR) studies were conducted by Marahiel and coworkers, who employed a chemoenzymatic approach to prepare variants of daptomycin.[254,255] A key finding of this work was the importance of each anionic residue. When aspartate residues were replaced with neutral asparagine residues effectively all activity was lost against *B. subtilis* PY79.[254]

Baltz and coworkers prepared several analogs through genetic engineering of nonribosomal peptide-synthetases.[256,257] A key result was that the Kyn13 residue could be exchanged for tryptophan with only a 2-fold loss in activity. Furthermore, substitution of Kyn13 with the hydrophobic residues isoleucine or valine yielded analogs of daptomycin that were moderately active in the presence of lung surfactant, which strongly inhibits the parent compound. Positions 8 and 11 were found to be amenable to substitution with serine/lysine or alanine/asparagine, respectively. Substitution of the 3MeGlu12 with glutamate resulted in a 16-fold reduction of activity against *S. aureus*.

Less than two dozen analogs of daptomycin have been reported using the chemoenzymatic and biosynthetic approaches over the last 17 years. This low number of analogs may be due to the limited substrate specificity of the enzymes and/or purification issues and/or low yields.

Recently a method has been developed for the direct modification of the Trp1 residue using aromatic prenyltransferase enzymes.[258] This allows for the introduction of a variety of alkyl or aryl substituents to several positions on the indole ring. Some of these analogs were highly active against Gram-(+) bacteria, including daptomycin-resistant strains of *E. faecalis* and *S. aureus*. It was later demonstrated that similarly modified analogs were active even if EDTA was added to the growth medium to sequester free calcium.[259] This suggests that the MOA of these hydrophobically modified analogs differs significantly from that of daptomycin since, which is entirely inactive without calcium.

Due to the limitations of the above approaches to the synthesis of daptomycin analogs, several groups have used total synthesis as a means for their preparation. The total chemical synthesis of daptomycin was first reported in a patent by Cubist Pharmaceuticals in 2006, and involved a labour-intensive solution-phase segment coupling approach.[251] In the following years, several groups developed improved syntheses of daptomycin and closely related analogs using primarily solid-phase peptide

synthesis strategies with some steps carried out in solution.[143–145,153,260,261] Some of these strategies were discussed in section 1.6.5.

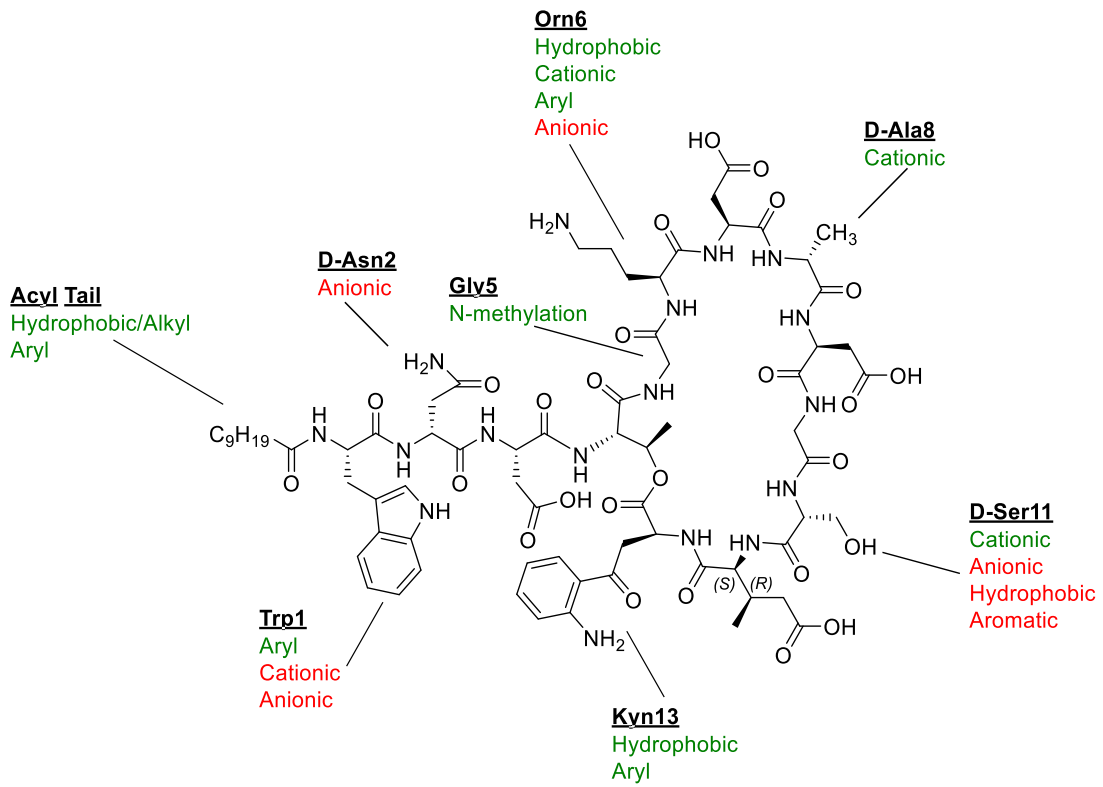

Figure 5.2 Viable (green) and non-viable (red) modifications to daptomycin summarized by Karas.[262]

A comprehensive review has been published recently which provides an impressive overview of nearly 350 analogs of daptomycin that have been prepared to date, and effectively amounts to a meta-analysis examining the SARs of daptomycin.[262] Upon examining these peptides, the authors categorized substitutions at each amino acid position, and determined the general trends in their effects on activity. Some of their findings are summarized in (Figure 5.2). Taking into account the findings of many researchers—including those mentioned above[256,257,263,264], and the Taylor group[119,145,152,265]—Karas et al.[262] make several claims regarding the SARs of daptomycin. They state that modifications to the calcium-binding DXDG motif (residues 7–10) are generally disfavoured, except for at position 8

(corresponding to X). Also, the stereochemistry of each of the D-amino acids is important to activity. In some cases, increasing the length of the fatty acyl tail confers increased activity, but also increases toxicity. Relatively few positions are amenable to even minor modifications. The residue found to be the most tolerant of modification is Orn6. As mentioned above, this has led to extensive modification at this position over the years.[249,253] Of particular relevance to this chapter is the finding that position 8 is amenable to substitution with a cationic D-Lys residue.[257,266] Position 11 was deemed amenable to substitution with cationic residues based on results of Taylor group member Ghufran Barnawi, which are reiterated and expanded-upon below.[265]

While examining the SARs of daptomycin, we performed an alanine scan on a daptomycin analog (Dap-E12W13) in which the non proteinogenic amino acids Kyn13 and 3MeGlu12 are exchanged for Trp and Glu, respectively.[119] When tested against *B. subtilis* 1046 this analog was found to be 5-fold less active than daptomycin. However, in contrast to any current method for the synthesis of daptomycin, this peptide could be prepared entirely on the solid phase using almost exclusively commercially available Fmoc-protected building blocks. This route allowed for the substitution of all residues save Thr4, whose side chain hydroxyl group is required for ring closure, and Asp9, which was replaced with Asn. By using Dap-E12W13 as a basis for SAR studies, we avoided the need for large quantities of 3MeGlu, which at the time was only accessible by low yielding 12-step syntheses.[143,144] The results of this alanine scan revealed that both Orn6 and D-Ser11 could be substituted with alanine—preserving the stereochemical configuration—while exhibiting only a 2 to 3-fold loss of activity. This suggested that these positions may be amenable to substitution. These findings were consistent with prior studies by Cubist Pharmaceuticals, who demonstrated that substitution of D-Ser11 in daptomycin with D-Ala resulted in no loss of activity.[257]

Further studies conducted in the Taylor group on analogs of Dap-E12-W13 established that the side chain of Thr4 is important for activity, since substitution with serine at position 4 resulted in complete

loss of activity against *B. subtilis*.[145] Substitution of Thr4 with a 2,3-diaminobutyic acid residue (replacing the ester bond with an amide bond) resulted in a significant reduction in activity regardless of the stereochemical configuration at the side chain.[152] Replacing Asp9 with Asn gave an analog that was inactive at the highest concentration tested (100 μg/mL).[265]

Very recently, Chow et al. conducted an alanine scan on daptomycin, substituting residues at positions 1–3, 6–9, 12, and 13.[263] Substitution of the glycine residues at positions 5 and 10 was not done due to concerns of epimerization during fragment coupling or cyclization, and position 11 had previously been examined as mentioned above. In general, the results of the alanine scan of daptomycin concurred with those for the analog Dap-E12-W13 (Figure 5.3). Both studies found that the exchange of Orn6 for Ala resulted in little to no loss of activity, while most other positions were not amenable to substitution. This is a strong indication that Dap-E12-W13 is a valid model system for studying the SARs of daptomycin.

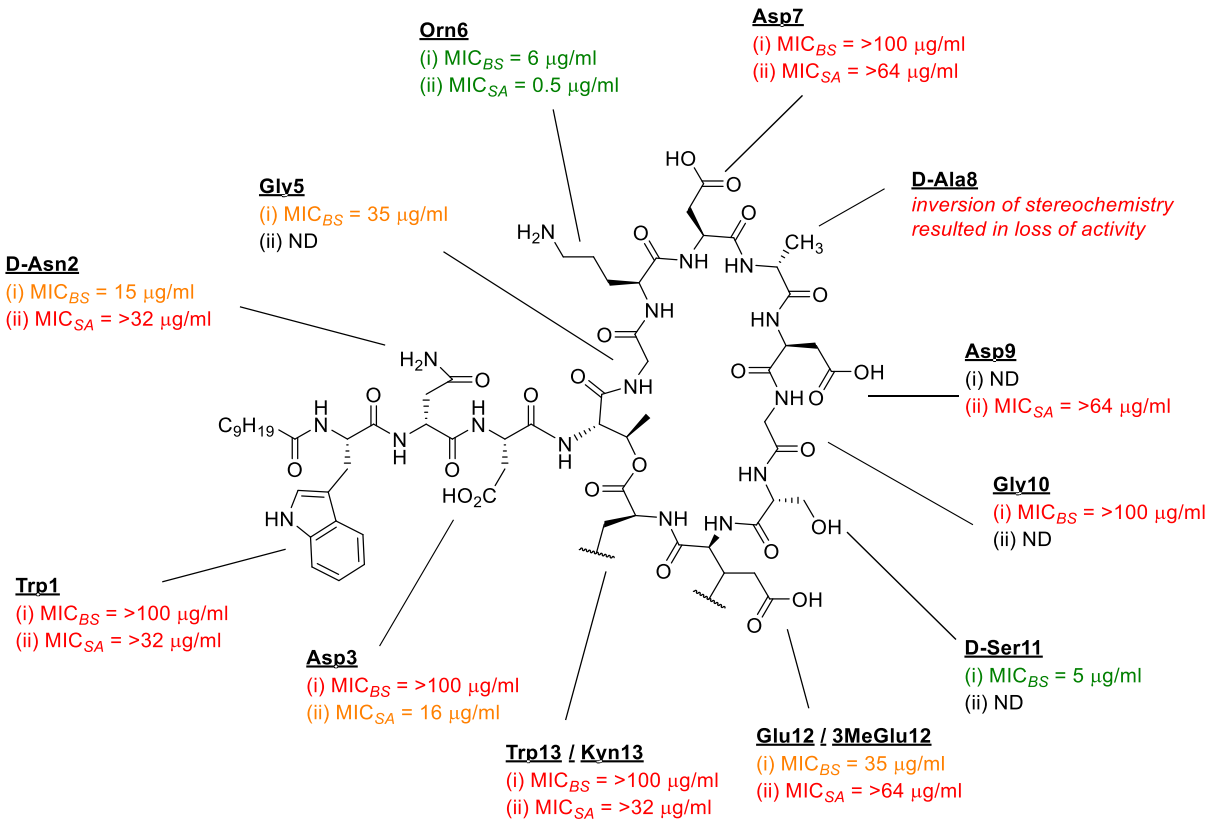

Figure 5.3 Alanine scan of daptomycin and a daptomycin analog. (i) Activity against *B. subtilis* 1046 (1.25 mM Ca^{+2}) of an analog of Dap-E12-W13 where the listed residue has been substituted with alanine.[119] (ii) Activity against *S. aureus* ATCC29213 (50 μg/ml Ca^{+2}) of an analog of daptomycin where the listed residue has been substituted with alanine.[263]

In addition to the alanine scan, Chow et al. prepared a large number of analogs with the aim of better understanding the SAR of daptomycin.[263] They incorporated each of the common amino acids at position 6, and determined that cationic or hydrophobic side chains were better tolerated. They also substituted a series of unnatural aryl amino acids at position 1. Two isomeric β-naphthyl-alanine residues resulted in highly active analogs, with MICs lower than that of daptomycin against certain strains of MRSA. This work also led to the discovery of kynomycin (Figure 5.4), which contains an *N*-methylated kynurenine residue at position 13 and is more active than daptomycin against several bacterial strains.[264]

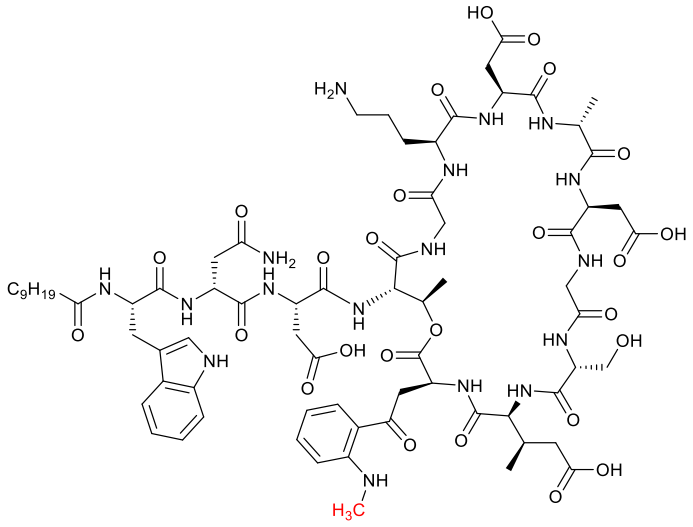

Figure 5.4 Structure of kynomycin. Aside from the extra methyl group attached to the kynurenine residue shown in red, kynomycin is identical to daptomycin.

Since Dap-E12-W13 naturally contains a D-alanine residue at position 8, we examined the importance of stereochemical configuration by substituting with L-Ala.[119] This substitution resulted in a large loss of activity, indicating that the configuration at this position is important for activity. This was further confirmed by Chow et al. who reported similar results when L-Ala was inserted at position 8 in daptomycin.[263] Previously, Cubist Pharmaceuticals had reported that D-Ala8 could be exchanged for D-Ser with little loss of activity.[257] These results suggest that position 8 may be amenable to substitution so long as the stereochemical configuration is maintained.

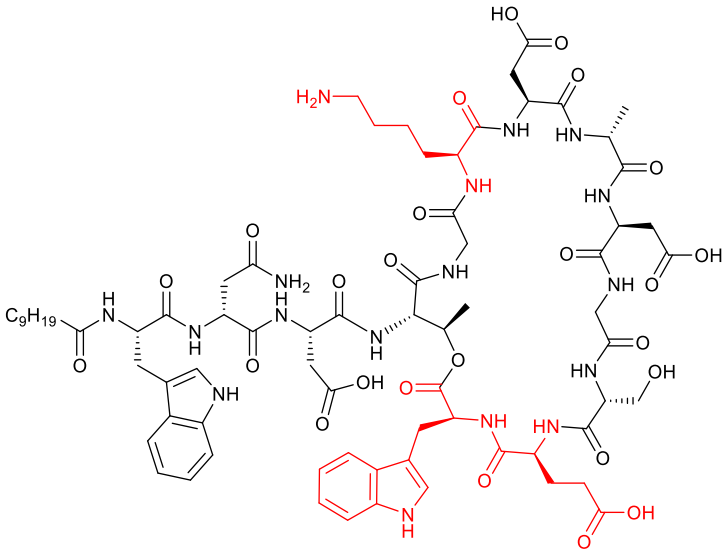

Figure 5.5 Structure and MIC of Dap-K6-E12-W13.

While examining the SARs of Dap-E12-W13, we found that substituting Orn6 with Lys provided an analog, Dap-K6-E12-W13 (Figure 5.5), that was only 2- to 3-fold less active than daptomycin against *B. subtilis* 1046. Therefore, we decided to use this analog as a scaffold for further SAR studies.

5.2.1 Research Objectives

The main objective of the research presented in this chapter was to determine the effect of amino acid substitutions at positions 8 and 11 on the activity of Dap-K6-E12-W13. The activity was determined in two ways: firstly, by determining the impact on the minimum inhibitory concentration (MIC) at which bacterial growth was inhibited, and secondly, we examined the effect on calcium-dependent insertion into model bacterial membranes. We hypothesized that increased calcium dependence would correspond to an increase in MIC.

For the sake of clarity and simplicity, in this chapter analogs may be referred to by the specific D-amino acid incorporated at either position 8 or 11. For example, DapK6-(D-Pro8)-E12W13 may be referred to as the D-Pro8 analog.

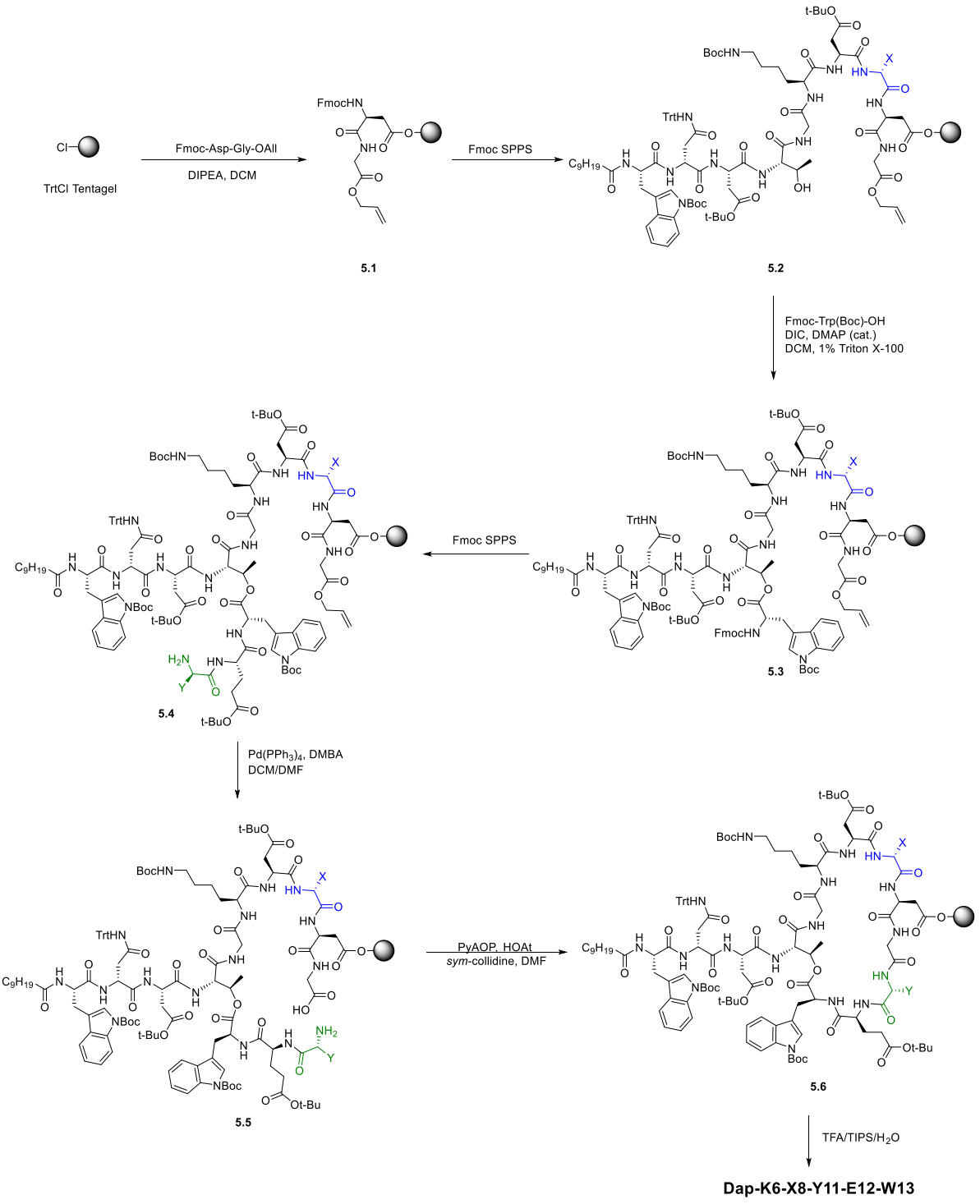

Scheme 5.1 Solid phase peptide synthesis of daptomycin analogs.

5.3 Results and Discussion

5.3.1 Synthesis of Dap-K6-E12-W13 Analogs

For the synthesis of analogs, we used an entirely on-resin Fmoc-SPPS method previously developed by the Taylor group for the synthesis of Dap-K6-E12-W13 (Scheme 5.1).[119] This route proved to be robust, and the majority of analogs were prepared without issues. One exception is Dap-K6-(D-D8)-E12-W13, the synthesis of which was unsuccessful. Aspartate residues are known to be problematic in peptide synthesis and the inclusion of three successive aspartate residues may account for premature termination.[267]

Synthesis of Dap-K6-(G8)-E12-W13 also failed initially. This was presumably due to aspartimide formation resulting from the introduction of a new Asp-Gly sequence.[267–269] However, inclusion of a backbone protecting group on the glycine residue effectively suppressed this side reaction. For the remaining analogs, routine side chain protecting groups[125] were sufficient to prepare the peptides according to the method outlined in Scheme 5.1. For peptides with sulphur-containing side chains, ethanedithiol (EDT) was included in the cleavage cocktail to prevent oxidation. Purity of the isolated peptides was generally very high (>95%) and yields typically fell between 3–12% based on resin loading capacity. In general, this method was reasonably efficient for the parallel synthesis of multiple analogs, and the synthesis up to peptide **5.2** could be easily performed using an automated peptide synthesizer.

5.3.2 *In Vitro* Biological Activity of Dap-K6-E12-W13 Analogs.

Minimum inhibitory concentrations of the analogs of Dap-K6-E12-W13 against *B. subtilis* at a 1.25 mM Ca^{2+} are shown in Table 5.1. To simplify comparisons to Dap-K6-E12-W13 in the following section, we use a rounded MIC value of 2 μg/ml (e.g. an MIC of 4 μg/ml corresponds to a 2-fold loss in activity). Several analogs were identified with MICs of 2–4 μg/ml, similar to that of the parent

compound (Figure 5.5). Other analogs are described as exhibiting moderate activity (8–16 μg/ml), poor activity (32–75 μg/ml), or are effectively inactive (≥ 100 μg/ml).

5.3.2.1 Position 8 Analogs

Changing the length of the side chain at position 8 had a negative, but moderate, impact on activity. Loss of a methyl group (Gly8, **5.10**) resulted in an 8-fold loss of activity. Extending the side chain by one (D-Abu8, **5.15**) or two (D-Nva8, **5.16**) methylene units resulted in a 4 or 8-fold loss of activity. A branched side chain (D-Val8, **5.7**) resulted in a further 16-fold loss of activity. Surprisingly, analog **5.30** with D-Met at this position was only 2-fold less active than the parent compound.

Inclusion of D-Pro (**5.12**) or Sar (**5.14**) at position 8 essentially abolished activity (MIC > 128 μg/ml). This is likely due to conformational changes caused by these *N*-alkyl amino acids. This indicates that the peptide's secondary structure is important to activity.

The inclusion of aromatic amino acids resulted in a moderate loss of activity. Peptide **5.17** (D-Trp8) was 8-fold less active, while peptide **5.19** (D-Tyr8) was only 4-fold less active. Inclusion of D-His was particularly detrimental, with **5.34** exhibiting a 16-fold reduction.

Aside from D-His, cationic substitutions were particularly well accommodated at position 8. Analogs bearing D-Lys (**5.38**) or D-Arg (**5.36**) were only 2-fold less active. Shortening of the cationic side chain (D-Orn, **5.40**) further reduced activity. The low activity of the D-His analog may then be explained by the combination of its short length and aryl character.

Peptide **5.22** (D-Ser8) was a moderate 4-fold less active. Inclusion of other neutral, polar amino acids (**5.24**, **5.26**, **5.28**) resulted in a greater loss of activity. Anionic D-Glu8 (**5.31**) was 8-fold less active.

5.3.2.2 Position 11 Analogs

At position 11, elimination of the side chain by including Gly (**5.11**) only resulted in a 2-fold reduction in activity. Analogs with branched side chains were poorly active (**5.8**, **5.9**). Like with position 8, inclusion of D-Pro11 (**5.13**) abolished activity. Aromatic (**5.18**, **5.20**, **5.21**) or anionic (**5.33**, **5.32**) side chains also resulted in analogs that were poorly active or inactive. D-Thr11 (**5.23**) was well accommodated, only giving a 2-fold reduction in activity. Interestingly, introducing a D-Gln residue (**5.27**) caused a 15-fold loss of activity, while the homologous D-Asn11 (**5.25**) was almost as active as the parent peptide. In aggrement with the latter result, Nguyen et al. have previously demonstrated that the analogous daptomycin derivative was only 2-fold less active against *S. aureus* than native daptomycin.[257] Again, cationic substitutions were well accommodated (**5.35**, **5.37**, **5.39**), though in contrast to position 8 this included D-His11. Notably the peptide with D-Arg at position 11 (**5.37**) was comparable in activity to the parent compound.

5.3.2.3 Further Substitution with Cationic Residues

Since analogs bearing cationic substitutions were quite active, we prepared analogs with these amino acids at both position 8 and 11 (**5.41**–**5.43**). With D-Lys8 and D-Arg11, **5.42** was comparable in activity to Dap-K6-E12-W13. The other analogs were only 2-fold less active. Hoping to improve antibacterial activity by further reducing the anionic character, we prepared an analog of **5.42** with Asp3 and Glu12 substituted with Asn and Gln, respectively. Unfortunately, this peptide, **5.44**, was 16-fold less active.

Table 5.1 *In vitro* antibacterial activity of Dap-K6-E12-W13 analogs

		Amino Acid Substitutions[a]		MIC[b] (µg/ml)
		D-X8	D-Y11	*Bacillus subtilis* 1046
Dap-K6-E12-W13		Ala	Ser	2
Alkyl	**5.7**	Val	—	32
	5.8	—	Val	30
	5.9	—	Leu	30
	5.10	Gly	—	16
	5.11	—	Gly	4
	5.12	Pro	—	>128
	5.13	—	Pro	>100
	5.14	Sar	—	>128
	5.15	Abu	—	8
	5.16	Nva	—	16
Aryl	**5.17**	Trp	—	16
	5.18	—	Trp	>100
	5.19	Tyr	—	8
	5.20	—	Tyr	75
	5.21	—	Phe	100
Neutral Polar	**5.22**	Ser	—	8
	5.23	—	Thr	4
	5.24	Asn	—	64
	5.25	—	Asn	2.5
	5.26	Gln	—	16
	5.27	—	Gln	30
Sulphur Containing [c]	**5.28**	Cys	—	16
	5.29	—	Cys	32
	5.30	Met	—	4
Anionic	**5.31**	Glu	—	16
	5.32	—	Glu	75
	5.33	—	Asp	30
Cationic	**5.34**	His	—	32
	5.35	—	His	4
	5.36	Arg	—	4
	5.37	—	Arg	2
	5.38	Lys	—	4
	5.39	—	Lys	8
	5.40	Orn	—	8
	5.41	Arg	Arg	4
	5.42	Lys	Arg	2
	5.43	Orn	Arg	4
Dap-N3-K6-Q12-W13	**5.44**	Lys	Arg	32

[a]If not indicated then D-Ala8 or D-Ser11 are present. [b]Minimum inhibitory concentrations (MICs) were defined as the peptide concentration at which no visible bacterial growth was observed in LB broth containing 1.25 mM Ca^{2+} following incubation at 37 °C. [c]1 mM DTE was added to prevent cysteine/methionine oxidation.

5.3.3 Calcium-Dependent Membrane Binding of Variants at Position 8 & 11

The intrinsic fluorescence of tryptophan, which bears an indole ring, has proved useful for the study of proteins by fluorescence spectroscopy. Fluorescence of the indole ring is strongly dependent on its local environment, and so is affected by solvent polarity.[270] In addition to general solvent effects, hydrogen bonding with the indole nitrogen can cause significant fluorescence quenching.[271] Certain amino acids also quench Trp fluorescence through either excited-state electron or proton transfer.[272] Of these, Cys and His have the strongest effect; but Gln, Asn, Glu, Asp, Lys and Tyr are all capable of quenching. Calcium-dependent insertion of Dap-K6-E12-W13 into liposomes corresponds to an increase in fluorescence at 354 nm with increasing calcium concentrations, shown in Figure 5.6. A similar increase in Kyn fluorescence is observed when daptomycin inserts into liposomes.[117,118,273] Previously reported procedures were modified to allow for fluorescence measurements in a 96-well plate using a plate reader. This allowed for more rapid analysis of each analog. Even higher throughput could easily be achieved by only measuring emission at a single wavelength of interest (354 nm for Trp) which would significantly reduce acquisition times. For Dap-K6-E12-W13, the results obtained using this new method (Figure 5.6) closely match those obtained previously using a conventional fluorescence spectrometer.[119]

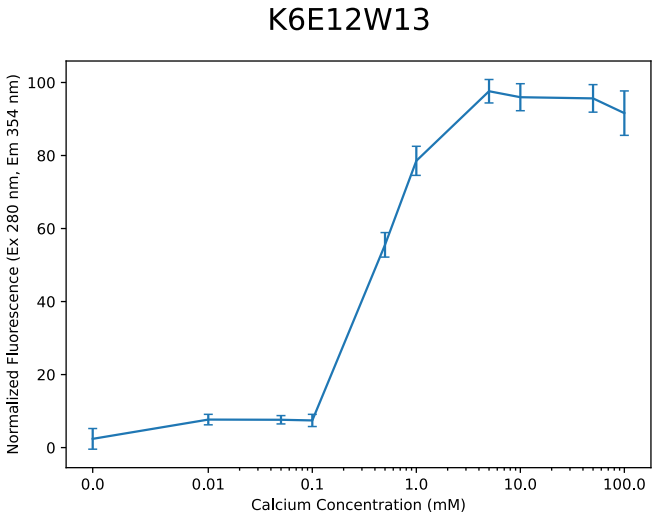

Figure 5.6 Membrane binding curve of Dap-K6-E12-W13. Calcium-dependent insertion into DMPC/DMPG (1:1) LUVs. Fluorescence values, including a peptide blank, are min/max normalized so that the highest intensity is 100.

Membrane binding curves of analogs bearing alkyl (**5.7**–**5.16**) or aryl (**5.17**–**5.21**) side chains are shown in Figure 5.7. Included in this category are glycine (**5.10**, **5.11**) and proline (**5.12**, **5.13**) residues. The majority of these analogs began to exhibit an increase in fluorescence at around 0.1 mM Ca^{2+} and maximum fluorescence between 1 and 10 mM Ca^{2+}.

Peptide **5.12** (D-Pro8), which is inactive, did not exhibit a significant increase in fluorescence until 10 mM Ca^{2+}. On the other hand, **5.13** (D-Pro11), showed increased fluorescence starting at 0.5–1 mM Ca^{2+}. At position 8, proline is situated in the DXDG Ca^{2+} binding motif and may induce a conformational change that reduces Ca^{2+} affinity, impeding insertion into liposomes. At position 11, D-Pro seems to have less of an impact on Ca^{2+} affinity. However, both analogs are inactive at 128 µg/ml indicating they are unable to adopt a biologically active conformation in the membrane. This clearly demonstrates that Ca^{2+}-dependent membrane binding, while important, is not the only factor that determines the activity of a daptomycin derivative.

Peptide **5.14** (Sar8) was similarly inactive and did not exhibit a Ca^{2+}-dependent increase in fluorescence. The amide methyl group of Sar8 likely disrupts the DXDG motif in a fashion similar to D-Pro8. On the other hand, peptide **5.10** (Gly8) was moderately active, indicating that this peptide is free to adopt both a conformation that can bind calcium.

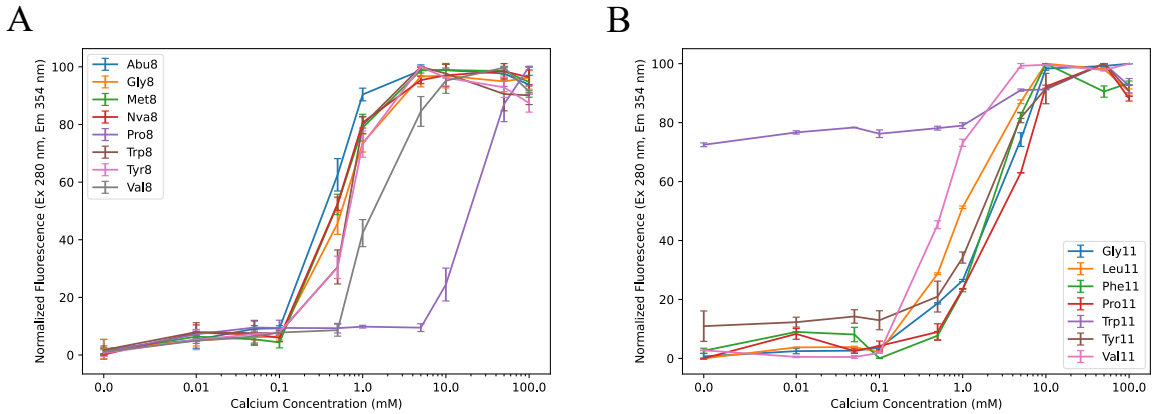

Figure 5.7 Membrane binding curves of Dap-K6-E12-W13 analogs with amino acids containing alkyl or aryl side chains. Calcium-dependent insertion into DMPC/DMPG (1:1). The amino acids listed in the legend are either at (**A**) position 8 or (**B**) position 11. All amino acids at positions 8 or 11 have D-stereochemistry, except for glycine.

The Gly11 analog (**5.11**) retained good antibacterial activity, while the Val11 (**5.8**) and Leu11 (**5.9**) analogs displayed poor activity. Interestingly, both Val11 and Leu11 showed detectable membrane binding at lower Ca^{2+} concentrations than the Gly11 analog (Figure 5.7B). This suggests that bulky residues may promote insertion into the membrane but interfere with some key aspect of the MOA such as aggregation or binding to some target.

The D-Trp11 analog (**5.18**), which was inactive at 100 µg/ml, exhibits a large increase in fluorescence compared to the minimum (peptide in buffer alone) when liposomes are added to the solution. Such an increase is seen for most peptides, but to a lesser extent. A second, small increase in fluorescence is also seen between 1 and 5 mM Ca^{2+}. The precise cause of this is unclear but may indicate that a Trp

residue in **5.18** inserts into the membrane even in the absence of Ca^{2+}, though this does not appear to translate to increased biological activity.

In contrast, for peptide **5.17** (D-Trp8), which was 8-fold less active than the parent peptide, the membrane binding curve was typical. It was virtually identical to that of **5.19** (D-Tyr8) which was only 4-fold less active.

The binding curves for analogs containing residues at position 8 or 11 that have polar side chains, either neutral (**5.22**–**5.27**) or anionic (**5.31**–**5.33**) are shown in Figure 5.8. Analogs bearing cysteine residues exhibited atypical membrane binding curves with high variance. This may be due to fluorescence quenching by the Cys residue, they are omitted here because no reliable conclusions can be drawn from such spectra alone. Most analogs exhibited typical Ca^{2+}-dependent membrane binding, with fluorescence intensity increasing between 0.1–0.5 mM Ca^{2+}, reaching maximum fluorescence from 5–10 mM Ca^{2+}. The cause of increased variation or a decrease in fluorescence (as with D-Asp11, **5.33**) at higher calcium concentrations is unknown but is most likely due to liposome instability or the formation of insoluble peptide aggregates. The behaviour of lipids/peptides at these Ca^{2+} concentrations (≥ 50 mM) is of little biological relevance and well outside the region of interest for this assay (0–10 mM). The addition of high concentrations of Ca^{2+} is, however, important for identifying interesting outliers such as the D-Pro8 analog.

One analog in this series, **5.32** (D-Glu11) required a higher concentration of Ca^{2+} (5 mM) before fluorescence began to increase. This analog was also the least active (MIC 75 µg/ml). This indicates that the analog has either reduced Ca^{2+} affinity or that once bound to Ca^{2+}, the complex has a reduced affinity for PG.

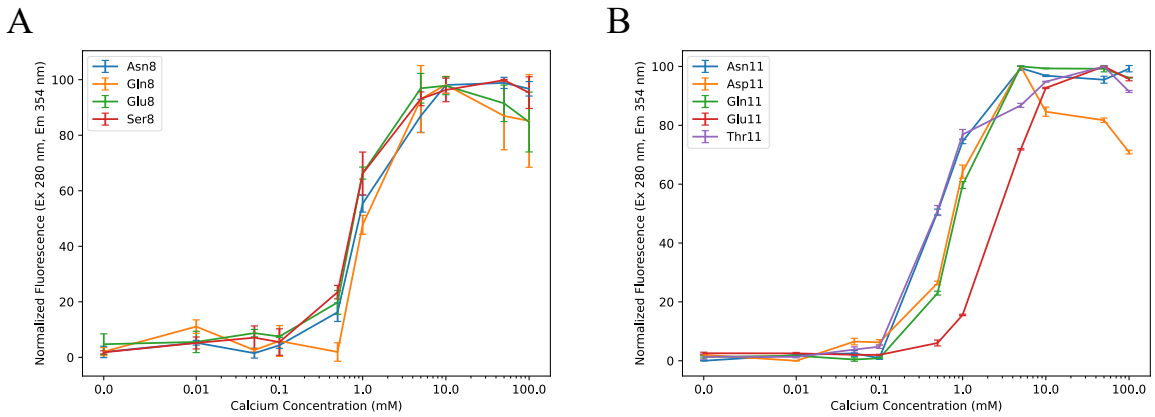

Figure 5.8 Membrane binding curves of Dap-K6-E12-W13 analogs with amino acids containing neutral polar or anionic side chains. Calcium-dependent insertion into DMPC/DMPG (1:1) LUVs. The amino acids listed in the legend are either at (**A**) position 8 or (**B**) position 11. All amino acids at positions 8 or 11 have D-stereochemistry.

Binding curves for analogs bearing cationic residues at positions 8 and 11 (**5.34**–**5.43**) are shown in Figure 5.9. For the most part these analogs exhibited biological activity approaching that of Dap-K6-E12-W13, and the membrane binding curves were similar. Most of these analogs exhibited an increase in fluorescence at 0.5 mM Ca^{2+}, approaching maximum fluorescence at 1–5 mM Ca^{2+}. An exception is **5.34** (D-His8), which was 16-fold less active, and fluorescence increased more gradually, requiring higher Ca^{2+} concentrations. The low fluorescence intensity of the His-containing analogs is likely due to the quenching effect mentioned above. Other exceptions were the analogs bearing D-Arg at either position 8 (**5.36**), or both 8 and 11 (**5.41**), for which fluorescence increased at very low Ca^{2+} concentration (0.05–0.1 mM) reaching a maximum at 1 mM Ca^{2++}. It appears that D-Arg at position 8 increases affinity for the liposomes, possibly due to electrostatic interactions of the cationic side chain with the phosphate head groups of the lipids. However, this does not translate to increased potency since these analogs are 2-fold less active than Dap-K6-E12-W13. Peptide **5.14** (Sar8) and peptide **5.44** did not exhibit calcium-dependent increases in fluorescence, the corresponding binding curves are provided in Appendix D.

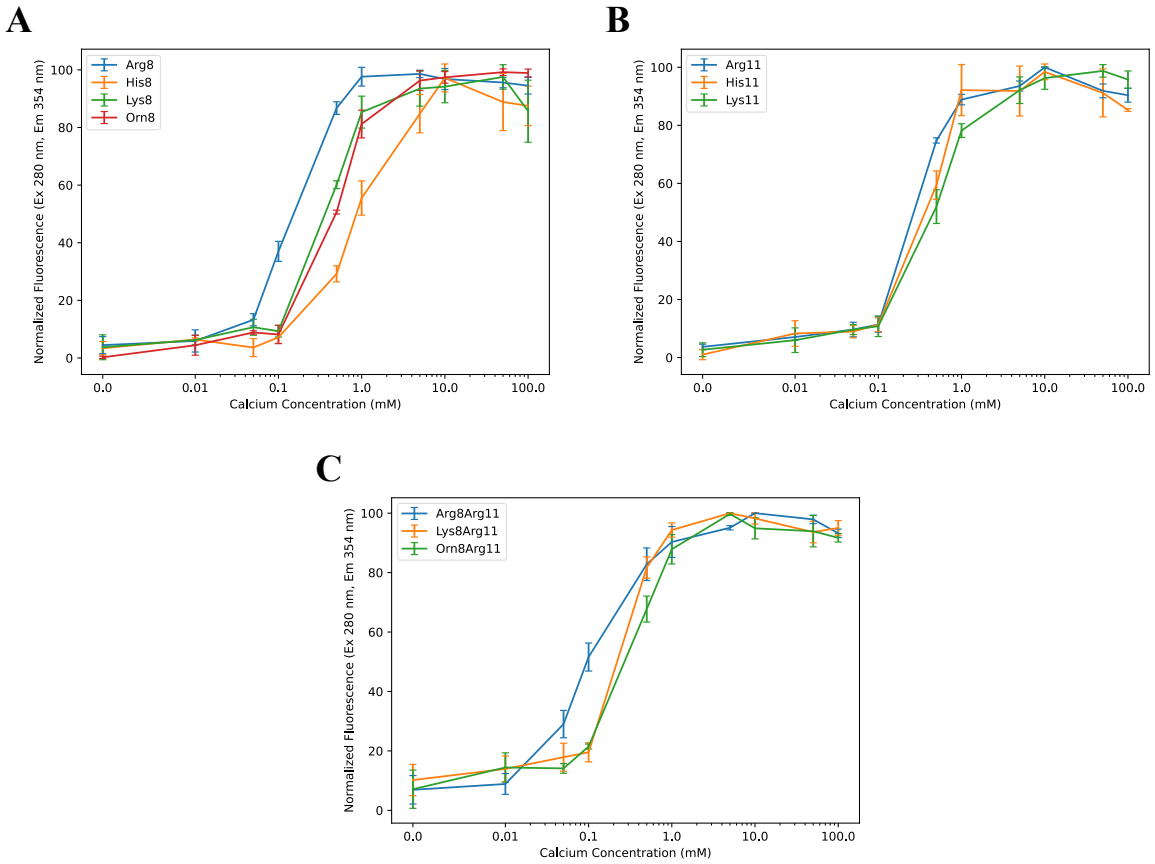

Figure 5.9 Membrane binding curves of Dap-K6-E12-W13 analogs with amino acids containing cationic side chains. Calcium-dependent insertion into DMPC/DMPG (1:1) LUVs results in an increase in the fluorescence of tryptophan. The amino acids listed in the legend are either at (**A**) position 8 or (**B**) position 11. All amino acids at positions 8 or 11 have D-stereochemistry.

The results of the antibacterial and membrane binding studies suggest that, in most cases, membrane insertion at low calcium concentrations is necessary for potent antimicrobial activity. However, membrane insertion at low concentration is not always accompanied by a low MIC. This is most clearly seen by directly comparing the MIC (Table 5.1) to the calcium concentration at which the peptide exhibits over 50% of its maximum fluorescence. This is comparison is shown in Figure 5.10. Here we see that all peptides with an MIC > 30 μg/ml reach 50% fluorescence at or above 1 mM Ca^{++}. Likewise,

with the exception of the Gly11 (**5.11**) analog, all peptides with MICs < 8 µg/ml reach 50% fluorescence at 0.5 mM Ca^{++}.

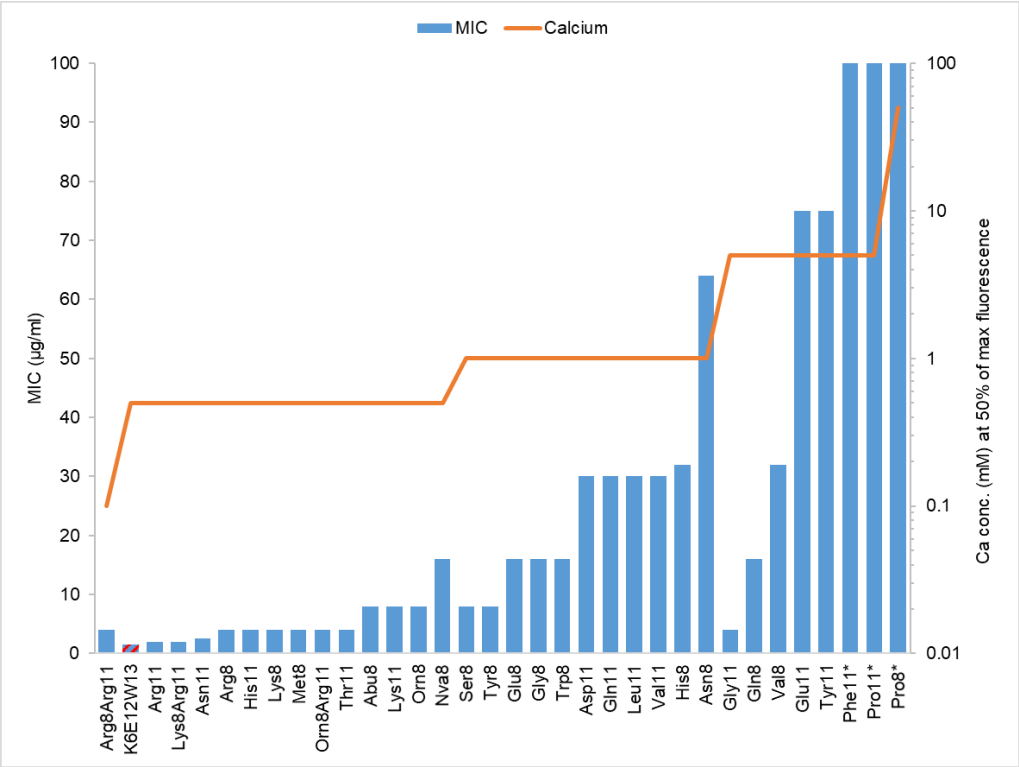

Figure 5.10 Correlation of MIC with the calcium concentration where 50% fluorescence occurs. The lowest concentration at which the fluorescence is greater than or equal to 50% of the maximum fluorescence is indicated by the orange line. The MIC of each analog is represented by the blue bars. The parent analog, Dap-K6-E12-W13 has been highlighted with red stripes. Other peptides are labelled according to the D-amino acids at either position 8 or 11. (*) Indicates that the MIC is ≥ 100 µg/ml.

5.3.4 Cationic Daptomyin Analogs.

Since analogs of Dap-K6-E12-W13 with cationic residues at positions 8 and 11 were comparably active to the parent peptide and some exhibited reduced Ca^{2+} dependence for membrane binding, we decided to prepare analogs of daptomycin with the same substitutions. Because of the kynurenine residue at position 13, we could not use the method in Scheme 5.1. Instead, these peptides were prepared using a

recently published method which makes use of a new Fmoc-SPPS compatible Kyn building block and an off-resin cyclization.[261] Preliminary MICs of these analogs (**5.45**–**5.49**) against *B. subtilis* 1046 are given in Table 5.2. So far, these analogs appear to be *more* active than daptomycin. Further screening of *in vitro* biological activity against several clinically relevant strains of *S. aureus* is underway.

Table 5.2 Preliminary MICs of cationic daptomycin analogs.

	MIC (μg/ml) at 1.25 mM Ca^{2+}					
Strain	Dap	Dap-D-Arg11 (**5.45**)	Dap-D-Arg8 (**5.46**)	Dap-D-Lys8 (**5.47**)	Dap-D-Arg8-D-Arg11 (**5.48**)	Dap-D-Lys8-D-Arg11 (**5.49**)
B. subtilis 1046	1	0.25	0.5	0.5	—	—

5.4 Conclusions & Future Work

The active analog of daptomycin, Dap-K6-E12-W13, was employed as a model system for studying the effect of amino acid substitutions at positions 8 and 11. We examined the effect on *in vitro* biological activity and Ca^{2+}-dependent insertion into model membranes. Position 8 is amenable to substitution with cationic residues Lys, Arg, or Orn, and the hydrophobic residue Met. Aromatic, anionic, or neutral-polar substitutions resulted in moderate to severe reductions in activity. Residues with alkyl side chains had a moderate impact on activity that was more pronounced if the side chain was branched (Val).

Cationic substitutions were also well accommodated at position 11, particularly Arg and His. The neutral polar residue Asn had little impact on activity but increasing the side chain length (Gln) or a negative charge (Asp, Glu) resulted in poor activity. Alkyl or aryl substituents also resulted in poor activity. Substitutions with amino acids that induce changes in the conformation of the peptide backbone had pronounced negative effects. These general trends with respect to antibacterial activity are summarized in Figure 5.11.

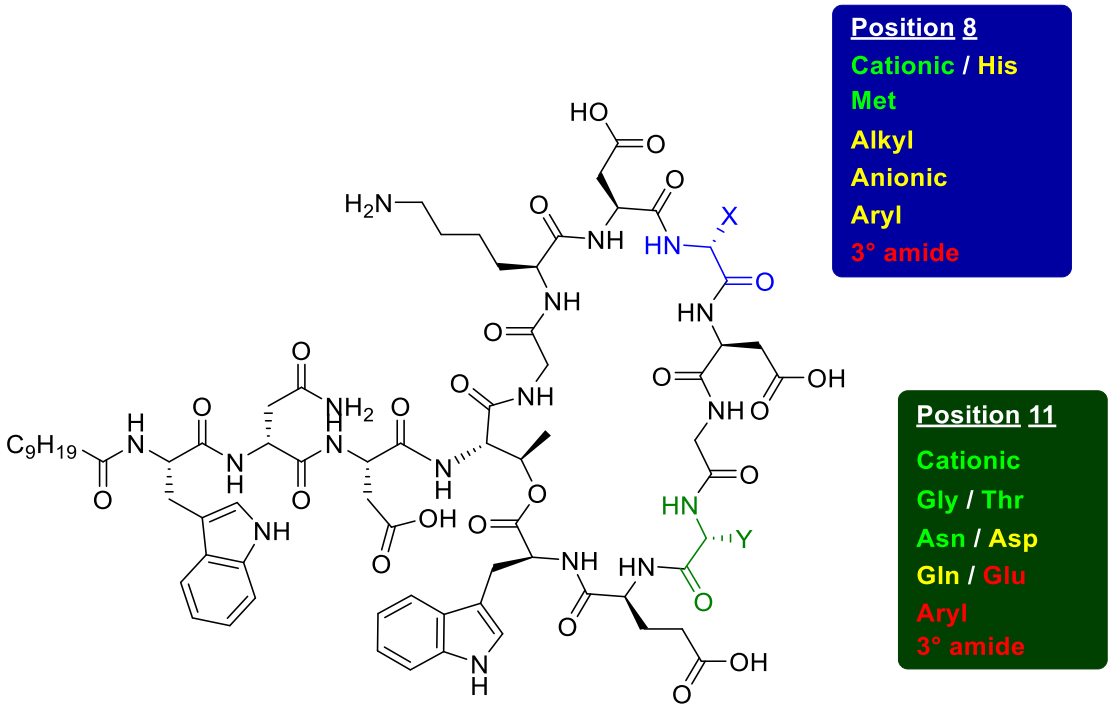

Figure 5.11 Summary of structure-activity relationships for position 8 and 11 analogs. Green: MIC 2–8 µg/ml; Yellow: MIC 8–32 µg/ml; Red: MIC > 32 µg/ml.

We found that good antibacterial activity was usually accompanied by insertion into membranes at low Ca^{2+} concentrations; however, membrane insertion at low Ca^{2+} did not always predict a low MIC. Studying the SARs of Dap-K6-E12-W13 led us to prepare daptomycin analogs with cationic residues at positions 8/11. The increased potency of these analogs compared to daptomycin is a clear indicator that studies on the model peptide Dap-K6-E12-W13 are of relevance to the natural product. Furthermore, our findings aligned closely with previous SAR studies on daptomycin described in section 5.2.

5.5 Experimental

5.5.1 General

The peptides were prepared as previously reported with minor variations to accommodate the substituted amino acids.[119] Analogs bearing substituted amino acids at position 11 (D-Asn11, D-Gln11, D-Thr11, Gly11, D-Asp11, D-Glu11, D-Leu11, D-Val11, D-Phe11, D-Tyr11, D-Trp11, D-Pro11) were prepared by group member Ghufran Barnawi, whose thesis contains experimental procedures for their preparation, characterization data, and MIC values.[265] Four position 11 analogs (D-Lys11, D-His11, D-Cys11, D-Arg11) were prepared by Ghufran Barnawi but purified and characterized by myself, so they are included below. Dap-K6-(D-Lys8, D-Arg11)-E12-W13 had previously been prepared by Ghufran Barnawi but was remade as described in this work. The remade peptide was much more active, which indicates an amino acid with the undesired stereochemistry had been previously been incorporated.

Select analogs were prepared and partially characterized by other group members. Certain position 8 analogs were prepared by Julian Marlyn (D-Met8, D-Pro8, D-Tyr8, D-Val8, D-Cys8, D-Ser8, D-Trp8) or Olivia Schnieder (D-Gln8, D-Glu8, D-His8, D-Arg8, D-Asn8). Calcium-dependent membrane-binding data for position 11 analogs using Method A (cuvette assay) instrument was collected by Sarah Schulz and David Beriashvili. Peptides **5.45**–**5.49** were prepared by Jeremy Goodyear and Ryan Moreira using Fmoc-MeGlu(*t*-Bu)-OH and Fmoc-Kyn(Boc)-OH prepared according to previously published procedures.[261,274]

Dap-K6-G8-E12-W13 (5.10). Beginning with attachment to TrtCl Tentagel resin (50 µmol, 1 equiv), the peptide was prepared using the method described by Barnawi et. al with only minor deviations.[119] At position 8, glycine was incorporated as Fmoc-(DMB)Gly-OH to prevent aspartimide formation. Following cyclization and resin-cleavage/global deprotection the crude peptide was purified by semi-

preparative RP-HPLC (linear gradient of 70:30 to 50:50 H_2O/MeCN + 0.1% TFA over 40 min). Collected fractions were lyophilized to give the desired peptide (4.6 mg, 6% yield). Purity of the peptide was verified by analytical RP-HPLC (t_R = 23.9 min, linear gradient of 90:10 to 10:90 H_2O/MeCN + 0.1% TFA over 40 min). HRMS (+ESI) *m/z*: $[M + 2H]^{+2}$ calcd for $C_{72}H_{101}N_{17}O_{25}$ 801.8572; found 801.8534.

Dap-N3-K6-D-K8-D-R11-Q12-W13 (5.41). Beginning with attachment to TrtCl Tentagel resin (50 µmol, 1 equiv), the peptide was prepared using the method described by Barnawi et. al with only minor deviations.[119] Fmoc-Asn-OH, Fmoc-D-Lys(Boc)-OH, Fmoc-D-Arg(Pbf)-OH, and Fmoc-Gln(Trt)-OH were incorporated at positions 3, 8, 11, and 12, respectively. Following cyclization and resin-cleavage/global deprotection the crude peptide was purified by semi-preparative RP-HPLC (linear gradient of 70:30 to 50:50 H_2O/MeCN + 0.1% TFA over 40 min). Collected fractions were lyophilized to give the desired peptide (6.3 mg, 7% yield). Purity of the peptide was verified by analytical RP-HPLC (t_R = 22.3 min, linear gradient of 90:10 to 10:90 H_2O/MeCN + 0.1% TFA over 40 min). HRMS (+ESI) *m/z*: $[M + 3H]^{+3}$ calcd for $C_{79}H_{120}N_{23}O_{22}$ 580.9654; found 580.9665.

Dap-K6-D-K8-E12-W13 (5.38). Beginning with attachment to TrtCl Tentagel resin (50 µmol, 1 equiv), the peptide was prepared using the method described by Barnawi et. al with only minor deviations.[119] Fmoc-D-Lys(Boc)-OH was incorporated at position 8. Following cyclization and resin-cleavage/global deprotection the crude peptide was purified by semi-preparative RP-HPLC (linear gradient of 60:40 to 50:50 H_2O/MeCN + 0.1% TFA over 40 min). Collected fractions were lyophilized to give the desired peptide (4.8 mg, 6% yield). Purity of the peptide was verified by analytical RP-HPLC (t_R = 28.6 min, linear gradient of 90:10 to 10:90 H_2O/MeCN + 0.1% TFA over 50 min). HRMS (+ESI) *m/z*: $[M + 2H]^{+2}$ calcd for $C_{76}H_{110}N_{18}O_{25}$ 837.3939; found 837.3927.

Dap-K6-D-K8-D-R11-E12-W13 (5.42). Beginning with attachment to TrtCl Tentagel resin (50 µmol, 1 equiv), the peptide was prepared using the method described by Barnawi et. al with only minor deviations.[119] Fmoc-D-Lys(Boc)-OH and Fmoc-D-Arg(Pbf)-OH were incorporated at positions 8 and 11, respectively. Following cyclization and resin-cleavage/global deprotection the crude peptide was purified by semi-preparative RP-HPLC (linear gradient of 60:40 to 50:50 H_2O/MeCN + 0.1% TFA over 40 min). Collected fractions were lyophilized to give the desired peptide (5.9 mg, 7% yield). Purity of the peptide was verified by analytical RP-HPLC (t_R = 27.7 min, linear gradient of 90:10 to 10:90 H_2O/MeCN + 0.1% TFA over 50 min). HRMS (+ESI) *m/z*: $[M + 2H]^{+2}$ calcd for $C_{79}H_{117}N_{21}O_{24}$ 871.9285; found 871.9265.

Dap-K6-D-Orn8-E12-W13 (5.40). Beginning with attachment to TrtCl Tentagel resin (50 µmol, 1 equiv), the peptide was prepared using the method described by Barnawi et. al with only minor deviations.[119] Fmoc-D-Orn(Boc)-OH was incorporated at position 8. Following cyclization and resin-cleavage/global deprotection the crude peptide was purified by semi-preparative RP-HPLC (linear gradient of 70:30 to 50:50 H_2O/MeCN + 0.1% TFA over 40 min). Collected fractions were lyophilized to give the desired peptide (5.5 mg, 7% yield). Purity of the peptide was verified by analytical RP-HPLC (t_R = 28.6 min, linear gradient of 90:10 to 10:90 H_2O/MeCN + 0.1% TFA over 50 min). HRMS (+ESI) *m/z*: $[M + 2H]^{+2}$ calcd for $C_{75}H_{108}N_{18}O_{25}$ 830.3861; found 830.3889.

Dap-K6-D-Orn8-D-R11-E12-W13 (5.43). Beginning with attachment to TrtCl Tentagel resin (50 µmol, 1 equiv), the peptide was prepared using the method described by Barnawi et. al with only minor deviations.[119] Fmoc-D-Orn(Boc)-OH and Fmoc-D-Arg(Pbf)-OH were incorporated at positions 8 and 11, respectively. Following cyclization and resin-cleavage/global deprotection the crude peptide was purified by semi-preparative RP-HPLC (linear gradient of 60:40 to 50:50 H_2O/MeCN + 0.1% TFA over 40 min). Collected fractions were lyophilized to give the desired peptide (6.0 mg, 7% yield). Purity of the peptide was verified by analytical RP-HPLC (t_R = 27.7 min, linear gradient of 90:10 to 10:90

H_2O/MeCN + 0.1% TFA over 50 min). HRMS (+ESI) *m/z*: $[M + 2H]^{+2}$ calcd for $C_{78}H_{115}N_{21}O_{24}$ 864.9206; found 864.9171.

Dap-K6-D-Nva8-E12-W13 (5.16). Beginning with attachment to TrtCl Tentagel resin (50 µmol, 1 equiv), the peptide was prepared using the method described by Barnawi et. al with only minor deviations.[119] Fmoc-D-Nva-OH was incorporated at position 8. Following cyclization and resin-cleavage/global deprotection the crude peptide was purified by semi-preparative RP-HPLC (linear gradient of 70:30 to 50:50 H_2O/MeCN + 0.1% TFA over 40 min). Collected fractions were lyophilized to give the desired peptide (8.1 mg, 10% yield). Purity of the peptide was verified by analytical RP-HPLC (t_R = 30.8 min, linear gradient of 90:10 to 10:90 H_2O/MeCN + 0.1% TFA over 50 min). HRMS (+ESI) *m/z*: $[M + 2H]^{+2}$ calcd for $C_{75}H_{107}N_{17}O_{25}$ 822.8807; found 822.8767.

Dap-K6-D-Abu8-E12-W13 (5.15). Beginning with attachment to TrtCl Tentagel resin (50 µmol, 1 equiv), the peptide was prepared using the method described by Barnawi et. al with only minor deviations.[119] Fmoc-D-Abu-OH was incorporated at position 8. Following cyclization and resin-cleavage/global deprotection the crude peptide was purified by semi-preparative RP-HPLC (linear gradient of 70:30 to 50:50 H_2O/MeCN + 0.1% TFA over 40 min). Collected fractions were lyophilized to give the desired peptide (9.8 mg, 12% yield). Purity of the peptide was verified by analytical RP-HPLC (t_R = 30.1 min, linear gradient of 90:10 to 10:90 H_2O/MeCN + 0.1% TFA over 50 min). HRMS (+ESI) *m/z*: $[M + 2H]^{+2}$ calcd for $C_{74}H_{105}N_{17}O_{25}$ 815.8728; found 815.8740.

Dap-K6-D-R8-D-R11-E12-W13 (5.41). Beginning with attachment to TrtCl Tentagel resin (50 µmol, 1 equiv), the peptide was prepared using the method described by Barnawi et. al with only minor deviations.[119] Fmoc-D-Arg(Pbf)-OH was incorporated at both position 8 and position 11. Following cyclization and resin-cleavage/global deprotection the crude peptide was purified by semi-preparative RP-HPLC (linear gradient of 70:30 to 50:50 H_2O/MeCN + 0.1% TFA over 40 min). Collected fractions

were lyophilized to give the desired peptide (3.6 mg, 4% yield). Purity of the peptide was verified by analytical RP-HPLC (t_R = 28.6 min, linear gradient of 90:10 to 10:90 H_2O/MeCN + 0.1% TFA over 50 min). HRMS (+ESI) *m/z*: $[M + 2H]^{+2}$ calcd for $C_{79}H_{117}N_{23}O_{24}$ 885.9315; found 885.9293.

Dap-K6-Sar8-E12-W13 (5.14). Beginning with attachment to TrtCl Tentagel resin (50 µmol, 1 equiv), the peptide was prepared using the method described by Barnawi et. al with only minor deviations.[119] Fmoc-Sar-OH was incorporated at position 8. Following cyclization and resin-cleavage/global deprotection the crude peptide was purified by semi-preparative RP-HPLC (linear gradient of 70:30 to 50:50 H_2O/MeCN + 0.1% TFA over 40 min). Collected fractions were lyophilized to give the desired peptide (7.1 mg, 9% yield). Purity of the peptide was verified by analytical RP-HPLC (t_R = 30.1 min, linear gradient of 90:10 to 10:90 H_2O/MeCN + 0.1% TFA over 50 min). HRMS (+ESI) *m/z*: $[M + 2H]^{+2}$ calcd for $C_{73}H_{103}N_{17}O_{25}$ 808.8650; found 808.8620.

Dap-K6-D-K11-E12-W13 (5.39). Was prepared by Ghufran Barnawi, incorporating Fmoc-D-Lys(Boc)-OH at position 11. Following resin-cleavage/global deprotection the crude peptide was purified by semi-preparative RP-HPLC (linear gradient of 70:30 to 60:40 H_2O/MeCN + 0.1% TFA over 40 min). Collected fractions were lyophilized to give the desired peptide (23.8 mg). Purity of the peptide was verified by analytical RP-HPLC (t_R = 25.3 min, linear gradient of 90:10 to 10:90 H_2O/MeCN + 0.1% TFA over 50 min). HRMS (+ESI) *m/z*: $[M + 2H]^{+2}$ calcd for $C_{76}H_{110}N_{18}O_{24}$ 829.3965; found 829.4003.

Dap-K6-D-H11-E12-W13 (5.35). Was prepared by Ghufran Barnawi, incorporating Fmoc-D-His(Trt)-OH at position 11. Following resin-cleavage/global deprotection the crude peptide was purified by semi-preparative RP-HPLC (linear gradient of 70:30 to 60:40 H_2O/MeCN + 0.1% TFA over 40 min). Collected fractions were lyophilized to give the desired peptide (13.2 mg). Purity of the peptide was

verified by analytical RP-HPLC (t_R = 25.5 min, linear gradient of 90:10 to 10:90 H_2O/MeCN + 0.1% TFA over 50 min). HRMS (+ESI) *m/z*: $[M + 2H]^{+2}$ calcd for $C_{76}H_{105}N_{19}O_{24}$ 833.8784; found 833.8753.

Dap-K6-D-C11-E12-W13 (5.29). Was prepared by Ghufran Barnawi, incorporating Fmoc-D-Cys(Trt)-OH at position 11. In this case 2.5% ethanedithiol (EDT) was added to the deprotection cocktail to prevent thiol oxidation. Following resin-cleavage/global deprotection the crude peptide was purified by semi-preparative RP-HPLC (linear gradient of 70:30 to 60:40 H_2O/MeCN + 0.1% TFA over 40 min). Collected fractions were lyophilized to give the desired peptide (13.8 mg). Purity of the peptide was verified by analytical RP-HPLC (t_R = 26.6 min, linear gradient of 90:10 to 10:90 H_2O/MeCN + 0.1% TFA over 50 min). HRMS (+ESI) *m/z*: $[M + H]^+$ calcd for $C_{73}H_{102}N_{17}O_{24}S$ 1632.6999; found 1632.6964.

Dap-K6-D-R11-E12-W13 (5.37). Was prepared by Ghufran Barnawi, incorporating Fmoc-D-Arg(Pbf)-OH at position 11. Following resin-cleavage/global deprotection the crude peptide was purified by semi-preparative RP-HPLC (linear gradient of 70:30 to 60:40 H_2O/MeCN + 0.1% TFA over 40 min). Collected fractions were lyophilized to give the desired peptide (12.5 mg). Purity of the peptide was verified by analytical RP-HPLC (t_R = 29.2 min, linear gradient of 90:10 to 10:90 H_2O/MeCN + 0.1% TFA over 50 min). HRMS (+ESI) *m/z*: $[M + 2H]^{+2}$ calcd for $C_{76}H_{110}N_{20}O_{24}$ 843.3995; found 843.4024.

Dap-K6-D-M8-E12-W13 (5.30). Was prepared by Julian Marlyn. Beginning with attachment to TrtCl Tentagel resin (50 µmol, 1 equiv), the peptide was prepared using the method described by Barnawi et. al with only minor deviations.[119] Fmoc-D-Met-OH was incorporated at position 8. In this case 2.5% EDT was added to the deprotection cocktail to prevent side chain oxidation. Following cyclization and resin-cleavage/global deprotection the crude peptide was purified by semi-preparative RP-HPLC (linear gradient of 70:30 to 50:50 H_2O/MeCN + 0.1% TFA over 40 min). Collected fractions were lyophilized to give the desired peptide. Purity of the peptide was verified by analytical RP-HPLC (t_R =

30.7 min, linear gradient of 90:10 to 10:90 H_2O/MeCN + 0.1% TFA over 50 min). HRMS (+ESI) *m/z*: $[M + H]^+$ calcd for $C_{75}H_{106}N_{17}O_{25}S$ 1676.7261; found 1676.7204.

Dap-K6-D-P8-E12-W13 (5.12). Was prepared by Julian Marlyn. Beginning with attachment to TrtCl Tentagel resin (50 µmol, 1 equiv), the peptide was prepared using the method described by Barnawi et. al with only minor deviations.[119] Fmoc-D-Pro-OH was incorporated at position 8. Following cyclization and resin-cleavage/global deprotection the crude peptide was purified by semi-preparative RP-HPLC (linear gradient of 70:30 to 50:50 H_2O/MeCN + 0.1% TFA over 40 min). Collected fractions were lyophilized to give the desired peptide. Purity of the peptide was verified by analytical RP-HPLC (t_R = 26.3 min, linear gradient of 90:10 to 10:90 H_2O/MeCN + 0.1% TFA over 50 min). HRMS (+ESI) *m/z*: $[M + H]^+$ calcd for $C_{75}H_{104}N_{17}O_{25}$ 1642.7384; found 1642.7321.

Dap-K6-D-Y8-E12-W13 (5.19). Was prepared by Julian Marlyn. Beginning with attachment to TrtCl Tentagel resin (50 µmol, 1 equiv), the peptide was prepared using the method described by Barnawi et. al with only minor deviations.[119] Fmoc-D-Tyr(*t*-Bu)-OH was incorporated at position 8. Following cyclization and resin-cleavage/global deprotection the crude peptide was purified by semi-preparative RP-HPLC (linear gradient of 70:30 to 50:50 H_2O/MeCN + 0.1% TFA over 40 min). Collected fractions were lyophilized to give the desired peptide. Purity of the peptide was verified by analytical RP-HPLC (t_R = 30.7 min, linear gradient of 90:10 to 10:90 H_2O/MeCN + 0.1% TFA over 50 min). HRMS (+ESI) *m/z*: $[M + H]^+$ calcd for $C_{79}H_{106}N_{17}O_{26}$ 1708.7489; found 1708.7424.

Dap-K6-D-V8-E12-W13 (5.7). Was prepared by Julian Marlyn. Beginning with attachment to TrtCl Tentagel resin (50 µmol, 1 equiv), the peptide was prepared using the method described by Barnawi et. al with only minor deviations.[119] Fmoc-D-Val-OH was incorporated at position 8. Following cyclization and resin-cleavage/global deprotection the crude peptide was purified by semi-preparative RP-HPLC (linear gradient of 70:30 to 50:50 H_2O/MeCN + 0.1% TFA over 40 min). Collected fractions were

lyophilized to give the desired peptide. Purity of the peptide was verified by analytical RP-HPLC (t_R = 26.9 min, linear gradient of 90:10 to 10:90 H_2O/MeCN + 0.1% TFA over 40 min). HRMS (+ESI) *m/z*: $[M + H]^+$ calcd for $C_{75}H_{106}N_{17}O_{25}$ 1644.7540; found 1644.7511.

Dap-K6-D-C8-E12-W13 (5.28). Was prepared by Julian Marlyn. Beginning with attachment to TrtCl Tentagel resin (50 µmol, 1 equiv), the peptide was prepared using the method described by Barnawi et. al with only minor deviations.[119] Fmoc-D-Cys(Trt)-OH was incorporated at position 8. In this case 2.5% EDT was added to the cleavage cocktail to prevent thiol oxidation. Following cyclization and resin-cleavage/global deprotection the crude peptide was purified by semi-preparative RP-HPLC (linear gradient of 70:30 to 50:50 H_2O/MeCN + 0.1% TFA over 40 min). Collected fractions were lyophilized to give the desired peptide. Purity of the peptide was verified by analytical RP-HPLC (t_R = 30.5 min, linear gradient of 90:10 to 10:90 H_2O/MeCN + 0.1% TFA over 50 min). HRMS (+ESI) *m/z*: $[M + H]^+$ calcd for $C_{73}H_{102}N_{17}O_{25}S$ 1648.6948; found 1648.6891.

Dap-K6-D-S8-E12-W13 (5.22). Was prepared by Julian Marlyn. Beginning with attachment to TrtCl Tentagel resin (50 µmol, 1 equiv), the peptide was prepared using the method described by Barnawi et. al with only minor deviations.[119] Fmoc-D-Ser(*t*-Bu)-OH was incorporated at position 8. Following cyclization and resin-cleavage/global deprotection the crude peptide was purified by semi-preparative RP-HPLC (linear gradient of 70:30 to 50:50 H_2O/MeCN + 0.1% TFA over 40 min). Collected fractions were lyophilized to give the desired peptide. Purity of the peptide was verified by analytical RP-HPLC (t_R = 26.0 min, linear gradient of 90:10 to 10:90 H_2O/MeCN + 0.1% TFA over 40 min). HRMS (+ESI) *m/z*: $[M + H]^+$ calcd for $C_{73}H_{102}N_{17}O_{26}$ 1632.7176; found 1632.7112.

Dap-K6-D-W8-E12-W13 (5.17). Was prepared by Julian Marlyn. Beginning with attachment to TrtCl Tentagel resin (50 µmol, 1 equiv), the peptide was prepared using the method described by Barnawi et. al with only minor deviations.[119] Fmoc-D-Trp(Boc)-OH was incorporated at position 8. Following

cyclization and resin-cleavage/global deprotection the crude peptide was purified by semi-preparative RP-HPLC (linear gradient of 70:30 to 50:50 H_2O/MeCN + 0.1% TFA over 40 min). Collected fractions were lyophilized to give the desired peptide. Purity of the peptide was verified by analytical RP-HPLC (t_R = 31.7 min, linear gradient of 90:10 to 10:90 H_2O/MeCN + 0.1% TFA over 50 min). HRMS (+ESI) *m/z*: $[M + H]^+$ calcd for $C_{81}H_{107}N_{18}O_{25}$ 1731.7649; found 1731.7600.

Dap-K6-D-Q8-E12-W13 (5.26). Was prepared by Olivia Schnieder. Beginning with attachment to TrtCl Tentagel resin (100 µmol, 1 equiv), the peptide was prepared using the method described by Barnawi et. al with only minor deviations.[119] Fmoc-D-Gln(Trt)-OH was incorporated at position 8. Following cyclization and resin-cleavage/global deprotection the crude peptide was purified by semi-preparative RP-HPLC (linear gradient of 70:30 to 50:50 H_2O/MeCN + 0.1% TFA over 40 min). Collected fractions were lyophilized to give the desired peptide (5 mg, 3% yield). Purity of the peptide was verified by analytical RP-HPLC (t_R = 23.7 min, linear gradient of 90:10 to 10:90 H_2O/MeCN + 0.1% TFA over 50 min). HRMS (+ESI) *m/z*: $[M + H]^+$ calcd for $C_{75}H_{105}N_{18}O_{26}$ 1673.7442; found 1673.7402.

Dap-K6-D-E8-E12-W13 (5.31). Was prepared by Olivia Schnieder. Beginning with attachment to TrtCl Tentagel resin (100 µmol, 1 equiv), the peptide was prepared using the method described by Barnawi et. al with only minor deviations.[119] Fmoc-D-Glu(*t*-Bu)-OH was incorporated at position 8. Following cyclization and resin-cleavage/global deprotection the crude peptide was purified by semi-preparative RP-HPLC (linear gradient of 70:30 to 50:50 H_2O/MeCN + 0.1% TFA over 40 min). Collected fractions were lyophilized to give the desired peptide (5 mg, 3% yield). Purity of the peptide was verified by analytical RP-HPLC (t_R = 24.1 min, linear gradient of 90:10 to 10:90 H_2O/MeCN + 0.1% TFA over 50 min). HRMS (+ESI) *m/z*: $[M + 2H]^{+2}$ calcd for $C_{75}H_{105}N_{17}O_{27}$ 837.8677; found 837.8718.

Dap-K6-D-H8-E12-W13 (5.34). Was prepared by Olivia Schnieder. Beginning with attachment to TrtCl Tentagel resin (100 µmol, 1 equiv), the peptide was prepared using the method described by Barnawi et. al with only minor deviations.[119] Fmoc-D-His(Trt)-OH was incorporated at position 8. Following cyclization and resin-cleavage/global deprotection the crude peptide was purified by semi-preparative RP-HPLC (linear gradient of 70:30 to 50:50 H_2O/MeCN + 0.1% TFA over 40 min). Collected fractions were lyophilized to give the desired peptide (17 mg, 10% yield). Purity of the peptide was verified by analytical RP-HPLC (t_R = 23.2 min, linear gradient of 90:10 to 10:90 H_2O/MeCN + 0.1% TFA over 50 min). HRMS (+ESI) *m/z*: $[M + 2H]^{+2}$ calcd for $C_{76}H_{105}N_{19}O_{25}$ 841.8759; found 841.8800.

Dap-K6-D-R8-E12-W13 (5.36). Was prepared by Olivia Schnieder. Beginning with attachment to TrtCl Tentagel resin (100 µmol, 1 equiv), the peptide was prepared using the method described by Barnawi et. al with only minor deviations.[119] Fmoc-D-Arg(Pbf)-OH was incorporated at position 8. Following cyclization and resin-cleavage/global deprotection the crude peptide was purified by semi-preparative RP-HPLC (linear gradient of 70:30 to 50:50 H_2O/MeCN + 0.1% TFA over 40 min). Collected fractions were lyophilized to give the desired peptide (10 mg, 6% yield). Purity of the peptide was verified by analytical RP-HPLC (t_R = 23.5 min, linear gradient of 90:10 to 10:90 H_2O/MeCN + 0.1% TFA over 50 min). HRMS (+ESI) *m/z*: $[M + 2H]^{+2}$ calcd for $C_{76}H_{110}N_{20}O_{25}$ 851.3970; found 851.3989.

Dap-K6-D-N8-E12-W13 (5.24). Was prepared by Olivia Schnieder. Beginning with attachment to TrtCl Tentagel resin (100 µmol, 1 equiv), the peptide was prepared using the method described by Barnawi et. al with only minor deviations.[119] Fmoc-D-Asn(Trt)-OH was incorporated at position 8. Following cyclization and resin-cleavage/global deprotection the crude peptide was purified by semi-preparative RP-HPLC (linear gradient of 70:30 to 50:50 H_2O/MeCN + 0.1% TFA over 40 min). Collected fractions were lyophilized to give the desired peptide (6 mg, 4% yield). Purity of the peptide

was verified by analytical RP-HPLC (t_R = 23.8 min, linear gradient of 90:10 to 10:90 H_2O/MeCN + 0.1% TFA over 50 min). HRMS (+ESI) *m/z*: $[M + H]^+$ calcd for $C_{74}H_{103}N_{18}O_{26}$ 1659.7285; found 1659.7218.

5.5.2 Preparation of Lipids

Large unilamellar vesicles (LUV) were prepared from either 1,2-dimyristoyl-sn-glycero-3-phospho-(1'-rac-glycerol) sodium salt (DMPG) and 1,2-dimyristoyl-sn-glycero-3-phosphocholine (DMPC) or 1,2-dioleoyl-sn-glycero-3-phospho-(1'-rac-glycerol) (DOPG) and 1,2-dioleoyl-sn-glycero-3-phosphocholine (DOPC) in a 1:1 molar ratio by polycarbonate membrane extrusion as previously described.[119] Mixtures of 1:1 1,2-dioctanoyl-sn-glycero-3-phospho-(1'-rac-glycerol) sodium salt (C8PG) and 1,2-dioctanoyl-sn-glycero-3-phosphocholine (C8PC) were prepared without the need for extrusion. The total lipid concentration was 5 mM in HEPES buffered saline (pH 7.4, 20 mM HEPES, 150 mM NaCl).

5.5.3 Ca-Dependent Membrane Binding Method A: single-cell fluorimeter.

Fluorescence emission spectra were acquired with a PTI QuantaMaster 4 instrument following a protocol that has been previously described.[104,119] Briefly, a pH 7.4 buffer solution containing LUVs at a concentration of 250 µM, peptide at 3 µM, 150 mM NaCl, and 20 mM HEPES was warmed to 37 °C. A calcium chloride solution was titrated in to give the desired final concentrations. Emission spectra were collected following a 3 min equilibration time.

5.5.4 Ca-Dependent Membrane Binding Method B: adapted for a microplate reader.

The previously reported protocol for membrane binding studies was modified for compatibility with a top-reading fluorescence plate reader, allowing or higher throughput analysis of the position 8 analog variants. Into each column of a Corning half-area 96-well black polystyrene microplate was dispensed 10 µl of saline-buffer (pH 7.5, 20 mM HEPES, 150 mM NaCl) containing 10-fold the desired final

calcium chloride concentration. Buffer containing no calcium was dispensed into the column corresponding to the peptide-blank (15 µl) and 0 mM Ca (10 µl). A 0.25 mM lipid solution was prepared from the 5 mM lipid stock and saline-buffer then 100 µl was added to each well in the column corresponding to the lipid-blank. From a 100 µM stock solution of peptide (in purified water or buffer) 36 µl was diluted to 1.02 ml with saline-buffer (Concentration of approximately 3.5 µM). Then 85 µl was added to the peptide-blank column. The plate and the peptide solutions were then warmed to 37 °C. To a warm peptide solution was added 55 µl of the 5 mM lipid stock, and immediately 90 µl was dispensed into the pre-loaded calcium containing wells. Measurement was delayed, allowing for an equilibration time of approximately 3 minutes for each well. The dispensation and measurement process was then repeated for the remaining rows. One peptide is analyzed per-row with calcium concentration varying across the columns.

Fluorescence was measured using a Tecan M1000 plate reader. To measure kynurenine fluorescence the excitation wavelength was 365 nm and emission was measured from 400–600 nm, the bandwidth for emission and excitation were set to 5 nm. To measure tryptophan fluorescence the excitation wavelength was 280 nm with a bandwidth of 2.5 nm and excitation was measured from 300–400 nm with a bandwidth of 5 nm. Measurements were taken with 100 flashes at 400 Hz and an integration time of 20 µs. The step size over the emission range was 3 nm. The signal gain was set to an appropriate level determined for the maximum emission at 100 mM calcium for DapK6E12W13.

5.5.5 Fluorescence Analysis

Before plotting the emission spectra, fluorescence values from the lipid-only blank were subtracted. Emission at a select wavelength (354 nm for Trp fluorescence, 475 nm for DMACA or DEACA fluorescence) and varying calcium concentrations were then Min/Max normalized before the average of two or three trials was plotted on a semi-log plot with a partial linear x-axis below 0.1 mM Ca.

Analysis was performed using Pandas, a python library, and plots were generated using Matplotlib.[275–278]

5.5.6 Minimum Inhibitory Concentration

Minimum inhibitory concentrations were determined by a broth microdilution assay.[162] B. subtilis 1046 cultures were grown overnight in LB broth followed by dilution to *ca.* 1×10^6 CFU/mL, determined by measuring optical density at 600 nm (OD_{600}). Diluted peptide solutions were prepared by serial dilutions in LB broth and, following inoculation with an equal volume of diluted bacterial culture, were incubated at 37 °C for 24h. The lowest peptide concentration with no detectable bacterial growth defined the MIC. Calcium chloride was included in the growth medium at a concentration of 1.25 mM.

Chapter 6
Summary and Future Work

6.1 Summary

The research presented in this thesis primarily concerns the cationic lipopeptide antibiotic paenibacterin. Total synthesis of paenibacterin (Chapter 2) using solid phase peptide synthesis was challenging due to a slow esterification between Ile13 and the side chain of Thr3. We were also unsuccessful in in finding conditions that would allow for the cyclization of paenibacterin on-resin. However, paenibacterin A1 was successfully synthesized by way of an off-resin cyclization. It was prepared in high yield and purity so long as a pseudoproline dipeptide was incorporated to disrupt aggregation. Using this method, we prepared the major component of natural paenibacterin bearing an anteiso acyl tail. We also prepared analogs of paenibacterin where the ester linkage was substituted for an amide linkage. These analogs all exhibited similar activity against both Gram-(+) and Gram-(−) bacteria.

We later developed an improved route to the synthesis of paenibacterin after discovering that the ester linkage could be made on a truncated linear precursor peptide without epimerization. This significantly improved the purity of the peptide following esterification. We used this method to prepare an economical analog of paenibacterin where costly D-Orn residues were replaced with D-Lys. Pleasingly this analog was as active or more active than natural paenibacterin A1. Using this Lys analog (PAK) as a scaffold we prepared a series of analogs to determine the structure-activity relationships of paenibacterin (Chapter 3). We examined two aspects: its cationic character, and hydrophobicity. To determine the importance of each cationic lysine residue they were replaced in-turn with alanine. We then prepared a series of doubly-substituted analogs. Against Gram-(−) bacteria Lys7 was found to be the least important to activity, while Lys1 and Lys2 were most important. Against Gram-(+) bacteria

the reduction in activity was minimal regardless of which lysine residue was replaced. This suggests that paenibacterin's MOA against Gram-(−), but not Gram-(+) bacteria depends on the interaction of several cationic side chains with specific molecules in the target membrane. We found that there was no loss in activity against Gram-(−) bacteria when the acyl tail was reduced to 10 carbons in length, whereas shortening of the tail from 13–10 carbon atoms resulted in a gradual decrease in activity against Gram-(+) bacteria. Analogs with a pentadecenoyl or acetyl tail were inactive against both. A fluorescent 1-pyrenebutyric acid tail was accommodated with only a 2-fold loss in activity. An analog with Trp at position 6 was active, which led us to conclude that this position was amenable to substitution with aromatic amino acids.

To facilitate mechanism of action studies of paenibacterin we desired to prepare analogs containing an efficient, environmentally sensitive fluorophore (Chapter 4). To this end we designed two amino acids that contained a 7-aminocoumarin fluorophore, whose quantum yield increases in apolar environments. These amino acids were compatible with Fmoc SPPS and were incorporated into paenibacterin with a minimal impact on activity. Using fluorescence spectroscopy and confocal microscopy we examined interactions between this fluorescent paenibacterin analog and model membranes, LPS, and live cells. This peptide was found to bind to liposomes, resulting in a large increase in fluorescence. Binding to sub-CMC LPS resulted in an unexpected quenching effect. Bacterial cells stained with this peptide were easily visible by confocal microscopy and allowed us to visualize paenibacterins interaction with the cells. We observed apparent localization of paenibacterin to the membrane of Gram-(−) bacteria, while it appeared to enter and disperse throughout Gram-(+) bacteria.

Finally, we conducted a limited SAR study of a daptomycin analog Dap-K6-E12-W13, substituting the amino acids at position 8 and 11 (Chapter 5). We found that most substitutions resulted in a significant reduction of *in vitro* biological activity but had little impact on calcium-dependent binding

to liposomes. Analogs with cationic residues at either position mostly exhibited good activity and membrane-binding at low calcium concentrations. We reasoned that these substitutions would also be well-tolerated in daptomycin itself. Indeed, preliminary results indicate that these analogs of daptomycin are more active than the parent compound.

6.2 Future Work

6.2.1 Broad Screening of Antibacterial Activity.

While conducting the research discussed in this chapter, we have prepared a small but not insignificant library of analogs of both paenibacterin and daptomycin. Many of the analogs exhibited good activity against our model bacteria *E. coli* K-12 and *B. subtilis* 1046, and so it is important that we examine the scope of their activity. A number of peptides have already been shared with external organizations better equipped to handle pathogenic bacteria, and the Taylor group hopes to soon be able to conduct broader screening in-house as well.

6.2.2 Study of Paenibacterin Aggregation Using Pyrene Excimer Fluorescence.

We prepared an analog of paenibacterin that contains a pyrene fluorophore (**3.26**). Similar analogs have been used to study lipopeptide antibiotic aggregation, e.g. to characterize the aggregation of daptomycin in membranes[113] or the lipopeptide A514145[114]. If pyrene fluorophores are in close proximity, they can form an excited dimer, detectable in the emission spectrum. Detection of these excimers when the Pba analog is added to model membranes would indicate that paenibacterin is forming aggregates as a part of its mechanism of action.

6.2.3 Further Labelling of Paenibacterin Analogs

In chapter 4 we labeled paenibacterin by incorporating DMACA and DEACA at a single position. In future work, DMACA will be incorporated at different positions, and the effect of liposomes/LPS on peptide fluorescence will be re-examined. Instead of substituting Val6, we will instead replace Val2

which will place the DMACA fluorophore in closer proximity to the acyl tail. Provided the analog is active, a change in fluorescence should better reflect the environment of the exocyclic portion of the peptide as it inserts into a membrane. In the literature, dansyl analogs of polymyxins or octapeptins typically incorporate the fluorophore at a position near the acyl tail (if labelled at a specific position).[229,279,280]

We will also compare the observations with the DMACA labelled peptides to results for analogs labelled with common fluorophores such as: dansyl—commonly used for studying polymyxin-like peptides[221,279], acrylodan/PRODAN—another polarity-sensitive fluorophore[281,282], or BODIPY which is not very environmentally sensitive and so should be valuable for examining localization within bacteria or even animal cells.[283,284] The results of chapter 3 suggest that any single lysine residue could likely be modified without much impact on activity.

6.2.4 Time-Lapse Microscopy

As mentioned in Chapter 4, we hope to examine the accumulation of fluorescently labelled paenibacterin in the membranes or cytosol of bacteria. This will be done using time-lapse confocal microscopy.[228,229]

6.2.5 Synergy of Short-Tailed Peptides

Finally, we hope to examine the ability of both paenibacterin and analogs to permeabilize the outer membrane of bacteria. As with the polymyxin B nonapeptides, we suspect that inactive analogs bearing truncated (pentanoyl, acetyl) tails may exhibit synergistic effects with other large membrane-impermeable antibiotics or serum complement.[76]

Bibliography

(1) Noden, M.; Moreira, R.; Huang, E.; Yousef, A.; Palmer, M.; Taylor, S. D. Total Synthesis of Paenibacterin and Its Analogues. *J. Org. Chem.* **2019**, *84* (9), 5339–5347. https://doi.org/10.1021/acs.joc.9b00364.

(2) Infectious Diseases Society of America. Bad Bugs, No Drugs: As Antibiotic Discovery Stagnates ... A Public Health Crisis Brews; 2004.

(3) Gilbert, D. N.; Guidos, R. J.; Boucher, H. W.; Talbot, G. H.; Spellberg, B.; Edwards, J. E.; Michael Scheld, W.; Bradley, J. S.; Bartlett As, J. G.; Infectious Diseases Society of America; Policy, I. P.; Infectious Diseases Society of America. The 10 X 20 Initiative: Pursuing a Global Commitment to Develop 10 New Antibacterial Drugs by 2020. *Clin. Infect. Dis.* **2010**, *50* (8), 1081–1083. https://doi.org/10.1086/652237.

(4) Rossolini, G. M.; Arena, F.; Pecile, P.; Pollini, S. Update on the Antibiotic Resistance Crisis. *Curr. Opin. Pharmacol.* **2014**, *18*, 56–60. https://doi.org/10.1016/j.coph.2014.09.006.

(5) Velkov, T.; Roberts, K. D.; Nation, R. L.; Thompson, P. E.; Li, J. Pharmacology of Polymyxins: New Insights into an "old" Class of Antibiotics. *Future Microbiol.* **2013**, *8* (6), 711–724. https://doi.org/10.2217/fmb.13.39.

(6) Falagas, M. E.; Rizos, M.; Bliziotis, I. A.; Rellos, K.; Kasiakou, S. K.; Michalopoulos, A. Toxicity after Prolonged (More than Four Weeks) Administration of Intravenous Colistin. *BMC Infect. Dis.* **2005**, *5*, 1. https://doi.org/10/ddkpm2.

(7) Shariati, A.; Dadashi, M.; Chegini, Z.; van Belkum, A.; Mirzaii, M.; Khoramrooz, S. S.; Darban-Sarokhalil, D. The Global Prevalence of Daptomycin, Tigecycline, Quinupristin/Dalfopristin, and Linezolid-Resistant Staphylococcus Aureus and Coagulase–Negative Staphylococci Strains: A Systematic Review and Meta-Analysis. *Antimicrob. Resist. Infect. Control* **2020**, *9* (1), 56. https://doi.org/10.1186/s13756-020-00714-9.

(8) Walkty, A.; Karlowsky, J. A.; Adam, H. J.; Lagacé-Wiens, P.; Baxter, M.; Mulvey, M. R.; McCracken, M.; Poutanen, S. M.; Roscoe, D.; Zhanel, G. G. Frequency of MCR-1-Mediated Colistin Resistance among Escherichia Coli Clinical Isolates Obtained from Patients in Canadian Hospitals (CANWARD 2008-2015). *CMAJ Open* **2016**, *4* (4), E641–E645. https://doi.org/10/gk4g9s.

(9) Strahl, H.; Errington, J. Bacterial Membranes: Structure, Domains, and Function. *Annu. Rev. Microbiol.* **2017**, *71* (1), 519–538. https://doi.org/10.1146/annurev-micro-102215-095630.

(10) Madigan, M.; Martinko, J.; Stahl, D.; Clark, D. P. *Brock Biology of Microorganisms*, 13th ed.; Pearson Education, 2012; p 63.

(11) Singer, S. J.; Nicolson, G. L. The Fluid Mosaic Model of the Structure of Cell Membranes. *Science* **1972**, *175* (4023), 720–731. https://doi.org/10.1126/science.175.4023.720.

(12) Kuk, A. C. Y.; Hao, A.; Guan, Z.; Lee, S.-Y. Visualizing Conformation Transitions of the Lipid II Flippase MurJ. *Nat. Commun.* **2019**, *10* (1), 1736. https://doi.org/10/gkc2f9.

(13) Ruiz, N. Bioinformatics Identification of MurJ (MviN) as the Peptidoglycan Lipid II Flippase in Escherichia Coli. *Proc. Natl. Acad. Sci. U. S. A.* **2008**, *105* (40), 15553–15557. https://doi.org/10.1073/pnas.0808352105.

(14) Kumar, S.; Rubino, F. A.; Mendoza, A. G.; Ruiz, N. The Bacterial Lipid II Flippase MurJ Functions by an Alternating-Access Mechanism. *J. Biol. Chem.* **2019**, *294* (3), 981–990. https://doi.org/10.1074/jbc.RA118.006099.

(15) Inoue, A.; Murata, Y.; Takahashi, H.; Tsuji, N.; Fujisaki, S.; Kato, J. I. Involvement of an Essential Gene, MviN, in Murein Synthesis in Escherichia Coli. *J. Bacteriol.* **2008**, *190* (21), 7298–7301. https://doi.org/10.1128/JB.00551-08.
(16) Lingwood, D.; Simons, K. Lipid Rafts as a Membrane-Organizing Principle. *Science* **2010**, *327* (5961), 46–50. https://doi.org/10.1126/science.1174621.
(17) López, D.; Kolter, R. Functional Microdomains in Bacterial Membranes. *Genes Dev.* **2010**, *24* (17), 1893–1902. https://doi.org/10.1101/gad.1945010.
(18) Müller, A.; Wenzel, M.; Strahl, H.; Grein, F.; Saaki, T. N. V.; Kohl, B.; Siersma, T.; Bandow, J. E.; Sahl, H.-G.; Schneider, T.; Hamoen, L. W. Daptomycin Inhibits Cell Envelope Synthesis by Interfering with Fluid Membrane Microdomains. *Proc. Natl. Acad. Sci.* **2016**, *113* (45), E7077–E7086. https://doi.org/10/f9ckmv.
(19) Benarroch, J. M.; Asally, M. The Microbiologist's Guide to Membrane Potential Dynamics. *Trends Microbiol.* **2020**, *28* (4), 304–314. https://doi.org/10.1016/j.tim.2019.12.008.
(20) Mulkidjanian, A. Y.; Dibrov, P.; Galperin, M. Y. The Past and Present of Sodium Energetics: May the Sodium-Motive Force Be with You. *Biochim. Biophys. Acta BBA - Bioenerg.* **2008**, *1777* (7), 985–992. https://doi.org/10/b9cdz4.
(21) Chopra, I. Molecular Mechanisms Involved in the Transport of Antibiotics into Bacteria. *Parasitology* **1988**, *96* (S1), S25–S44. https://doi.org/10/drdc7n.
(22) Dassa, E.; Bouige, P. The ABC of ABCs: A Phylogenetic and Functional Classification of ABC Systems in Living Organisms. *Res. Microbiol.* **2001**, *152* (3), 211–229. https://doi.org/10/c67r3n.
(23) Sohlenkamp, C.; Geiger, O. Bacterial Membrane Lipids: Diversity in Structures and Pathways. *FEMS Microbiol. Rev.* **2015**, *40* (1), 133–159. https://doi.org/10.1093/femsre/fuv008.
(24) Barreteau, H.; Kovač, A.; Boniface, A.; Sova, M.; Gobec, S.; Blanot, D. Cytoplasmic Steps of Peptidoglycan Biosynthesis. *FEMS Microbiol. Rev.* **2008**, *32* (2), 168–207. https://doi.org/10.1111/j.1574-6976.2008.00104.x.
(25) van Heijenoort, J. Lipid Intermediates in the Biosynthesis of Bacterial Peptidoglycan. *Microbiol. Mol. Biol. Rev.* **2007**, *71* (4), 620–635. https://doi.org/10.1128/mmbr.00016-07.
(26) Ruiz, N. Lipid Flippases for Bacterial Peptidoglycan Biosynthesis. *Lipid Insights* **2015**, *2015*, 21–31. https://doi.org/10.4137/Lpi.s31783.
(27) Lovering, A. L.; Safadi, S. S.; Strynadka, N. C. J. Structural Perspective of Peptidoglycan Biosynthesis and Assembly. *Annu. Rev. Biochem.* **2012**, *81* (1), 451–478. https://doi.org/10.1146/annurev-biochem-061809-112742.
(28) Percy, M. G.; Gründling, A. Lipoteichoic Acid Synthesis and Function in Gram-Positive Bacteria. *Annu. Rev. Microbiol.* **2014**, *68* (1), 81–100. https://doi.org/10.1146/annurev-micro-091213-112949.
(29) Brown, S.; Santa Maria, J. P.; Walker, S. Wall Teichoic Acids of Gram-Positive Bacteria. *Annu. Rev. Microbiol.* **2013**, *67* (1), 313–336. https://doi.org/10.1146/annurev-micro-092412-155620.
(30) Egan, A. J. F.; Jean, N. L.; Koumoutsi, A.; Bougault, C. M.; Biboy, J.; Sassine, J.; Solovyova, A. S.; Breukink, E.; Typas, A.; Vollmer, W.; Simorre, J. P. Outer-Membrane Lipoprotein LpoB Spans the Periplasm to Stimulate the Peptidoglycan Synthase PBP1B. *Proc. Natl. Acad. Sci. U. S. A.* **2014**, *111* (22), 8197–8202. https://doi.org/10.1073/pnas.1400376111.
(31) Heine, H.; Rietschel, E. T.; Ulmer, A. J. The Biology of Endotoxin. *Appl. Biochem. Biotechnol. - Part B Mol. Biotechnol.* **2001**, *19* (3), 279–296. https://doi.org/10.1385/MB:19:3:279.

(32) Alexander, C.; Rietschel, E. T. Bacterial Lipopolysaccharides and Innate Immunity. *J. Endotoxin Res.* **2001**, *7* (3), 167–202. https://doi.org/10.1179/096805101101532675.
(33) Sperandeo, P.; Martorana, A. M.; Polissi, A. The Lipopolysaccharide Transport (Lpt) Machinery: A Nonconventional Transporter for Lipopolysaccharide Assembly at the Outer Membrane of Gram-Negative Bacteria. *J. Biol. Chem.* **2017**, *292* (44), 17981–17990. https://doi.org/10.1074/jbc.R117.802512.
(34) Konovalova, A.; Kahne, D. E.; Silhavy, T. J. Outer Membrane Biogenesis. *Annu. Rev. Microbiol.* **2017**, *71* (1), 539–556. https://doi.org/10.1146/annurev-micro-090816-093754.
(35) Okuda, S.; Sherman, D. J.; Silhavy, T. J.; Ruiz, N.; Kahne, D. Lipopolysaccharide Transport and Assembly at the Outer Membrane: The PEZ Model. *Nat. Rev. Microbiol.* **2016**, *14* (6), 337–345. https://doi.org/10.1038/nrmicro.2016.25.
(36) Martin-Loeches, I.; Dale, G. E.; Torres, A. Murepavadin: A New Antibiotic Class in the Pipeline. *Expert Rev. Anti Infect. Ther.* **2018**, *16* (4), 259–268. https://doi.org/10.1080/14787210.2018.1441024.
(37) Steckbeck, J. D.; Deslouches, B.; Montelaro, R. C. Antimicrobial Peptides: New Drugs for Bad Bugs? *Expert Opin. Biol. Ther.* **2014**, *14* (1), 11–14. https://doi.org/10.1517/14712598.2013.844227.
(38) Hancock, R. E. W.; Lehrer, R. Cationic Peptides: A New Source of Antibiotics. *Trends Biotechnol.* **1998**, *16* (2), 82–88. https://doi.org/10.1016/S0167-7799(97)01156-6.
(39) Zhao, P.; Xue, Y.; Gao, W.; Li, J.; Zu, X.; Fu, D.; Bai, X.; Zuo, Y.; Hu, Z.; Zhang, F. Bacillaceae -Derived Peptide Antibiotics since 2000. *Peptides* **2018**, *101* (December 2017), 10–16. https://doi.org/10.1016/j.peptides.2017.12.018.
(40) Cochrane, S. A.; Vederas, J. C. Lipopeptides from Bacillus and Paenibacillus Spp.: A Gold Mine of Antibiotic Candidates. *Med. Res. Rev.* **2016**, *36* (1), 4–31. https://doi.org/10.1002/med.21321.
(41) Guo, Y.; Huang, E.; Yuan, C.; Zhang, L.; Yousef, A. E. Isolation of a Paenibacillus Sp. Strain and Structural Elucidation of Its Broad-Spectrum Lipopeptide Antibiotic. *Appl. Environ. Microbiol.* **2012**, *78* (9), 3156–3165. https://doi.org/10.1128/AEM.07782-11.
(42) Huang, E.; Guo, Y.; Yousef, A. E. Biosynthesis of the New Broad-Spectrum Lipopeptide Antibiotic Paenibacterin in Paenibacillus Thiaminolyticus OSY-SE. *Res. Microbiol.* **2014**, *165* (3), 243–251. https://doi.org/10.1016/j.resmic.2014.02.002.
(43) Huang, E.; Yousef, A. E. The Lipopeptide Antibiotic Paenibacterin Binds to the Bacterial Outer Membrane and Exerts Bactericidal Activity through Cytoplasmic Membrane Damage. *Appl. Environ. Microbiol.* **2014**, *80* (9), 2700–2704. https://doi.org/10.1128/AEM.03775-13.
(44) Jenssen, H.; Hamill, P.; Hancock, R. E. W. Peptide Antimicrobial Agents. *Clin. Microbiol. Rev.* **2006**, *19* (3), 491–511. https://doi.org/10/cp8c89.
(45) Huang, E.; Yousef, A. E. Paenibacterin, a Novel Broad-Spectrum Lipopeptide Antibiotic, Neutralises Endotoxins and Promotes Survival in a Murine Model of Pseudomonas Aeruginosa-Induced Sepsis. *Int. J. Antimicrob. Agents* **2014**, *44* (1), 74–77. https://doi.org/10.1016/j.ijantimicag.2014.02.018.
(46) Waxman, D. J.; Strominger, J. L. Penicillin-Binding Proteins and the Mechanism of Action of Beta-Lactam Antibiotics. *Annu. Rev. Biochem.* **1983**, *52*, 825–869. https://doi.org/10.1146/annurev.bi.52.070183.004141.
(47) Zhang, L.; Dhillon, P.; Yan, H.; Farmer, S.; Hancock, R. E. W. Interactions of Bacterial Cationic Peptide Antibiotics with Outer and Cytoplasmic Membranes OfPseudomonas Aeruginosa Interactions of Bacterial Cationic Peptide Antibiotics with Outer and Cytoplasmic Membranes of Pseudomonas Aeruginosa. *Antimicrob Agents Chemother* **2000**, *44* (12), 3317–3321. https://doi.org/10.1128/AAC.44.12.3317-3321.2000.Updated.

(48) Li, R.; Du, W.; Yang, J.; Liu, Z.; Yousef, A. E. Control of Listeria Monocytogenes Biofilm by Paenibacterin, a Natural Antimicrobial Lipopeptide. *Food Control* **2018**, *84*, 529–535. https://doi.org/10.1016/j.foodcont.2017.08.031.

(49) Abdelhamid, A. G.; Yousef, A. E. The Microbial Lipopeptide Paenibacterin Disrupts Desiccation Resistance in Salmonella Enterica Serovars Tennessee and Eimsbuettel. *Appl. Environ. Microbiol.* **2019**, *85* (14). https://doi.org/10.1128/AEM.00739-19.

(50) Felnagle, E. A.; Jackson, E. E.; Chan, Y. A.; Podevels, A. M.; Berti, A. D.; McMahon, M. D.; Thomas, M. G. Nonribosomal Peptide Synthetases Involved in the Production of Medically Relevant Natural Products. *Mol. Pharm.* **2008**, *5* (2), 191–211. https://doi.org/10.1021/mp700137g.

(51) Marahiel, M. A. Working Outside the Protein-Synthesis Rules: Insights into Non-Ribosomal Peptide Synthesis. *J. Pept. Sci.* **2009**, *15* (12), 799–807. https://doi.org/10.1002/psc.1183.

(52) Taylor, S. D.; Palmer, M. The Action Mechanism of Daptomycin. *Bioorg. Med. Chem.* **2016**, *24* (24), 6253–6268. https://doi.org/10.1016/j.bmc.2016.05.052.

(53) Shaheen, M.; Li, J.; Ross, A. C.; Vederas, J. C.; Jensen, S. E. Paenibacillus Polymyxa PKB1 Produces Variants of Polymyxin B-Type Antibiotics. *Chem. Biol.* **2011**, *18* (12), 1640–1648. https://doi.org/10.1016/j.chembiol.2011.09.017.

(54) Choi, S.-K.; Park, S.-Y.; Kim, R.; Kim, S.-B.; Lee, C.-H.; Kim, J. F.; Park, S.-H. Identification of a Polymyxin Synthetase Gene Cluster of Paenibacillus Polymyxa and Heterologous Expression of the Gene in Bacillus Subtilis. *J. Bacteriol.* **2009**, *191* (10), 3350–3358. https://doi.org/10.1128/JB.01728-08.

(55) Zheng, J.; Knolhoff, A. M.; Brown, E. W.; Croley, T. R. ANTIMICROBIAL PEPTIDES, PHARMACEUTICAL COMPOSITIONS, AND METHODS OF USE THEREOF. US10906940B2, 02 2021.

(56) Li, Y.-X. X.; Zhong, Z.; Zhang, W.-P. P.; Qian, P.-Y. Y. Discovery of Cationic Nonribosomal Peptides as Gram-Negative Antibiotics through Global Genome Mining. *Nat. Commun.* **2018**, *9* (1), 3273–3273. https://doi.org/10.1038/s41467-018-05781-6.

(57) Knolhoff, A. M.; Zheng, J.; McFarland, M. A.; Luo, Y.; Callahan, J. H.; Brown, E. W.; Croley, T. R. Identification and Structural Characterization of Naturally-Occurring Broad-Spectrum Cyclic Antibiotics Isolated from Paenibacillus. *J. Am. Soc. Mass Spectrom.* **2015**, *26* (10), 1768–1779. https://doi.org/10.1007/s13361-015-1190-2.

(58) Bergen, P. J.; Li, J.; Rayner, C. R.; Nation, R. L. Colistin Methanesulfonate Is an Inactive Prodrug of Colistin against Pseudomonas Aeruginosa. *Antimicrob. Agents Chemother.* **2006**, *50* (6), 1953–1958. https://doi.org/10.1128/AAC.00035-06.

(59) Velkov, T.; Thompson, P. E.; Nation, R. L.; Li, J. Structure-Activity Relationships of Polymyxin Antibiotics. *J. Med. Chem.* **2010**, *53* (5), 1898–1916. https://doi.org/10.1021/jm900999h.

(60) Abdelraouf, K.; Braggs, K. H.; Yin, T.; Truong, L. D.; Hu, M.; Tam, V. H. Characterization of Polymyxin B-Induced Nephrotoxicity: Implications for Dosing Regimen Design. *Antimicrob. Agents Chemother.* **2012**, *56* (9), 4625–4629. https://doi.org/10.1128/AAC.00280-12.

(61) Bader, J.; Teuber, M. Action of Polymyxin B on Bacterial Membranes, I. Binding to the O-Antigenic Lipopolysaccharide of Salmonella Typhimurium. *Z. Für Naturforschung C* **1973**, *28* (7–8), 425–433. https://doi.org/10/gmcb3d.

(62) Nikaido, H. Molecular Basis of Bacterial Outer Membrane Permeability Revisited. *Microbiol. Mol. Biol. Rev. MMBR* **2003**, *67* (4), 593–656. https://doi.org/10.1128/MMBR.67.4.593.

(63) Pristovšek, P.; Kidrič, J. Solution Structure of Polymyxins B and E and Effect of Binding to Lipopolysaccharide: An NMR and Molecular Modeling Study. *J. Med. Chem.* **1999**, *42* (22), 4604–4613. https://doi.org/10.1021/jm991031b.
(64) van der Meijden, B.; Robinson, J. A. Synthesis of a Polymyxin Derivative for Photolabeling Studies in the Gram-Negative Bacterium Escherichia Coli. *J. Pept. Sci.* **2015**, *21* (3), 231–235. https://doi.org/10.1002/psc.2736.
(65) Suchanek, M.; Radzikowska, A.; Thiele, C. Photo-Leucine and Photo-Methionine Allow Identification of Protein-Protein Interactions in Living Cells. *Nat. Methods* **2005**, *2* (4), 261–267. https://doi.org/10.1038/nmeth752.
(66) Schindler, P. R. G.; Teuber, M. Action of Polymyxin B on Bacterial Membranes: Morphological Changes in the Cytoplasm and in the Outer Membrane of Salmonella Typhimurium and Escherichia Coli B. *Antimicrob. Agents Chemother.* **1975**, *8* (1), 95–104. https://doi.org/10.1128/AAC.8.1.95.
(67) Kanazawa, K.; Sato, Y.; Ohki, K.; Okimura, K.; Uchida, Y.; Shindo, M.; Sakura, N. Contribution of Each Amino Acid Residue in Polymyxin B3 to Antimicrobial and Lipopolysaccharide Binding Activity. *Chem. Pharm. Bull.* **2009**, *57* (3), 240–244. https://doi.org/10.1248/cpb.57.240.
(68) Okimura, K.; Ohki, K.; Sato, Y.; Ohnishi, K.; Sakura, N. Semi-Synthesis of Polymyxin B (2-10) and Colistin (2-10) Analogs Employing the Trichloroethoxycarbonyl (Troc) Group for Side Chain Protection of α, γ-Diaminobutyric Acid Residues. *Chem. Pharm. Bull.* **2007**, *55* (12), 1724–1730. https://doi.org/10.1248/cpb.55.1724.
(69) Clausell, A.; Rabanal, F.; Garcia-Subirats, M.; Asunción Alsina, M.; Cajal, Y. Membrane Association and Contact Formation by a Synthetic Analogue of Polymyxin B and Its Fluorescent Derivatives. *J. Phys. Chem. B* **2006**, *110* (9), 4465–4471. https://doi.org/10/dtkr4z.
(70) Shi, Y.; Cromie, M. J.; Hsu, F. F.; Turk, J.; Groisman, E. A. PhoP-Regulated Salmonella Resistance to the Antimicrobial Peptides Magainin 2 and Polymyxin B. *Mol. Microbiol.* **2004**, *53* (1), 229–241. https://doi.org/10.1111/j.1365-2958.2004.04107.x.
(71) Breazeale, S. D.; Ribeiro, A. A.; McClerren, A. L.; Raetz, C. R. H. H. A Formyltransferase Required for Polymyxin Resistance in Escherichia Coli and the Modification of Lipid A with 4-Amino-4-Deoxy-L-Arabinose: Identification and Function of UDP-4-Deoxy-4-Formamido-L-Arabinose. *J. Biol. Chem.* **2005**, *280* (14), 14154–14167. https://doi.org/10.1074/jbc.M414265200.
(72) Hinchliffe, P.; Yang, Q. E.; Portal, E.; Young, T.; Li, H.; Tooke, C. L.; Carvalho, M. J.; Paterson, N. G.; Brem, J.; Niumsup, P. R.; Tansawai, U.; Lei, L.; Li, M.; Shen, Z.; Wang, Y.; Schofield, C. J.; Mulholland, A. J.; Shen, J.; Fey, N.; Walsh, T. R.; Spencer, J. Insights into the Mechanistic Basis of Plasmid-Mediated Colistin Resistance from Crystal Structures of the Catalytic Domain of MCR-1. *Sci. Rep.* **2017**, *7* (January), 39392–39392. https://doi.org/10.1038/srep39392.
(73) Vaara, M.; Vaara, T. Sensitization of Gram-Negative Bacteria to Antibiotics and Complement by a Nontoxic Oligopeptide. *Nature* **1983**, *303* (5917), 526–528. https://doi.org/10.1038/303526a0.
(74) Viljanen, P.; Vaara, M. Susceptibility of Gram-Negative Bacteria to Polymyxin B Nonapeptide. *Antimicrob. Agents Chemother.* **1984**, *25* (6), 701–705. https://doi.org/10.1128/AAC.25.6.701.
(75) Vaara, M.; Viljanen, P. Binding of Polymyxin B Nonapeptide to Gram-Negative Bacteria. *Antimicrob. Agents Chemother.* **1985**, *27* (4), 548–554. https://doi.org/10.1128/AAC.27.4.548.

(76) Vaara, M. Agents That Increase the Permeability of the Outer Membrane. *Microbiol. Rev.* **1992**, *56* (3), 395–411. https://doi.org/10.1128/mmbr.56.3.395-411.1992.
(77) Tsubery, H.; Ofek, I.; Cohen, S.; Fridkin, M. Structure - Function Studies of Polymyxin B Nonapeptide: Implications to Sensitization of Gram-Negative Bacteria. *J. Med. Chem.* **2000**, *43* (16), 3085–3092. https://doi.org/10.1021/jm0000057.
(78) Vaara, M.; Siikanen, O.; Apajalahti, J.; Fox, J.; Frimodt-Møller, N.; He, H.; Poudyal, A.; Li, J.; Nation, R. L.; Vaara, T. A Novel Polymyxin Derivative That Lacks the Fatty Acid Tail and Carries Only Three Positive Charges Has Strong Synergism with Agents Excluded by the Intact Outer Membrane. *Antimicrob. Agents Chemother.* **2010**, *54* (8), 3341–3346. https://doi.org/10.1128/AAC.01439-09.
(79) Velkov, T.; Li, J.; Roberts, K. D.; Li, J. Rediscovering the Octapeptins. *Nat. Prod. Rep.* **2017**, *34* (3), 295–309. https://doi.org/10.1039/C6NP00113K.
(80) Meyers, E.; Parker, W. L.; Brown, W. E.; Linnett, P.; Strominger, J. L. Em49: A New Polypeptide Antibiotic Active Against Cell Membranes. *Ann. N. Y. Acad. Sci.* **1974**, *235* (1), 493–501. https://doi.org/10.1111/j.1749-6632.1974.tb43286.x.
(81) Han, M.-L. L.; Shen, H.-H. H.; Hansford, K. A.; Schneider, E. K.; Sivanesan, S.; Roberts, K. D.; Thompson, P. E.; Le Brun, A. P.; Zhu, Y.; Sani, M.-A. A.; Separovic, F.; Blaskovich, M. A. T. T.; Baker, M. A.; Moskowitz, S. M.; Cooper, M. A.; Li, J.; Velkov, T. Investigating the Interaction of Octapeptin A3 with Model Bacterial Membranes. *ACS Infect. Dis.* **2017**, *3* (8), 606–619. https://doi.org/10.1021/acsinfecdis.7b00065.
(82) Velkov, T.; Gallardo-Godoy, A.; Swarbrick, J. D.; Blaskovich, M. A. T.; Elliott, A. G.; Han, M.; Thompson, P. E.; Roberts, K. D.; Huang, J. X.; Becker, B.; Butler, M. S.; Lash, L. H.; Henriques, S. T.; Nation, R. L.; Sivanesan, S.; Sani, M. A.; Separovic, F.; Mertens, H.; Bulach, D.; Seemann, T.; Owen, J.; Li, J.; Cooper, M. A. Structure, Function, and Biosynthetic Origin of Octapeptin Antibiotics Active against Extensively Drug-Resistant Gram-Negative Bacteria. *Cell Chem. Biol.* **2018**, *25* (4), 380-391.e5. https://doi.org/10.1016/j.chembiol.2018.01.005.
(83) Hancock, R. E. W.; Haney, E. F.; Gill, E. E. The Immunology of Host Defence Peptides: Beyond Antimicrobial Activity. *Nat. Rev. Immunol.* **2016**, *16* (5), 321–334. https://doi.org/10/f8ktg8.
(84) Wimley, W. C. Describing the Mechanism of Antimicrobial Peptide Action with the Interfacial Activity Model. *ACS Chem. Biol.* **2010**, *5* (10), 905–917. https://doi.org/10.1021/cb1001558.
(85) Andersson, D. I.; Hughes, D.; Kubicek-Sutherland, J. Z. Mechanisms and Consequences of Bacterial Resistance to Antimicrobial Peptides. *Drug Resist. Updat.* **2016**, *26*, 43–57. https://doi.org/10.1016/j.drup.2016.04.002.
(86) Papagianni, M. Ribosomally Synthesized Peptides with Antimicrobial Properties: Biosynthesis, Structure, Function, and Applications. *Biotechnol. Adv.* **2003**, *21* (6), 465–499. https://doi.org/10.1016/S0734-9750(03)00077-6.
(87) Melo, M. N.; Ferre, R.; Castanho, M. A. R. B. Antimicrobial Peptides: Linking Partition, Activity and High Membrane-Bound Concentrations. *Nat. Rev. Microbiol.* **2009**, *7* (3), 245–250. https://doi.org/10.1038/nrmicro2095.
(88) Baumann, G.; Mueller, P. A Molecular Model of Membrane Excitability. *J. Supramol. Struct.* **1974**, *2* (5–6), 538–557. https://doi.org/10.1002/jss.400020504.
(89) Ludtke, S. J.; He, K.; Heller, W. T.; Harroun, T. A.; Yang, L.; Huang, H. W. Membrane Pores Induced by Magainin †. *Biochemistry* **1996**, *35* (43), 13723–13728. https://doi.org/10.1021/bi9620621.

(90) Pouny, Y.; Rapaport, D.; Mor, A.; Nicolas, P.; Shai, Y. Interaction of Antimicrobial Dermaseptin and Its Fluorescently Labeled Analogs with Phospholipid Membranes. *Biochemistry* **1992**, *31* (49), 12416–12423. https://doi.org/10.1021/bi00164a017.

(91) Duong, L.; Gross, S. P.; Siryaporn, A. Developing Antimicrobial Synergy With AMPs. *Front. Med. Technol.* **2021**, *3*. https://doi.org/10/gk4g9r.

(92) Srinivas, N.; Jetter, P.; Ueberbacher, B. J.; Werneburg, M.; Zerbe, K.; Steinmann, J.; Van der Meijden, B.; Bernardini, F.; Lederer, A.; Dias, R. L. A.; Misson, P. E.; Henze, H.; Zumbrunn, J.; Gombert, F. O.; Obrecht, D.; Hunziker, P.; Schauer, S.; Ziegler, U.; Kach, A.; Eberl, L.; Riedel, K.; DeMarco, S. J.; Robinson, J. A. Peptidomimetic Antibiotics Target Outer-Membrane Biogenesis in Pseudomonas Aeruginosa. *Science* **2010**, *327* (5968), 1010–1013. https://doi.org/10.1126/science.1182749.

(93) Shankaramma, S. C.; Athanassiou, Z.; Zerbe, O.; Moehle, K.; Mouton, C.; Bernardini, F.; Vrijbloed, J. W.; Obrecht, D.; Robinson, J. A. Macrocyclic Hairpin Mimetics of the Cationic Antimicrobial Peptide Protegrin I: A New Family of Broad-Spectrum Antibiotics. *ChemBioChem* **2002**, *3* (11), 1126–1133. https://doi.org/10.1002/1439-7633(20021104)3:11<1126::AID-CBIC1126>3.0.CO;2-I.

(94) Robinson, J. A.; Shankaramma, S. C.; Jetter, P.; Kienzl, U.; Schwendener, R. A.; Vrijbloed, J. W.; Obrecht, D. Properties and Structure–Activity Studies of Cyclic β-Hairpin Peptidomimetics Based on the Cationic Antimicrobial Peptide Protegrin I. *Bioorg. Med. Chem.* **2005**, *13* (6), 2055–2064. https://doi.org/10.1016/j.bmc.2005.01.009.

(95) Schmidt, J.; Patora-Komisarska, K.; Moehle, K.; Obrecht, D.; Robinson, J. A. Structural Studies of β-Hairpin Peptidomimetic Antibiotics That Target LptD in Pseudomonas Sp. *Bioorg. Med. Chem.* **2013**, *21* (18), 5806–5810. https://doi.org/10.1016/j.bmc.2013.07.013.

(96) Yeaman, M. R.; Yount, N. Y. Mechanisms of Antimicrobial Peptide Action and Resistance. *Pharmacol. Rev.* **2003**, *55* (1), 27–55. https://doi.org/10.1124/pr.55.1.2.

(97) Li, M.; Cha, D. J.; Lai, Y.; Villaruz, A. E.; Sturdevant, D. E.; Otto, M. The Antimicrobial Peptide-Sensing System Aps of Staphylococcus Aureus. *Mol. Microbiol.* **2007**, *66* (5), 1136–1147. https://doi.org/10.1111/j.1365-2958.2007.05986.x.

(98) Andrä, J.; Goldmann, T.; Ernst, C. M.; Peschel, A.; Gutsmann, T. Multiple Peptide Resistance Factor (MprF)-Mediated Resistance of Staphylococcus Aureus against Antimicrobial Peptides Coincides with a Modulated Peptide Interaction with Artificial Membranes Comprising Lysyl- Phosphatidylglycerol. *J. Biol. Chem.* **2011**, *286* (21), 18692–18700. https://doi.org/10.1074/jbc.M111.226886.

(99) Chen, F. J.; Lauderdale, T. L.; Lee, C. H.; Hsu, Y. C.; Huang, I. W.; Hsu, P. C.; Yang, C. S. Effect of a Point Mutation in MprF on Susceptibility to Daptomycin, Vancomycin, and Oxacillin in an MRSA Clinical Strain. *Front. Microbiol.* **2018**, *9* (MAY), 1–12. https://doi.org/10.3389/fmicb.2018.01086.

(100) Pilonieta, M. C.; Erickson, K. D.; Ernst, R. K.; Detweiler, C. S. A Protein Important for Antimicrobial Peptide Resistance, YdeI/OmdA, Is in the Periplasm and Interacts with OmpD/NmpC. *J. Bacteriol.* **2009**, *191* (23), 7243–7252. https://doi.org/10.1128/JB.00688-09.

(101) Li, Z.; Cao, Y.; Yi, L.; Liu, J. H.; Yang, Q. Emergent Polymyxin Resistance: End of an Era? *Open Forum Infect. Dis.* **2019**, *6* (10), 1–10. https://doi.org/10.1093/ofid/ofz368.

(102) Liu, Y. Y.; Wang, Y.; Walsh, T. R.; Yi, L. X.; Zhang, R.; Spencer, J.; Doi, Y.; Tian, G.; Dong, B.; Huang, X.; Yu, L. F.; Gu, D.; Ren, H.; Chen, X.; Lv, L.; He, D.; Zhou, H.; Liang, Z.; Liu, J. H.; Shen, J. Emergence of Plasmid-Mediated Colistin Resistance Mechanism MCR-1 in Animals and Human Beings in China: A Microbiological and Molecular

Biological Study. *Lancet Infect. Dis.* **2016**, *16* (2), 161–168. https://doi.org/10.1016/S1473-3099(15)00424-7.
(103) Wood, T. M.; Martin, N. I. The Calcium-Dependent Lipopeptide Antibiotics: Structure, Mechanism, & Medicinal Chemistry. *MedChemComm* **2019**, *10* (5), 634–646. https://doi.org/10.1039/C9MD00126C.
(104) Taylor, R.; Butt, K.; Scott, B.; Zhang, T.; Muraih, J. K.; Mintzer, E.; Taylor, S.; Palmer, M. Two Successive Calcium-Dependent Transitions Mediate Membrane Binding and Oligomerization of Daptomycin and the Related Antibiotic A54145. *Biochim. Biophys. Acta - Biomembr.* **2016**, *1858* (9), 1999–2005. https://doi.org/10.1016/j.bbamem.2016.05.020.
(105) Straus, S. K.; Hancock, R. E. W. Mode of Action of the New Antibiotic for Gram-Positive Pathogens Daptomycin: Comparison with Cationic Antimicrobial Peptides and Lipopeptides. *Biochim. Biophys. Acta - Biomembr.* **2006**, *1758* (9), 1215–1223. https://doi.org/10.1016/j.bbamem.2006.02.009.
(106) Silverman, J. A.; Perlmutter, N. G.; Shapiro, H. M. Correlation of Daptomycin Bactericidal Activity and Membrane Depolarization in Staphylococcus Aureus. *Antimicrob. Agents Chemother.* **2003**, *47* (8), 2538–2544. https://doi.org/10/dttg8r.
(107) Ho, S. W.; Jung, D.; Calhoun, J. R.; Lear, J. D.; Okon, M.; Scott, W. R. P.; Hancock, R. E. W.; Straus, S. K. Effect of Divalent Cations on the Structure of the Antibiotic Daptomycin. *Eur. Biophys. J.* **2008**, *37* (4), 421–433. https://doi.org/10/bnztmx.
(108) Ball, L.-J.; Goult, C. M.; Donarski, J. A.; Micklefield, J.; Ramesh, V. NMR Structure Determination and Calcium Binding Effects of Lipopeptide Antibiotic Daptomycin. *Org. Biomol. Chem.* **2004**, *2* (13), 1872–1878. https://doi.org/10/dd5h2p.
(109) Scott, W. R. P.; Baek, S.-B.; Jung, D.; Hancock, R. E. W.; Straus, S. K. NMR Structural Studies of the Antibiotic Lipopeptide Daptomycin in DHPC Micelles. *Biochim. Biophys. Acta BBA - Biomembr.* **2007**, *1768* (12), 3116–3126. https://doi.org/10/fskwwn.
(110) Muthaiyan, A.; Silverman, J. A.; Jayaswal, R. K.; Wilkinson, B. J. Transcriptional Profiling Reveals That Daptomycin Induces the Staphylococcus Aureus Cell Wall Stress Stimulon and Genes Responsive to Membrane Depolarization. *Antimicrob. Agents Chemother.* **2008**, *52* (3), 980–990. https://doi.org/10/bstwqt.
(111) Muraih, J. K.; Pearson, A.; Silverman, J.; Palmer, M. Oligomerization of Daptomycin on Membranes. *Biochim. Biophys. Acta BBA - Biomembr.* **2011**, *1808* (4), 1154–1160. https://doi.org/10/bmxrv8.
(112) Muraih, J. K.; Palmer, M. Estimation of the Subunit Stoichiometry of the Membrane-Associated Daptomycin Oligomer by FRET. *Biochim. Biophys. Acta BBA - Biomembr.* **2012**, *1818* (7), 1642–1647. https://doi.org/10/f3z3x8.
(113) Muraih, J. K.; Harris, J.; Taylor, S. D.; Palmer, M. Characterization of Daptomycin Oligomerization with Perylene Excimer Fluorescence: Stoichiometric Binding of Phosphatidylglycerol Triggers Oligomer Formation. *Biochim. Biophys. Acta - Biomembr.* **2012**, *1818* (3), 673–678. https://doi.org/10.1016/j.bbamem.2011.10.027.
(114) Zhang, T. H.; Taylor, S. D.; Palmer, M.; Duhamel, J. Membrane Binding and Oligomerization of the Lipopeptide A54145 Studied by Pyrene Fluorescence. *Biophys. J.* **2016**, *111* (6), 1267–1277. https://doi.org/10.1016/j.bpj.2016.07.018.
(115) Zhang, T.; Muraih, J. K.; MacCormick, B.; Silverman, J.; Palmer, M. Daptomycin Forms Cation- and Size-Selective Pores in Model Membranes. *Biochim. Biophys. Acta BBA - Biomembr.* **2014**, *1838* (10), 2425–2430. https://doi.org/10/f6fx5b.
(116) Zhang, T. H.; Muraih, J. K.; Tishbi, N.; Herskowitz, J.; Victor, R. L.; Silverman, J.; Uwumarenogie, S.; Taylor, S. D.; Palmer, M.; Mintzer, E. Cardiolipin Prevents Membrane

Translocation and Permeabilization by Daptomycin. *J. Biol. Chem.* **2014**, *289* (17), 11584–11591. https://doi.org/10.1074/jbc.M114.554444.
(117) Lakey, J. H.; Ptak, M. Fluorescence Indicates a Calcium-Dependent Interaction between the Lipopeptide Antibiotic LY 146032 and Phospholipid Membranes. *Biochemistry* **1988**, *27* (13), 4639–4645. https://doi.org/10.1021/bi00413a009.
(118) Beriashvili, D.; Taylor, R.; Kralt, B.; Abu Mazen, N.; Taylor, S. D.; Palmer, M. Mechanistic Studies on the Effect of Membrane Lipid Acyl Chain Composition on Daptomycin Pore Formation. *Chem. Phys. Lipids* **2018**, *216* (August), 73–79. https://doi.org/10.1016/j.chemphyslip.2018.09.015.
(119) Barnawi, G.; Noden, M.; Taylor, R.; Lohani, C.; Beriashvili, D.; Palmer, M.; Taylor, S. D. S. D. An Entirely Fmoc Solid Phase Approach to the Synthesis of Daptomycin Analogs. *Pept. Sci.* **2019**, *111* (1), 1–10. https://doi.org/10.1002/bip.23094.
(120) Grein, F.; Müller, A.; Scherer, K. M.; Liu, X.; Ludwig, K. C.; Klöckner, A.; Strach, M.; Sahl, H. G.; Kubitscheck, U.; Schneider, T. Ca2+-Daptomycin Targets Cell Wall Biosynthesis by Forming a Tripartite Complex with Undecaprenyl-Coupled Intermediates and Membrane Lipids. *Nat. Commun.* **2020**, *11* (1), 1–11. https://doi.org/10.1038/s41467-020-15257-1.
(121) Fischer, A.; Yang, S.-J.; Bayer, A. S.; Vaezzadeh, A. R.; Herzig, S.; Stenz, L.; Girard, M.; Sakoulas, G.; Scherl, A.; Yeaman, M. R.; Proctor, R. A.; Schrenzel, J.; François, P. Daptomycin Resistance Mechanisms in Clinically Derived Staphylococcus Aureus Strains Assessed by a Combined Transcriptomics and Proteomics Approach. *J. Antimicrob. Chemother.* **2011**, *66* (8), 1696–1711. https://doi.org/10/cqm985.
(122) Bayer, A. S.; Schneider, T.; Sahl, H. G. Mechanisms of Daptomycin Resistance in Staphylococcus Aureus: Role of the Cell Membrane and Cell Wall. *Ann. N. Y. Acad. Sci.* **2013**, *1277* (1), 139–158. https://doi.org/10.1111/j.1749-6632.2012.06819.x.
(123) Merrifield, R. B. Solid Phase Peptide Synthesis. I. The Synthesis of a Tetrapeptide. *J. Am. Chem. Soc.* **1963**, *85* (14), 2149–2154. https://doi.org/10.1021/ja00897a025.
(124) Isidro-Llobet, A.; Álvarez, M.; Albericio, F. Amino Acid-Protecting Groups. *Chem. Rev.* **2009**, *109* (6), 2455–2504. https://doi.org/10.1021/cr800323s.
(125) Amblard, M.; Fehrentz, J.-A.; Martinez, J.; Subra, G. Methods and Protocols of Modern Solid Phase Peptide Synthesis. *Mol. Biotechnol.* **2006**, *33* (3), 239–254. https://doi.org/10.1385/MB:33:3:239.
(126) Behrendt, R.; White, P.; Offer, J. Advances in Fmoc Solid-Phase Peptide Synthesis. *J. Pept. Sci.* **2016**, *22* (1), 4–27. https://doi.org/10.1002/psc.2836.
(127) *Peptide Synthesis*; Hussein, W. M., Skwarczynski, M., Toth, I., Eds.; Methods in Molecular Biology; Springer US: New York, NY, 2020; Vol. 2103. https://doi.org/10.1007/978-1-0716-0227-0.
(128) Coin, I.; Beyermann, M.; Bienert, M. Solid-Phase Peptide Synthesis: From Standard Procedures to the Synthesis of Difficult Sequences. *Nat. Protoc.* **2007**, *2* (12), 3247–3256. https://doi.org/10.1038/nprot.2007.454.
(129) Paradís-Bas, M.; Tulla-Puche, J.; Albericio, F. The Road to the Synthesis of "Difficult Peptides." *Chem. Soc. Rev.* **2016**, *45* (3), 631–654. https://doi.org/10.1039/C5CS00680E.
(130) *Fmoc Solid Phase Peptide Synthesis: A Practical Approach*; Chan, W. C., White, P. D., Eds.; The practical approach series; Oxford University Press: New York, 2000.
(131) Wöhr, T.; Wahl, F.; Nefzi, A.; Rohwedder, B.; Sato, T.; Sun, X.; Mutter, M.; Lausanne, C.-. Pseudo-Prolines as a Solubilizing, Structure-Disrupting Protection Technique in Peptide Synthesis. *J. Am. Chem. Soc.* **1996**, *118* (39), 9218–9227. https://doi.org/10.1021/ja961509q.

(132) Wöhr, T.; Mutter, M. Pseudo-Prolines in Peptide Synthesis: Direct Insertion of Serine and Threonine Derived Oxazolidines in Dipeptides. *Tetrahedron Lett.* **1995**, *36* (22), 3847–3848. https://doi.org/10.1016/0040-4039(95)00667-2.
(133) Haack, T.; Mutter, M. Serine Derived Oxazolidines as Secondary Structure Disrupting, Solubilizing Building Blocks in Peptide Synthesis. *Tetrahedron Lett.* **1992**, *33* (12), 1589–1592. https://doi.org/10.1016/S0040-4039(00)91681-2.
(134) Postma, T. M.; Albericio, F. Cysteine Pseudoprolines for Thiol Protection and Peptide Macrocyclization Enhancement in Fmoc-Based Solid-Phase Peptide Synthesis. *Org. Lett.* **2014**, *16* (6), 1772–1775. https://doi.org/10.1021/ol5004725.
(135) Nepomniaschiy, N.; Grimminger, V.; Cohen, A.; Digiovanni, S.; Lashuel, H. A.; Brik, A. Switch Peptide via Staudinger Reaction. *Org. Lett.* **2008**, *10* (22), 5243–5246. https://doi.org/10.1021/ol802268e.
(136) Itoh, H.; Inoue, M. Full Solid-Phase Total Synthesis of Macrocyclic Natural Peptides Using Four-Dimensionally Orthogonal Protective Groups. *Org. Biomol. Chem.* **2019**, *17* (27), 6519–6527. https://doi.org/10.1039/c9ob01130g.
(137) Cherkupally, P.; Acosta, G. A.; Ramesh, S.; De La Torre, B. G.; Govender, T.; Kruger, H. G.; Albericio, F. Solid-Phase Peptide Synthesis (SPPS), C-Terminal vs. Side-Chain Anchoring: A Reality or a Myth. *Amino Acids* **2014**, *46* (8), 1827–1838. https://doi.org/10.1007/s00726-014-1746-7.
(138) Thakkar, A.; Trinh, T. B.; Pei, D. Global Analysis of Peptide Cyclization Efficiency. *ACS Comb. Sci.* **2013**, *15* (2), 120–129. https://doi.org/10/f4k7hq.
(139) Sharma, S. K.; Wu, A. D.; Chandramouli, N.; Fotsch, C.; Kardash, G.; Bair, K. W. Solid-Phase Total Synthesis of Polymyxin B1. *J. Pept. Res.* **1999**, *53* (5), 501–506. https://doi.org/10.1034/j.1399-3011.1999.00045.x.
(140) Ramesh, S.; Govender, T.; Kruger, H. G.; Albericio, F.; de la Torre, B. G. An Improved and Efficient Strategy for the Total Synthesis of a Colistin-like Peptide. *Tetrahedron Lett.* **2016**, *57* (17), 1885–1888. https://doi.org/10/f8kcbk.
(141) Xu, W. L.; Cui, A. L.; Hu, X. X.; You, X. F.; Li, Z. R.; Zheng, J. S. A New Strategy for Total Solid-Phase Synthesis of Polymyxins. *Tetrahedron Lett.* **2015**, *56* (33), 4796–4799. https://doi.org/10.1016/j.tetlet.2015.06.056.
(142) Tsakos, M.; Schaffert, E. S.; Clement, L. L.; Villadsen, N. L.; Poulsen, T. B. Ester Coupling Reactions – an Enduring Challenge in the Chemical Synthesis of Bioactive Natural Products. *Nat. Prod. Rep.* **2015**, *32* (4), 605–632. https://doi.org/10.1039/C4NP00106K.
(143) Lam, H. Y.; Zhang, Y.; Liu, H.; Xu, J.; Wong, C. T. T.; Xu, C.; Li, X. Total Synthesis of Daptomycin by Cyclization via a Chemoselective Serine Ligation. *J. Am. Chem. Soc.* **2013**, *135* (16), 6272–6279. https://doi.org/10.1021/ja4012468.
(144) Lohani, C. R.; Taylor, R.; Palmer, M.; Taylor, S. D. Solid-Phase Total Synthesis of Daptomycin and Analogs. *Org. Lett.* **2015**, *17* (3), 748–751. https://doi.org/10.1021/acs.orglett.5b00043.
(145) Lohani, C. R.; Taylor, R.; Palmer, M.; Taylor, S. D. Solid-Phase Synthesis and in Vitro Biological Activity of a Thr4→Ser4 Analog of Daptomycin. *Bioorg. Med. Chem. Lett.* **2015**, *25* (23), 5490–5494. https://doi.org/10.1016/j.bmcl.2015.10.072.
(146) Lohani, C. R.; Soley, J.; Kralt, B.; Palmer, M.; Taylor, S. D. α-Azido Esters in Depsipeptide Synthesis: C-O Bond Cleavage during Azido Group Reduction. *J. Org. Chem.* **2016**, *81* (23), 11831–11840. https://doi.org/10.1021/acs.joc.6b02309.
(147) Lohani, C. R.; Rasera, B.; Scott, B.; Palmer, M.; Taylor, S. D. α-Azido Acids in Solid-Phase Peptide Synthesis: Compatibility with Fmoc Chemistry and an Alternative Approach to the

Solid Phase Synthesis of Daptomycin Analogs. *J. Org. Chem.* **2016**, *81* (6), 2624–2628. https://doi.org/10.1021/acs.joc.5b02882.

(148) Wodtke, R.; Ruiz-Gómez, G.; Kuchar, M.; Teresa Pisabarro, M.; Novotná, P.; Urbanová, M.; Steinbach, J.; Pietzsch, J.; Löser, R. Cyclopeptides Containing the DEKS Motif as Conformationally Restricted Collagen Telopeptide Analogues: Synthesis and Conformational Analysis. *Org. Biomol. Chem.* **2015**, *13* (6), 1878–1896. https://doi.org/10/gj6kh8.

(149) Davies, J. S. The Cyclization of Peptides and Depsipeptides. *J. Pept. Sci.* **2003**, *9* (8), 471–501. https://doi.org/10/bwqcnv.

(150) White, C. J.; Yudin, A. K. Contemporary Strategies for Peptide Macrocyclization. *Nat. Chem.* **2011**, *3* (7), 509–524. https://doi.org/10/fbmmb3.

(151) We elected to use oxyma/COMU/NMM to install residues 4-10 as we found these conditions provide a very high quality product. Thr3, Val2, D-Orn1 and the lipid all have to be installed in the presence of the free Thr side chain. We found that guanidinium coupling reagents will react, albeit slowly, with the OH group in Thr; therefore, we switched to DIC for introducing these residues as well as residues 11 and 12.

(152) Moreira, R.; Barnawi, G.; Beriashvili, D.; Palmer, M.; Taylor, S. D. The Effect of Replacing the Ester Bond with an Amide Bond and of Overall Stereochemistry on the Activity of Daptomycin. *Bioorg. Med. Chem.* **2019**, *27* (1), 240–246. https://doi.org/10.1016/j.bmc.2018.12.004.

(153) Hart, P. T.; Kleijn, L. H. J.; De Bruin, G.; Oppedijk, S. F.; Kemmink, J.; Martin, N. I. A Combined Solid- and Solution-Phase Approach Provides Convenient Access to Analogues of the Calcium-Dependent Lipopeptide Antibiotics. *Org. Biomol. Chem.* **2014**, *12* (6), 913–918. https://doi.org/10.1039/c3ob42238k.

(154) We anticipated that the rate of reduction of the azido group in the peptide containing Daba(N3) (peptide 9 containing Daba(N3) in place of Dapa(N3)) would be slower than that of the less sterically hindered Dapa residue, and thus treated the peptide containing Daba(N3) with DTT/DIPEA for 16 h.

(155) Pícha, J.; Buděšínský, M.; Macháčková, K.; Collinsová, M.; Jiráček, J. Optimized Syntheses of Fmoc Azido Amino Acids for the Preparation of Azidopeptides. *J. Pept. Sci.* **2017**, *23* (3), 202–214. https://doi.org/10/gj6kh7.

(156) Lau, Y. H.; Spring, D. R. Efficient Synthesis of Fmoc-Protected Azido Amino Acids. *Synlett* **2011**, *2011* (13), 1917–1919. https://doi.org/10/fs9rhk.

(157) De Vleeschouwer, M.; Sinnaeve, D.; Van Den Begin, J.; Coenye, T.; Martins, J. C.; Madder, A. Rapid Total Synthesis of Cyclic Lipodepsipeptides as a Premise to Investigate Their Self-Assembly and Biological Activity. *Chem. - Eur. J.* **2014**, *20* (25), 7766–7775. https://doi.org/10.1002/chem.201402066.

(158) Biermann, U.; Metzger, J. O. Alkylation of Alkenes: Ethylaluminum Sesquichloride-Mediated Hydro-Alkyl Additions with Alkyl Chloroformates and Di-Tert-Butylpyrocarbonate. *J. Am. Chem. Soc.* **2004**, *126* (33), 10319–10330. https://doi.org/10/fm4jqx.

(159) Gude, M.; Ryf, J.; White, P. D. An Accurate Method for the Quantitation of Fmoc-Derivatized Solid Phase Supports. *Lett. Pept. Sci.* **2002**, *9* (4–5), 203–206. https://doi.org/10.1007/BF02538384.

(160) Levinson, A. M.; McGee, J. H.; Roberts, A. G.; Creech, G. S.; Wang, T.; Peterson, M. T.; Hendrickson, R. C.; Verdine, G. L.; Danishefsky, S. J. Total Chemical Synthesis and Folding of All- l and All- d Variants of Oncogenic KRas(G12V). *J. Am. Chem. Soc.* **2017**, *139* (22), 7632–7639. https://doi.org/10.1021/jacs.7b02988.

(161) Jacobsen, M. T.; Petersen, M. E.; Ye, X.; Galibert, M.; Lorimer, G. H.; Aucagne, V.; Kay, M. S. A Helping Hand to Overcome Solubility Challenges in Chemical Protein Synthesis. *J. Am. Chem. Soc.* **2016**, *138* (36), 11775–11782. https://doi.org/10.1021/jacs.6b05719.
(162) Wiegand, I.; Hilpert, K.; Hancock, R. E. W. Agar and Broth Dilution Methods to Determine the Minimal Inhibitory Concentration (MIC) of Antimicrobial Substances. *Nat. Protoc.* **2008**, *3* (2), 163–175. https://doi.org/10.1038/nprot.2007.521.
(163) Koh, J. J.; Lin, S.; Beuerman, R. W.; Liu, S. Recent Advances in Synthetic Lipopeptides as Anti-Microbial Agents: Designs and Synthetic Approaches. *Amino Acids* **2017**, *49* (10), 1653–1677. https://doi.org/10.1007/s00726-017-2476-4.
(164) Fang, Y.; Zhong, W.; Wang, Y.; Xun, T.; Lin, D.; Liu, W.; Wang, J.; Lv, L.; Liu, S.; He, J. Tuning the Antimicrobial Pharmacophore to Enable Discovery of Short Lipopeptides with Multiple Modes of Action. *Eur. J. Med. Chem.* **2014**, *83*, 36–44. https://doi.org/10/f6fjng.
(165) Rabanal, F.; Cajal, Y. Recent Advances and Perspectives in the Design and Development of Polymyxins. *Nat. Prod. Rep.* **2017**, *34* (7), 886–908. https://doi.org/10/gk4g9n.
(166) Akhoundsadegh, N.; Belanger, C. R.; Hancock, R. E. W. Outer Membrane Interaction Kinetics of New Polymyxin B Analogs in Gram-Negative Bacilli. *Antimicrob. Agents Chemother.* **2019**, *63* (10), 1–13. https://doi.org/10.1128/AAC.00935-19.
(167) Gallardo-Godoy, A.; Hansford, K. A.; Muldoon, C.; Becker, B.; Elliott, A. G.; Huang, J. X.; Pelingon, R.; Butler, M. S.; Blaskovich, M. A. T.; Cooper, M. A. Structure-Function Studies of Polymyxin B Lipononapeptides. *Molecules* **2019**, *24* (3), 553. https://doi.org/10/gk4g9p.
(168) Tsukamoto, Fh.; Kondo, Y. Facile and Selective Cleavage of Allyl Ethers Based on Palladium(0)-Catalyzed Allylic Alkylation of N,N'-Dimethylbarbituric Acid. 3. https://doi.org/10/cj283r.
(169) Giltrap, A. M.; Haeckl, F. P. J.; Kurita, K. L.; Linington, R. G.; Payne, R. J. Total Synthesis of Skyllamycins A–C. *Chem. – Eur. J.* **2017**, *23* (60), 15046–15049. https://doi.org/10/gj6kh6.
(170) Giltrap, A. M.; Haeckl, F. P. J.; Kurita, K. L.; Linington, R. G.; Payne, R. J. Synthetic Studies Toward the Skyllamycins: Total Synthesis and Generation of Simplified Analogues. *J. Org. Chem.* **2018**, *83* (13), 7250–7270. https://doi.org/10/gdw5mm.
(171) Barlos, K.; Gatos, D.; Kallitsis, J.; Papaphotiu, G.; Sotiriu, P.; Wenqing, Y.; Schäfer, W. Darstellung geschützter peptid-fragmente unter einsatz substituierter triphenylmethyl-harze. *Tetrahedron Lett.* **1989**, *30* (30), 3943–3946. https://doi.org/10/bbrv6r.
(172) Morris, M. A.; Malek, M.; Hashemian, M. H.; Nguyen, B. T.; Manuse, S.; Lewis, K.; Nowick, J. S. A Fluorescent Teixobactin Analogue. *ACS Chem. Biol.* **2020**, *15* (5), 1222–1231. https://doi.org/10.1021/acschembio.9b00908.
(173) Chico, D. E.; Given, R. L.; Miller, B. T. Binding of Cationic Cell-Permeable Peptides to Plastic and Glass. *Peptides* **2003**, *24* (1), 3–9. https://doi.org/10.1016/S0196-9781(02)00270-X.
(174) Sharafi, T.; Ardebili, A. Plastic Binding Feature of Polymyxins: The Effect on MIC Susceptibility Measurements. *Infect. Drug Resist.* **2019**, *12*, 2649–2653. https://doi.org/10/gj6kjm.
(175) Kavanagh, A.; Ramu, S.; Gong, Y.; Cooper, M. A.; Blaskovich, M. A. T. Effects of Microplate Type and Broth Additives on Microdilution MIC Susceptibility Assays. *Antimicrob. Agents Chemother.* **2018**, *63* (1), e01760-18, /aac/63/1/AAC.01760-18.atom. https://doi.org/10/gj6kh5.
(176) Lavis, L. D.; Raines, R. T. Bright Ideas for Chemical Biology. *ACS Chem. Biol.* **2008**, *3* (3), 142–155. https://doi.org/10.1021/cb700248m.

(177) Sahoo, H. Fluorescent Labeling Techniques in Biomolecules: A Flashback. *RSC Adv.* **2012**, *2* (18), 7017–7029. https://doi.org/10.1039/C2RA20389H.
(178) Royer, C. A. Probing Protein Folding and Conformational Transitions with Fluorescence. *Chem. Rev.* **2006**, *106* (5), 1769–1784. https://doi.org/10.1021/cr0404390.
(179) Ghisaidoobe, A.; Chung, S. Intrinsic Tryptophan Fluorescence in the Detection and Analysis of Proteins: A Focus on Förster Resonance Energy Transfer Techniques. *Int. J. Mol. Sci.* **2014**, *15* (12), 22518–22538. https://doi.org/10.3390/ijms151222518.
(180) Qiu, J.; Kirsch, L. E. Evaluation of Lipopeptide (Daptomycin) Aggregation Using Fluorescence, Light Scattering, and Nuclear Magnetic Resonance Spectroscopy. *J. Pharm. Sci.* **2014**, *103* (3), 853–861. https://doi.org/10/gkd67b.
(181) Krueger, A. T.; Imperiali, B. Fluorescent Amino Acids: Modular Building Blocks for the Assembly of New Tools for Chemical Biology. *ChemBioChem* **2013**, *14* (7), 788–799. https://doi.org/10.1002/cbic.201300079.
(182) Cheng, Z.; Kuru, E.; Sachdeva, A.; Vendrell, M. Fluorescent Amino Acids as Versatile Building Blocks for Chemical Biology. *Nat. Rev. Chem.* **2020**, *4* (6), 275–290. https://doi.org/10.1038/s41570-020-0186-z.
(183) Harkiss, A. H.; Sutherland, A. Recent Advances in the Synthesis and Application of Fluorescent α-Amino Acids. *Org. Biomol. Chem.* **2016**, *14* (38), 8911–8921. https://doi.org/10.1039/c6ob01715k.
(184) Loving, G. S.; Sainlos, M.; Imperiali, B. Monitoring Protein Interactions and Dynamics with Solvatochromic Fluorophores. *Trends Biotechnol.* **2010**, *28* (2), 73–83. https://doi.org/10.1016/j.tibtech.2009.11.002.
(185) Wang, J.; Xie, J.; Schultz, P. G. A Genetically Encoded Fluorescent Amino Acid. *J. Am. Chem. Soc.* **2006**, *128* (27), 8738–8739. https://doi.org/10/dxt6hp.
(186) Vázquez, M. E.; Rothman, D. M.; Imperiali, B. A New Environment-Sensitive Fluorescent Amino Acid for Fmoc-Based Solid Phase Peptide Synthesis. *Org. Biomol. Chem.* **2004**, *2* (14), 1965–1966. https://doi.org/10/cm3x23.
(187) Loving, G.; Imperiali, B. A Versatile Amino Acid Analogue of the Solvatochromic Fluorophore 4- *N,N* -Dimethylamino-1,8-Naphthalimide: A Powerful Tool for the Study of Dynamic Protein Interactions. *J. Am. Chem. Soc.* **2008**, *130* (41), 13630–13638. https://doi.org/10.1021/ja804754y.
(188) Nitz, M.; Mezo, A. R.; Ali, M. H.; Imperiali, B. Enantioselective Synthesis and Application of the Highly Fluorescent and Environment-Sensitive Amino Acid 6-(2-Dimethylaminonaphthoyl) Alanine (DANA). *Chem. Commun.* **2002**, *17* (17), 1912–1913. https://doi.org/10.1039/b205224e.
(189) Cohen, B. E. Probing Protein Electrostatics with a Synthetic Fluorescent Amino Acid. *Science* **2002**, *296* (5573), 1700–1703. https://doi.org/10.1126/science.1069346.
(190) Koopmans, T.; Van Haren, M.; Van Ufford, L. Q.; Beekman, J. M.; Martin, N. I. A Concise Preparation of the Fluorescent Amino Acid L-(7-Hydroxycoumarin-4- Yl) Ethylglycine and Extension of Its Utility in Solid Phase Peptide Synthesis. *Bioorg. Med. Chem.* **2013**, *21* (2), 553–559. https://doi.org/10.1016/j.bmc.2012.10.055.
(191) Kuhn, S. M.; Rubini, M.; Müller, M. A.; Skerra, A. Biosynthesis of a Fluorescent Protein with Extreme Pseudo-Stokes Shift by Introducing a Genetically Encoded Non-Natural Amino Acid Outside the Fluorophore. *J. Am. Chem. Soc.* **2011**, *133* (11), 3708–3711. https://doi.org/10/c8xgjf.
(192) Cottam Jones, J. M.; Harris, P. W. R.; Scanlon, D. B.; Forbes, B. E.; Brimble, M. A.; Abell, A. D. Fluorescent IGF-II Analogues for FRET-Based Investigations into the Binding of IGF-II to the IGF-1R. *Org. Biomol. Chem.* **2016**, *14* (9), 2698–2705. https://doi.org/10/f8sz3j.

(193) Wagner, B. D. The Use of Coumarins as Environmentally-Sensitive Fluorescent Probes of Heterogeneous Inclusion Systems. *Molecules* **2009**, *14* (1), 210–237. https://doi.org/10.3390/molecules14010210.
(194) Cao, D.; Liu, Z.; Verwilst, P.; Koo, S.; Jangjili, P.; Kim, J. S.; Lin, W. Coumarin-Based Small-Molecule Fluorescent Chemosensors. *Chem. Rev.* **2019**, *119* (18), 10403–10519. https://doi.org/10/gkrg9v.
(195) Mukherjee, T.; Rao, K.; Mittal, J. Photodecomposition of Coumarin Laser Dyes in Different Solvent Systems. *Indian J. Chem. -Sect. IJC-A* **1986**, *25* (11), 993–1000.
(196) Jones, G.; Jackson, W. R.; Choi, C. Y.; Bergmark, W. R. Solvent Effects on Emission Yield and Lifetime for Coumarin Laser Dyes. Requirements for a Rotatory Decay Mechanism. *J. Phys. Chem.* **1985**, *89* (2), 294–300. https://doi.org/10.1021/j100248a024.
(197) von Trebra, R. J.; Koch, T. H. Photochemistry of Coumarin Laser Dyes: The Role of Singlet Oxygen in the Photo-Oxidation of Coumarin 311. *J. Photochem.* **1986**, *35* (1), 33–46. https://doi.org/10.1016/0047-2670(86)87115-5.
(198) Lopez Arbeloa, T.; Lopez Arbeloa, F.; Tapia, M. J.; Lopez Arbeloa, I. Hydrogen-Bonding Effect on the Photophysical Properties of 7-Aminocoumarin Derivatives. *J. Phys. Chem.* **1993**, *97* (18), 4704–4707. https://doi.org/10.1021/j100120a024.
(199) Lakowicz, J. R. Solvent and Environmental Effects. In *Principles of Fluorescence Spectroscopy*; Lakowicz, J. R., Ed.; Springer US: Boston, MA, 2006; pp 205–235. https://doi.org/10.1007/978-0-387-46312-4_6.
(200) Rettig, W. Charge Separation in Excited States of Decoupled Systems—TICT Compounds and Implications Regarding the Development of New Laser Dyes and the Primary Process of Vision and Photosynthesis. *Angew. Chem. Int. Ed. Engl.* **1986**, *25* (11), 971–988. https://doi.org/10/c6ttmv.
(201) Jones, G.; Jackson, W. R.; Halpern, A. M. Medium Effects on Fluorescence Quantum Yields and Lifetimes for Coumarin Laser Dyes. *Chem. Phys. Lett.* **1980**, *72* (2), 391–395. https://doi.org/10/bdxqfz.
(202) Wirtz, L.; Kazmaier, U. A Mild Titanium-Catalyzed Synthesis of Functionalized Amino Coumarins as Fluorescence Labels. *Eur. J. Org. Chem.* **2011**, *2011* (35), 7062–7065. https://doi.org/10.1002/ejoc.201101117.
(203) Wirtz, L.; Auerbach, D.; Jung, G.; Kazmaier, U. Fluorescence Labeling of Amino Acids and Peptides with 7-Aminocoumarins. *Synthesis* **2012**, *44* (13), 2005–2012. https://doi.org/10.1055/s-0031-1291145.
(204) Verma, P.; Pal, H. Intriguing H-Aggregate and H-Dimer Formation of Coumarin-481 Dye in Aqueous Solution As Evidenced from Photophysical Studies. *J. Phys. Chem. A* **2012**, *116* (18), 4473–4484. https://doi.org/10/f3zj73.
(205) Ogawa, M.; Kosaka, N.; Choyke, P. L.; Kobayashi, H. H-Type Dimer Formation of Fluorophores: A Mechanism for Activatable, in Vivo Optical Molecular Imaging. *ACS Chem. Biol.* **2009**, *4* (7), 535–546. https://doi.org/10/cpw68m.
(206) Valdes-Aguilera, O.; Neckers, D. C. Aggregation Phenomena in Xanthene Dyes. *Acc. Chem. Res.* **1989**, *22* (5), 171–177. https://doi.org/10/df3t63.
(207) Bollmann, S.; Löllmann, M.; Sauer, M.; Doose, S. Dimer Formation of Organic Fluorophores Reports on Biomolecular Dynamics under Denaturing Conditions. *Phys. Chem. Chem. Phys.* **2011**, *13* (28), 12874. https://doi.org/10/cpjdcd.
(208) Brun, M.-P.; Bischoff, L.; Garbay, C. A Very Short Route to Enantiomerically Pure Coumarin-Bearing Fluorescent Amino Acids. *Angew. Chem. Int. Ed.* **2004**, *43* (26), 3432–3436. https://doi.org/10.1002/anie.200454116.

(209) Kele, P.; Sui, G.; Huo, Q.; Leblanc, R. M. Highly Enantioselective Synthesis of a Fluorescent Amino Acid. *Tetrahedron Asymmetry* **2000**, *11* (24), 4959–4963. https://doi.org/10.1016/S0957-4166(00)00459-6.
(210) Sui, G.; Kele, P.; Orbulescu, J.; Huo, Q.; Leblanc, R. M. Synthesis of a Coumarin Based Fluorescent Amino Acid. *Lett. Pept. Sci.* **2001**, *8* (1), 47–51. https://doi.org/10.1007/BF02443578.
(211) v. Pechmann, H.; Schaal, M. Studien Über Cumarine. – II. Ueber Dasp - Dimethylamido- β-Methylcumarin Und Einige Homologe. *Berichte Dtsch. Chem. Ges.* **1899**, *32* (3), 3690–3696. https://doi.org/10.1002/cber.189903203161.
(212) Li, Z.; Su, K.; Jiang, Z.; Yu, Y.; You, Q.; Zhang, X. Photoactivatable Prolyl Hydroxylase 2 Inhibitors for Stabilizing the Hypoxia-Inducible Factor with Light. *J. Med. Chem.* **2019**, *62* (16), 7583–7588. https://doi.org/10.1021/acs.jmedchem.9b00688.
(213) Dastlik, K. A.; Sundermeier, U.; Johns, D. M.; Chen, Y.; Williams, R. M. An Improved Synthesis of Optically Pure 4-Boc-5,6-Diphenylmorpholin-2-One and 4-Cbz-5,6-Diphenylmorpholin-2-One. *Synlett* **2005**, No. 4, 693–696. https://doi.org/10/frjfdp.
(214) Belokon, Yuri. N.; Bakhmutov, V. I.; Chernoglazova, N. I.; Kochetkov, K. A.; Vitt, S. V.; Garbalinskaya, N. S.; Belikov, V. M. General Method for the Asymmetric Synthesis of α-Amino Acids via Alkylation of the Chiral Nickel(<scp>II</Scp>) Schiff Base Complexes of Glycine and Alanine. *J Chem Soc Perkin Trans 1* **1988**, *58* (2), 305–312. https://doi.org/10.1039/P19880000305.
(215) Fujii, K.; Ikai, Y.; Mayumi, T.; Oka, H.; Suzuki, M.; Harada, K. I. A Nonempirical Method Using LC/MS for Determination of the Absolute Configuration of Constituent Amino Acids in a Peptide: Elucidation of Limitations of Marfey's Method and of Its Separation Mechanism. *Anal. Chem.* **1997**, *69* (16), 3346–3352. https://doi.org/10.1021/ac9701795.
(216) Marfey, P. Determination OfD-Amino Acids. II. Use of a Bifunctional Reagent, 1,5-Difluoro-2,4-Dinitrobenzene. *Carlsberg Res. Commun.* **1984**, *49* (6), 591. https://doi.org/10/cmsnkv.
(217) Szókán, G.; Mezö, G.; Hudecz, F. Application of Marfey's Reagent in Racemization Studies of Amino Acids and Peptides. *J. Chromatogr. A* **1988**, *444*, 115–122. https://doi.org/10/fr8wx9.
(218) Bhushan, R.; Bruckner, H. Marfey's Reagent for Chiral Amino Acid Analysis: A Review. *Amino Acids* **2004**, *27* (3–4), 231–247. https://doi.org/10.1007/s00726-004-0118-0.
(219) Soloshonok, V. A.; Cai, C.; Hruby, V. J.; Van Meervelt, L.; Mischenko, N. Stereochemically Defined C-Substituted Glutamic Acids and Their Derivatives. 1. An Efficient Asymmetric Synthesis of (2S,3S)-3-Methyl- and - 3-Trifluoromethylpyroglutamic Acids. *Tetrahedron* **1999**, *55* (41), 12031–12044. https://doi.org/10.1016/S0040-4020(99)00711-5.
(220) McInerney, M. P.; Roberts, K. D.; Thompson, P. E.; Li, J.; Nation, R. L.; Velkov, T.; Nicolazzo, J. A. Quantitation of Polymyxin–Lipopolysaccharide Interactions Using an Image-Based Fluorescent Probe. *J. Pharm. Sci.* **2016**, *105* (2), 1006–1010. https://doi.org/10.1016/j.xphs.2015.10.028.
(221) Moore, R. A.; Bates, N. C.; Hancock, R. E. W. Interaction of Polycationic Antibiotics with Pseudomonas Aeruginosa Lipopolysaccharide and Lipid A Studied by Using Dansyl-Polymyxin. *Antimicrob. Agents Chemother.* **1986**, *29* (3), 496–500. https://doi.org/10.1128/AAC.29.3.496.
(222) Yu, L.; Tan, M.; Ho, B.; Ding, J. L.; Wohland, T. Determination of Critical Micelle Concentrations and Aggregation Numbers by FLuorescence Correlation Spectroscopy: Aggregation of a Lipopolysaccharide. *Anal. Chim. Acta* **2006**, 10.

(223) Santos, N. C.; Silva, A. C.; Castanho, M. A. R. B.; Martins-Silva, J.; Saldanha, C. Evaluation of Lipopolysaccharide Aggregation by Light Scattering Spectroscopy. *ChemBioChem* **2003**, *4* (1), 96–100. https://doi.org/10.1002/cbic.200390020.

(224) Lepper, P.; Held, T.; Schneider, E.; Bölke, E.; Gerlach, H.; Trautmann, M. Clinical Implications of Antibiotic-Induced Endotoxin Release in Septic Shock. *Intensive Care Med.* **2002**, *28* (7), 824–833. https://doi.org/10.1007/s00134-002-1330-6.

(225) Gutsmann, T.; Razquin-Olazarán, I.; Kowalski, I.; Kaconis, Y.; Howe, J.; Bartels, R.; Hornef, M.; Schürholz, T.; Rössle, M.; Sanchez-Gómez, S.; Moriyon, I.; Martinez de Tejada, G.; Brandenburg, K. New Antiseptic Peptides To Protect against Endotoxin-Mediated Shock. *Antimicrob. Agents Chemother.* **2010**, *54* (9), 3817–3824. https://doi.org/10.1128/AAC.00534-10.

(226) Kirikae, T.; Hirata, M.; Yamasu, H.; Kirikae, F.; Tamura, H.; Kayama, F.; Nakatsuka, K.; Yokochi, T.; Nakano, M. Protective Effects of a Human 18-Kilodalton Cationic Antimicrobial Protein (CAP18)-Derived Peptide against Murine Endotoxemia. *Infect. Immun.* **1998**, *66* (5), 1861–1868. https://doi.org/10.1128/IAI.66.5.1861-1868.1998.

(227) Skinner, S. O.; Sepúlveda, L. A.; Xu, H.; Golding, I. Measuring MRNA Copy Number in Individual Escherichia Coli Cells Using Single-Molecule Fluorescent in Situ Hybridization. *Nat. Protoc.* **2013**, *8* (6), 1100–1113. https://doi.org/10.1038/nprot.2013.066.

(228) Young, J. W.; Locke, J. C. W.; Altinok, A.; Rosenfeld, N.; Bacarian, T.; Swain, P. S.; Mjolsness, E.; Elowitz, M. B. Measuring Single-Cell Gene Expression Dynamics in Bacteria Using Fluorescence Time-Lapse Microscopy. *Nat. Protoc.* **2012**, *7* (1), 80–88. https://doi.org/10.1038/nprot.2011.432.

(229) Deris, Z. Z.; Swarbrick, J. D.; Roberts, K. D.; Azad, M. A. K.; Akter, J.; Horne, A. S.; Nation, R. L.; Rogers, K. L.; Thompson, P. E.; Velkov, T.; Li, J. Probing the Penetration of Antimicrobial Polymyxin Lipopeptides into Gram-Negative Bacteria. *Bioconjug. Chem.* **2014**, *25* (4), 750–760. https://doi.org/10.1021/bc500094d.

(230) Drouet, F.; Noisier, A. F. M.; Harris, C. S.; Furkert, D. P.; Brimble, M. A. A Convenient Method for the Asymmetric Synthesis of Fluorinated α-Amino Acids from Alcohols. *Eur. J. Org. Chem.* **2014**, *2014* (6), 1195–1201. https://doi.org/10.1002/ejoc.201301718.

(231) Ueki, H.; Ellis, T. K.; Martin, C. H.; Boettiger, T. U.; Bolene, S. B.; Soloshonok, V. A. Improved Synthesis of Proline-Derived Ni(II) Complexes of Glycine: Versatile Chiral Equivalents of Nucleophilic Glycine for General Asymmetric Synthesis of α-Amino Acids. *J. Org. Chem.* **2003**, *68* (18), 7104–7107. https://doi.org/10.1021/jo0301494.

(232) Belokon', Y. N.; Tararov, V. I.; Maleev, V. I.; Savel'eva, T. F.; Ryzhov, M. G. Improved Procedures for the Synthesis of (S)-2-[N-(N'-Benzyl- Prolyl)Amino]Benzophenone (BPB) and Ni(II) Complexes of Schiff's Bases Derived from BPB and Amino Acids. *Tetrahedron Asymmetry* **1998**, *9* (23), 4249–4252. https://doi.org/10.1016/S0957-4166(98)00449-2.

(233) Zhou, J.; Lin, X.; Ji, X.; Xu, S.; Liu, C.; Dong, X.; Zhao, W. Azetidine-Containing Heterospirocycles Enhance the Performance of Fluorophores. *Org. Lett.* **2020**, *22* (11), 4413–4417. https://doi.org/10.1021/acs.orglett.0c01414.

(234) Hoelzel, C. A.; Hu, H.; Wolstenholme, C. H.; Karim, B. A.; Munson, K. T.; Jung, K. H.; Zhang, H.; Liu, Y.; Yennawar, H. P.; Asbury, J. B.; Li, X.; Zhang, X. A General Strategy to Enhance Donor-Acceptor Molecules Using Solvent-Excluding Substituents. *Angew. Chem. Int. Ed.* **2020**, *59* (12), 4785–4792. https://doi.org/10.1002/anie.201915744.

(235) Eaton, D. F. Reference Materials for Fluorescence Measurement. *Pure Appl. Chem.* **1988**, *60* (7), 1107–1114. https://doi.org/10/cr7mp6.

(236) Rhys Williams, A. T.; A. Winfield, S.; N. Miller, J. Relative Fluorescence Quantum Yields Using a Computer-Controlled Luminescence Spectrometer. *Analyst* **1983**, *108* (1290), 1067–1071. https://doi.org/10/dg5s8n.
(237) Yvon, H. J.; others. A Guide to Recording Fluorescence Quantum Yields. *HORIBA Jobin Yvon Inc Stanmore Middx. UK* **2012**.
(238) Rumble, J. R., editor. *CRC Handbook of Chemistry and Physics (Internet Version)*, 102nd ed.; CRC Press/Taylor & Francis: Boca Raton, FL, 2021.
(239) Kubin, R. F.; Fletcher, A. N. The Effect of Oxygen on the Fluorescence Quantum Yields of Some Coumarin Dyes in Ethanol. *Chem. Phys. Lett.* **1983**, *99* (1), 49–52. https://doi.org/10/dt6sst.
(240) Phosphate-Buffered Saline (PBS): *Cold Spring Harb. Protoc.* **2006**, *2006* (1), pdb.rec8247. https://doi.org/10.1101/pdb.rec8247.
(241) Debono, M.; Barnhart, M.; Carrell, C. B.; Hoffmann, J. A.; Occolowitz, J. L.; Abbott, B. J.; Fukuda, D. S.; Hamill, R. L.; Biemann, K.; Herlihy, W. C. A21978C, a Complex of New Acidic Peptide Antibiotics: Isolation, Chemistry, and Mass Spectral Structure Elucidation. *J. Antibiot. (Tokyo)* **1987**, *40* (6), 761–777. https://doi.org/10.7164/antibiotics.40.761.
(242) Kosmidis, C.; Levine, D. P. Daptomycin: Pharmacology and Clinical Use. *Expert Opin. Pharmacother.* **2010**, *11* (4), 615–625. https://doi.org/10.1517/14656561003598893.
(243) Kelesidis, T.; Humphries, R.; Uslan, D. Z.; Pegues, D. A. Daptomycin Nonsusceptible Enterococci: An Emerging Challenge for Clinicians. *Clin. Infect. Dis.* **2011**, *52* (2), 228–234. https://doi.org/10.1093/cid/ciq113.
(244) Albarillo, F. S.; Medina, R. E.; Joyce, C. S.; Darji, H.; Santarossa, M. Daptomycin-Resistant VRE Infections: A Descriptive Analysis at a Single Academic Centre. *Infect. Dis.* **2021**, *53* (5), 393–395. https://doi.org/10.1080/23744235.2021.1881153.
(245) Hayden, M. K.; Rezai, K.; Hayes, R. A.; Lolans, K.; Quinn, J. P.; Weinstein, R. A. Development of Daptomycin Resistance In Vivo in Methicillin-Resistant *Staphylococcus Aureus*. *J. Clin. Microbiol.* **2005**, *43* (10), 5285–5287. https://doi.org/10/fbdzpd.
(246) Osorio, C.; Garzón, L.; Jaimes, D.; Silva, E.; Bustos, R.-H. Impact on Antibiotic Resistance, Therapeutic Success, and Control of Side Effects in Therapeutic Drug Monitoring (TDM) of Daptomycin: A Scoping Review. *Antibiotics* **2021**, *10* (3), 263. https://doi.org/10.3390/antibiotics10030263.
(247) Tran, T. T.; Munita, J. M.; Arias, C. A. Mechanisms of Drug Resistance: Daptomycin Resistance: Daptomycin Resistance. *Ann. N. Y. Acad. Sci.* **2015**, *1354* (1), 32–53. https://doi.org/10.1111/nyas.12948.
(248) Bhuiyan, M. S.; Jiang, J.-H.; Kostoulias, X.; Theegala, R.; Lieschke, G. J.; Peleg, A. Y. The Resistance to Host Antimicrobial Peptides in Infections Caused by Daptomycin-Resistant Staphylococcus Aureus. *Antibiot. Basel Switz.* **2021**, *10* (2). https://doi.org/10.3390/antibiotics10020096.
(249) Siedlecki, J.; Hill, J.; Parr, I.; Yu, X.; Morytko, M.; Zhang, Y.; Silverman, J.; Controneo, N.; Laganas, V.; Li, T.; Li, J.; Keith, D.; Shimer, G.; Finn, J. Array Synthesis of Novel Lipodepsipeptide. *Bioorg. Med. Chem. Lett.* **2003**, *13* (23), 4245–4249. https://doi.org/10/fb5zzt.
(250) He, Y.; Li, J.; Yin, N.; Herradura, P. S.; Martel, L.; Zhang, Y.; Pearson, A. L.; Kulkarni, V.; Mascio, C.; Howland, K.; Silverman, J. A.; Keith, D. D.; Metcalf, C. A. Reduced Pulmonary Surfactant Interaction of Daptomycin Analogs via Tryptophan Replacement with Alternative Amino Acids. *Bioorg. Med. Chem. Lett.* **2012**, *22* (19), 6248–6251. https://doi.org/10.1016/j.bmcl.2012.08.013.

(251) Alexander, D. C.; Baltz, R. H.; Brian, P.; Coeffet-Le, G. M.-F.; Doekel, S.; He, X.; Kulkarni, V.; Leitheiser, C.; Miao, V. P. W.; Nguyen, K. T.; Parr, I. B.; Ritz, D.; Zhang, Y. Antiinfective Lipopeptides. WO2006110185A3, October 25, 2007.
(252) Pearson, A. L.; Metcalf III, C. A.; Li, J. Novel Antibacterial Agents for the Treatment of Gram Positive Infections. WO2010075215A1, July 1, 2010.
(253) Hill, J.; Siedlecki, J.; Parr, I.; Morytko, M.; Yu, X.; Zhang, Y.; Silverman, J.; Controneo, N.; Laganas, V.; Li, T.; Lai, J.-J.; Keith, D.; Shimer, G.; Finn, J. Synthesis and Biological Activity of N-Acylated Ornithine Analogues of Daptomycin. *Bioorg. Med. Chem. Lett.* **2003**, *13* (23), 4187–4191. https://doi.org/10/cgxk7p.
(254) Grünewald, J.; Sieber, S. A.; Mahlert, C.; Linne, U.; Marahiel, M. A. Synthesis and Derivatization of Daptomycin: A Chemoenzymatic Route to Acidic Lipopeptide Antibiotics. *J. Am. Chem. Soc.* **2004**, *126* (51), 17025–17031. https://doi.org/10/frkfn9.
(255) Kopp, F.; Grünewald, J.; Mahlert, C.; Marahiel, M. A. Chemoenzymatic Design of Acidic Lipopeptide Hybrids: New Insights into the Structure−Activity Relationship of Daptomycin and A54145. *Biochemistry* **2006**, *45* (35), 10474–10481. https://doi.org/10/d2n9zd.
(256) Nguyen, K. T.; He, X.; Alexander, D. C.; Li, C.; Gu, J.-Q.; Mascio, C.; Praagh, A. V.; Mortin, L.; Chu, M.; Silverman, J. A.; Brian, P.; Baltz, R. H. Genetically Engineered Lipopeptide Antibiotics Related to A54145 and Daptomycin with Improved Properties. *Antimicrob. Agents Chemother.* **2010**, *54* (4), 1404–1413. https://doi.org/10/dqfj92.
(257) Nguyen, K. T.; Ritz, D.; Gu, J.-Q.; Alexander, D.; Chu, M.; Miao, V.; Brian, P.; Baltz, R. H. Combinatorial Biosynthesis of Novel Antibiotics Related to Daptomycin. *Proc. Natl. Acad. Sci.* **2006**, *103* (46), 17462–17467. https://doi.org/10/cgmhfd.
(258) Scull, E. M.; Bandari, C.; Johnson, B. P.; Gardner, E. D.; Tonelli, M.; You, J.; Cichewicz, R. H.; Singh, S. Chemoenzymatic Synthesis of Daptomycin Analogs Active against Daptomycin-Resistant Strains. *Appl. Microbiol. Biotechnol.* **2020**, *104* (18), 7853–7865. https://doi.org/10/gj6kjj.
(259) Mupparapu, N.; Lin, Y.-H. C.; Kim, T. H.; Elshahawi, S. I. Regiospecific Synthesis of Calcium-Independent Daptomycin Antibiotics Using a Chemoenzymatic Method. *Chem. – Eur. J.* **2021**, *27* (12), 4176–4182. https://doi.org/10/gj6kjh.
(260) Xu, B.; Hermant, Y.; Yang, S. H.; Harris, P. W. R.; Brimble, M. A. A Versatile Boc Solid Phase Synthesis of Daptomycin and Analogues Using Site Specific, On-Resin Ozonolysis to Install the Kynurenine Residue. *Chem. - Eur. J.* **2019**, *25* (62), 14101–14107. https://doi.org/10.1002/chem.201903725.
(261) Moreira, R.; Wolfe, J.; Taylor, S. D. A High-Yielding Solid-Phase Total Synthesis of Daptomycin Using a Fmoc SPPS Stable Kynurenine Synthon. *Org. Biomol. Chem.* **2021**, *19* (14), 3144–3153. https://doi.org/10/gj6kjk.
(262) Karas, J. A.; Carter, G. P.; Howden, B. P.; Turner, A. M.; Paulin, O. K. A.; Swarbrick, J. D.; Baker, Mark. A.; Li, J.; Velkov, T. Structure–Activity Relationships of Daptomycin Lipopeptides. *J. Med. Chem.* **2020**, *63* (22), 13266–13290. https://doi.org/10/gkc2gk.
(263) Chow, H. Y.; Po, K. H. L.; Jin, K.; Qiao, G.; Sun, Z.; Ma, W.; Ye, X.; Zhou, N.; Chen, S.; Li, X. Establishing the Structure–Activity Relationship of Daptomycin. *ACS Med. Chem. Lett.* **2020**, *11* (7), 1442–1449. https://doi.org/10/gj6kkf.
(264) Chow, H. Y.; Po, K. H. L.; Gao, P.; Blasco, P.; Wang, X.; Li, C.; Ye, L.; Jin, K.; Chen, K.; Chan, E. W. C.; You, X.; Yi Tsun Kao, R.; Chen, S.; Li, X. Methylation of Daptomycin Leading to the Discovery of Kynomycin, a Cyclic Lipodepsipeptide Active against Resistant Pathogens. *J. Med. Chem.* **2020**, *63* (6), 3161–3171. https://doi.org/10/gkc2gh.
(265) Barnawi, Ghufran. Structure-Activity Relationship Studies on Daptomycin. Master's Thesis, UWSpace, 2018.

(266) Baltz, R. H. Combinatorial Biosynthesis of Cyclic Lipopeptide Antibiotics: A Model for Synthetic Biology to Accelerate the Evolution of Secondary Metabolite Biosynthetic Pathways. *ACS Synth. Biol.* **2014**, *3* (10), 748–758. https://doi.org/10.1021/sb3000673.
(267) Samson, D.; Rentsch, D.; Minuth, M.; Meier, T.; Loidl, G. The Aspartimide Problem Persists: Fluorenylmethyloxycarbonyl-Solid-Phase Peptide Synthesis (Fmoc-SPPS) Chain Termination Due to Formation of N-Terminal Piperazine-2,5-Diones. *J. Pept. Sci.* **2019**, *25* (7), 1–11. https://doi.org/10.1002/psc.3193.
(268) Mergler, M.; Dick, F.; Sax, B.; Weiler, P.; Vorherr, T. The Aspartimide Problem in Fmoc-Based SPPS. Part I. *J. Pept. Sci.* **2003**, *9* (1), 36–46. https://doi.org/10.1002/psc.430.
(269) Yang, Y.; Sweeney, W. V.; Schneider, K.; Thörnqvist, S.; Chait, B. T.; Tam, J. P. Aspartimide Formation in Base-Driven 9-Fluorenylmethoxycarbonyl Chemistry. *Tetrahedron Lett.* **1994**, *35* (52), 9689–9692. https://doi.org/10.1016/0040-4039(94)88360-2.
(270) Lakowicz, J. R. Protein Fluorescence. In *Principles of Fluorescence Spectroscopy*; Lakowicz, J. R., Ed.; Springer US: Boston, MA, 2006. https://doi.org/10.1007/978-0-387-46312-4.
(271) Gryczynski, I.; Wiczk, W.; Johnson, M. L.; Lakowicz, J. R. Lifetime Distributions and Anisotropy Decays of Indole Fluorescence in Cyclohexane/Ethanol Mixtures by Frequency-Domain Fluorometry. *Biophys. Chem.* **1988**, *32* (2), 173–185. https://doi.org/10/cg5485.
(272) Chen, Y.; Barkley, M. D. Toward Understanding Tryptophan Fluorescence in Proteins. *Biochemistry* **1998**, *37* (28), 9976–9982. https://doi.org/10/bf4rwv.
(273) Jung, D.; Rozek, A.; Okon, M.; Hancock, R. E. W. Structural Transitions as Determinants of the Action of the Calcium-Dependent Antibiotic Daptomycin. *Chem. Biol.* **2004**, *11* (7), 949–957. https://doi.org/10/fr6kbt.
(274) Moreira, R.; Taylor, S. D. Highly Efficient and Enantioselective Syntheses of (2S,3R)-3-Alkyl- and Alkenylglutamates from Fmoc-Protected Garner's Aldehyde. *Amino Acids* **2020**, *52* (6–7), 987–998. https://doi.org/10.1007/s00726-020-02868-7.
(275) The pandas development team. Pandas-Dev/Pandas: Pandas. Zenodo February 2020. https://doi.org/10.5281/zenodo.3509134.
(276) McKinney, W. Data Structures for Statistical Computing in Python. In *Proceedings of the 9th Python in Science Conference*; van der Walt, S., Millman, J., Eds.; 2010; pp 56–61. https://doi.org/10.25080/Majora-92bf1922-00a.
(277) Hunter, J. D. Matplotlib: A 2D Graphics Environment. *Comput. Sci. Eng.* **2007**, *9* (3), 90–95. https://doi.org/10.1109/MCSE.2007.55.
(278) Caswell, T. A.; Droettboom, M.; Lee, A.; Hunter, J.; Firing, E.; de Andrade, E. S.; Hoffmann, T.; Stansby, D.; Klymak, J.; Varoquaux, N.; Nielsen, J. H.; Root, B.; Elson, P.; May, R.; Dale, D.; Lee, J.-J.; Seppänen, J. K.; McDougall, D.; Straw, A.; Hobson, P.; Gohlke, C.; Yu, T. S.; Ma, E.; Vincent, A. F.; Silvester, S.; Moad, C.; Kniazev, N.; hannah; Ernest, E. Matplotlib/Matplotlib: REL: V3.2.2. Zenodo June 2020. https://doi.org/10.5281/zenodo.3898017.
(279) Newton, B. A. A Fluorescent Derivative of Polymyxin: Its Preparation and Use in Studying the Site of Action of the Antibiotic. *J. Gen. Microbiol.* **1955**, *12* (2), 226–236. https://doi.org/10/czzqqz.
(280) Soon, R. L.; Velkov, T.; Chiu, F.; Thompson, P. E.; Kancharla, R.; Roberts, K.; Larson, I.; Nation, R. L.; Li, J. Design, Synthesis, and Evaluation of a New Fluorescent Probe for Measuring Polymyxin–Lipopolysaccharide Binding Interactions. *Anal. Biochem.* **2011**, *409* (2), 273–283. https://doi.org/10.1016/j.ab.2010.10.033.
(281) Prendergast, F. G.; Meyer, M.; Carlson, G. L.; Iida, S.; Potter, J. D. Synthesis, Spectral Properties, and Use of 6-Acryloyl-2-Dimethylaminonaphthalene (Acrylodan). A Thiol-

Selective, Polarity-Sensitive Fluorescent Probe. *J. Biol. Chem.* **1983**, *258* (12), 7541–7544. https://doi.org/10/gk45p7.
(282) Mims, M. P.; Sturgis, C. B.; Sparrow, J. T.; Morrisett, J. D. Acrylodan Can Label Amino as Well as Sulfhydryl Groups: Results with Low-Density Lipoprotein, Lipoprotein[a], and Lipid-Free Proteins. *Biochemistry* **1993**, *32* (35), 9215–9220. https://doi.org/10/b8brjn.
(283) Johnson, I. D. *Molecular Probes Handbook: A Guide to Fluorescent Probes and Labeling Technologies*; Life Technologies Corporation, 2010.
(284) Sabnis, R. W. *Handbook of Fluorescent Dyes and Probes: Sabnis/Handbook of Fluorescent Dyes and Probes*; John Wiley & Sons, Inc: Hoboken, NJ, USA, 2015. https://doi.org/10.1002/9781119007104.

Appendix A

Characterization of Chapter 2 Compounds[i]

[i] Reproduced in part with permission from "Noden, M.; Moreira, R.; Huang, E.; Yousef, A.; Palmer, M.; Taylor, S. D. Total Synthesis of Paenibacterin and Its Analogues. *J. Org. Chem.* **2019**, *84* (9), 5339–5347. http://pubs.acs.org/articlesonrequest/AOR-9JJKmajHkFRVKFaYMZSr". Copyright © 2019 American Chemical Society.

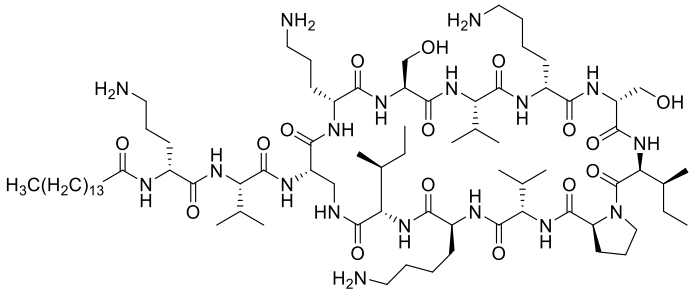

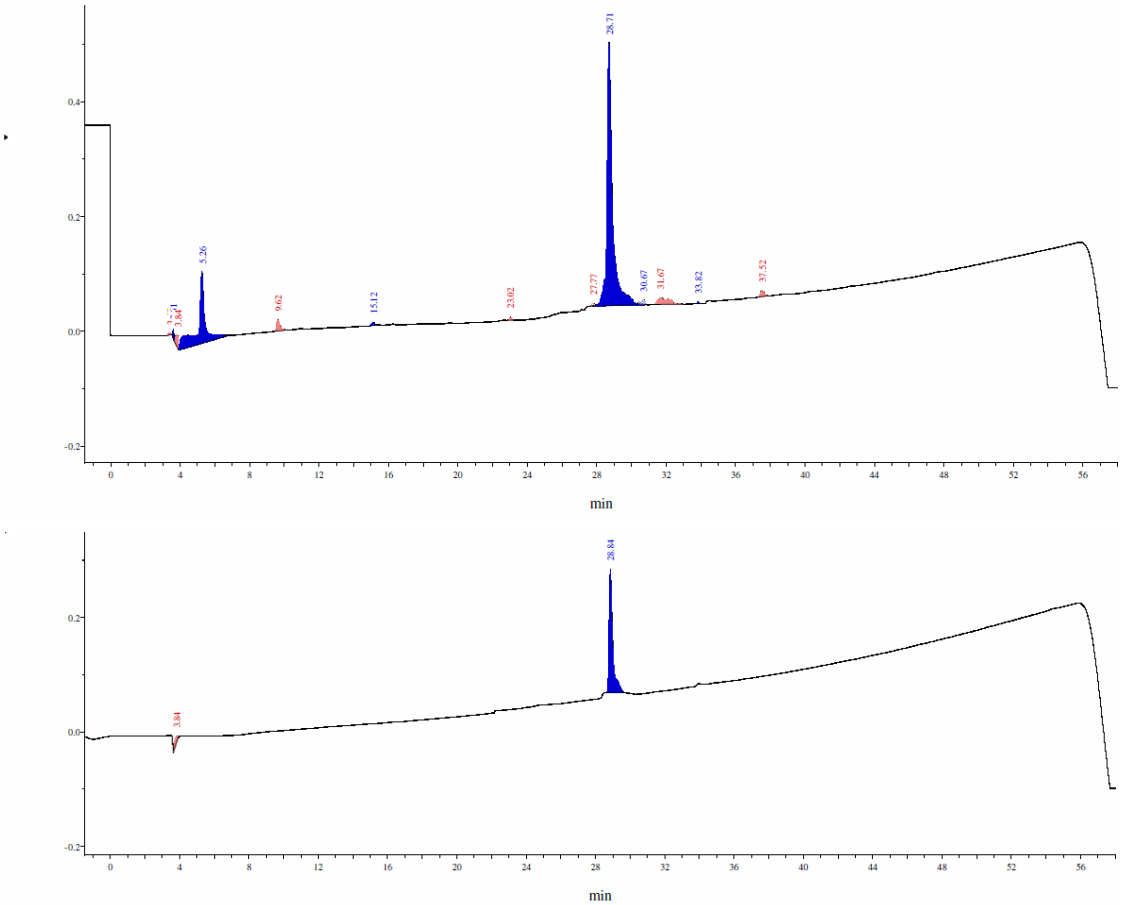

Figure A.1 HPLC chromatogram of crude (top) and pure (bottom) PA1-Dapa. Linear gradient of 10:90 CH_3CN:H_2O (0.2% TFA) to 90:10 CH_3CN:H_2O (0.2% TFA) in 50 min (λ = 220 nm).

Elemental composition search on mass 795.55876

m/z= 790.55876-800.55876

m/z	Theo. Mass	Delta (ppm)	RDB equiv.	Composition
795.55876	795.55833	0.54	14.5	$C_{80}H_{148}O_{17}N_{15}$
	795.55766	1.38	15.0	$C_{78}H_{146}O_{16}N_{18}$
	795.55632	3.07	10.5	$C_{75}H_{148}O_{19}N_{17}$
	795.55565	3.91	11.0	$C_{73}H_{146}O_{18}N_{20}$
	795.56194	-3.99	10.5	$C_{74}H_{148}O_{18}N_{19}$

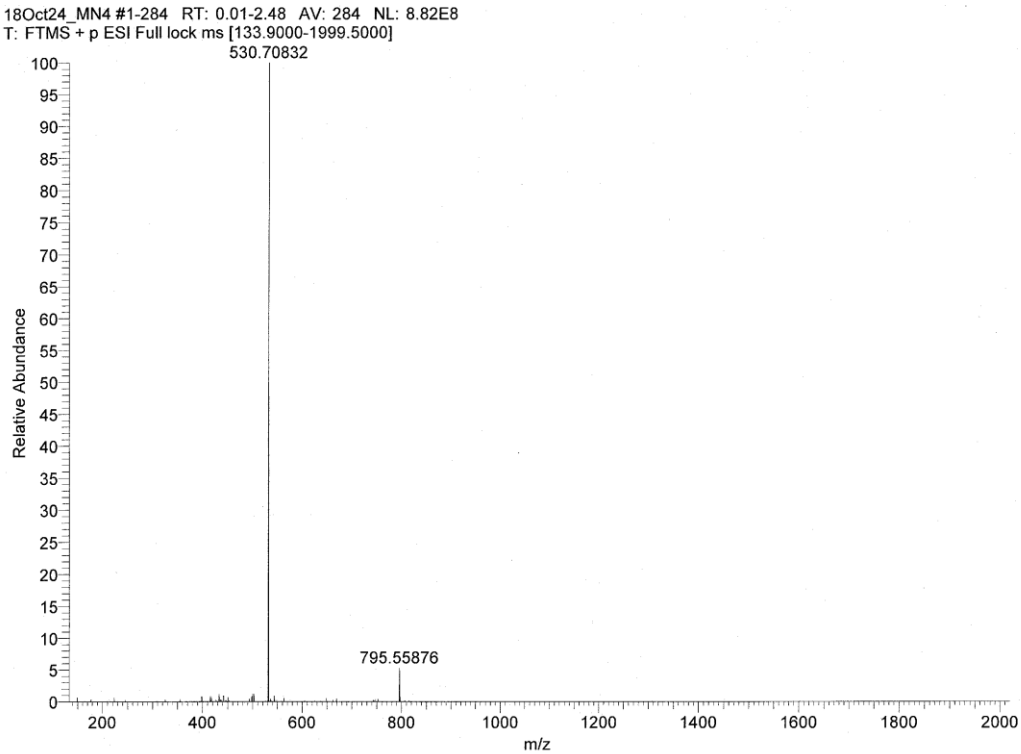

Figure A.2. ESI-(+) HRMS of pure PA1-Dapa. The peak at *m/z* = 795.55876 corresponds to the doubly charged species. The HRMS data for the peak at *m/z* = 795.55876 is also shown. The peak at *m/z* = 530.70832 corresponds to the triply charged species.

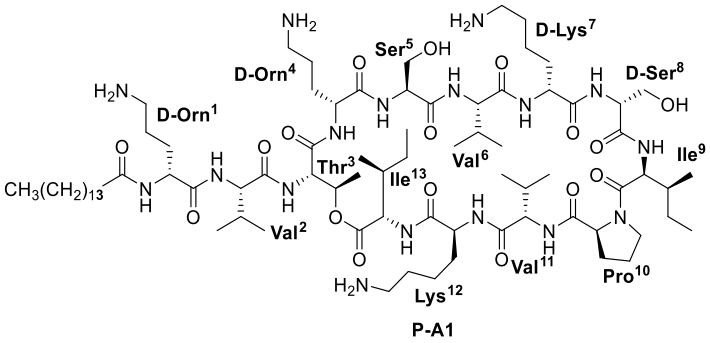

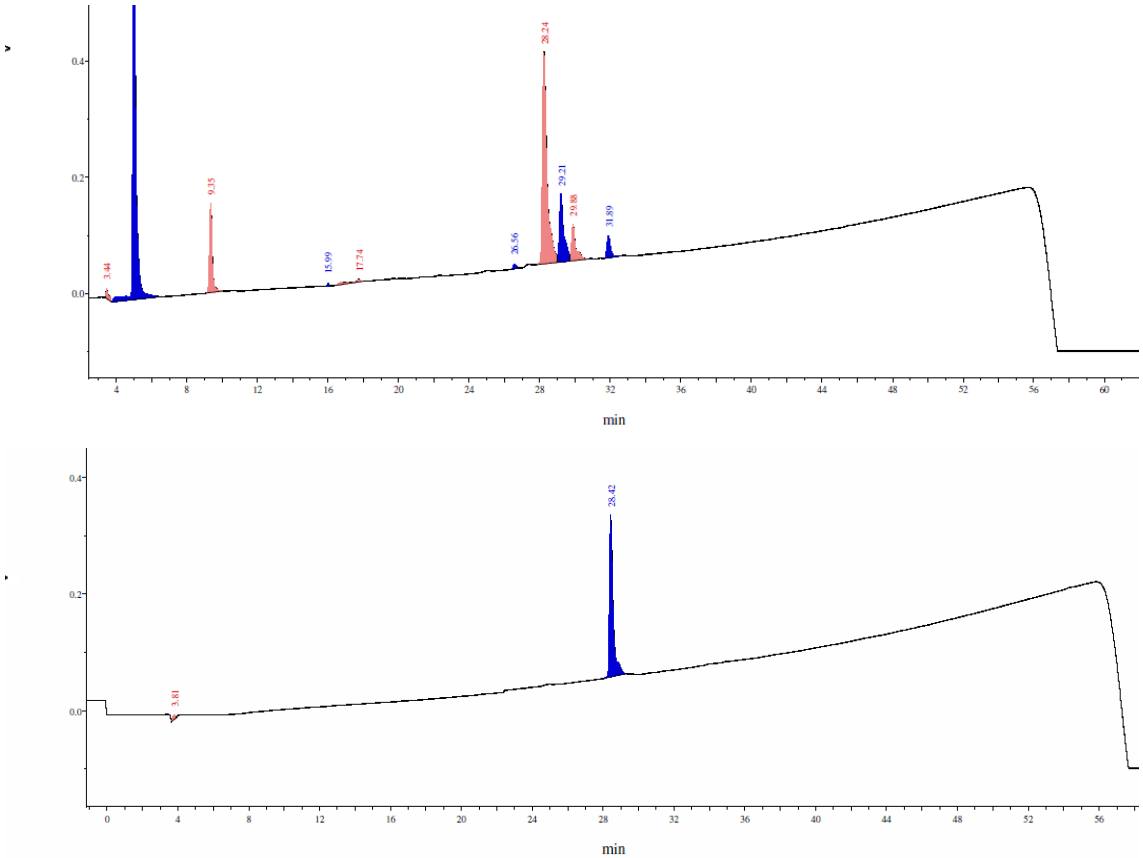

Figure A.3. HPLC chromatogram of crude (top) and pure (bottom) PA1 prepared as described in Scheme 2.6. Linear gradient of 10:90 CH_3CN:H_2O (0.2% TFA) to 90:10 CH_3CN:H_2O (0.2% TFA) in 50 min (λ = 220 nm). In the top chromatogram, PA1 elutes at 28.2 min and the epimer of PA1 elutes at 29.2 min.

Elemental composition search on mass 803.05870

m/z= 798.05870-808.05870

m/z	Theo. Mass	Delta (ppm)	RDB equiv.	Composition
803.05870	803.05951	-1.00	19.0	$C_{84}H_{147}O_{15}N_{15}$
	803.05749	1.50	15.0	$C_{79}H_{147}O_{17}N_{17}$
	803.05682	2.34	15.5	$C_{77}H_{145}O_{16}N_{20}$

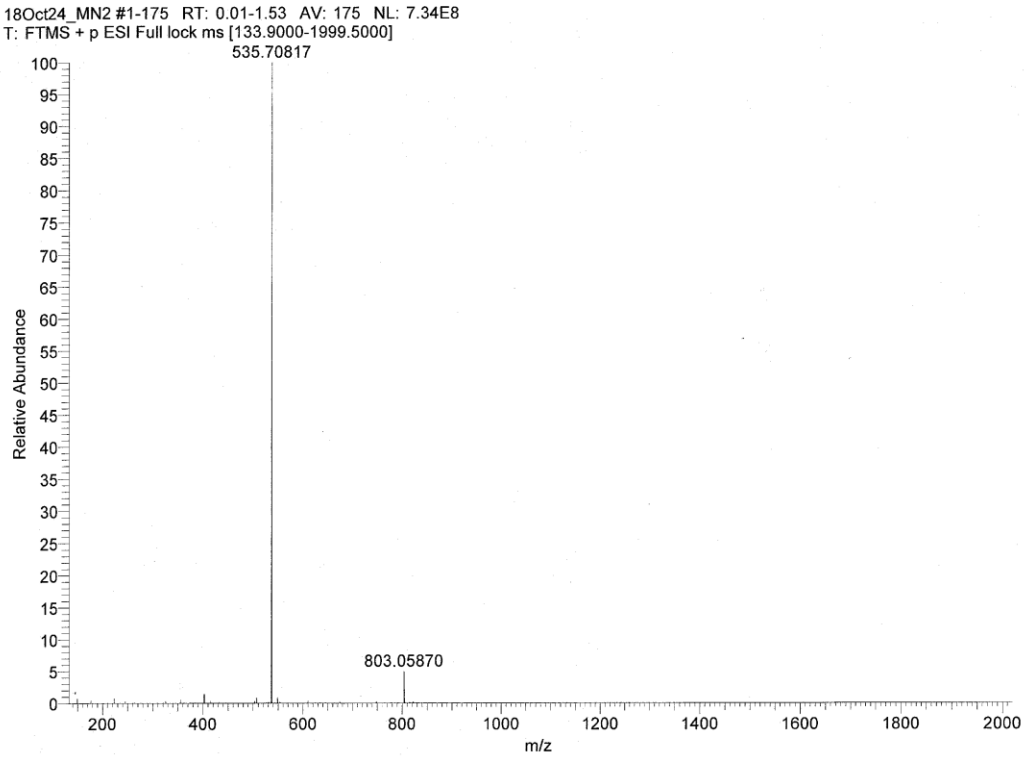

Figure A.4. ESI-(+) HRMS of pure PA1 prepared as described in Scheme 2.6. The peak at *m/z* = 803.05870 corresponds to the doubly charged species. The HRMS data for the peak at *m/z* = 803.05870 is also shown. The peak at *m/z* = 535.70817 corresponds to the triply charged species.

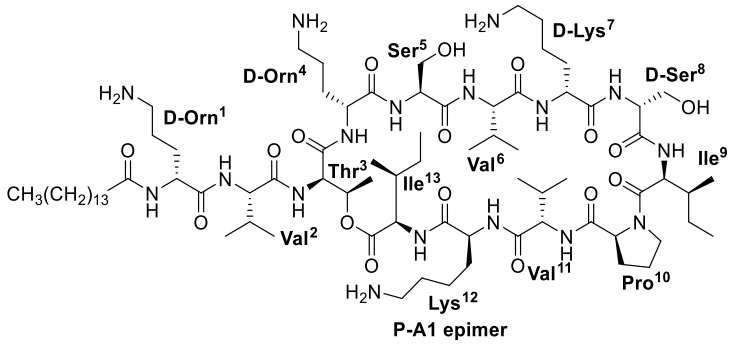

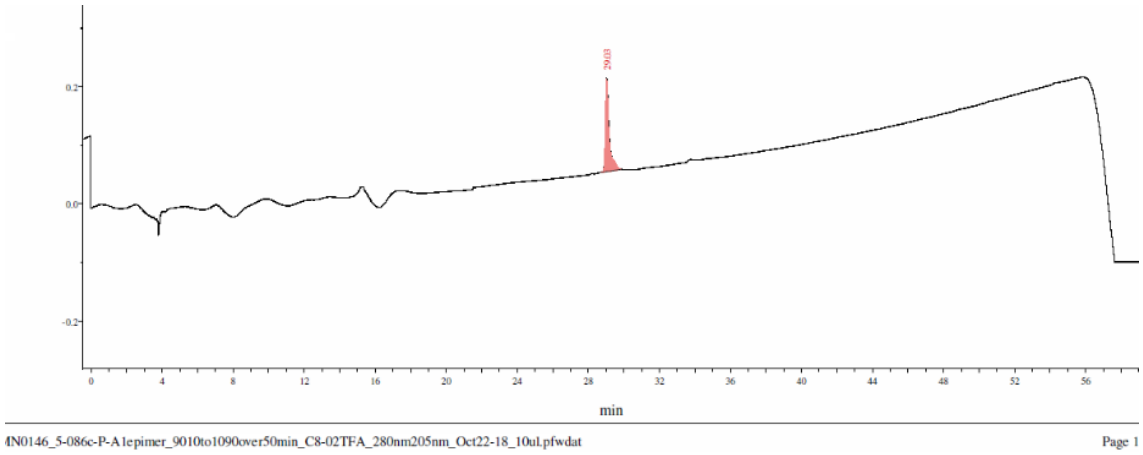

Figure A.5. HPLC chromatogram of pure PA1-epimer . Linear gradient of 10:90 CH_3CN:H_2O (0.2% TFA) to 90:10 CH_3CN:H_2O (0.2% TFA) in 50 min (λ = 220 nm).

Elemental composition search on mass 803.05849

m/z= 798.05849-808.05849

m/z	Theo. Mass	Delta (ppm)	RDB equiv.	Composition
803.05849	803.05749	1.24	15.0	$C_{79}H_{147}O_{17}N_{17}$
	803.05951	-1.26	19.0	$C_{84}H_{147}O_{15}N_{15}$
	803.05682	2.08	15.5	$C_{77}H_{145}O_{16}N_{20}$
	803.05615	2.91	10.5	$C_{76}H_{149}O_{20}N_{16}$

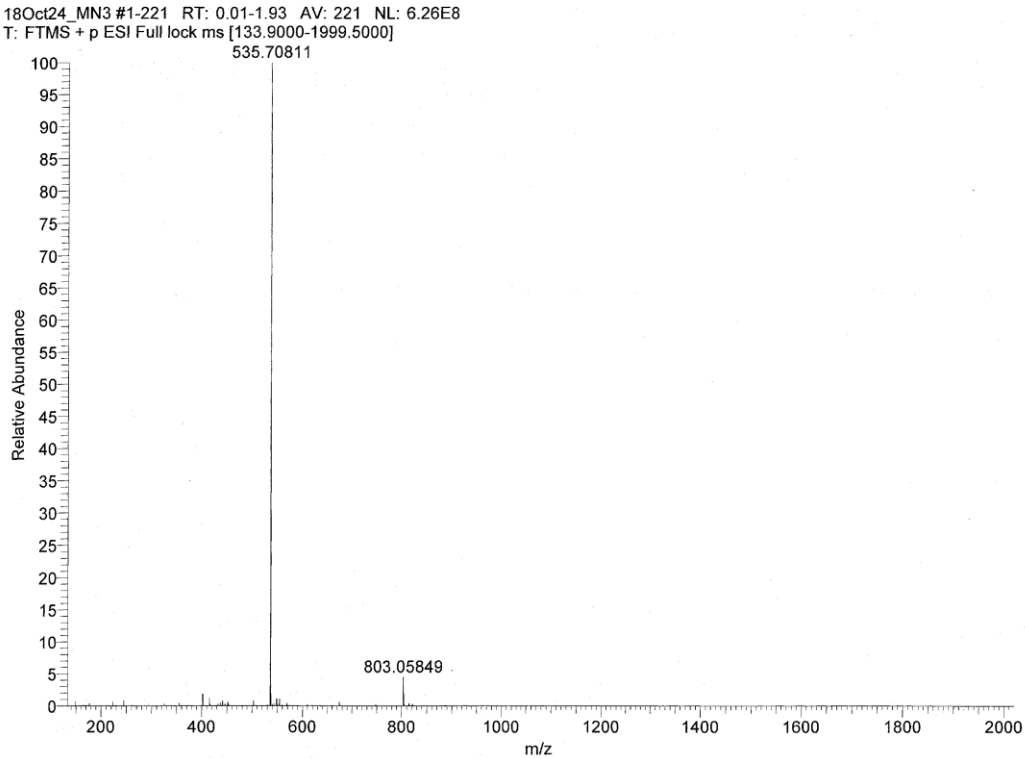

Figure A.6. ESI-(+) HRMS of pure PA1-epimer. The peak at *m/z* = 803.05849 corresponds to the doubly charged species. The HRMS data for the peak at *m/z* = 803.05849 is also shown. The peak at *m/z* = 535.70811 corresponds to the triply charged species.

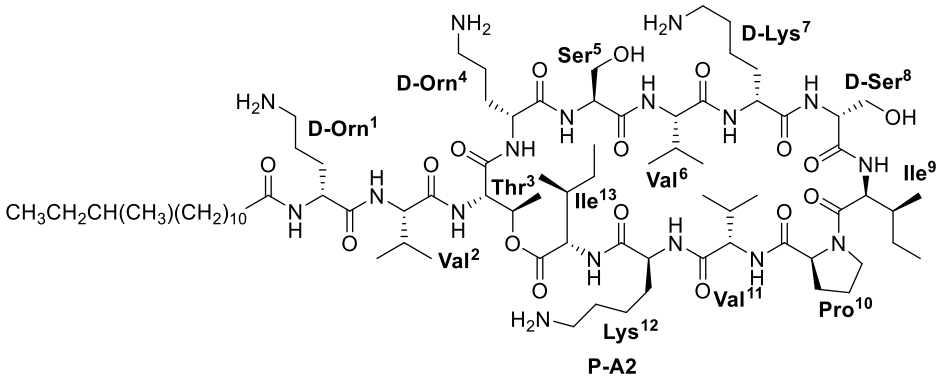

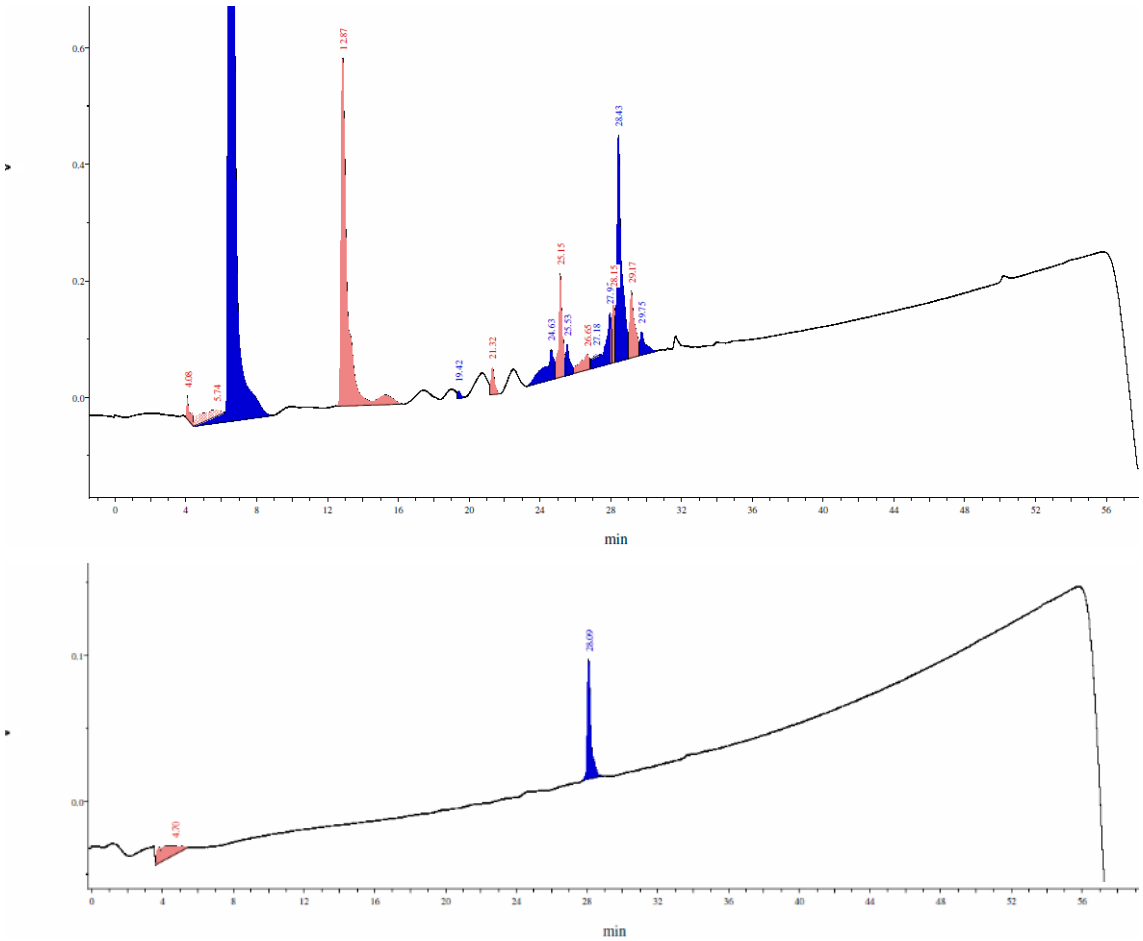

Figure A.7. HPLC chromatogram of crude (top) and pure (bottom) PA2. Linear gradient of 10:90 CH_3CN:H_2O (0.2% TFA) to 90:10 CH_3CN:H_2O (0.2% TFA) in 50 min (λ = 220 nm).

Elemental composition search on mass 803.06055

m/z= 798.06055-808.06055

m/z	Theo. Mass	Delta (ppm)	RDB equiv.	Composition
803.06055	803.06311	-3.19	15.0	$C_{78}H_{147}O_{16}N_{19}$
	803.05749	3.80	15.0	$C_{79}H_{147}O_{17}N_{17}$
	803.06378	-4.03	14.5	$C_{80}H_{149}O_{17}N_{16}$
	803.05682	4.64	15.5	$C_{77}H_{145}O_{16}N_{20}$

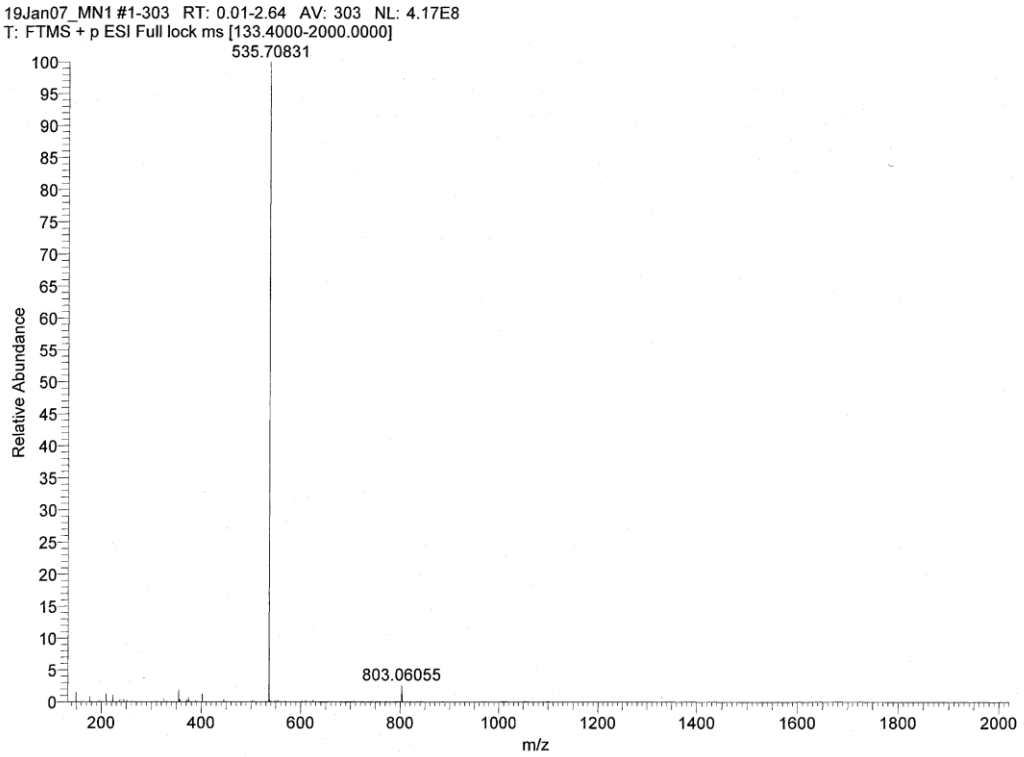

Figure A.8. ESI-(+) HRMS of pure PA2. The peak at *m/z* = 803.06055 corresponds to the doubly charged species. The HRMS data for the peak at *m/z* = 803.06055 is also shown. The peak at *m/z* = 535.70831 corresponds to the triply charged species.

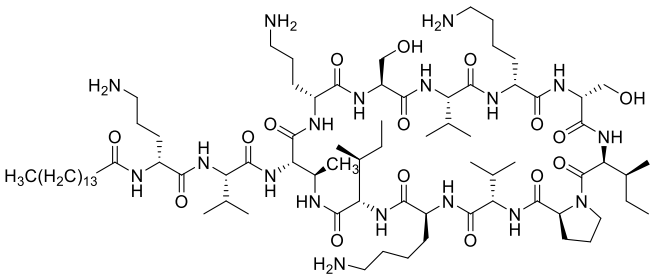

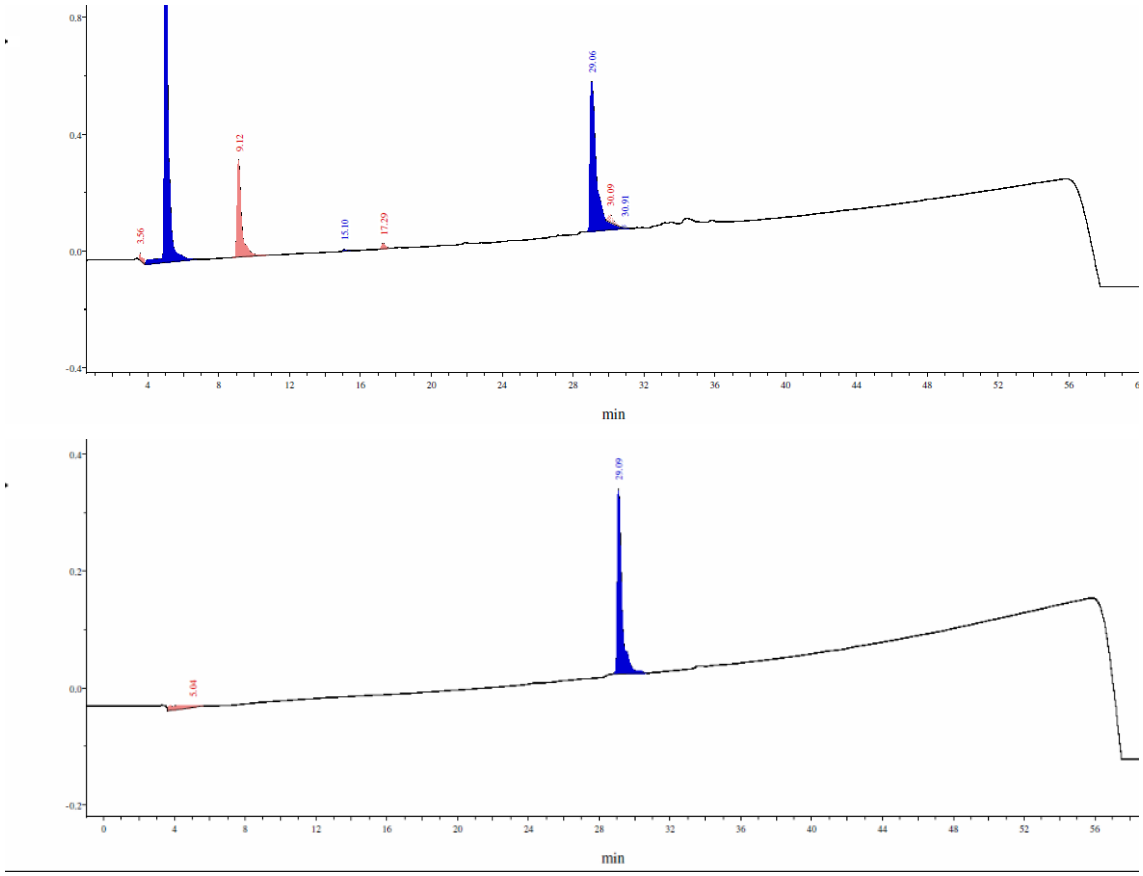

Figure A.9. HPLC chromatogram of crude (top) and pure (bottom) PA1-Daba . Linear gradient of 10:90 CH_3CN:H_2O (0.2% TFA) to 90:10 CH_3CN:H_2O (0.2% TFA) in 50 min (λ = 220 nm).

Elemental composition search on mass 802.56883

m/z= 797.56883-807.56883

m/z	Theo. Mass	Delta (ppm)	RDB equiv.	Composition
802.56883	802.57110	-2.83	15.0	$C_{78}H_{148}O_{15}N_{20}$
	802.56616	3.33	14.5	$C_{81}H_{150}O_{17}N_{15}$
	802.57177	-3.67	14.5	$C_{80}H_{150}O_{16}N_{17}$
	802.56549	4.17	15.0	$C_{79}H_{148}O_{16}N_{18}$

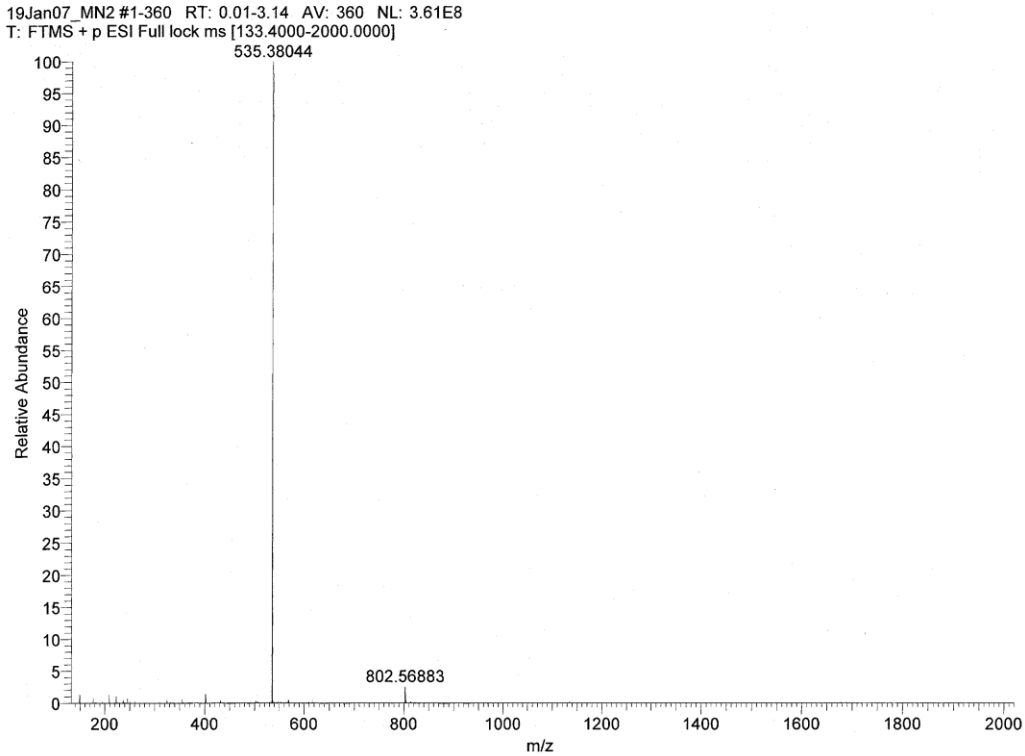

Figure A.10. ESI-(+) HRMS of pure PA1-Daba. The peak at *m/z* = 802.56883 corresponds to the doubly charged species. The HRMS data for the peak at *m/z* = 803.56883 is also shown. The peak at *m/z* = 535.38044 corresponds to the triply charged species

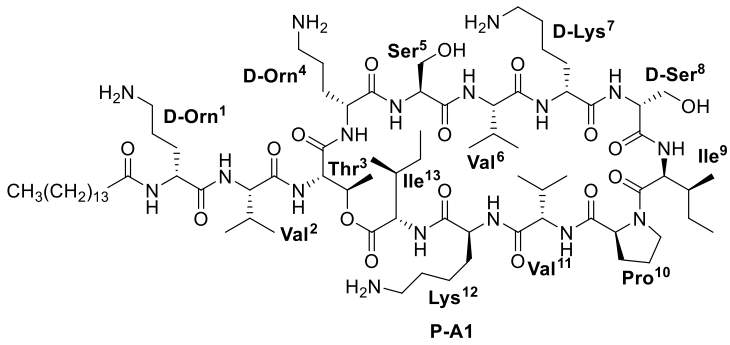

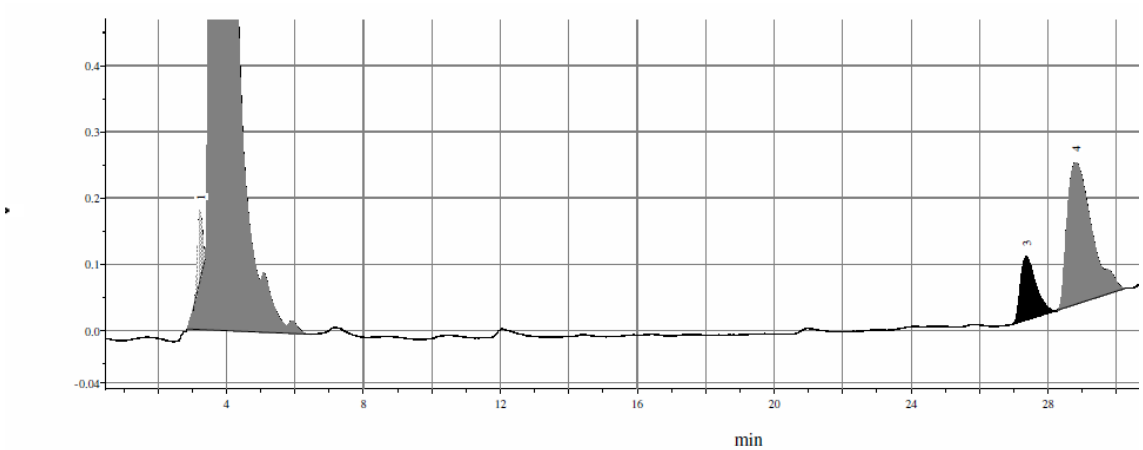

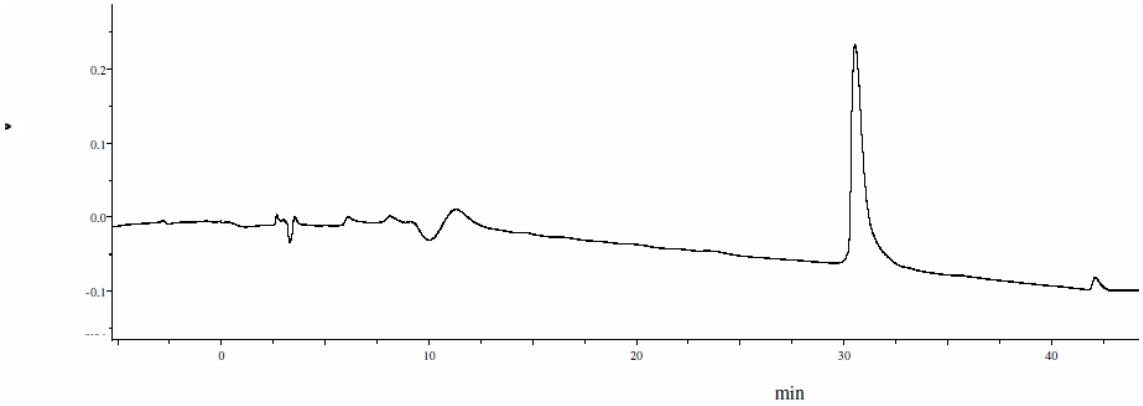

Figure A.11. HPLC chromatogram of crude PA1prepared as described in Scheme 2.3. (top) Chromatogram of the crude product. PA1 elutes at 27 min (peak 3), with its epimer and the linear peptide eluding at 29 min (peak 4). (linear gradient of 70:30 CH_3CN:H_2O + 0.1% TFA to 50:50 CH_3CN:H_2O + 0.1% TFA in 25 min (λ = 220 nm); (bottom) HPLC chromatogram of purified PA1 (t_R = 30.5 min, linear gradient of 90:10 CH_3CN:H_2O + 0.1% TFA to 70:30 CH_3CN:H_2O + 0.1% TFA in 40 min (λ = 220 nm)).

emental composition search on mass 1605.10799

m/z= 1600.10799-1610.10799

m/z	Theo. Mass	Delta (ppm)	RDB equiv.	Composition
1605.10799	1605.10771	0.17	15.5	$C_{79}H_{146}O_{17}N_{17}$
	1605.10637	1.01	16.0	$C_{77}H_{144}O_{16}N_{20}$
	1605.10503	1.84	11.0	$C_{76}H_{148}O_{20}N_{16}$
	1605.11173	-2.33	19.5	$C_{84}H_{146}O_{15}N_{15}$

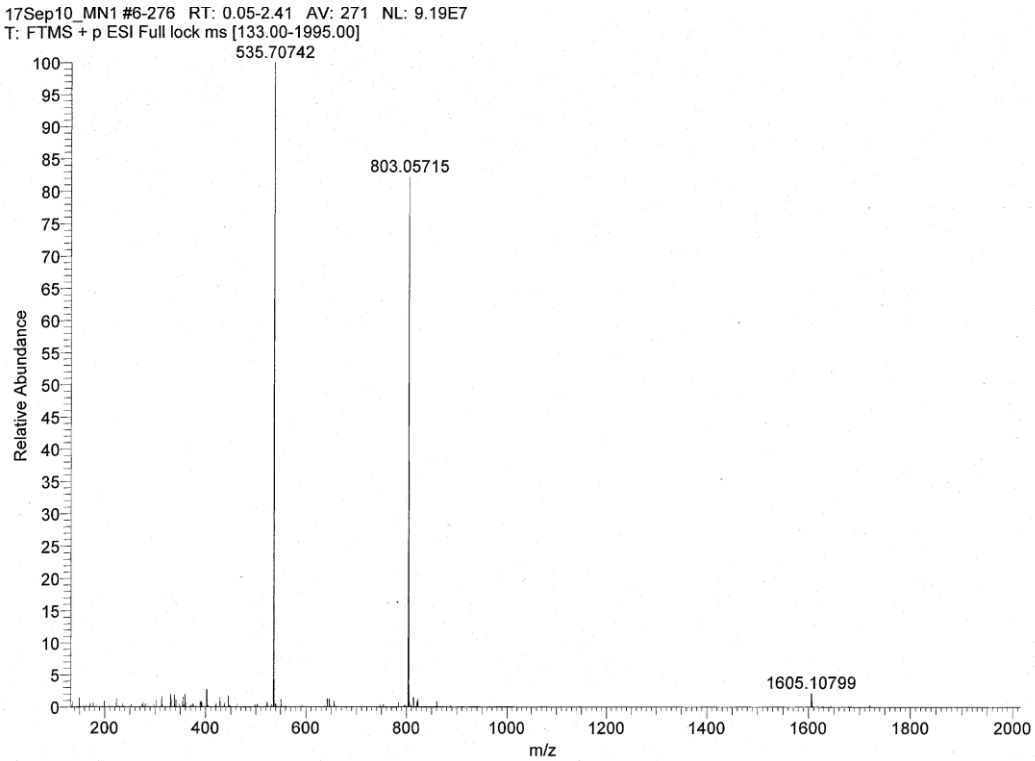

Figure A.12. ESI-(+) HRMS of pure PA1 prepared as described in Scheme 2.3. The HRMS data for the peak at *m/z* = 1605.10799 is also shown

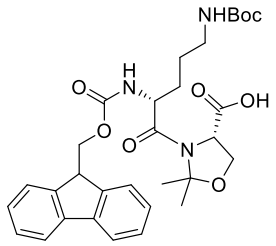

Fmoc-D-Orn(Boc)-Ser($\Psi^{Me,Me}$Pro)OH

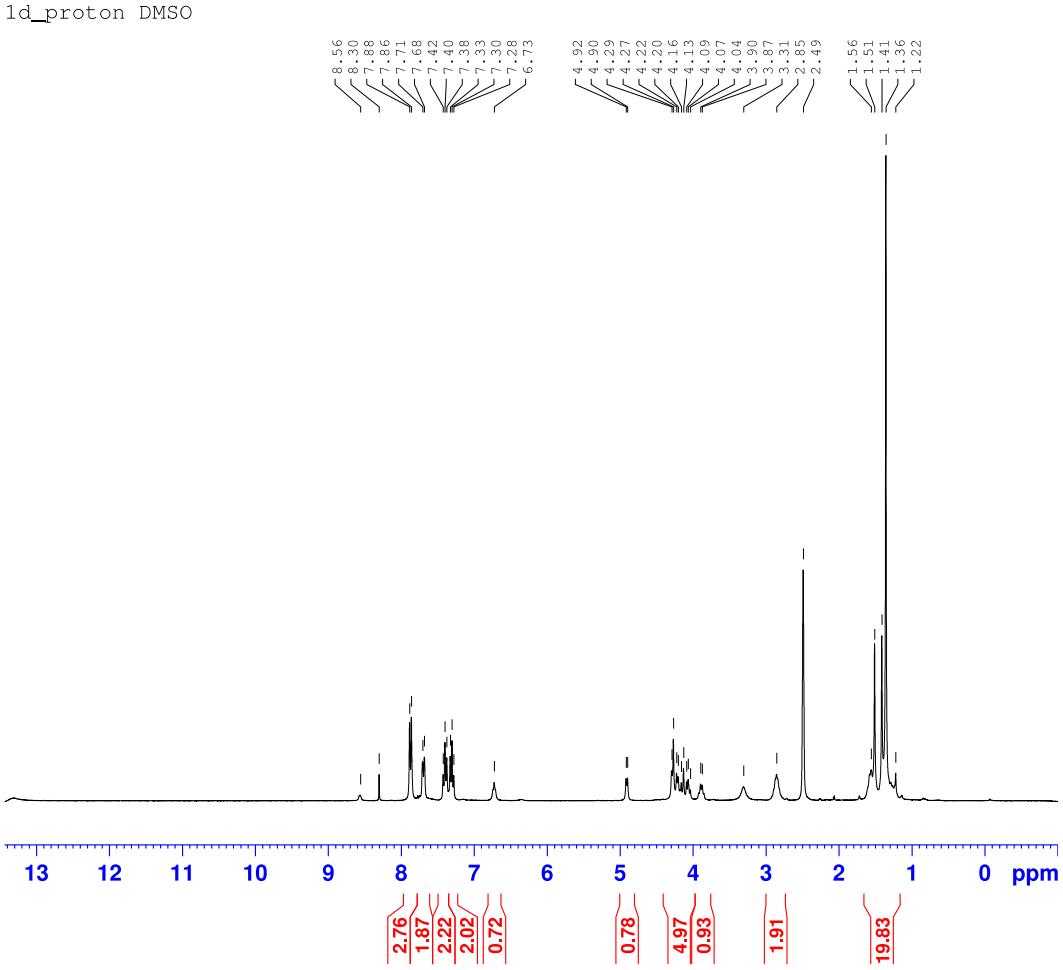

Figure A.13. ^{1}**H NMR of Fmoc-D-Orn(Boc)-Ser($\Psi^{Me,Me}$Pro)-OH (300 MHz, DMSO-*d*6)**

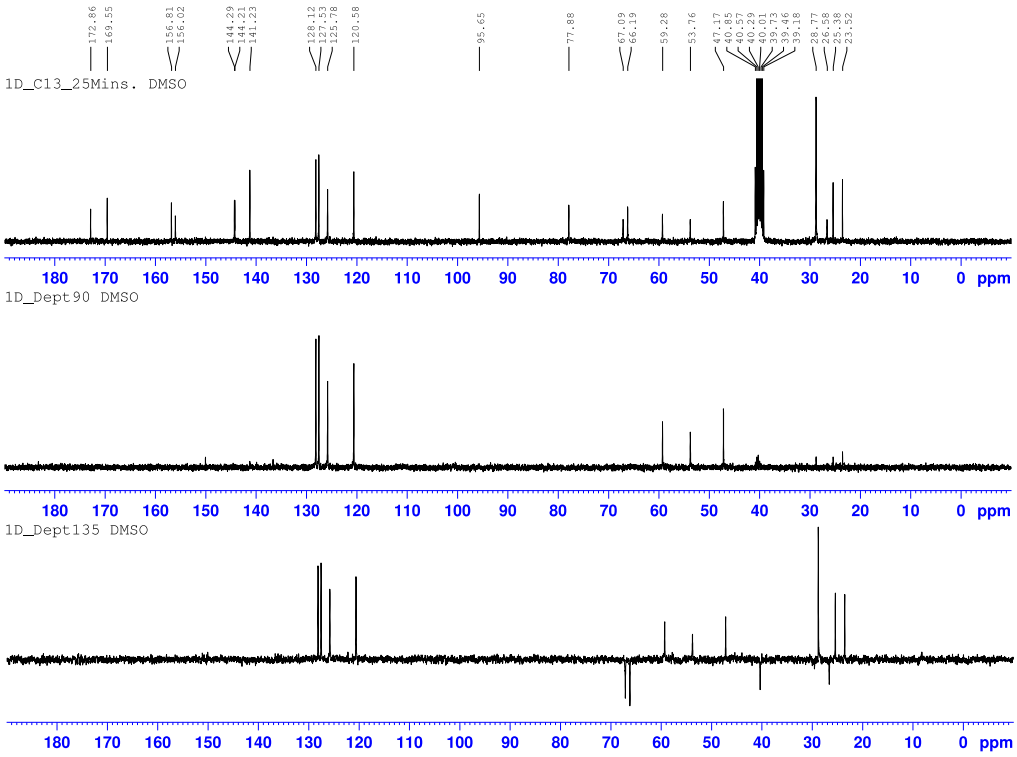

Figure A.14. $^{13}C\{^{1}H\}$ and DEPT NMR of Fmoc-D-Orn(Boc)-Ser($\Psi^{Me,\,Me}$Pro)-OH (75 MHz, DMSO-*d*6)

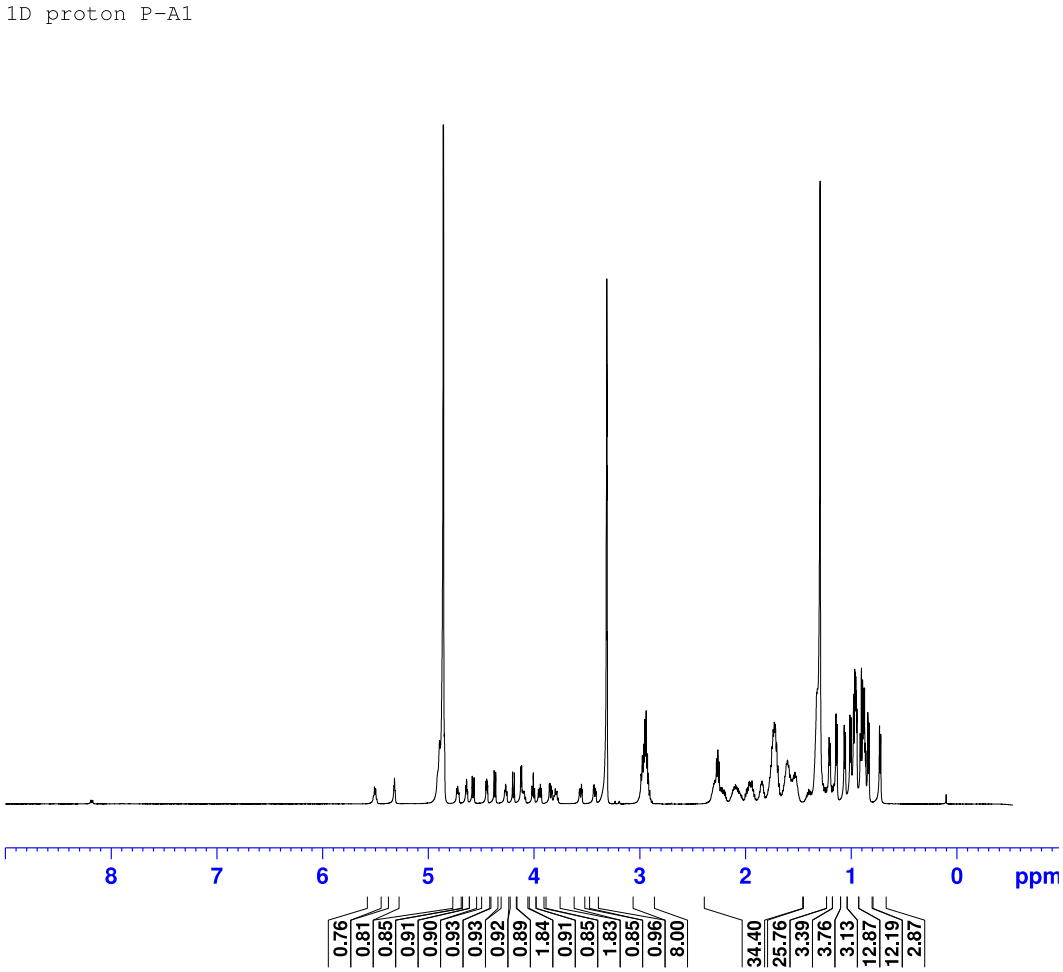

Figure A.15. ^{1}H-NMR spectrum of PA1 prepared as described in Scheme 2.6 (600 MHz, CD_3OD)

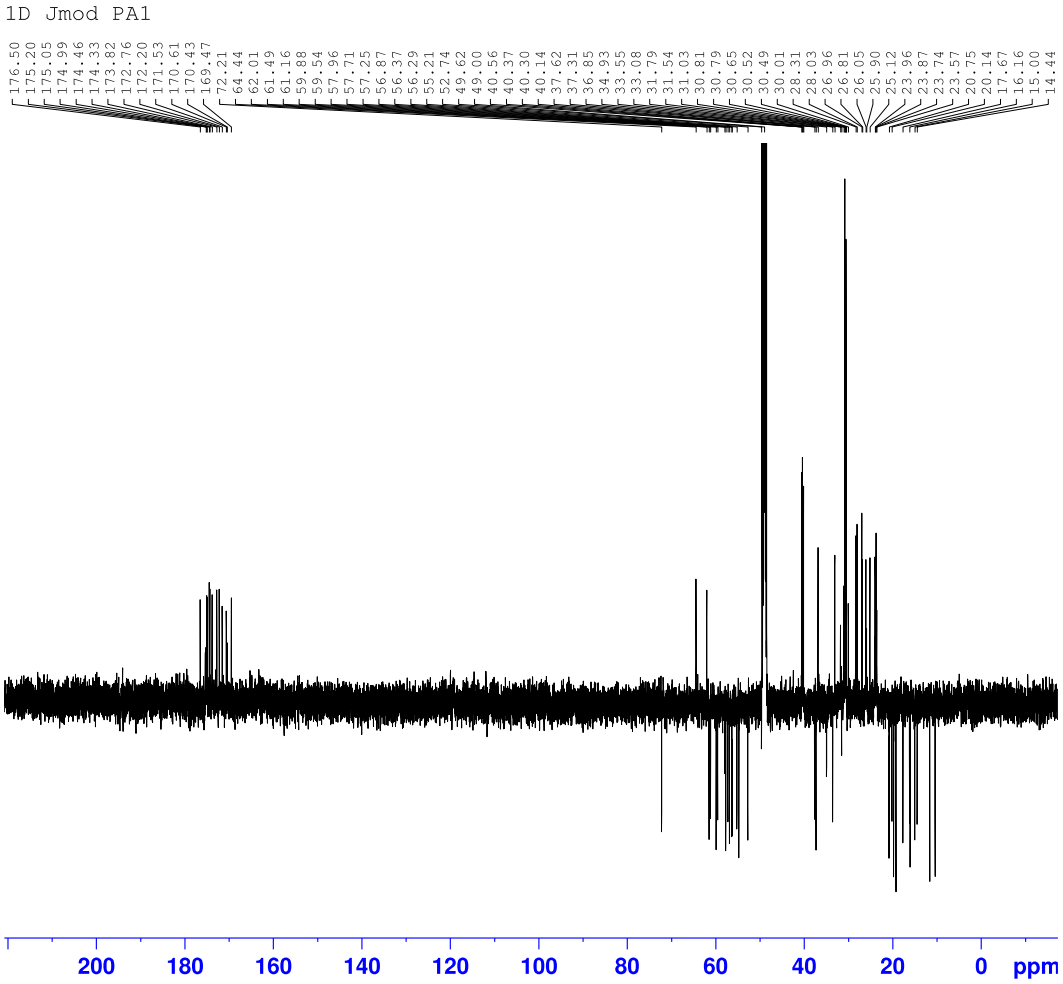

Figure A.16. ^{13}C-JMOD spectrum of PA1 prepared as described in Scheme 2.6 (125 MHz, CD_3OD)

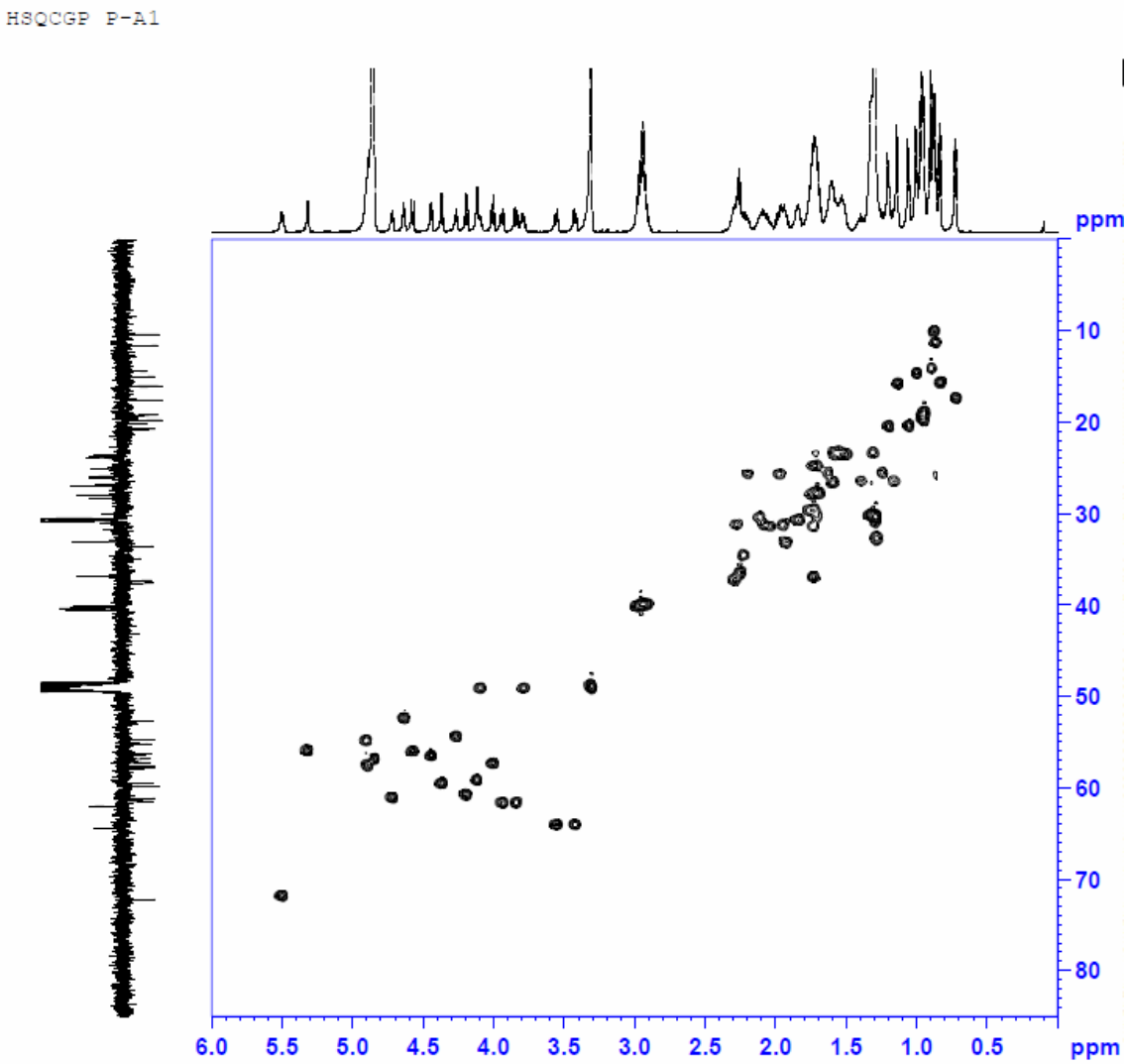

Figure A.17. ^{1}H-^{13}C HSQC of PA1 prepared as described in Scheme 2.6 (600 MHz, CD_3OD)

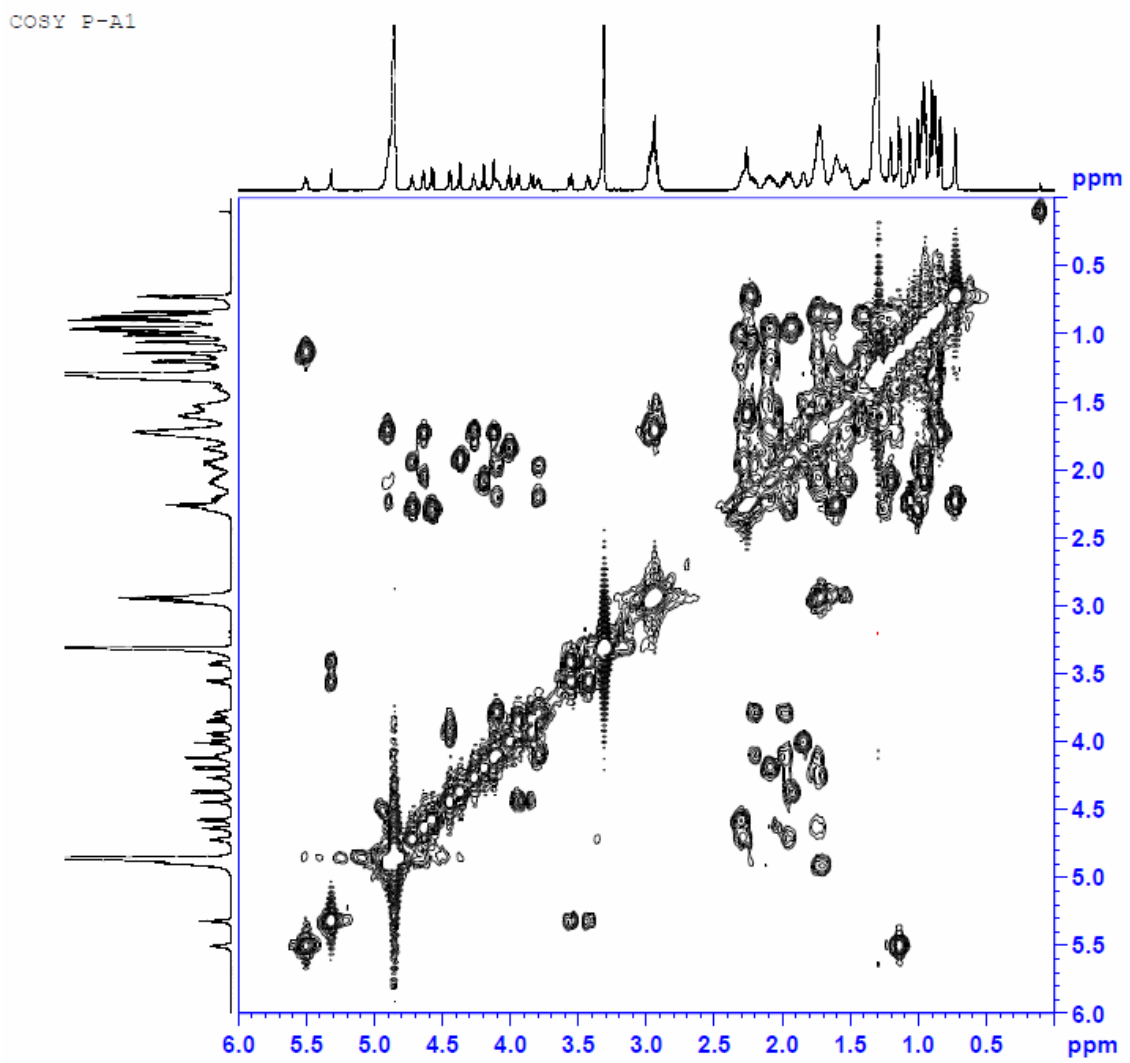

Figure A.18. ^{1}H-COSY of PA1 prepared as described in Scheme 2.6 (600 MHz, CD_3OD)

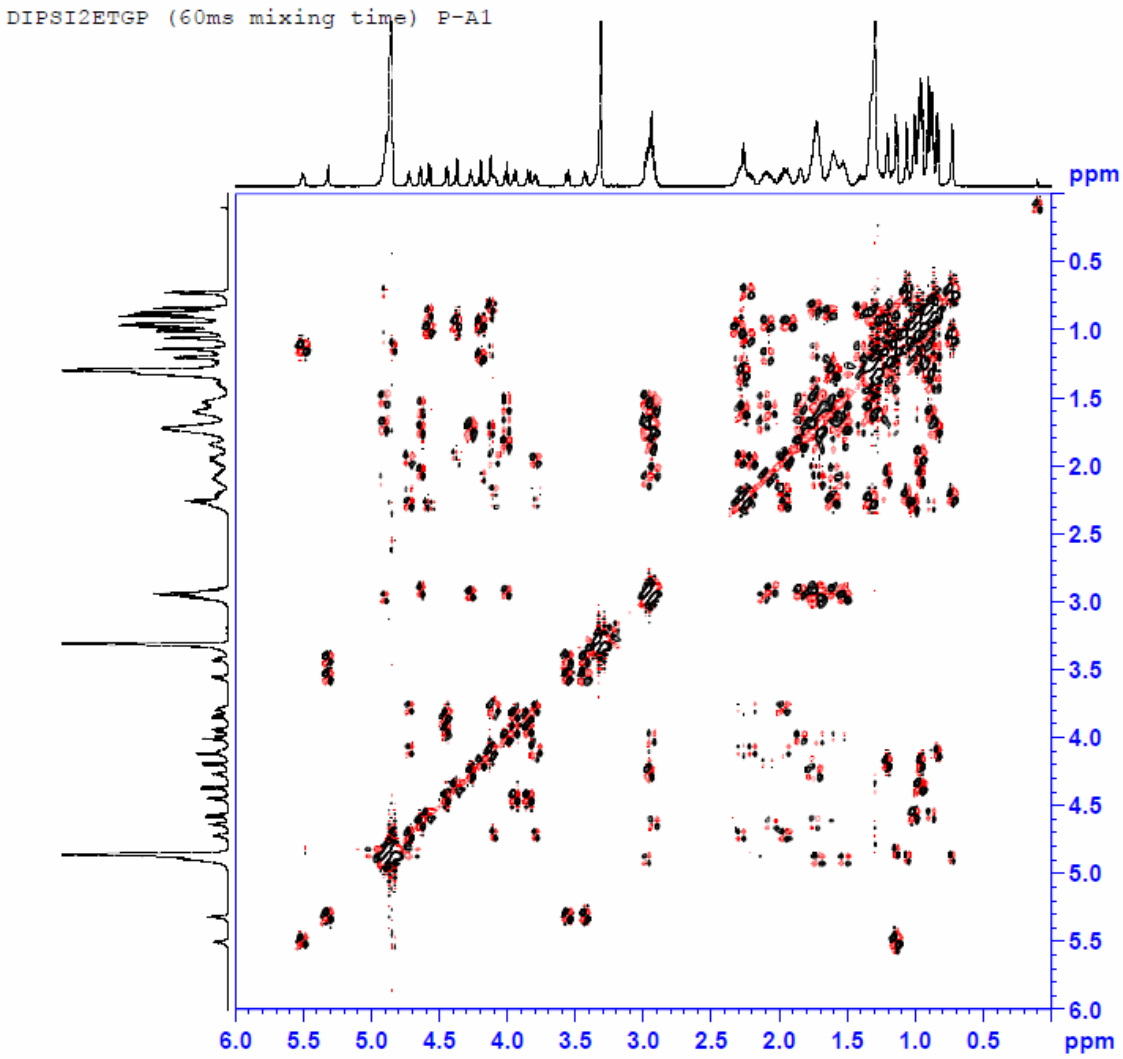

Figure A.19. ^{1}H-TOCSY of PA1 prepared as described in Scheme 2.6 (600 MHz, CD_3OD)

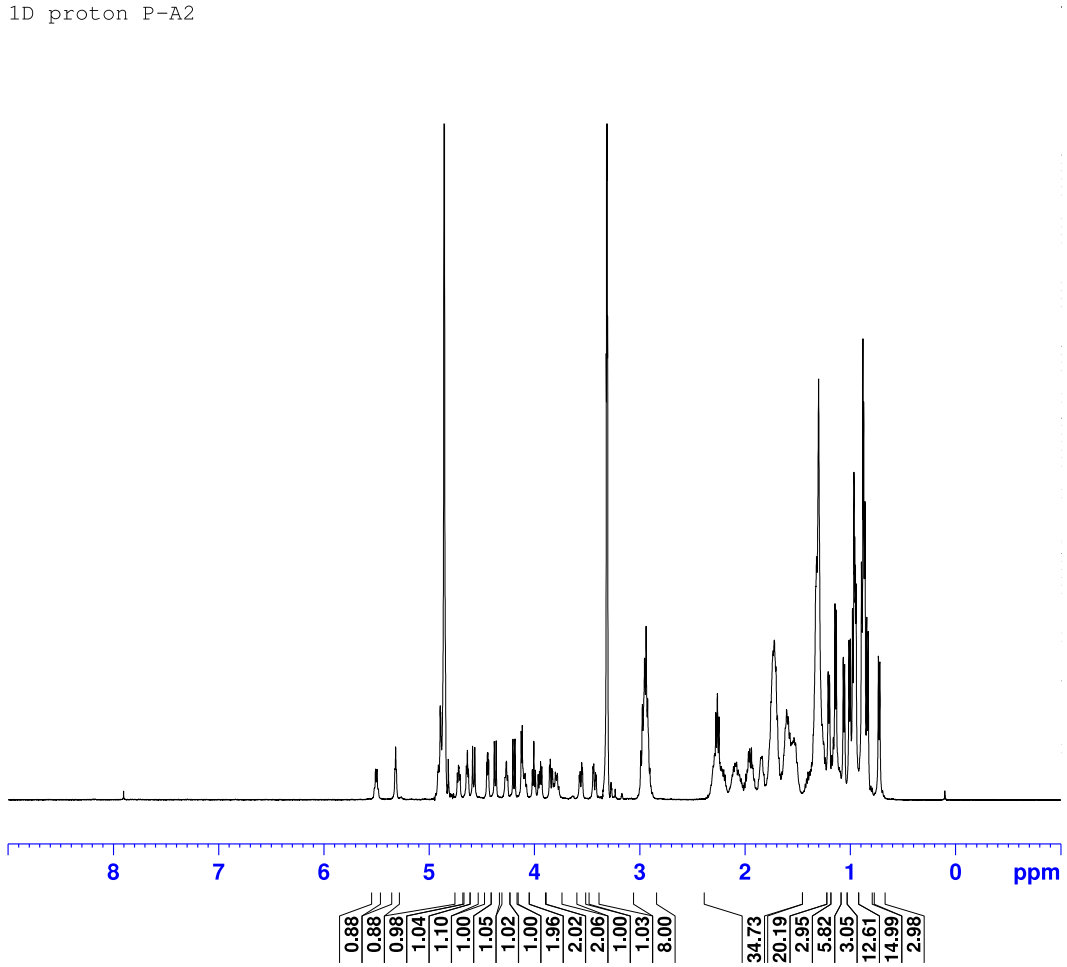

Figure A.20. ^{1}H-NMR spectrum of PA2 (500 MHz, CD_3OD)

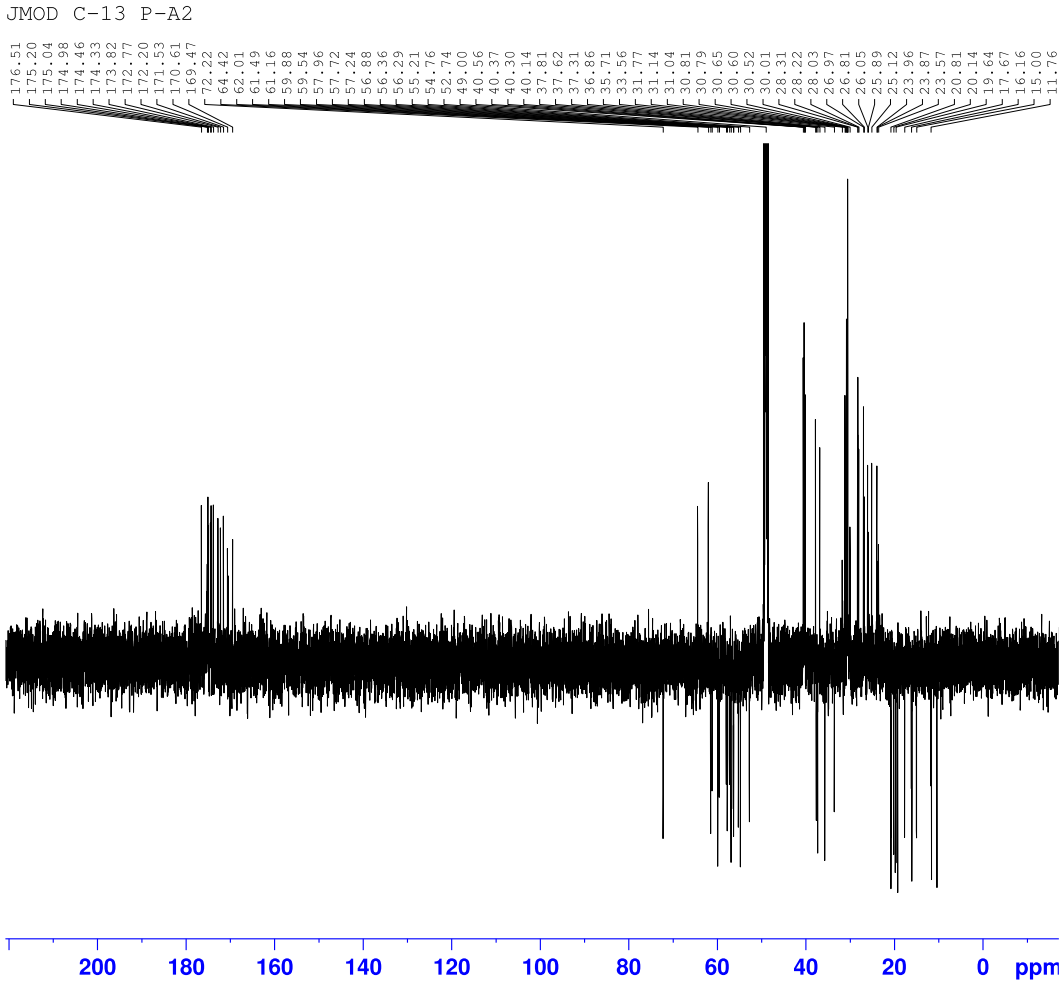

Figure A.21. ^{13}C-JMOD spectrum of PA2 (125 MHz, CD_3OD)

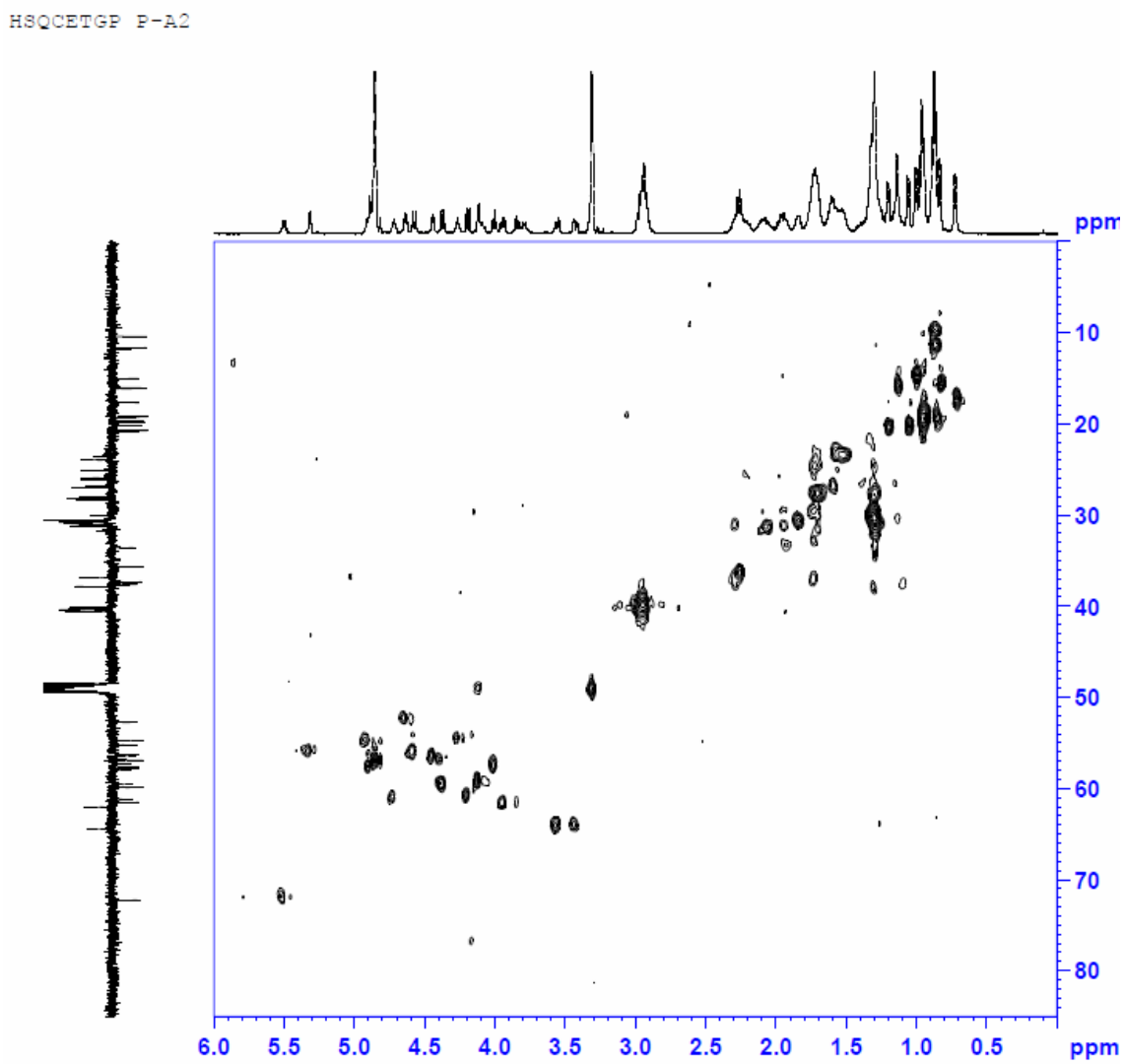

Figure A.22. ^{1}H-^{13}C HSQC of PA2 (500 MHz, CD_3OD)

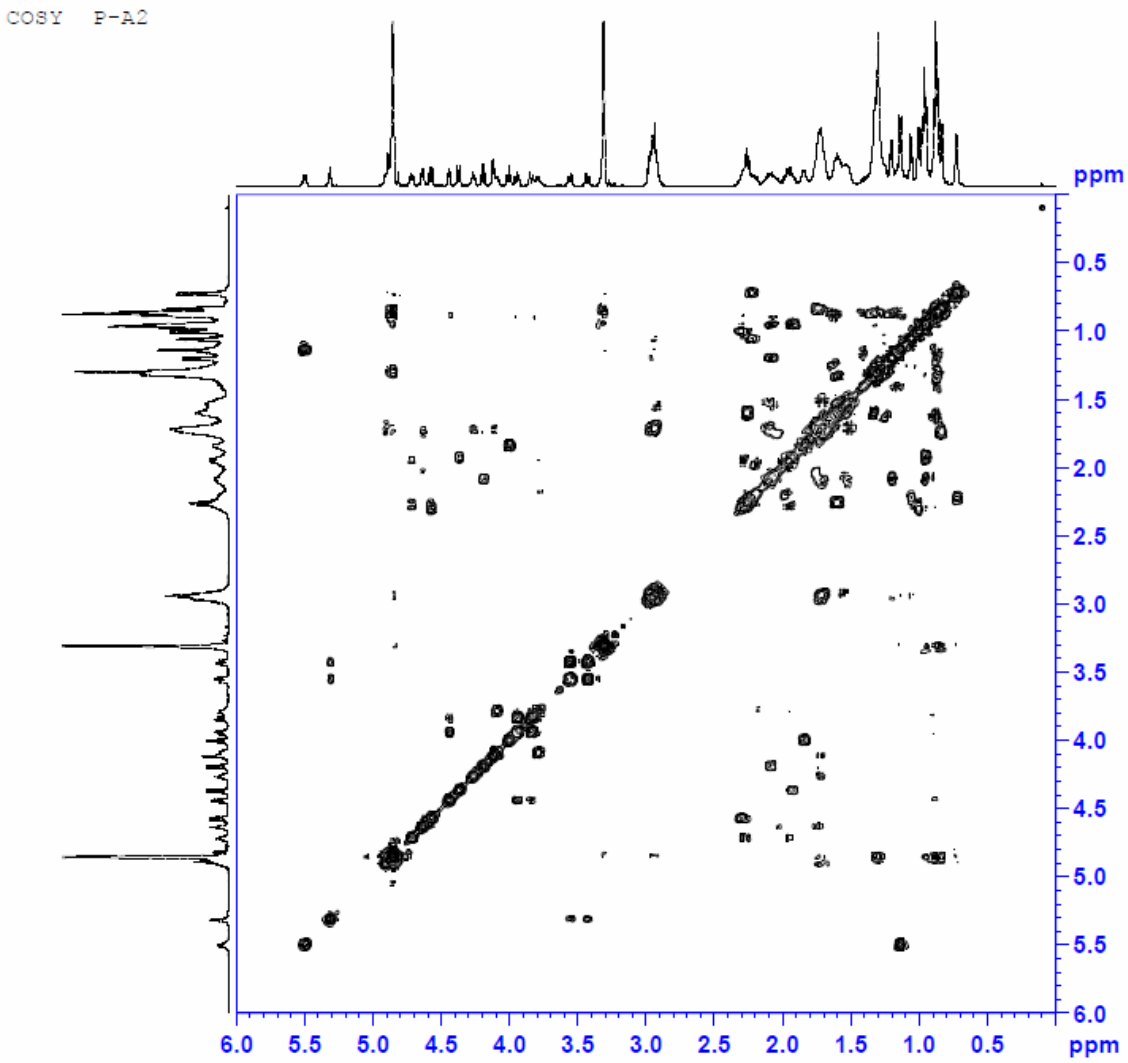

Figure A.23. ^{1}H-COSY of PA2 (500 MHz, CD_3OD)

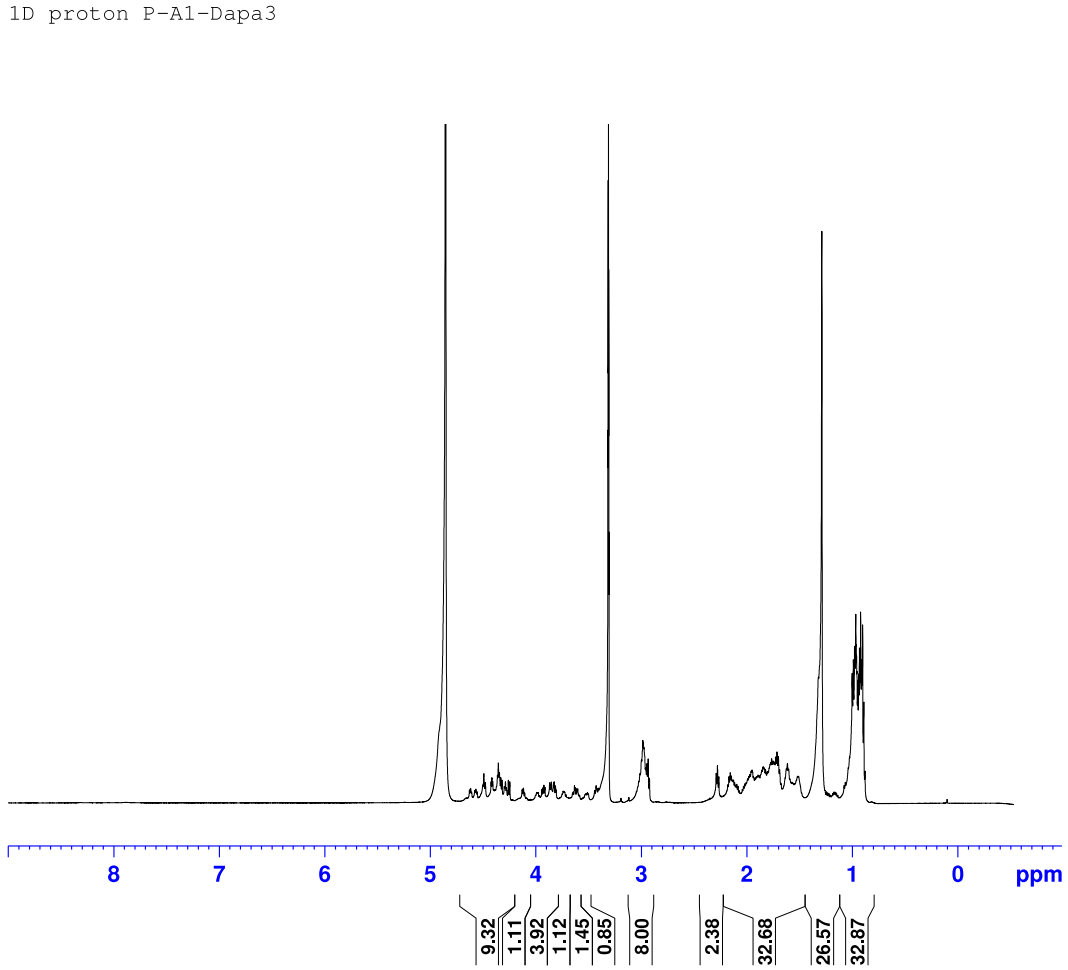

Figure A.24. ^{1}H-NMR spectrum of PA1-Dapa (600 MHz, CD_3OD)

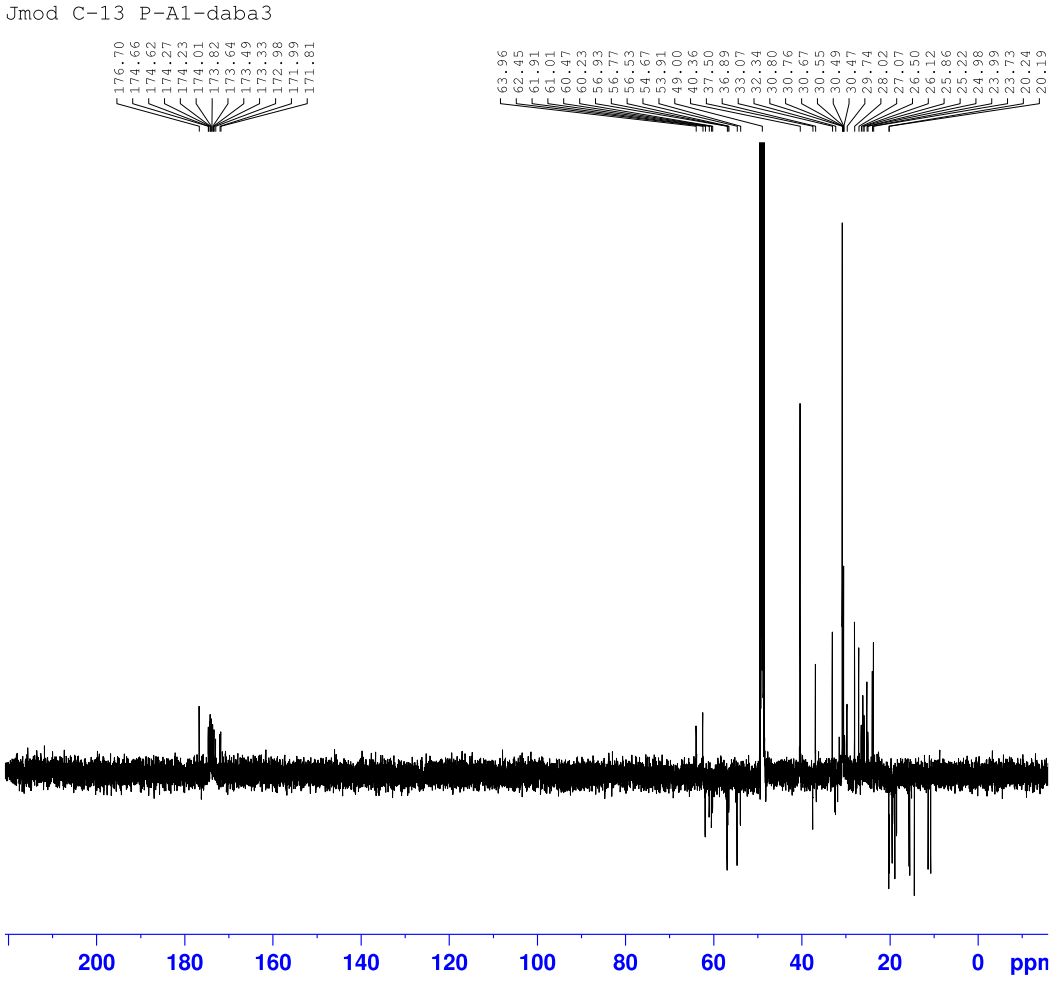

Figure S25. ^{13}C-JMOD spectrum of PA1-Dapa (125 MHz, CD_3OD)

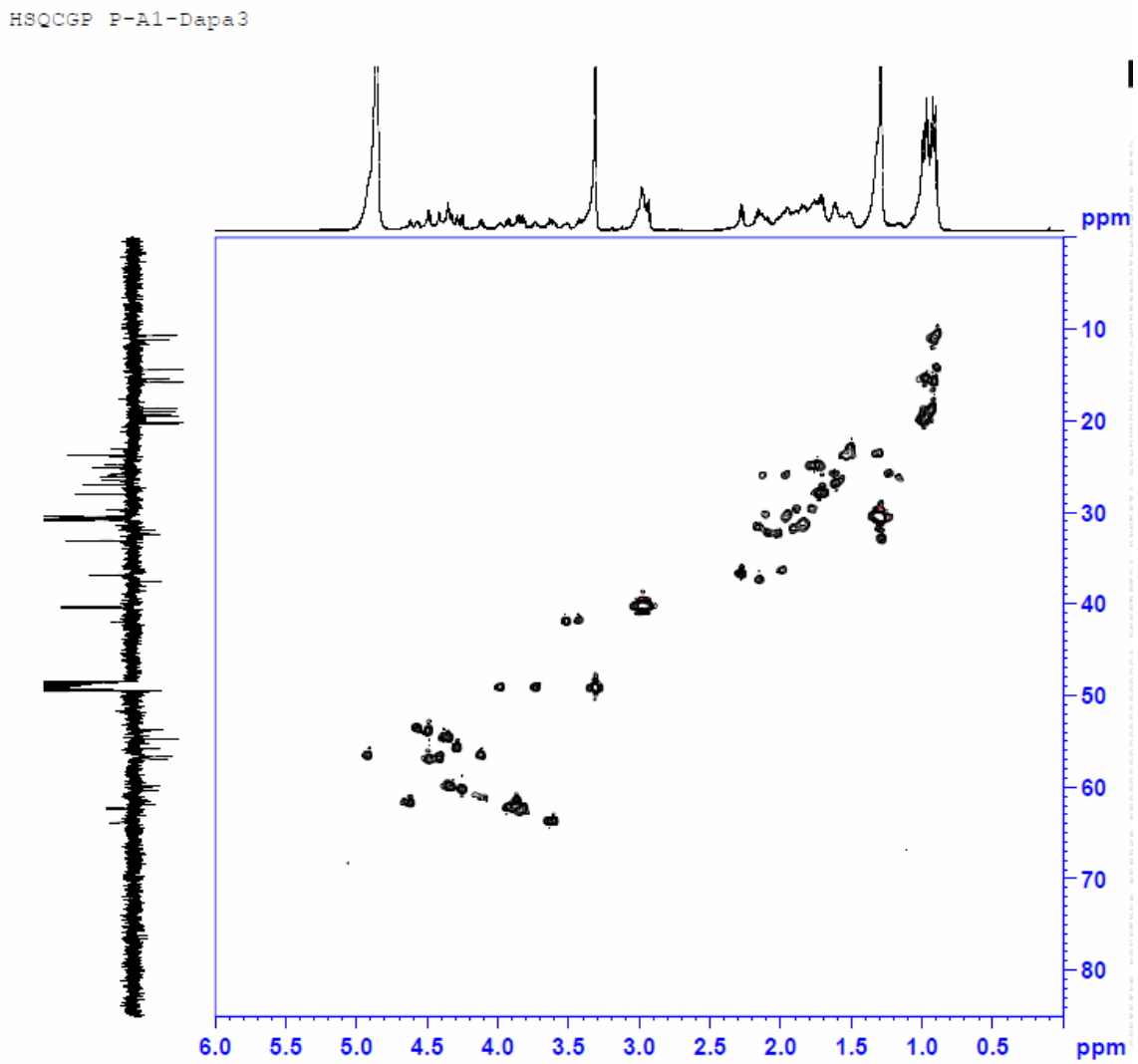

Figure A.25. ^{1}H-^{13}C HSQC of PA1-Dapa (600 MHz, CD_3OD)

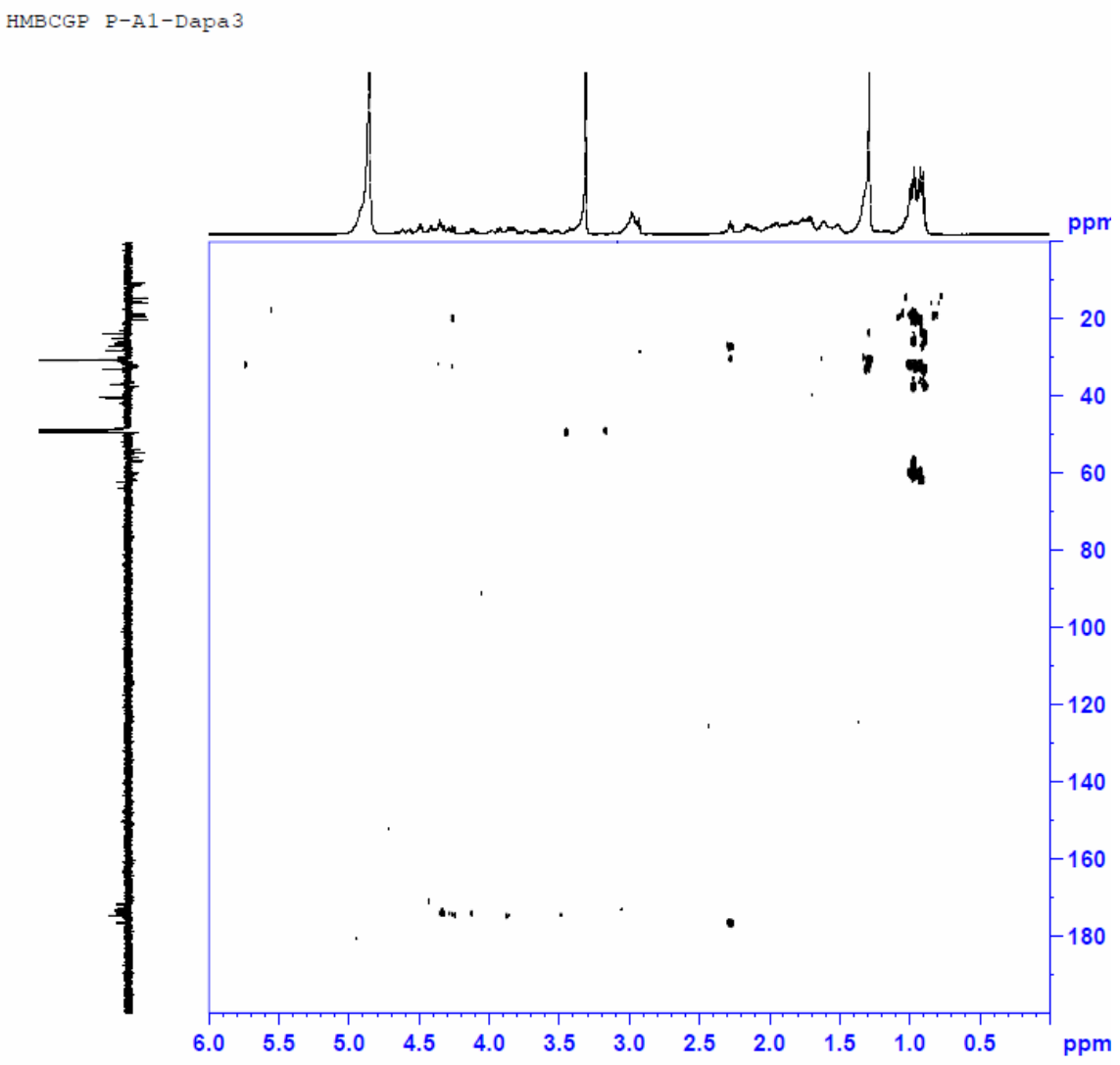

Figure A.26. ^{1}H-^{13}C HMBC of PA1-Dapa (500 MHz, CD_3OD)

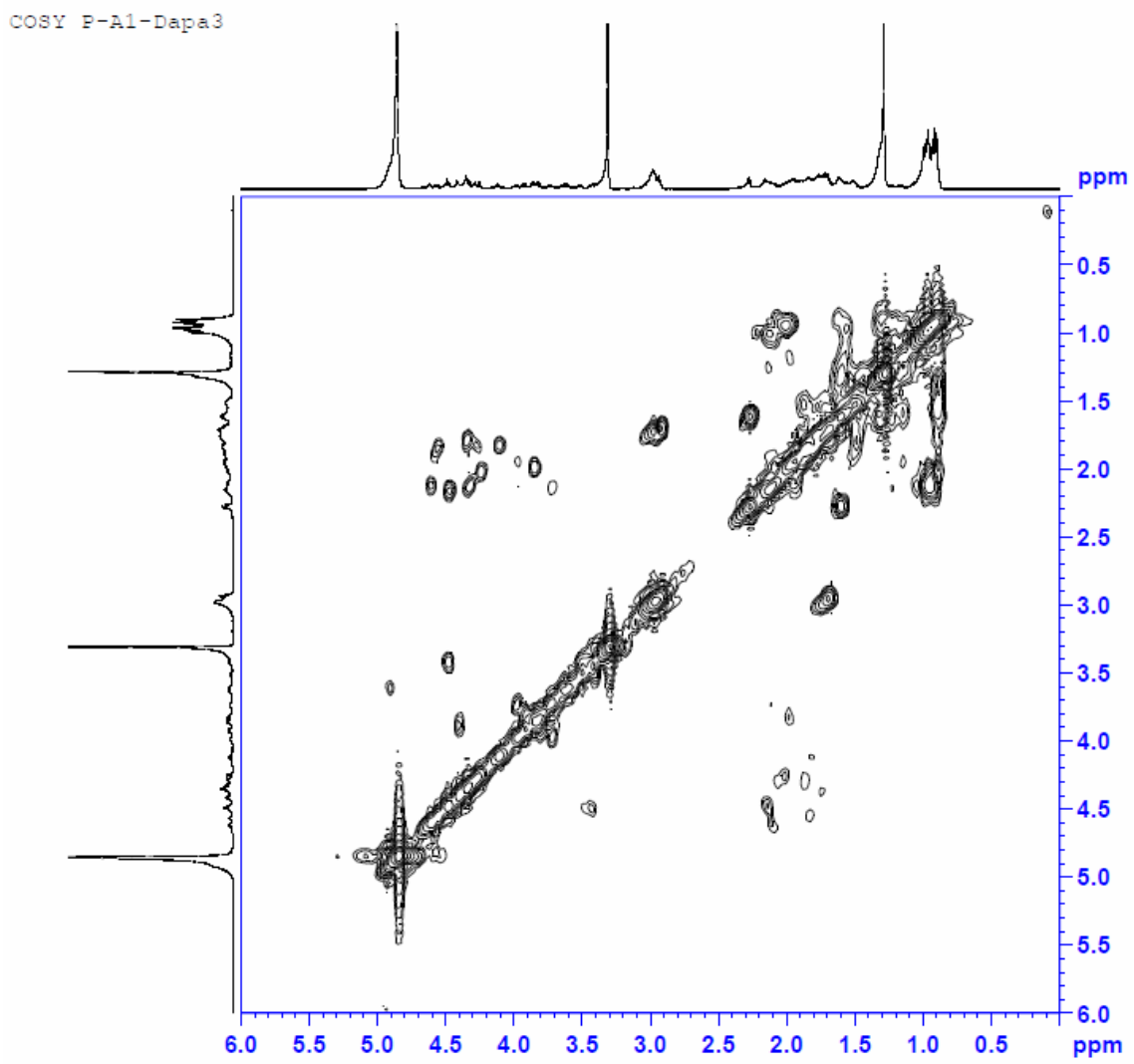

Figure A.27. ^{1}H-COSY of PA1-Dapa (600 MHz, CD_3OD)

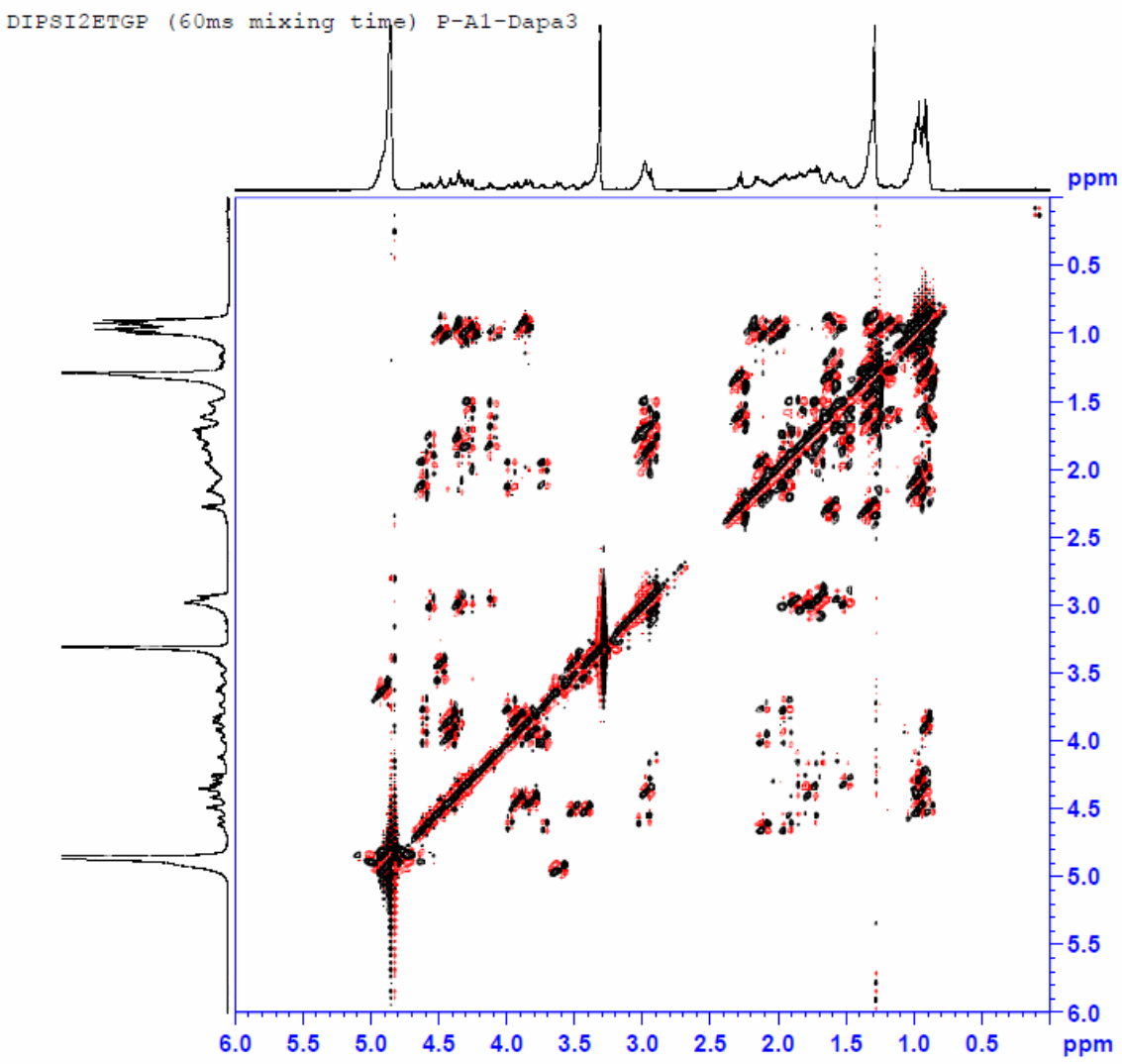

Figure A.28. ^{1}H-TOCSY of PA1-Dapa (600 MHz, CD_3OD)

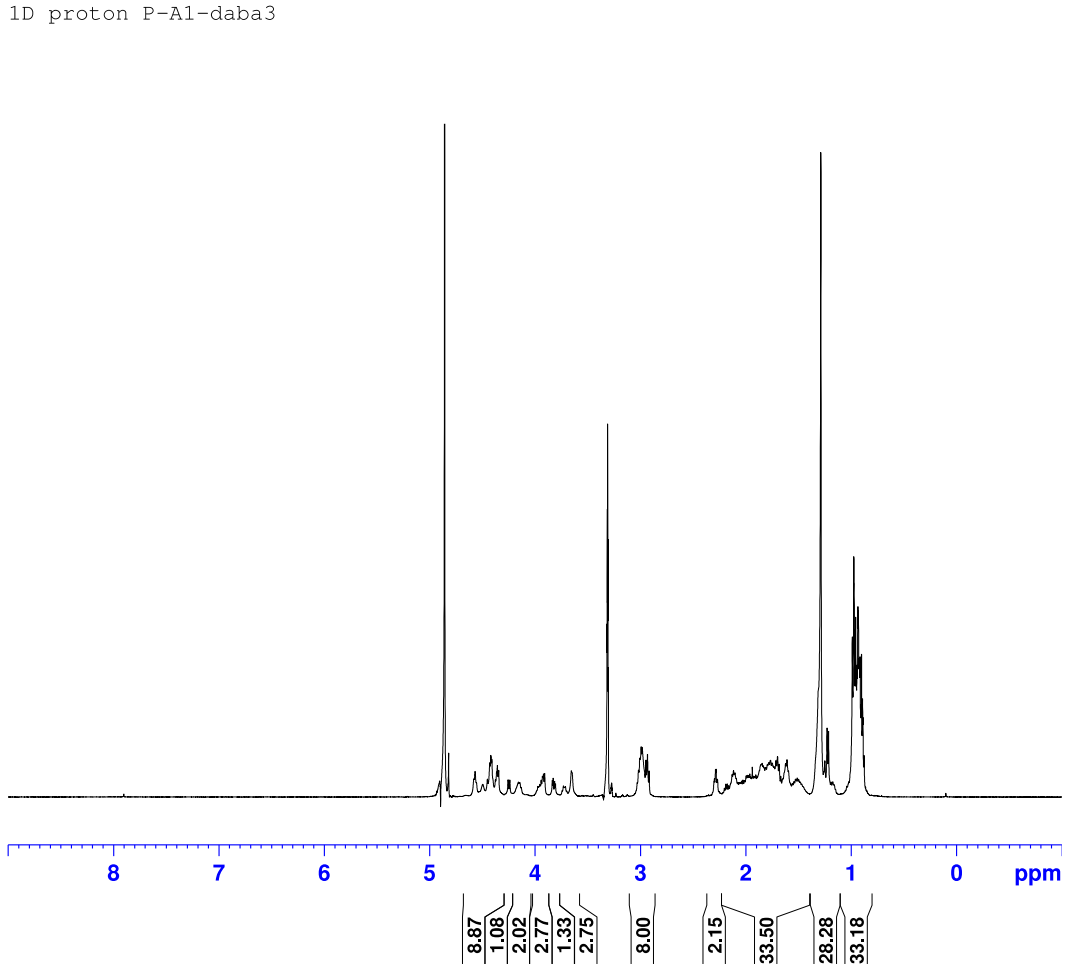

Figure A.29. ^{1}H-NMR spectrum of PA1-Daba (500 MHz, CD_3OD)

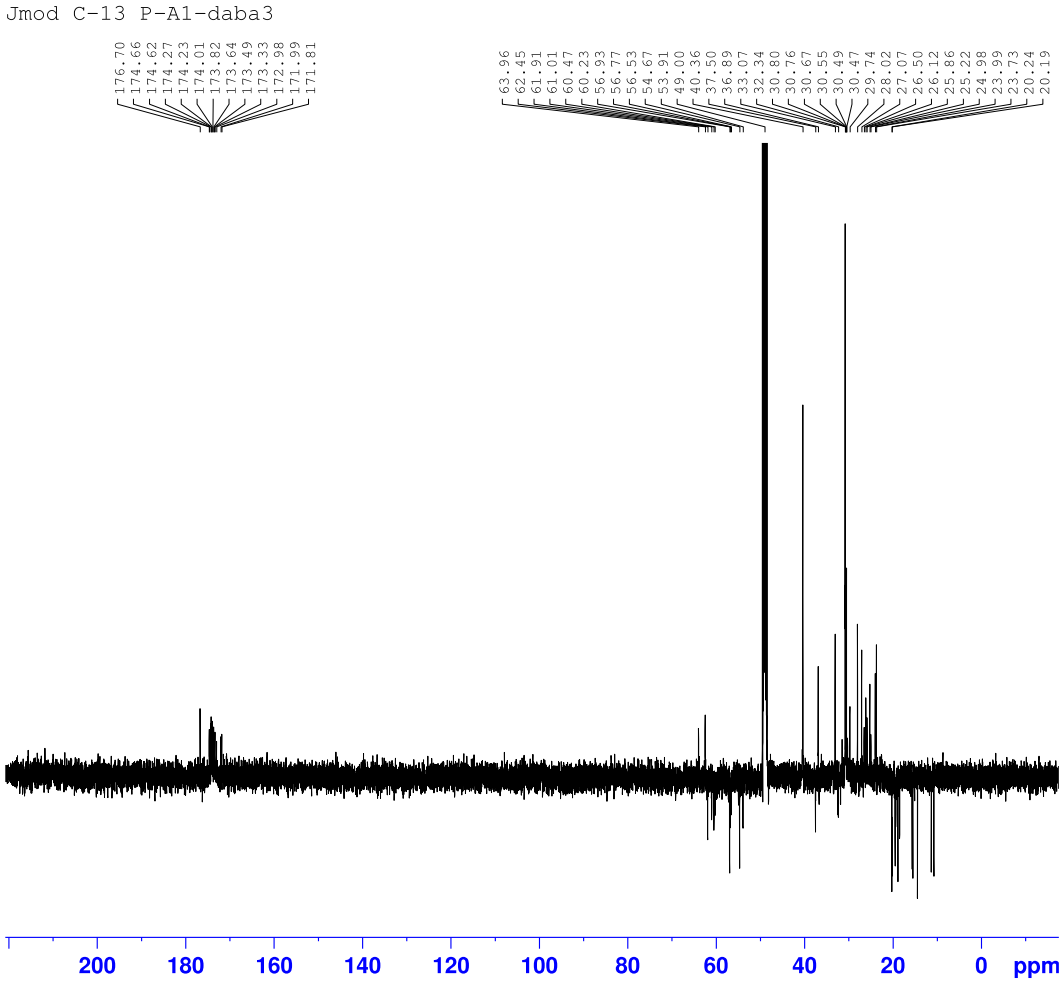

Figure A.30. ^{13}C-JMOD spectrum of PA1-Daba (125 MHz, CD_3OD)

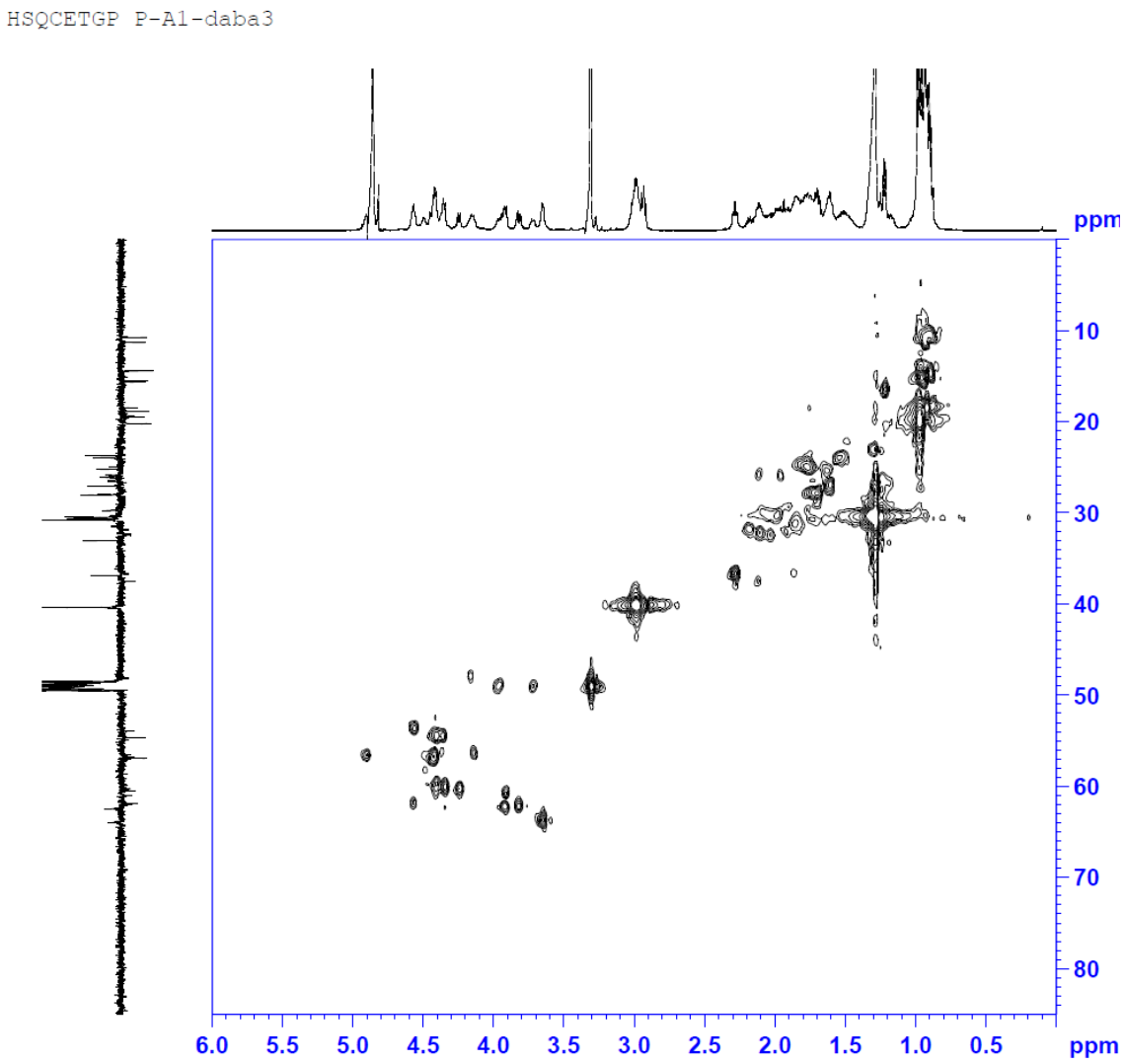

Figure A.31. ^{1}H-^{13}C HSQC of PA1-Daba (500 MHz, CD_3OD)

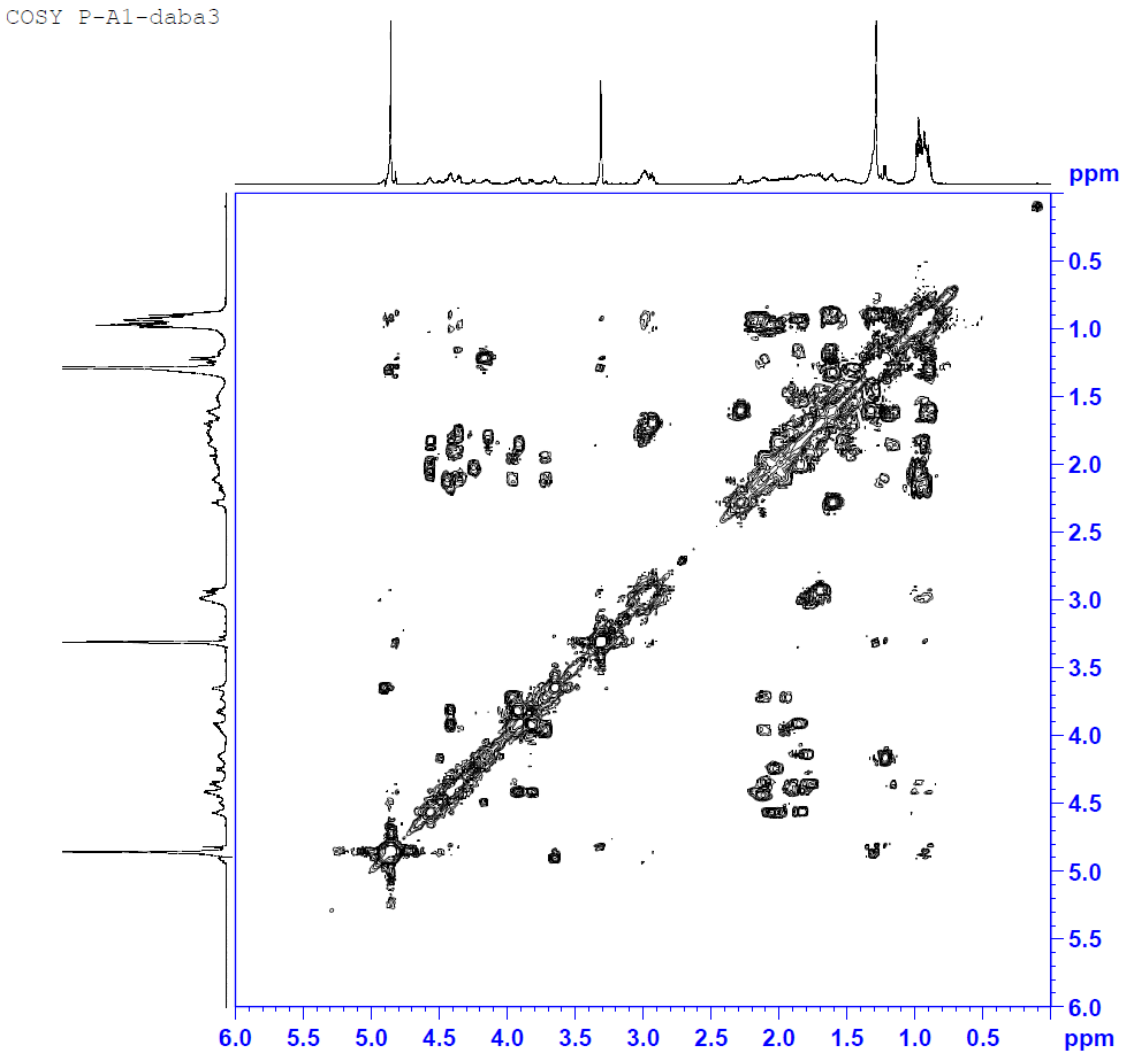

Figure A.32. ^{1}H-COSY of PA1-Daba (500 MHz, CD_3OD)

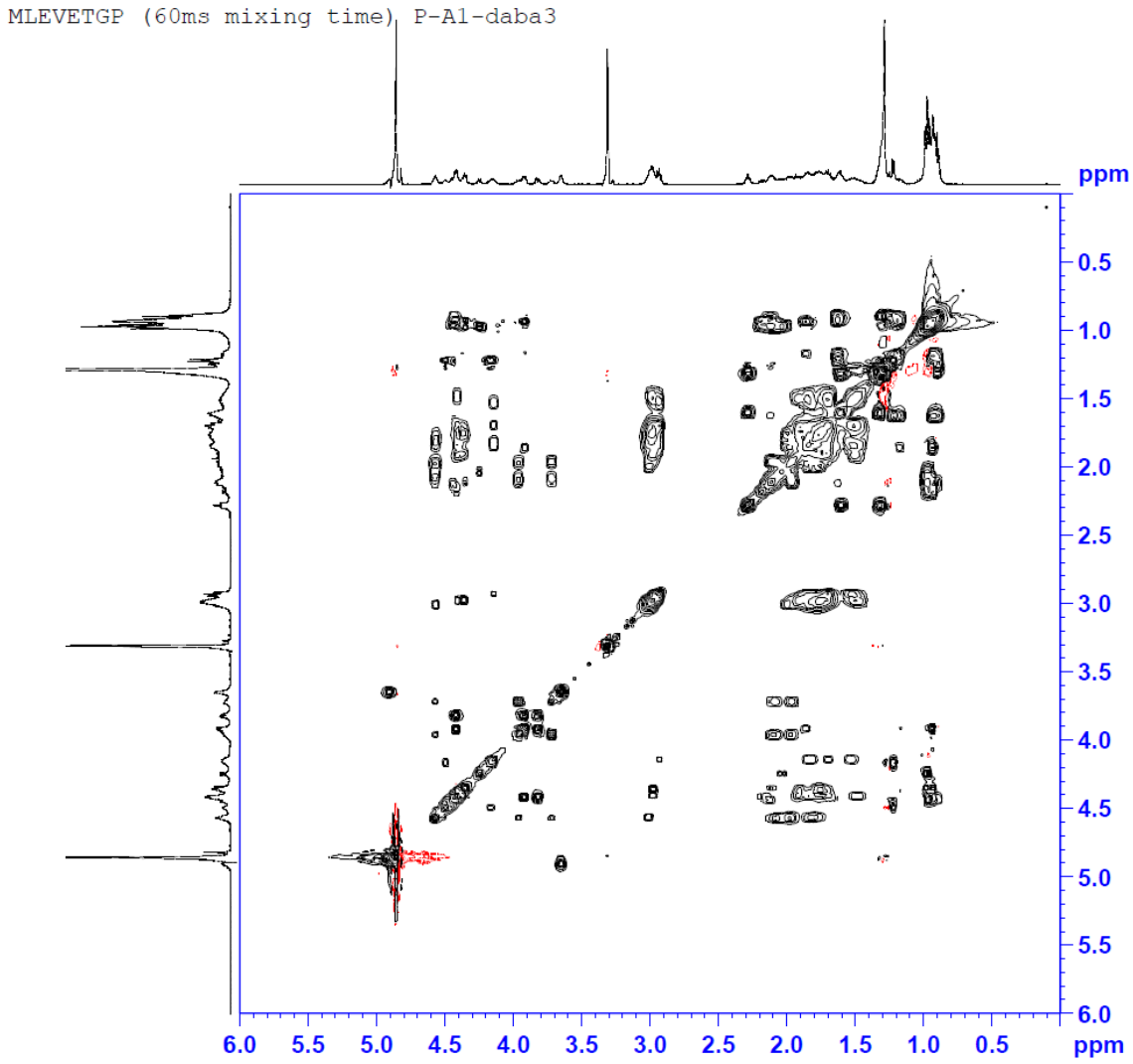

Figure A.33. ^{1}H-TOCSY of PA1-Daba (500 MHz, CD_3OD)

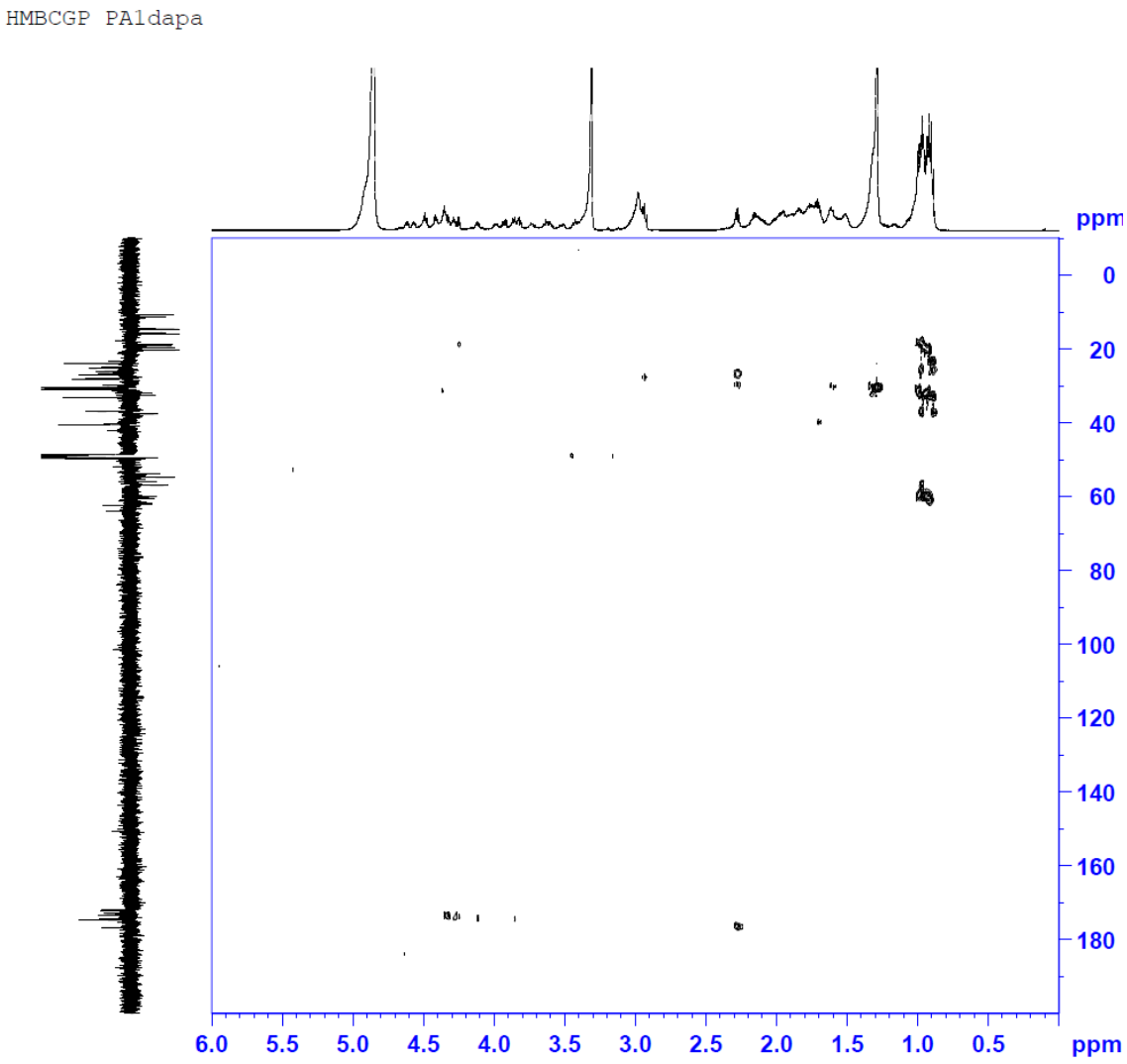

Figure A.34. ^{1}H-^{13}C HMBC of PA1-Daba (500 MHz, CD_3OD)

Table A.1 HSQC peak coordinates for PA1 and PA2

		Paenibacterin (Guo *et al.*)[41]		PA1 (this work)		PA2 (this work)	
		^{1}H	^{13}C	^{1}H	^{13}C	^{1}H	^{13}C
D-Orn1	CH^{α}	4.27	54.61	4.27	54.46	4.27	54.40
	CH_2^{β}	1.77	29.91	1.74	29.54	1.73	29.65
		1.73	29.91				
	CH_2^{γ}	1.72	24.99	1.73	24.69	1.72	24.63
	CH_2^{δ}	2.94	39.99	**2.94**	**39.90**	**2.95**	**39.84**
Val2	CH^{α}	4.19	61.03	4.19	60.77	4.21	60.71
	CH_2^{β}	2.08	31.42	2.08	31.32	2.07	31.27
	$CH_3^{\gamma 1}$	1.20	20.65	1.20	20.48	1.20	20.43
	$CH_3^{\gamma 2}$	0.95	19.94	0.96	19.51	**0.95**	**19.46**
Thr3	CH^{α}	4.84	57.12	4.84	56.89	4.86	56.99
	CH_2^{β}	5.49	72.10	5.51	71.77	5.52	71.87
	CH_3^{γ}	1.14	16.02	1.14	15.79	1.14	15.90
D-Orn4	CH^{α}	4.64	52.62	4.63	52.36	4.65	52.30
	CH_2^{β}	2.05	31.61	1.74	31.49	1.71	31.59
		1.74	31.61				
	CH_2^{γ}	1.58	23.37	**1.53**	**23.56**	**1.53**	**23.34**
		1.55	23.37				
	CH_2^{δ}	2.92	40.12	**2.94**	**39.90**	**2.95**	**39.84**
Ser5	CH^{α}	5.32	56.13	5.32	55.92	5.34	55.86
	CH_2^{β}	3.55	64.32	3.55	64.00	3.44	63.95
		3.42	64.32	3.42	64.00	3.57	64.11
Val6	CH^{α}	4.37	59.75	4.37	59.47	4.39	59.42
	CH_2^{β}	1.93	33.44	1.93	33.10	1.92	33.37
	$CH_3^{\gamma 1}$	0.97	19.64	**0.96**	**19.51**	**0.95**	**19.46**
	$CH_3^{\gamma 2}$	0.95	19.09	**0.96**	**19.51**	**0.95**	**19.46**
D-Lys7	CH^{α}	4.00	57.59	4.01	57.37	4.01	57.47
	CH_2^{β}	1.84	30.90	1.84	30.68	1.84	30.62

		Paenibacterin (Guo *et al.*)[41]		PA1 (this work)		PA2 (this work)	
D-Lys7	CH_2^{γ}	1.58	23.80	**1.53**	**23.56**	**1.53**	**23.34**
		1.54	23.80				
	CH_2^{δ}	1.71	27.86	1.71	27.76	1.71	27.71
	CH_2^{ε}	2.94	40.21	**2.94**	**39.90**	**2.95**	**39.84**
D-Ser8	CH^{α}	4.44	56.75	4.45	56.40	4.46	56.34
	CH_2^{β}	3.94	61.88	3.84	61.58	3.86	61.52
		3.84	61.88	3.94	61.58	3.95	61.52
Ile9	CH^{α}	4.57	56.22	4.58	55.92	4.60	55.86
	CH_2^{β}	2.30	37.49	2.30	37.31	2.27	36.44
	CH_3^{γ}	1.00	14.87	1.01	14.50	1.01	14.60
	CH_2^{γ}	1.63	25.77	1.63	25.50		
		1.25	25.77	1.24	25.50		
	CH_3^{δ}	0.88	10.24	0.88	9.97	0.88	9.91
Pro10	CH^{α}	4.72	61.36	4.72	61.09	4.74	61.03
	CH_2^{β}	2.28	31.43	2.29	31.16	1.94	31.07
		1.95	31.43	1.95	31.16	2.29	31.04
	CH_2^{γ}	2.20	25.93	2.19	25.66		
		1.97	25.93	1.97	25.66		
	CH_2^{δ}	4.09	49.33	4.10	49.12	4.13	49.06
		3.78	49.33	3.79	49.12		
Val11	CH^{α}	4.89	57.85	4.89	57.53	4.91	57.47
	CH_2^{β}	2.23	34.81	2.23	34.56		
	$CH_3^{\gamma 1}$	1.06	20.62	1.06	20.32	1.06	20.43
	$CH_3^{\gamma 2}$	0.73	17.55	0.72	17.25	0.72	17.19
Lys12	CH^{α}	4.90	55.05	4.91	54.78	4.92	54.72
	CH_2^{β}	2.11	30.58	2.12	30.35		
		1.70	30.58				
Lys12	CH_2^{γ}	1.51	23.70	**1.53**	**23.56**	**1.53**	**23.34**
	CH_2^{δ}	1.72	28.02	**1.71**	**27.76**	**1.71**	**27.71**
	CH_2^{ε}	2.98	40.40	**2.94**	**39.90**	**2.95**	**39.84**

		Paenibacterin (Guo *et al.*)[41]		PA1 (this work)		PA2 (this work)	
Ile13	CH^{α}	4.11	59.42	4.12	59.15	4.13	59.09
	CH_2^{β}	1.73	37.18	1.74	36.99	1.73	37.09
	CH_3^{γ}	0.84	15.88	0.84	15.63	0.82	15.57
	CH_2^{γ}	1.40	26.68	1.16	26.47		
		1.16	26.68	1.40	26.47		
	CH_3^{δ}	0.87	11.40	0.86	11.26	**0.86**	**11.20**

Note: Bolded peaks overlap with one or more other peaks

Table A.2. Acyl tail HSQC coordinates

	Anteiso (Guo *et al*)[41]			PA2, anteiso	
	^{1}H	^{13}C		^{1}H	^{13}C
C^{1}		176.43	C^{1}		176.51
CH_2^{2}	2.26	36.73	CH_2^{2}	**2.27**	**36.44**
CH_2^{3}	1.60	26.84	CH_2^{3}	1.60	26.74
CH_2^{4}	1.32	30.39	CH_2^{4-10}	1.31	30.29
CH_2^{5-10}	1.29	30.74	CH_2^{11}	1.31	27.87
CH_2^{11}	1.29	28.34	CH^{12}	1.01	37.58
CH^{12}	1.17	40.10	$CH_3^{12\text{-}Me}$	0.86	19.29
CH_2^{13}	1.52	29.04	CH_2^{13}		
$CH_3^{14,15}$	0.88	22.92	CH_3^{14}	**0.86**	**11.20**

	PA1, linear			PA1-Dapa, linear			PA1-Daba, linear	
	^{1}H	^{13}C		^{1}H	^{13}C		^{1}H	^{13}C
C^{1}		176.50	C^{1}		176.66	C^{1}		176.70
CH_2^{2}	2.26	36.50	CH_2^{2}	2.28	36.77	CH_2^{2}	2.28	36.56
CH_2^{3}	1.59	26.63	CH_2^{3}	1.61	26.90	CH_2^{3}	1.60	26.85
CH_2^{4-12}	1.30	30.35	CH_2^{4-12}	1.29	30.62	CH_2^{4-12}	1.29	30.41
CH^{13}	1.28	32.62	CH^{13}	1.29	32.89	CH^{13}		
CH_2^{14}	1.31	23.23	CH_2^{14}	1.31	23.58	CH_2^{14}	1.29	22.97
CH_3^{15}	0.90	14.01	CH_3^{15}	0.90	14.28	CH_3^{15}	0.97	13.75

Note: Bolded peaks overlap with one or more other peaks

Table A.3. HSQC peak coordinates for PA1-Dapa[3] and PA1 Daba[3]

PA1-Dapa				PA1-Daba			
Residue		**^{1}H**	**^{13}C**	**Residue**		**^{1}H**	**^{13}C**
D-Orn 1 & 2	$CH^{\alpha'}$	4.57	53.59	D-Orn 1 & 2	$CH^{\alpha'}$	4.56	53.55
	$CH_2^{\beta'}$	1.84	31.11		$CH_2^{\beta''}$	1.87	31.22
	$CH^{\alpha''}$	4.36	54.57		$CH^{\alpha''}$	4.36	54.52
	$CH_2^{\beta''}$	1.89	29.65		$CH_2^{\beta'}$	1.90	29.28
		1.77	29.65			1.71	29.12
	CH_2^{γ}	1.76	24.96		CH_2^{γ}	1.77	24.91
	CH_2^{δ}	2.97	40.33		CH_2^{δ}	2.98	40.12
Val 2 & 6	CH^{α}	4.34	59.90	Val 2 & 6	$CH^{\alpha'}$	4.43	56.78
	CH_2^{β}	2.09	32.24		$CH_2^{\beta'}$	2.19	31.71
		2.15	31.59		$CH^{\alpha''}$	4.35	60.02
	CH_3^{γ}	0.99	19.94		$CH_2^{\beta''}$	2.11	32.19
		0.95	19.30		CH_3^{γ}	0.97	19.90
Dapa3	CH^{α}	4.50	53.92	Daba3	CH^{α}	4.49	58.21
	CH_2^{β}	3.52	41.95		CH_2^{β}	4.17	47.88
		3.43	41.78		CH_3^{γ}	1.21	16.50
Ser5	CH^{α}	4.92	56.51	Ser5	CH^{α}	4.90	56.46
	CH_2^{β}	3.63	63.79		CH_2^{β}	3.65	63.58
D-Lys7 & L-Lys12	$CH^{\alpha'}$	4.12	56.51	D-Lys7 & L-Lys12	$CH^{\alpha''}$	4.14	56.30
	$CH^{\alpha''}$	4.29	55.70		$CH^{\alpha'}$	4.40	54.36
	CH_2^{β}	1.84	31.11		CH_2^{β}	1.87	31.22
	CH_2^{γ}	1.55	23.83		CH_2^{γ}	1.55	23.94
		1.51	23.02				
	CH_2^{δ}	1.71	27.87		CH_2^{δ}	1.71	27.82
	CH_2^{ε}	2.97	40.33		CH_2^{ε}	2.98	40.12
D-Ser8	CH^{α}	4.42	56.83	D-Ser8	CH^{α}	4.42	59.69
	CH_2^{β}	3.82	62.33		CH_2^{β}	3.82	62.12
D-Ser8		3.93	62.17	D-Ser8		3.92	62.12
Ile9	CH^{α}	4.49	56.99	Ile9	CH^{α}	4.43	56.78

PA1-Dapa				PA1-Daba			
Ile9 (*cont.*)	CH_2^{β}	2.15	37.42	Ile9 (*cont.*)	CH_2^{β}	2.13	37.37
	CH_3^{γ}	0.98	15.41		CH_3^{γ}	0.97	15.04
	CH_2^{γ}	1.62	25.77		CH_2^{γ}	1.63	25.40
		1.24	25.77				
	CH_3^{δ}	0.90	10.72		CH_3^{δ}	0.90	10.51
Pro10	CH^{α}	4.62	61.68	Pro10	CH^{α}	4.57	61.80
	CH_2^{β}	2.11	30.30		CH_2^{β}	2.06	30.08
		1.95	30.31			1.98	30.09
	CH_2^{γ}	2.13	26.09		CH_2^{γ}	2.11	25.72
		1.96	25.93			1.97	25.88
	CH_2^{δ}	3.99	49.06		CH_2^{δ}	3.96	48.85
		3.73	49.23			3.73	49.02
Val11	CH^{α}	4.25	60.23	Val11	CH^{α}	4.25	60.18
	CH_2^{β}	2.02	32.40		CH_2^{β}	2.03	32.35
	CH_3^{γ}	0.93	18.65		CH_3^{γ}	0.93	18.44
Ile13	CH^{α}	3.86	61.36	Ile13	CH^{α}	3.92	60.83
	CH_2^{β}	2.00	36.28		CH_2^{β}	1.87	36.56
	CH_3^{γ}	0.91	15.74		CH_3^{γ}	0.90	14.56
	CH_2^{γ}	1.16	26.25		CH_2^{γ}	1.63	25.40
	CH_3^{δ}	0.91	11.04		CH_3^{δ}	0.94	11.00

Appendix B

Characterization of Chapter 3 Compounds

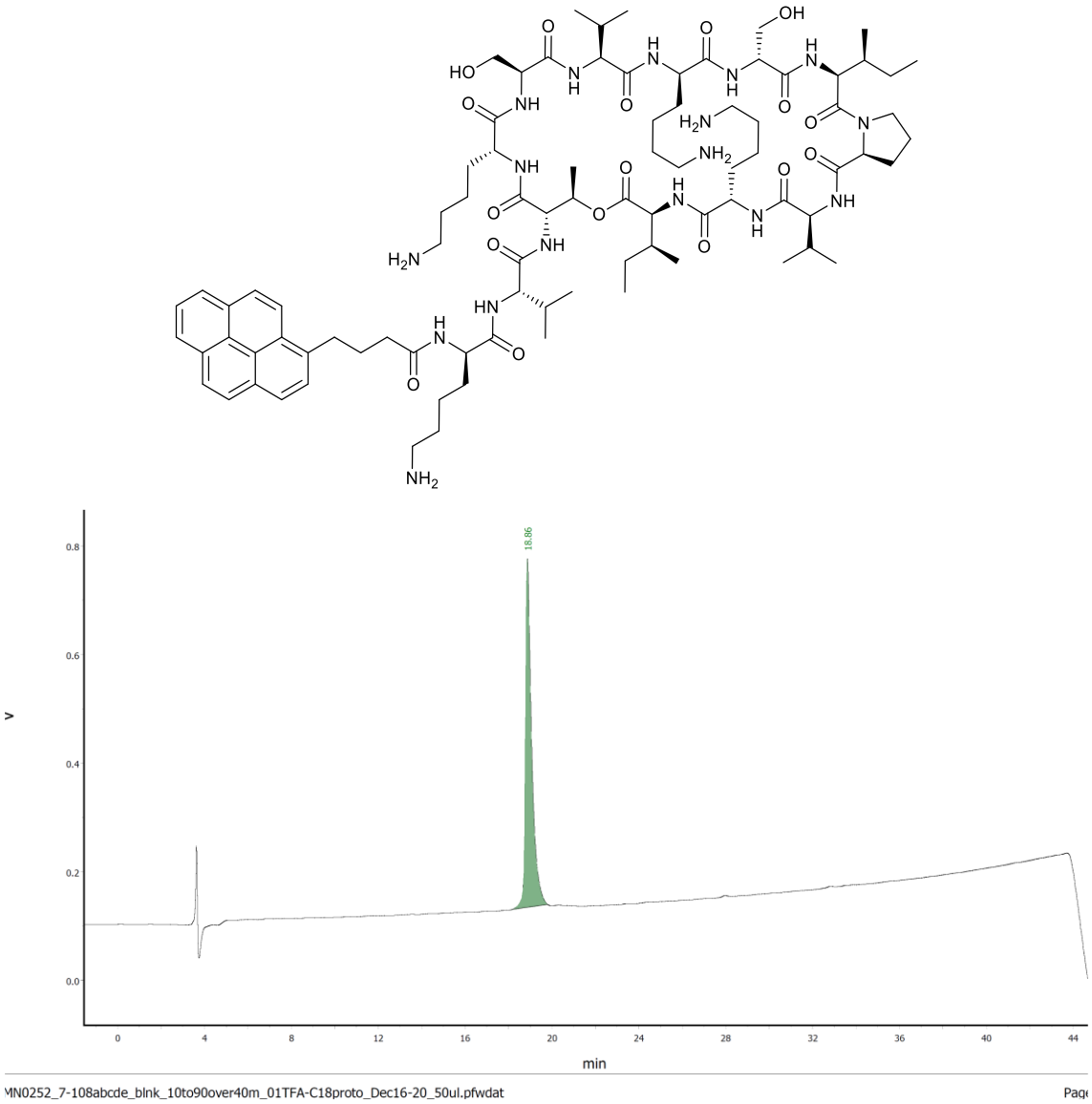

Figure B.1 Analytical RP-HPLC of PA(Pba tail)-D-K1-D-K4 (3.26**).** Linear gradient of 10:90 to 90:10 MeCN/H2O (0.1% TFA) over 40 min (λ = 220 nm). C18 proto, 5 µm, 250 × 4.6 mm.

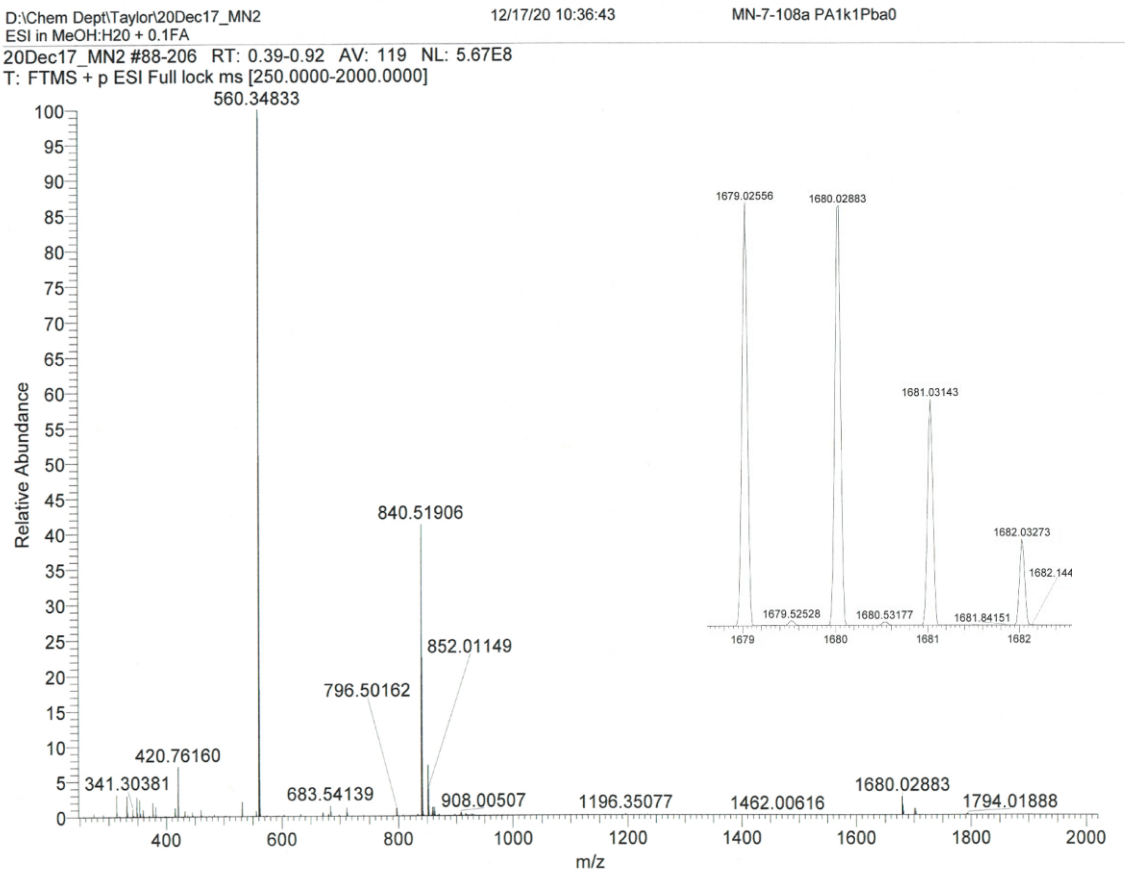

Elemental composition search on mass 1679.02556

m/z= 1674.02556-1684.02556

m/z	Theo. Mass	Delta (ppm)	RDB equiv.	Composition
1679.02556	1679.02946	-2.32	27.5	$C_{86}H_{136}O_{17}N_{17}$
	1679.01689	5.17	28.0	$C_{85}H_{134}O_{17}N_{18}$
	1679.04204	-9.81	27.0	$C_{87}H_{138}O_{17}N_{16}$
	1679.00565	11.86	28.0	$C_{86}H_{134}O_{18}N_{16}$
	1679.05327	-16.50	27.0	$C_{86}H_{138}O_{16}N_{18}$

Figure B.2 HRMS (+ESI) of PA(Pba tail)-D-K1-D-K4 (3.26).

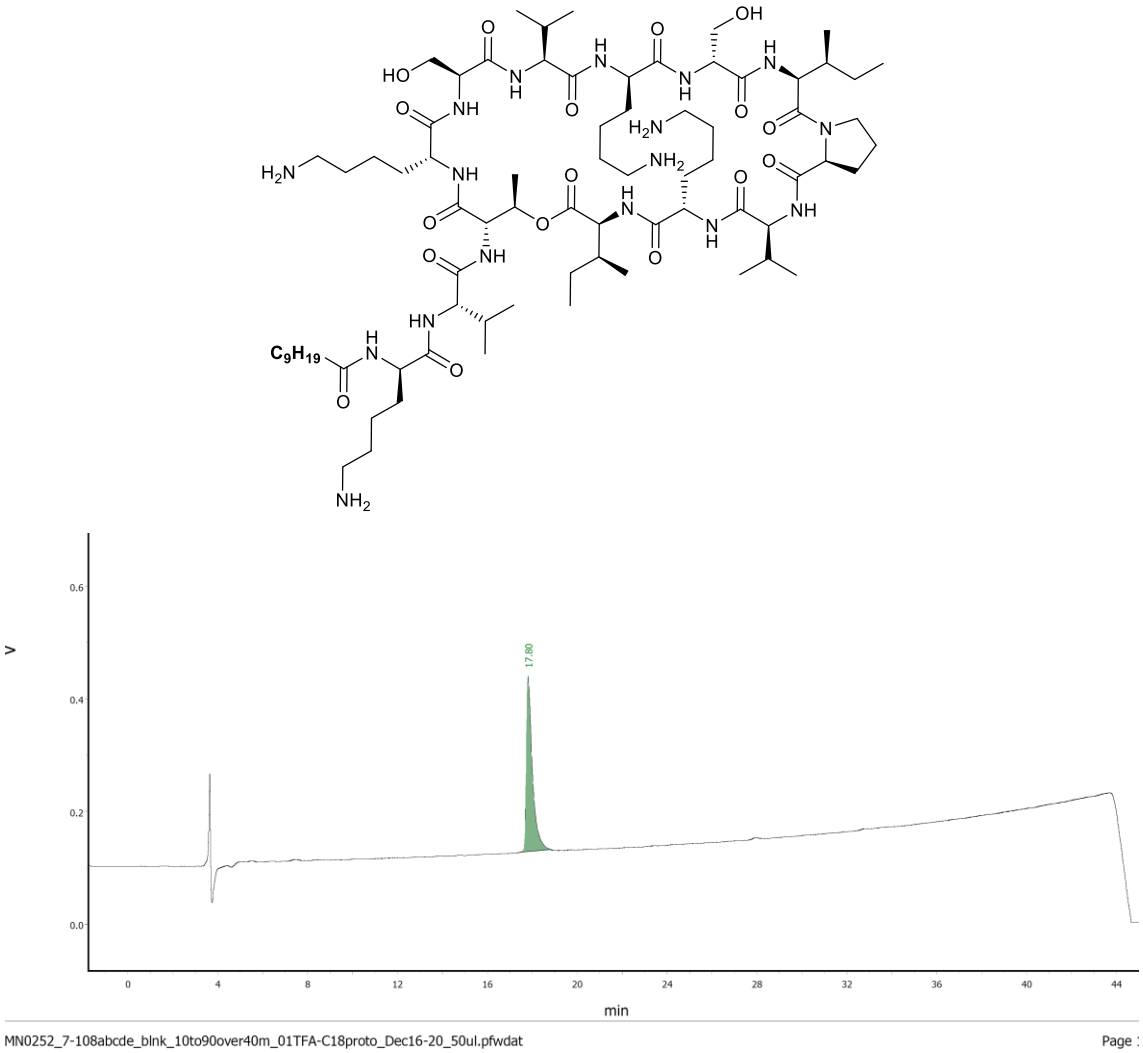

Figure B.3 Analytical RP-HPLC of PA(C10 tail)-D-K1-D-K4 (3.23). Linear gradient of 10:90 to 90:10 MeCN/H2O (0.1% TFA) over 40 min (λ = 220 nm). C18 proto, 5 µm, 250 × 4.6 mm.

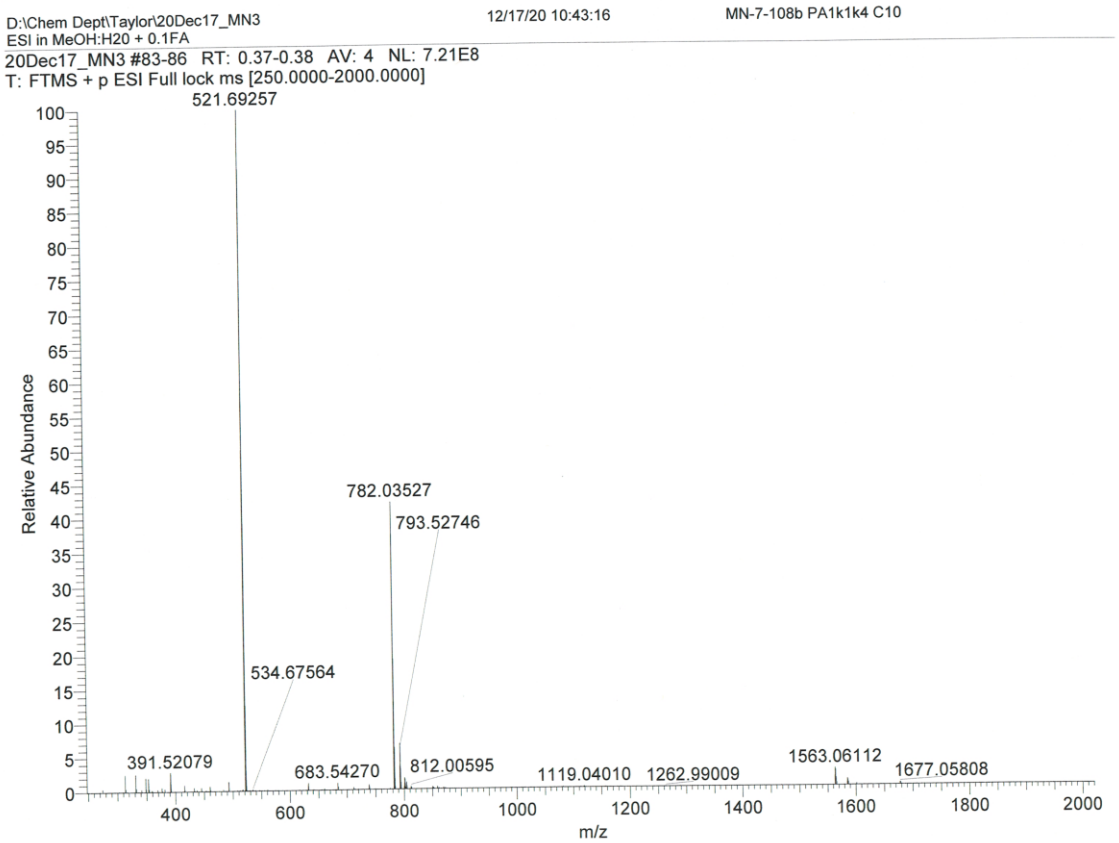

Elemental composition search on mass 1563.06112

m/z= 1558.06112-1568.06112

m/z	Theo. Mass	Delta (ppm)	RDB equiv.	Composition
1563.06112	1563.06076	0.23	15.5	$C_{76}H_{140}O_{17}N_{17}$
	1563.07334	-7.82	15.0	$C_{77}H_{142}O_{17}N_{16}$
	1563.04819	8.27	16.0	$C_{75}H_{138}O_{17}N_{18}$
	1563.08457	-15.00	15.0	$C_{76}H_{142}O_{16}N_{18}$
	1563.03695	15.46	16.0	$C_{76}H_{138}O_{18}N_{16}$

Figure B.4 HRMS (+ESI) of PA(C10 tail)-D-K1-D-K4 (3.23).

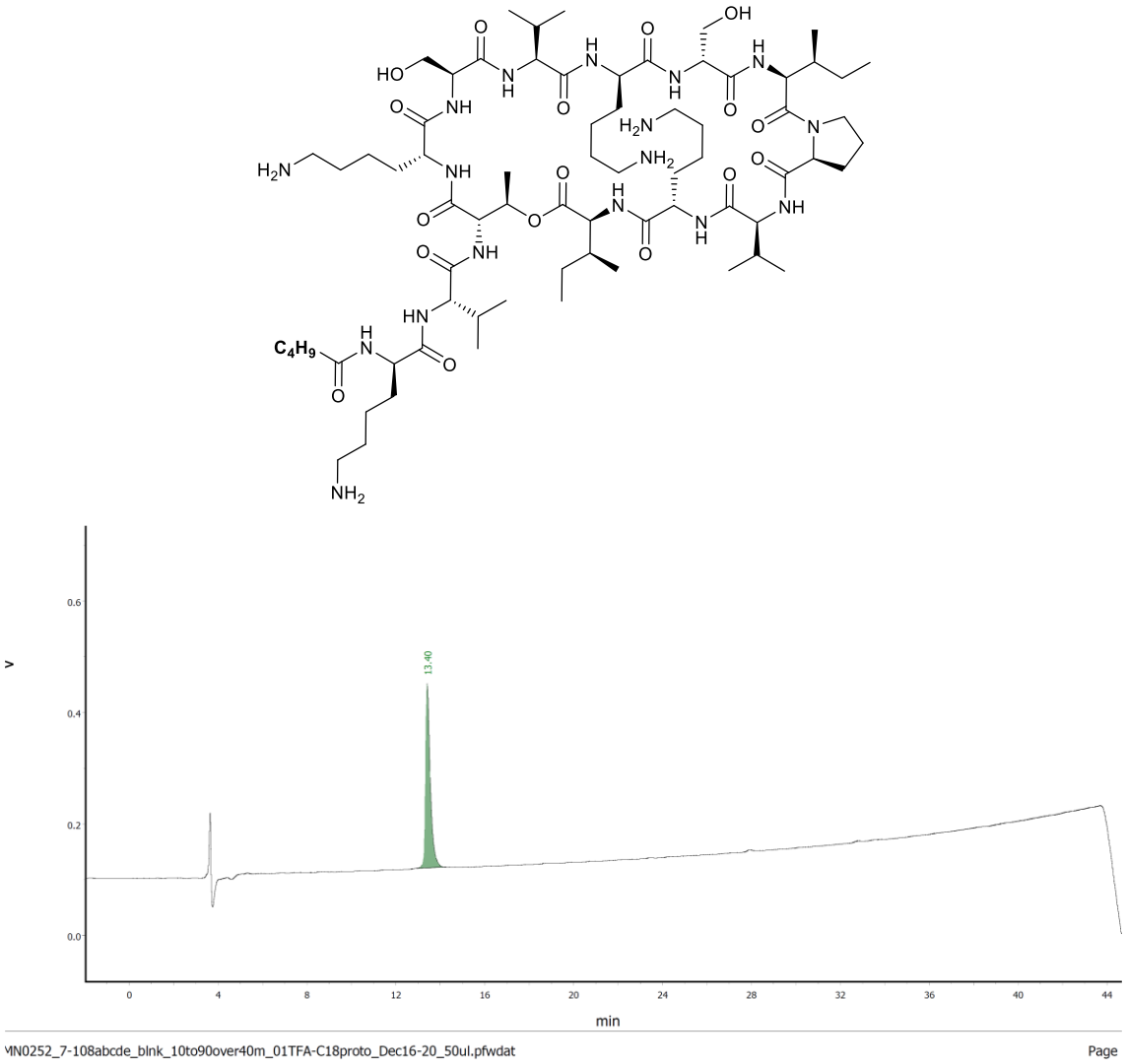

Figure B.5 Analytical RP-HPLC of PA(C5 tail)-D-K1-D-K4 (3.24). Linear gradient of 10:90 to 90:10 MeCN/H2O (0.1% TFA) over 40 min (λ = 220 nm). C18 proto, 5 µm, 250 × 4.6 mm.

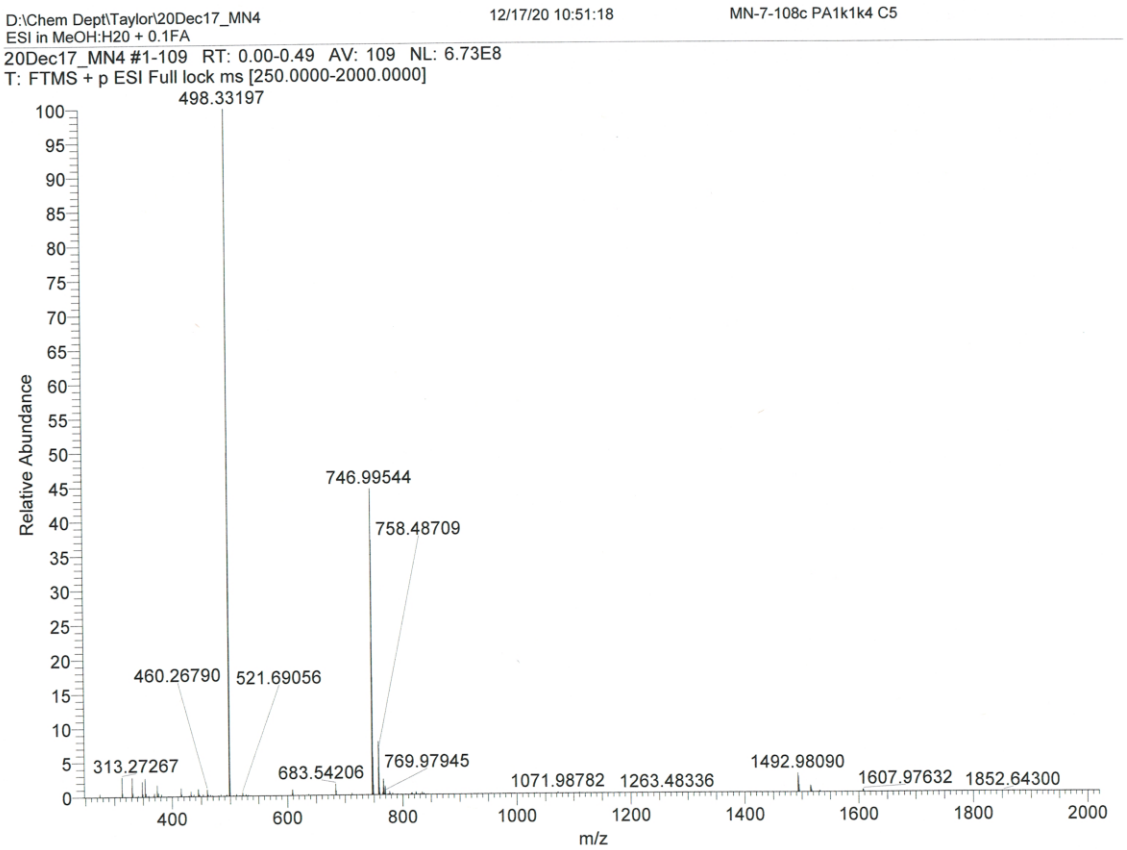

Elemental composition search on mass 1492.98090

m/z= 1487.98090-1497.98090

m/z	Theo. Mass	Delta (ppm)	RDB equiv.	Composition
1492.98090	1492.98251	-1.08	15.5	$C_{71}H_{130}O_{17}N_{17}$
	1492.96994	7.34	16.0	$C_{70}H_{128}O_{17}N_{18}$
	1492.99509	-9.50	15.0	$C_{72}H_{132}O_{17}N_{16}$
	1492.95870	14.87	16.0	$C_{71}H_{128}O_{18}N_{16}$
	1493.00632	-17.03	15.0	$C_{71}H_{132}O_{16}N_{18}$

Figure B.6 HRMS (+ESI) of PA(C5 tail)-D-K1-D-K4 (3.24).

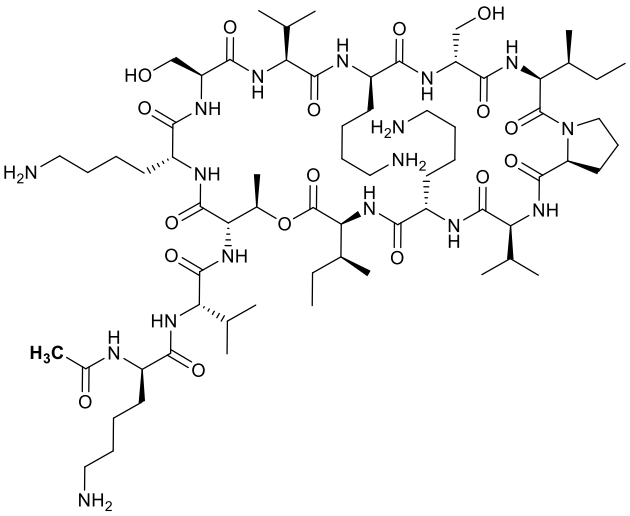

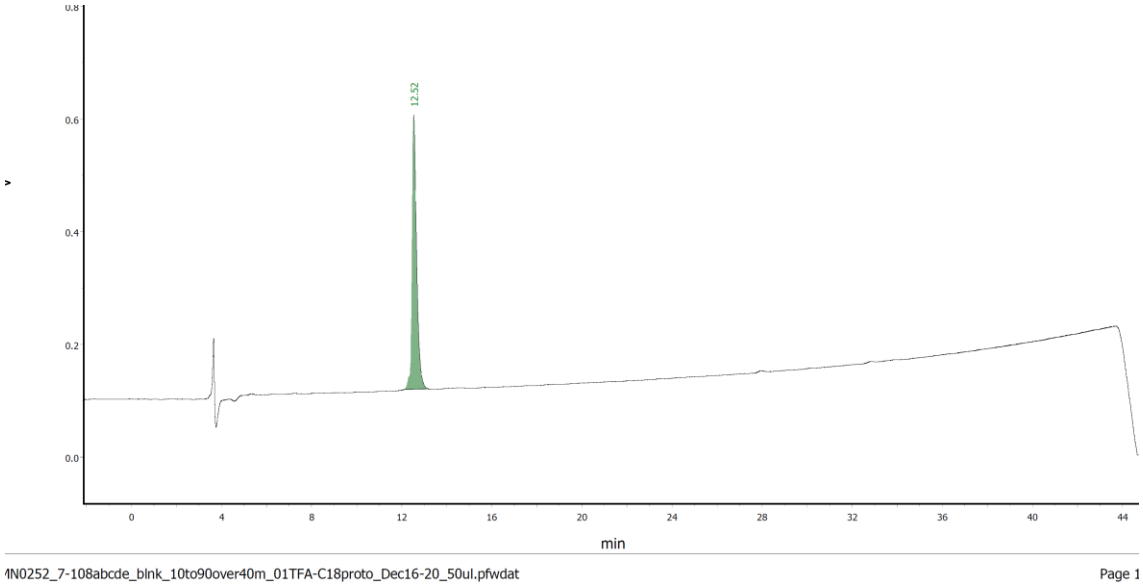

Figure B.7 Analytical RP-HPLC of PA(C2 tail)-D-K1-D-K4 (3.25). Linear gradient of 10:90 to 90:10 MeCN/H2O (0.1% TFA) over 40 min (λ = 220 nm). C18 proto, 5 µm, 250 × 4.6 mm.

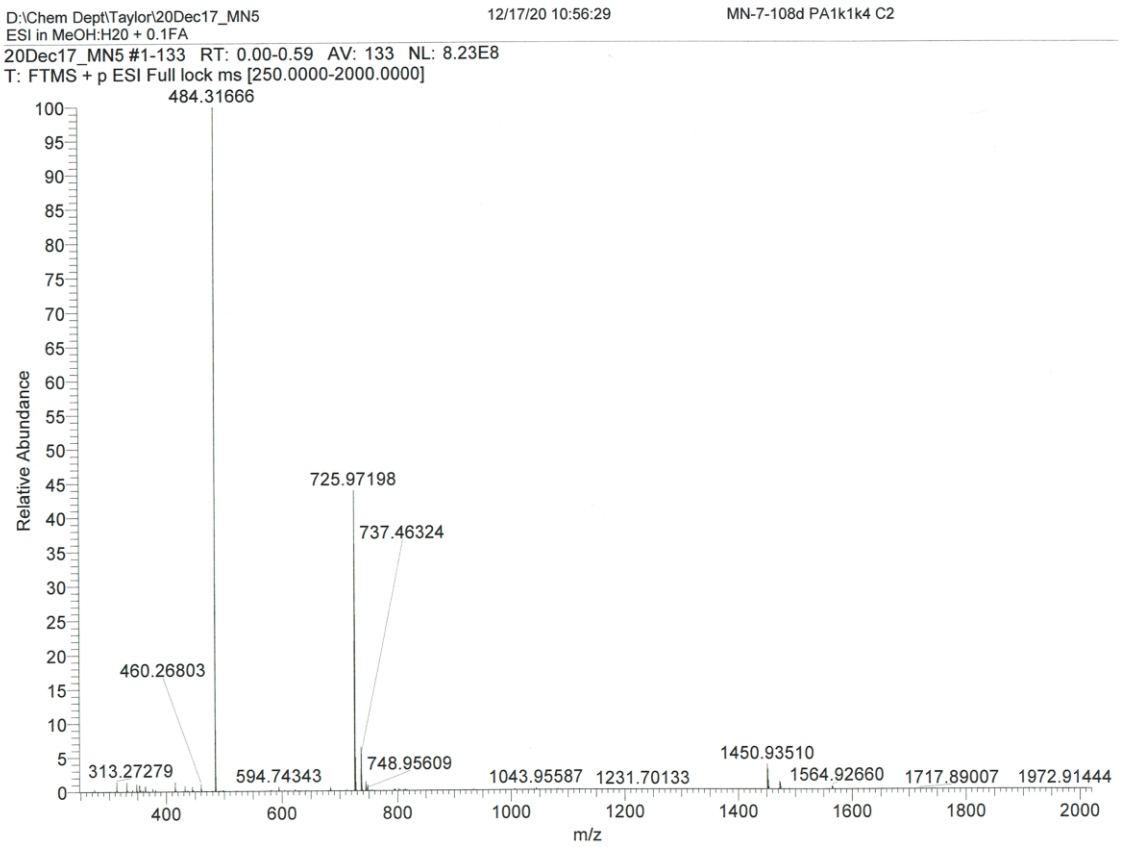

Elemental composition search on mass 1450.93510

m/z= 1445.93510-1455.93510

m/z	Theo. Mass	Delta (ppm)	RDB equiv.	Composition
1450.93510	1450.93556	-0.32	15.5	$C_{68}H_{124}O_{17}N_{17}$
	1450.92299	8.35	16.0	$C_{67}H_{122}O_{17}N_{18}$
	1450.91175	16.09	16.0	$C_{68}H_{122}O_{18}N_{16}$

Figure B.8 HRMS (+ESI) of PA(C2 tail)-D-K1-D-K4 (3.25).

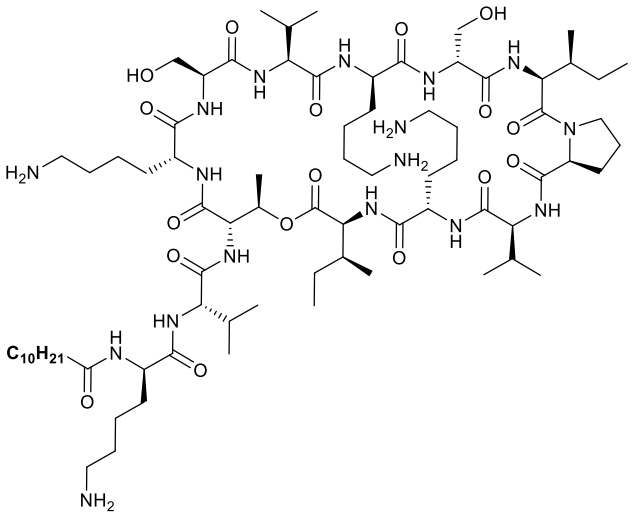

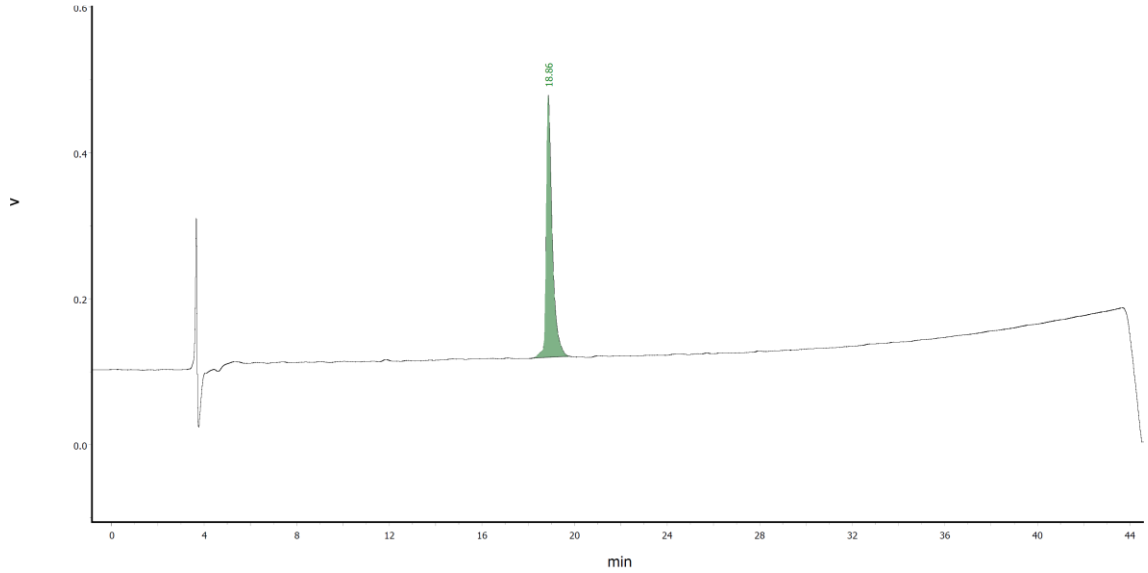

Figure B.9 Analytical RP-HPLC of PA(C11 tail)-D-K1-D-K4 (3.22). Linear gradient of 10:90 to 90:10 MeCN/H2O (0.1% TFA) over 40 min (λ = 220 nm). C18 proto, 5 µm, 250 × 4.6 mm.

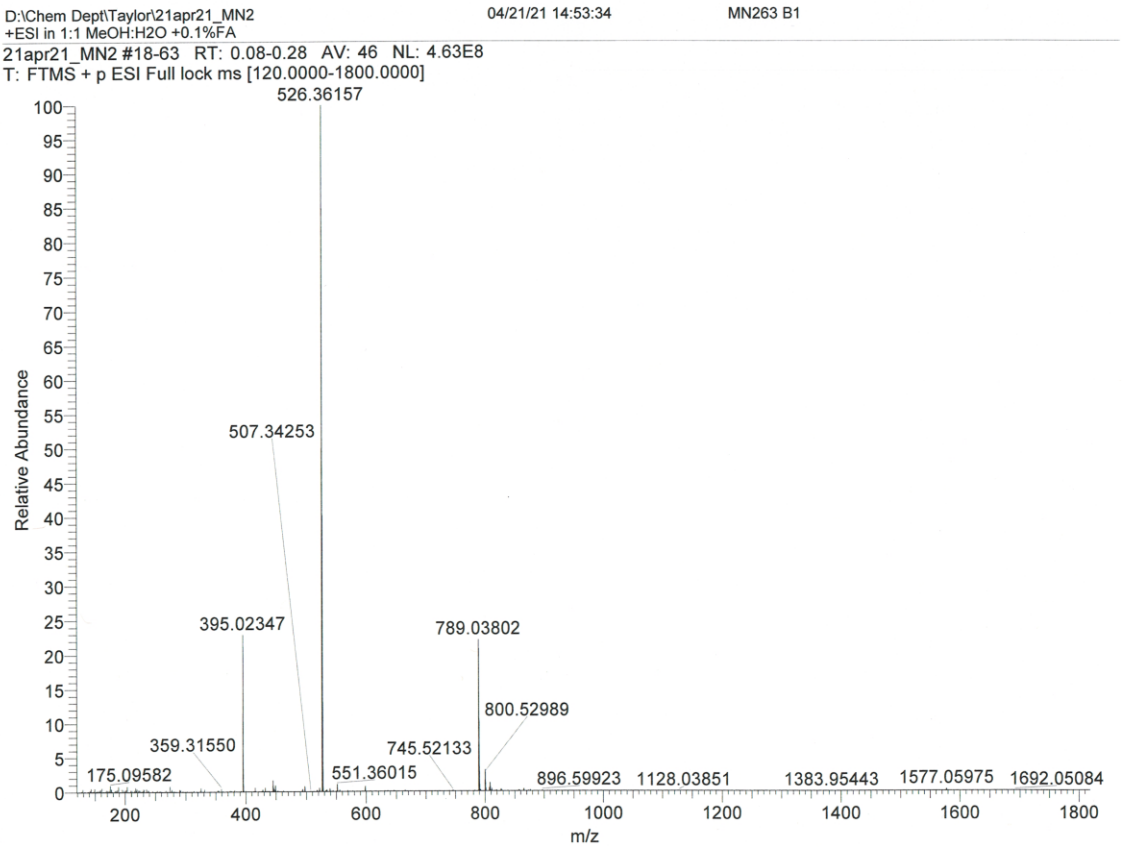

Elemental composition search on mass 526.36157

m/z= 521.36157-531.36157

m/z	Theo. Mass	Delta (ppm)	RDB equiv.	Composition
526.36157	526.36366	-3.96	14.5	$C_{77}H_{144}O_{17}N_{17}$
	526.37578	-27.00	13.5	$C_{78}H_{148}O_{16}N_{17}$

Figure B.10 HRMS (+ESI) of PA(C11 tail)-D-K1-D-K4 (3.22).

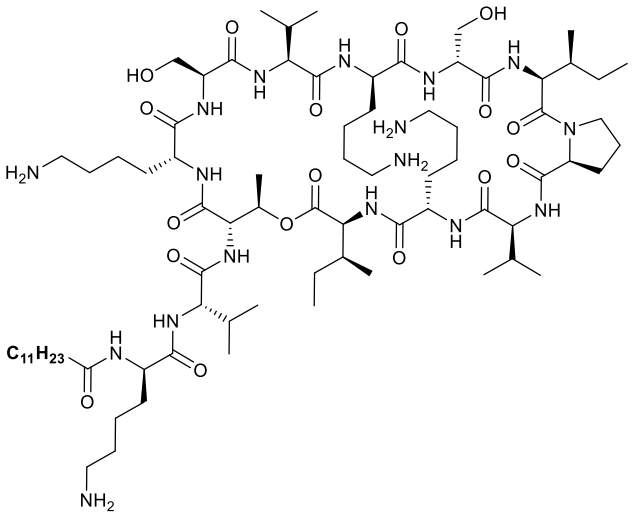

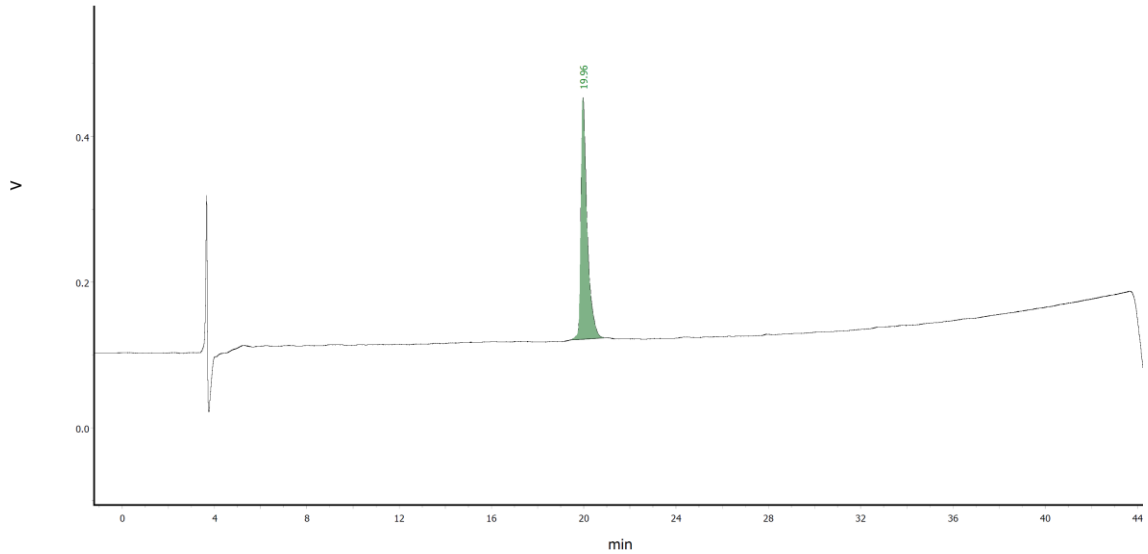

Figure B.11 Analytical RP-HPLC of PA(C12 tail)-D-K1-D-K4 (3.21**).** Linear gradient of 10:90 to 90:10 MeCN/H2O (0.1% TFA) over 40 min (λ = 220 nm). C18 proto, 5 µm, 250 × 4.6 mm.

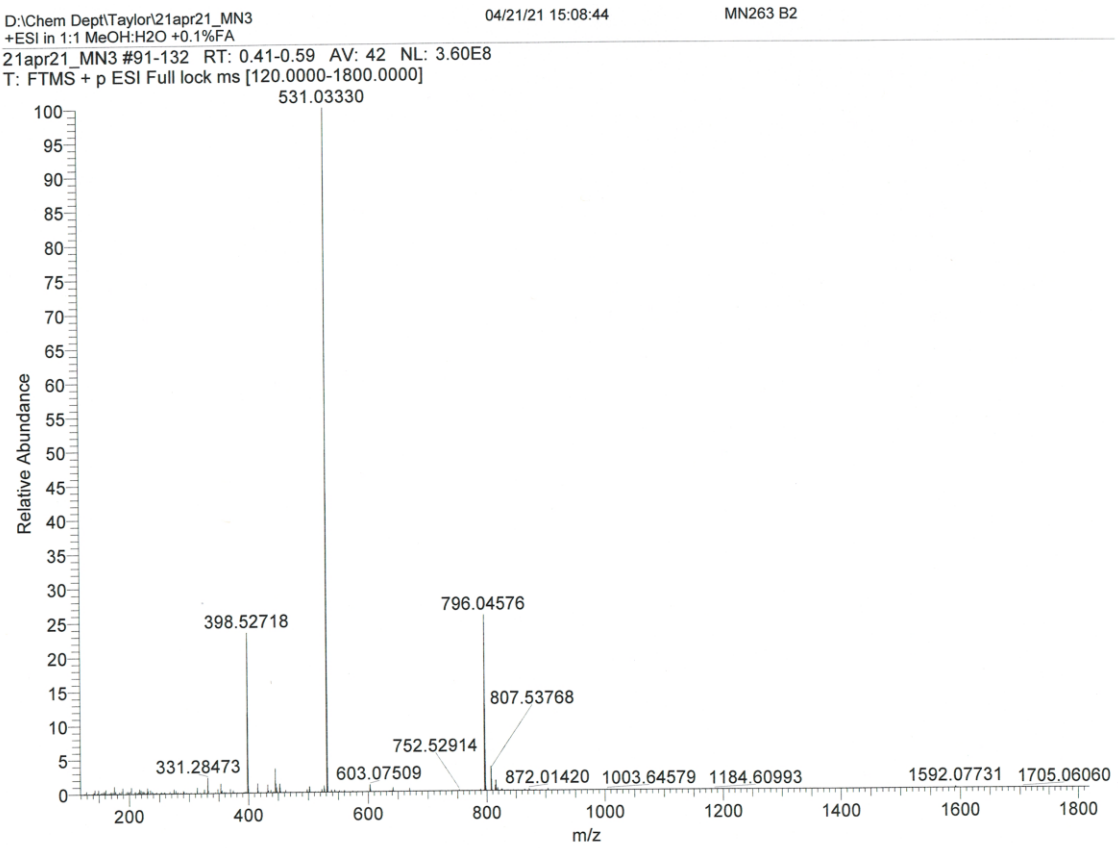

Elemental composition search on mass 531.03330

m/z= 526.03330-536.03330

m/z	Theo. Mass	Delta (ppm)	RDB equiv.	Composition
531.03330	531.03554	-4.22	14.5	$C_{78}H_{146}O_{17}N_{17}$

Figure B.12 HRMS (+ESI) of PA(C12 tail)-D-K1-D-K4 (3.21).

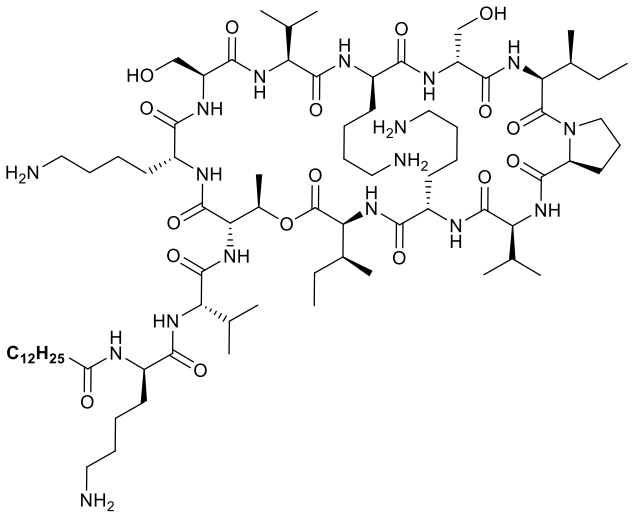

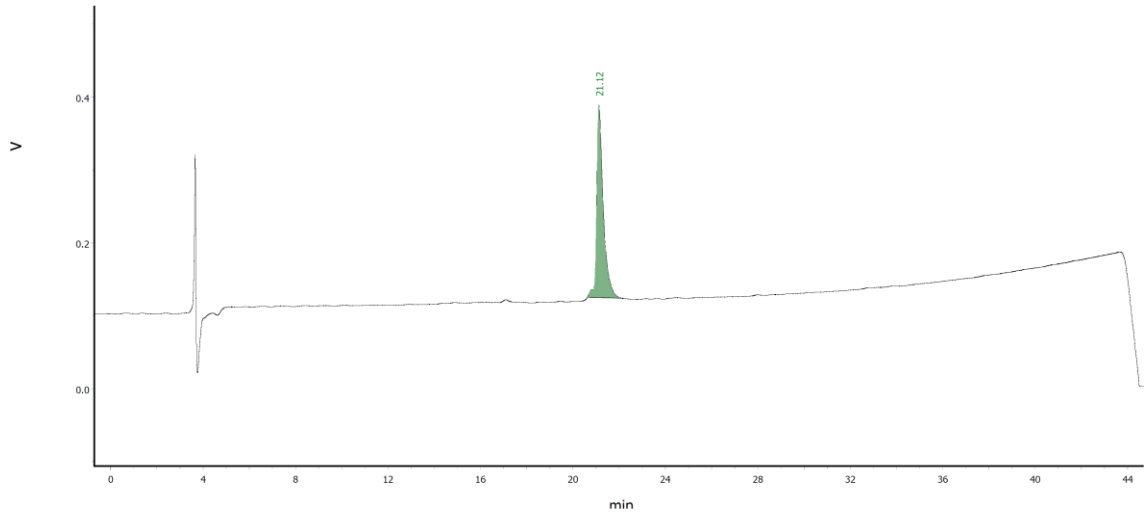

Figure B.13 Analytical RP-HPLC of PA(C13 tail)-D-K1-D-K4 (3.20). Linear gradient of 10:90 to 90:10 MeCN/H2O (0.1% TFA) over 40 min (λ = 220 nm). C18 proto, 5 µm, 250 × 4.6 mm.

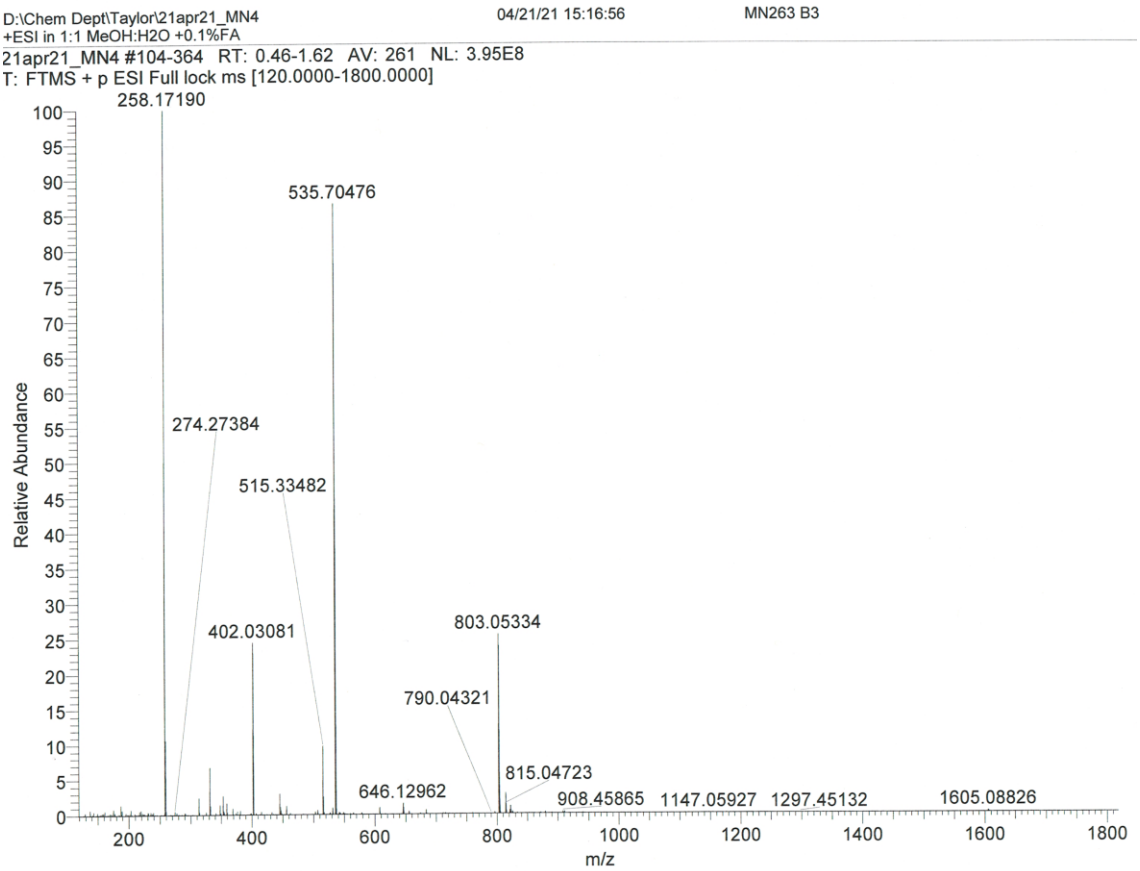

Figure B.14 HRMS (+ESI) of PA(C13 tail)-D-K1-D-K4 (3.20).

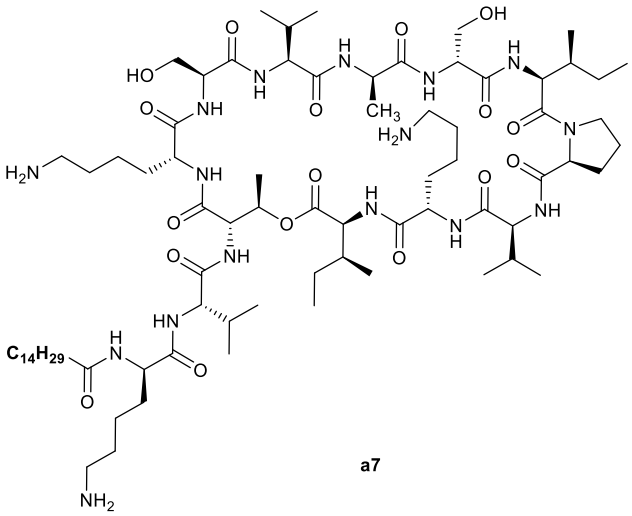

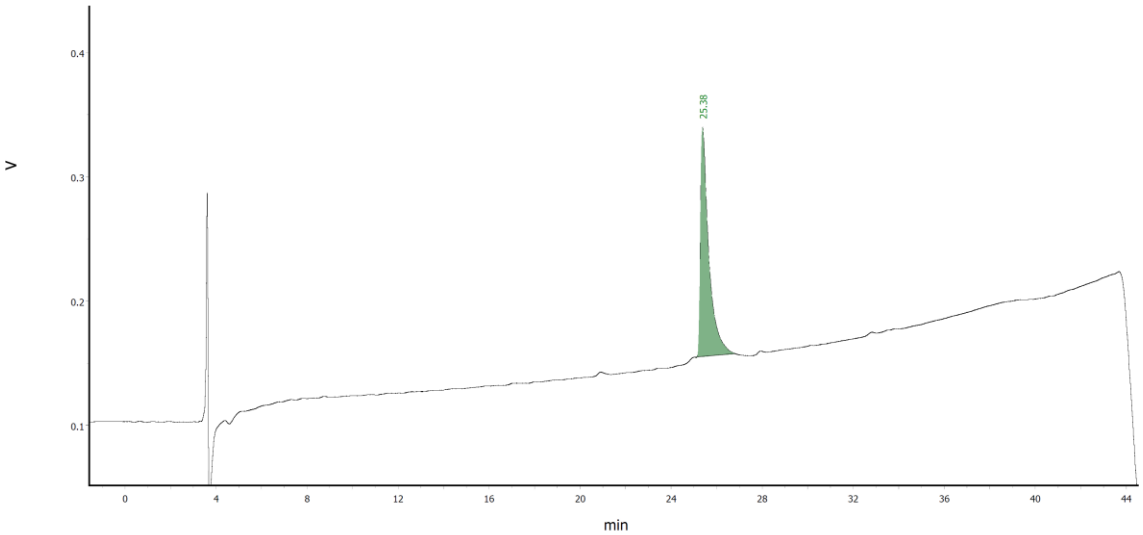

Figure B.15 Analytical RP-HPLC of PA1-D-K1-D-K4-D-A7 (3.27). Linear gradient of 10:90 to 90:10 MeCN/H2O (0.1% TFA) over 40 min (λ = 220 nm). C18 proto, 5 µm, 250 × 4.6 mm.

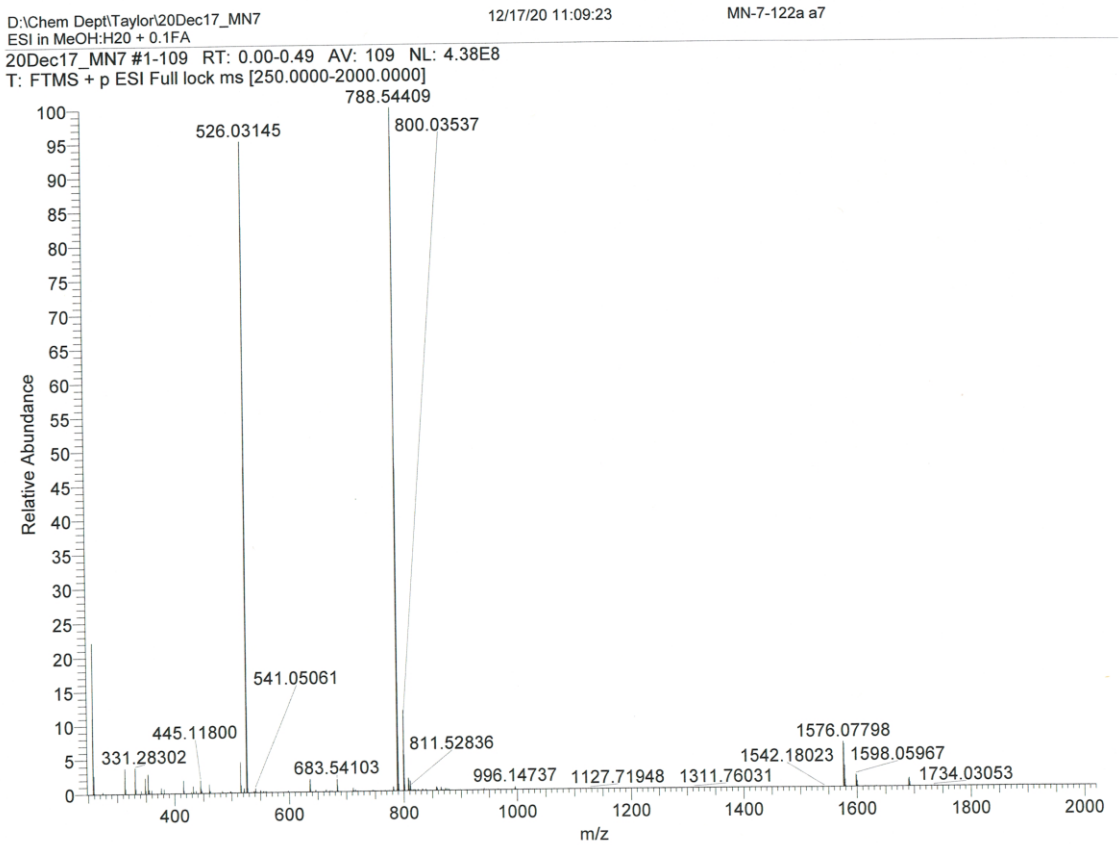

Elemental composition search on mass 1576.07798

m/z= 1571.07798-1581.07798

m/z	Theo. Mass	Delta (ppm)	RDB equiv.	Composition
1576.07798	1576.08116	-2.02	15.5	$C_{78}H_{143}O_{17}N_{16}$
	1576.06859	5.96	16.0	$C_{77}H_{141}O_{17}N_{17}$
	1576.09240	-9.15	15.5	$C_{77}H_{143}O_{16}N_{18}$
	1576.05601	13.94	16.5	$C_{76}H_{139}O_{17}N_{18}$
	1576.10497	-17.13	15.0	$C_{78}H_{145}O_{16}N_{17}$

Figure B.16 HRMS (+ESI) of PA1-D-K1-D-K4-D-A7 (3.27).

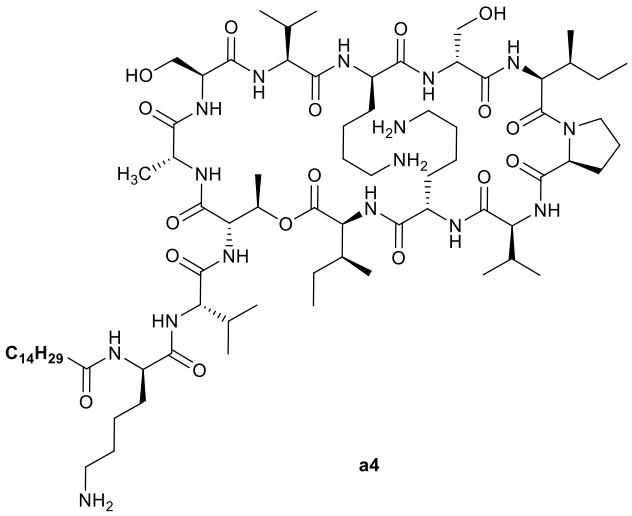

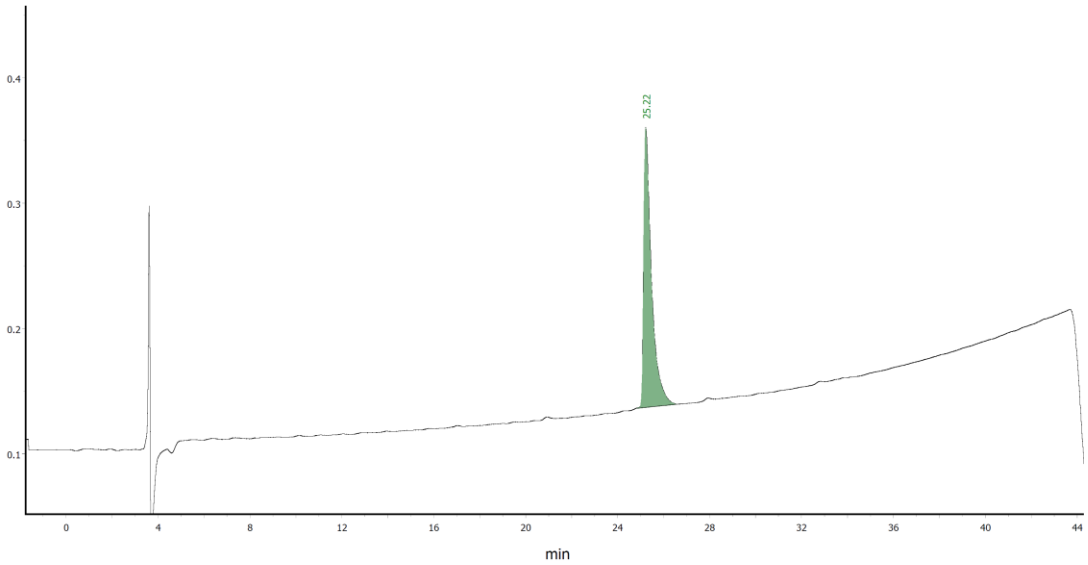

Figure B.17 Analytical RP-HPLC of PA1-D-K1-D-A4 (3.28). Linear gradient of 10:90 to 90:10 MeCN/H2O (0.1% TFA) over 40 min (λ = 220 nm). C18 proto, 5 µm, 250 × 4.6 mm.

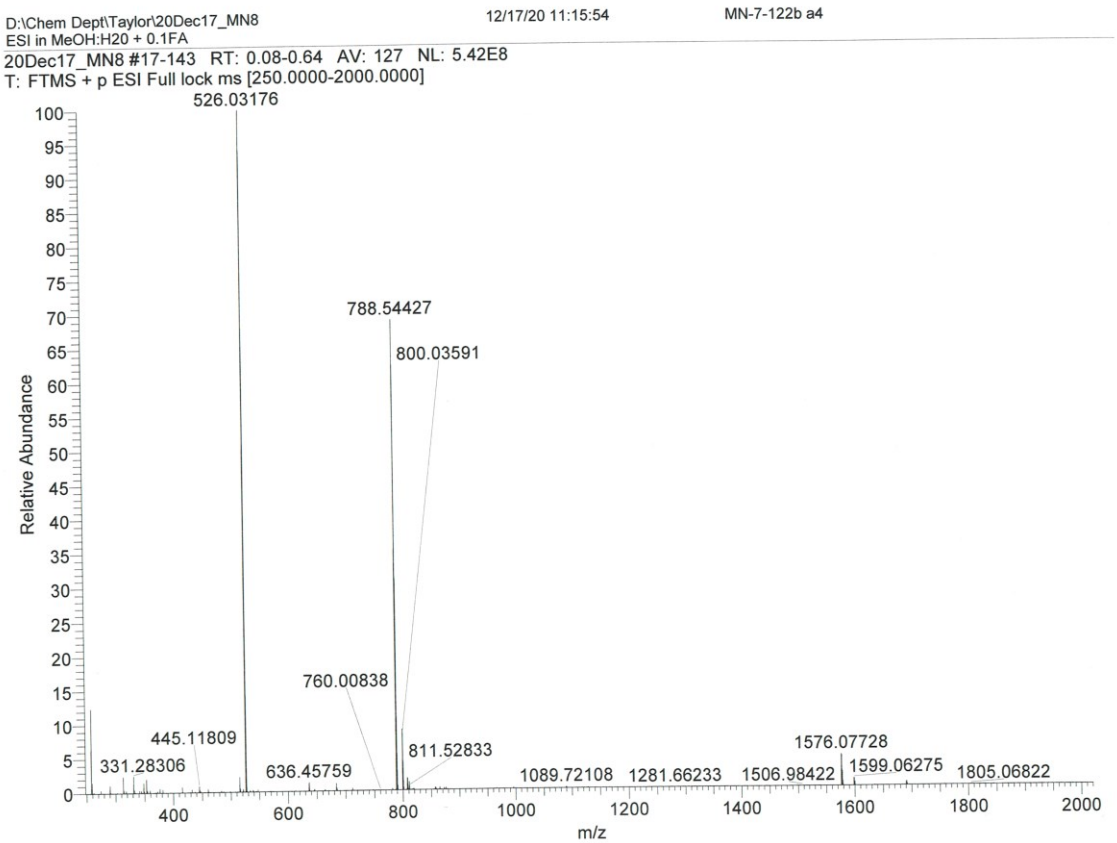

Elemental composition search on mass 1576.07728

m/z= 1571.07728-1581.07728

m/z	Theo. Mass	Delta (ppm)	RDB equiv.	Composition
1576.07728	1576.08116	-2.46	15.5	$C_{78}H_{143}O_{17}N_{16}$
	1576.06859	5.52	16.0	$C_{77}H_{141}O_{17}N_{17}$
	1576.09240	-9.59	15.5	$C_{77}H_{143}O_{16}N_{18}$
	1576.05601	13.49	16.5	$C_{76}H_{139}O_{17}N_{18}$
	1576.10497	-17.57	15.0	$C_{78}H_{145}O_{16}N_{17}$

Figure B.18 HRMS (+ESI) of PA1-D-K1-D-A4 (3.28).

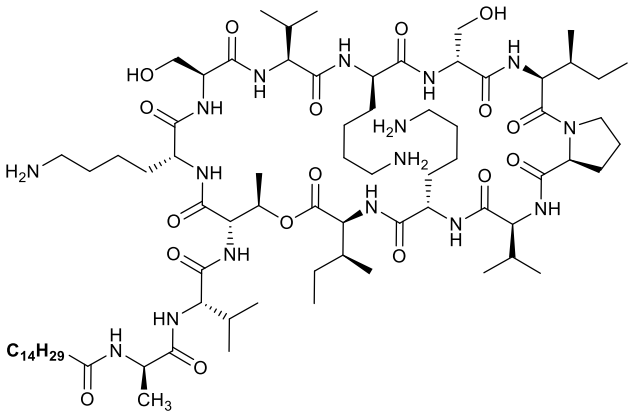

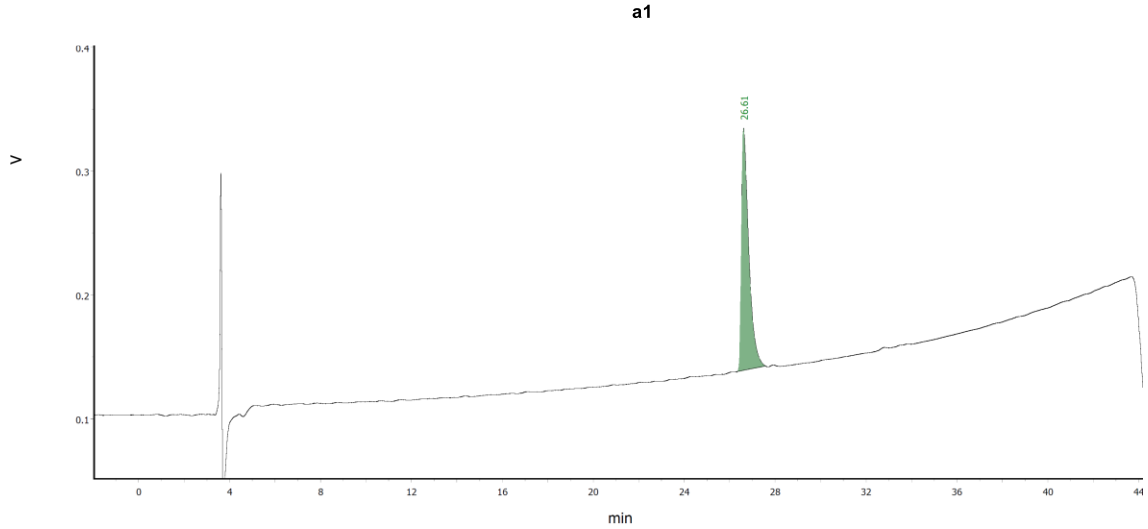

Figure B.19 Analytical RP-HPLC of PA1--D-A1-D-K4 (3.29). Linear gradient of 10:90 to 90:10 MeCN/H2O (0.1% TFA) over 40 min (λ = 220 nm). C18 proto, 5 µm, 250 × 4.6 mm.

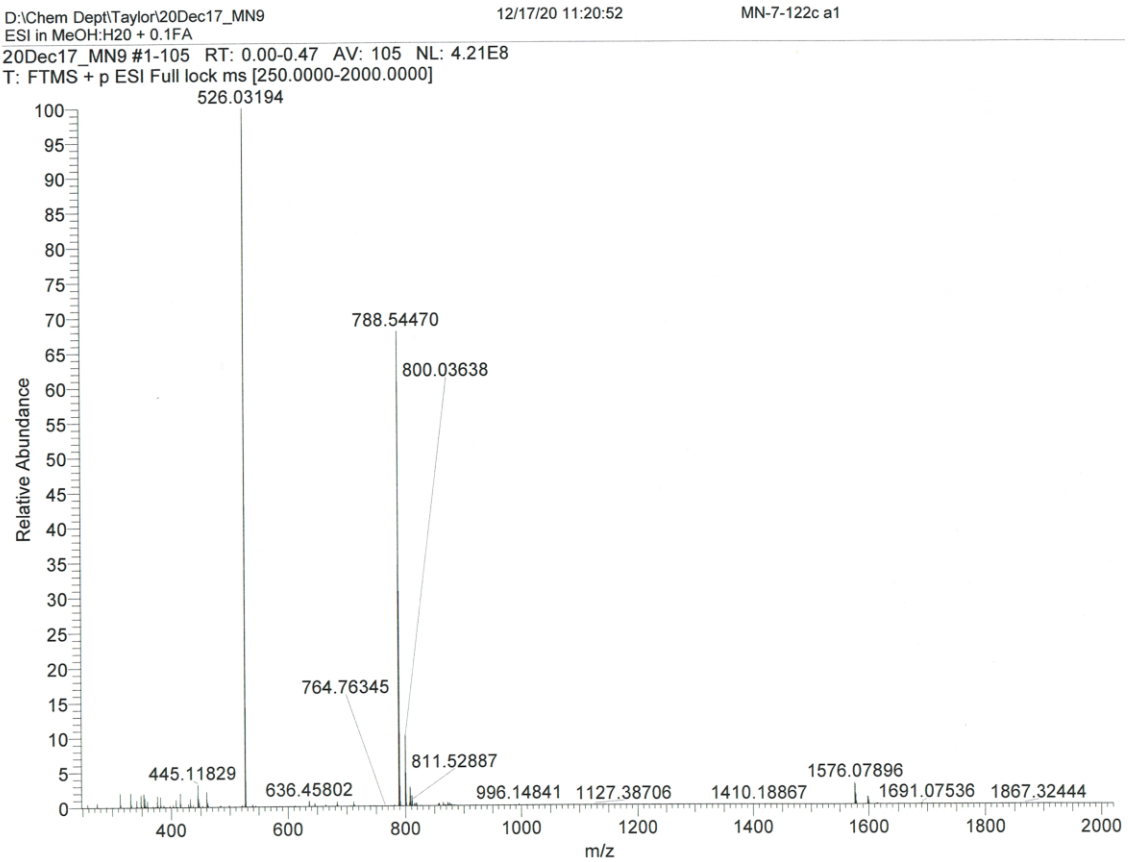

Elemental composition search on mass 1576.07896

m/z= 1571.07896-1581.07896

m/z	Theo. Mass	Delta (ppm)	RDB equiv.	Composition
1576.07896	1576.08116	-1.40	15.5	$C_{78}H_{143}O_{17}N_{16}$
	1576.06859	6.58	16.0	$C_{77}H_{141}O_{17}N_{17}$
	1576.09240	-8.53	15.5	$C_{77}H_{143}O_{16}N_{18}$
	1576.05601	14.56	16.5	$C_{76}H_{139}O_{17}N_{18}$
	1576.10497	-16.50	15.0	$C_{78}H_{145}O_{16}N_{17}$

Figure B.20 HRMS (+ESI) of PA1-D-A1-D-K4 (3.29).

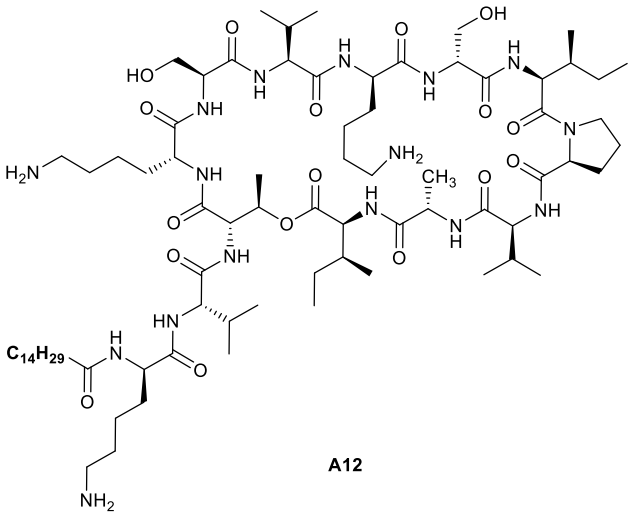

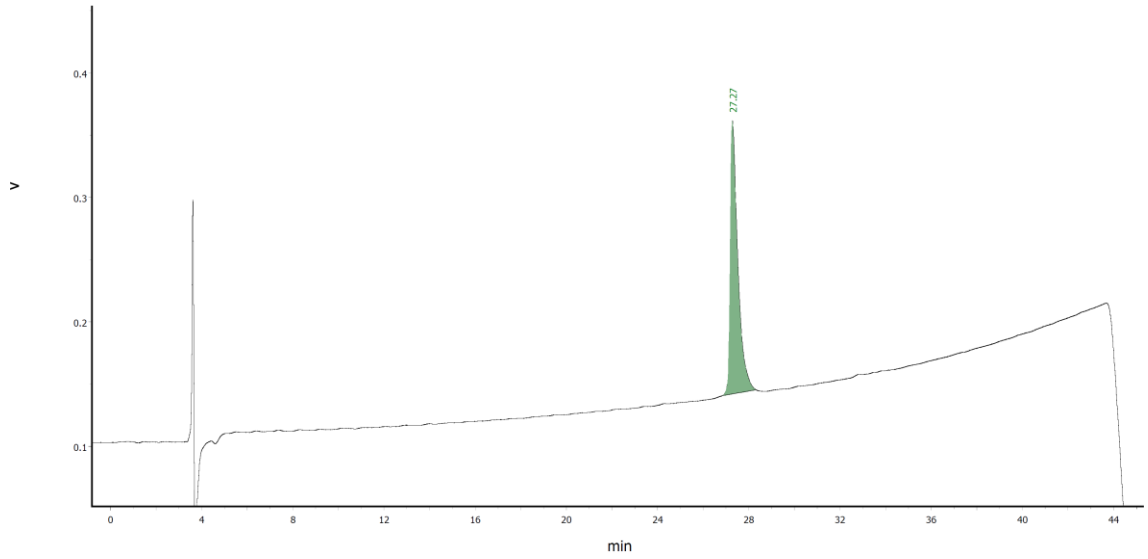

Figure B.21 Analytical RP-HPLC of PA1-D-K1-D-K4-A12 (3.30). Linear gradient of 10:90 to 90:10 MeCN/H2O (0.1% TFA) over 40 min (λ = 220 nm). C18 proto, 5 µm, 250 × 4.6 mm.

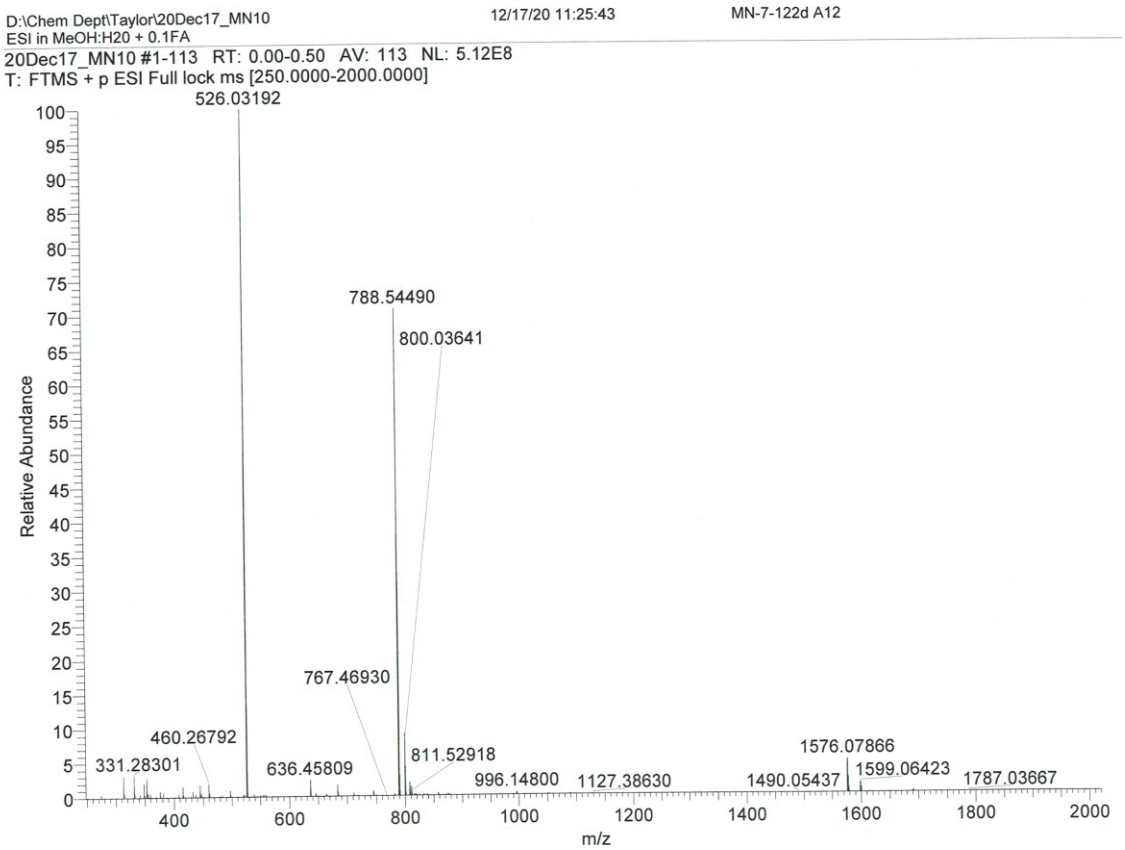

Elemental composition search on mass 1576.07866

m/z= 1571.07866-1581.07866

m/z	Theo. Mass	Delta (ppm)	RDB equiv.	Composition
1576.07866	1576.08116	-1.59	15.5	$C_{78}H_{143}O_{17}N_{16}$
	1576.06859	6.39	16.0	$C_{77}H_{141}O_{17}N_{17}$
	1576.09240	-8.72	15.5	$C_{77}H_{143}O_{16}N_{18}$
	1576.05601	14.37	16.5	$C_{76}H_{139}O_{17}N_{18}$
	1576.10497	-16.69	15.0	$C_{78}H_{145}O_{16}N_{17}$

Figure B.22 HRMS (+ESI) of PA1-D-K1-D-K4-A12 (3.30).

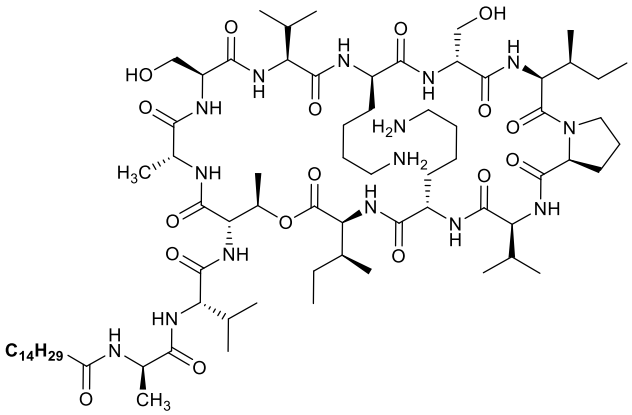

a1a4

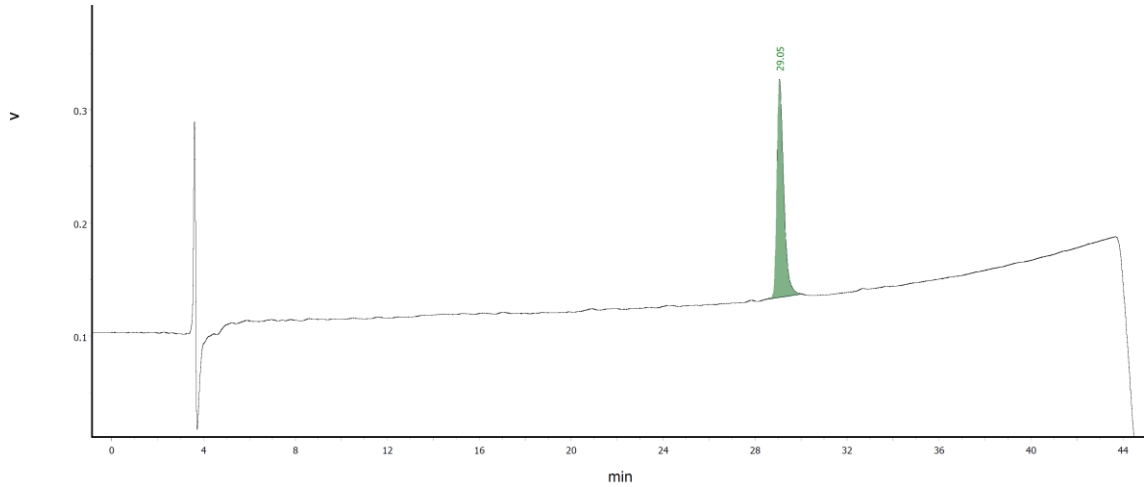

Figure B.23 Analytical RP-HPLC of PA1-D-A1-D-A4 (3.31). Linear gradient of 10:90 to 90:10 MeCN/H2O (0.1% TFA) over 40 min (λ = 220 nm). C18 proto, 5 µm, 250 × 4.6 mm.

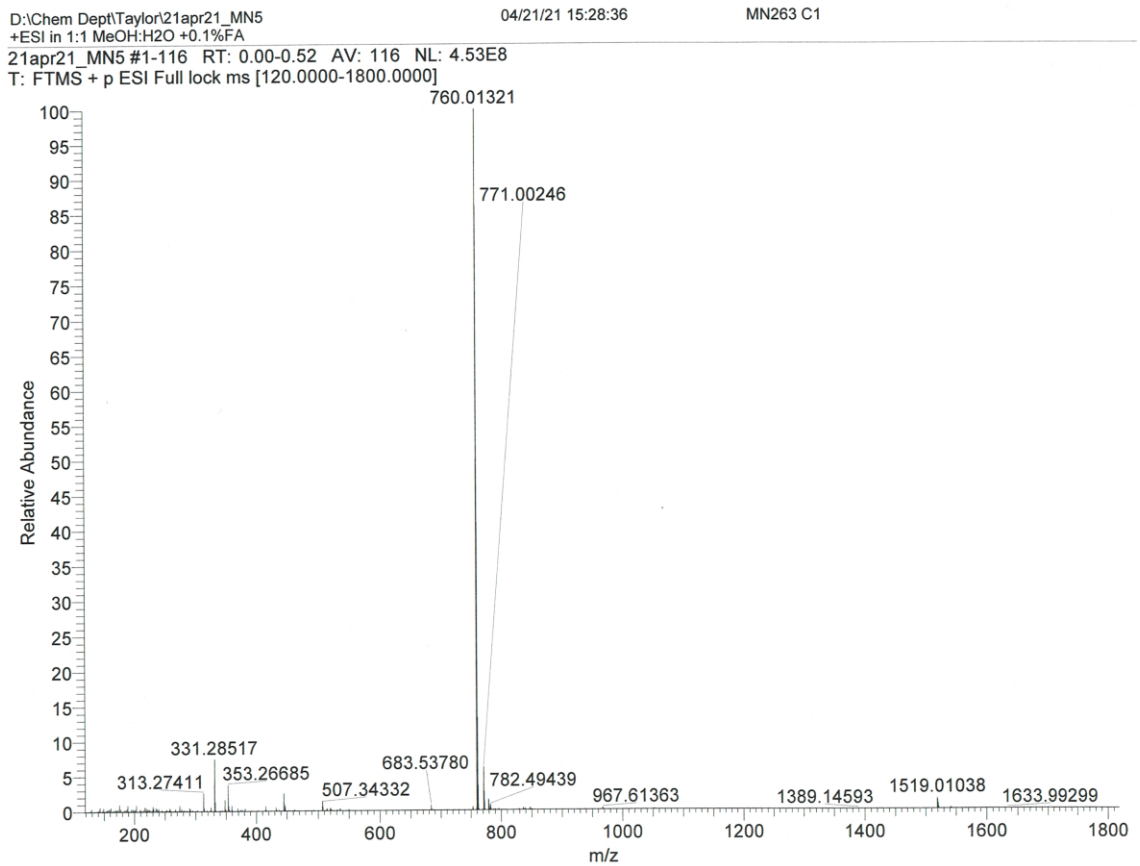

Elemental composition search on mass 760.01321

m/z= 755.01321-765.01321

m/z	Theo. Mass	Delta (ppm)	RDB equiv.	Composition
760.01321	760.01530	-2.74	15.0	$C_{75}H_{137}O_{17}N_{15}$
	760.02091	-10.13	15.0	$C_{74}H_{137}O_{16}N_{17}$
	760.02720	-18.41	14.5	$C_{75}H_{139}O_{16}N_{16}$

Figure B.24 HRMS (+ESI) of PA1-D-A1-D-A4 (3.31).

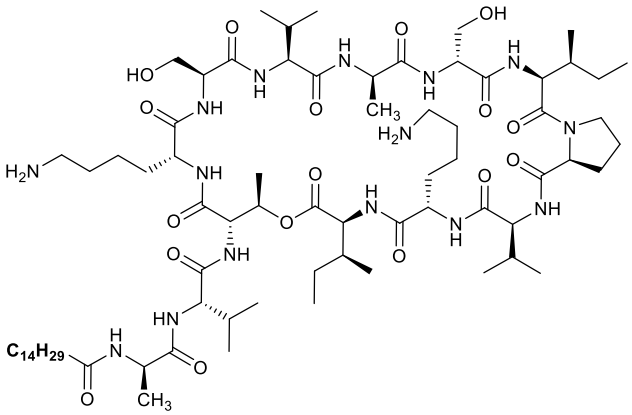

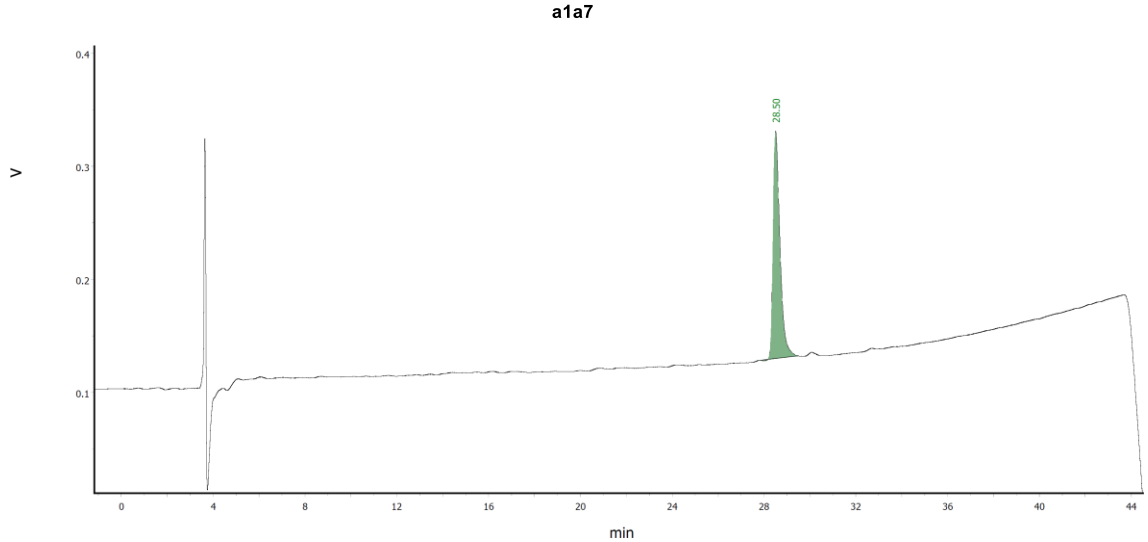

Figure B.25 Analytical RP-HPLC of PA1-D-A1-D-K4-D-A7 (3.32). Linear gradient of 10:90 to 90:10 MeCN/H2O (0.1% TFA) over 40 min (λ = 220 nm). C18 proto, 5 µm, 250 × 4.6 mm.

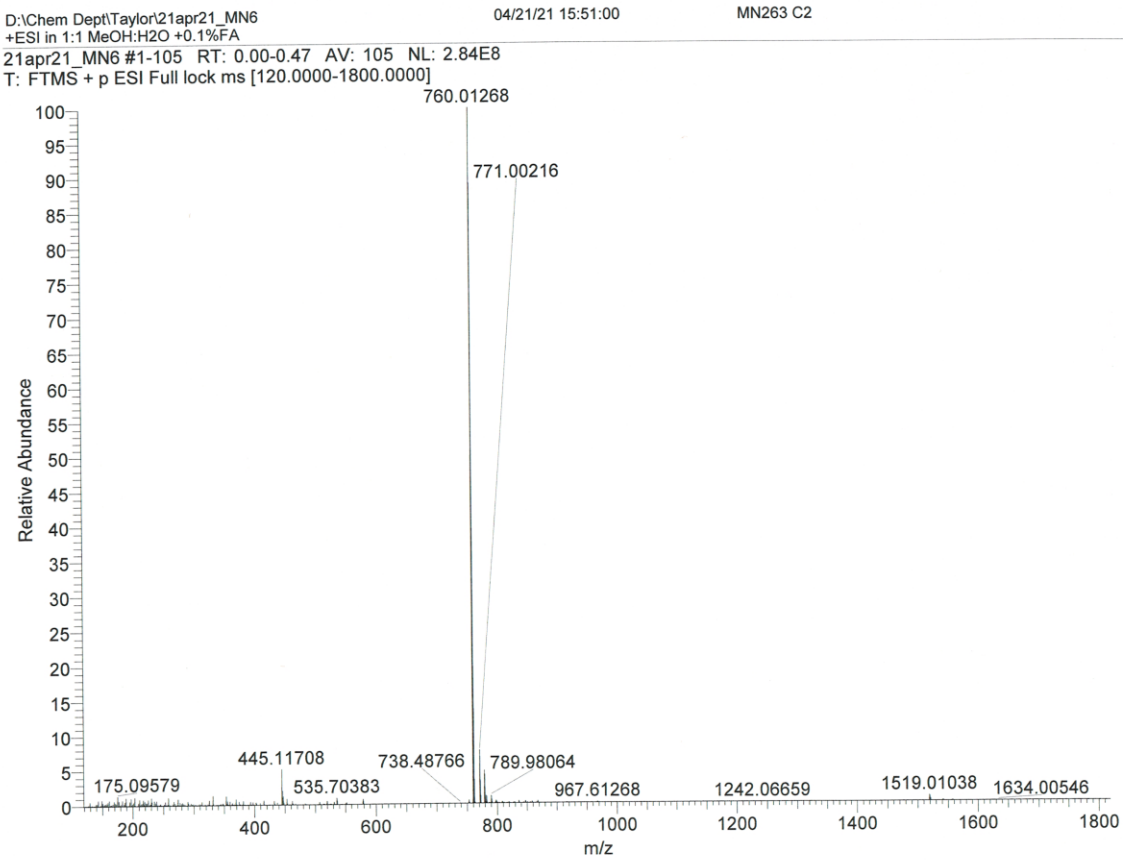

Elemental composition search on mass 760.01268

m/z= 755.01268-765.01268

m/z	Theo. Mass	Delta (ppm)	RDB equiv.	Composition
760.01268	760.01530	-3.44	15.0	$C_{75}H_{137}O_{17}N_{15}$

Figure B.26 HRMS (+ESI) of PA1-D-A1-D-K4-D-A7 (3.32).

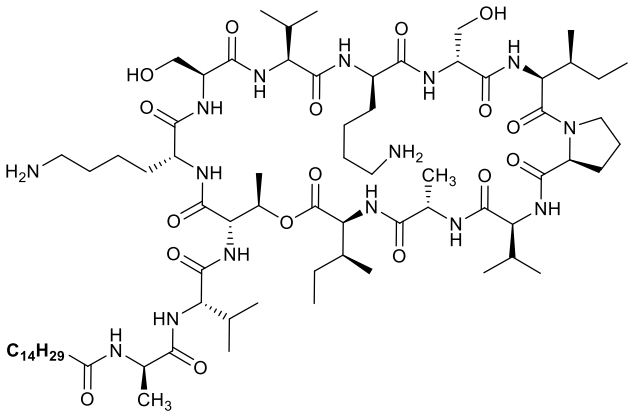

a1A12

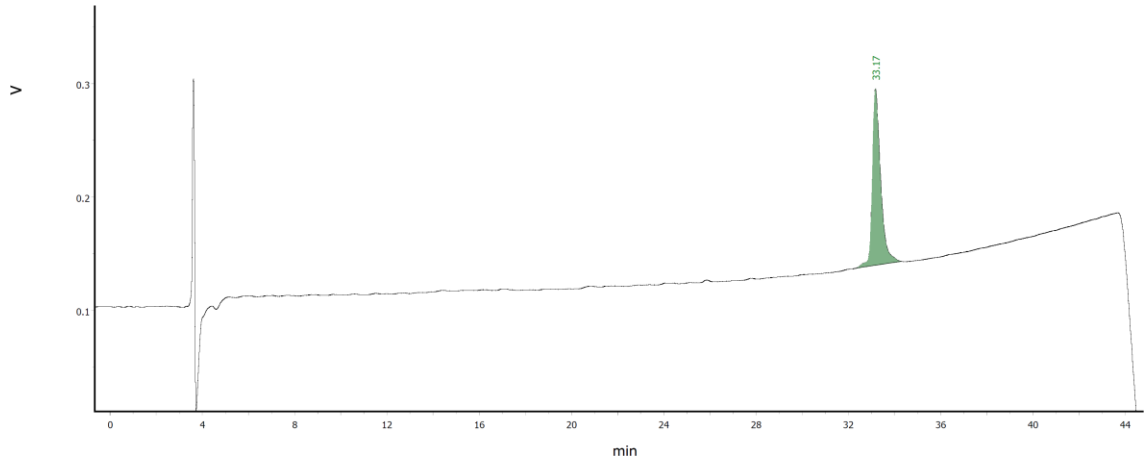

Figure B.27 Analytical RP-HPLC of PA1-D-A1-D-K4-A12 (3.33). Linear gradient of 10:90 to 90:10 MeCN/H2O (0.1% TFA) over 40 min (λ = 220 nm). C18 proto, 5 µm, 250 × 4.6 mm.

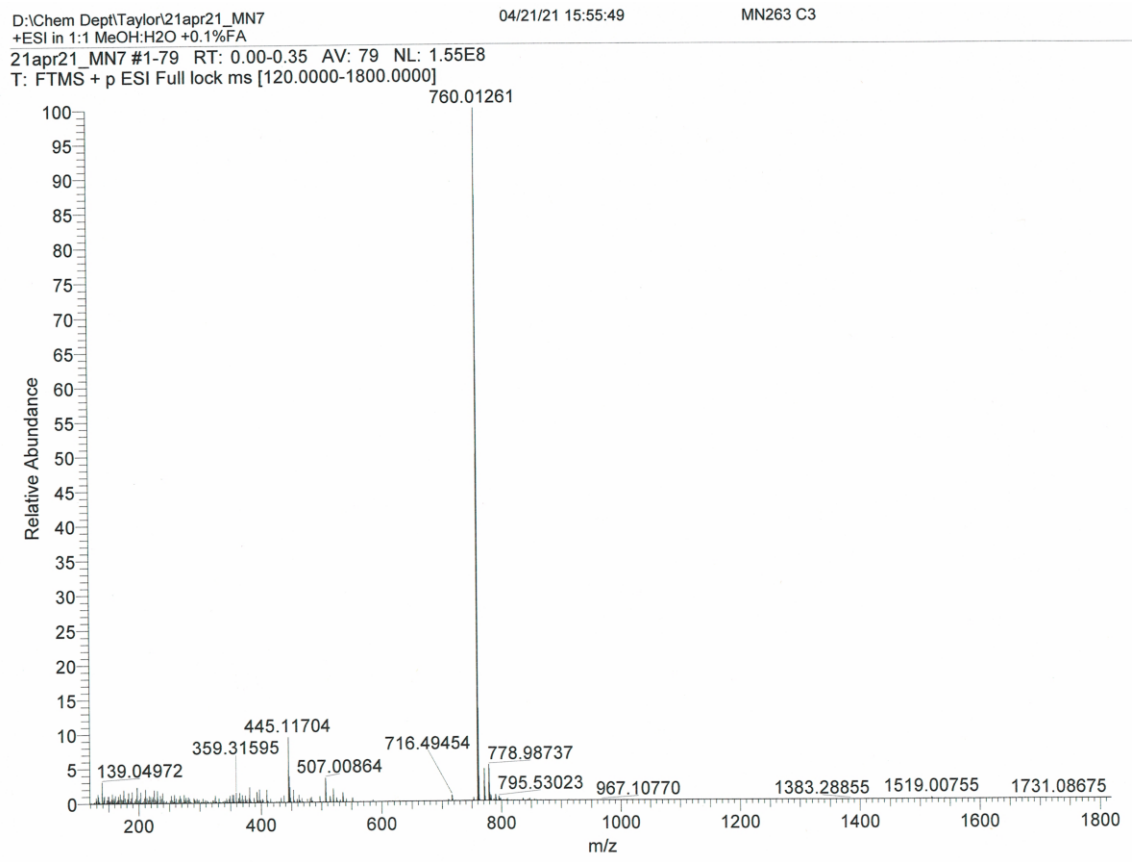

Elemental composition search on mass 760.01261

m/z= 755.01261-765.01261

m/z	Theo. Mass	Delta (ppm)	RDB equiv.	Composition
760.01261	760.01530	-3.53	15.0	$C_{75}H_{137}O_{17}N_{15}$

Figure B.28 HRMS (+ESI) of PA1-D-A1-D-K4-A12 (3.33).

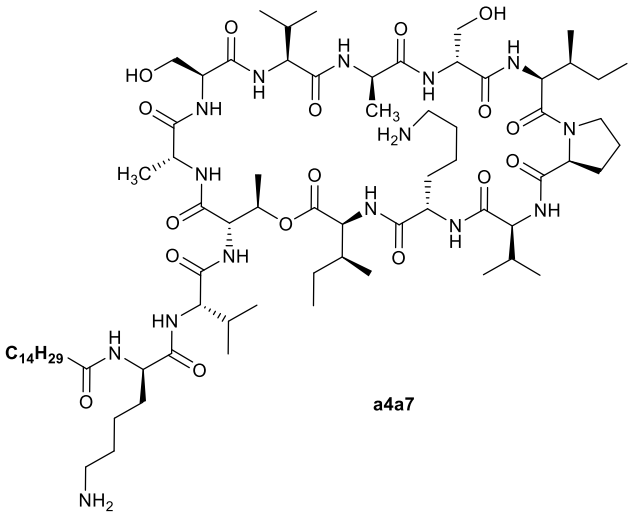

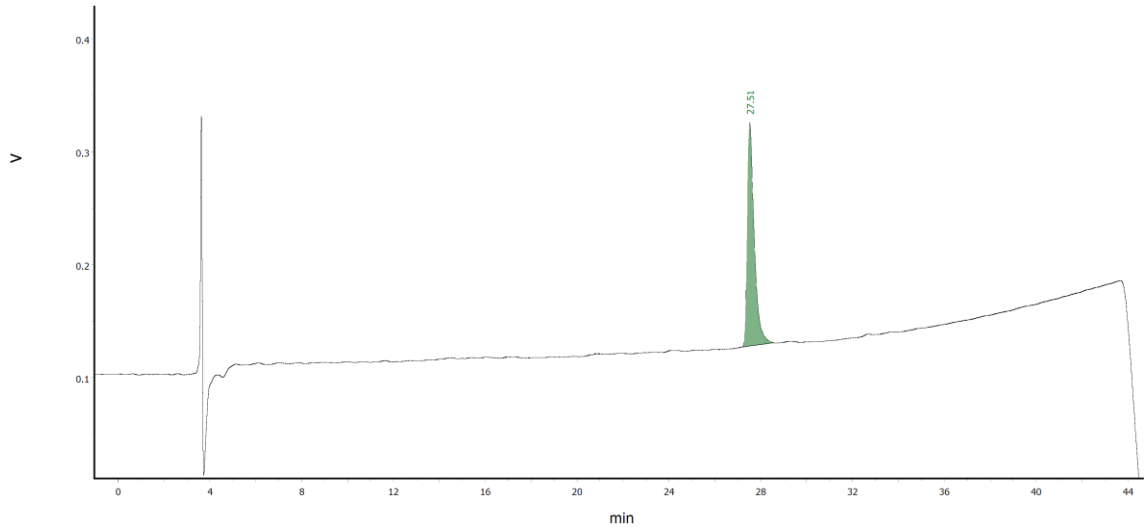

Figure B.29 Analytical RP-HPLC of PA1-D-K1-D-A4-D-A7 (3.34). Linear gradient of 10:90 to 90:10 MeCN/H2O (0.1% TFA) over 40 min (λ = 220 nm). C18 proto, 5 µm, 250 × 4.6 mm.

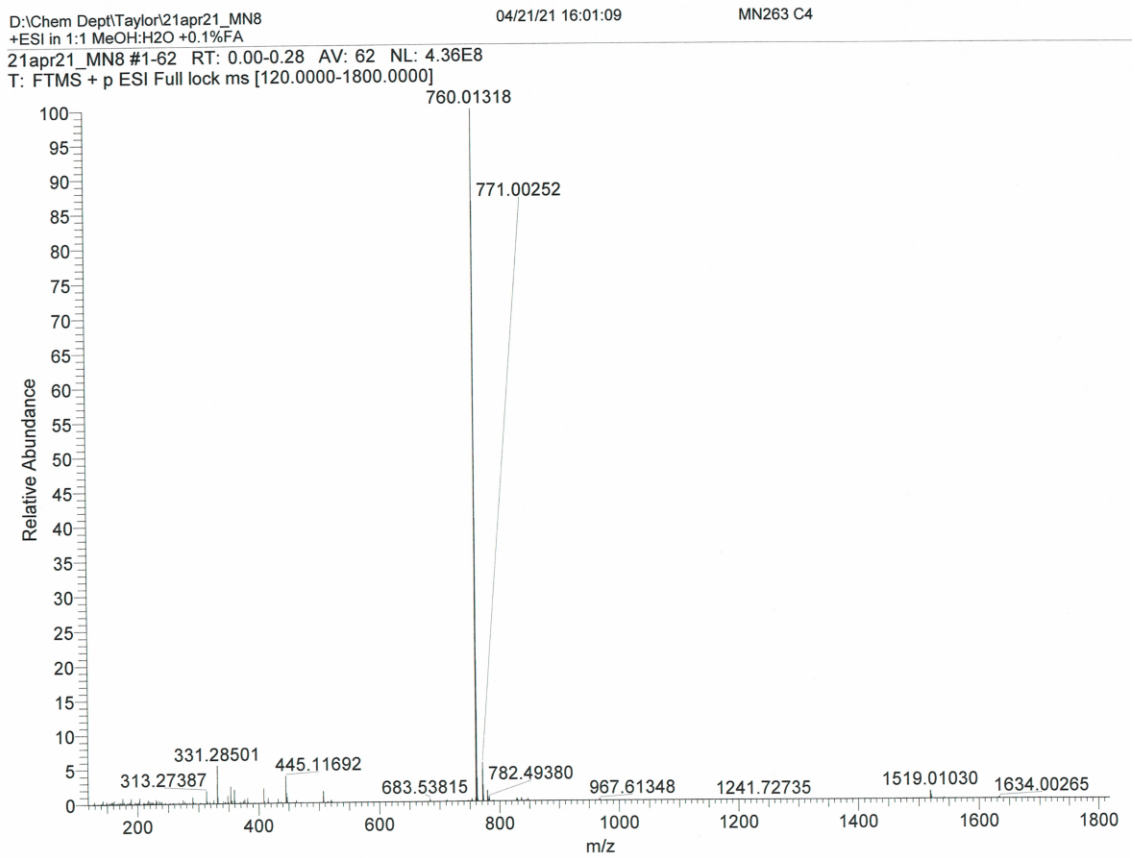

Elemental composition search on mass 760.01318

m/z= 755.01318-765.01318

m/z	Theo. Mass	Delta (ppm)	RDB equiv.	Composition
760.01318	760.01530	-2.78	15.0	$C_{75}H_{137}O_{17}N_{15}$

Figure B.30 HRMS (+ESI) of PA1-D-K1-D-A4-D-A7 (3.34).

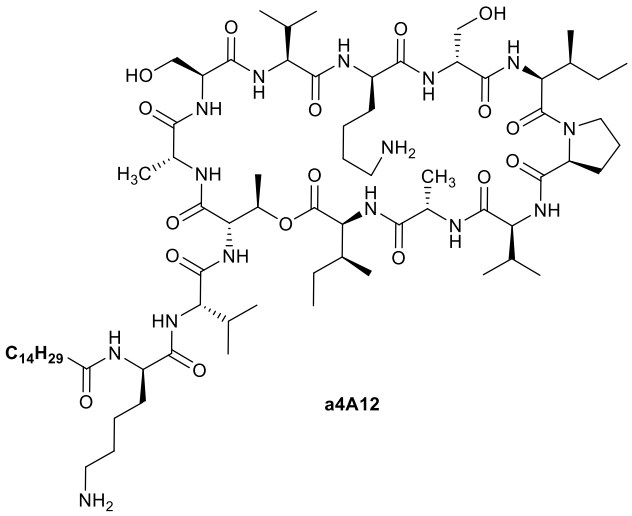

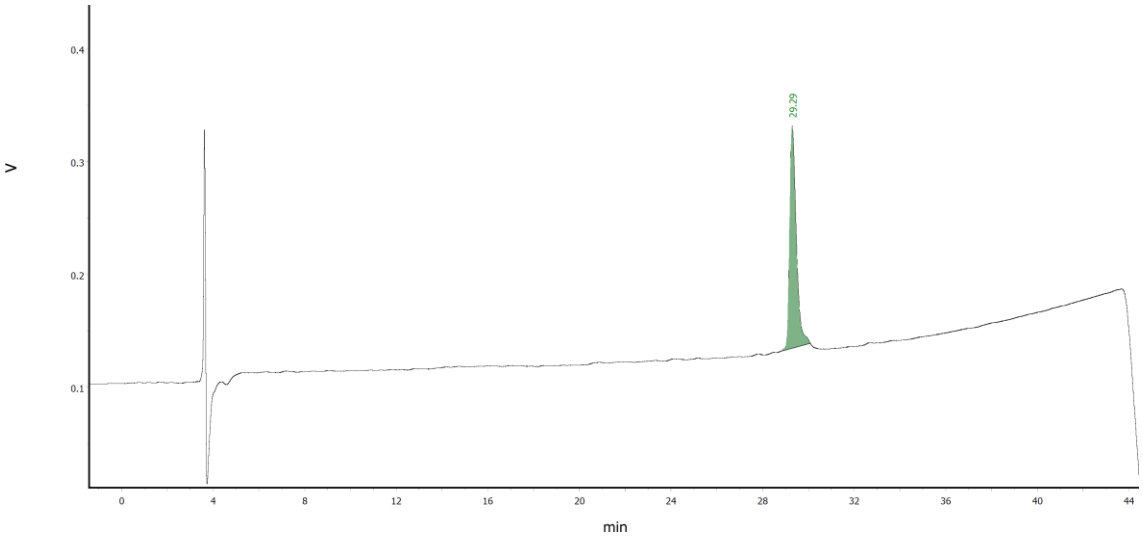

Figure B.31 Analytical RP-HPLC of PA1-D-K1-D-A4-A12 (3.35). Linear gradient of 10:90 to 90:10 MeCN/H2O (0.1% TFA) over 40 min (λ = 220 nm). C18 proto, 5 µm, 250 × 4.6 mm.

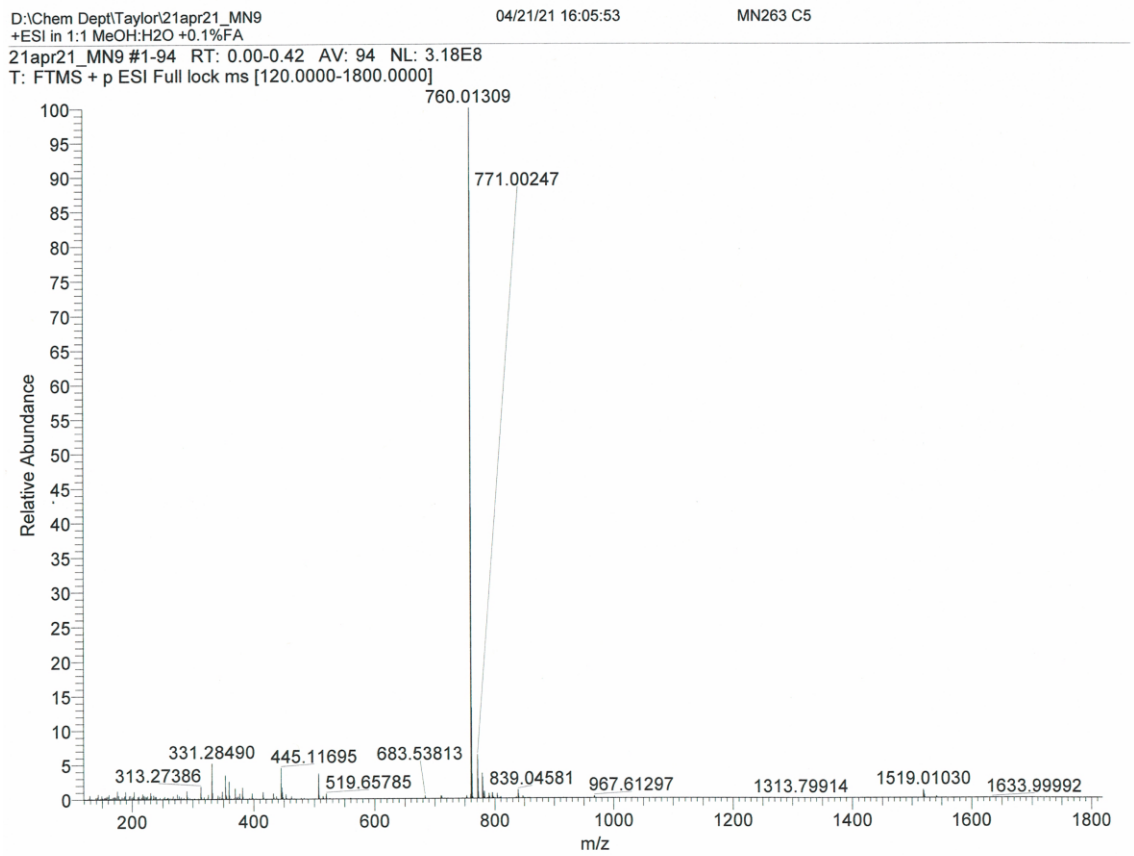

Elemental composition search on mass 760.01309

m/z= 755.01309-765.01309

m/z	Theo. Mass	Delta (ppm)	RDB equiv.	Composition
760.01309	760.01530	-2.90	15.0	$C_{75}H_{137}O_{17}N_{15}$

Figure B.32 HRMS (+ESI) of PA1-D-K1-D-A4-A12 (3.35).

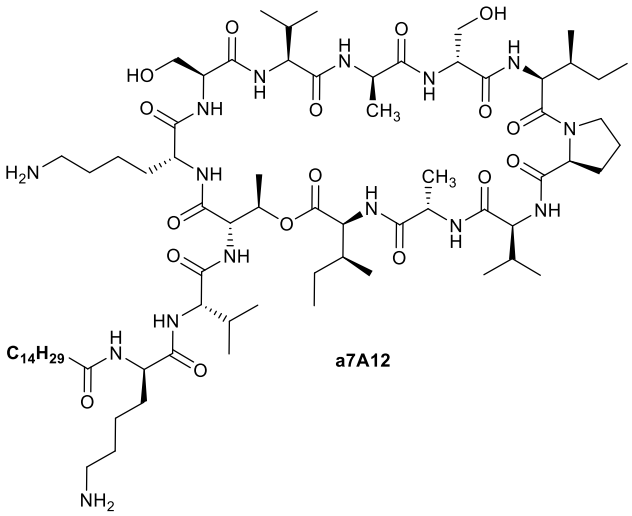

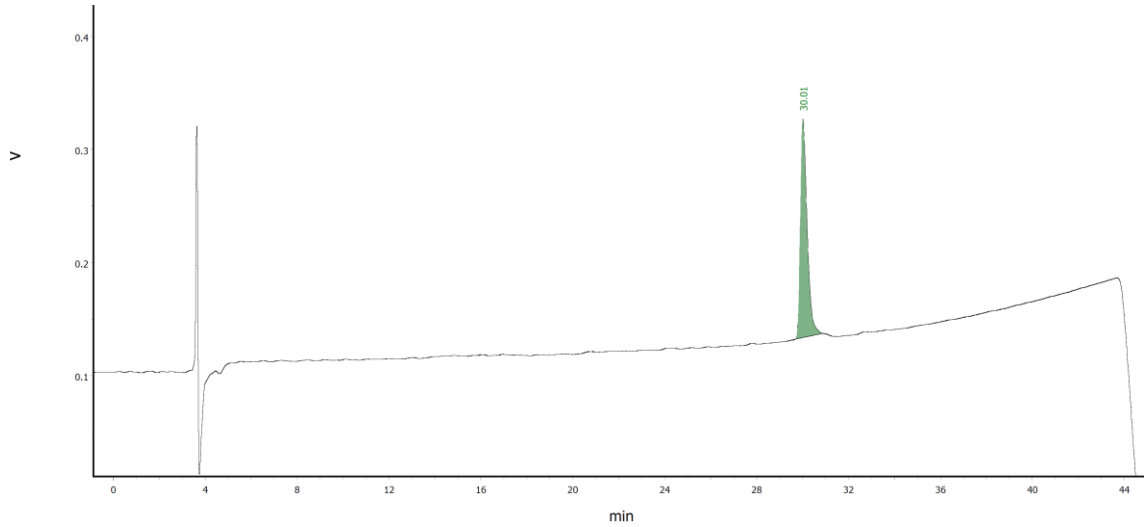

Figure B.33 Analytical RP-HPLC of PA1-D-K1-D-K4-D-A7-A12 (3.36). Linear gradient of 10:90 to 90:10 MeCN/H2O (0.1% TFA) over 40 min (λ = 220 nm). C18 proto, 5 µm, 250 × 4.6 mm.

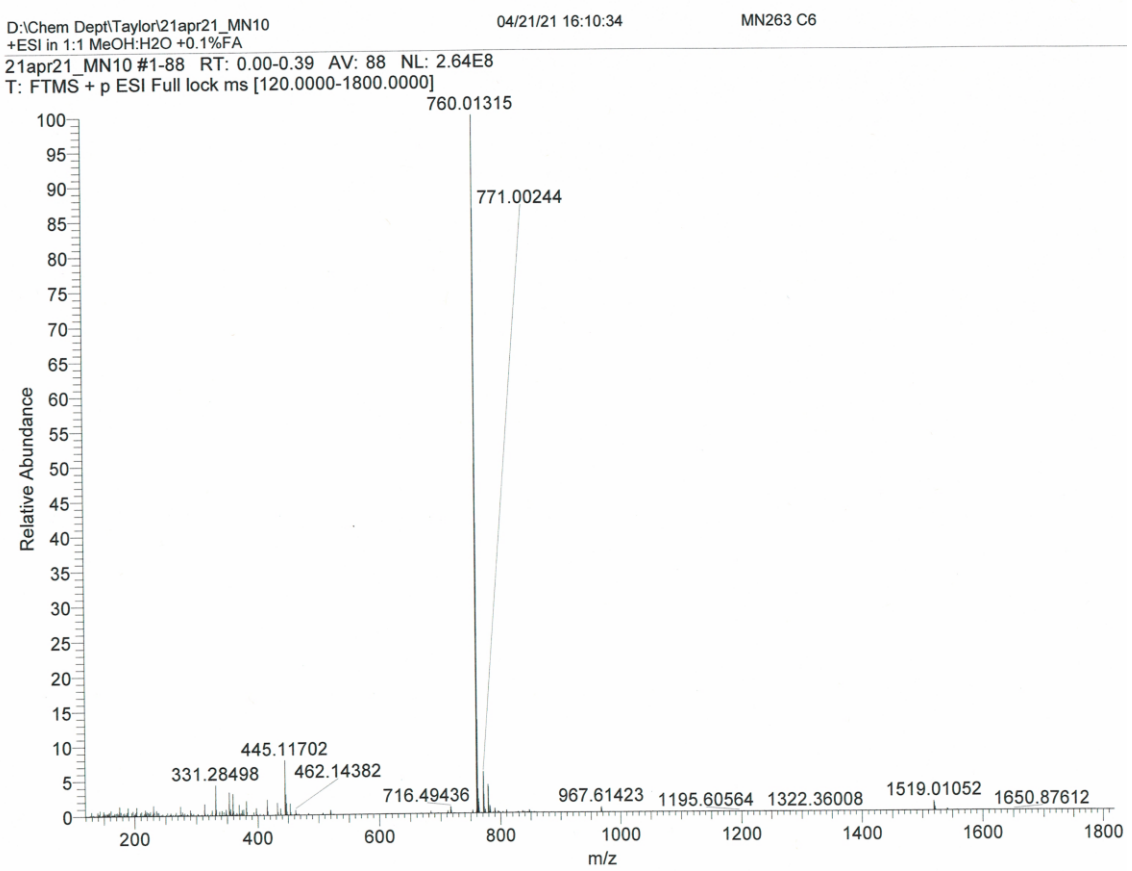

Elemental composition search on mass 760.01315

m/z= 755.01315-765.01315

m/z	Theo. Mass	Delta (ppm)	RDB equiv.	Composition
760.01315	760.01530	-2.82	15.0	$C_{75}H_{137}O_{17}N_{15}$

Figure B.34 HRMS (+ESI) of PA1-D-K1-D-K4-D-A7-A12 (3.36).

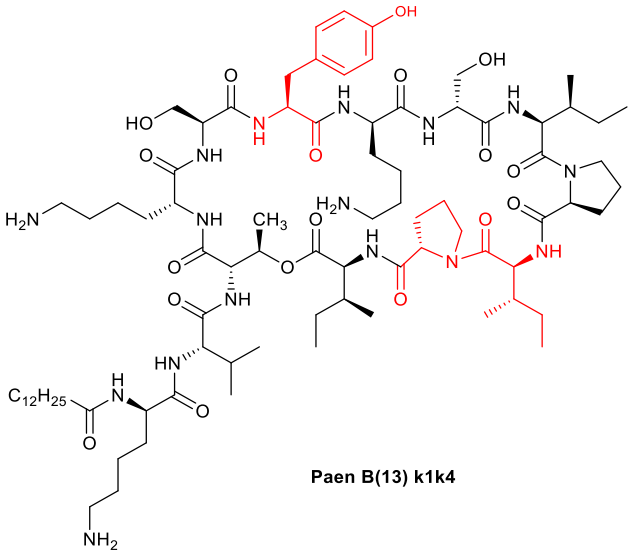

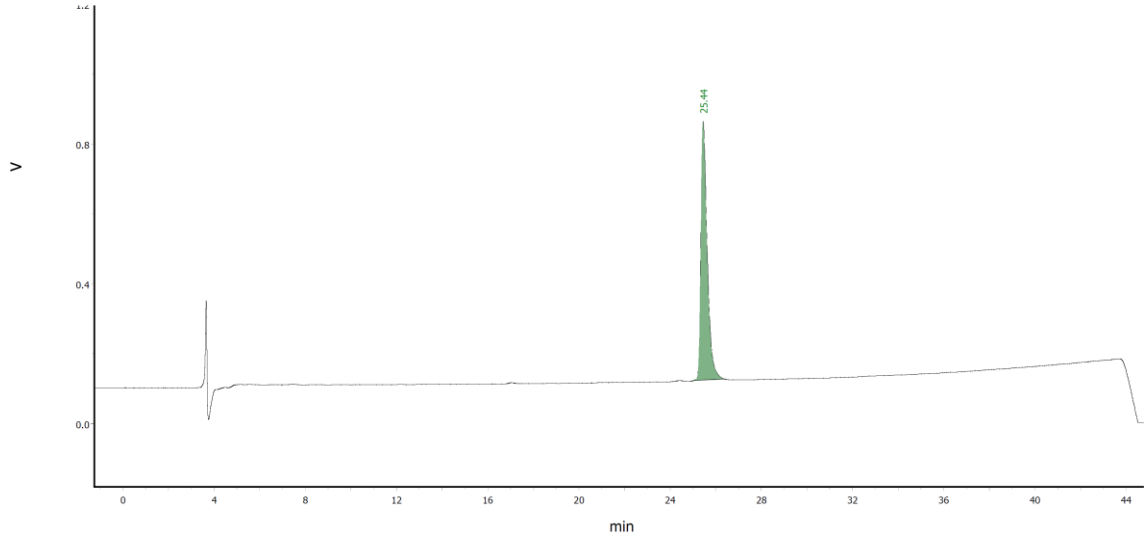

Figure B.35 Analytical RP-HPLC of PB1-D-K1-D-K4 (3.38). Linear gradient of 10:90 to 90:10 MeCN/H2O (0.1% TFA) over 40 min (λ = 220 nm). C18 proto, 5 µm, 250 × 4.6 mm.

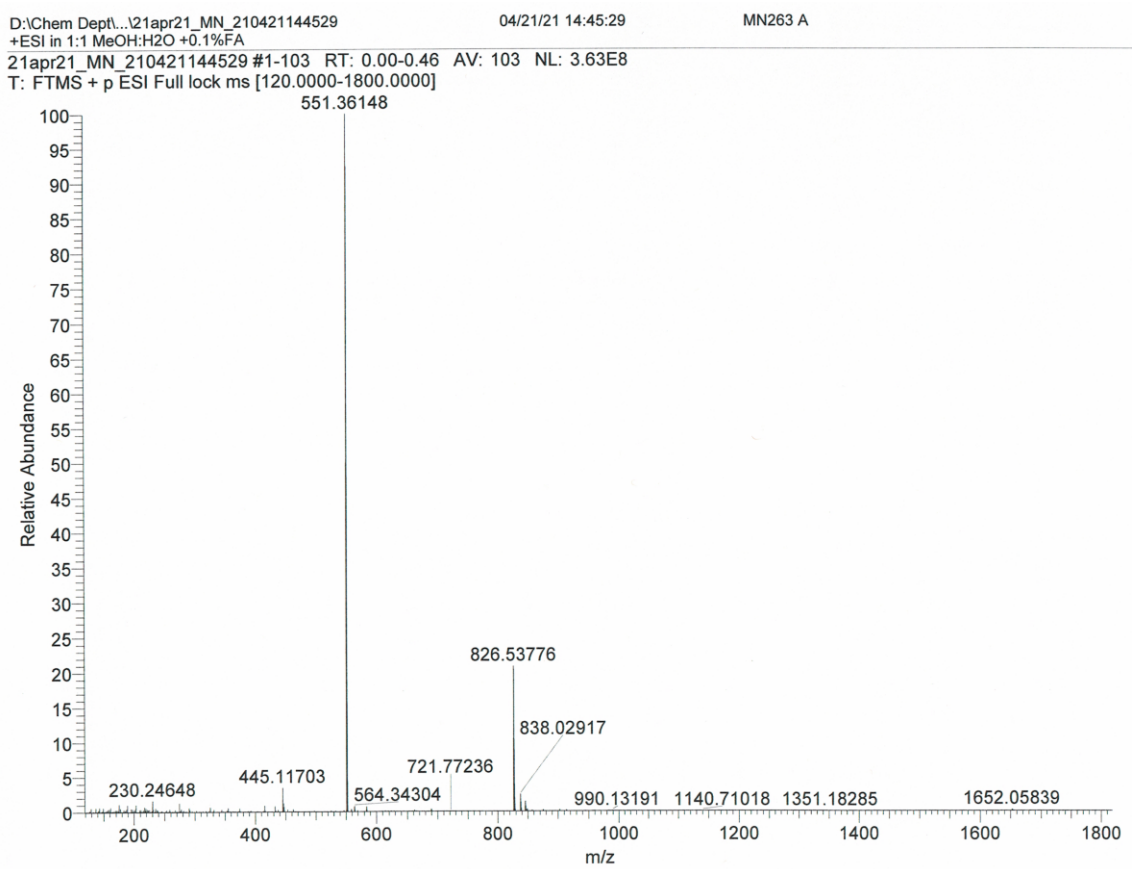

Elemental composition search on mass 551.36148

m/z= 546.36148-556.36148

m/z	Theo. Mass	Delta (ppm)	RDB equiv.	Composition
551.36148	551.36354	-3.74	19.5	$C_{83}H_{145}O_{18}N_{16}$

Figure B.36 HRMS (+ESI) of PB1-D-K1-D-K4 (3.38).

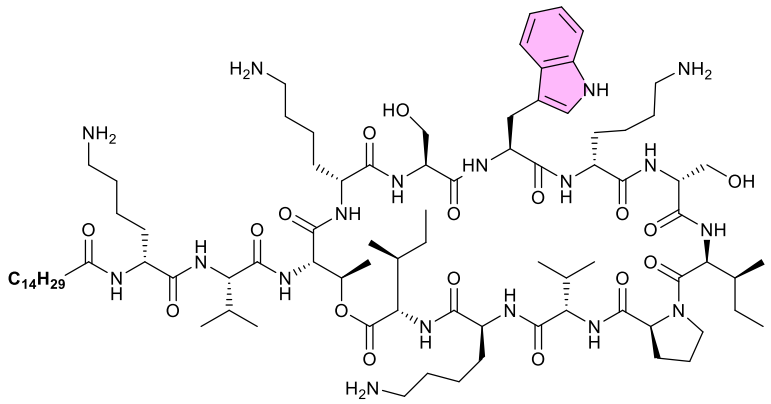

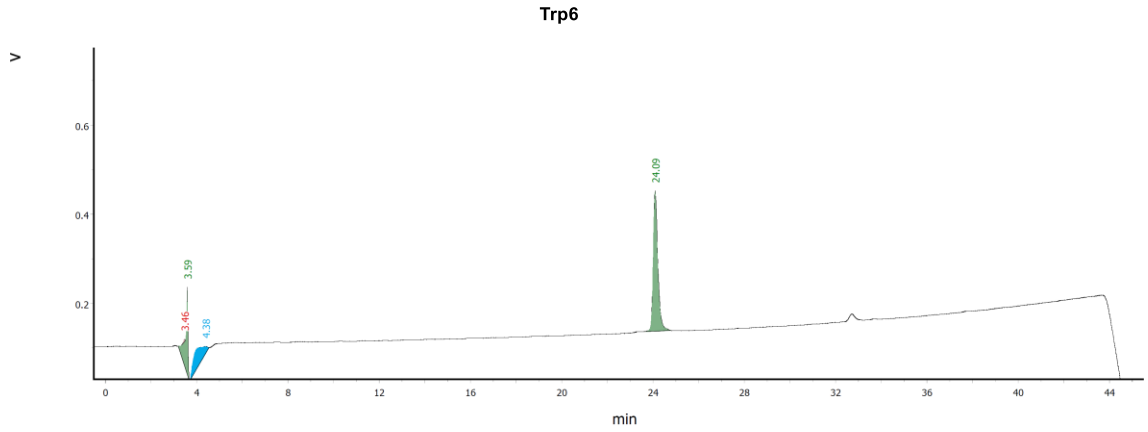

Figure B.37 Analytical RP-HPLC of PA1-D-K1-D-K4-W6 (3.40). Linear gradient of 10:90 to 90:10 MeCN/H2O (0.1% TFA) over 40 min (λ = 220 nm). C18 proto, 5 µm, 250 × 4.6 mm.

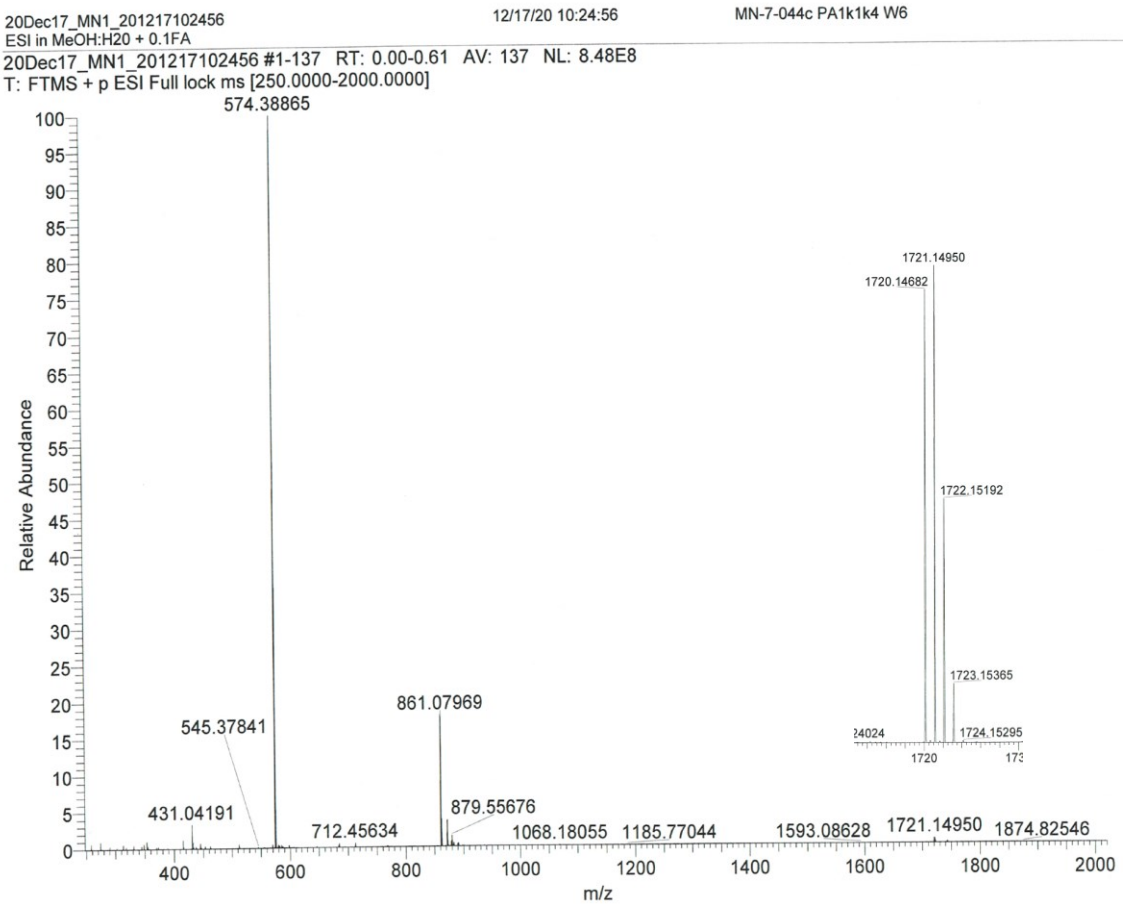

Elemental composition search on mass 1720.14682

m/z= 1715.14682-1725.14682

m/z	Theo. Mass	Delta (ppm)	RDB equiv.	Composition
1720.14682	1720.14991	-1.80	21.5	$C_{87}H_{151}O_{17}N_{18}$
	1720.13868	4.73	21.5	$C_{88}H_{151}O_{18}N_{16}$
	1720.16249	-9.11	21.0	$C_{88}H_{153}O_{17}N_{17}$
	1720.12610	12.04	22.0	$C_{87}H_{149}O_{18}N_{17}$
	1720.11353	19.36	22.5	$C_{86}H_{147}O_{18}N_{18}$

Figure B.38 HRMS (+ESI) of PA1-D-K1-D-K4-W6 (3.40).

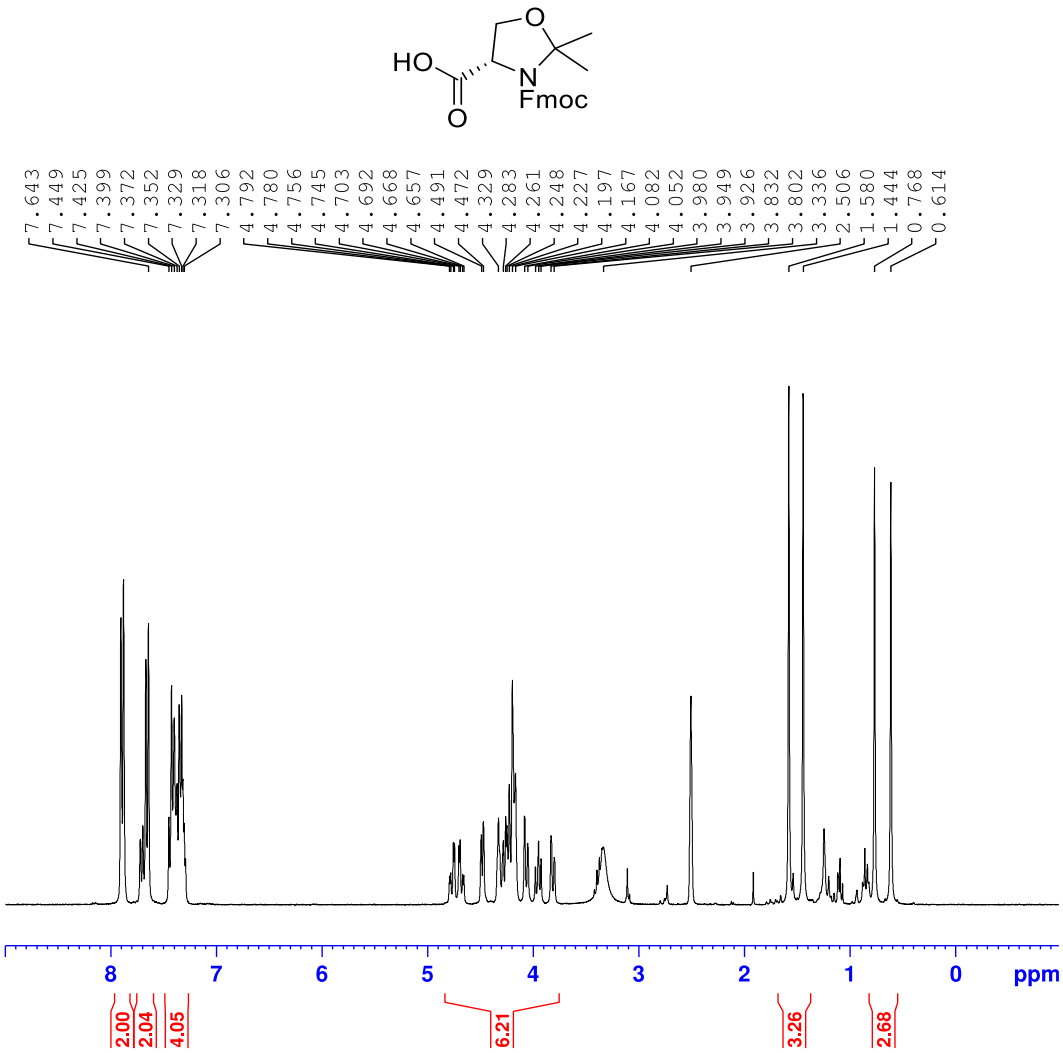

Figure B.39 ^{1}H NMR (300 MHz, $(CD_3)_2SO$) of compound 3.7

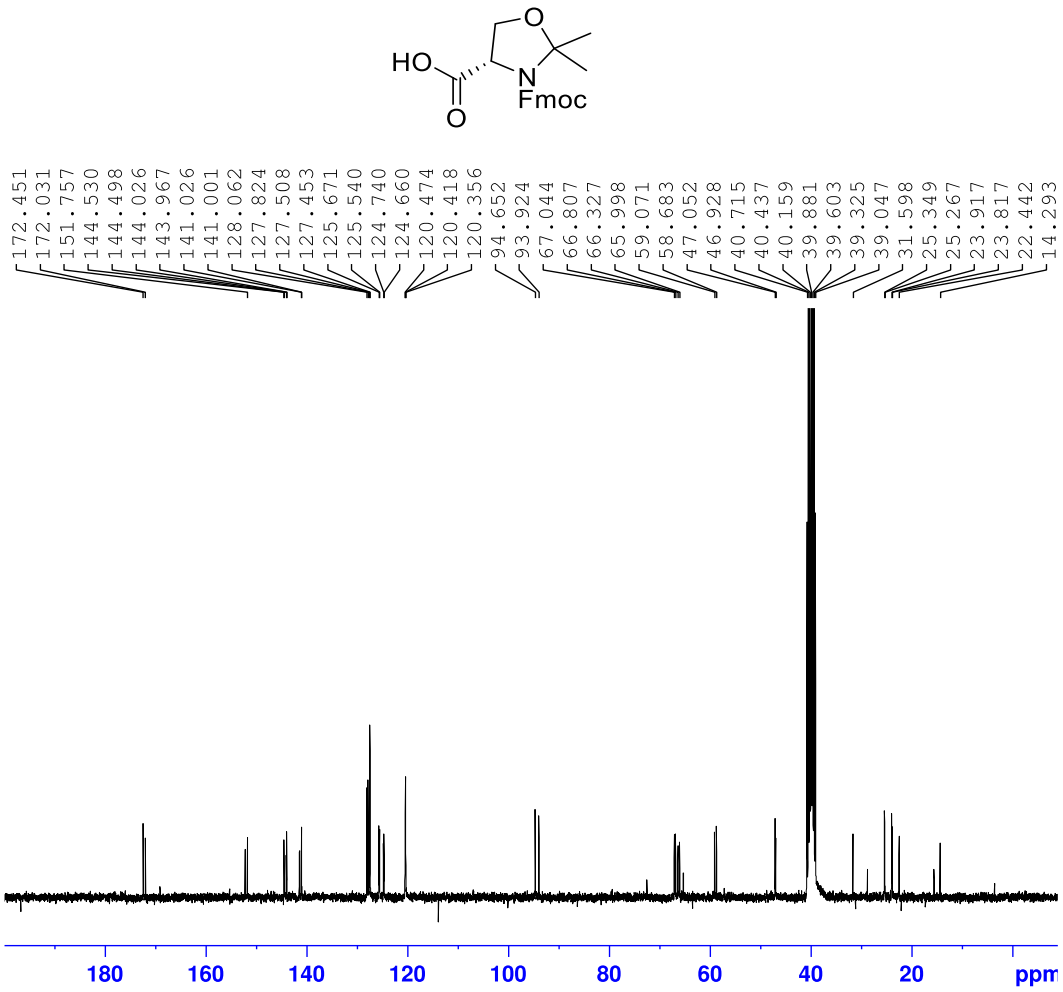

Figure B.40 ^{13}C NMR (75 MHz, $(CD_3)_2SO$) of compound 3.7

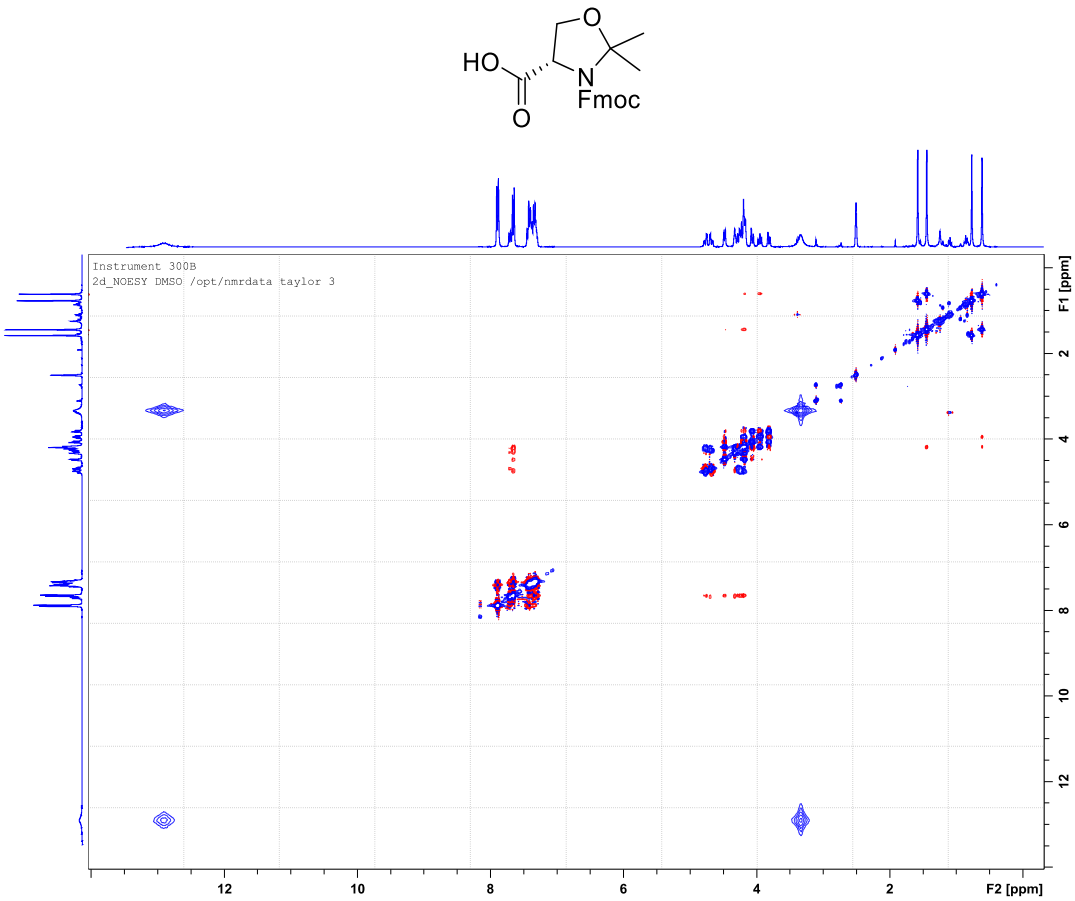

Figure B.41 ^{1}H NOESY (300 MHz, $(CD_3)_2SO$) of compound 3.7

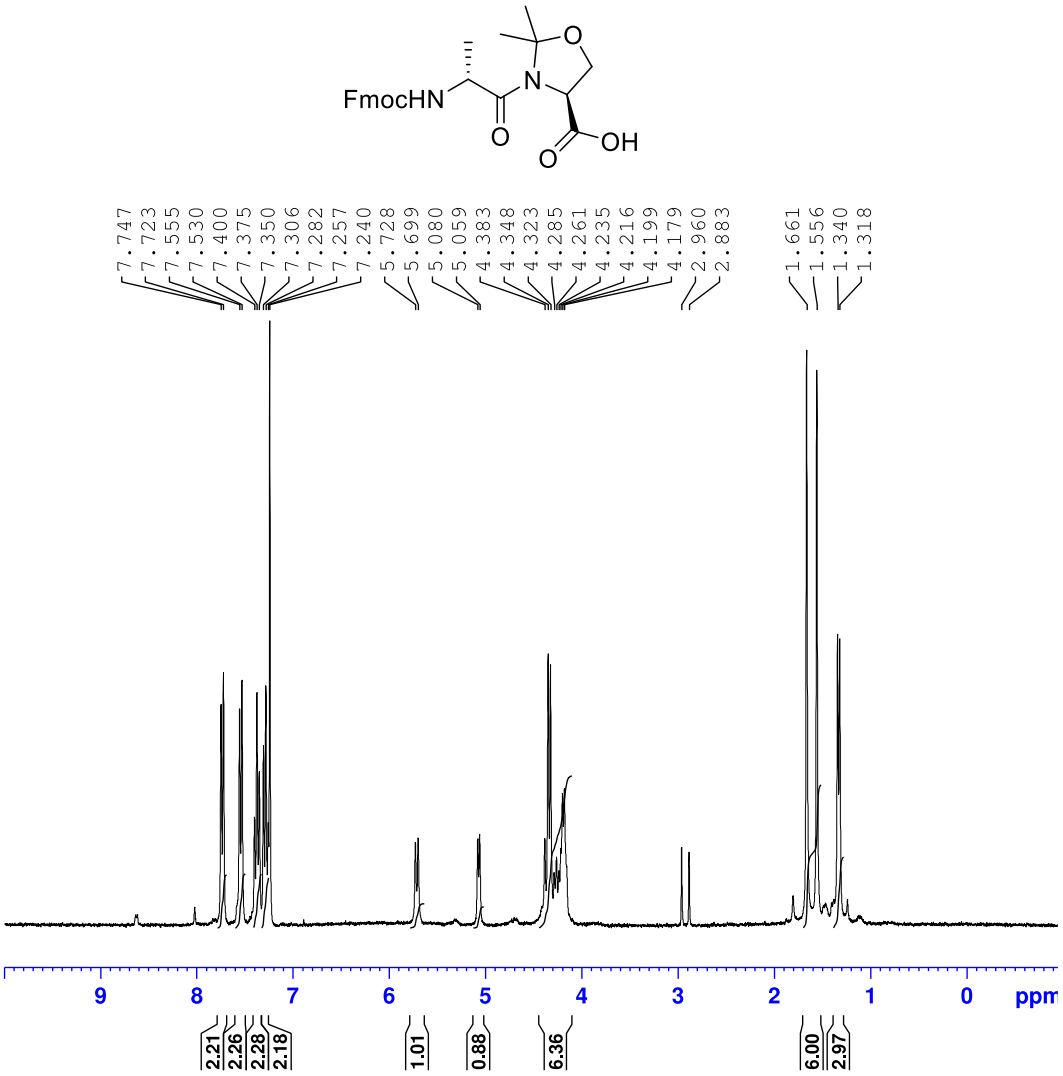

Figure B.42 ^{1}H NMR (300 MHz, $CDCl_3$) of Fmoc-Ser($\Psi^{Me,Me}$Pro)-OH

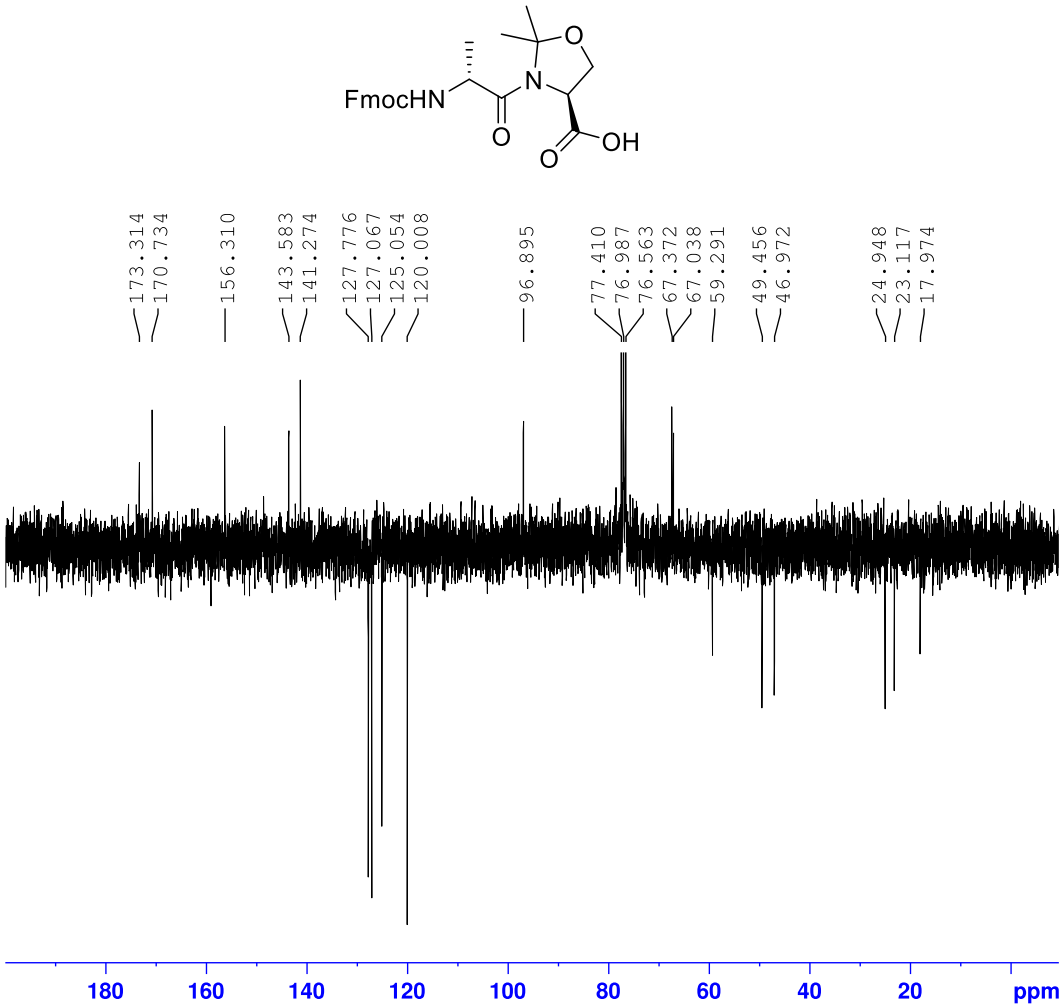

Figure B.43 ^{13}C NMR (75 MHz, $CDCl_3$) of Fmoc-Ser($\Psi^{Me,Me}$Pro)-OH

Appendix C

Characterization of Chapter 4 Compounds[i]

[i]Reproduced (adapted) with permission from "Noden, M.; Taylor, S. D. Enantioselective Synthesis and Application of Small and Environmentally Sensitive Fluorescent Amino Acids for Probing Biological Interactions. *J. Org. Chem.* **2021**, *86* (17), 11407–11418.". Copyright © 2021 American Chemical Society.

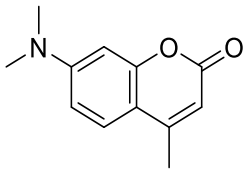

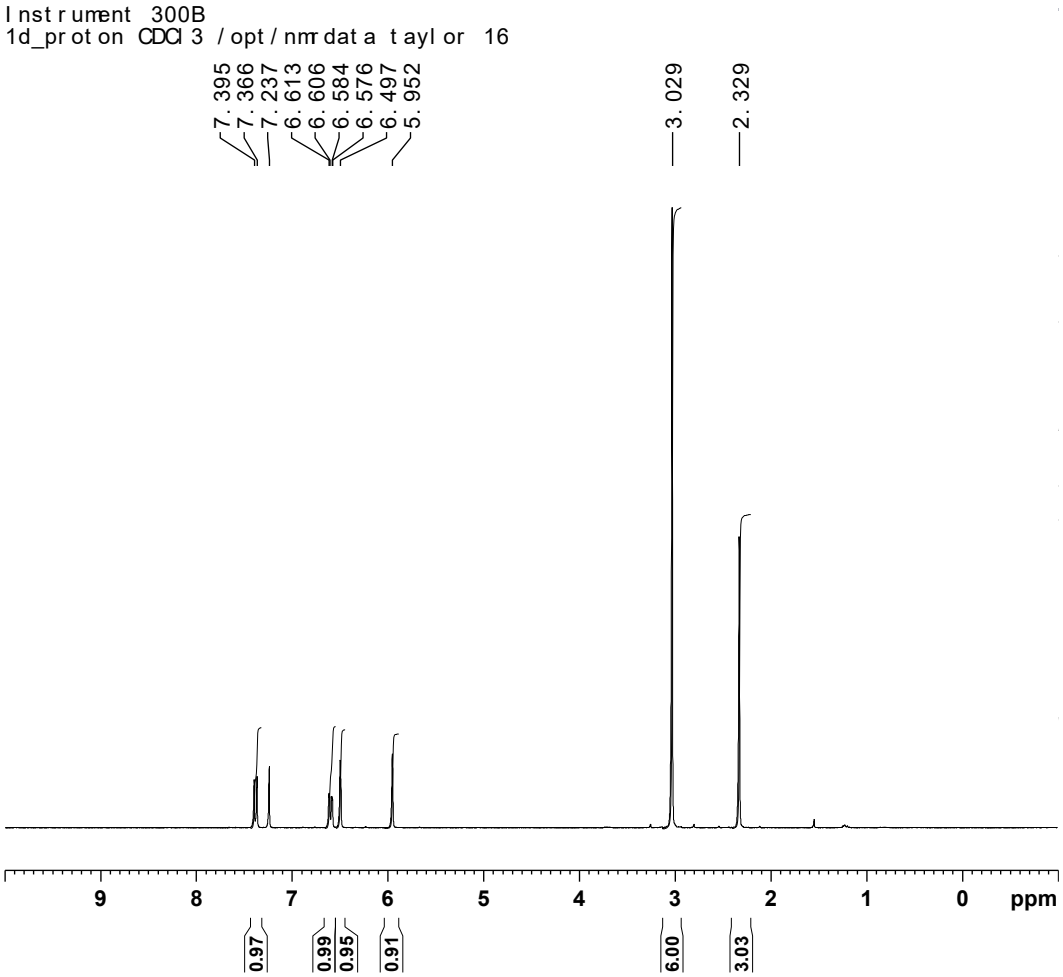

Figure C.1 ^{1}H NMR ($CDCl_3$, 300 MHz) of compound 4.9

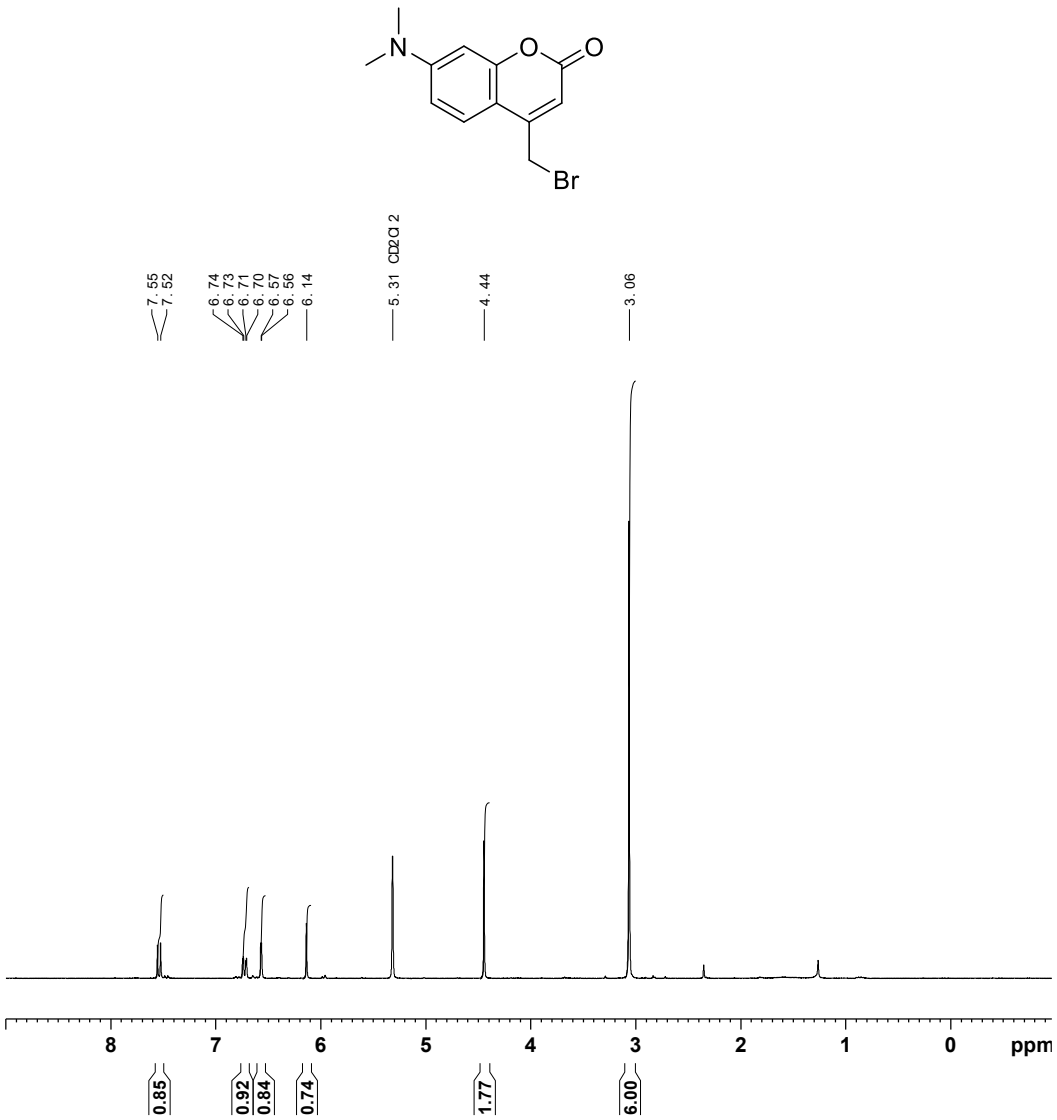

Figure C.2 ^{1}H NMR (CD_2Cl_2, 300 MHz) of compound 4.11

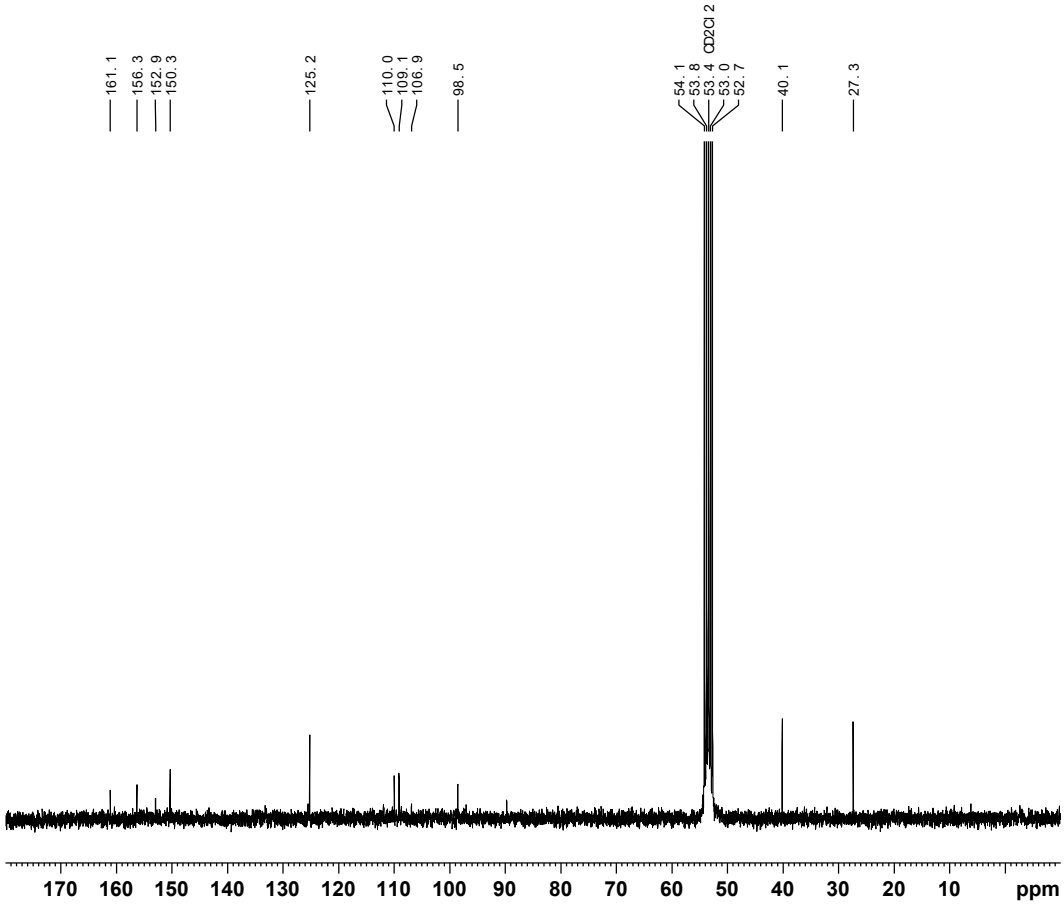

Figure C.3 $^{13}C\{^{1}H\}$ NMR (CD_2Cl_2, 75 MHz) of compound 4.11

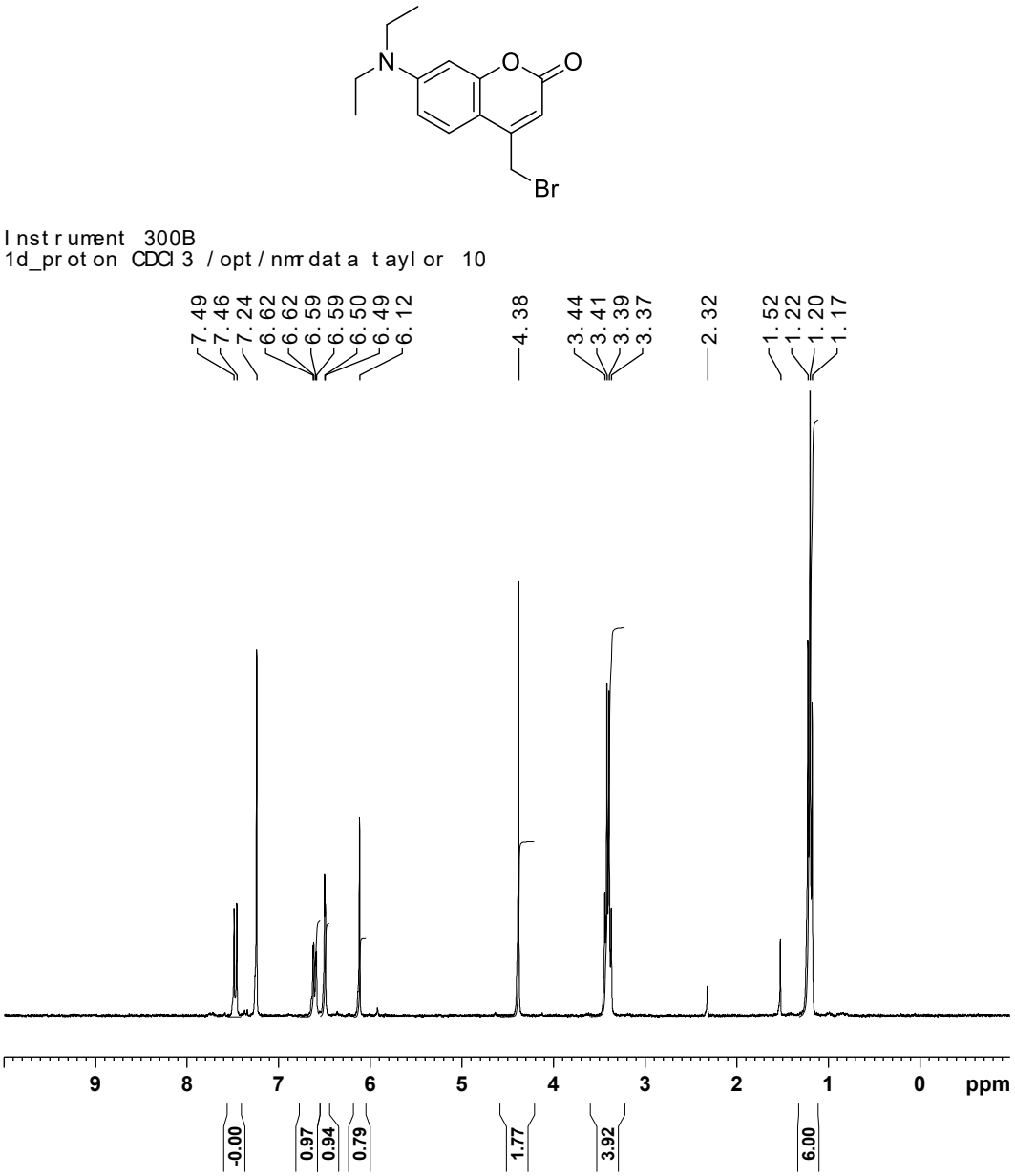

Figure C.4 ^{1}H NMR ($CDCl_3$, 300 MHz) of compound 4.12

Figure C.5 $^{13}C\{^{1}H\}$ NMR ($CDCl_3$, 75 MHz) of compound 4.12

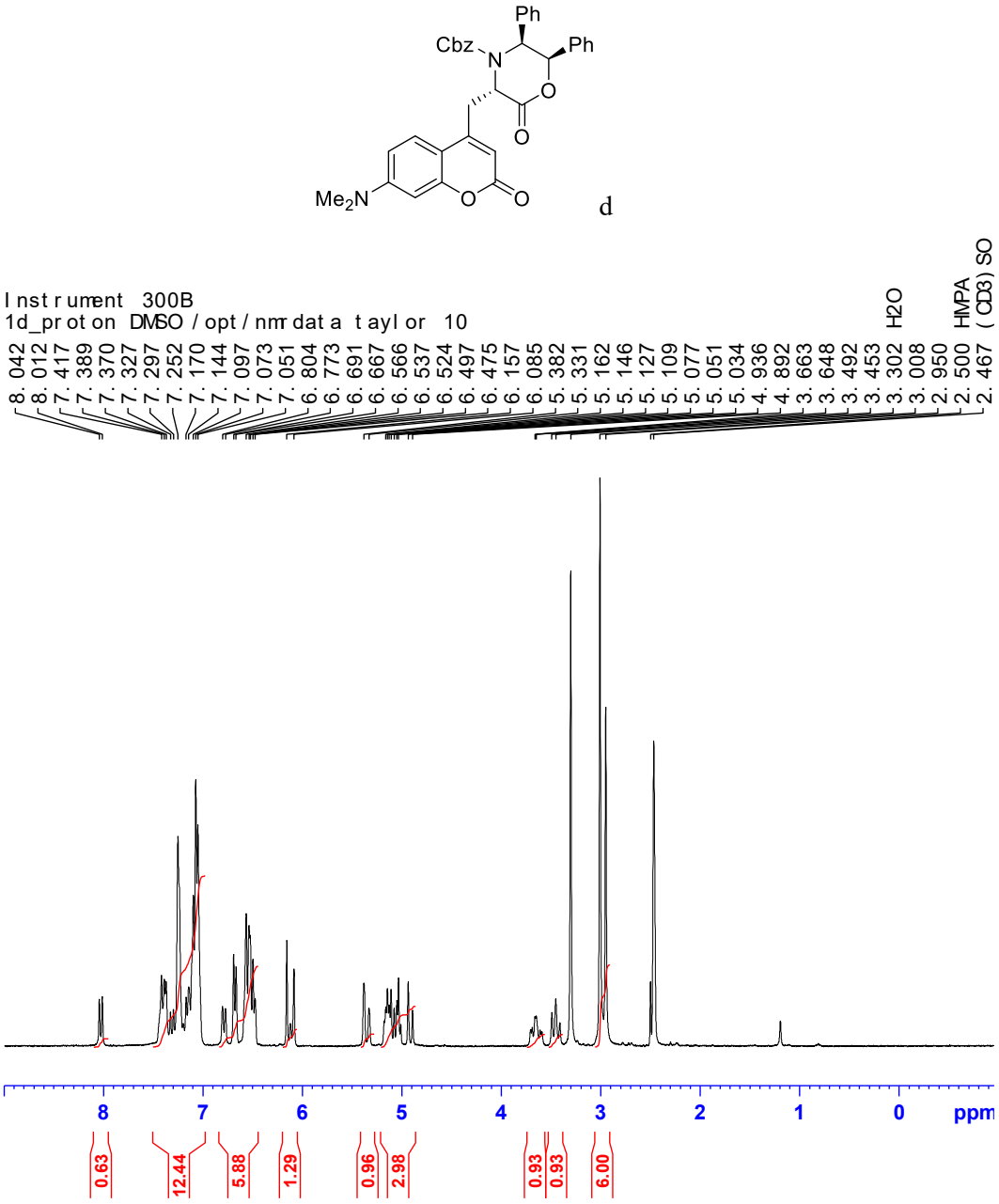

Figure C.6 ^{1}H NMR ($(CD_3)_2SO$, 300 MHz) of compound 4.13

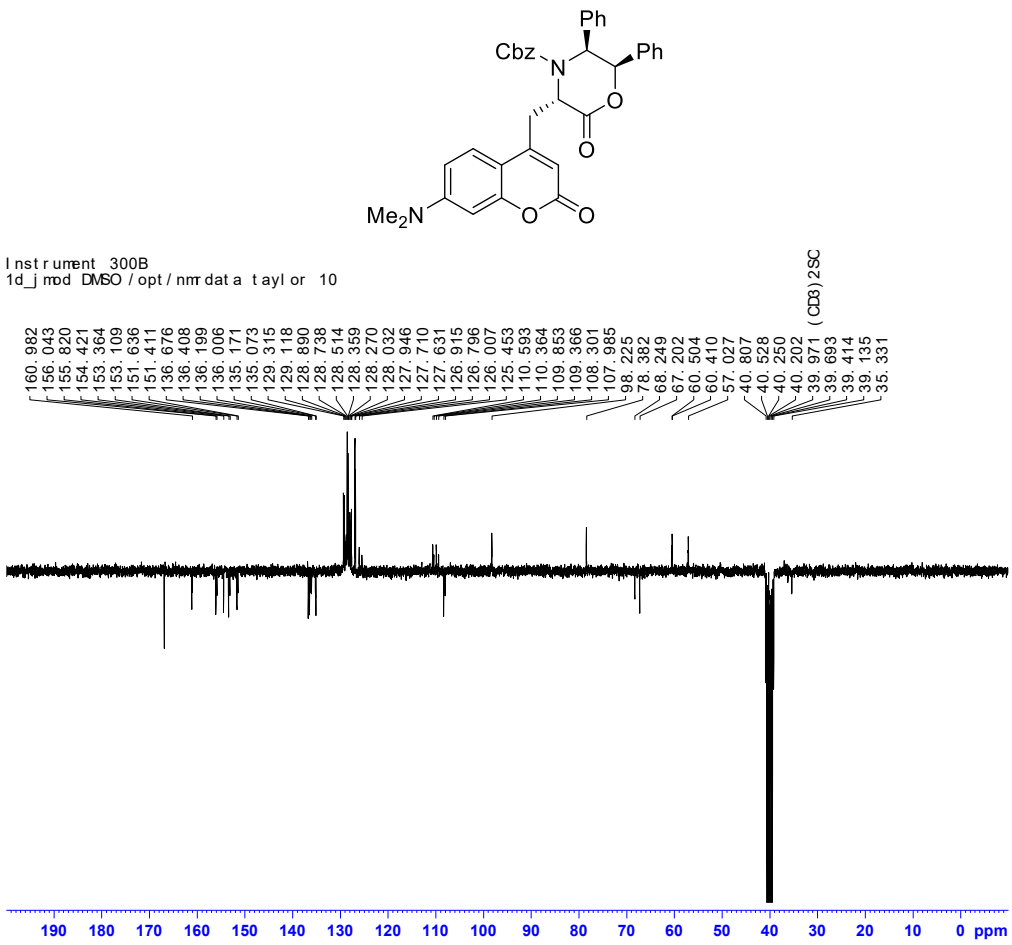

Figure C.7 $^{13}C\{^{1}H\}$ NMR ($(CD_3)_2SO$, 75 MHz) of compound 4.13

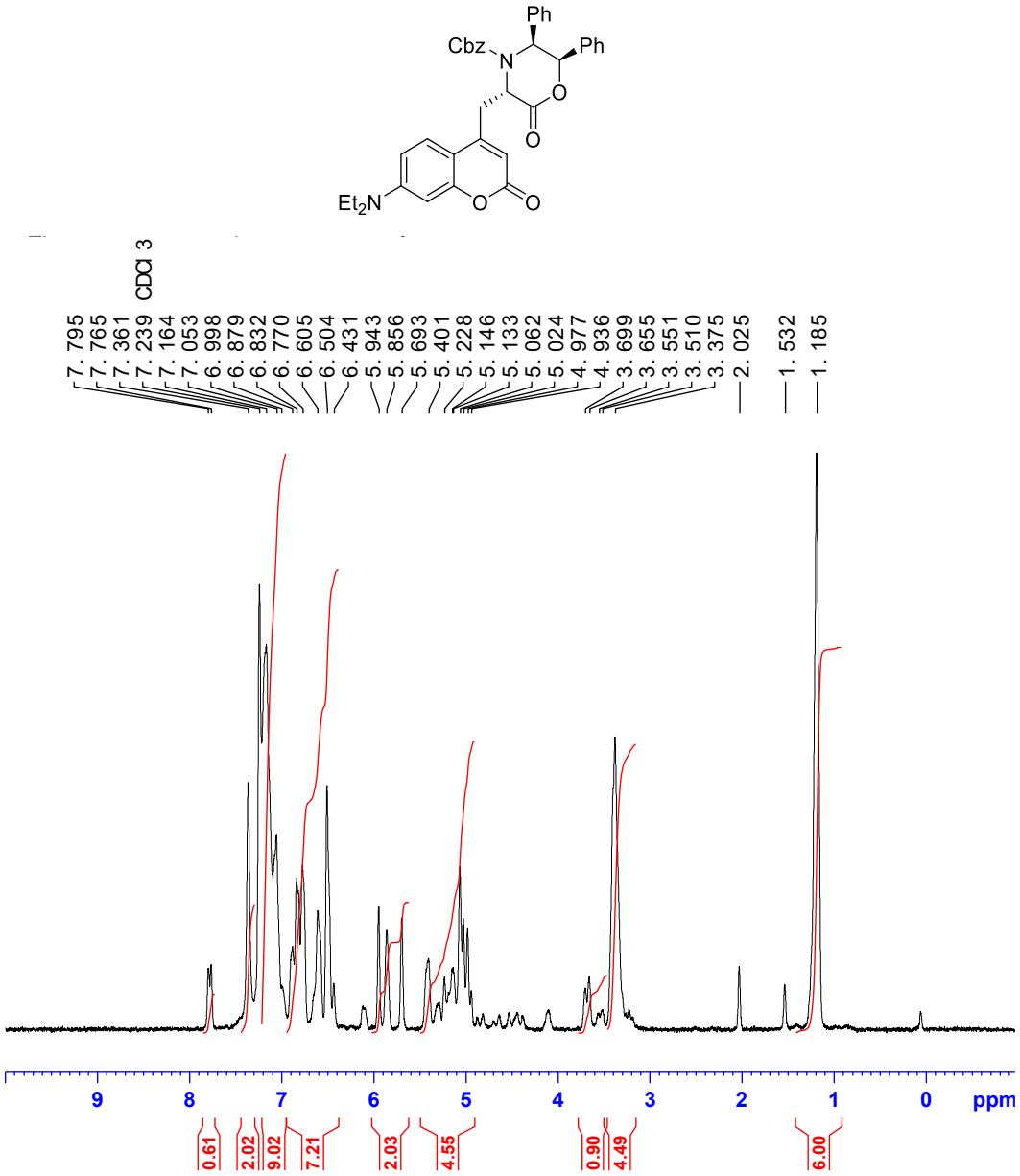

Figure C.8 ^{1}H NMR ($CDCl_3$, 500 MHz) of compound 4.14

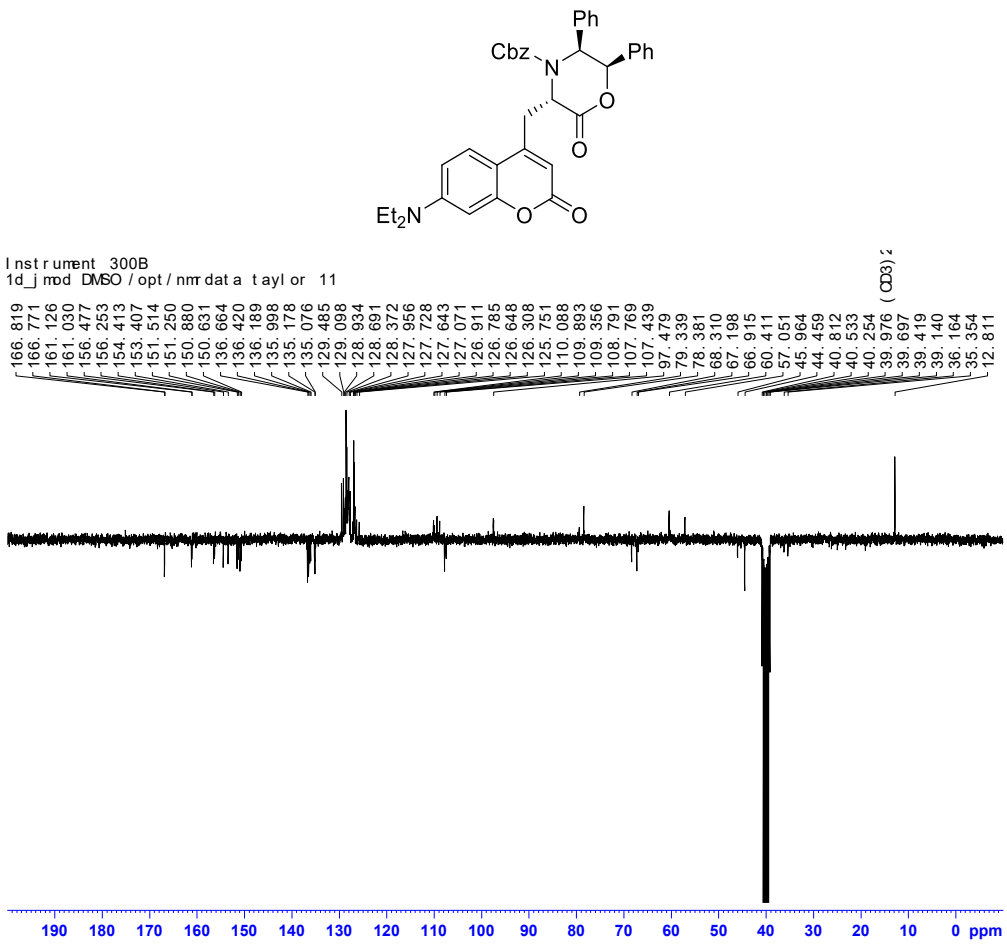

Figure C.9 $^{13}C\{^{1}H\}$ NMR ($CDCl_3$, 75 MHz) of compound 4.14

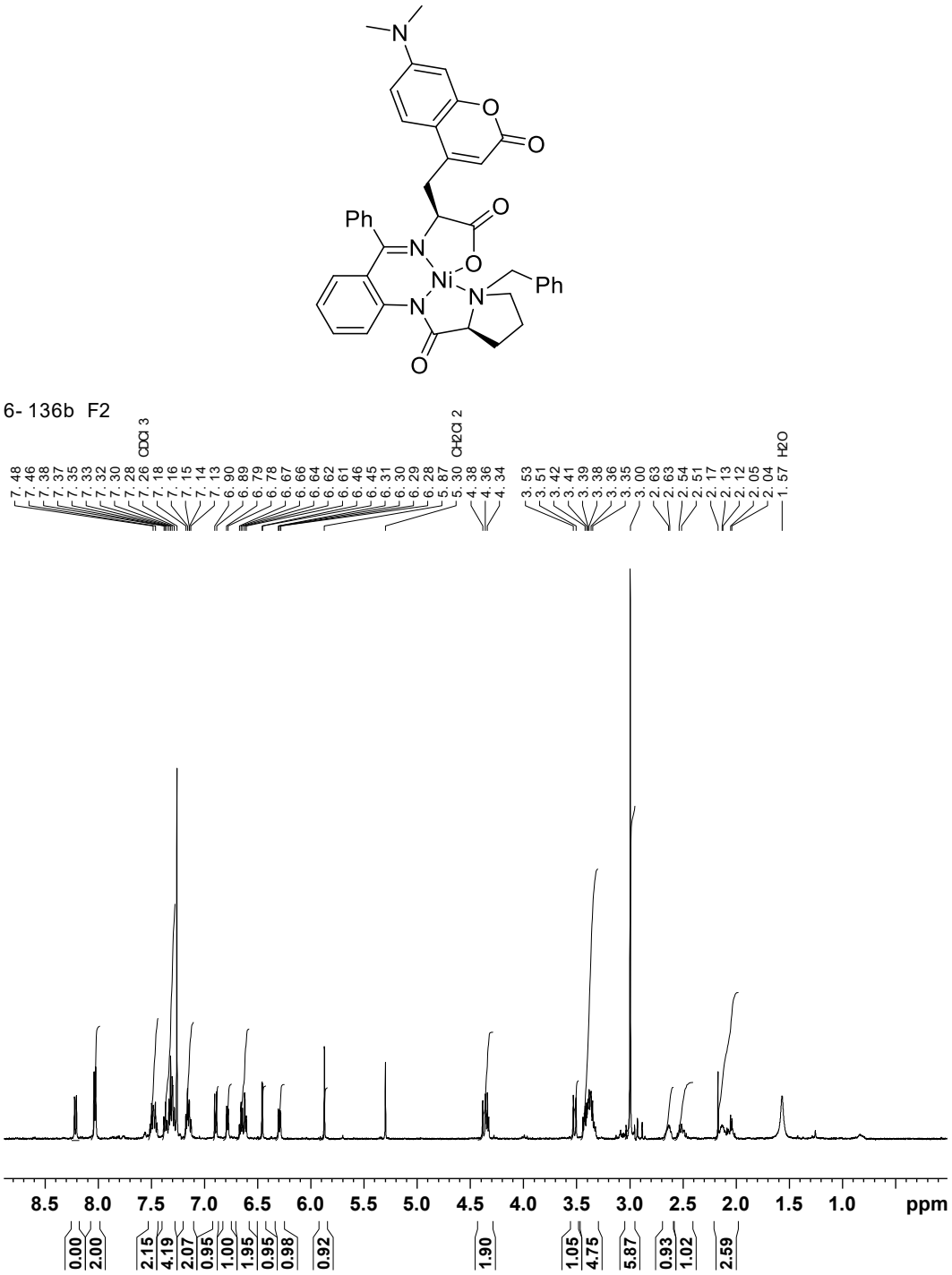

Figure C.10 ^{1}H NMR ($CDCl_3$, 500 MHz) of compound 4.16

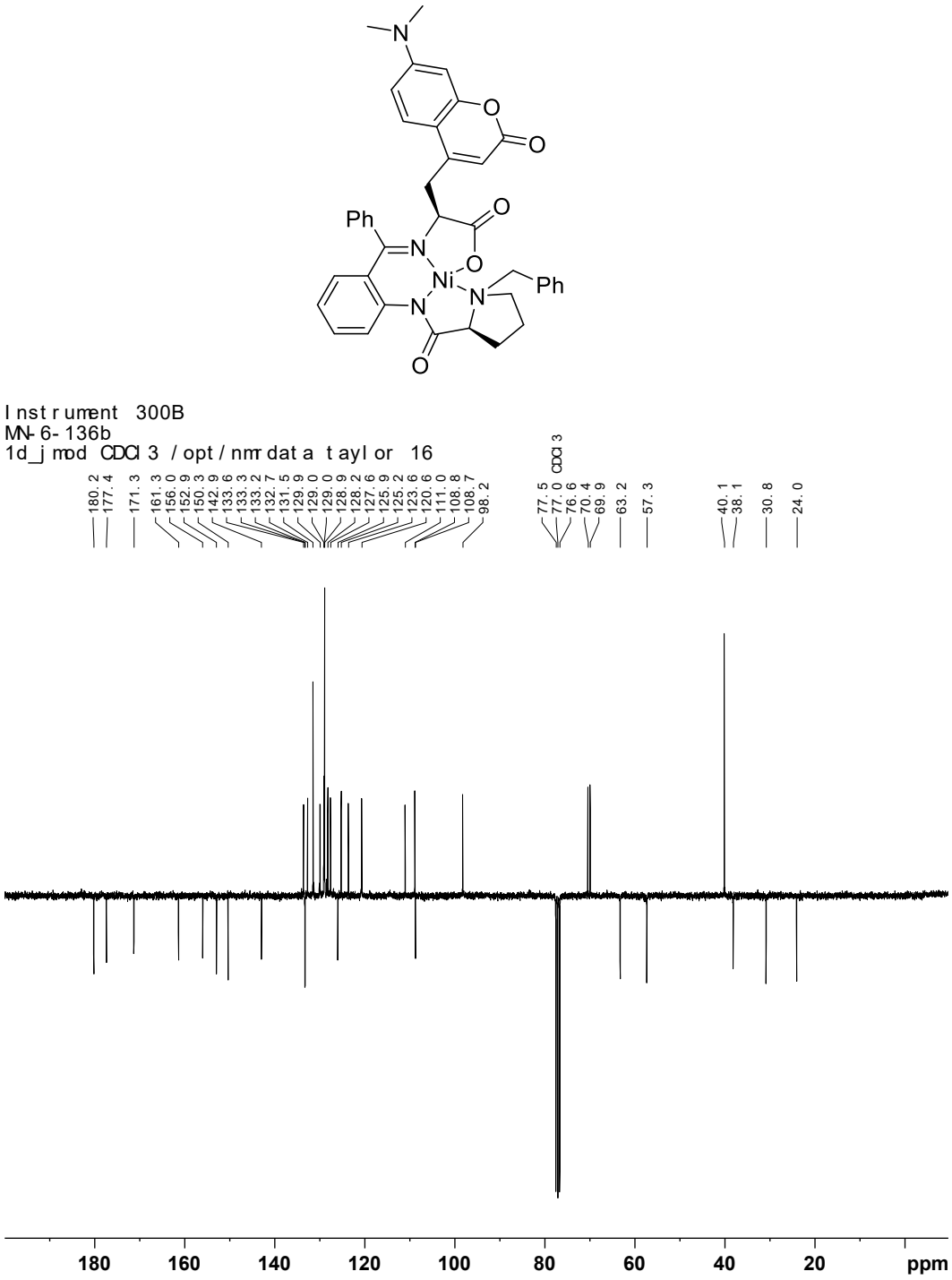

Figure C.11 $^{13}C\{^{1}H\}$ NMR ($CDCl_3$, 75 MHz) of compound 4.16

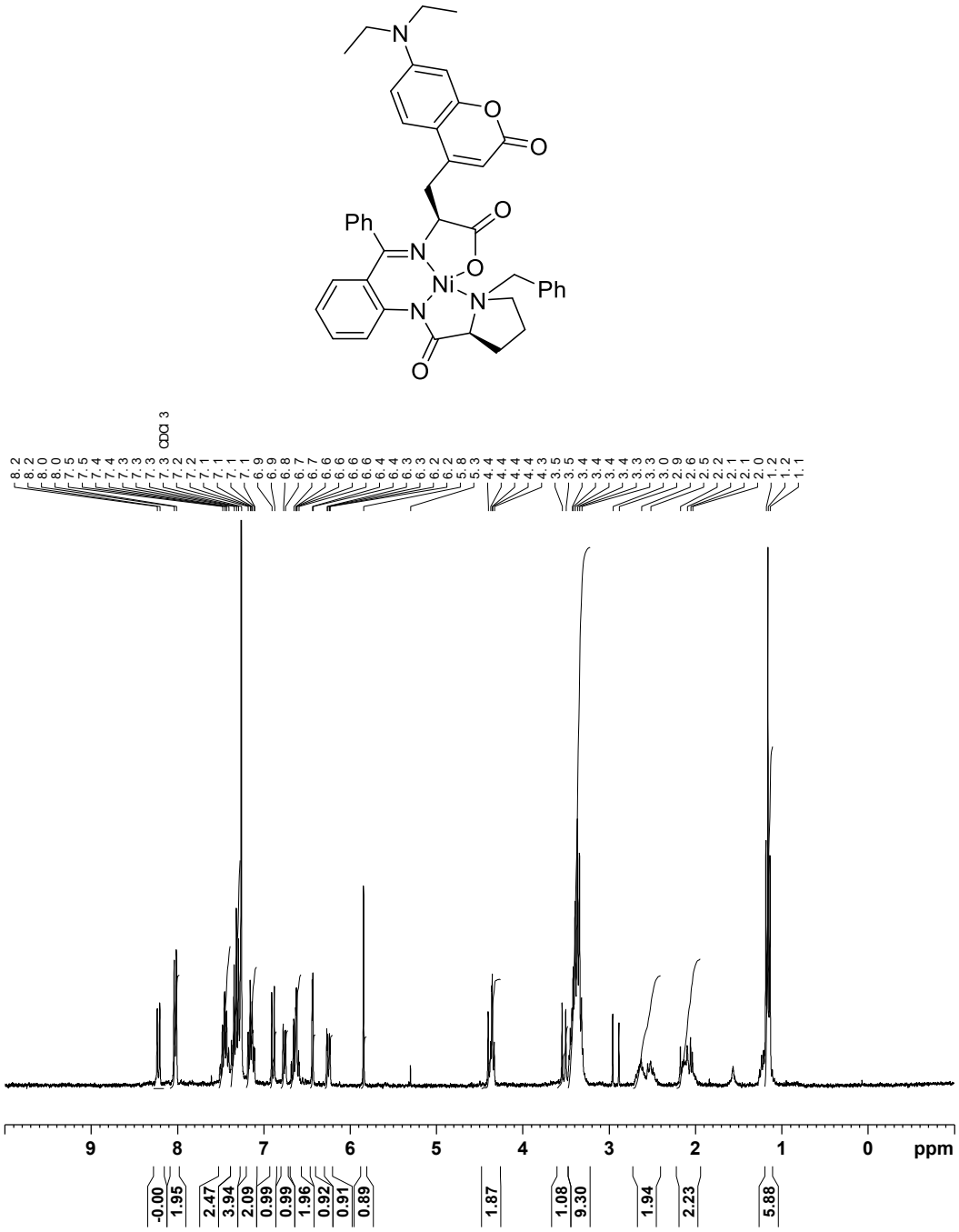

Figure C.12 ^{1}H NMR ($CDCl_3$, 300 MHz) of compound 4.17

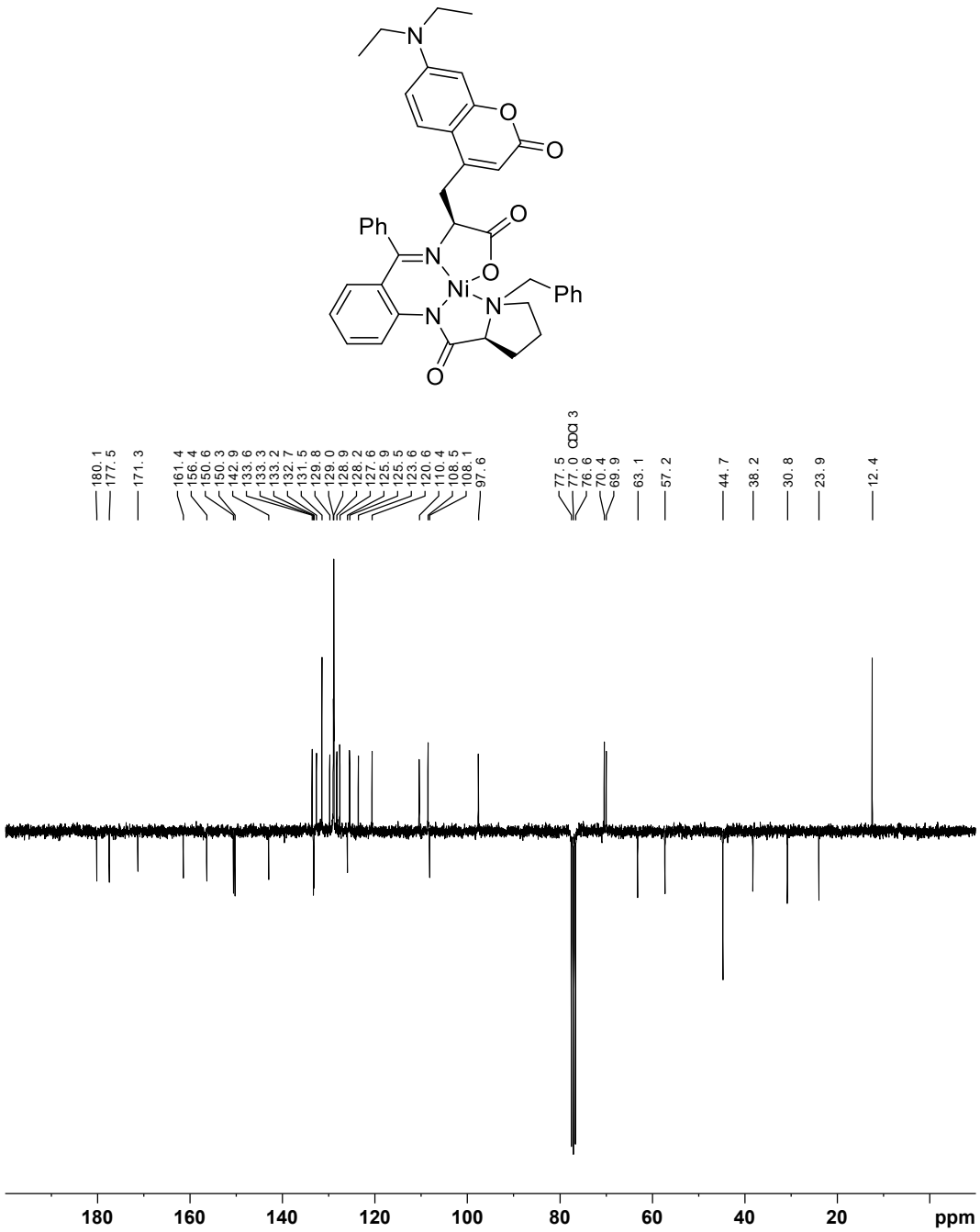

Figure C.13 $^{13}C\{^{1}H\}$ NMR ($CDCl_3$, 75 MHz) of compound 4.17

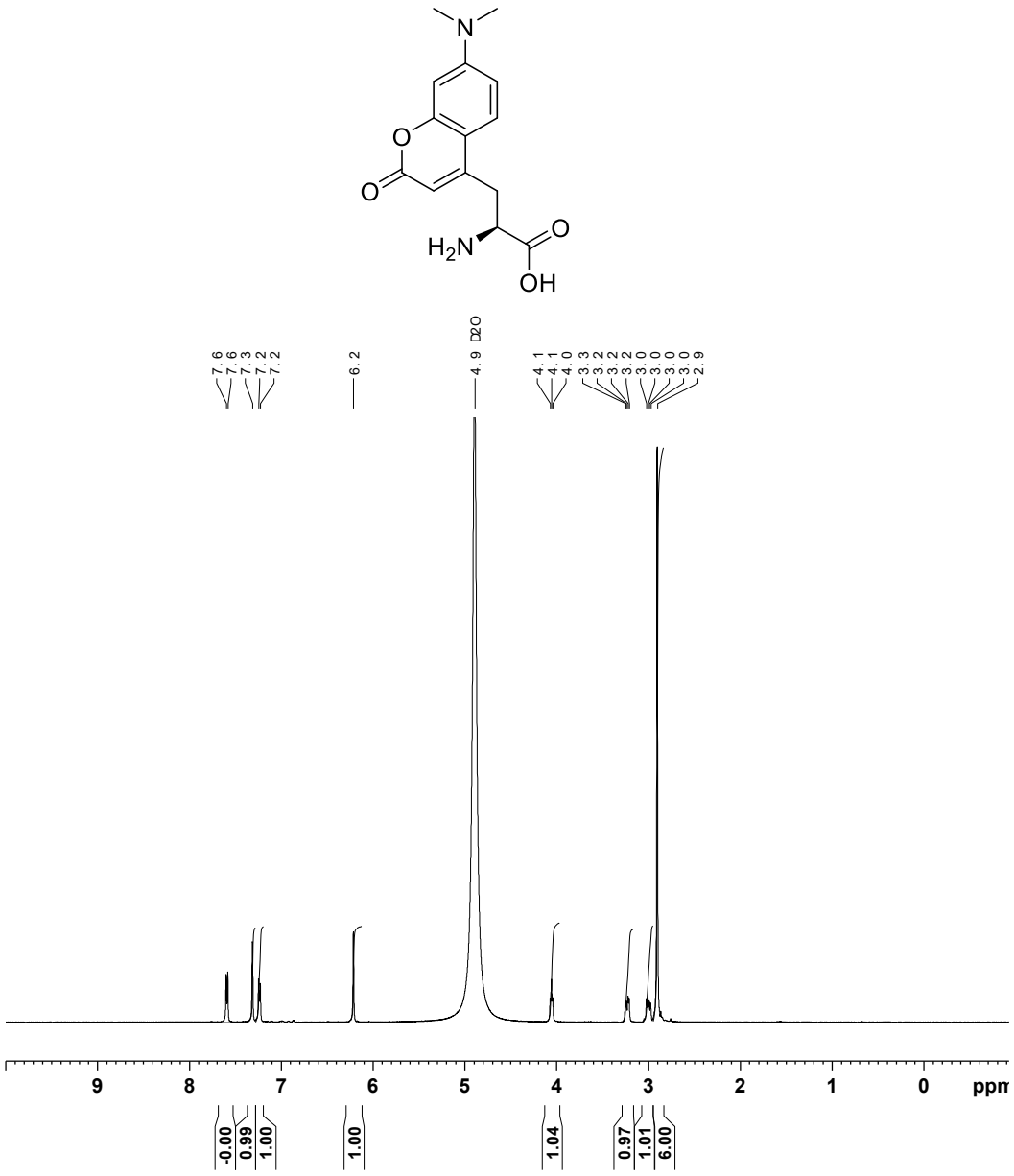

Figure C.14 ^{1}H NMR (D_2O with 5% DCl, 500 MHz) of DMACA (4.7)

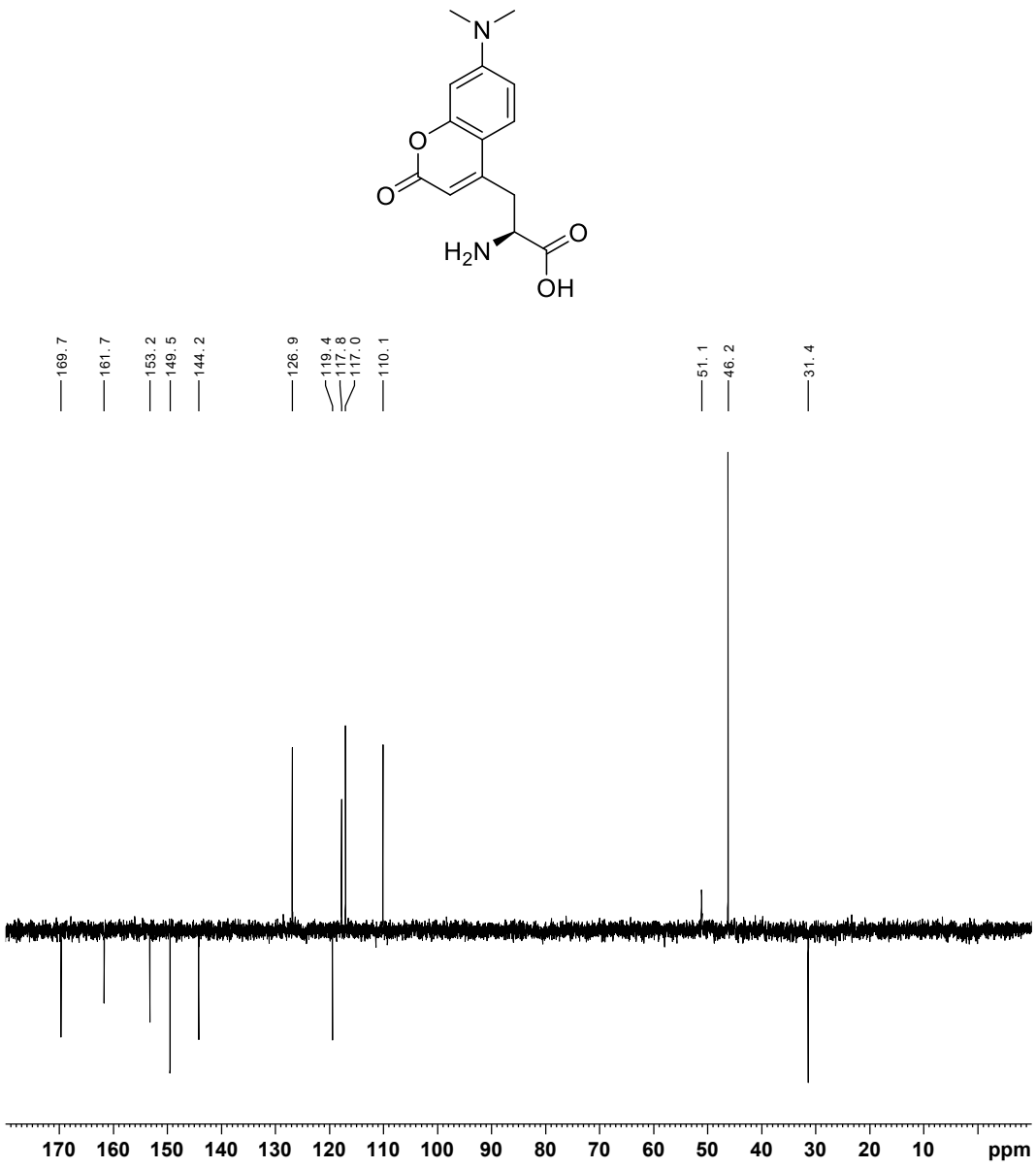

Figure C.15 $^{13}C\{^{1}H\}$ NMR (D_2O with 5% DCl, 75 MHz) of DMACA (4.7)

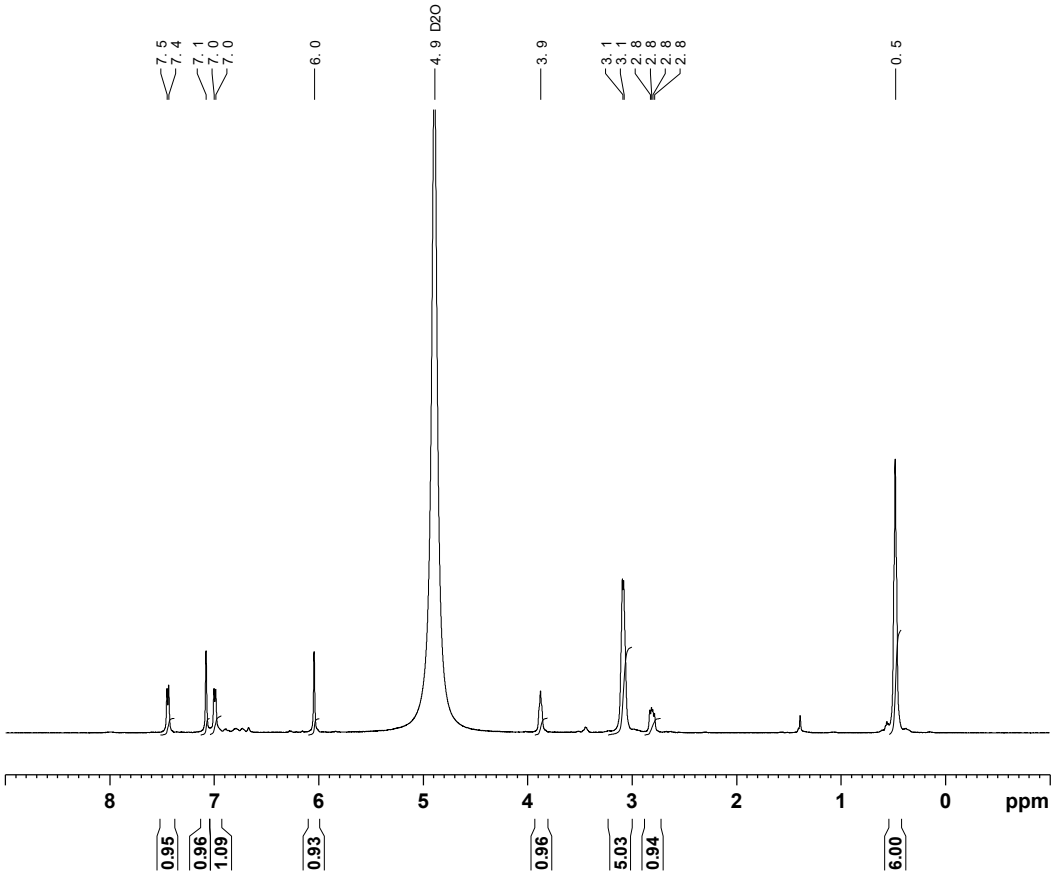

Figure SC.16 ^{1}H NMR (D_2O with 5% DCl, 500 MHz) of DEACA (4.8)

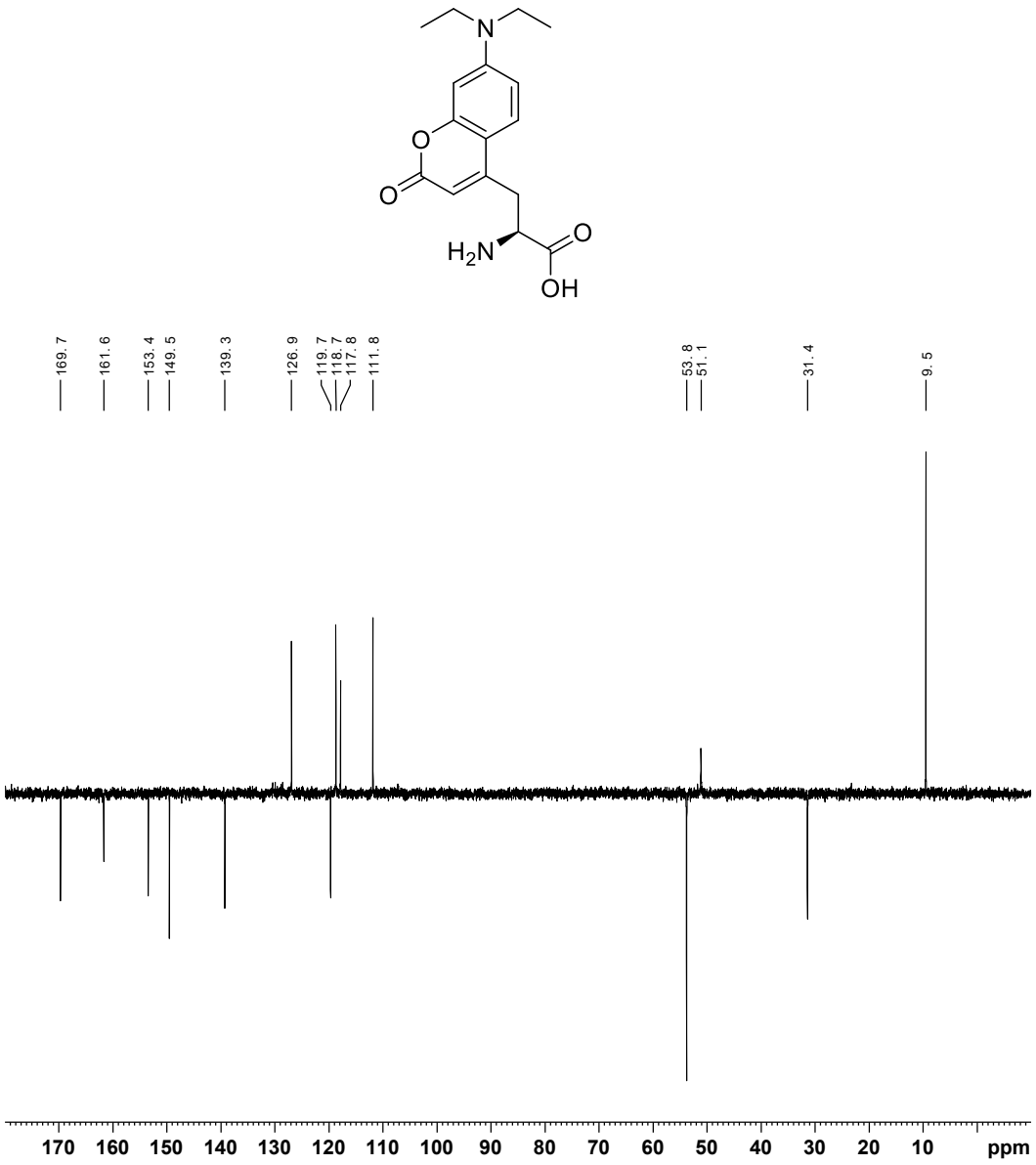

Figure C.17 $^{13}C\{^{1}H\}$ NMR (D_2O with 5% DCl, 75 MHz) of DEACA (4.8)

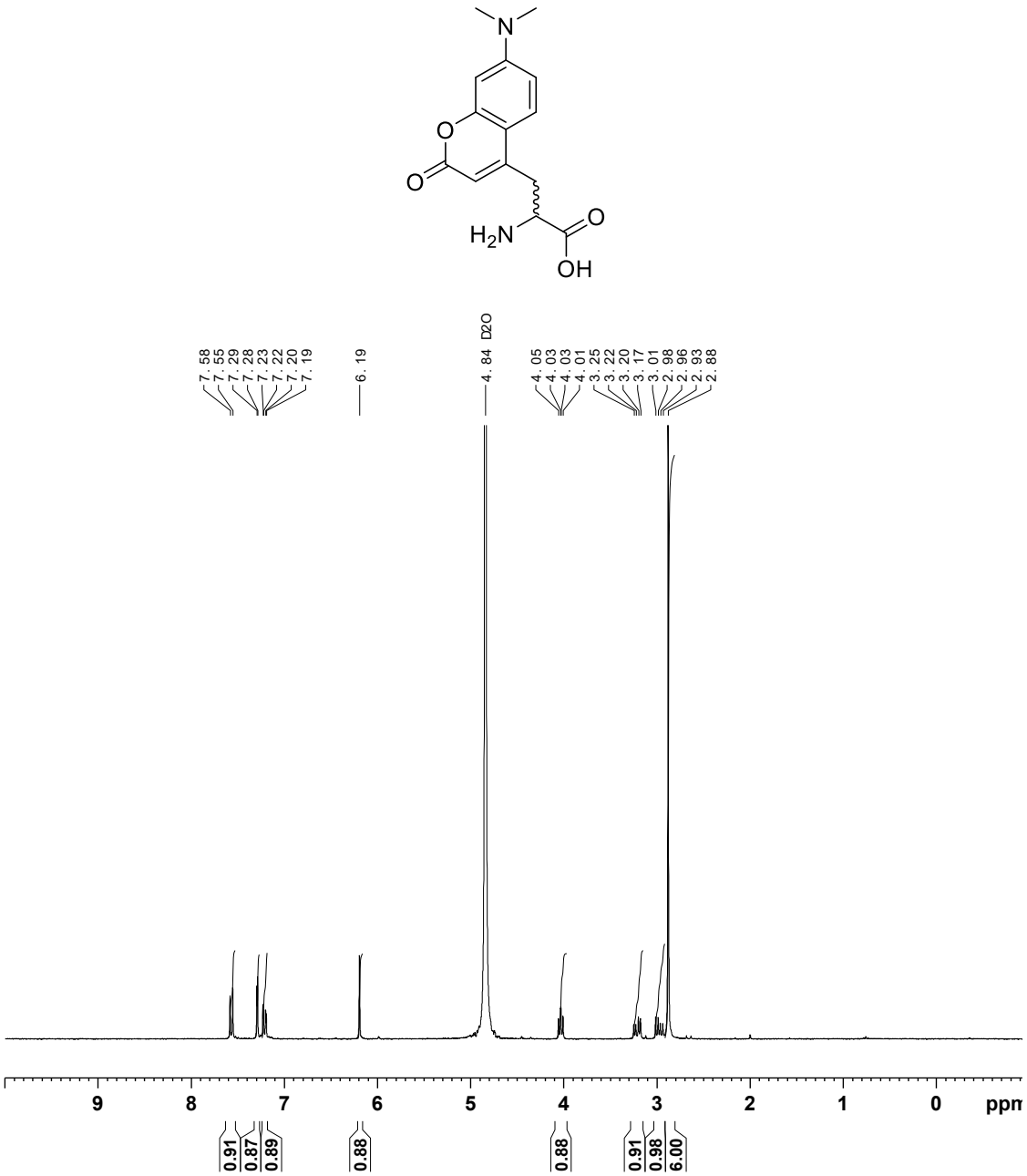

Figure C.18 ^{1}H NMR (D_2O with 5% DCl, 300 MHz) of racemic DMACA

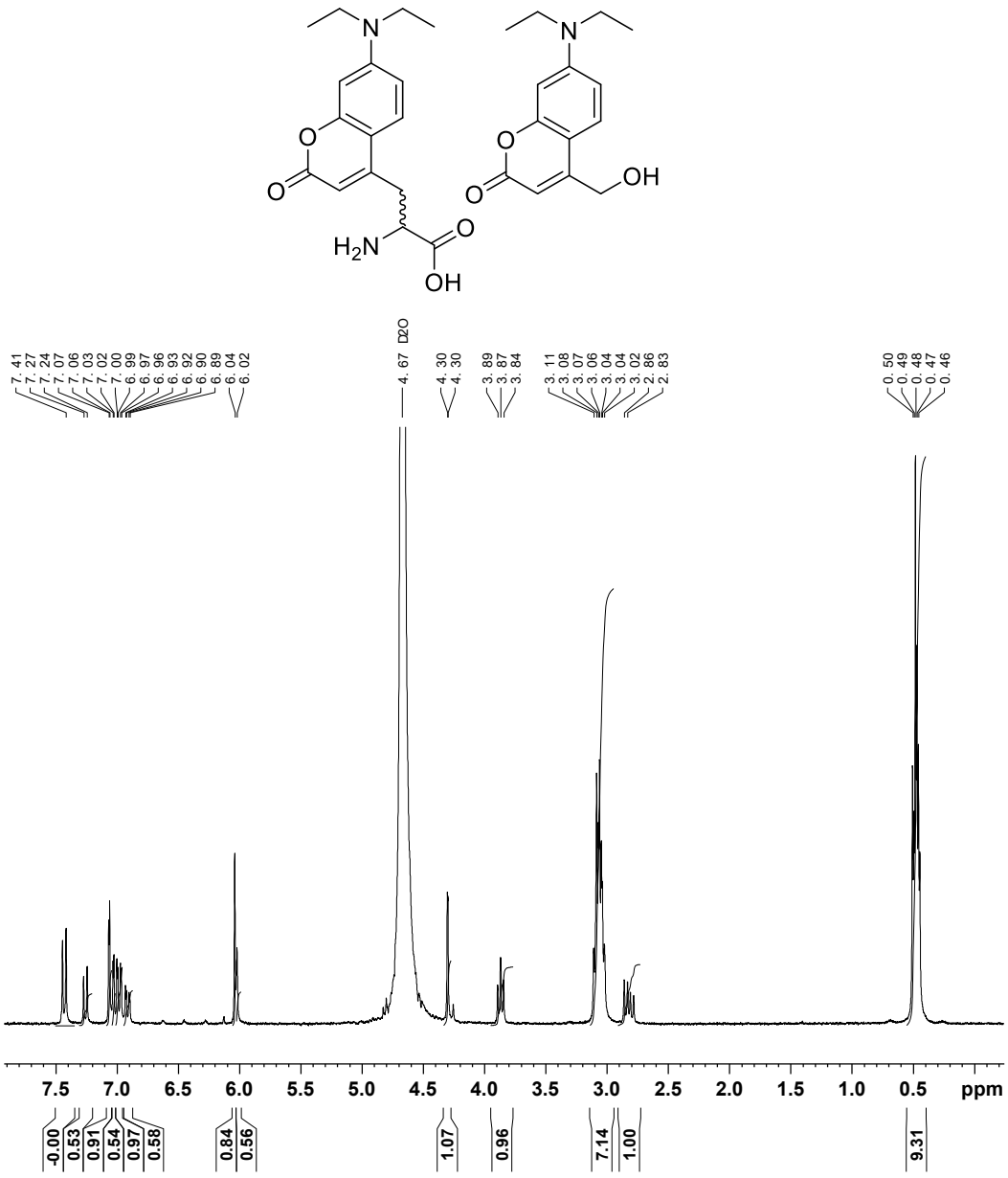

Figure C.19 ^{1}H NMR (D_2O with 5% DCl, 300 MHz) of racemic DEACA and 7-diethylamino-4-(hydroxymethyl)coumarin

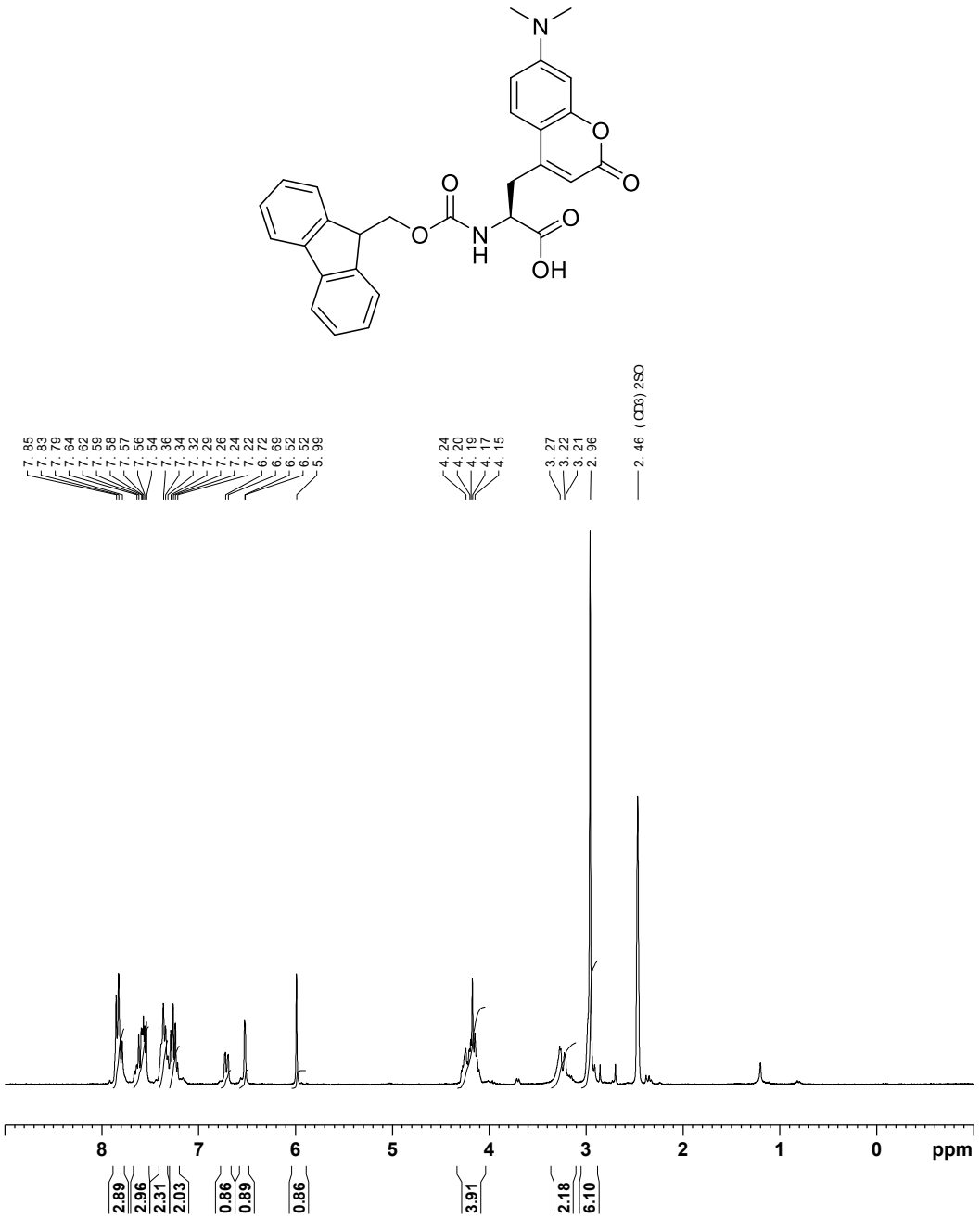

Figure C.20 ^{1}H NMR ($(CD_3)_2SO$, 300 MHz) of Fmoc-DMACA (4.18)

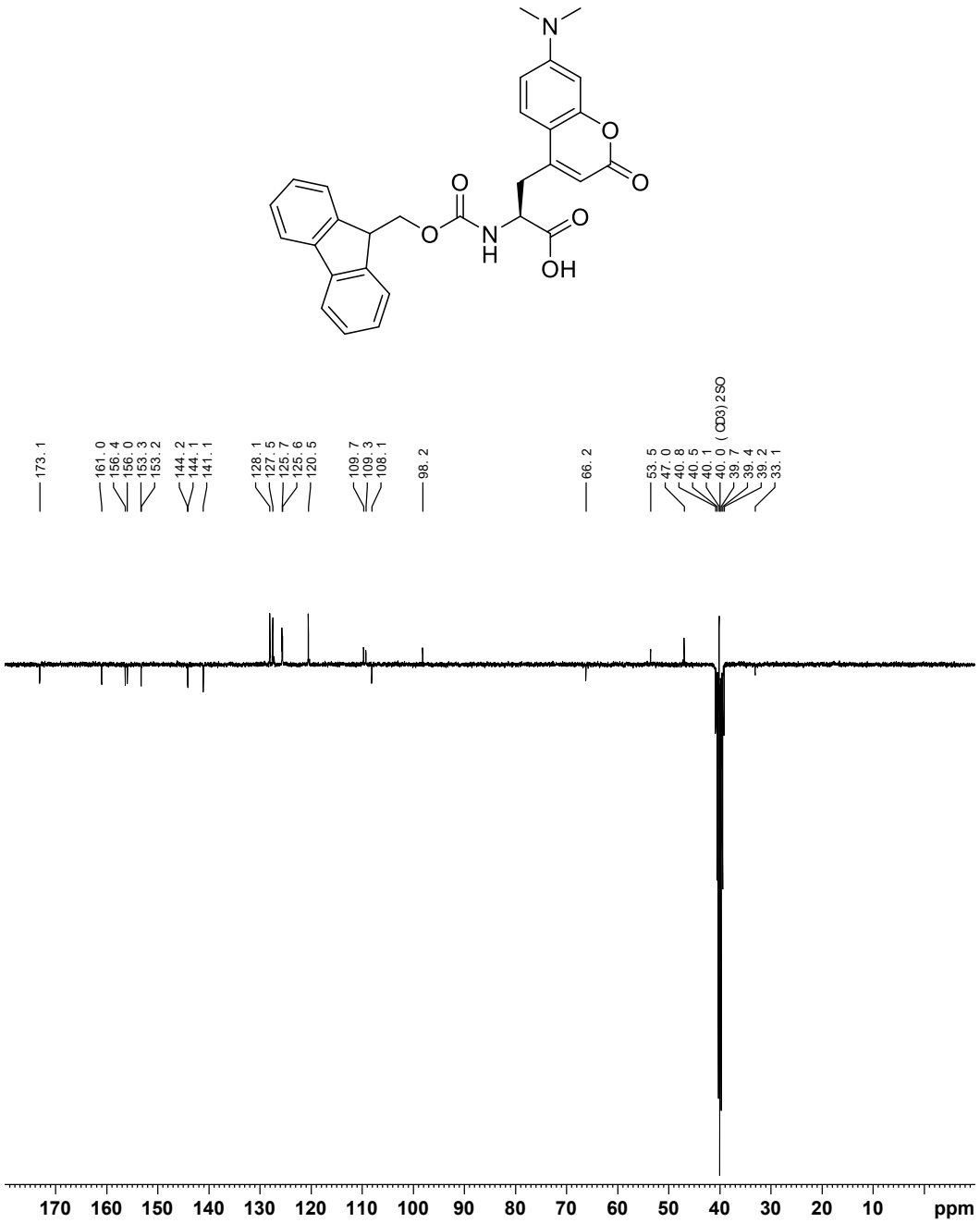

Figure C.21 $^{13}C\{^{1}H\}$ NMR ($(CD_3)_2SO$, 75 MHz) of Fmoc-DMACA (4.18)

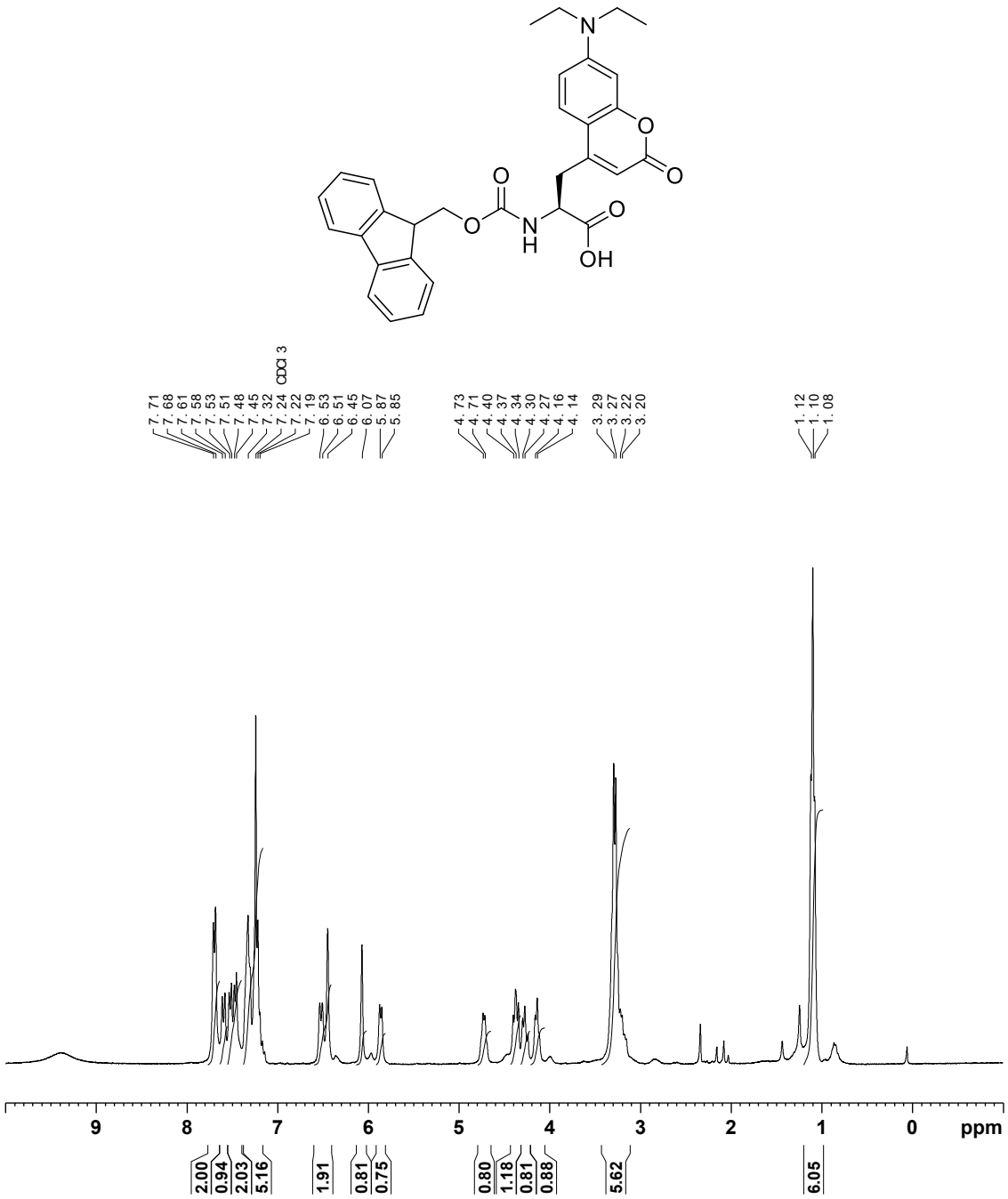

Figure C.22 ^{1}H NMR ($CDCl_3$, 300 MHz) of Fmoc-DEACA (4.19)

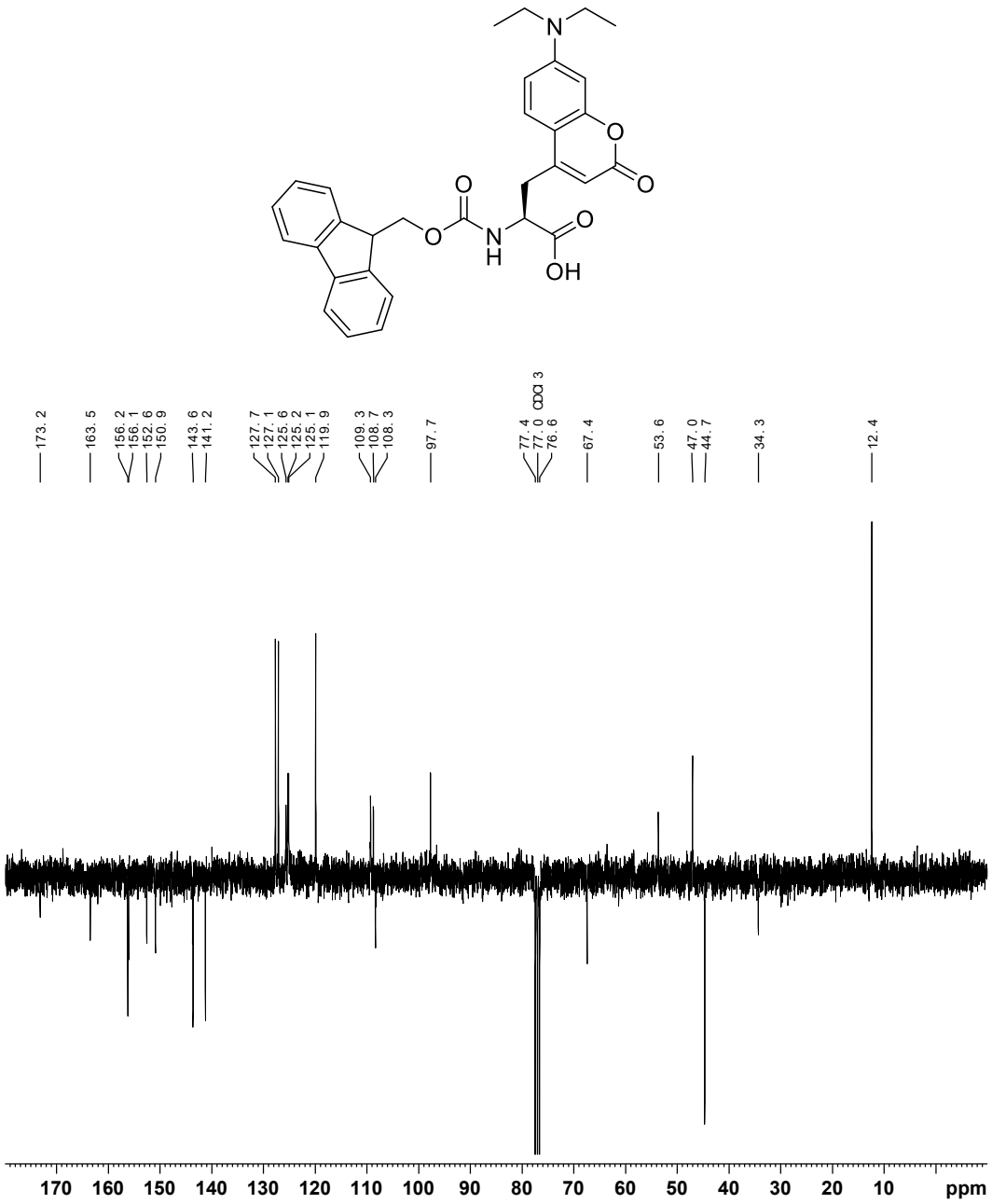

Figure C.23 $^{13}C\{^{1}H\}$ NMR ($CDCl_3$,75 MHz) of Fmoc-DEACA (4.19)

Figure C.24 ^{1}H NMR ($(CD_3)_2SO$, 300 MHz) of Fmoc-D-Lys(Boc)-Ser($\Psi^{Me,Me}$Pro)-OH

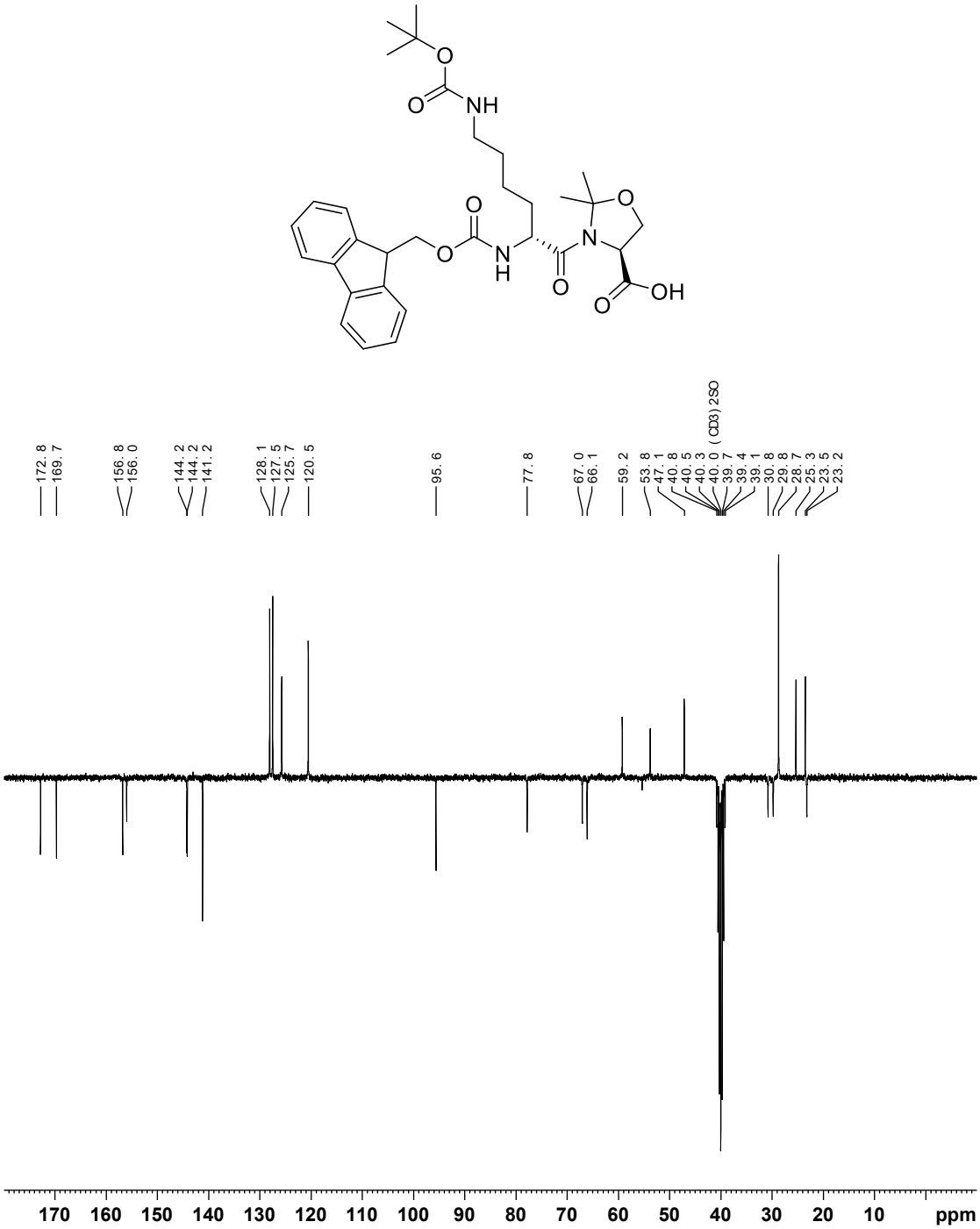

Figure C.25 $^{13}C\{^{1}H\}$ NMR ($(CD_3)_2SO$, 75 MHz) of Fmoc-D-Lys(Boc)-Ser($\Psi^{Me,Me}$Pro)-OH

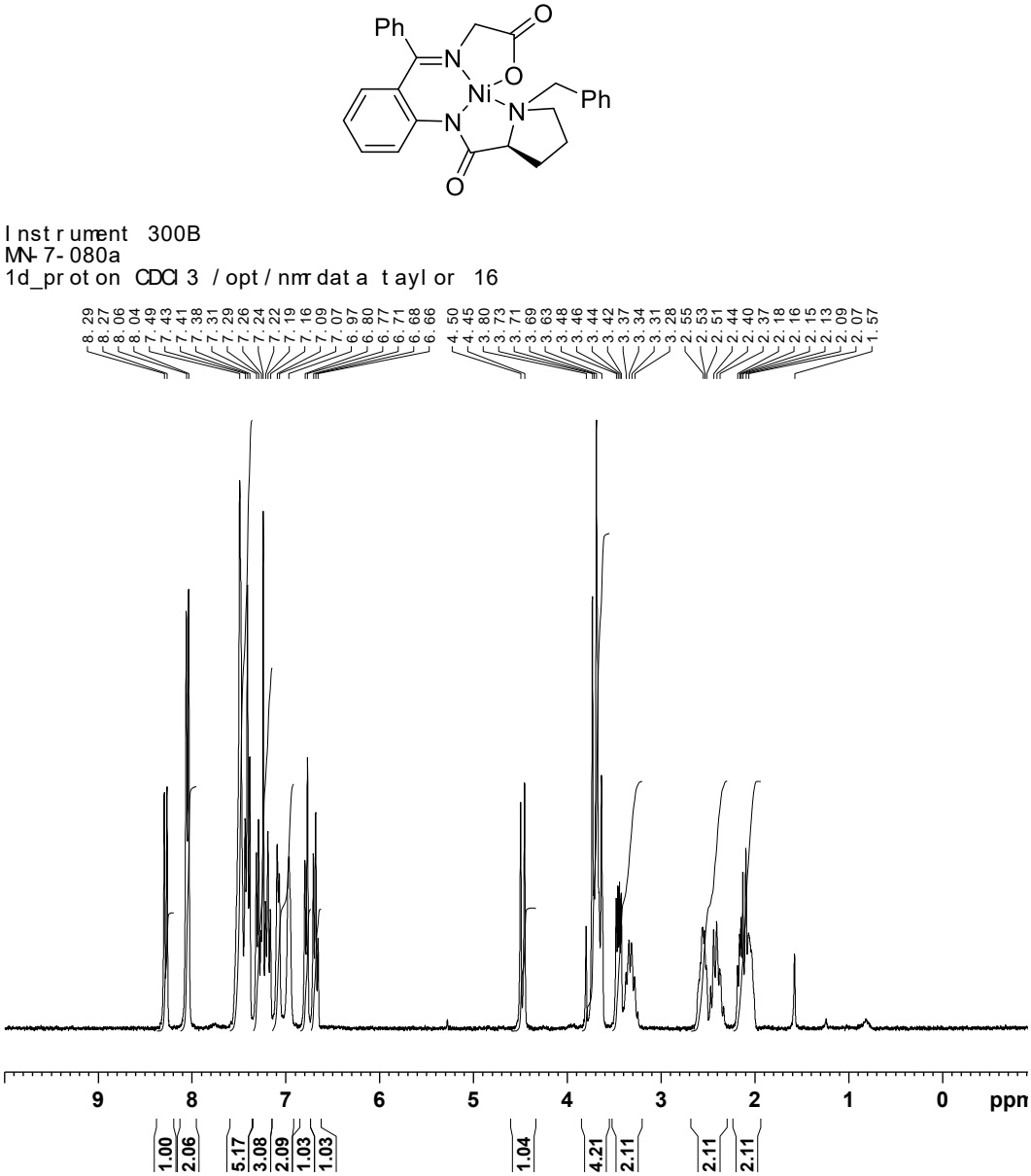

Figure C.26 ^{1}H NMR ($CDCl_3$, 300 MHz) of compound 4.15

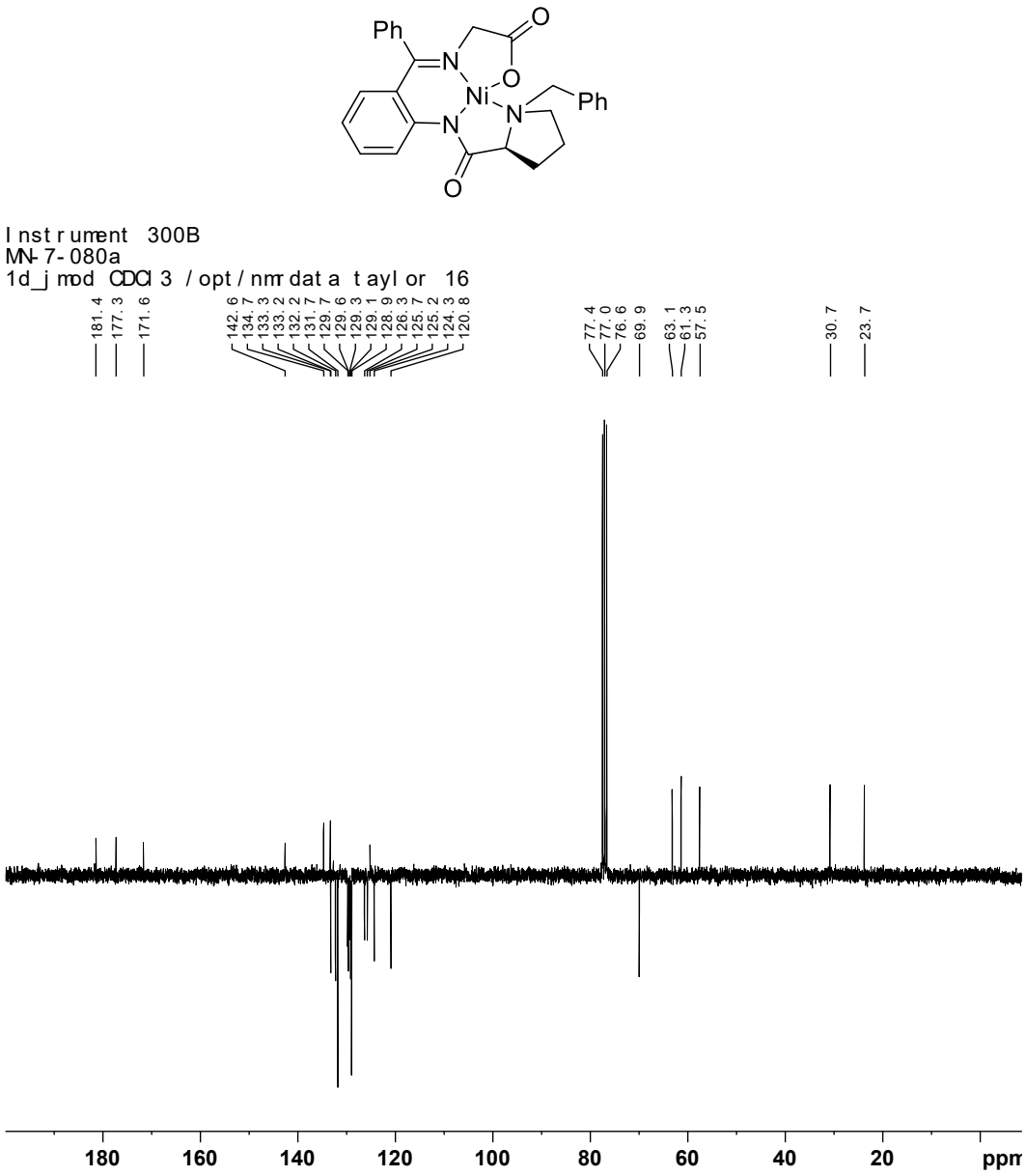

Figure C.27 $^{13}C\{^{1}H\}$ NMR ($CDCl_3$,75 MHz) of compound 4.15

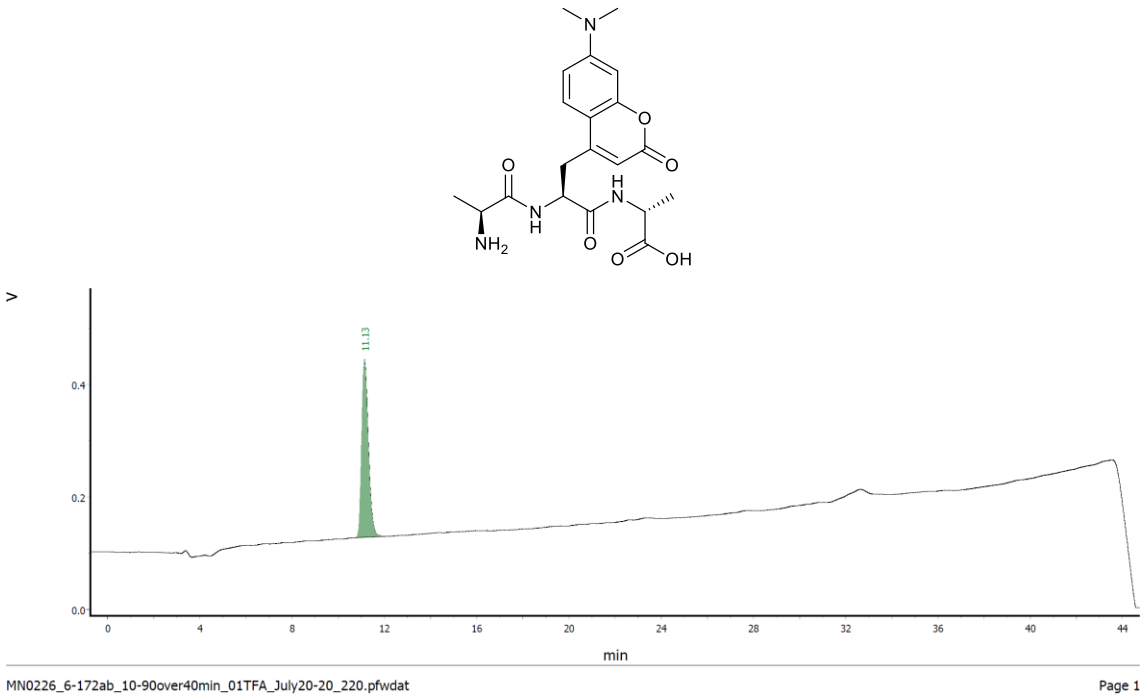

Figure C.28 Analytical RP-HPLC of Ala-DMACA-Ala (4.20). Linear gradient of 10:90 to 90:10 MeCN/H_2O (0.1% TFA) over 40 min (λ = 220 nm). C18 proto, 5 µm, 250 × 4.6 mm.

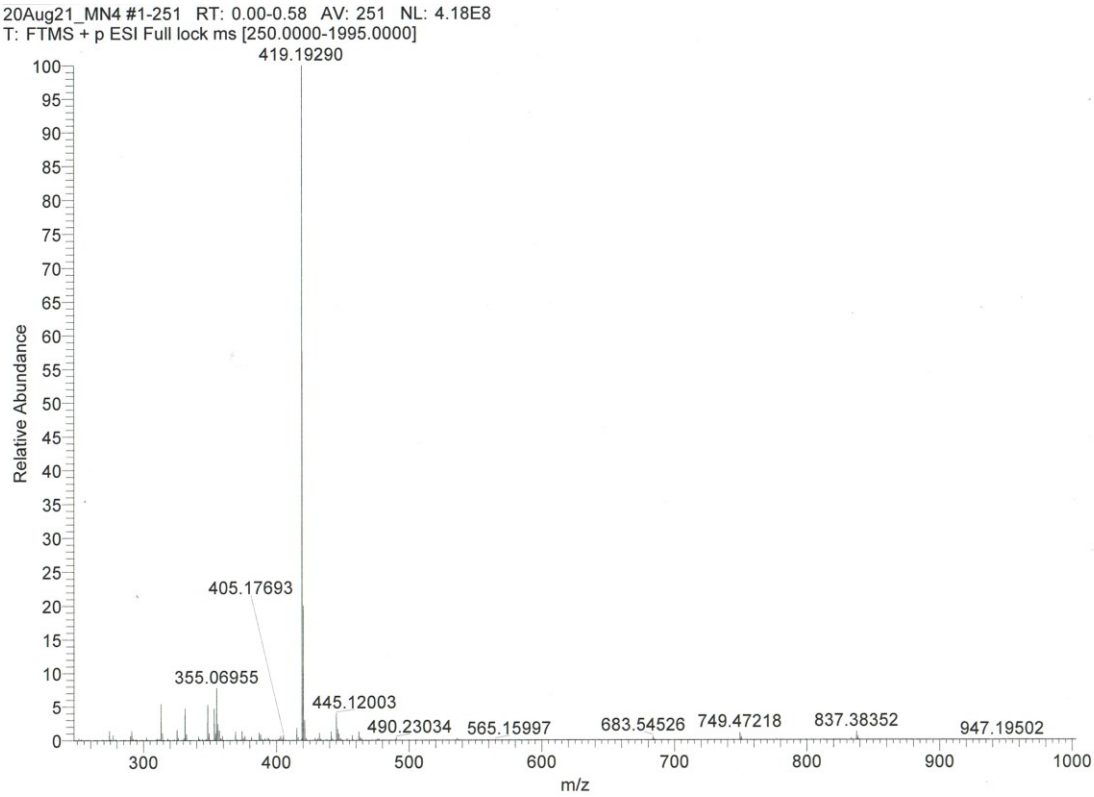

Figure C.29 HRMS (ESI+) of Ala-DMACA-Ala (4.20).

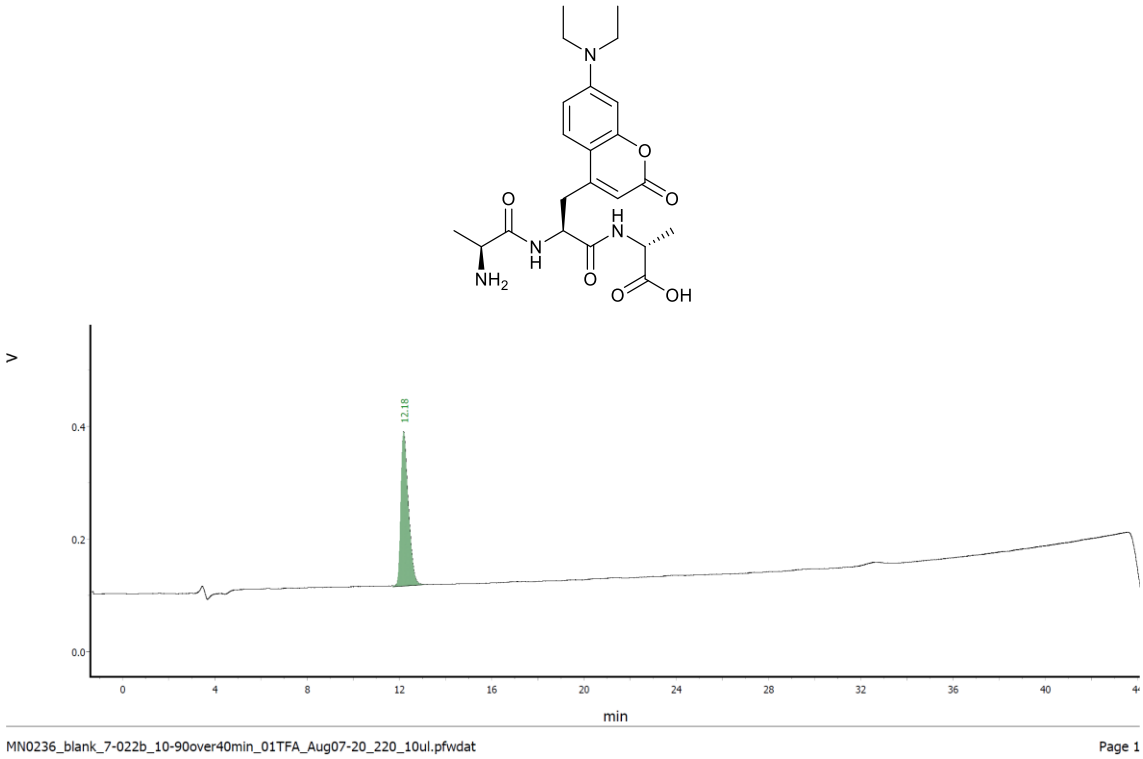

Figure C.30 Analytical RP-HPLC of Ala-DEACA-Ala (4.21). Linear gradient of 10:90 to 90:10 MeCN/H_2O (0.1% TFA) over 40 min (λ = 220 nm); C18 proto, 5 µm, 250 × 4.6 mm.

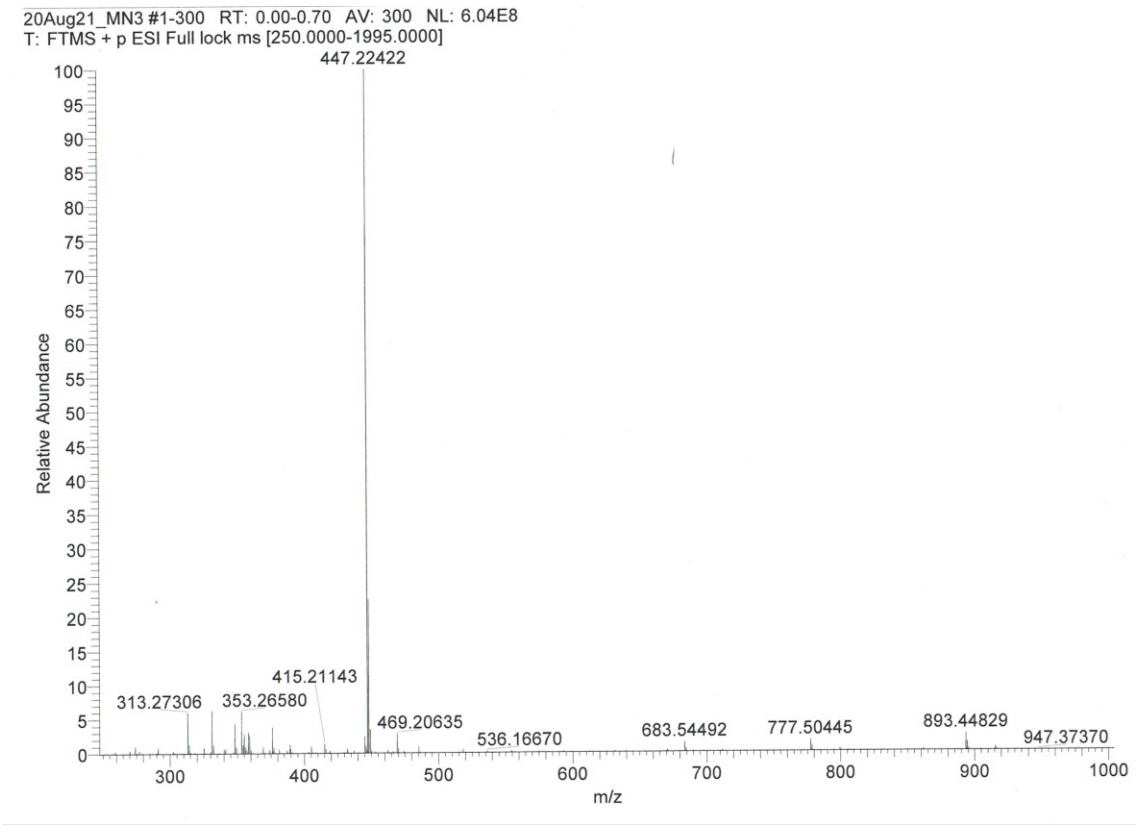

Figure C.31 HRMS (ESI+) of Ala-DEACA-Ala (4.21).

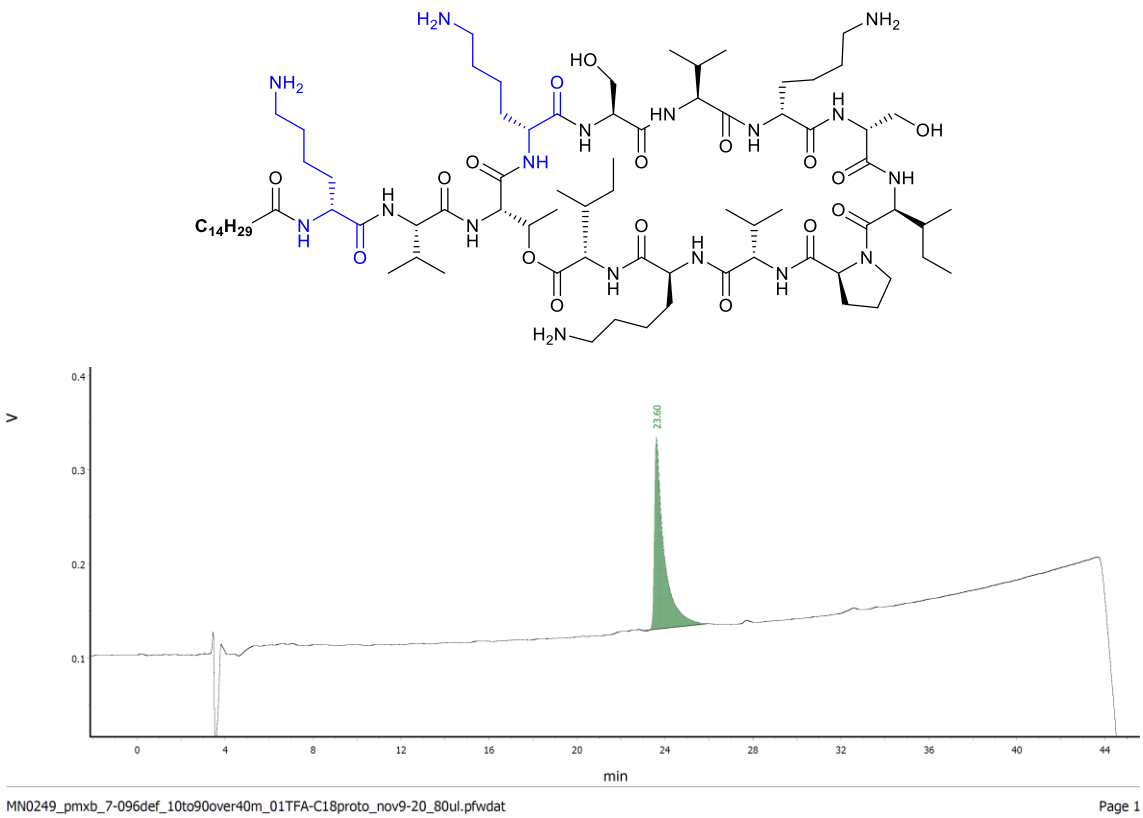

Figure C.32 Analytical RP-HPLC of PA1-D-K1-D-K4 (4.25). Linear gradient of 10:90 to 90:10 MeCN/H_2O (0.1% TFA) over 40 min (λ = 220 nm). C18 proto, 5 µm, 250 × 4.6 mm.

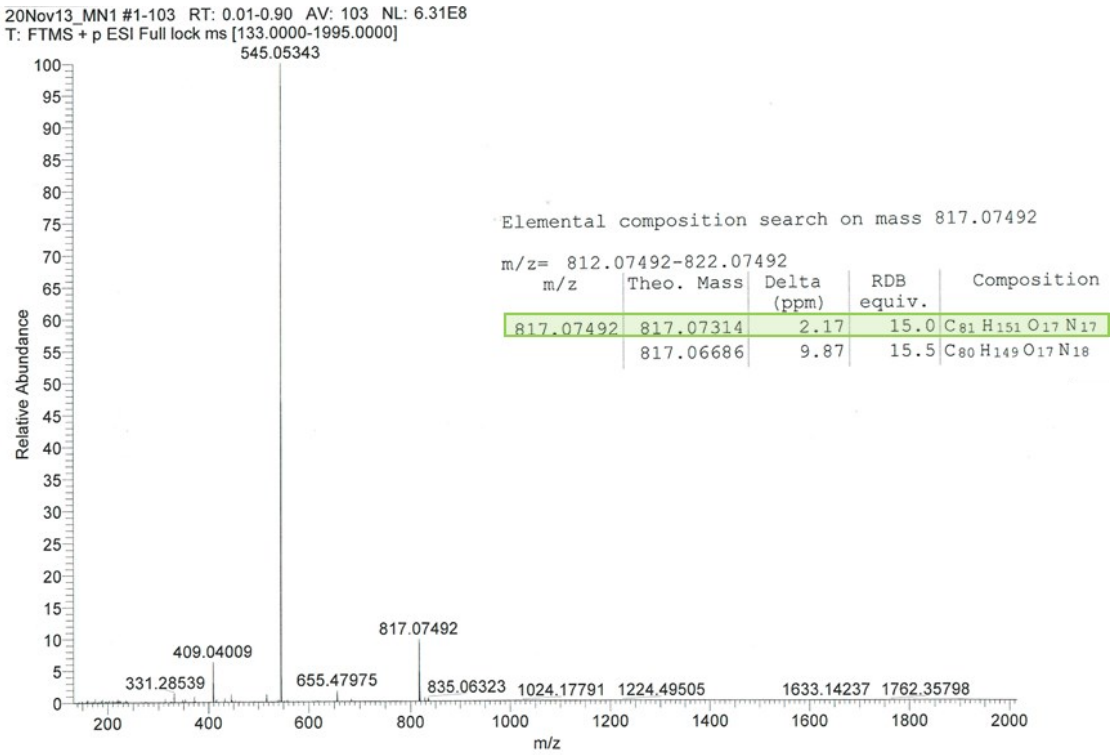

Figure C.33 HRMS (+ESI) of PA1-D-K1-D-K4 (4.25).

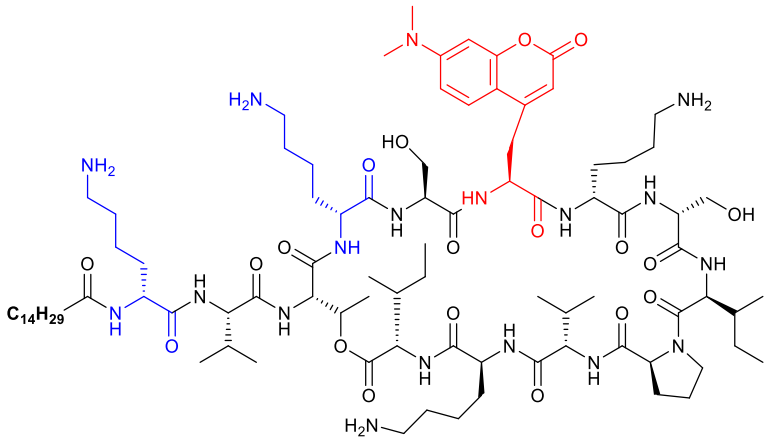

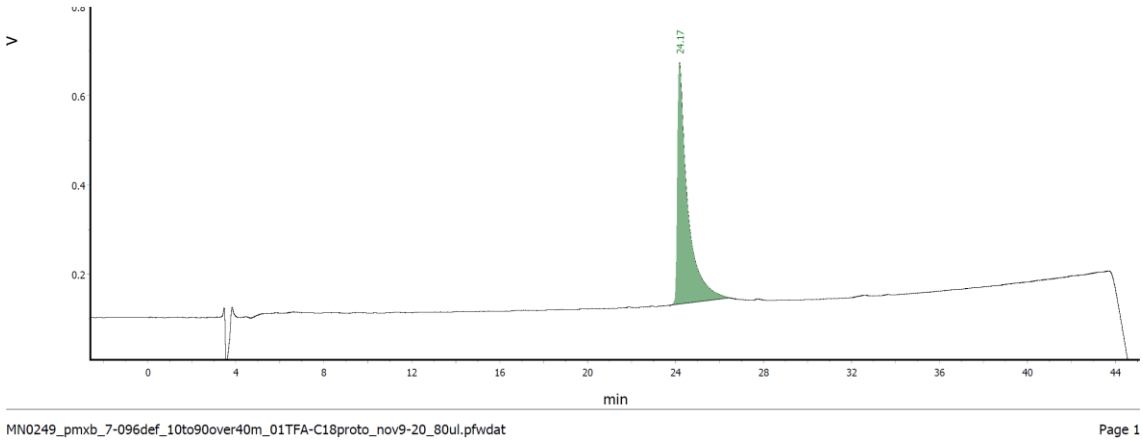

Figure C.34 Analytical RP-HPLC of PA1-D-K1-D-K4-DMACA6 (4.26). Linear gradient of 10:90 to 90:10 MeCN/H_2O (0.1% TFA) over 40 min (λ = 220 nm). C18 proto, 5 µm, 250 × 4.6 mm.

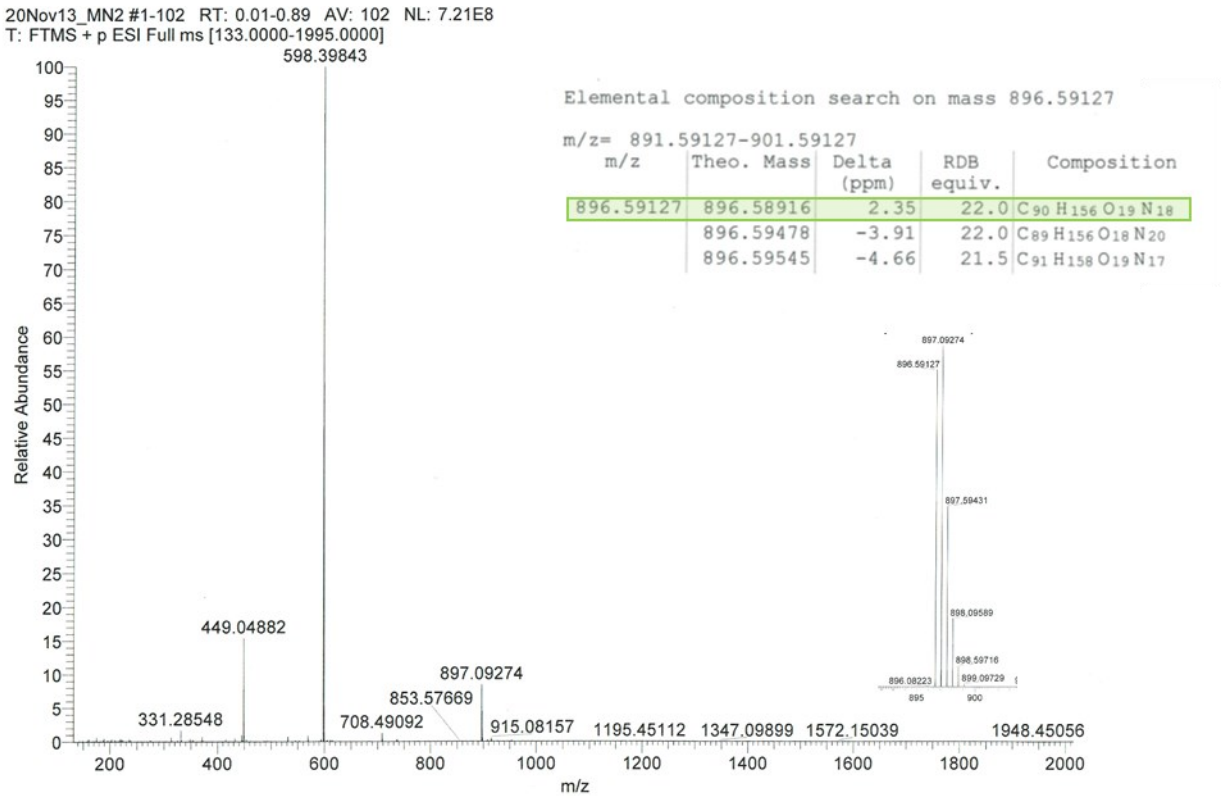

Figure C.35 HRMS (+ESI) of PA1-D-K1-D-K4-DMACA6 (4.26).

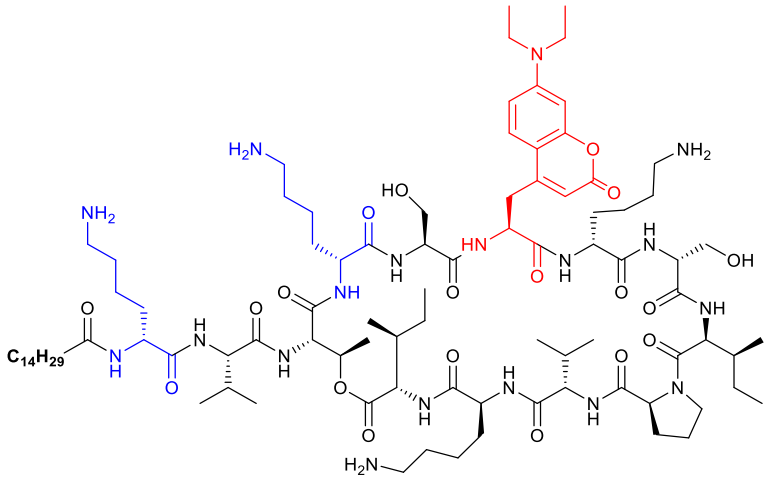

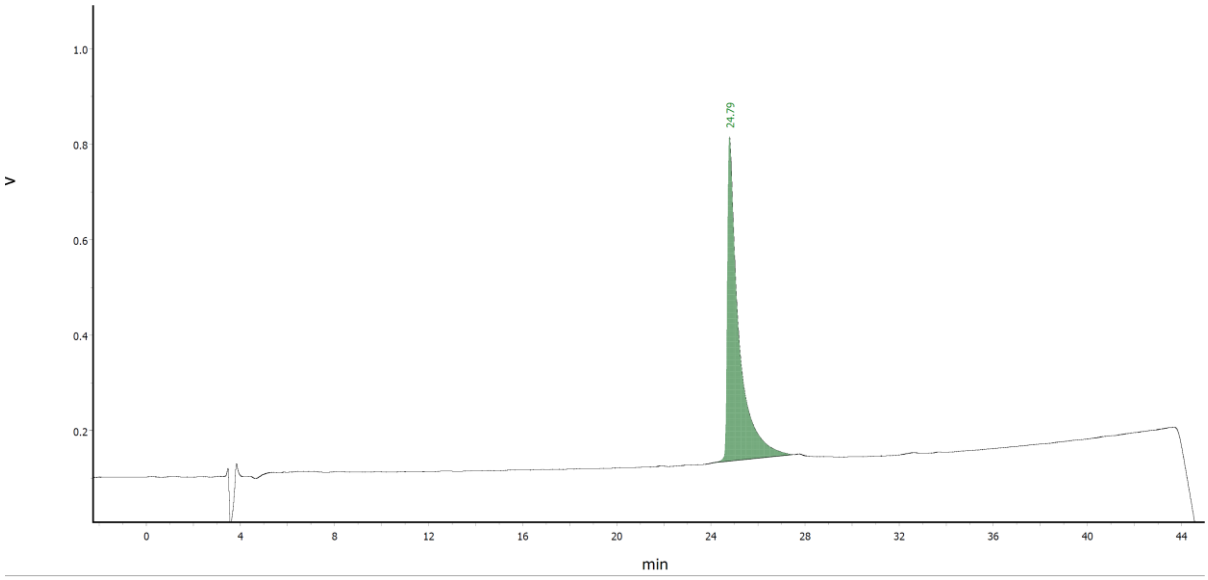

Figure C.36 Analytical RP-HPLC of PA1-D-K1-D-K4-DEACA6 (4.27). Linear gradient of 10:90 to 90:10 MeCN/H_2O (0.1% TFA) over 40 min (λ = 220 nm). C18 proto, 5 µm, 250 × 4.6 mm.

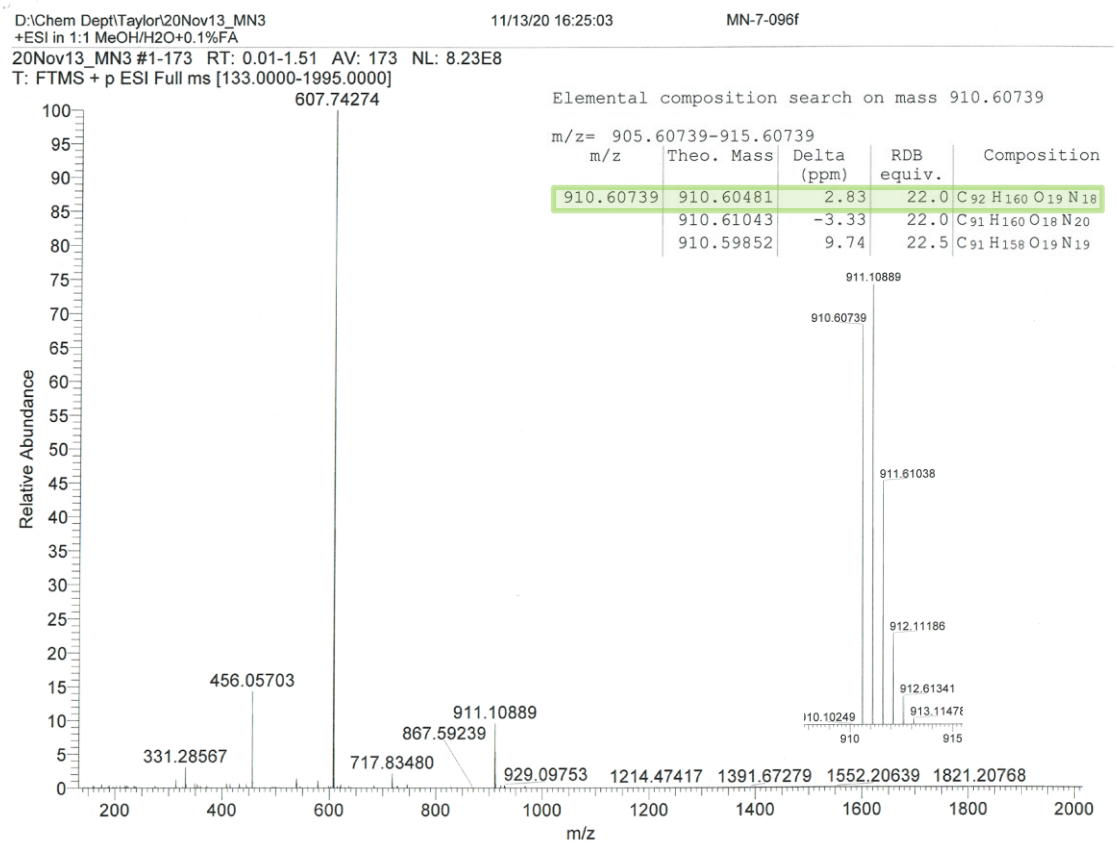

Figure C.37 HRMS (+ESI) of PA1-D-K1-D-K4-DMACA6 (4.27).

Appendix D

Characterization and Fluorescence Data for Chapter 5 Compounds

D.1 HPLC and MS data for peptides

Table D.1 Summary of high resolution ESI-MS characterization data

Peptide	Formula [M]	*m/z* $[M+1H]^+$	*m/z* $[M+2H]^{+2}$	*m/z* $[M+3H]^{+3}$	Observed m/z	Δ ppm
Dap-K6k11E12W13	$C_{76}H_{108}N_{18}O_{24}$		829.39647		829.40028	4.59
Dap-K6h11E12W13	$C_{76}H_{103}N_{19}O_{24}$		833.87844		833.87527	-3.81
Dap-K6c11E12W13	$C_{73}H_{101}N_{17}O_{24}S$	1632.69988			1632.69641	-2.13
Dap-K6r11E12W13	$C_{76}H_{108}N_{20}O_{24}$		843.39954		843.40244	3.43
Dap-K6m8E12W13	$C_{75}H_{105}N_{17}O_{25}S$	1676.72610			1676.72042	-3.39
Dap-K6p8E12W13	$C_{75}H_{103}N_{17}O_{25}$	1642.73838			1642.73213	-3.80
Dap-K6y8E12W13	$C_{79}H_{105}N_{17}O_{26}$	1708.74894			1708.74238	-3.84
Dap-K6v8E12W13	$C_{75}H_{105}N_{17}O_{25}$	1644.75403			1644.75111	-1.77
Dap-K6c8E12W13	$C_{73}H_{101}N_{17}O_{25}S$	1648.69480			1648.68909	-3.46
Dap-K6s8E12W13	$C_{73}H_{101}N_{17}O_{26}$	1632.71764			1632.71123	-3.93
Dap-K6w8E12W13	$C_{81}H_{106}N_{18}O_{25}$	1731.76493			1731.76000	-2.85
Dap-K6q8E12W13	$C_{75}H_{104}N_{18}O_{26}$	1673.74419			1673.74016	-2.41
Dap-K6e8E12W13	$C_{75}H_{103}N_{17}O_{27}$		837.86774		837.87181	4.86
Dap-K6h8E12W13	$C_{76}H_{103}N_{19}O_{25}$		841.87590		841.88003	4.90
Dap-K6r8E12W13	$C_{76}H_{108}N_{20}O_{25}$		851.39700		851.39890	2.23
Dap-K6n8E12W13	$C_{74}H_{102}N_{18}O_{26}$	1659.72854			1659.72175	-4.09
Dap-K6k8E12W13	$C_{76}H_{108}N_{18}O_{25}$		837.39393		837.39271	-1.45
Dap-K6k8r11E12W13	$C_{79}H_{115}N_{21}O_{24}$		871.92847		871.92653	-2.22
Dap-K6o8E12W13	$C_{75}H_{106}N_{18}O_{25}$		830.38610		830.38885	3.31
Dap-K6o8r11E12W13	$C_{78}H_{113}N_{21}O_{24}$		864.92064		864.91714	-4.05
Dap-K6(nva8)E12W13	$C_{75}H_{105}N_{17}O_{25}$		822.88065		822.87674	-4.75
Dap-K6(abu8)E12W13	$C_{74}H_{103}N_{17}O_{25}$		815.87283		815.87396	1.39
Dap-K6r8r11E12W13	$C_{79}H_{115}N_{23}O_{24}$		885.93154		885.92928	-2.55
Dap-K6(Sar8)E12W13	$C_{73}H_{101}N_{17}O_{25}$		808.86500		808.86197	-3.75
Dap-K6G8E12W13	$C_{72}H_{99}N_{17}O_{25}$		801.85718		801.85344	-4.66
Dap-N3K6k8r11Q12W13	$C_{79}H_{117}N_{23}O_{22}$			580.96539	580.96648	1.87

Note: *lower-case letters indicate the amino acid has D-stereochemistry*

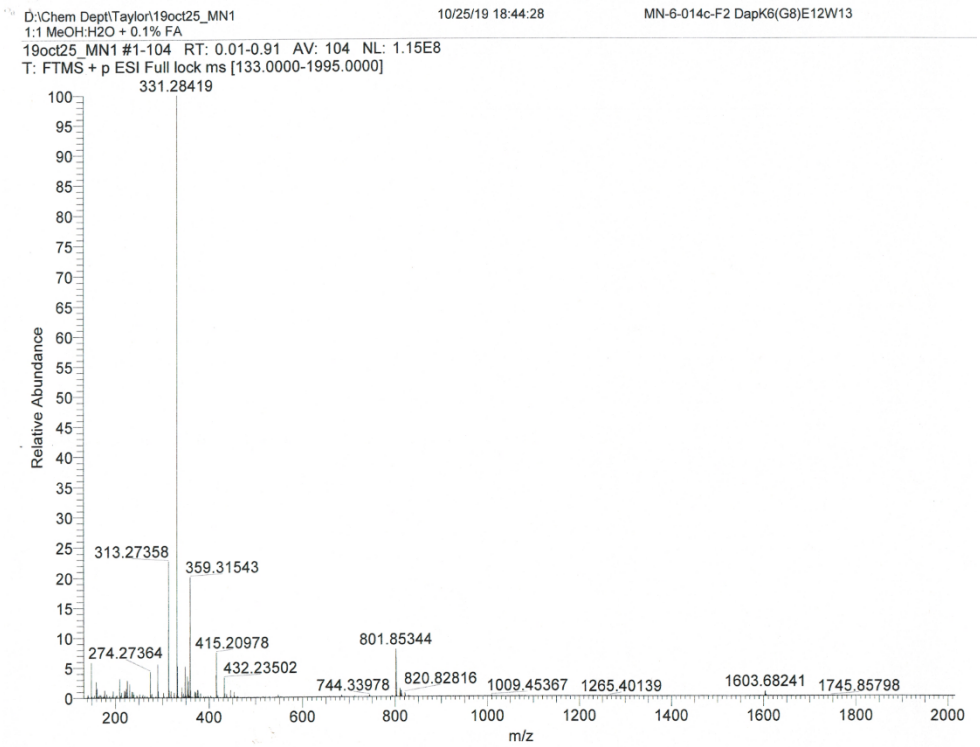

Figure D.1 HRMS (+ESI) of Dap-K6-(G8)-E12-W13

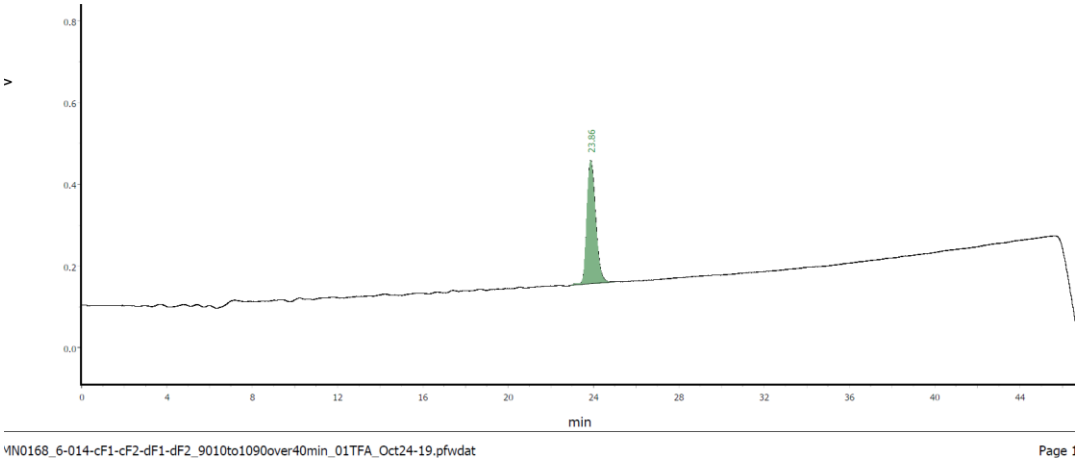

Figure D.2 Analytical RP-HPLC of Dap-K6-(G8)-E12-W13 Linear gradient of 10:90 CH_3CN:H_2O (0.1% TFA) to 90:10 CH_3CN:H_2O (0.1% TFA) over 40 min (λ = 220 nm)

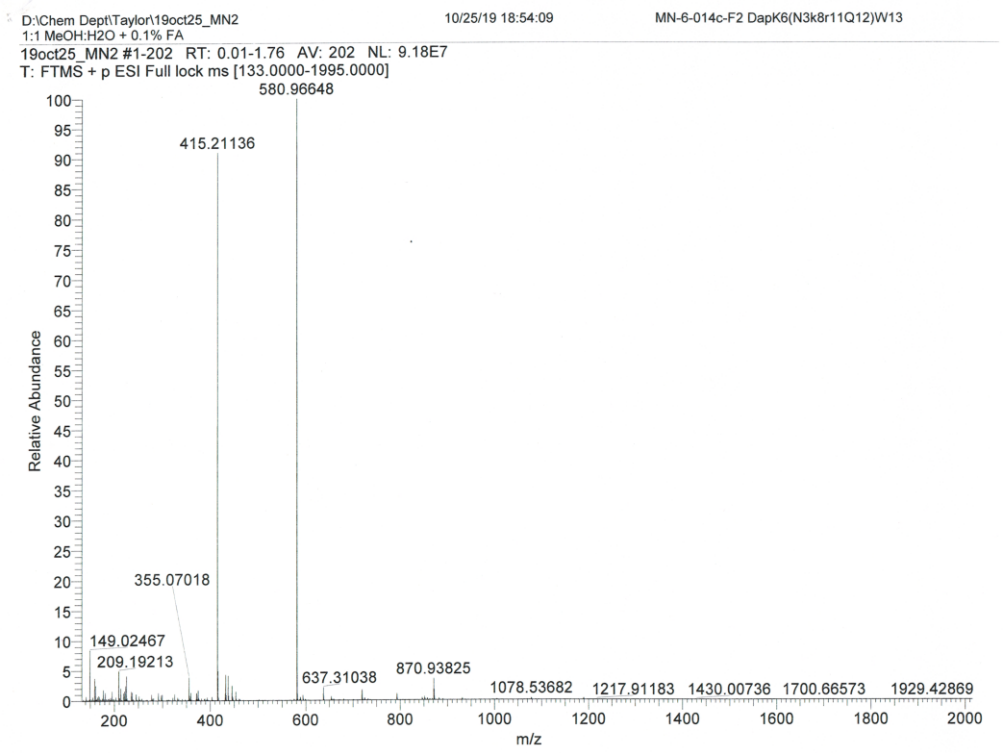

Figure D.3 HRMS (+ESI) of Dap-N3-K6-(D-K8, D-R11)-Q12-W13

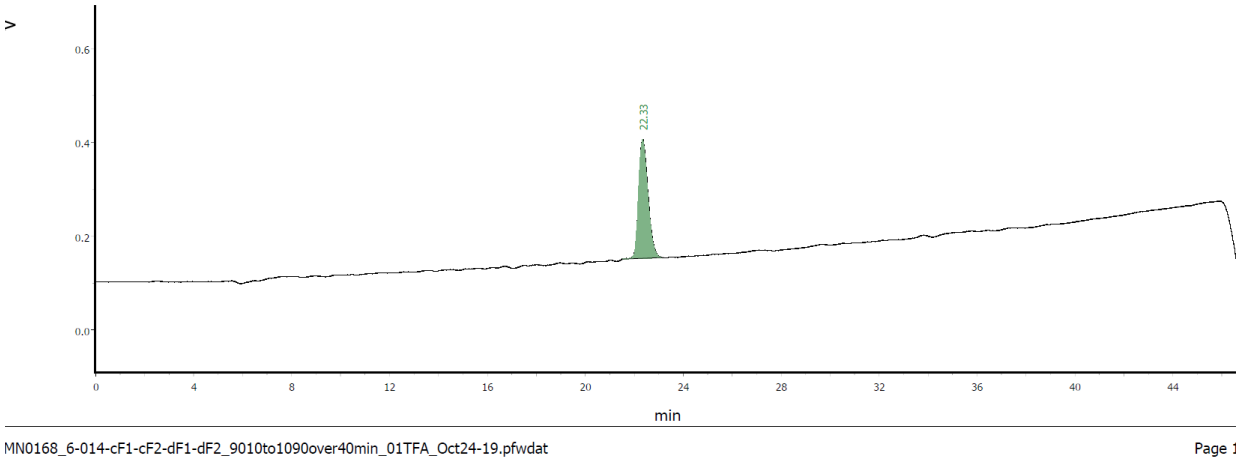

Figure D.4 Analytical RP-HPLC of Dap-N3-K6-(D-K8, D-R11)-Q12-W13 Linear gradient of 10:90 CH_3CN:H_2O (0.1% TFA) to 90:10 CH_3CN:H_2O (0.1% TFA) over 40 min (λ = 220 nm)

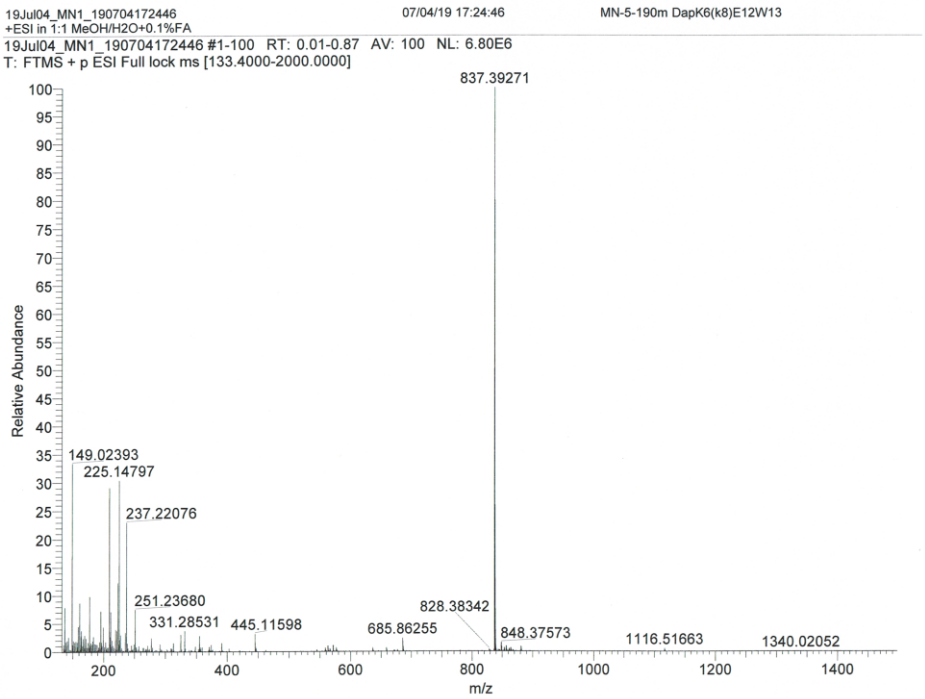

Figure D.5 HRMS (+ESI) of Dap-K6-(D-K8)-E12-W13

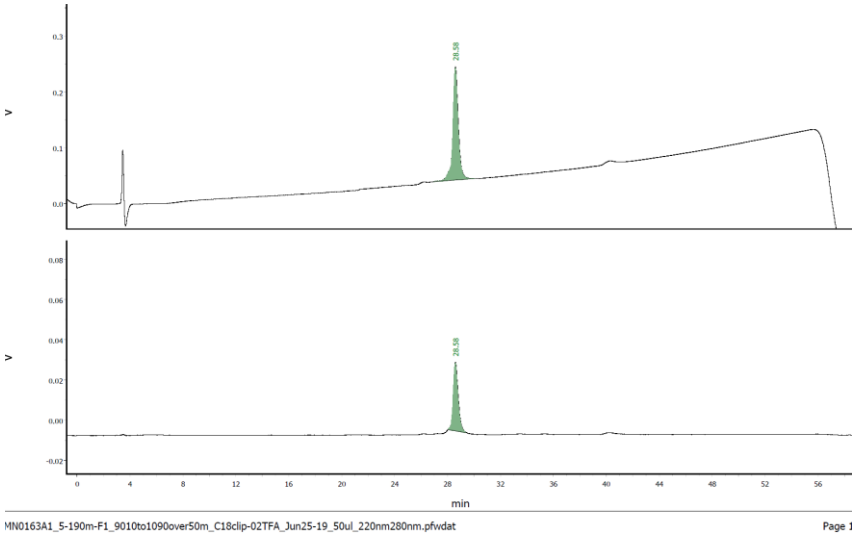

Figure D.6 Analytical RP-HPLC of Dap-K6-(D-K8)-E12-W13 Linear gradient of 10:90 CH_3CN:H_2O (0.1% TFA) to 90:10 CH_3CN:H_2O (0.1% TFA) over 50 min (λ_{top} = 220 nm, λ_{bottom} = 280 nm)

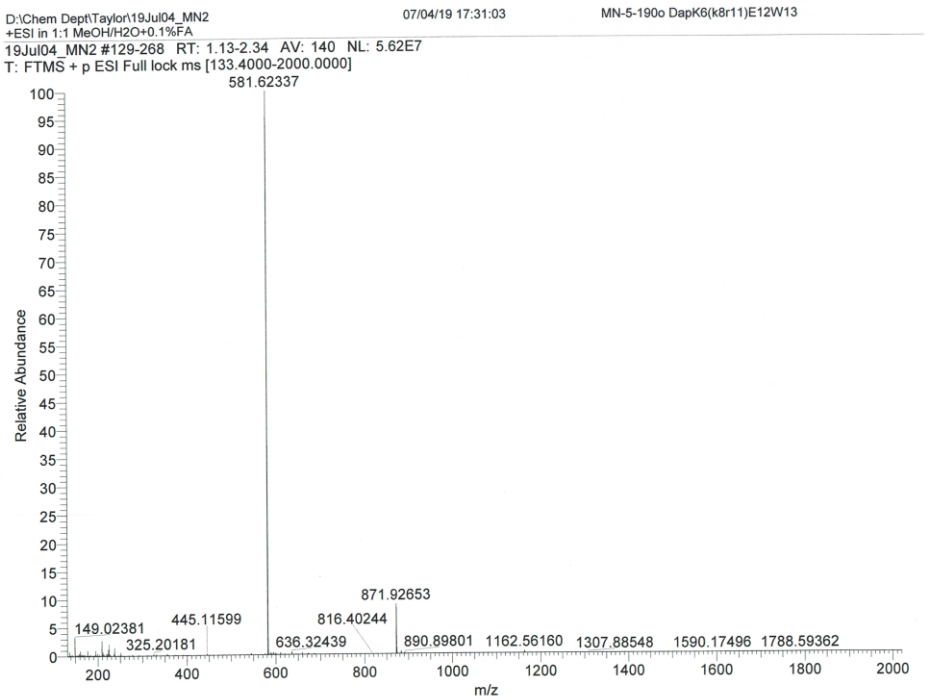

Figure D.7 HRMS (+ESI) of Dap-K6-(D-K8, D-R11)-E12-W13

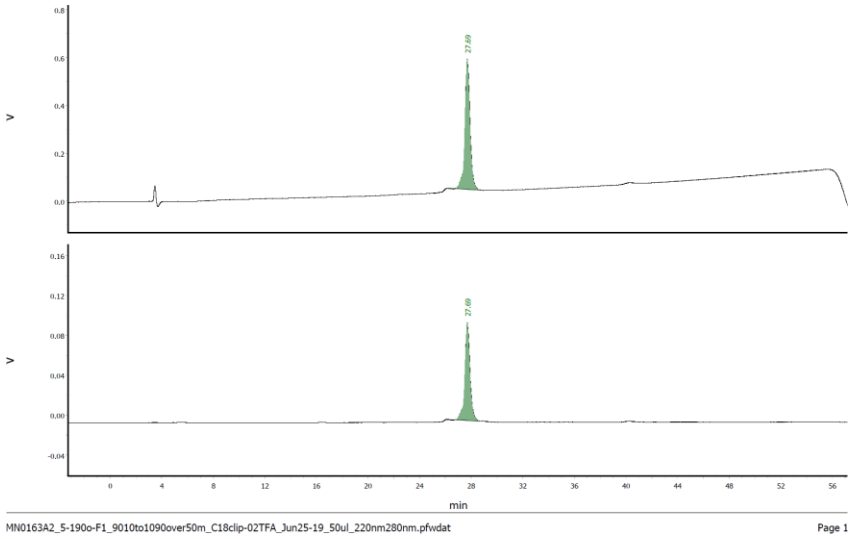

Figure D.8 Analytical RP-HPLC of Dap-K6-(D-K8, D-R11)-E12-W13 Linear gradient of 10:90 $CH_3CN:H_2O$ (0.1% TFA) to 90:10 $CH_3CN:H_2O$ (0.1% TFA) over 50 min (λ_{top} = 220 nm, λ_{bottom} = 280 nm)

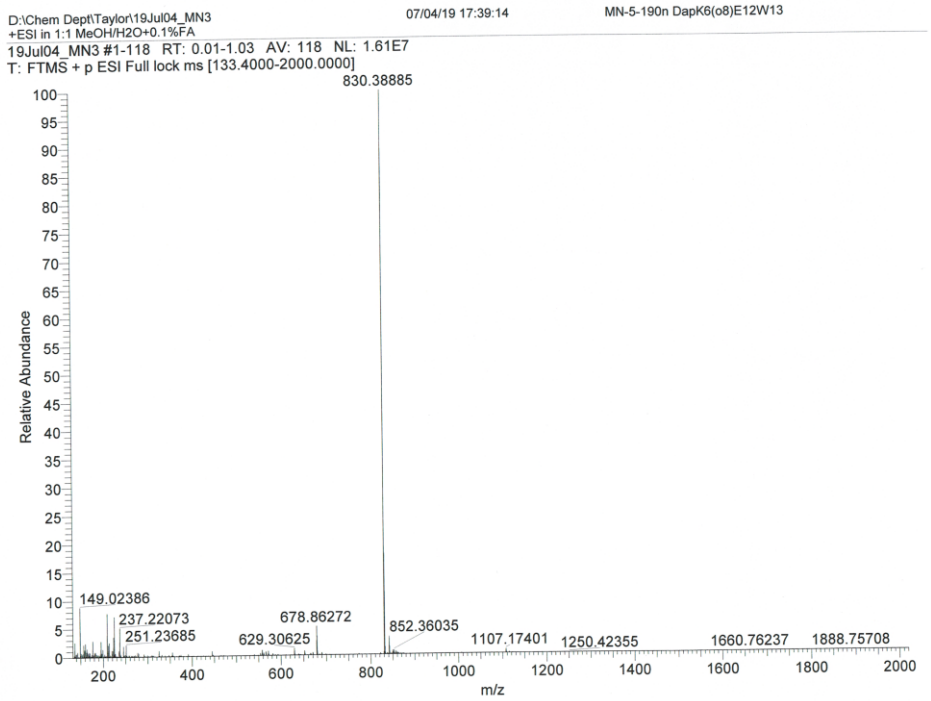

Figure D.9 HRMS (+ESI) of Dap-K6-(D-Orn8)-E12-W13

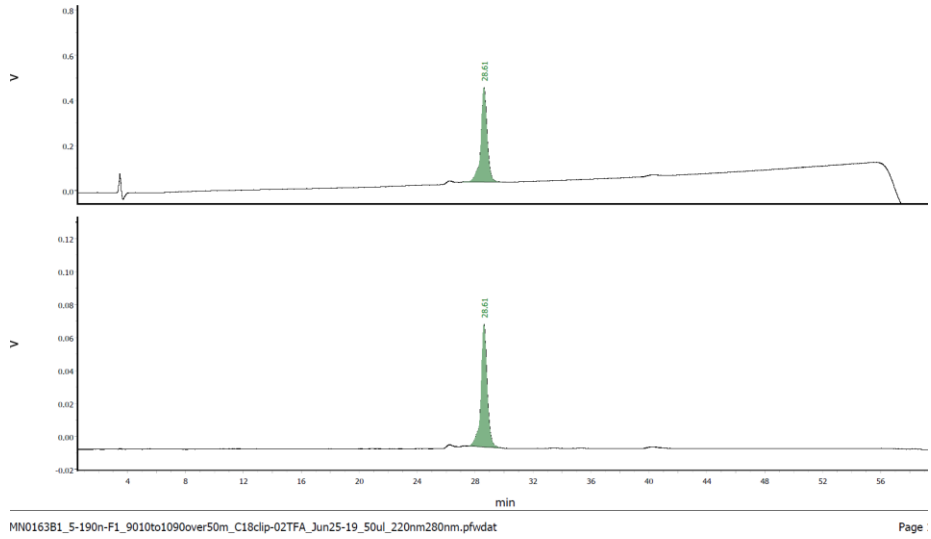

Figure D.10 Analytical RP-HPLC of Dap-K6-(D-Orn8)-E12-W13 Linear gradient of 10:90 $CH_3CN:H_2O$ (0.1% TFA) to 90:10 $CH_3CN:H_2O$ (0.1% TFA) over 50 min (λ_{top} = 220 nm, λ_{bottom} = 280 nm)

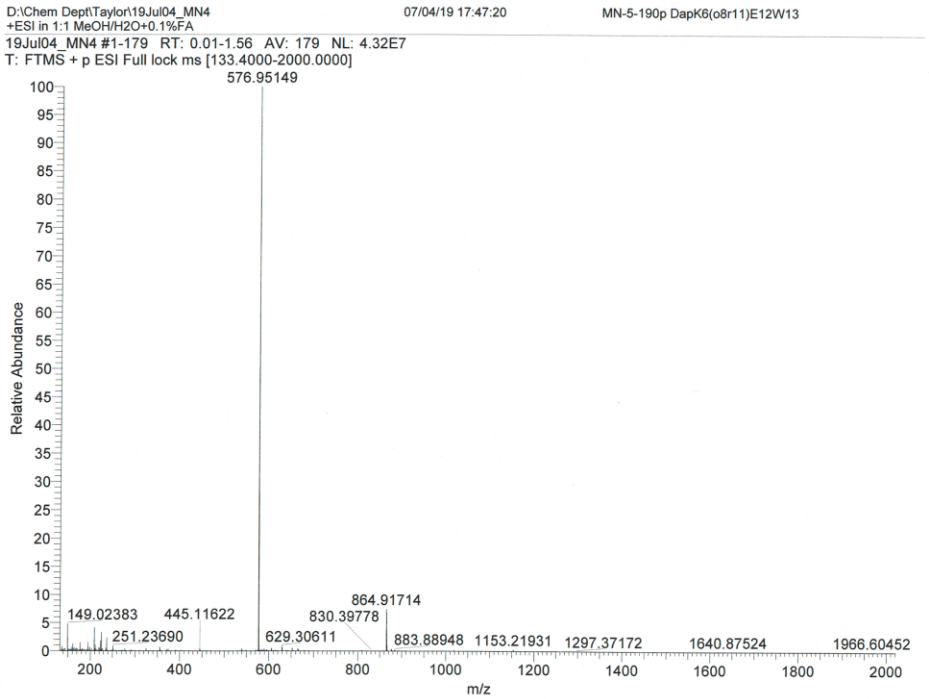

Figure D.11 HRMS (+ESI) of Dap-K6-(D-Orn8, D-R11)-E12-W13

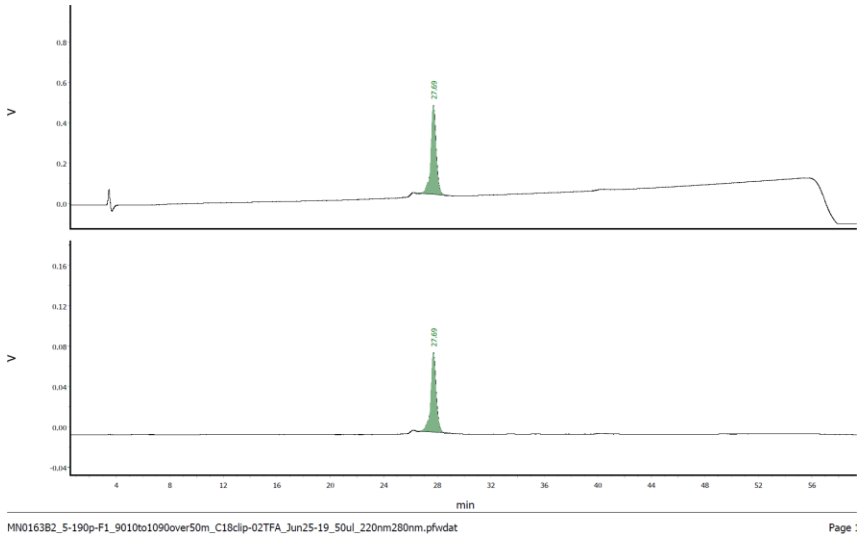

Figure D.12 Analytical RP-HPLC of Dap-K6-(D-Orn8, D-R11)-E12-W13 Linear gradient of 10:90 CH_3CN:H_2O (0.1% TFA) to 90:10 CH_3CN:H_2O (0.1% TFA) over 50 min (λ_{top} = 220 nm, λ_{bottom} = 280 nm)

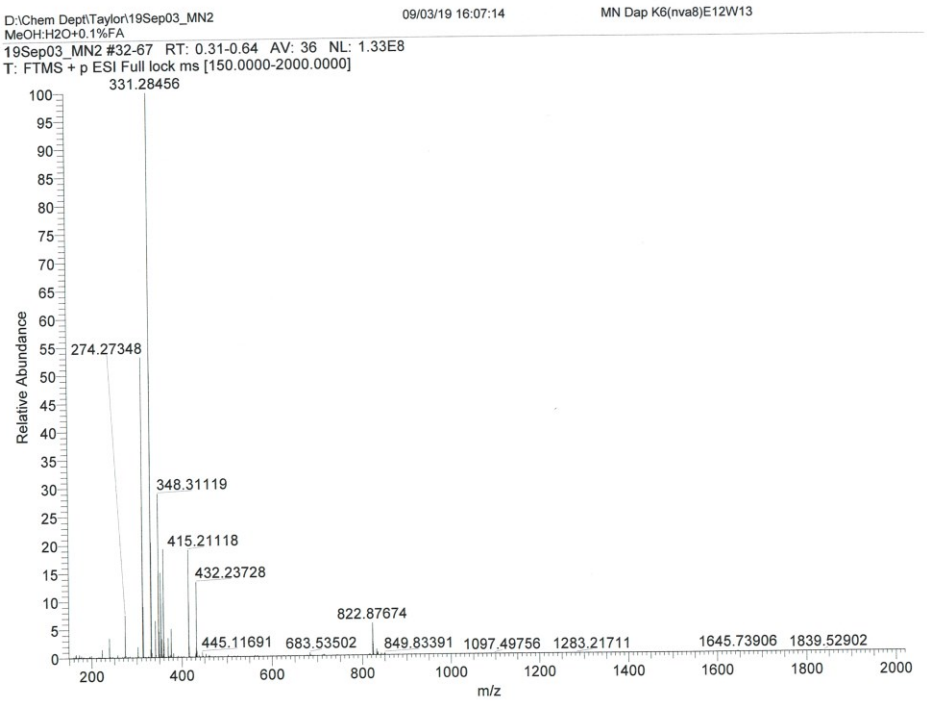

Figure D.13 HRMS (+ESI) of Dap-K6-(D-Nva8)-E12-W13

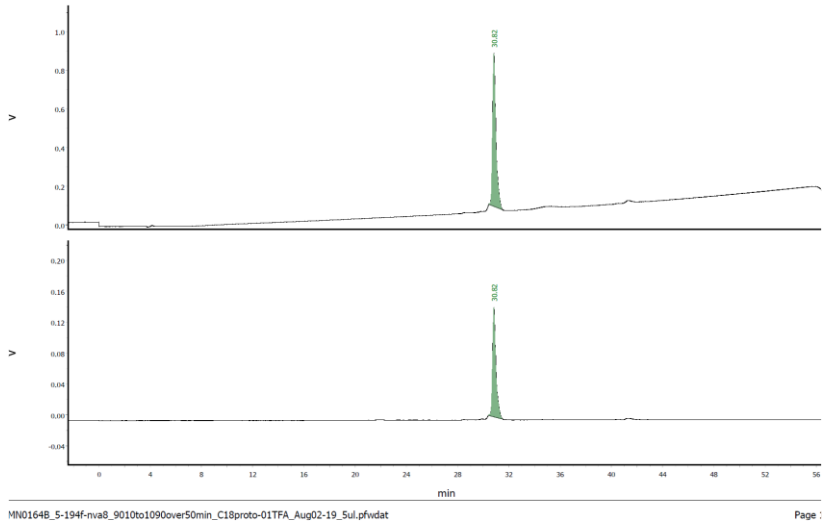

Figure D.14 Analytical RP-HPLC of Dap-K6-(D-Nva8)-E12-W13 Linear gradient of 10:90 $CH_3CN:H_2O$ (0.1% TFA) to 90:10 $CH_3CN:H_2O$ (0.1% TFA) over 50 min (λ_{top} = 220 nm, λ_{bottom} = 280 nm)

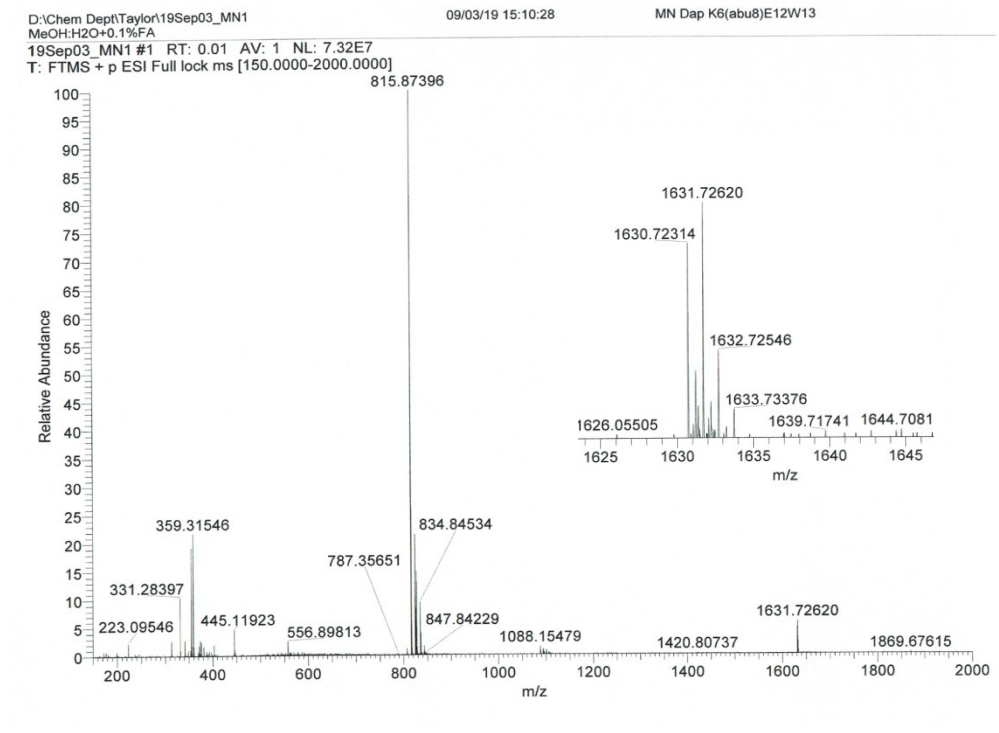

Figure D.15 HRMS (+ESI) of Dap-K6-(D-Abu8)-E12-W13

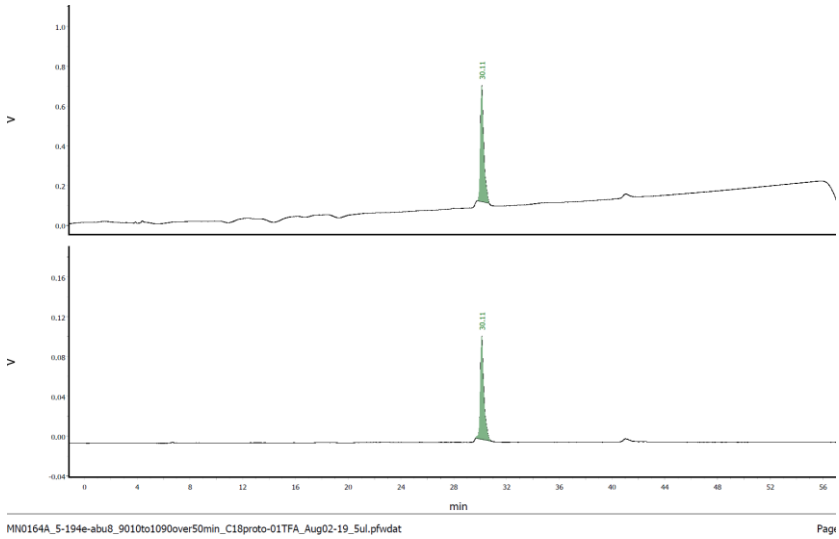

Figure D.16 Analytical RP-HPLC of Dap-K6-(D-Abu8)-E12-W13 Linear gradient of 10:90 $CH_3CN:H_2O$ (0.1% TFA) to 90:10 $CH_3CN:H_2O$ (0.1% TFA) over 50 min (λ_{top} = 220 nm, λ_{bottom} = 280 nm)

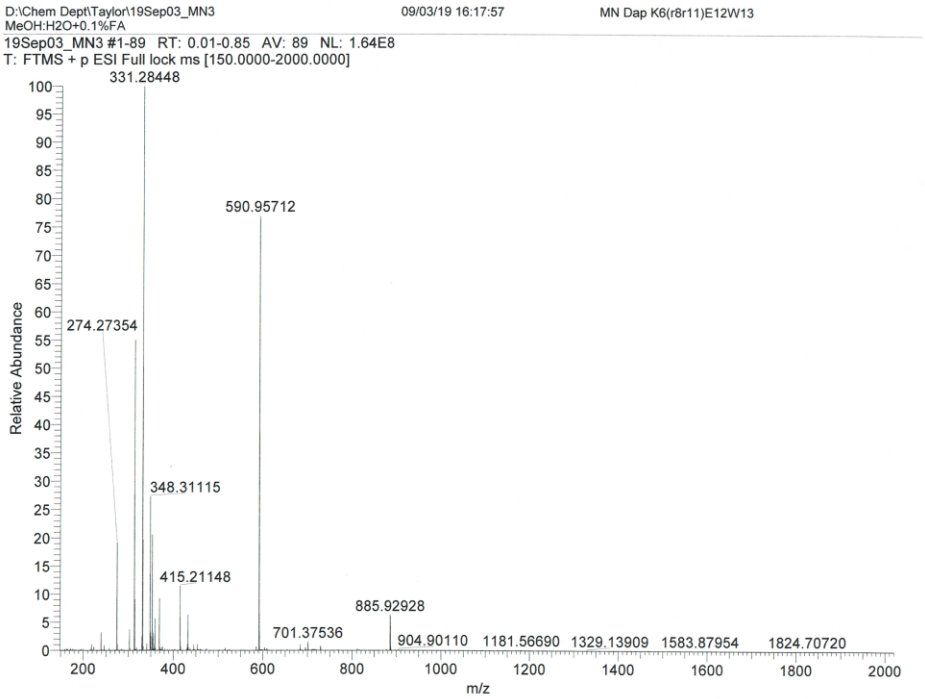

Figure D.17 HRMS (+ESI) of Dap-K6-(D-R8, D-R11)-E12-W13

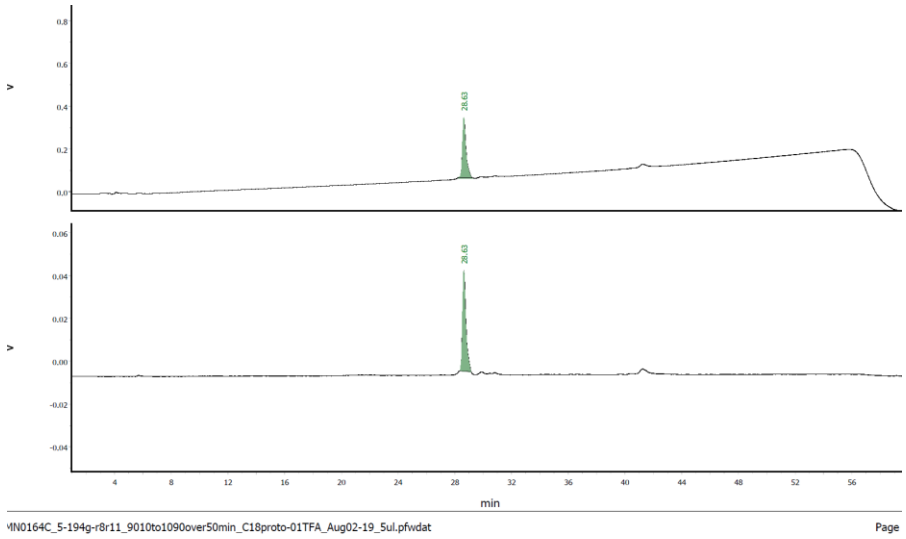

Figure D.18 Analytical RP-HPLC of Dap-K6-(D-R8, D-R11)-E12-W13 Linear gradient of 10:90 $CH_3CN:H_2O$ (0.1% TFA) to 90:10 $CH_3CN:H_2O$ (0.1% TFA) over 50 min (λ_{top} = 220 nm, λ_{bottom} = 280 nm)

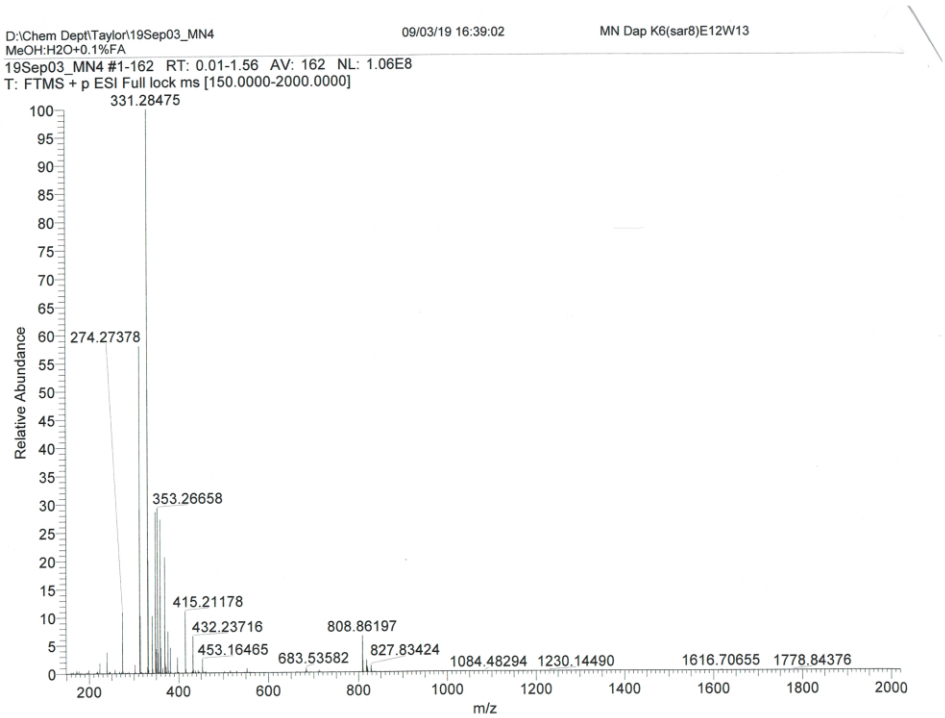

Figure D.19 HRMS (+ESI) of Dap-K6-(Sar8)-E12-W13

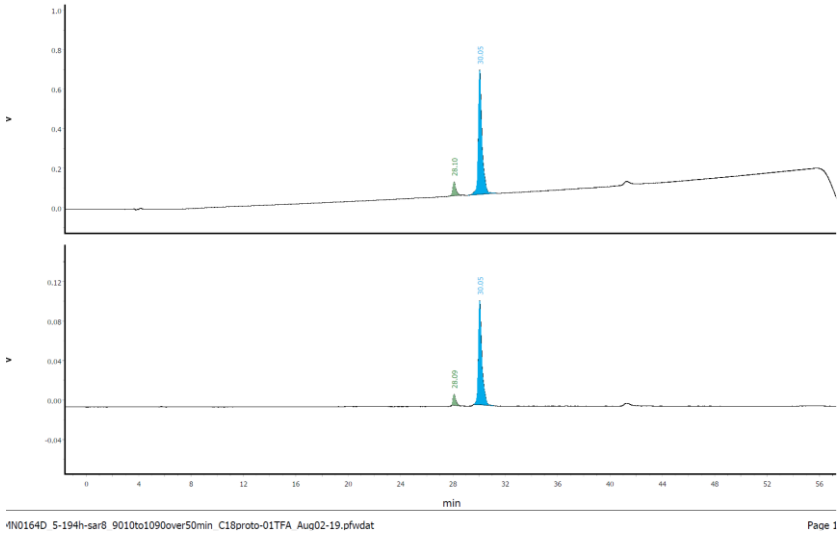

Figure D.20 Analytical RP-HPLC of Dap-K6-(Sar8)-E12-W13 Linear gradient of 10:90 CH_3CN:H_2O (0.1% TFA) to 90:10 CH_3CN:H_2O (0.1% TFA) over 50 min (λ_{top} = 220 nm, λ_{bottom} = 280 nm)

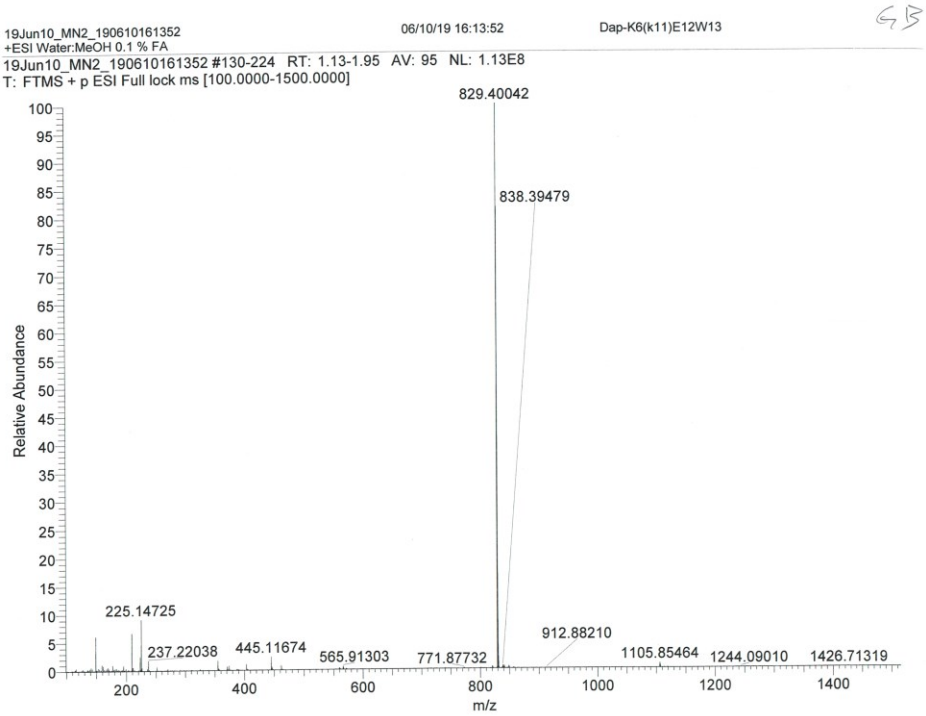

Figure D.21 HRMS (+ESI) of Dap-K6-(D-K11)-E12-W13

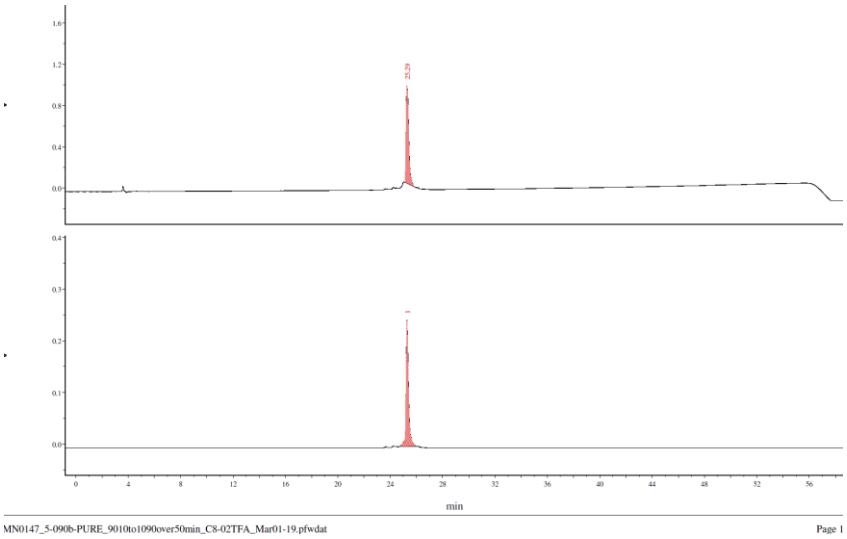

Figure D.22 Analytical RP-HPLC of Dap-K6-(D-K11)-E12-W13 Linear gradient of 10:90 CH_3CN:H_2O (0.1% TFA) to 90:10 CH_3CN:H_2O (0.1% TFA) over 50 min (λ_{top} = 220 nm, λ_{bottom} = 280 nm)

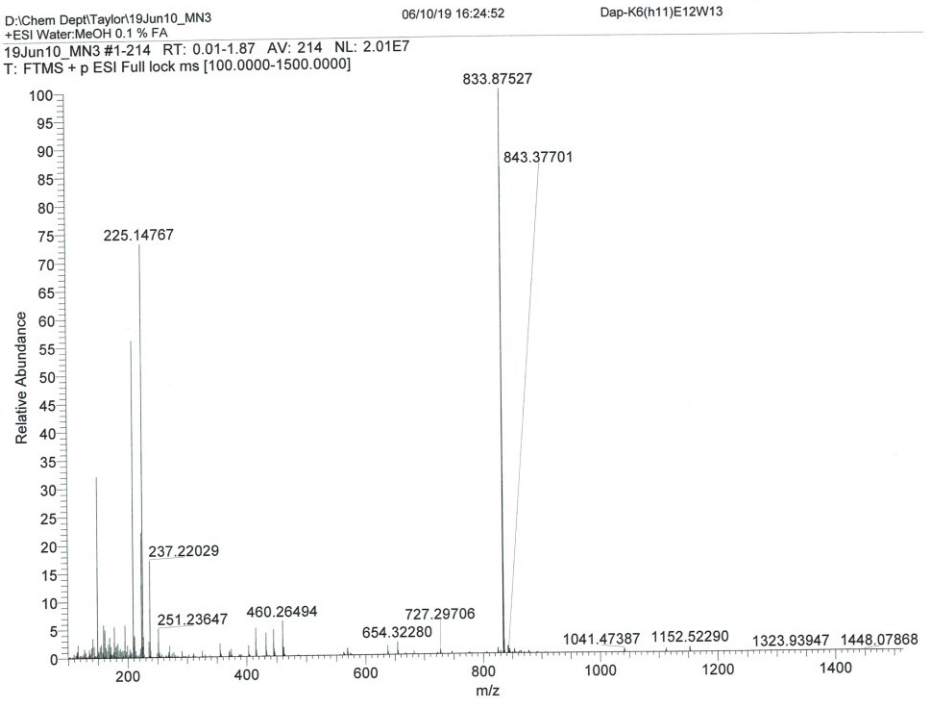

Figure D.23 HRMS (+ESI) of Dap-K6-(D-H11)-E12-W13

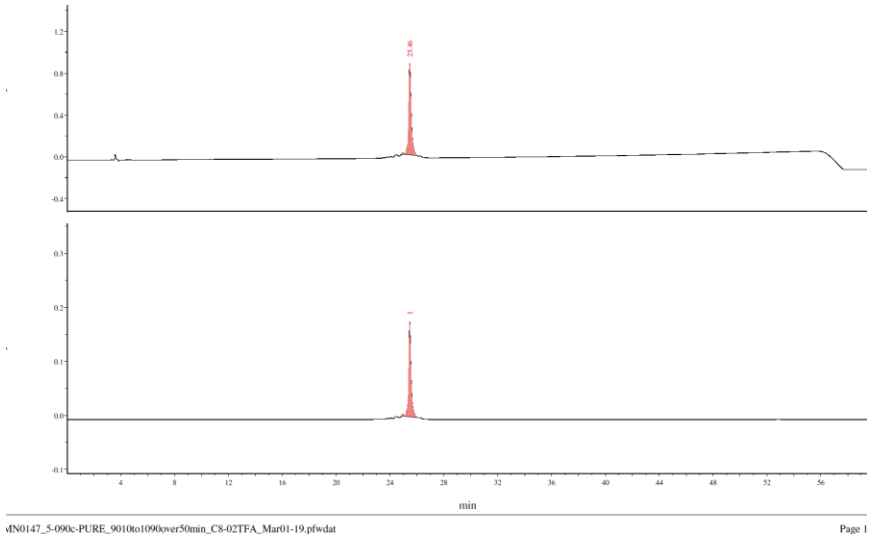

Figure D.24 Analytical RP-HPLC of Dap-K6-(D-H11)-E12-W13 Linear gradient of 10:90 CH_3CN:H_2O (0.1% TFA) to 90:10 CH_3CN:H_2O (0.1% TFA) over 50 min (λ_{top} = 220 nm, λ_{bottom} = 280 nm)

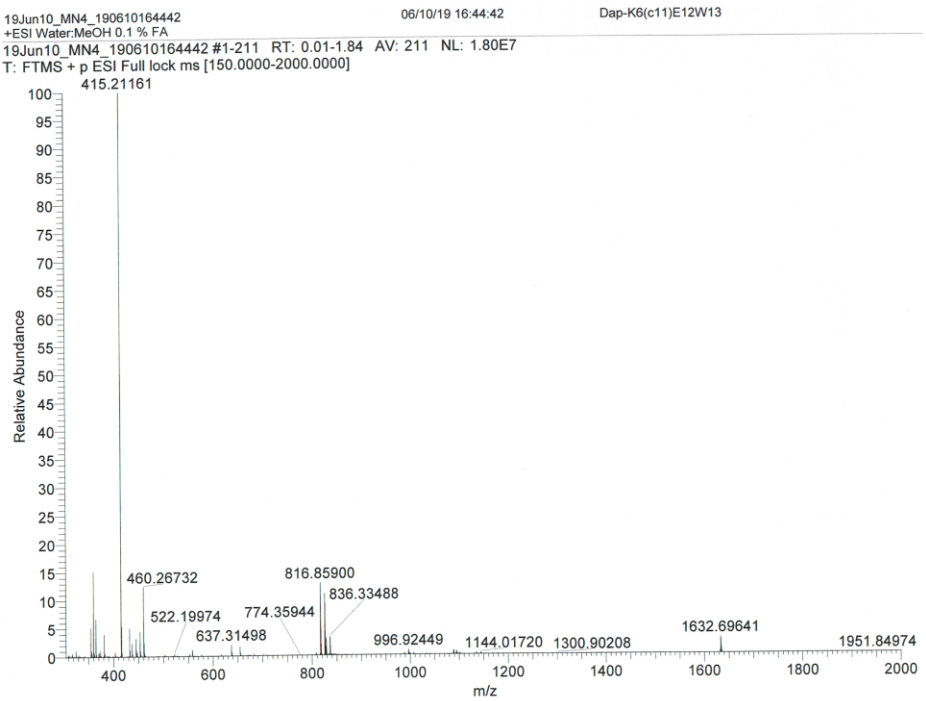

Figure D.25 HRMS (+ESI) of Dap-K6-(D-C11)-E12-W13

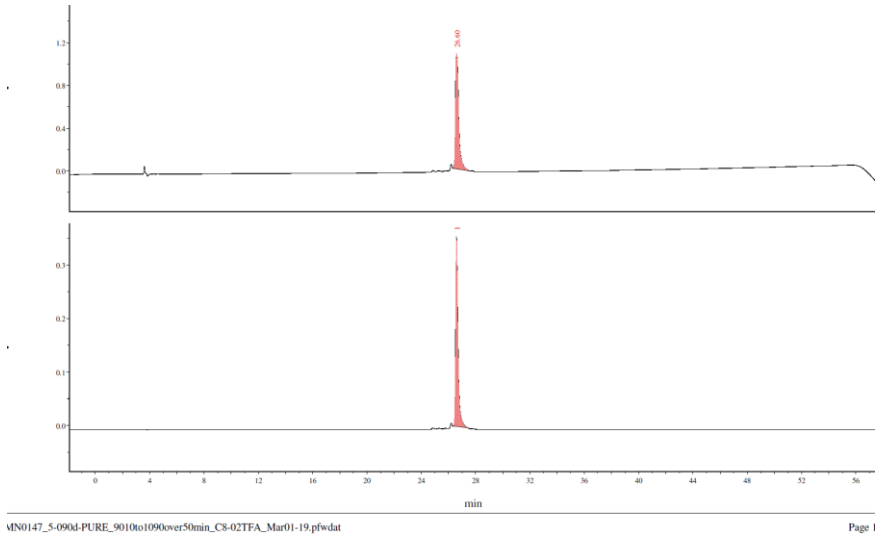

Figure D.26 Analytical RP-HPLC of Dap-K6-(D-C11)-E12-W13 Linear gradient of 10:90 CH_3CN:H_2O (0.1% TFA) to 90:10 CH_3CN:H_2O (0.1% TFA) over 50 min (λ_{top} = 220 nm, λ_{bottom} = 280 nm)

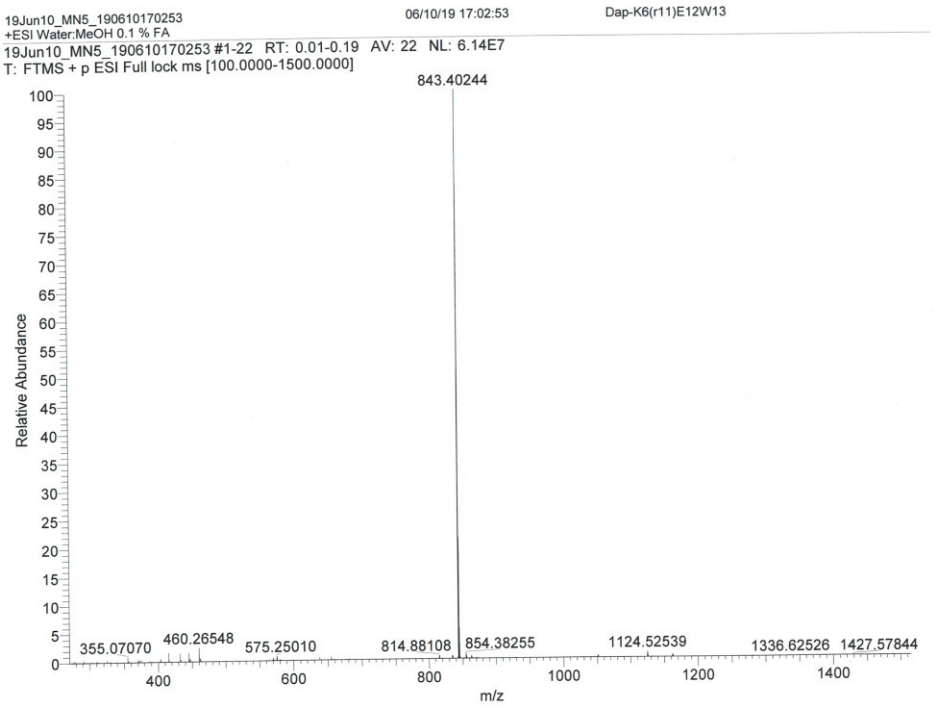

Figure D.27 HRMS (+ESI) of Dap-K6-(D-R11)-E12-W13

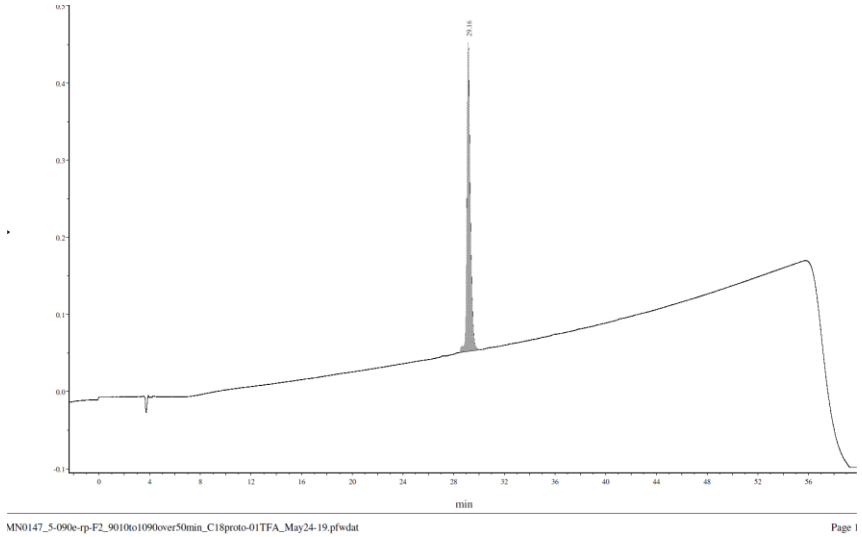

Figure D.28 Analytical RP-HPLC of Dap-K6-(D-R11)-E12-W13 Linear gradient of 10:90 $CH_3CN:H_2O$ (0.1% TFA) to 90:10 $CH_3CN:H_2O$ (0.1% TFA) over 50 min ($\lambda = 220$ nm)

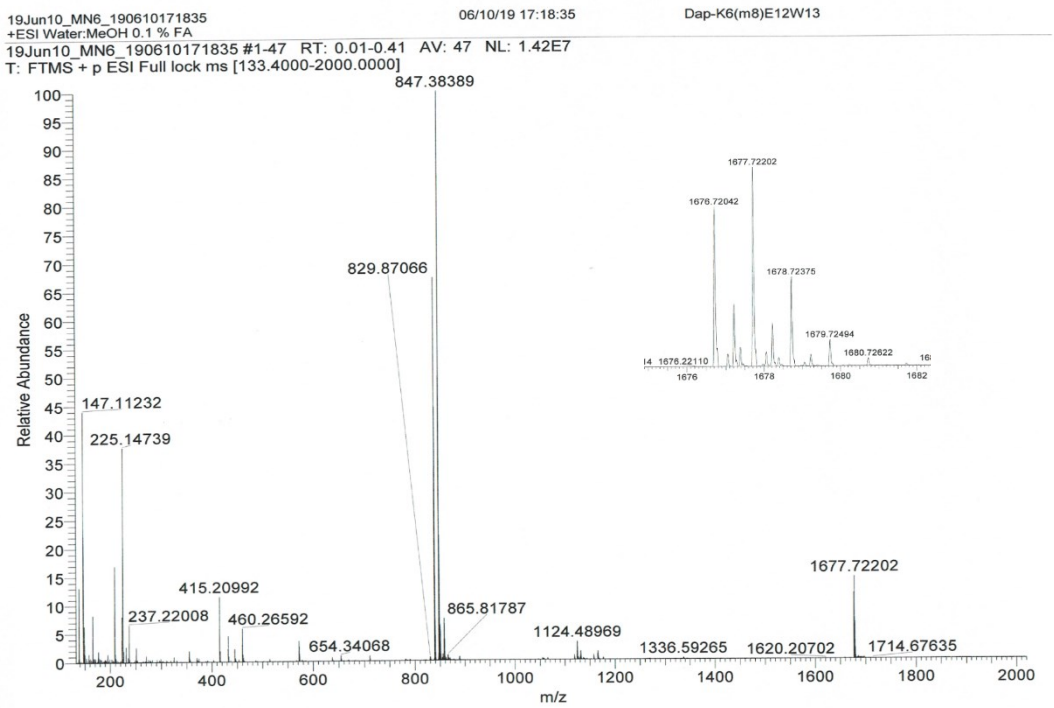

Figure D.29 HRMS (+ESI) of Dap-K6-(D-M8)-E12-W13

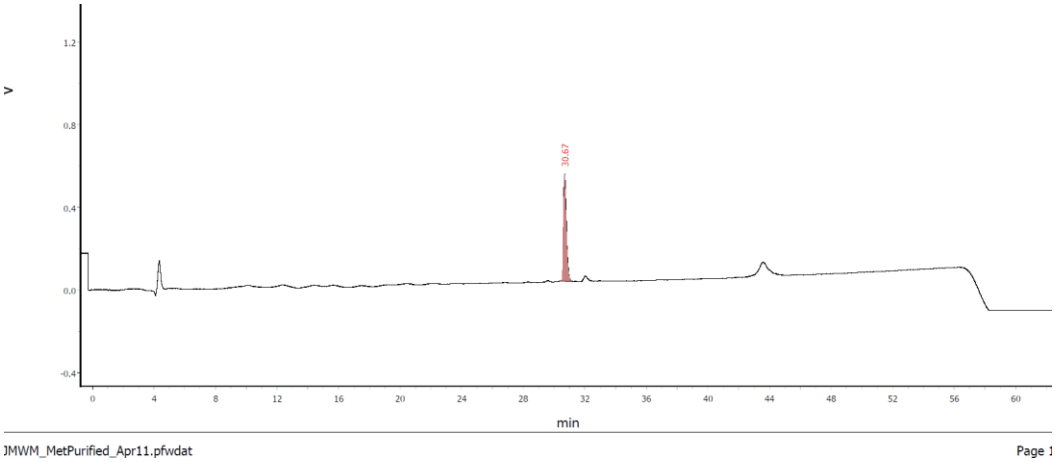

Figure D.30 Analytical RP-HPLC of Dap-K6-(D-M8)-E12-W13 Linear gradient of 10:90 $CH_3CN:H_2O$ (0.1% TFA) to 90:10 $CH_3CN:H_2O$ (0.1% TFA) over 50 min (λ = 220 nm)

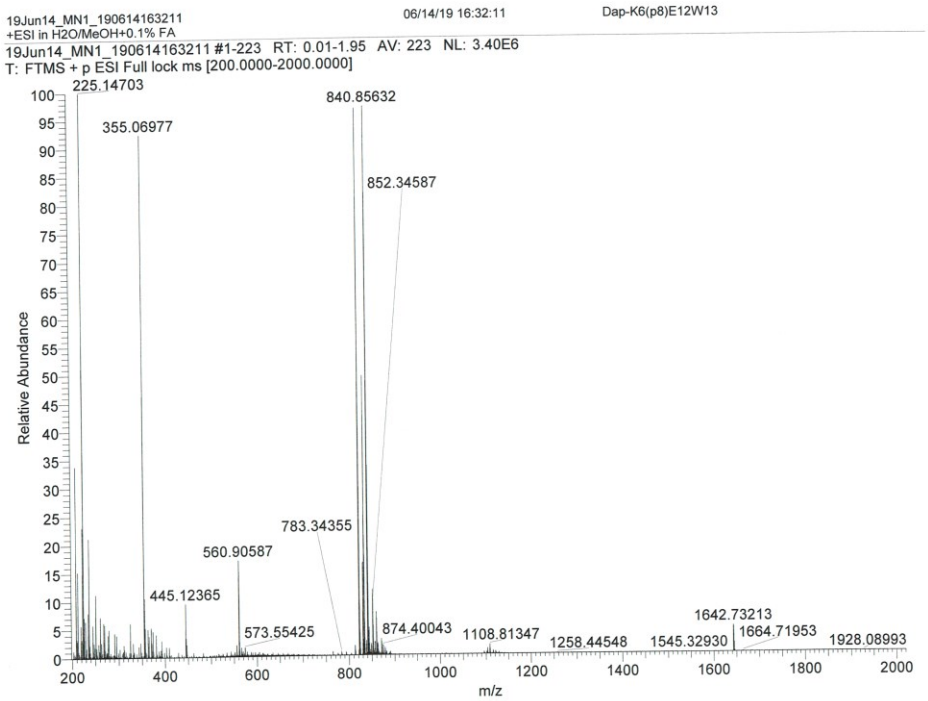

Figure D.31 HRMS (+ESI) of Dap-K6-(D-P8)-E12-W13

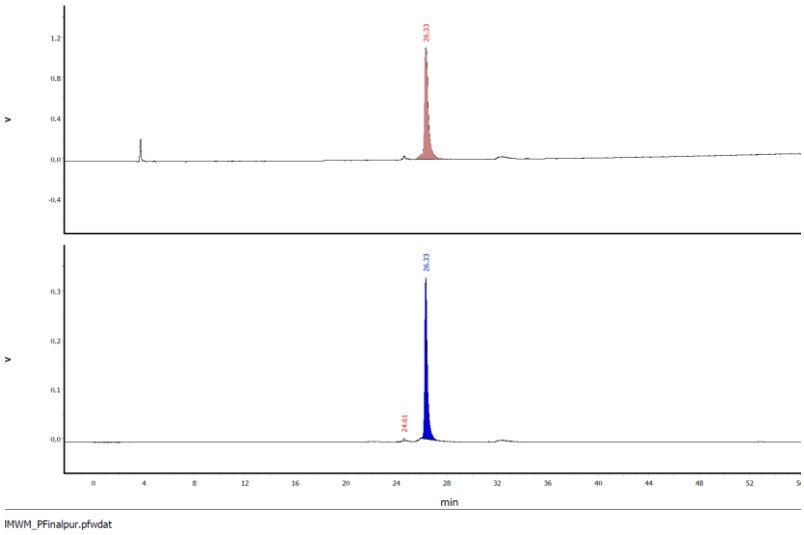

Figure D.32 Analytical RP-HPLC of Dap-K6-(D-P8)-E12-W13 Linear gradient of 10:90 $CH_3CN:H_2O$ (0.1% TFA) to 90:10 $CH_3CN:H_2O$ (0.1% TFA) over 50 min (λ_{top} = 220 nm, λ_{bottom} = 280 nm)

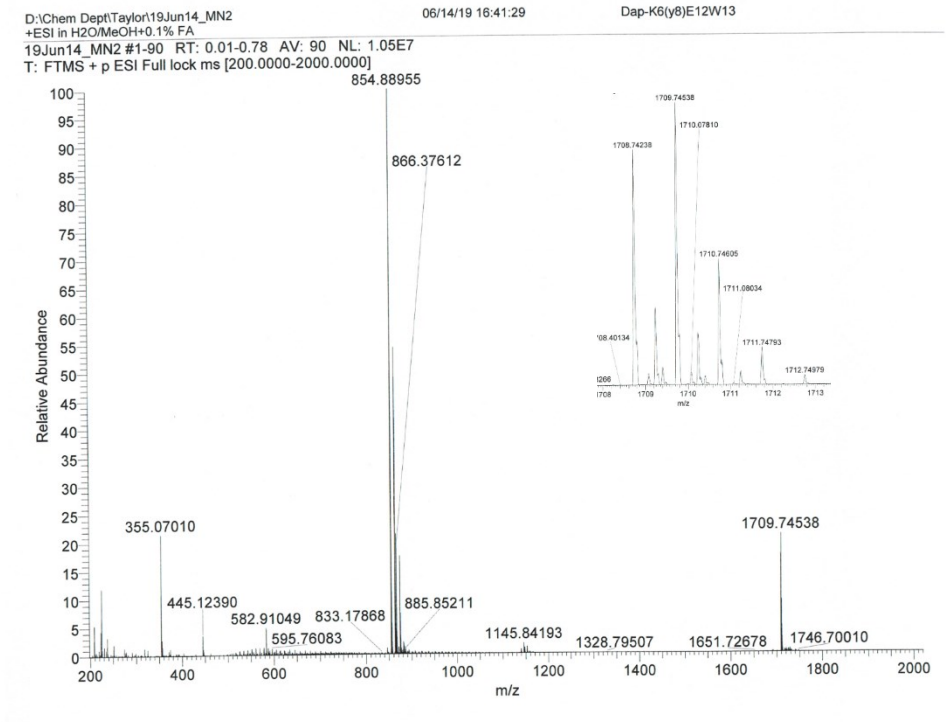

Figure D.33 HRMS (+ESI) of Dap-K6-(D-Y8)-E12-W13

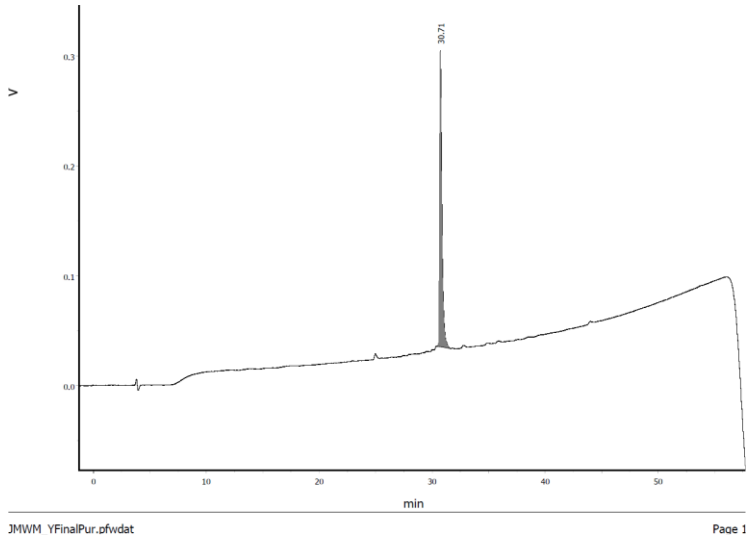

Figure D.34 Analytical RP-HPLC of Dap-K6-(D-Y8)-E12-W13 Linear gradient of 10:90 $CH_3CN:H_2O$ (0.1% TFA) to 90:10 $CH_3CN:H_2O$ (0.1% TFA) over 50 min (λ = 220 nm)

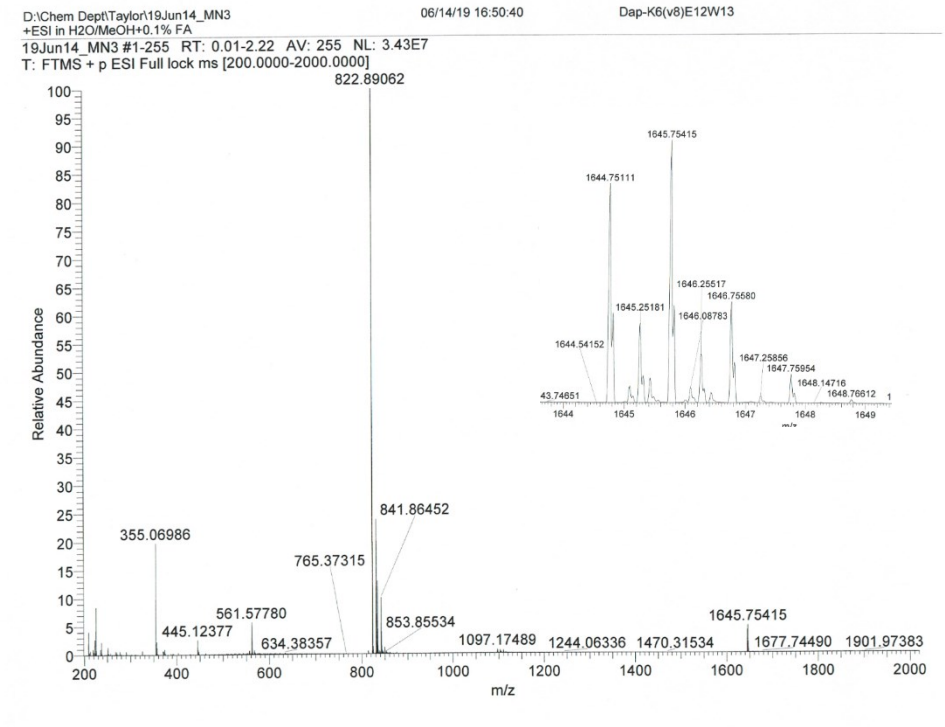

Figure D.35 HRMS (+ESI) of Dap-K6-(D-V8)-E12-W13

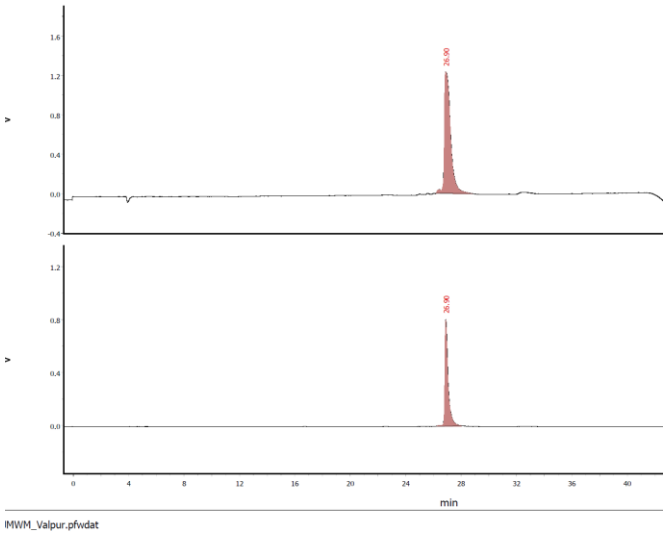

Figure D.36 Analytical RP-HPLC of Dap-K6-(D-V8)-E12-W13 Linear gradient of 10:90 $CH_3CN:H_2O$ (0.1% TFA) to 90:10 $CH_3CN:H_2O$ (0.1% TFA) over 40 min (λ_{top} = 220 nm, λ_{bottom} = 280 nm)

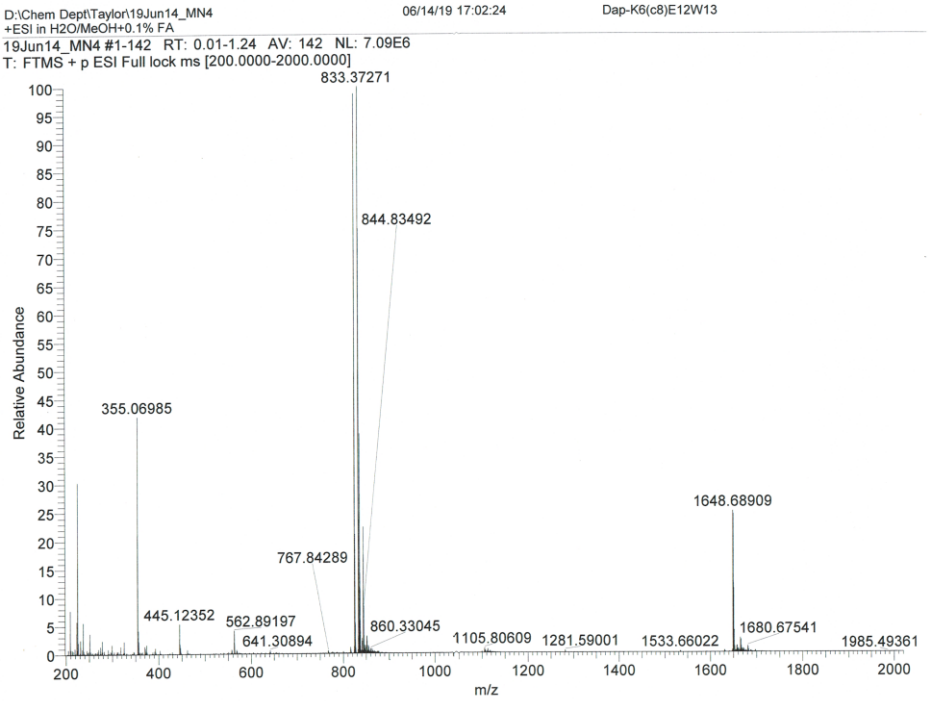

Figure D.37 HRMS (+ESI) of Dap-K6-(D-C8)-E12-W13

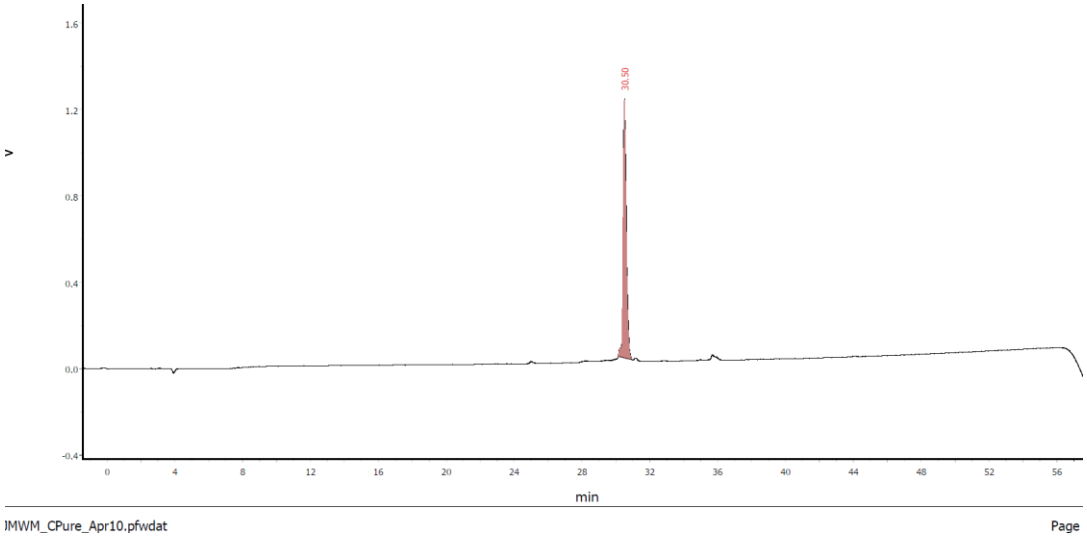

Figure D.38 Analytical RP-HPLC of Dap-K6-(D-C8)-E12-W13 Linear gradient of 10:90 $CH_3CN:H_2O$ (0.1% TFA) to 90:10 $CH_3CN:H_2O$ (0.1% TFA) over 50 min (λ = 220 nm)

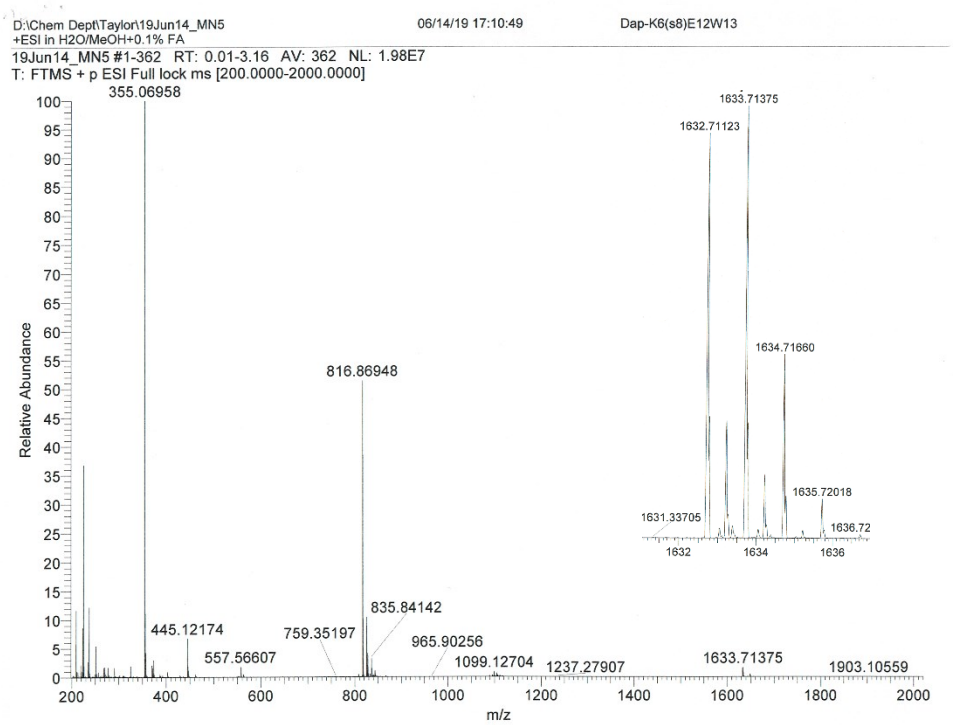

Figure D.39 HRMS (+ESI) of Dap-K6-(D-S8)-E12-W13

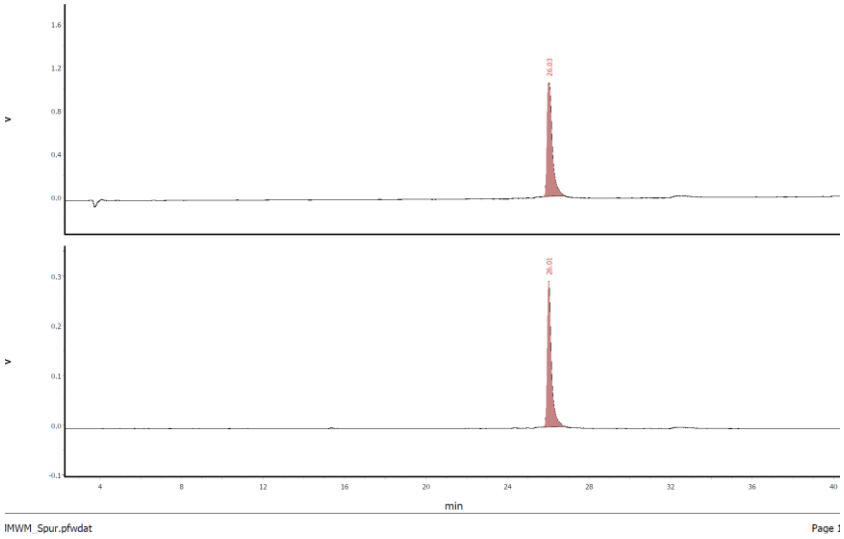

Figure D.40 Analytical RP-HPLC of Dap-K6-(D-S8)-E12-W13 Linear gradient of 10:90 $CH_3CN:H_2O$ (0.1% TFA) to 90:10 $CH_3CN:H_2O$ (0.1% TFA) over 50 min (λ_{top} = 220 nm, λ_{bottom} = 280 nm)

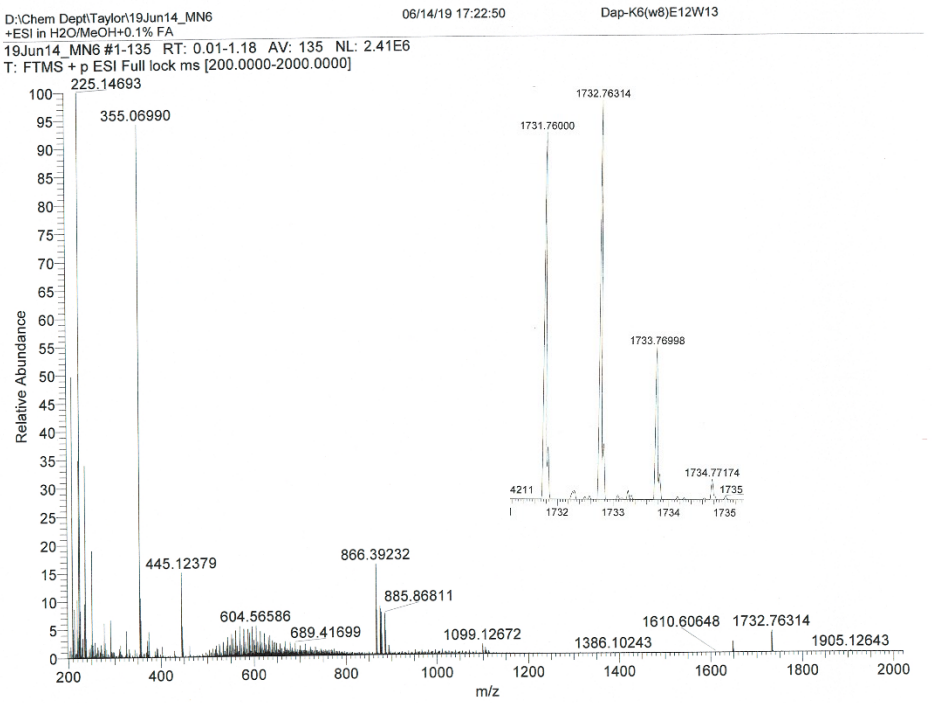

Figure D.41 HRMS (+ESI) of Dap-K6-(D-W8)-E12-W13

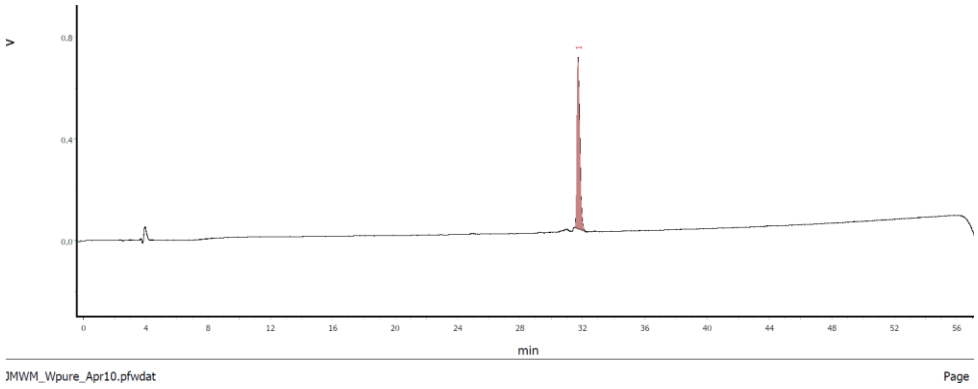

Figure D.42 Analytical RP-HPLC of Dap-K6-(D-W8)-E12-W13 Linear gradient of 10:90 $CH_3CN:H_2O$ (0.1% TFA) to 90:10 $CH_3CN:H_2O$ (0.1% TFA) over 50 min (λ = 220 nm)

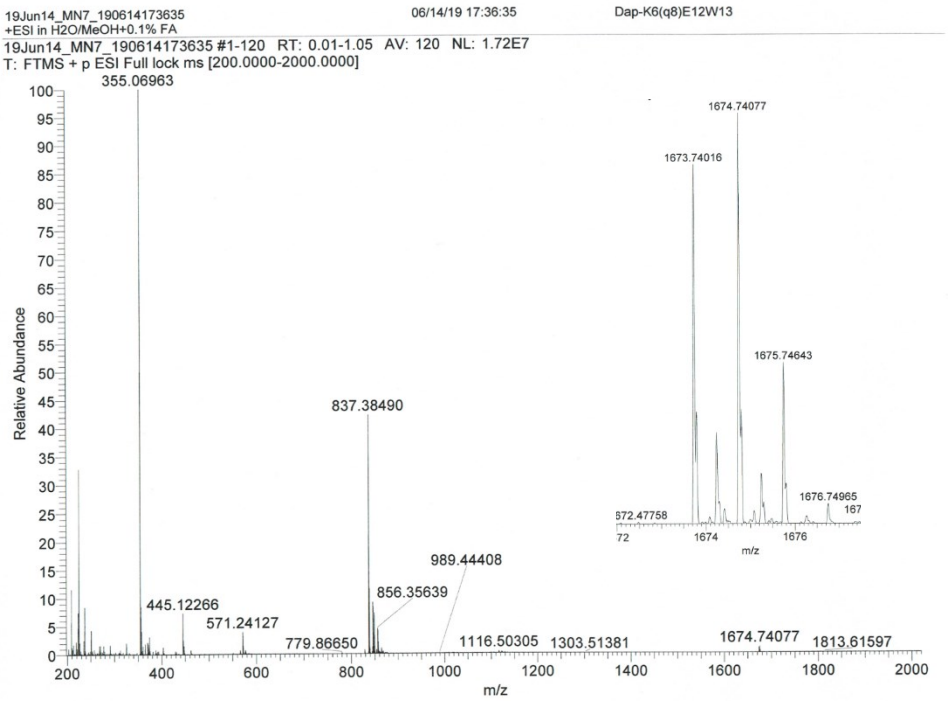

Figure D.43 HRMS (+ESI) of Dap-K6-(D-Q8)-E12-W13

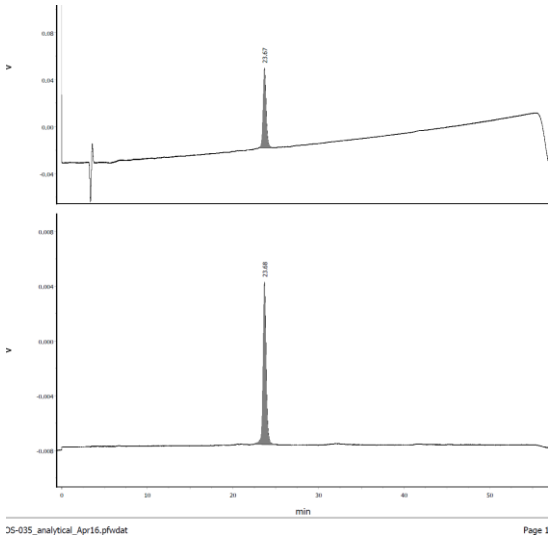

Figure D.44 Analytical RP-HPLC of Dap-K6-(D-Q8)-E12-W13 Linear gradient of 10:90 CH_3CN:H_2O (0.1% TFA) to 90:10 CH_3CN:H_2O (0.1% TFA) over 50 min (λ_{top} = 220 nm, λ_{bottom} = 280 nm)

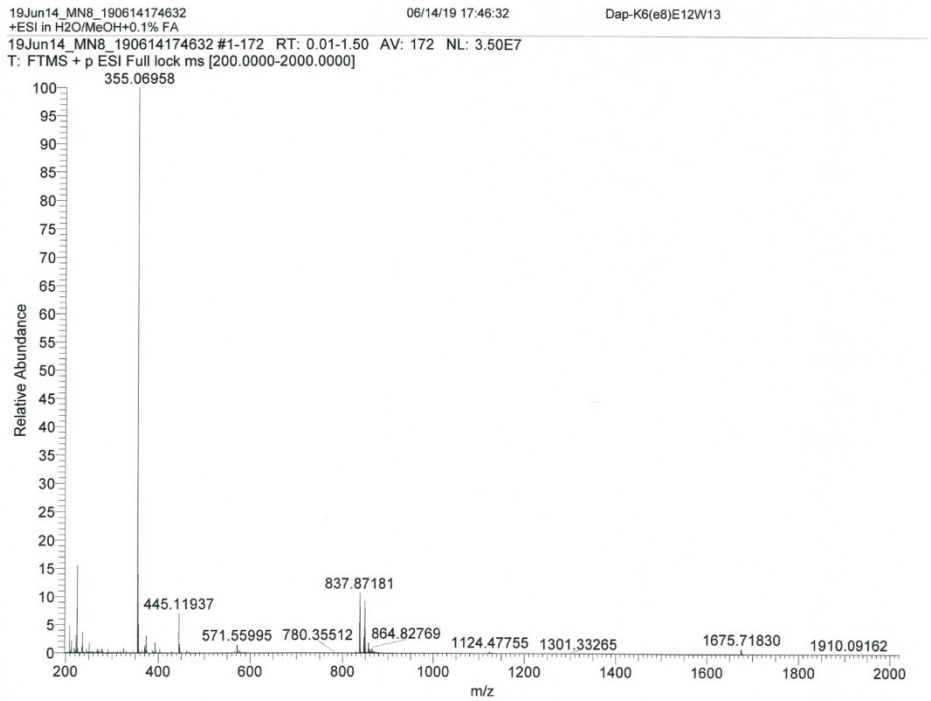

Figure D.45 HRMS (+ESI) of Dap-K6-(D-E8)-E12-W13

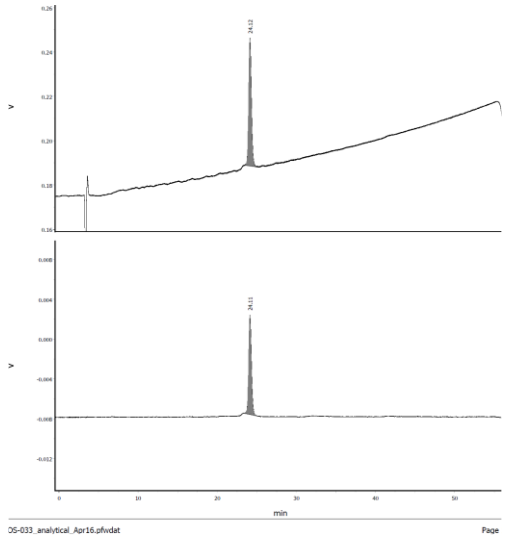

Figure D.46 Analytical RP-HPLC of Dap-K6-(D-E8)-E12-W13 Linear gradient of 10:90 CH_3CN:H_2O (0.1% TFA) to 90:10 CH_3CN:H_2O (0.1% TFA) over 50 min (λ_{top} = 220 nm, λ_{bottom} = 280 nm)

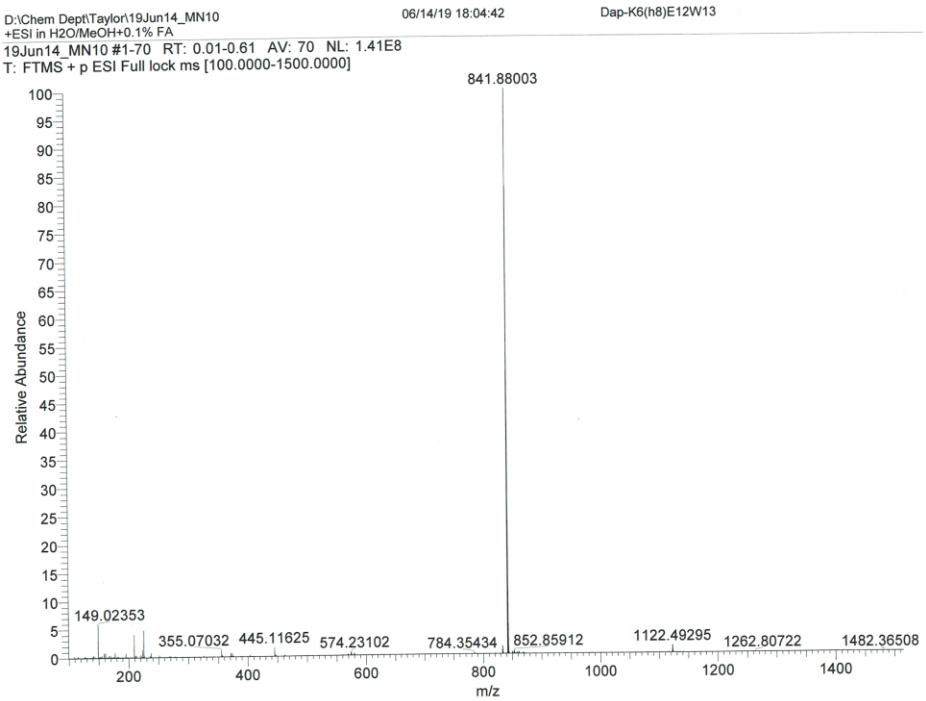

Figure D.47 HRMS (+ESI) of Dap-K6-(D-H8)-E12-W13

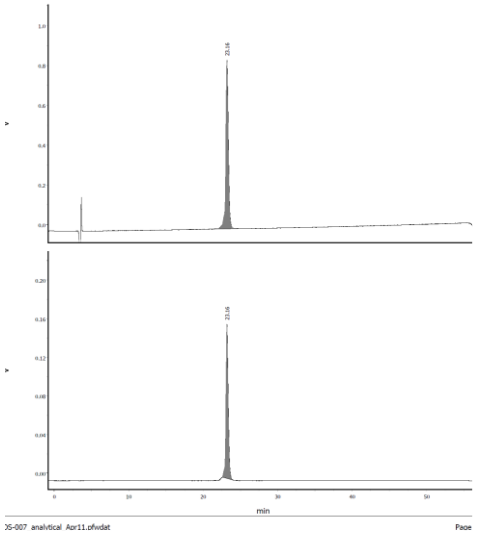

Figure D.48 Analytical RP-HPLC of Dap-K6-(D-H8)-E12-W13 Linear gradient of 10:90 $CH_3CN:H_2O$ (0.1% TFA) to 90:10 $CH_3CN:H_2O$ (0.1% TFA) over 50 min (λ_{top} = 220 nm, λ_{bottom} = 280 nm)

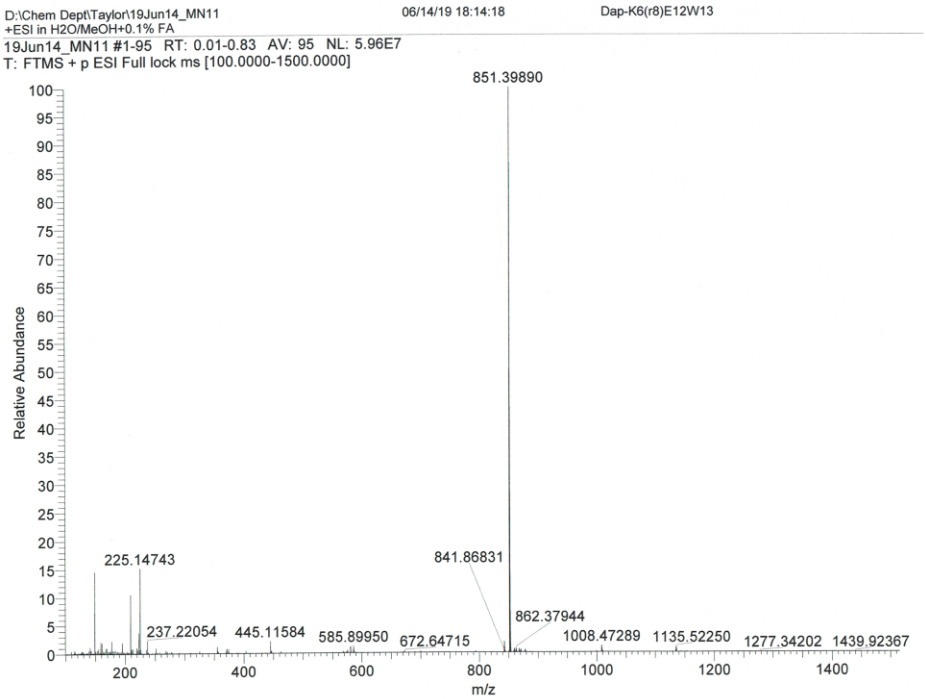

Figure D.49 HRMS (+ESI) of Dap-K6-(D-R8)-E12-W13

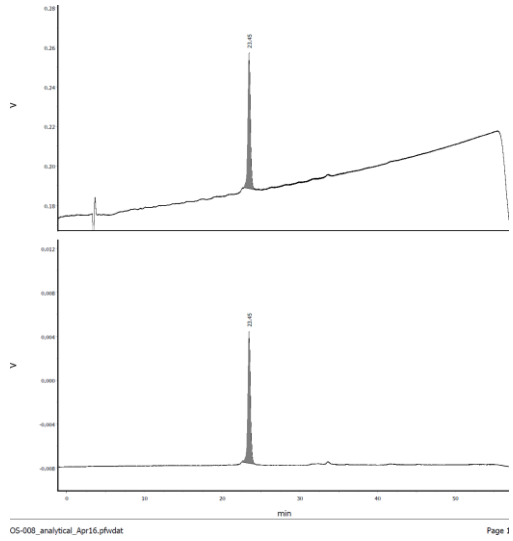

Figure D.50 Analytical RP-HPLC of Dap-K6-(D-R8)-E12-W13 Linear gradient of 10:90 $CH_3CN:H_2O$ (0.1% TFA) to 90:10 $CH_3CN:H_2O$ (0.1% TFA) over 50 min (λ_{top} = 220 nm, λ_{bottom} = 280 nm)

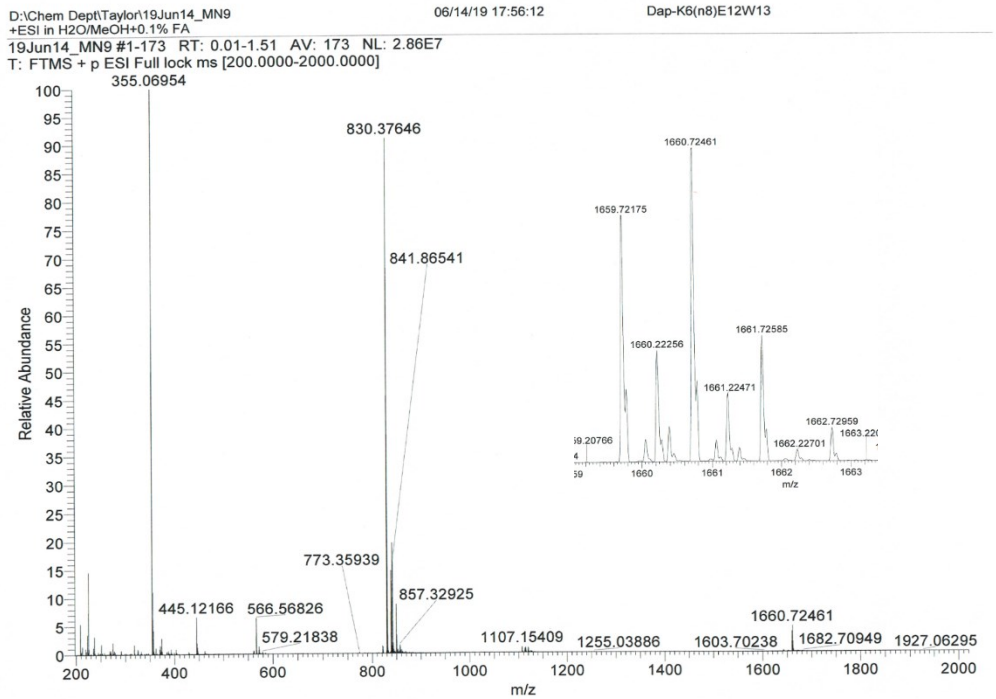

Figure D.51 HRMS (+ESI) of Dap-K6-(D-N8)-E12-W13

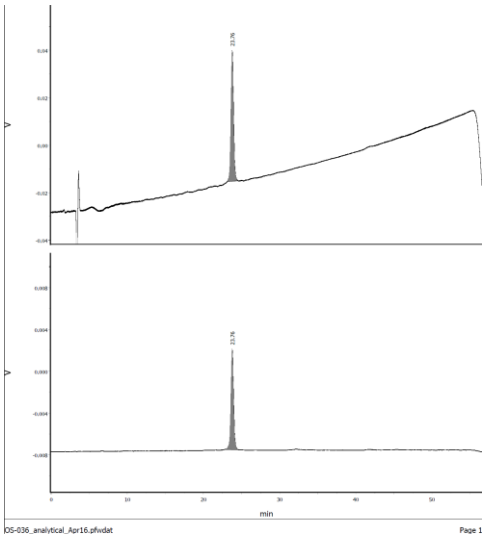

Figure D.52 Analytical RP-HPLC of Dap-K6-(D-N8)-E12-W13 Linear gradient of 10:90 CH_3CN:H_2O (0.1% TFA) to 90:10 CH_3CN:H_2O (0.1% TFA) over 50 min (λ_{top} = 220 nm, λ_{bottom} = 280 nm)

D.2 Emission Spectra

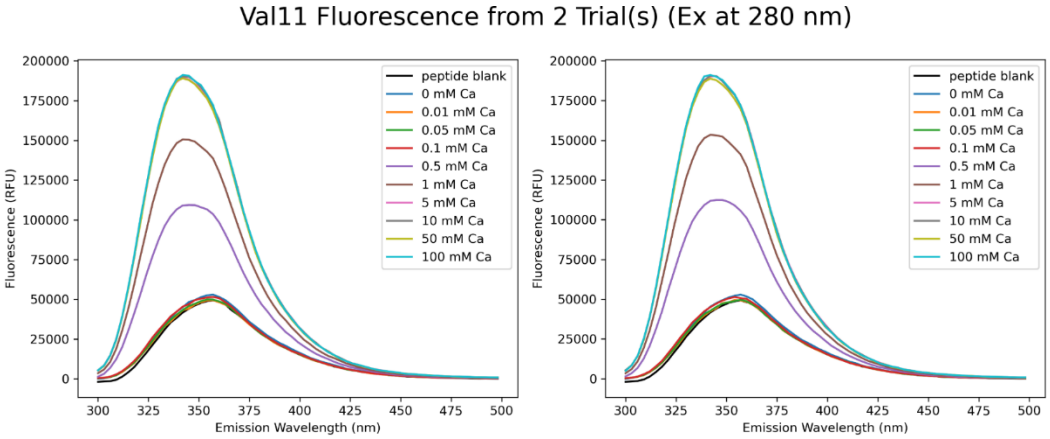

Figure D.53 Dap-K6-(D-V11)-E12-W13 membrane binding emission spectra Aquired on PTI Quantamaster 4 instrument at 37 °C.

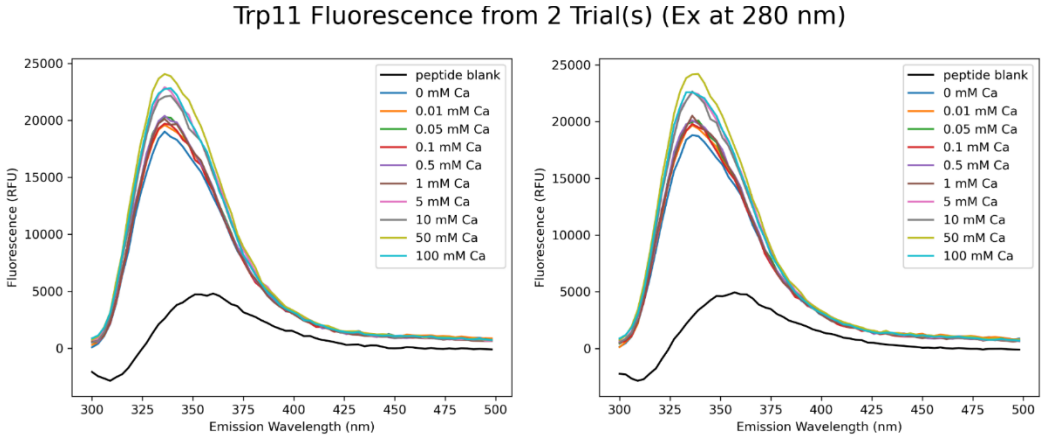

Figure D.54 Dap-K6-(D-W11)-E12-W13 membrane binding emission spectra Aquired on PTI Quantamaster 4 instrument at 37 °C.

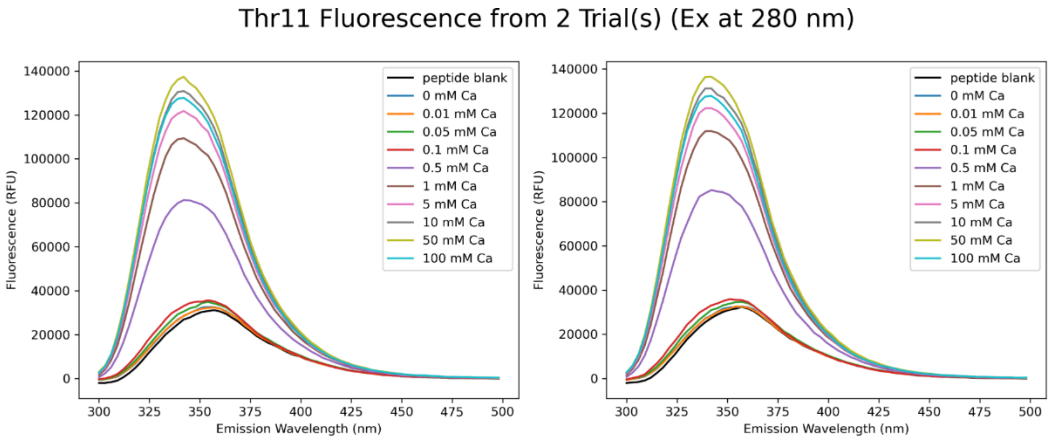

Figure D.55 Dap-K6-(D-T11)-E12-W13 membrane binding emission spectra Aquired on PTI Quantamaster 4 instrument at 37 °C.

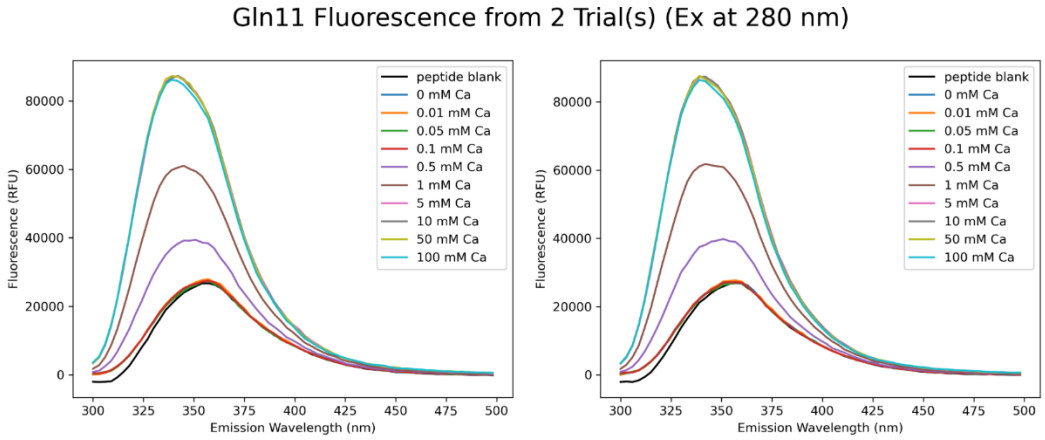

Figure D.56 Dap-K6-(D-Q11)-E12-W13 membrane binding emission spectra Aquired on PTI Quantamaster 4 instrument at 37 °C.

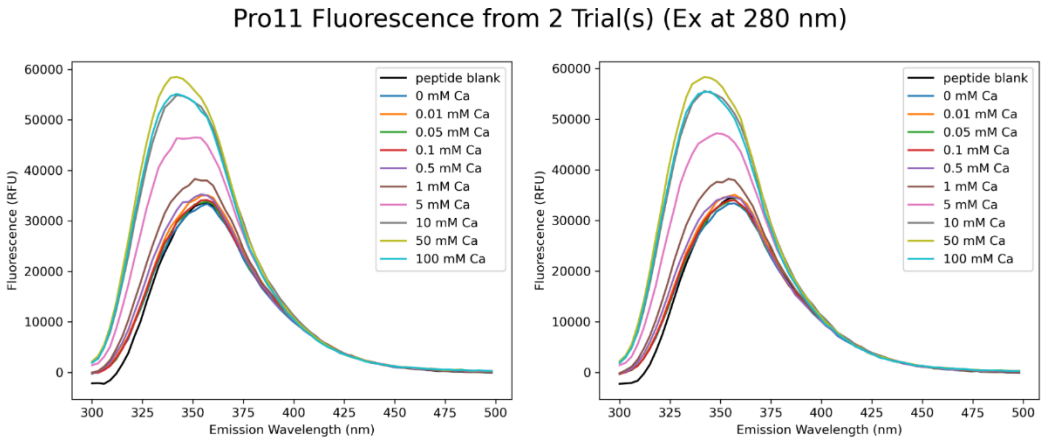

Figure D.57 Dap-K6-(D-P11)-E12-W13 membrane binding emission spectra Aquired on PTI Quantamaster 4 instrument at 37 °C.

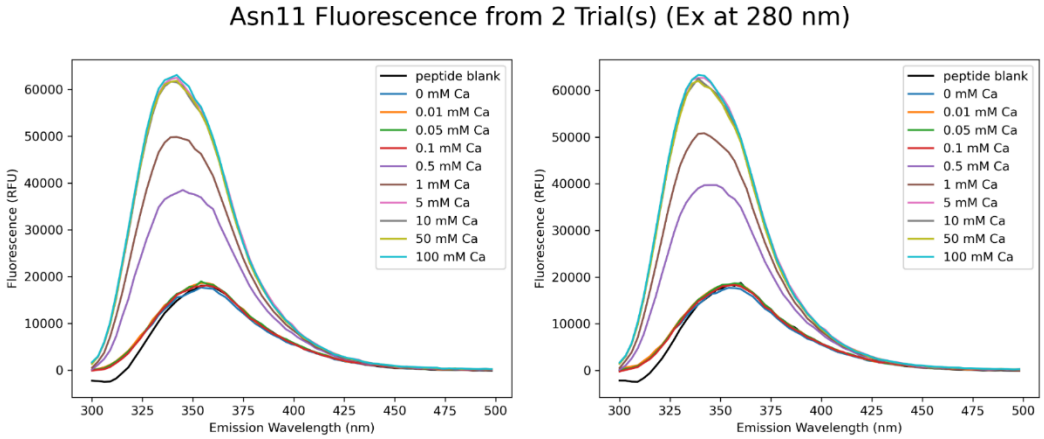

Figure D.58 Dap-K6-(D-N11)-E12-W13 membrane binding emission spectra Aquired on PTI Quantamaster 4 instrument at 37 °C.

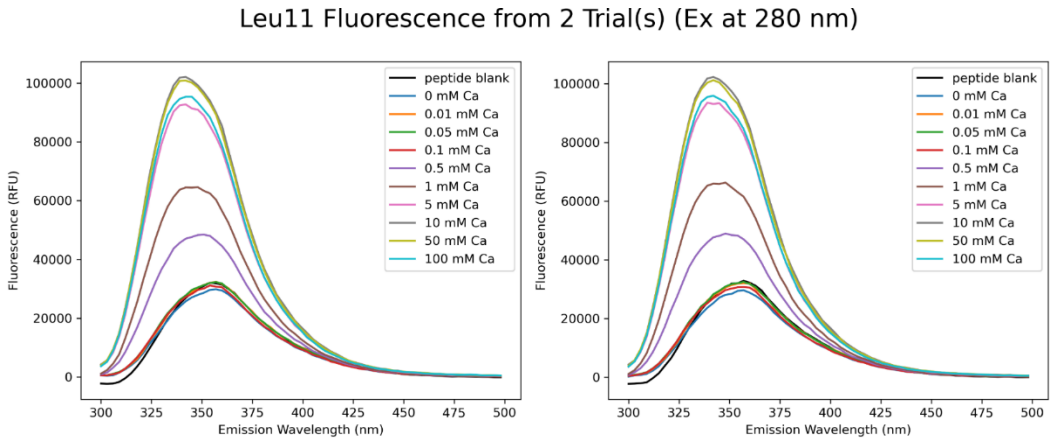

Figure D.59 Dap-K6-(D-L11)-E12-W13 membrane binding emission spectra Aquired on PTI Quantamaster 4 instrument at 37 °C.

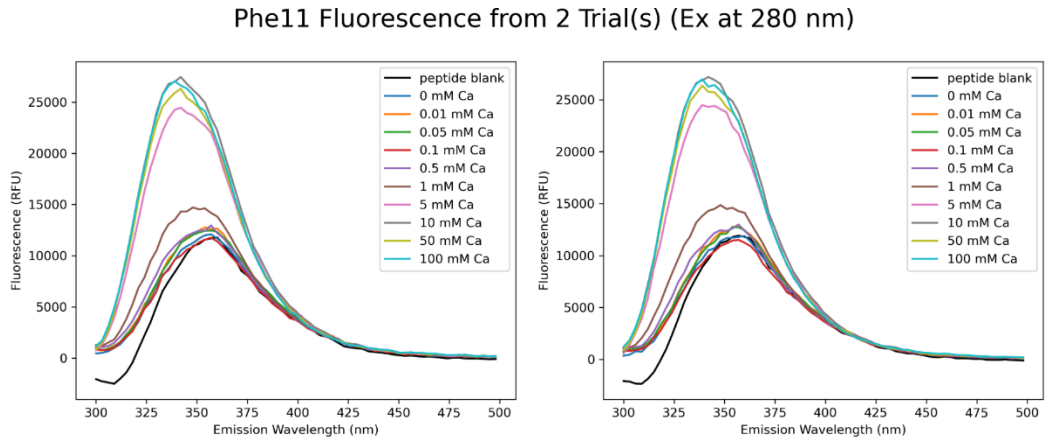

Figure D.60 Dap-K6-(D-F11)-E12-W13 membrane binding emission spectra Aquired on PTI Quantamaster 4 instrument at 37 °C.

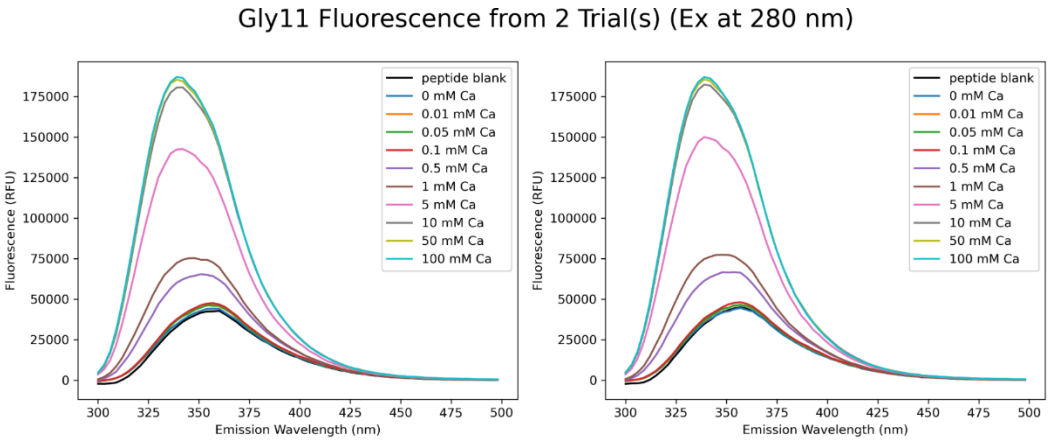

Figure D.61 Dap-K6-(G11)-E12-W13 membrane binding emission spectra Aquired on PTI Quantamaster 4 instrument at 37 °C.

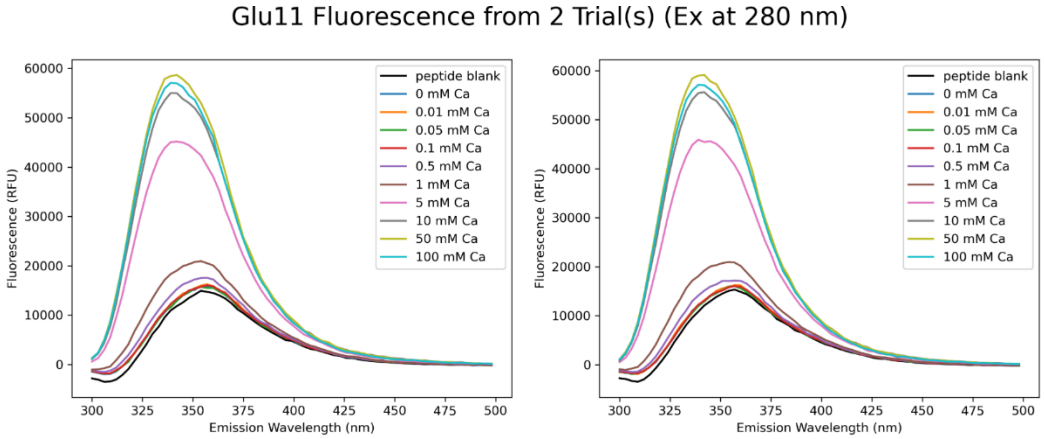

Figure D.62 Dap-K6-(D-E11)-E12-W13 membrane binding emission spectra Aquired on PTI Quantamaster 4 instrument at 37 °C.

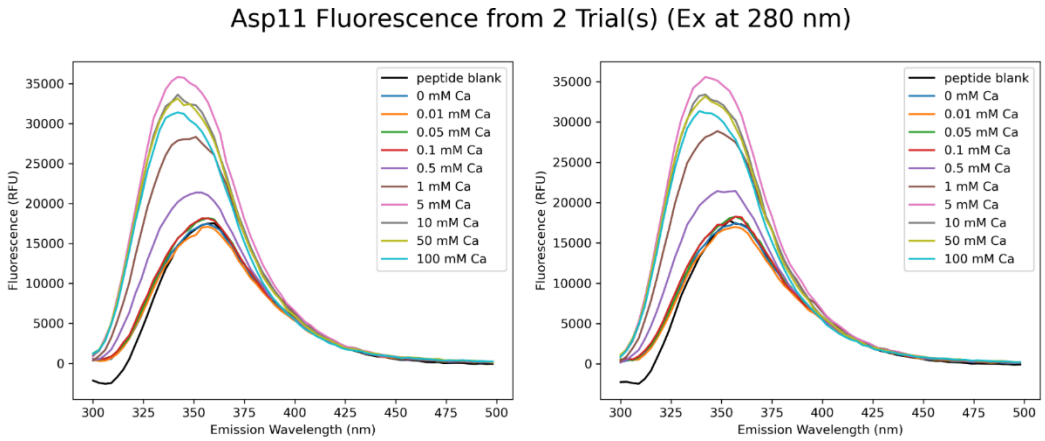

Figure D.63 Dap-K6-(D-D11)-E12-W13 membrane binding emission spectra Aquired on PTI Quantamaster 4 instrument at 37 °C.

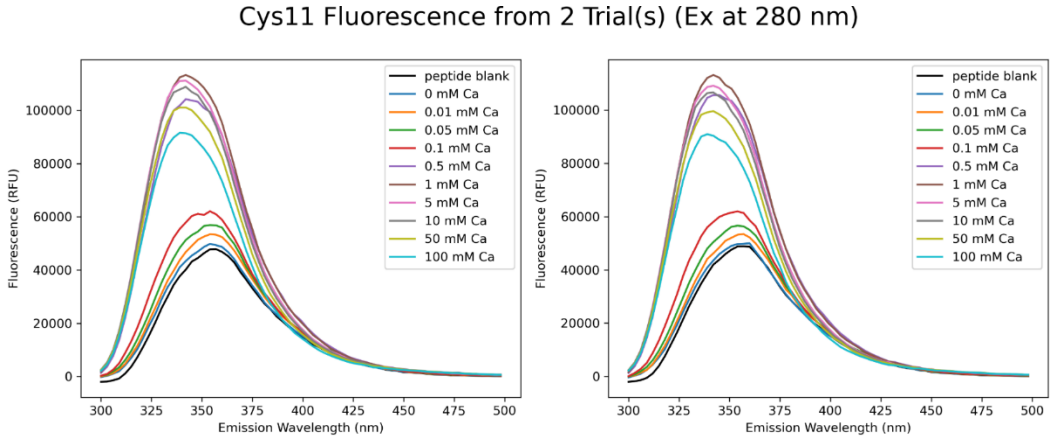

Figure D.64 Dap-K6-(D-C11)-E12-W13 membrane binding emission spectra Aquired on PTI Quantamaster 4 instrument at 37 °C.

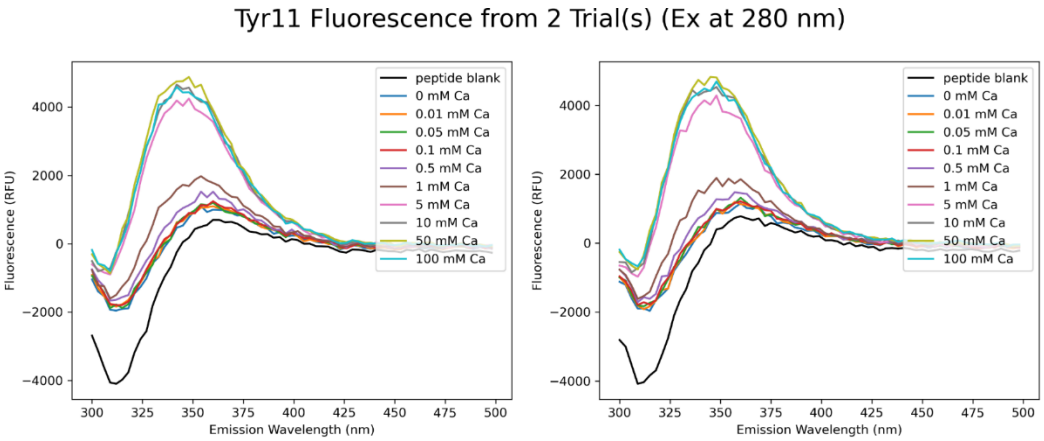

Figure D.65 Dap-K6-(D-Y11)-E12-W13 membrane binding emission spectra Aquired on PTI Quantamaster 4 instrument at 37 °C.

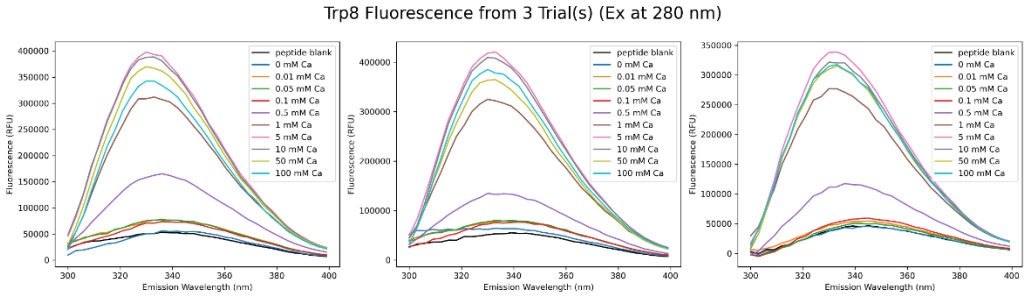

Figure D.66 Dap-K6-(D-W8)-E12-W13 membrane binding emission spectra Aquired on TECAN M1000 instrument at 37 °C.

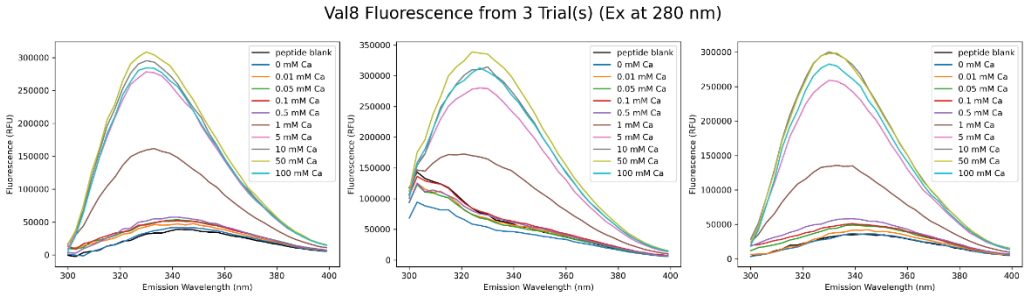

Figure D.67 Dap-K6-(D-V8)-E12-W13 membrane binding emission spectra Aquired on TECAN M1000 instrument at 37 °C.

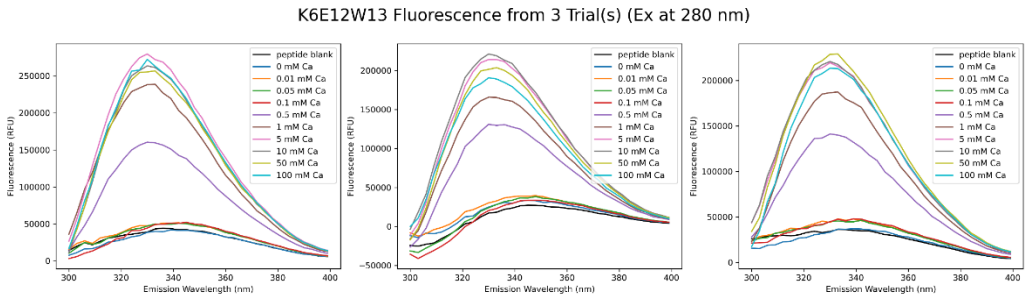

Figure D.68 Dap-K6-E12-W13 membrane binding emission spectra Aquired on TECAN M1000 instrument at 37 °C.

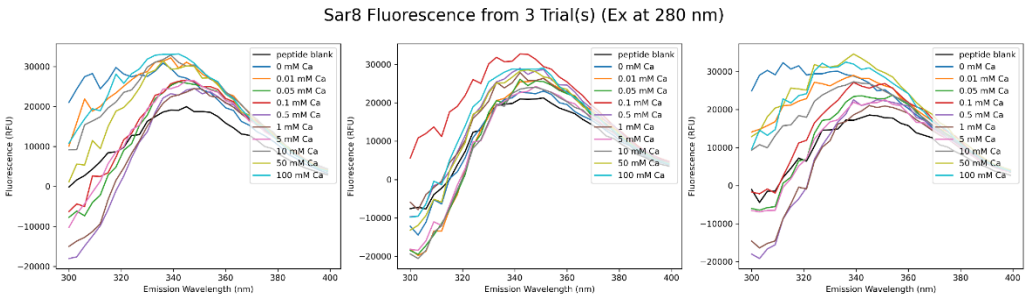

Figure D.69 Dap-K6-(Sar8)-E12-W13 membrane binding emission spectra Aquired on TECAN M1000 instrument at 37 °C.

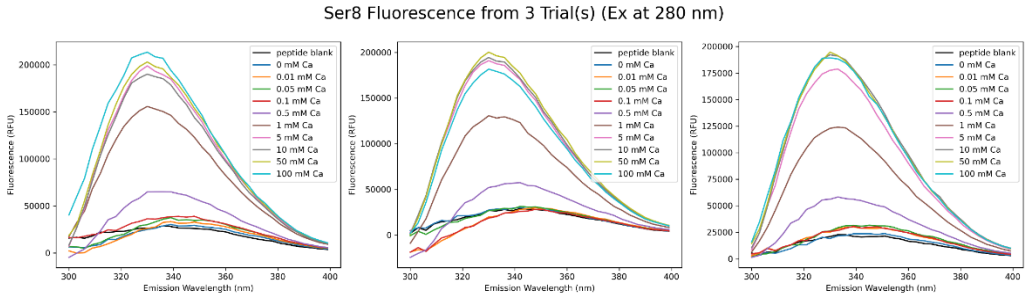

Figure D.70 Dap-K6-(D-S8)-E12-W13 membrane binding emission spectra Aquired on TECAN M1000 instrument at 37 °C.

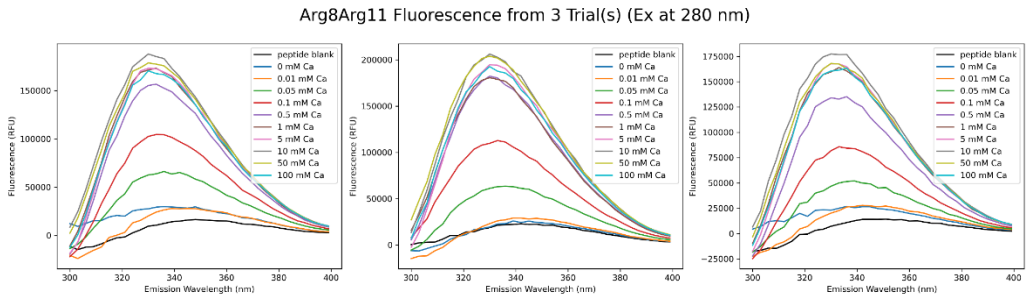

Figure D.71 Dap-K6-(D-R8, D-R11)-E12-W13 membrane binding emission spectra Aquired on TECAN M1000 instrument at 37 °C.

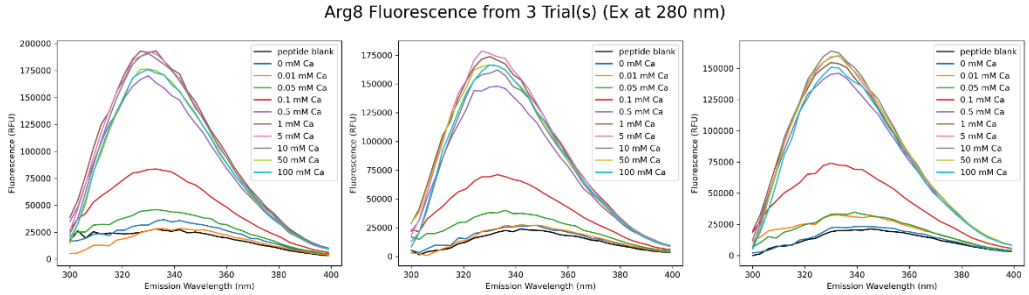

Figure D.72 Dap-K6-(D-R8)-E12-W13 membrane binding emission spectra Aquired on TECAN M1000 instrument at 37 °C.

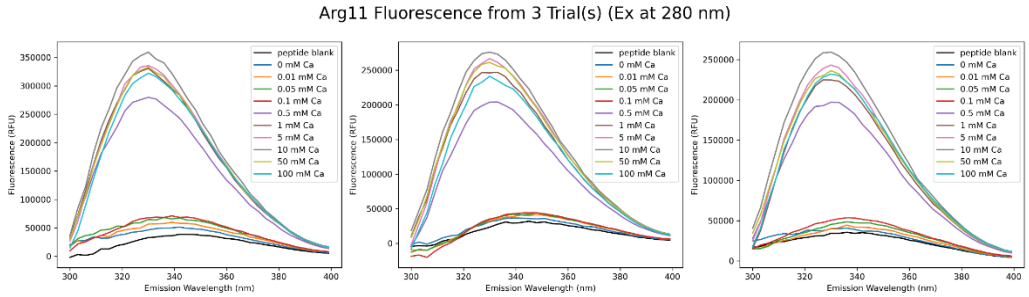

Figure D.73 Dap-K6-(D-R11)-E12-W13 membrane binding emission spectra Aquired on TECAN M1000 instrument at 37 °C.

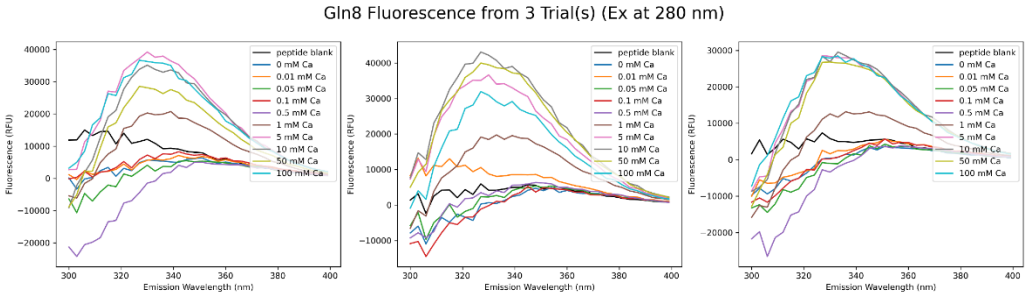

Figure D.74 Dap-K6-(D-Q8)-E12-W13 membrane binding emission spectra Aquired on TECAN M1000 instrument at 37 °C.

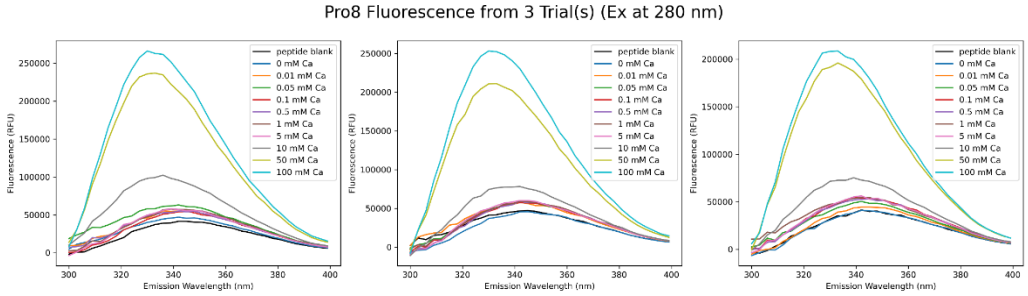

Figure D.75 Dap-K6-(D-P8)-E12-W13 membrane binding emission spectra Aquired on TECAN M1000 instrument at 37 °C.

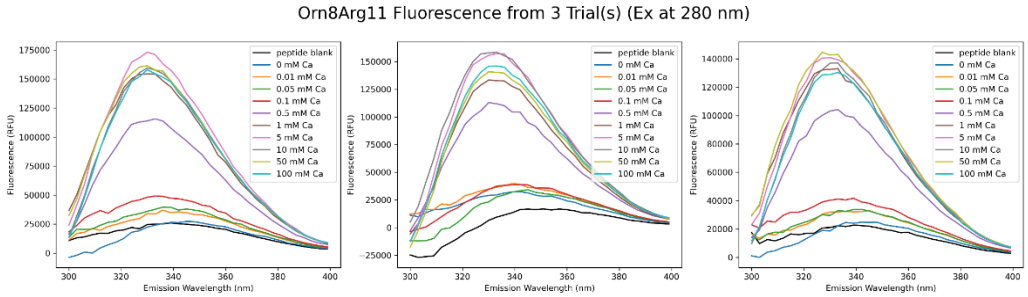

Figure D.76 Dap-K6-(D-Orn8, D-R11)-E12-W13 membrane binding emission spectra Aquired on TECAN M1000 instrument at 37 °C.

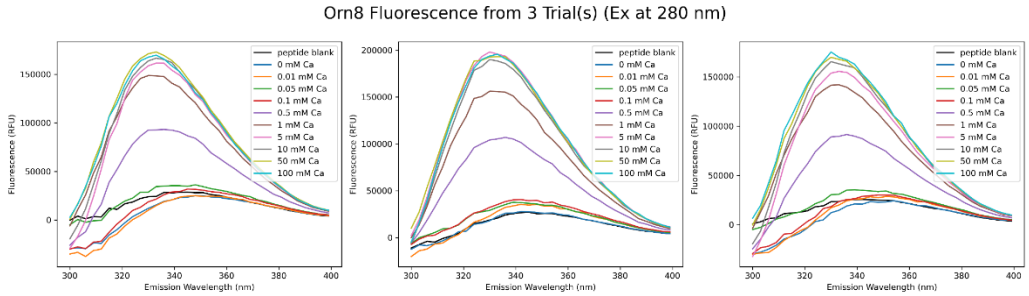

Figure D.77 Dap-K6-(D-Orn8)-E12-W13 membrane binding emission spectra Aquired on TECAN M1000 instrument at 37 °C.

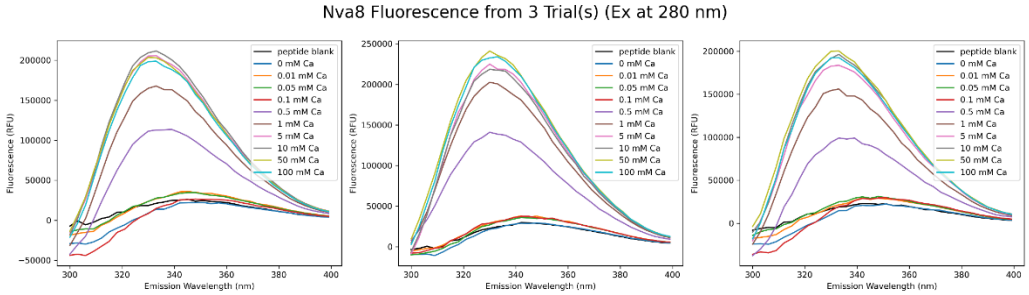

Figure D.78 Dap-K6-(D-Nva8)-E12-W13 membrane binding emission spectra Aquired on TECAN M1000 instrument at 37 °C.

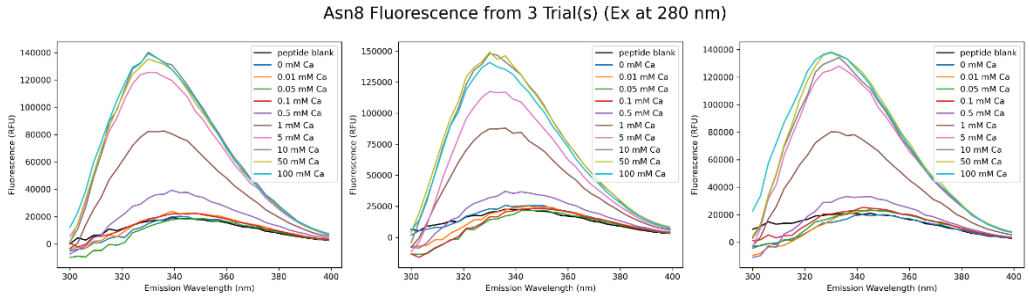

Figure D.79 Dap-K6-(D-N8)-E12-W13 membrane binding emission spectra Aquired on TECAN M1000 instrument at 37 °C.

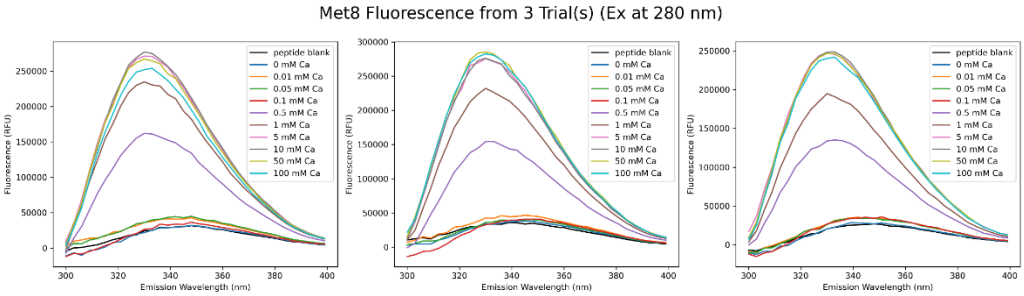

Figure D.80 Dap-K6-(D-M8)-E12-W13 membrane binding emission spectra Aquired on TECAN M1000 instrument at 37 °C.

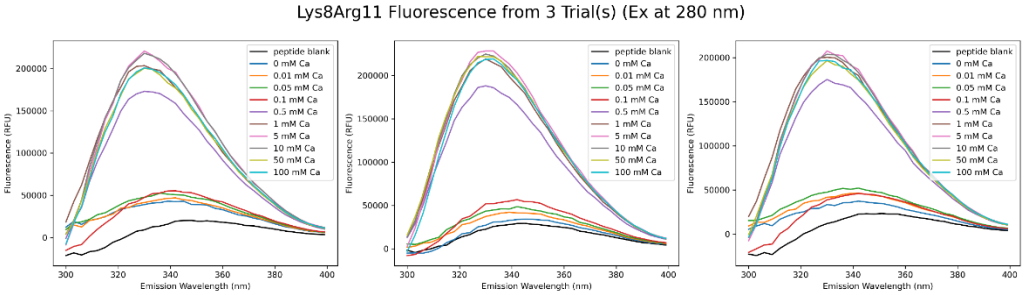

Figure D.81 Dap-K6-(D-K8, D-R11)-E12-W13 membrane binding emission spectra Aquired on TECAN M1000 instrument at 37 °C.

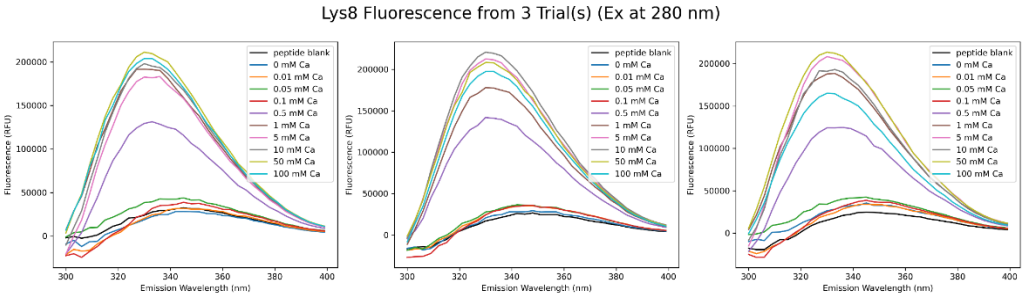

Figure D.82 Dap-K6-(D-K8)-E12-W13 membrane binding emission spectra Aquired on TECAN M1000 instrument at 37 °C.

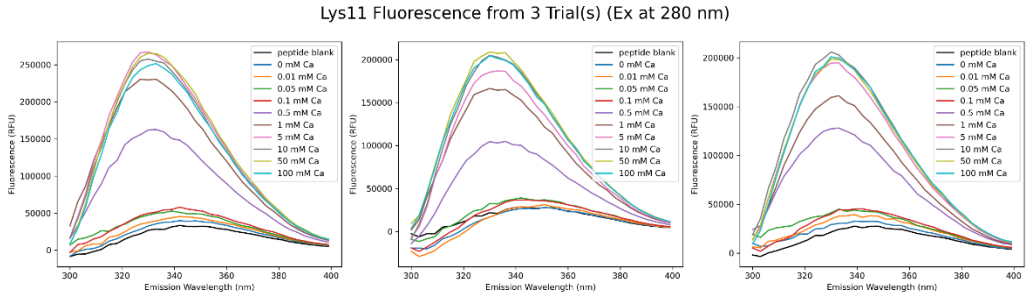

Figure D.83 Dap-K6-(D-K11)-E12-W13 membrane binding emission spectra Aquired on TECAN M1000 instrument at 37 °C.

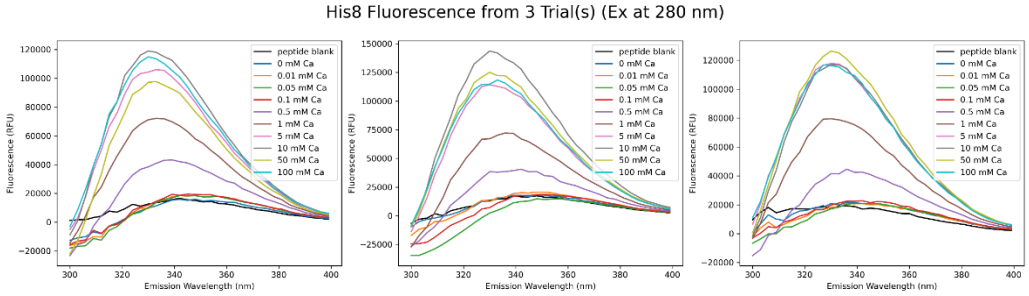

Figure D.84 Dap-K6-(D-H8)-E12-W13 membrane binding emission spectra Aquired on TECAN M1000 instrument at 37 °C.

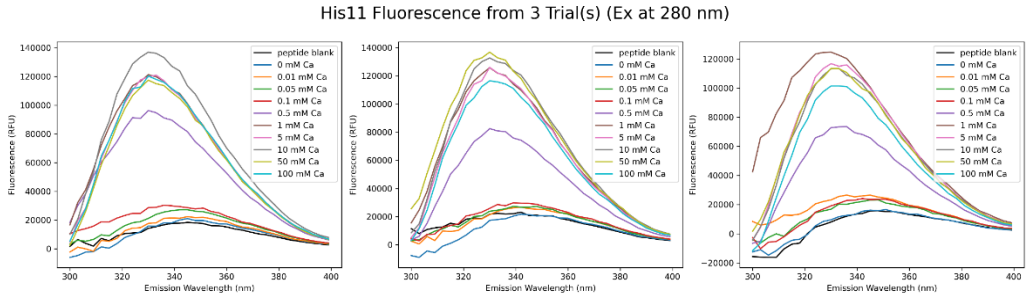

Figure D.85 Dap-K6-(D-H11)-E12-W13 membrane binding emission spectra Aquired on TECAN M1000 instrument at 37 °C.

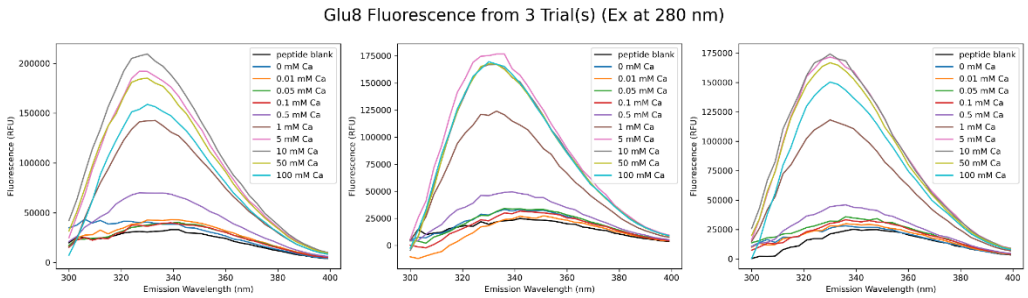

Figure D.86 Dap-K6-(D-Glu8)-E12-W13 membrane binding emission spectra Aquired on TECAN M1000 instrument at 37 °C.

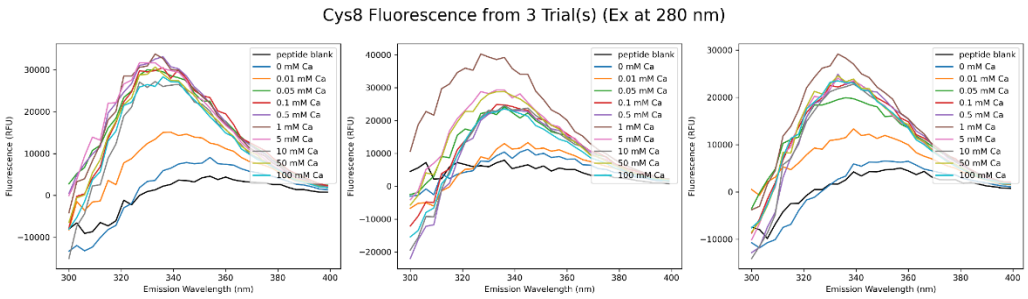

Figure D.87 Dap-K6-(D-C8)-E12-W13 membrane binding emission spectra Aquired on TECAN M1000 instrument at 37 °C.

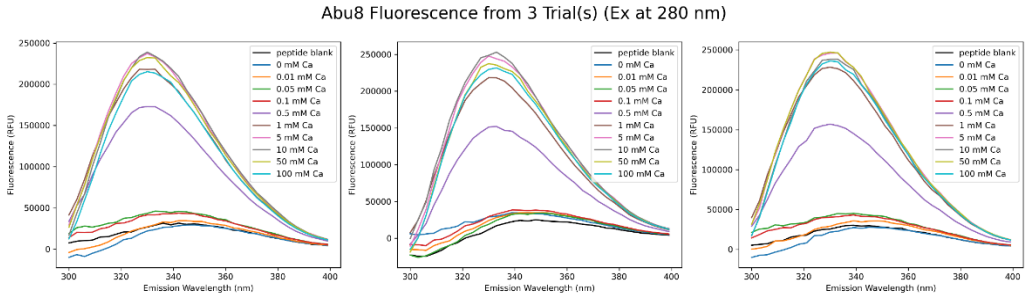

Figure D.88 Dap-K6-(D-Abu8)-E12-W13 membrane binding emission spectra Aquired on TECAN M1000 instrument at 37 °C.

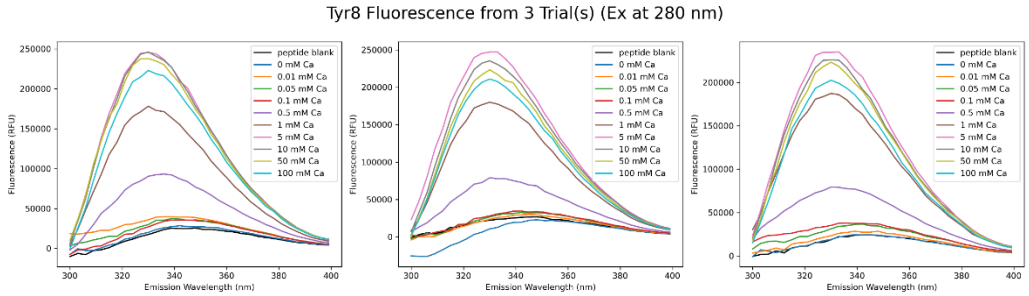

Figure D.89 Dap-K6-(D-Y8)-E12-W13 membrane binding emission spectra Aquired on TECAN M1000 instrument at 37 °C.

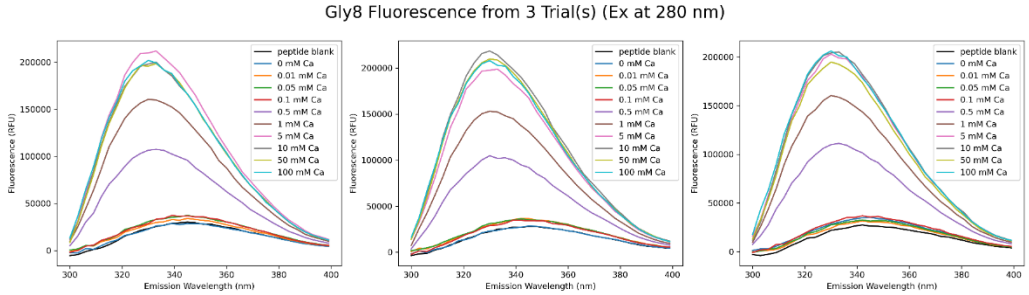

Figure D.90 Dap-K6-(G8)-E12-W13 membrane binding emission spectra Aquired on TECAN M1000 instrument at 37 °C.

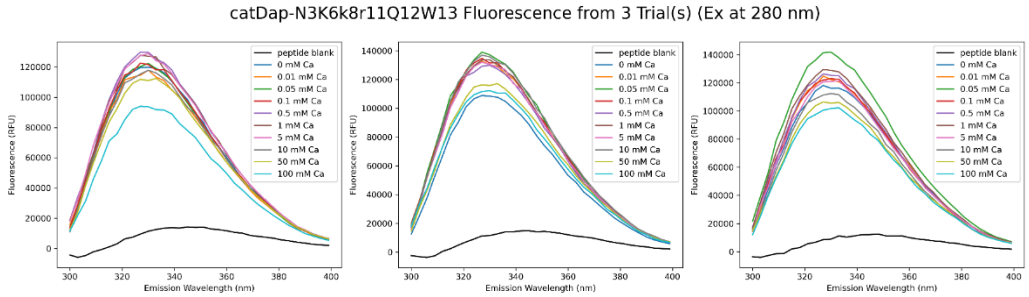

Figure D.91 Dap-N3-K6-(D-K8, D-R11)-Q12-W13 membrane binding emission spectra Aquired on TECAN M1000 instrument at 37 °C.

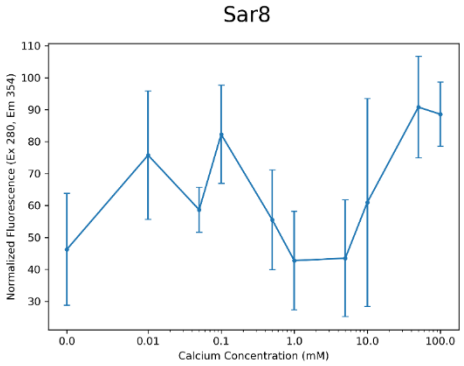

Figure D.92 Dap-K6-(D-Sar)-E12-W13 membrane binding curve No increase in fluorescence observed.

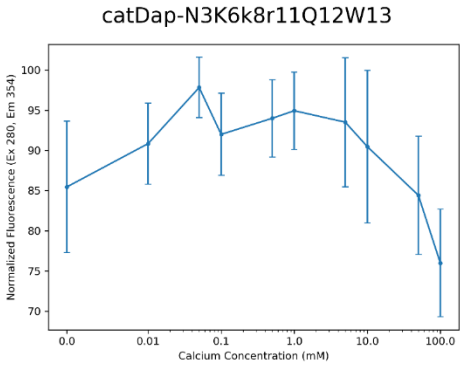

Figure D.93 Dap-N3-K6-(D-K8, D-R11)-Q12-W13 membrane binding curve No increase in fluorescence observed

Appendix E

Letters of Copyright Permission

Permission for manuscript included in Chapter 2.

Copyright Clearance Center RightsLink®

Home | Help | Live Chat | Sign in | Create Account

ACS Publications
Most Trusted. Most Cited. Most Read.

Total Synthesis of Paenibacterin and Its Analogues

Author: Michael Noden, Ryan Moreira, En Huang, et al
Publication: The Journal of Organic Chemistry
Publisher: American Chemical Society
Date: May 1, 2019

Copyright © 2019, American Chemical Society

PERMISSION/LICENSE IS GRANTED FOR YOUR ORDER AT NO CHARGE

This type of permission/license, instead of the standard Terms & Conditions, is sent to you because no fee is being charged for your order. Please note the following:

- Permission is granted for your request in both print and electronic formats, and translations.
- If figures and/or tables were requested, they may be adapted or used in part.
- Please print this page for your records and send a copy of it to your publisher/graduate school.
- Appropriate credit for the requested material should be given as follows: "Reprinted (adapted) with permission from (COMPLETE REFERENCE CITATION). Copyright (YEAR) American Chemical Society." Insert appropriate information in place of the capitalized words.
- One-time permission is granted only for the use specified in your request. No additional uses are granted (such as derivative works or other editions). For any other uses, please submit a new request.

BACK CLOSE WINDOW

Permission for manuscript included in Chapter 4.

CCC RightsLink®

Home | Help | Live Chat | Sign in | Create Account

ACS Publications
Most Trusted. Most Cited. Most Read.

Enantioselective Synthesis and Application of Small and Environmentally Sensitive Fluorescent Amino Acids for Probing Biological Interactions

Author: Michael Noden, Scott D. Taylor
Publication: The Journal of Organic Chemistry
Publisher: American Chemical Society
Date: Sep 1, 2021

Copyright © 2021, American Chemical Society

PERMISSION/LICENSE IS GRANTED FOR YOUR ORDER AT NO CHARGE

This type of permission/license, instead of the standard Terms and Conditions, is sent to you because no fee is being charged for your order. Please note the following:

- Permission is granted for your request in both print and electronic formats, and translations.
- If figures and/or tables were requested, they may be adapted or used in part.
- Please print this page for your records and send a copy of it to your publisher/graduate school.
- Appropriate credit for the requested material should be given as follows: "Reprinted (adapted) with permission from (COMPLETE REFERENCE CITATION). Copyright (YEAR) American Chemical Society." Insert appropriate information in place of the capitalized words.
- One-time permission is granted only for the use specified in your RightsLink request. No additional uses are granted (such as derivative works or other editions). For any uses, please submit a new request.

If credit is given to another source for the material you requested from RightsLink, permission must be obtained from that source.

BACK CLOSE WINDOW

Permission for Table 1.1:

ELSEVIER LICENSE
TERMS AND CONDITIONS

Jun 06, 2021

This Agreement between Michael Noden ("You") and Elsevier ("Elsevier") consists of your license details and the terms and conditions provided by Elsevier and Copyright Clearance Center.

License Number	5083141013127
License date	Jun 06, 2021
Licensed Content Publisher	Elsevier
Licensed Content Publication	International Journal of Antimicrobial Agents
Licensed Content Title	Paenibacterin, a novel broad-spectrum lipopeptide antibiotic, neutralises endotoxins and promotes survival in a murine model of Pseudomonas aeruginosa-induced sepsis
Licensed Content Author	En Huang,Ahmed E. Yousef
Licensed Content Date	Jul 1, 2014
Licensed Content Volume	44
Licensed Content Issue	1
Licensed Content Pages	4
Start Page	74
End Page	77
Type of Use	reuse in a thesis/dissertation
Portion	figures/tables/illustrations
Number of figures/tables/illustrations	1
Format	both print and electronic
Are you the author of this Elsevier article?	No
Will you be translating?	No
Title	Synthesis and Study of Cyclic Lipopeptide Antibiotics
Institution name	University of Waterloo
Expected presentation date	Sep 2021
Portions	Table 1
Requestor Location	Michael Noden 35 Waverly Rd Kitchener, ON N2G2E1 Canada Attn: Michael Noden
Publisher Tax ID	GB 494 6272 12
Total	**0.00 CAD**
Terms and Conditions	